Science

22 December 2006 | $10

Breakthrough of the Year

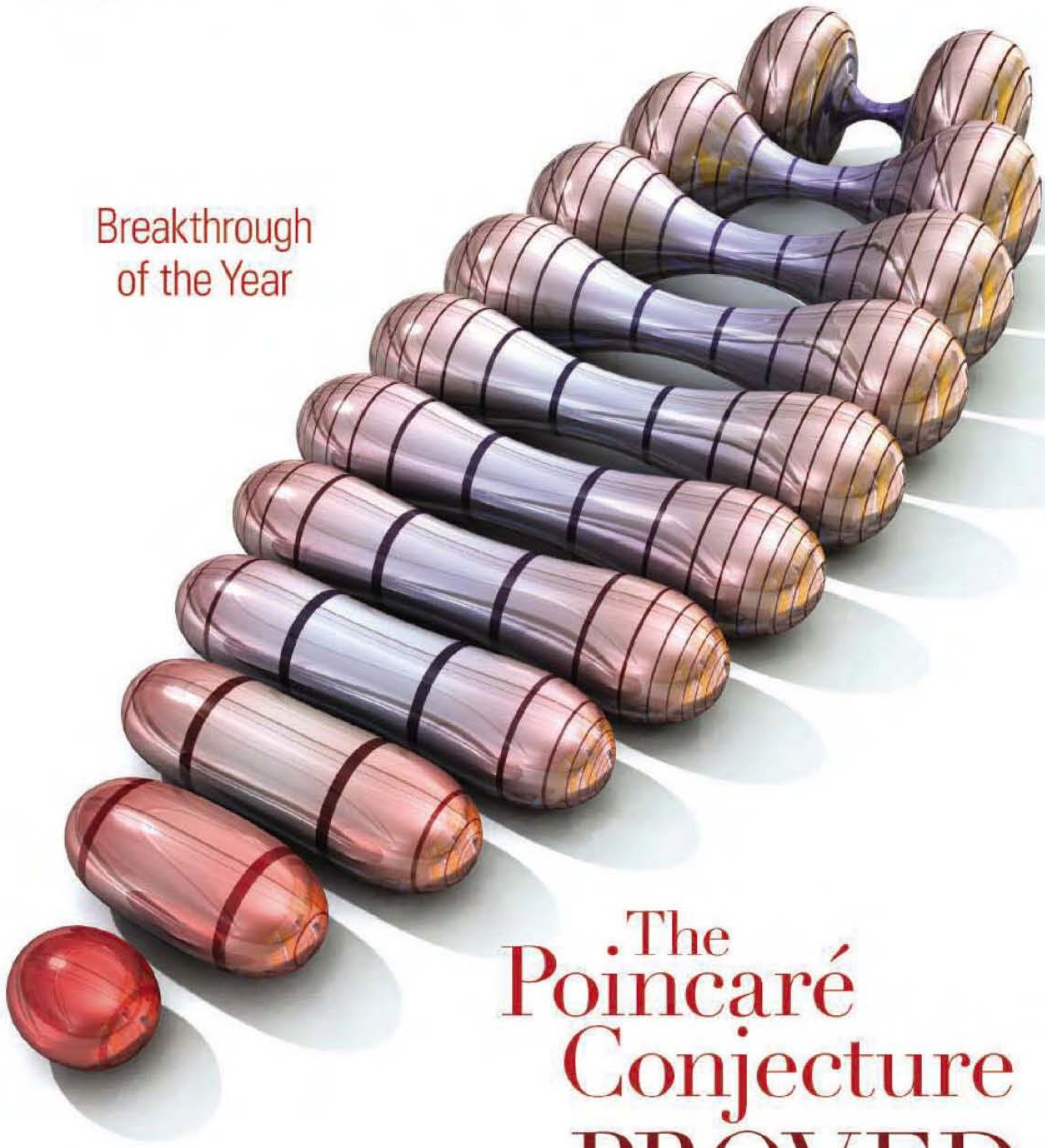

The Poincaré Conjecture PROVED

AAAS

CONTENTS

Volume 314, Issue 5807

COVER

To prove the Poincaré Conjecture, Grigori Perelman used the equations for Ricci flow—a procedure for transforming irregular spaces into uniform ones. In this two-dimensional example, the equations prescribe that negatively curved regions (blue) must expand while positively curved regions (red) contract. Over time, the original dumbbell-shaped surface evolves into a sphere. See the Breakthrough of the Year special section beginning on page 1848.

Image: Cameron Slayden/cosmocyte.com, based on data provided by Robert Sinclair

DEPARTMENTS

EDITORIAL

SPECIAL SECTION

Breakthrough of the Year

WINNER

RUNNERS-UP

OTHER FEATURES


1852

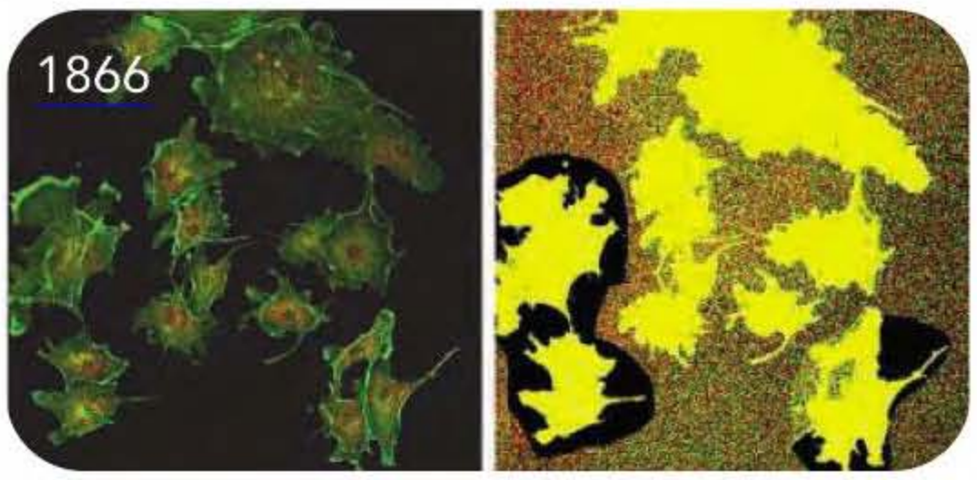
1866

NEWS OF THE WEEK

NEWS FOCUS

CONTENTS continued >>

SCIENCE EXPRESS

www.sciencexpress.org

PLANT SCIENCE

Nuclear Activity of MLA Immune Receptors Links Isolate-Specific and Basal Disease-Resistance Responses
Q.-H. Shen et al.
Plant immune receptors that detect pathogen attack trigger resistance responses by derepressing a transcriptional regulatory loop.
10.1126/science.1136372

GENETICS

A "Silent" Polymorphism in the *MDR*1 Gene Changes Substrate Specificity
C. Kimchi-Sarfaty et al.
A rare, but synonymous, codon in alleles of a drug-resistance gene can change translation kinetics and so produce a conformationally distinct protein species.
10.1126/science.1135308

PERSPECTIVE: SNPs, Silent But Not Invisible
A. A. Komar
10.1126/science.1138239

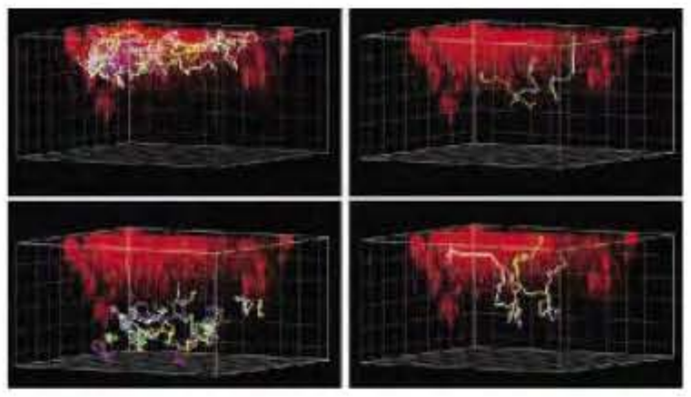

IMMUNOLOGY

Imaging of Germinal Center Selection Events During Affinity Maturation
C. D. C. Allen, T. Okada, H. L. Tang, J. G. Cyster
During selection of immune cells that make high-affinity antibodies within lymph nodes, the cells are highly mobile and seem to compete for help from other immune cells.
10.1126/science.1136736

CHEMISTRY

Chemical and Spectroscopic Evidence for an Fe^{V}-Oxo Complex
F. Tiago de Oliveira et al.
A high valent state of iron implicated in many enzymatic and environmental oxidations has been characterized in a stable compound at low temperature.
10.1126/science.1133417

LETTERS

BOOKS *ET AL.*

EDUCATION FORUM

PERSPECTIVES

BREVIA

EVOLUTION

MOLECULAR BIOLOGY

RESEARCH ARTICLES

CLIMATE CHANGE

VIROLOGY

BIOCHEMISTRY

CONTENTS continued **>>**

Science

REPORTS

ADVANCING SCIENCE, SERVING SOCIETY

SCIENCE (ISSN 0036-8075) is published weekly on Friday, except the last week in December, by the American Association for the Advancement of Science, 1200 New York Avenue, NW, Washington, DC 20005. Periodicals Mail postage (publication No. 484460) paid at Washington, DC, and additional mailing offices. Domestic individual membership and subscription (51 issues): $139 ($74 allocated to subscription). Domestic institutional subscription (51 issues): $650; Foreign postage extra: Mexico, Caribbean (surface mail) $55; other countries (air assist delivery) $85. First class, airmail, student, and emeritus rates on request. Canadian rates with GST available upon request, GST #1254 88122. Publications Mail Agreement Number 1069624. **Printed in the U.S.A.**

Change of address: Allow 4 weeks, giving old and new addresses and 8-digit account number. **Postmaster:** Send change of address to AAAS, P.O. Box 96178, Washington, DC 20090–6178. **Single-copy sales:** $10.00 current issue, $15.00 back issue prepaid includes surface postage; bulk rates on request. The identification code for *Science* is 0036-8075. *Science* is indexed in the *Reader's Guide to Periodical Literature* and in several specialized indexes.

CONTENTS continued **>>**

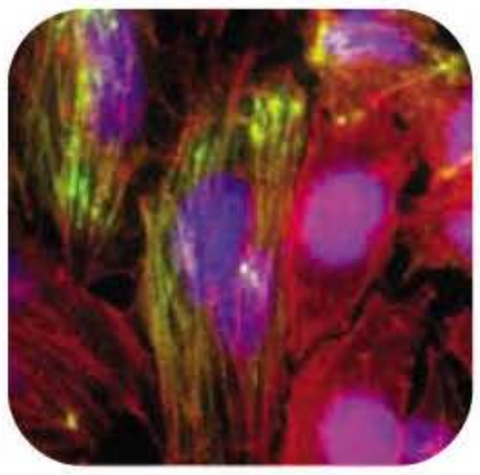

Cellular architecture breaks down.

SCIENCE**NOW**

www.sciencenow.org DAILY NEWS COVERAGE

A Genetic Culprit for Pancreatic Cancer
Afflicted family provides clues to origins of disease.

No Pain Is Science's Gain
Children who don't hurt help researchers identify critical pain protein.

Hysteria Is All in Your Head
But it is real, according to a new study of the cryptic disorder.

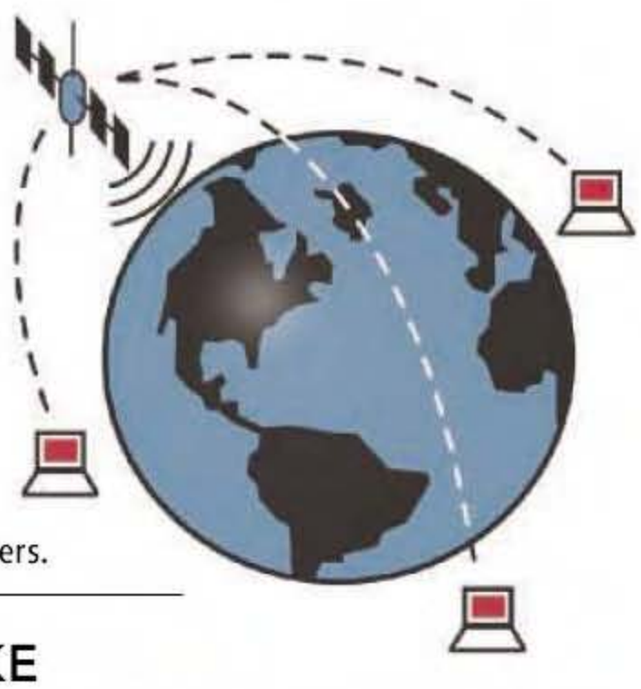

Discussions without borders.

SCIENCE'S **STKE**

www.stke.org SIGNAL TRANSDUCTION KNOWLEDGE ENVIRONMENT

FORUM: Questions and Controversies in Zinc Signaling
Read about new evidence for zinc in synaptic transmission and the link between zinc and apoptosis.

MY STKE
Take advantage of personalization tools to help you work more efficiently.

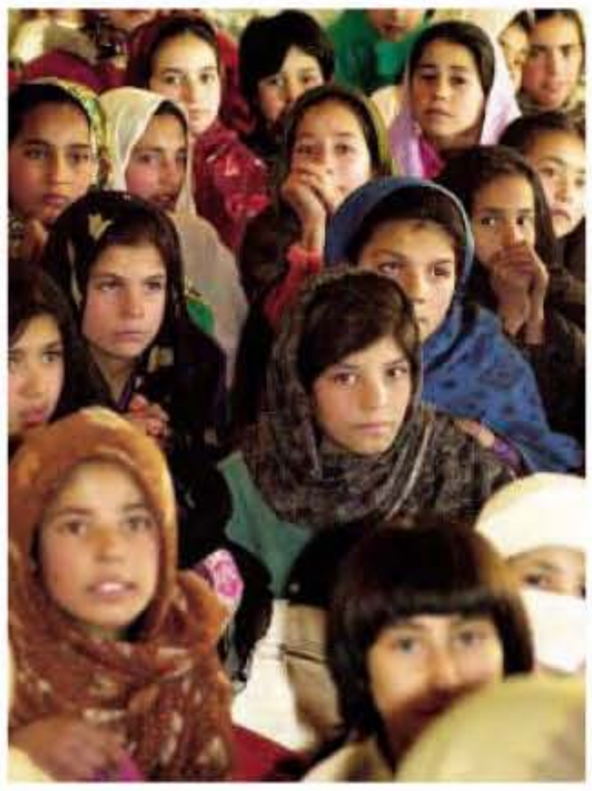

Science applied to humanitarian needs.

SCIENCE **CAREERS**

www.sciencecareers.org CAREER RESOURCES FOR SCIENTISTS

FRANCE: Science in an International and Humanitarian Context
L. Dicks
UNESCO offers young scientists a chance to apply their work to humanitarian needs.

US: A Model Archaeologist
P. Shulman
Former fashion model Amanda Adams helps unravel the secrets of geographic sites.

MISCINET: Managing Your Money While in College
R. Arnette
It is important to keep track of your finances and manage your money wisely during your college years.

SCIENCE**PODCAST**

Listen to the 22 December *Science* Podcast to hear about the best, worst, and most unusual science stories of 2006.
www.sciencemag.org/about/podcast.dtl

Separate individual or institutional subscriptions to these products may be required for full-text access.

EDITED BY STELLA HURTLEY AND PHIL SZUROMI

<< Be Prepared

Reproduction and population growth are driven by the availability of resources. **Boutin *et al.*** (p. 1928) provide evidence that two species of squirrel adjust their reproductive investment to match future increases in seed production, rather than simply tracking current or past seed production. Thus, reproductive investment of seed eaters can respond to future food availability, which creates an intriguing parallel in reproductive strategies between trees and the animals that consume their seed.

Looking Closely at Oligocene Climate

Changes in solar forcing caused by Earth's orbital motion not only have direct effects on climate but can also exert indirect effects on greenhouse gases such as CO_2. **Pälike *et al.*** (p. 1894) assembled a detailed, 13-million-year–long record of oxygen and carbon isotopes that span the entire Oligocene, a key period of Earth's transformation from a warm world essentially free of high-latitude ice sheets to one with persistent glaciation in Antarctica. Using a box model of the carbon cycle, they show how the global carbon cycle can amplify long-term solar forcing and attenuate shorter-term ones in a manner controlled mainly by the residence time of carbon in the oceans.

Death of a Solar System

At the end of its life, a star like the Sun blows away all of its outer layers and compresses into a white dwarf. **Gänsicke *et al.*** (p. 1908) have spotted the remnant debris from a planetary or asteroidal system orbiting a white dwarf. The disk of material is rich in heavy elements (metals) and shows a double-peaked emission line profile characteristic of material in orbit around a star.

Gently Probing Spins

Photoluminescent and charge-injection methods can determine single electron spin states but do not leave the spin state intact. For quantum information processing based on the spin storage and manipulation, the states need to be left intact after measurement. **Berezovsky *et al.*** (p. 1916, published online 9 November) describe the use of optical Kerr rotation that can probe the spin state of a single electron on a quantum dot nondestructively.

A Gulf Between Two Gaps

In the high-temperature superconductors, the onset of superconductivity is preceded by a region known as the pseudogap, particularly in underdoped samples. The relation of the pseudogap to superconductivity has been controversial, in part because different experiments have generated conflicting results. With improvements in sample quality and using an optimized, angle-resolved photoemission spectroscopy technique, **Tanaka *et al.*** (p. 1910, published online 16 November) reveal the presence of two gaps with different doping dependence, one gap with the pseudogap and the other with the superconducting gap. **Valla *et al.*** (p. 1914, published online 16 November) present results of a photoemission and scanning tunneling microscopy study on a nonsuperconducting cuprate that still exhibits the *d*-wave signature of its superconducting cousins. The results suggest that the pseudogap regime is formed as electrons pair up, but without the global coherence associated with the superconducting state. These results, which suggest that the pseudogap and superconducting gap coexist but are not related, should have implications for understanding superconductivity mechanisms (see the Perspective by **Millis** and the 17 November news story by **Service**).

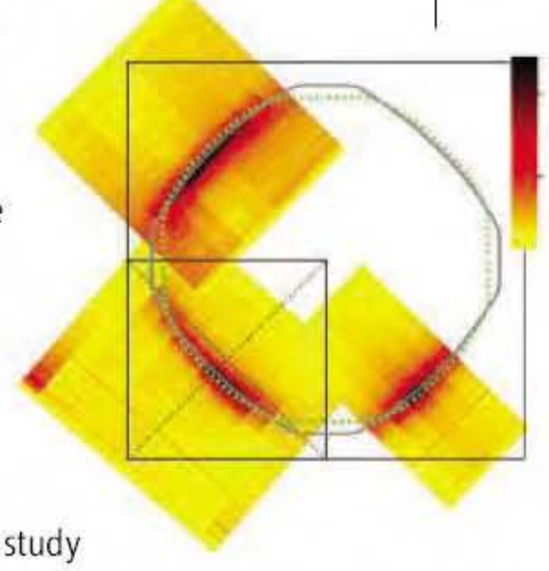

Seismic Seafloor Seep

Most of Earth's crust is created at mid-ocean ridges in eruptions of lava. **Tolstoy *et al.*** (p. 1920, published online 23 November; see the Perspective by **Chadwick**) have captured the seismic signature of a diking event as veins of lava broke through to the surface along the East Pacific Rise for 6 hours in January 2006. Their array of seismic detectors on the site monitored a gradual rise in seismic activity during the years leading up to the event and its waning thereafter.

The Origin of New Species

Homoploid hybrid speciation, the origin of a new species as a result of hybridization between two distinct species, is relatively rare in animals. **Gompert *et al.*** (p. 1923, published online 30 November), demonstrate that an adaptation to an extreme alpine environment has facilitated homoploid hybrid speciation in the *Lycaeides* butterflies of western North America. The hybrid species possesses a mosaic genome that is a mixture of the parental genomes and is reproductively isolated from both of the parental species.

European Giants

Enormous dinosaurs are the hallmark of many visions of prehistory, but fossil evidence for these giants has been limited to the New World and Africa. **Royo-Torres *et al.*** (p. 1925) now describe a specimen of a huge dinosaur (40 to 48 metric tons) recovered from Upper Jurassic to Lower Cretaceous rocks in Spain. The specimen represents a new clade of sauropods that seems

Continued on page 1839

CREDITS (TOP TO BOTTOM): PHILIPPE HENRY, WWW.PHILIPPE-HENRY.COM; VALLA *ET AL.*

Continued from page 1837

to have distinctly more primitive limb and bone structure than other giant sauropods found on other continents in Jurassic and Cretaceous rocks. Thus, enormous size arose in other groups of dinosaurs aside from the neosauropods.

Immunity and Influenza

Seasonal influenza exhibits high morbidity and mortality worldwide, so understanding its phylogenetics and dynamics is important. Despite its high mutation rate, there is limited observed diversity of influenza, perhaps because of generalized strain-transcendent immunity, but there is no evidence for generalized immunity in humans. However, there is evidence of antigenic clusters that sweep through the global human community between successive seasons. **Koelle *et al.*** (p. 1898; see the Perspective by **van Nimwegen**) introduce a phylodynamic model that allows for differences between influenza's genetic and antigenic properties and show that influenza's characteristic phylogeny can arise from cluster-specific immunity alone.

Details Define Double Duty

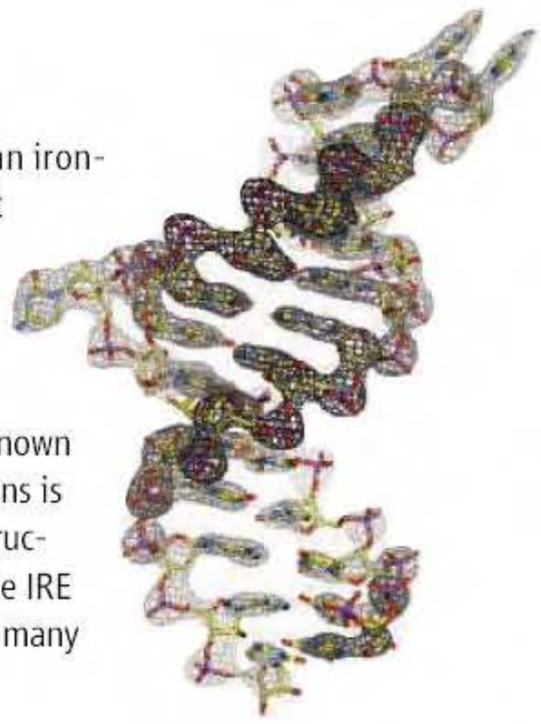

Iron regulatory protein 1 (IRP1) is a dual-function protein. With an iron-sulfur cluster bound, it is a cytosolic aconitase enzyme, but without it, IRP1 binds iron-responsive elements (IREs) in messenger RNA and regulates the expression of genes involved in iron transport, storage, and utilization. **Walden *et al.*** (p. 1903; see the Perspective by **Rouault**) now describe the structure of IRP1 bound to ferritin H IRE at 2.8 angstrom resolution and compare it with the known structure of cytosolic aconitase. The switch between the two functions is coupled to large-scale domain rearrangements, from a compact structure in the aconitase to an extended structure that interacts with the IRE at two sites. The RNA binding and enzyme active sites overlap with many amino acids that serve different roles in each state.

Small, But Not Overlooked

From a fragment of DNA obtained during a metagenomic study of a microbial community living in acid mine drainage, **Baker *et al.*** (p. 1933) have obtained evidence for a low-abundance lineage of archaea they call ARMAN (Archaeal Richmond Mine Acidophilic Nanoorganism). The DNA fragment carries a ribosomal RNA gene that indicates the organism's deep divergence from other archaeal groups. Members of the ARMAN group carry a gene encoding a pyrophosphatase that can be used in extracting energy from pyrite. Visualization with fluorescent in situ hybridization has revealed very small, ribosome-packed, irregularly shaped cells.

What's in a Vaccine?

After vaccination, the efficiency with which protective antibodies are produced often depends on the presence of an adjuvant, a substance that promotes activation of antibody-producing B cells. It has been anticipated that Toll-like receptors (TLRs) might be major players in mediating the effects of adjuvants. However, **Gavin *et al.*** (p. 1936; see the news story by **Wickelgren**) now find that the known TLR pathways do not modulate B cell responses and so adjuvants containing TLR ligands must depend on other properties. Such a revision to thinking about the effects of TLR on B cell responses will likely refocus current thinking about vaccine development.

The Pacemaker in the Pituitary

Endogenous annual rhythms drive many long-term cycles in physiology and behavior in long-lived vertebrates, but the anatomical and cellular basis of such rhythm generation remains a mystery. **Lincoln *et al.*** (p. 1941) analyzed prolactin secretion and its associated biological changes in sheep whose pituitary gland had been surgically disconnected from the central nervous system. Melatonin secretion by the pineal gland regulated the hormonal effect. Timer cells in the pituitary possess melatonin receptors that permit their regulation by the duration of the melatonin signal. These timer cells, in turn, drive the prolactin synthesizing and secreting cells, which themselves lack melatonin receptors.

CREDIT: WALDEN *ET AL.*

Donald Kennedy is the Editor-in-Chief of *Science*.

Breakthrough of the Year

LAST YEAR, EVOLUTION WAS THE BREAKTHROUGH OF THE YEAR; WE FOUND IT FULL OF NEW developments in understanding how new species originate. But we did get a complaint or two that perhaps we were just paying extra attention to the lively political/religious debate that was taking place over the issue, particularly in the United States.

Perish the thought! Our readers can relax this year: Religion and politics are off the table, and *n*-dimensional geometry is on instead. This year's Breakthrough salutes the work of a lone, publicity-shy Russian mathematician named Grigori Perelman, who was at the Steklov Institute of Mathematics of the Russian Academy of Sciences until 2005. The work is very technical but has received unusual public attention because Perelman appears to have proven the Poincaré Conjecture, a problem in topology whose solution will earn a $1 million prize from the Clay Mathematics Institute. That's only if Perelman survives what's left of a 2-year gauntlet of critical attack required by the Clay rules, but most mathematicians think he will.

The analysis supplied by Dana Mackenzie on p. 1848 struck me as a fascinating exploration, full of metaphors suggesting a multidisciplinary dimension in Perelman's analysis. He first got interested in Ricci flow, a process by which topological regions of high curvature flow into regions of lower curvature. He also identified a quantity, which he called "entropy," that increased during the flow, providing a gradient. Tight spots in spatial connections block the application of these rules to dimensions higher than two, so Perelman dealt with these through "surgical intervention." This story is rich with borrowings: from fluid mechanics, thermodynamics, and even surgery! It's hard to deal with a three-dimensional object in four-dimensional space. Perelman's solution is a stunning triumph of intellect. Alas, it has led to bitter controversy, involving others but not Perelman.

Of course, in any Breakthrough year we are obliged to have a Breakdown. This time around, we had to blow the whistle on ourselves. In recognizing this as a year in which scientific fraud took center stage, it was clear that we had to lead with the story involving the retraction of two of our own papers, an event that drew worldwide press attention and required us to ask for an outside evaluation of how we had handled the papers. That brought us some tough news about how competitive the scientific enterprise has become, and the consequential incentive to push (or shred) the ethical envelope.

On the positive side, it was a rich year for important experimental studies. My favorites include some new explanations for how species originate, one of the daunting post-Darwinian puzzles. Among other examples, there is a clear case for speciation through hybridization, an exception to the more general rule that hybrids either don't make it or are reproductively incompetent. Because I like coastlines, when I see new evidence about sea-level rise, I pay attention. This year we got new measures of rates of glacial melting at both ends of the globe: in Greenland, where rates are in hundreds of gigatons a year, and in Antarctica, where drainage by ice streams is accelerating. I also follow the Neanderthal story, because it's interesting to ponder how different human species—now thought from archaeological evidence to have overlapped for perhaps 10,000 years—might have interacted. New sequencing of the Neanderthal genome indicates that the point of divergence is nearly half a million years old and opens up a wealth of comparisons with the human genome sequence. The question everyone asks—"Did they have sex?"—is still open, though barely.

All in all, it's not been a bad year. The predictions we made in 2005 of "Areas to Watch" turned out pretty well. We said RNA interference would be an active sector—good call. Cosmic-ray capture didn't work out, but there was the predicted level of activity on the "small worlds" of microbial communities. We predicted lots of activity on high-temperature superconductivity, and there were more applications, although less new theory. The worst miss was the prediction that the ivory-billed woodpecker would be re-found. Come on, birders, give us some help out there; a good photo, please, not the skin.

– Donald Kennedy

10.1126/science.1138510

EDITORS' CHOICE

EDITED BY GILBERT CHIN AND JAKE YESTON

GENETICS

Color Convergence in Columbines

Anthocyanins are pigment molecules commonly found in red, blue, and purple flowers. Columbine flowers are imbued with anthocyanins, and this plant is known to have undergone a recent and rapid divergence, most likely as a result of strong selection by pollinators for floral traits such as color.

Using a phylogenetic framework, Whittall *et al.* have investigated the convergent loss—that is, the loss of the same trait across multiple evolutionary lineages—of anthocyanin biosynthesis in columbines, which has resulted in flowers that are yellow or white. They found six independent losses (four fixed and two polymorphic) and no gains of floral anthocyanins. Quantitating the anthocyanin precursors in three species without anthocyanin loss and eight species with loss demonstrated that the loss of anthocyanin correlated with a broad convergence in the reduced expression of genes that occur in the later stages of the biosynthetic pathway. Additionally, two of these genes are regulated by a single gene and demonstrated a correlated reduction of expression in five lineages, suggesting that the mutation causing anthocyanin loss is a regulatory component and not a structural one (enzyme). These data show that there is an evolutionary constraint on some of the genes in anthocyanin biosynthesis, most likely because upstream intermediates are also useful in protecting plants against UV damage, insects, and pathogens. — LMZ

Mol. Ecol. **15**, 4645 (2006).

CHEMISTRY

Taste and Timing

Modern water treatment protocols have gone a long way toward the efficient elimination of toxic contaminants in municipal supplies. However, certain benign impurities may remain and give rise to unpleasant tastes or odors. One challenge in adopting a general strategy for treating such "T&O" compounds is their varying proportions in different water sources. Effective remediation thus requires detailed knowledge of the distinct chemistry of each substance.

Toward this end, Peter and von Gunten present a systematic study of the oxidation kinetics of 11 common organic T&O contaminants by both ozone and hydroxyl radicals. The targets, spanning a variety of alcohols, aldehydes, ketones, and ethers, were treated individually with the oxidants in ultrapure water, and measured rate constants were then used to predict the degradation kinetics observed in spiked samples of natural water from two different lakes. In general, the predictions and measurements showed strong agreement. Five of the compounds were very efficiently oxidized by ozone, with rate constants of ~10^5 $M^{-1}s^{-1}$. Trihaloanisoles proved the most resistant to preliminary ozonation but were rapidly degraded by hydroxyl radicals. The authors note that hydroxyl radical protocols would need to be applied carefully to avoid excessive production of toxic bromate ions from residual aqueous bromide salts. — JSY

Environ. Sci. Technol. 10.1021/es061687b (2006).

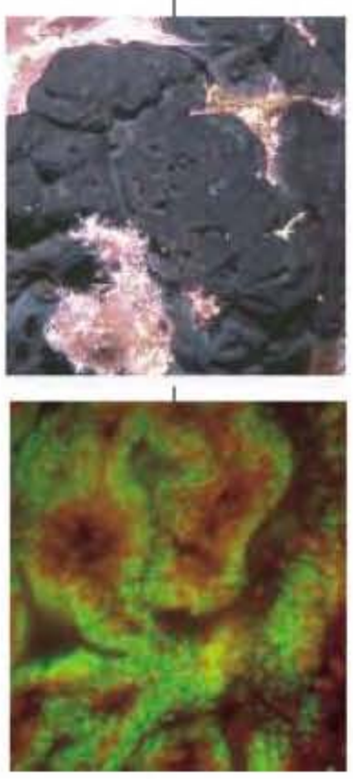

The Pacific sponge *Corticium* (top), and resident bacteria (green) and archaea (red).

ECOLOGY

Mopping Up Little Helpers

Sponges (Porifera) hold an interesting evolutionary position (sitting between the choanoflagellates and other animals), being conglomerations of cells, with some functional and morphological differentiation, loosely organized around a spongocoel cavity. Many sponges host an array of prokaryotes, some of which may accumulate passively as the sponge filters seawater; indeed, one view is that the sponge cells serve merely as an inert scaffold for prokaryote communities.

However, Sharp *et al.* show in a 3-year study that this association can persist beyond happenstance. They find that sponge embryos travel with a contingent of prokaryotes that are inherited vertically, implying that there are selective mechanisms of transmission and recruitment. Like the somatic cells of the sponge, the prokaryotic denizens display a functional differentiation, with some specializing in sulfur oxidation or nitrogen fixation, and they probably contribute to mutualistic nutrient cycling within the sponge. Furthermore, some of the bacteria appear to produce bioactive compounds, which may aid host defenses. — CA

Appl. Environ. Microbiol. 10.1128/AEM.01493-06 (2006).

APPLIED PHYSICS

Copper Confinement

As microelectronic circuitry continues to shrink, and devices are packed onto chips at increasingly higher densities, two main concerns must be addressed: heat dissipation and interconnection reliability. Copper has therefore begun to replace aluminum as the metal of choice for on-chip wiring, on account of both its lower resistivity (which reduces heat generation) and its resistance to electromigration. However, Cu tends to diffuse rapidly into silicon, generating electronic traps within the Si bandgap that are detrimental to device performance. To address this shortcoming, the use of diffusion barriers between Si and Cu is being explored. The materials composing such barriers must be compatible with the fabri-

CREDITS (TOP TO BOTTOM): JOHANN SCHUMACHER/PETER ARNOLD; SHARP ET AL., APPL. ENVIRON. MICROBIOL. 10.1128/AEM.01493-06 (2006)

cation process and also resistant to recrystallization during the high-temperature processing steps, a typical cause of failure. Hafnium nitride (HfN_x), with a melting temperature exceeding 3300°C, has attracted strong interest in this vein. Rawal *et al*. have investigated the combined use of thin layers of Ge/HfN_x as a diffusion barrier. They find that the bilayer system is more effective than a single HfN_x barrier layer, a result that they attribute to the ready reaction of Ge with Cu to form Cu_3Ge, thereby immobilizing much of the Cu that could otherwise diffuse through the HfN_x layer. — ISO

Appl. Phys. Lett. **89**, 231914 (2006).

GEOLOGY

Glass at a Crash Site

Hundreds of thousands of years ago, Stone Age peoples inhabited the Dakhleh Oasis, in central western Egypt, when the ancient landscape included lakes. The area has attracted substantial archaeological and geological investigation, and

The present-day Dakhleh Oasis.

one unresolved mystery has been the origin of unusual darkly colored glass, termed "Dakhleh glass," found at the site. Osinski *et al.* have probed the glass using x-ray fluorescence techniques, isotopic analysis, and electron microscopy. Its chemical composition (in particular, an anomalously high proportion of CaO and Al_2O_3) differs from that of all known volcanic glasses, and there is no evidence of volcanism in the region. The authors argue that the glass was probably created through a meteorite impact occurring 100,000 to 200,000 years ago. The energy of the impact would have fused the local carbonate and sandstone rocks into glass. The imprints of plant stems and leaves from that time were also uncovered in the glass, but no signs of shock metamorphosis were evident. Because an impact crater has not yet been located, the authors note the possibility of an aerial burst; in either case, such an event would have devastated the local population. — JB

Earth Planet. Sci. Lett. 10.1016/j.epsl.2006.10.039 (2006).

CREDIT: OSINSKI *ET AL.*, *EARTH PLANET. SCI. LETT.* 10.1016/J.EPSL.2006.10.039 (2006)

ECOLOGY/EVOLUTION

A Conservation of Clouds

DNA sequencing and careful morphometric analysis can reveal hidden differences between populations of organisms originally considered members of a single species, which can lead to their reclassification as two or more species. Such taxonomic splitting can have important implications for conservation if, for example, an already rare species turns out to be two or more even rarer ones.

The clouded leopard, *Neofelis nebulosa*, is such an example. This increasingly rare animal is found in the tropical forests of Southeast Asia, with the subspecies *N .n. nebulosa* occurring on the mainland and the subspecies *N. n. diardii* on the islands of Borneo and Sumatra. Buckley-Beason *et al.* compared nuclear and mitochondrial DNA sequences from several mainland and island individuals, and they concluded that the genetic differences were at least as great as those among other large cat species (lion, tiger, leopard, jaguar, and snow leopard). Kitchener *et al.* compared the coat patterns of a larger sample of individuals and found clear evidence for two distinct groups on the basis of the size and shape of the clouds on the shoulders of these animals; they recommend that the clouded leopard now become two distinct species, *N. nebulosa* and *N. diardii*. — AMS

Curr. Biol. **16**, 2371; 2377 (2006).

PSYCHOLOGY

'Tis the Season

Although the giving of gifts is a common activity at this time of year, giving a gift certificate has become an allowable substitute for giving money, which is generally regarded as unseemly. In order to explore whether money can serve not only as a useful instrument (for the purchase of material goods) but also as a valued resource, Briers *et al.* have carried out a series of experiments to see whether an unfulfilled desire for food (or money) might make one more tight-fisted (or more voracious). People who were hungry behaved less generously toward a charity (Médecins Sans Frontières) and in public goods games than those who had just eaten cake; conversely, people who were told to imagine being desirous of a substantial payoff (being in such a state was confirmed by how much their estimates of the size of a coin were skewed to be larger than actual) consumed more M&M's than those who were focused on a modest windfall. These results linking the rewarding character of food to that of money dovetail neatly with a recent study (Vohs *et al.*, Reports, p. 1154, 17 November 2006) that demonstrated money's value as a means of enhancing one's self-sufficiency and social independence. — GJC

Psychol. Sci. **17**, 939 (2006).

www.sciencemag.org

Science

1200 New York Avenue, NW
Washington, DC 20005
Editorial: 202-326-6550, FAX 202-289-7562
News: 202-326-6500, FAX 202-371-9227

Bateman House, 82-88 Hills Road
Cambridge, UK CB2 1LQ
+44 (0) 1223 326500, FAX +44 (0) 1223 326501

Subscription Services For change of address, missing issues, new orders and renewals, and payment questions: 866-434-AAAS (2227) or 202-326-6417, FAX 202-842-1065. Mailing addresses: AAAS, P.O. Box 96178, Washington, DC 20090-6178 or AAAS Member Services, 1200 New York Avenue, NW, Washington, DC 20005

Institutional Site Licenses please call 202-326-6755 for any questions or information

Reprints: Author Inquiries 800-635-7181
Commercial Inquiries 803-359-4578
Corrections 202-326-6501

Permissions 202-326-7074, FAX 202-682-0816

Member Benefits Bookstore: AAAS/BarnesandNoble.com bookstore www.aaas.org/bn; Car purchase discount: Subaru VIP Program 202-326-6417; Credit Card: MBNA 800-847-7378; Car Rentals: Hertz 800-654-2200 CDP#343457, Dollar 800-800-4000 #AA1115; AAAS Travels: Betchart Expeditions 800-252-4910; Life Insurance: Seabury & Smith 800-424-9883; Other Benefits: AAAS Member Services 202-326-6417 or www.aaasmember.org.

science_editors@aaas.org (for general editorial queries)
science_letters@aaas.org (for queries about letters)
science_reviews@aaas.org (for returning manuscript reviews)
science_bookrevs@aaas.org (for book review queries)

Published by the American Association for the Advancement of Science (AAAS), *Science* serves its readers as a forum for the presentation and discussion of important issues related to the advancement of science, including the presentation of minority or conflicting points of view, rather than by publishing only material on which a consensus has been reached. Accordingly, all articles published in *Science*—including editorials, news and comment, and book reviews—are signed and reflect the individual views of the authors and not official points of view adopted by the AAAS or the institutions with which the authors are affiliated.

AAAS was founded in 1848 and incorporated in 1874. Its mission is to advance science and innovation throughout the world for the benefit of all people. The goals of the association are to: foster communication among scientists, engineers and the public; enhance international cooperation in science and its applications; promote the responsible conduct and use of science and technology; foster education in science and technology for everyone; enhance the science and technology workforce and infrastructure; increase public understanding and appreciation of science and technology; and strengthen support for the science and technology enterprise.

Information for Contributors

See pages 102 and 103 of the 6 January 2006 issue or access www.sciencemag.org/feature/contribinfo/home.shtml

From Red to Dead >>

There has been talk for decades about replenishing the rapidly shrinking Dead Sea, between Israel and Jordan, by channeling water from the Red Sea.

Last week, the two countries and the Palestinian Authority agreed at a meeting in Jordan to study the idea. The World Bank is rounding up donors to finance a 2-year, $15.5 million analysis of the feasibility of transferring water 180 kilometers through Jordan via a canal from the Gulf of Aqaba.

The Dead Sea's water level is now sinking by about a meter a year, accelerated by draw-offs from its main source, the Jordan River, as well as an 80-year dry phase in the Middle East. In addition to stemming the decline, a water transfer would open opportunities for hydropower and desalination, both of which could harness the 400-meter drop between the Red and Dead seas.

Environmentalists say the project, estimated to cost $5 billion and take a decade, would disrupt numerous ecosystems. The biggest risk is salinization of groundwater near the canal, says Boston University geologist Farouk El-Baz. But he says "it's a good idea" that could help ease political problems by boosting the economy.

He Said, She Said

The use of irregular verbs such as "run" or "bring" reveals how boys and girls employ slightly different strategies in language-learning, say psychologists at Georgetown University in Washington, D.C.

As tots learn new words, they tend to "overregularize" verbs—that is, apply the past tense "-ed" even to irregular ones, saying "holded" instead of "held," for example.

To see whether the sexes differ, Michael Ullman and colleagues analyzed transcripts of utterances by 25 children—10 girls and 15 boys—between the ages of 2 and 5. Because girls learn words faster and are more verbally fluent than boys, Ullman's team suspected that the girls would be better at irregular verbs. But they found that the girls overregularized more than three times as often as did the boys.

By comparing how the tots handled words that sound similar, the researchers claim they could distinguish whether the children were using associative strategies or following rules in deciding verb endings. When boys overregularize, they are more likely to use rule-governed, or "procedural," memory, the researchers report in the November issue of *Developmental Science*. But girls are more likely to go with associations—for example, because the past tense of blink is blinked, sink would become "sinked."

Harvard University cognitive psychologist Steven Pinker says that although the study is small, it adds to evidence that males and females sometimes use "different mixtures of underlying processes" to arrive at the same results. He calls regular and irregular verbs "a good model organism for contrasting the roles of computation [rule-following] with memory [association] in cognition."

CREDITS (TOP TO BOTTOM): NASA; KAREN KASMAUSKI/CORBIS; AMNH/DENIS FININ

MONKEYS IN THE LAB

Apes have been out-of-bounds for researchers in the United Kingdom since 1997. Will monkeys follow?

In view of increasingly vocal—and violent—protests over using monkeys in biomedical studies, the Medical Research Council asked a group led by Oxford University geneticist David Weatherall to do a thorough assessment of the scientific value of such research.

The report, issued last week, reaffirms the need for these primates, saying there is "a strong scientific case" for using monkeys in studies of communicable diseases such as AIDS, malaria, and tuberculosis, as well as disparate subjects such as vision, endometriosis, and memory. The group concluded that although alternative approaches such as cell biology and noninvasive imaging hold promise, monkey experiments remain the best approach in these areas.

Weatherall hopes the report will give the public some solid facts to consider. "There's a strong feeling in the U.K. that we have got to create a better public debate in this field," he says. "It has really got to a stage of quite extreme violence." Whether the report will cool down the U.K.'s animal wars remains to be seen. Animal activists promptly pounced on the report. And Vicky Robinson, head of a group that advises the government on reducing animals in research, said it did not go far enough in exploring alternatives.

NETWATCH >>

At Home With Troglodytes

***Homo heidelbergensis* from Atapuerca.**

The Atapuerca hills in northern Spain have been alive with the sound of picks and shovels, as archaeologists disinter the oldest hominid fossils in Europe and other important remains. Read about the history of the excavations at this site from the University of Burgos in Spain and the Atapuerca Foundation. The pages profile locales such as the Gran Dolina cavern, which has yielded 800,000-year-old skull fragments and other bones that may belong to a new human species, *Homo antecessor*. For the latest dig news, check out the report on this year's finds, which include the first nearly complete human skull unearthed in the area in more than a decade. The site also features a timeline that lets you cruise through 6 million years of human evolution, pausing at milestones such as the invention of tools some 2.5 million years ago and the settlement of Europe about 1 million years ago. >> www.atapuerca.com

EDITED BY KELLI WHITLOCK BURTON

Three Q's

Ten months after the two top editors of the *Canadian Medical Association Journal* (*CMAJ*) were fired amid conflicts over editorial independence (*Science*, 24 March, p. 1695), Canada's premier scientific publication has picked a new editor. Ottawa epidemiologist and blood-transfusion expert **Paul Hébert** will take over next month in a move that Robert Fletcher of Harvard University calls "the beginning of the healing process for what was a very troubling episode."

Q: Will *CMAJ* face continuing conflict over editorial independence from the association?

No. I've decided to give the CMA access to the editorials before the journal goes to print. But the association will not be allowed to change them. The association simply requested the ability to prepare responses to the editorials in advance. But it will be a cold day in hell before people start telling me what to do. And there's no way the CMA wants to repeat history.

Q: What shape is *CMAJ* in as you take over?

Very strong submissions continue to pour in. The journal continues to make news week after week with high-impact studies.

Q: Where do you want to lead the journal?

I want to craft a patient-centered research focus, as opposed to a basic-science research focus. I think the journal that will be of greatest use to the members and to the public will focus on health-services research, clinical-practice research, and policy research.

CREDITS (TOP TO BOTTOM): *CMAJ*; DAMIAN DOVARGANES/AP PHOTO

Got a tip for this page? E-mail people@aaas.org

IN THE NEWS

DOLL UNDER ATTACK. The late Oxford University epidemiologist Richard Doll, whose work in the 1950s helped demonstrate that smoking causes lung cancer, received consultancy fees from chemical companies whose products he was evaluating, according to recent revelations. Relying on documents Doll donated to the Wellcome Trust's library in London, the *Guardian* newspaper reported earlier this month that the scientist received up to $1500 per day from Monsanto during the 1980s and nearly $30,000 from the Chemical Manufacturers Association and two chemical companies for a report that largely cleared vinyl chloride as a cancer agent.

The heads of the Medical Research Council and the Royal Society, among others, have rushed to the defense of Doll, who died last year. They say there's no evidence that the payments compromised his research. But Richard Horton, editor of *The Lancet* and an outspoken advocate of high ethical standards, labels their response a "defensive overreaction," adding that potential conflicts of interest should be disclosed even if they did not violate the standards of the day.

AWARDS

MOVING DAY. Ten scientists working at research powerhouses around the world will be setting up their labs across Europe under a new program run by the European Molecular Biology Organization (EMBO). The EMBO installation grants, $66,000 annually for 3 to 5 years and funded by member nations, are intended to strengthen science across the continent. The first cohort will open labs in Poland, Portugal, Turkey, Croatia, the Czech Republic, and Estonia.

Creating new labs in this way will help boost science in Europe, but more must be done, says Marcin Nowotny, a postdoc at the U.S. National Institute of Diabetes and Digestive and Kidney Diseases, who is moving to the International Institute of Molecular and Cellular Biology in Warsaw, Poland. Young researchers also need support from established scientists, Nowotny adds.

Movers >>

FAMILY-FRIENDLY CLIMATE. The head of geosciences at the National Science Foundation is going to work next month for her Silicon Valley–based entrepreneur son on a start-up venture that's part of a new wave of "greentech" companies. Margaret Leinen, who has led the $700 million directorate for 7 years, announced this month that she will be joining Climos, a San Francisco–based research company backed by her 38-year-old son, Dan Whaley. In 1994, Whaley co-founded an online travel reservations company that was sold in 2000 for $750 million.

Leinen, a paleoclimatologist and former dean of oceanography at the University of Rhode Island, will become the chief scientific officer for Climos, which CEO Whaley says is investigating "a number of promising natural processes to mitigate climate change." Leinen, who will open a Washington, D.C., office for the company, says that she hopes her efforts will build ties between environmental scientists and industry. "I'm also thrilled to have the chance to work with my son."

The Poincaré Conjecture—PROVED

The solution of a century-old mathematics problem turns out to be a bittersweet prize

TO MATHEMATICIANS, GRIGORI PERELMAN'S proof of the Poincaré conjecture qualifies at least as the Breakthrough of the Decade. But it has taken them a good part of that decade to convince themselves that it was for real. In 2006, nearly 4 years after the Russian mathematician released the first of three papers outlining the proof, researchers finally reached a consensus that Perelman had solved one of the subject's most venerable problems. But the solution touched off a storm of controversy and drama that threatened to overshadow the brilliant work.

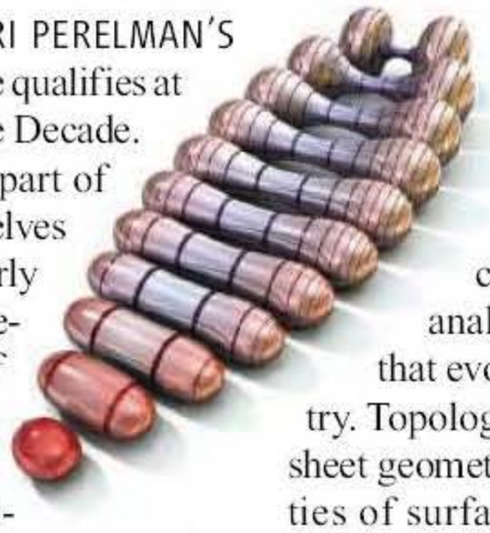

Perelman's proof has fundamentally altered two distinct branches of mathematics. First, it solved a problem that for more than a century was the indigestible seed at the core of topology, the mathematical study of abstract shape. Most mathematicians expect that the work will lead to a much broader result, a proof of the geometrization conjecture: essentially, a "periodic table" that brings clarity to the study of three-dimensional spaces, much as Mendeleev's table did for chemistry.

While bringing new *results* to topology, Perelman's work brought new *techniques* to geometry. It cemented the central role of geometric evolution equations, powerful machinery for transforming hard-to-work-with spaces into more-manageable ones. Earlier studies of such equations always ran into "singularities" at which the equations break down. Perelman dynamited that roadblock.

"This is the first time that mathematicians have been able to understand the structure of singularities and the development of such a complicated system," said Shing-Tung Yau of Harvard University at a lecture in Beijing this summer. "The methods developed … should shed light on many natural systems, such as the Navier-Stokes equation [of fluid dynamics] and the Einstein equation [of general relativity]."

Unruly spaces

Henri Poincaré, who posed his problem in 1904, is generally regarded as the founder of topology, the first mathematician to clearly distinguish it from analysis (the branch of mathematics that evolved from calculus) and geometry. Topology is often described as "rubber-sheet geometry," because it deals with properties of surfaces that can undergo arbitrary amounts of stretching. Tearing and its opposite, sewing, are not allowed.

Our bodies, and most of the familiar objects they interact with, have three dimensions. Their surfaces, however, have only two. As far as topology is concerned, two-dimensional surfaces with no boundary (those that wrap around and close in on themselves, as our skin does) have essentially only one distinguishing feature: the number of holes in the surface. A surface with no holes is a sphere; a surface with one hole is a torus; and so on. A sphere can never be turned into a torus, or vice versa.

Three-dimensional objects with 2D surfaces, however, are just the beginning. For example, it is possible to define curved 3D spaces as boundaries of 4D objects. Human beings can only dimly visualize such spaces, but mathematicians can use symbolic notation to describe them and explore their properties. Poincaré developed an ingenious tool, called the "fundamental group," for detecting holes, twists, and other features in spaces of *any* dimension. He conjectured that a 3D space cannot hide any interesting topology from the fundamental group. That is, a 3D space with a "trivial" fundamental group must be a hypersphere: the boundary of a ball in 4D space.

Enigma. Perelman (*top*) solved Poincaré's problem.

Although simple to state, Poincaré's conjecture proved maddeningly difficult to prove. By the early 1980s, mathematicians had proved analogous statements for spaces of every dimension higher than three—but not for the original one that Poincaré had pondered.

To make progress, topologists reached for a tool they had neglected: a way to specify distance. They set about recombining topology with geometry. In 1982, William Thurston (now of Cornell University) theorized that every 3D space can be carved up so that each piece has a unique uniform geometry, and that those geometries come in only eight possible types. This hypothesis became known as the geometrization conjecture.

If true, Thurston's insight would solve the Poincaré conjecture, because a sphere is the only one of the eight geometries that admits a trivial fundamental group. In 1982, Richard Hamilton (now of Columbia University) proposed a possible strategy for proving it: Start with any lumpy space, and then let it flow toward a uniform one. The result would be a tidy "geometrized" space à la Thurston. To guide the flow, Hamilton proposed a geometric evolution equation modeled after the heat equation of physics and named it "Ricci flow" in

CREDITS (TOP TO BOTTOM): CAMERON SLAYDEN/*SCIENCE*; EPA/CORBIS; HULTON-DEUTSCH COLLECTION/CORBIS

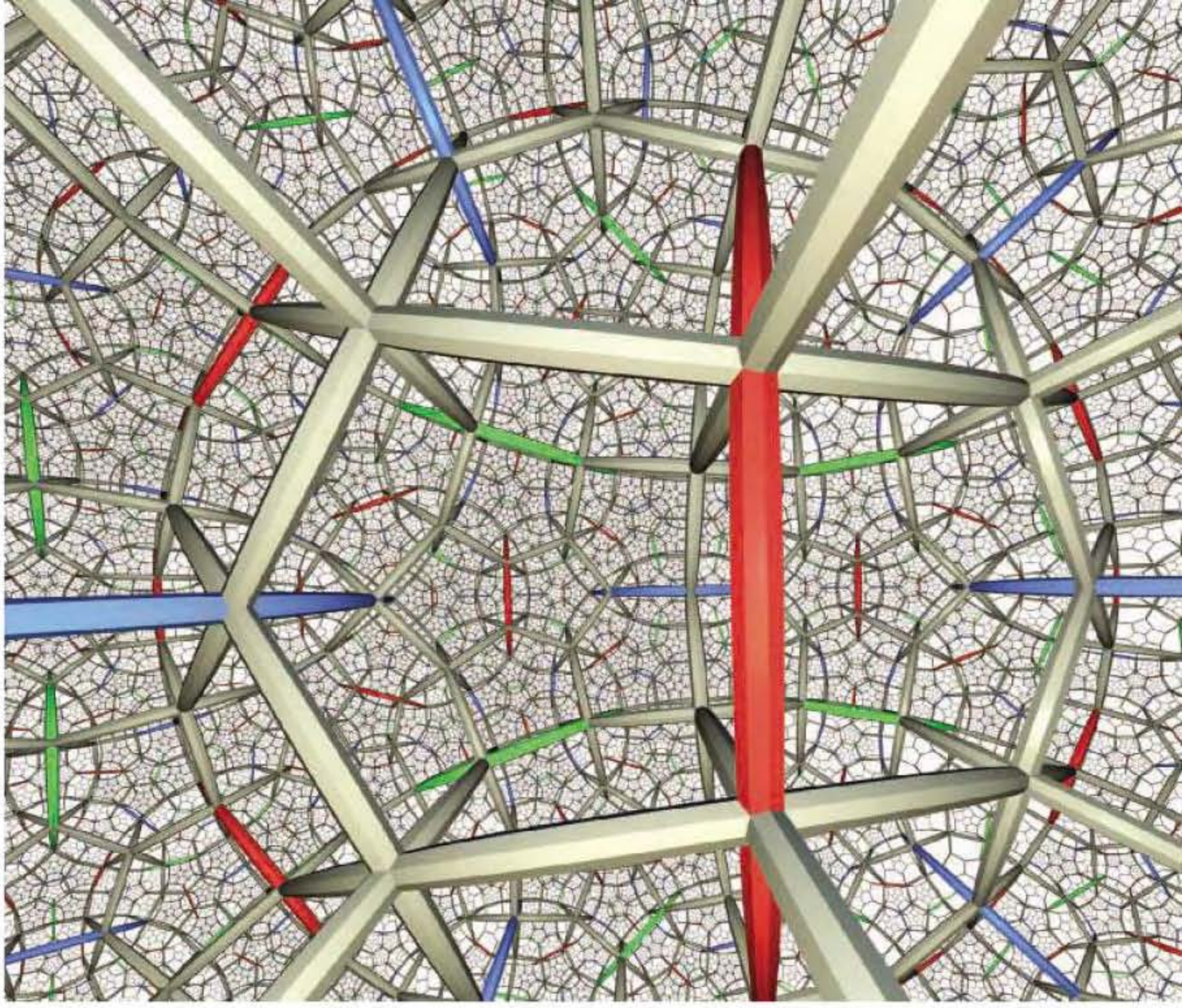

Fascinating. A computer rendering of a 3D space with uniform hyperbolic geometry.

honor of Gregorio Ricci-Curbastro, an early differential geometer. In Ricci flow, regions of high curvature tend to diffuse out into the regions of lower curvature, until the space has equal curvature throughout.

Hamilton's strategy works perfectly in 2D surfaces. Slender "necks," like the one seen on the cover of this issue, always expand. In 3D spaces, however, Ricci flow can run into snags. Necks sometimes pinch off, separating the space into regions with different uniform geometries. Although Hamilton did a great deal of pioneering work on Ricci flow, he could not tame the singularities. As a result, the whole program of research seemed to run aground in the mid-1990s. In 2000, when the Clay Mathematics Institute named the Poincaré conjecture as one of its $1 million Millennium Prize problems, most mathematicians believed that no breakthrough was in sight.

The breakthrough

In fact, Perelman was already well on his way to a solution. In 1995, the 29-year-old St. Petersburg native had returned to Russia after a 3-year sojourn in the United States, where he had met Hamilton and learned about Ricci flow. For the next 7 years, he remained mostly incommunicado. Then, in November 2002, Perelman posted on the Internet the first of three preprints outlining a proposed proof of the geometrization conjecture.

To experts, it was immediately clear that Perelman had made a major breakthrough. It was in the title of the first section of the first paper: "Ricci Flow as a Gradient Flow." Perelman had spotted an important detail that Hamilton had missed: a quantity that always increases during the flow, giving it a direction. By analogy with statistical mechanics, the mathematics underlying the laws of thermodynamics, Perelman called the quantity "entropy."

The entropy ruled out specific singularities that had stymied Hamilton. To reach a safe harbor, however, Perelman still had to identify the remaining types of singularities that might cause problems. He had to show that they occurred one at a time instead of accumulating in an infinite pileup. Then, for each singularity, he had to show how to prune and smooth it before it could sabotage Ricci flow. Those steps would be enough to prove Poincaré. To complete the geometrization conjecture, Perelman had to show, additionally, that the "Ricci flow with surgery" procedure could be continued for an infinitely long time.

CREDIT: CHARLES GUNN/TECHNICAL UNIVERSITY BERLIN

BREAKTHROUGH ONLINE

For an expanded version of this section, with references and links, see www.sciencemag.org/sciext/btoy2006

In 2003, when Perelman revisited the United States to lecture on his work, many mathematicians doubted that he could have pulled off all of these feats. By 2006, however, the mathematical community had finally caught up. Three separate manuscripts, each more than 300 pages in length, filled in key missing details of Perelman's proof.

Two of the papers—one authored by Bruce Kleiner and John Lott of the University of Michigan, Ann Arbor, the other by John Morgan of Columbia University and Gang Tian of the Massachusetts Institute of Technology in Cambridge—stopped short of the geometrization conjecture, because Perelman's explanation of the final step had been too sketchy. (Both groups are still working on it.) They did, however, include enough math to nail down the Poincaré conjecture.

The third paper, by Huai-Dong Cao of Lehigh University in Bethlehem, Pennsylvania, and Xi-Ping Zhu of Zhongshan University in Guangzhou, China, was less circumspect. Cao and Zhu claimed to have "the first written account of a complete proof of the Poincaré conjecture and the geometrization conjecture of Thurston." This summer, the International Mathematical Union (IMU) decided to award Perelman the Fields Medal, traditionally considered the highest honor in mathematics.

Anticlimax

Since then, the rosy glow of triumph has taken on darker hues. On 22 August, IMU President John Ball announced that Perelman had declined the Fields Medal. In an interview in *The New Yorker*, the reclusive mathematician said he was retiring from mathematics, disenchanted by unspecified lapses in "ethical standards" by colleagues. The *New Yorker* article also painted an unflattering portrait of Yau, intimating that he had claimed too much credit for his protégés Cao and Zhu.

In the ensuing months, hard feelings have abounded. Certain mathematicians claimed that their quotes were distorted in the *New Yorker*, and Yau threatened to sue. Kleiner and Lott complained that Cao and Zhu had copied a proof of theirs and claimed it as original, and the latter pair grudgingly printed an erratum acknowledging Kleiner and Lott's priority.

This fall, the American Mathematical Society attempted to organize an all-star panel on the Poincaré and geometrization conjectures at its January 2007 meeting in New Orleans, Louisiana. According to Executive Director John Ewing, the effort fell apart when Lott refused to share the stage with Zhu. Ewing still hopes to organize such an event "at some time in the future." For the time being, however, the animosity continues to make it hard for mathematicians to celebrate their greatest breakthrough of the new millennium.

–DANA MACKENZIE

Dana Mackenzie is a freelance science writer in Santa Cruz, California.

Family feud. DNA confirms that Neandertals split from modern humans 450,000 years ago.

2 DIGGING OUT FOSSIL DNA. This year, on the 150th anniversary of the discovery of the Neandertal type specimen, researchers in Europe and the United States transformed the study of this ancient human by sequencing more than 1 million bases of Neandertal DNA. In November, two groups, one decoding 65,000 Neandertal bases and the other a million bases, showed that researchers can now find sequence changes between modern and ancient humans, differences that may reveal key steps in our evolution. The studies concluded that Neandertals diverged from our own ancestors at least 450,000 years ago—approximately the time suggested by fossil and mitochondrial DNA studies. One group's data also suggest that Neandertals and modern humans may have interbred. In the works are a very rough draft of the complete Neandertal genome sequence and, as more fossils become available to sequencers, the development of bacterial libraries containing DNA from several Neandertals.

This breakthrough owes a large debt to earlier sequencing feats that demonstrated the potential of a new approach called metagenomics for deciphering ancient DNA, both human and nonhuman, and of faster sequencing technologies. For metagenomics, a technique developed for assessing microbial diversity, all the DNA in a sample is sequenced, and then sophisticated computer programs pull out only the target DNA based on its similarity to the sequence of a closely related extant organism.

In January 2006, researchers combined metagenomics with a new rapid sequencing technique called pyrosequencing, which uses pulses of light to read the sequence of thousands of bases at once, to get a whopping 13 million bases from a 27,000-year-old mammoth. The same sample also yielded another 15 million bases from bacteria, fungi, viruses, soil microbes, and plants—DNA that will provide clues about this giant mammal's environment. With those two advances, ancient DNA sequencing is off and running.

<< The Runners-Up

3 SHRINKING ICE. Glaciologists nailed down an unsettling observation this year: The world's two great ice sheets—covering Greenland and Antarctica—are indeed losing ice to the oceans, and losing it at an accelerating pace. Researchers don't understand why the massive ice sheets are proving so sensitive to an as-yet-modest warming of air and ocean water. The future of the ice sheets is still rife with uncertainty, but if the unexpectedly rapid shrinkage continues, low-lying coasts around the world—including New Orleans, South Florida, and much of Bangladesh—could face inundation within a couple of centuries rather than millennia.

This disturbing breakthrough rests on decades of measurements by airborne laser altimeters and orbiting radars, and, more recently, by a pair of satellites that measure ice mass directly by its gravitational pull. Different techniques and even different analyses of the same data disagree about just how much ice volume is changing. All of them, however,

Bye-bye. The great ice sheets are losing ice to melting and icebergs faster than it forms.

CREDITS (TOP TO BOTTOM): FRANK FRANKLIN II/AP; RICHARD ALLEY/PENN STATE UNIVERSITY; (CRYSTAL BALLS) TERRY SMITH

Scorecard 2006

How well did the editors forecast the year's Areas to Watch? The record shows that some of their crystal balls were clouded by wishful thinking.

Avian influenza. Research on flu drugs, vaccines, and epidemiology flourished in 2006, as did studies of the genetic changes that might turn avian influenza into a pandemic. But tracking the worldwide H5N1 outbreak is still difficult because researchers and countries hoard field samples and viral sequences.

Gravity rules. Gravitational-wave fans will have to wait. The Laser Interferometer Gravitational-Wave Observatory in the United States and the smaller GEO-600 facility in Germany won't publish results until early 2007. Not bad news—just no news.

RNAi-based treatments. The gene-silencing technology boasted promising clinical-trial results in macular degeneration and respiratory syncytial virus, won a Nobel Prize, and enticed drug giant Merck to pay $1.1 billion for a small biotech company focused on RNAi treatments. But safety worries still loom: A hepatitis B study of RNAi in mice reported that dozens of animals died from treatment.

Catching rays. The massive Pierre Auger Observatory in Argentina seems sure to answer fundamental questions about the highest-energy cosmic rays, such as whether their interactions with the afterglow of the big bang limit their energy and whether they originate from point sources in the sky. But not in 2006, as we predicted. Some answers will likely come at a major conference in Merida, Mexico, in July.

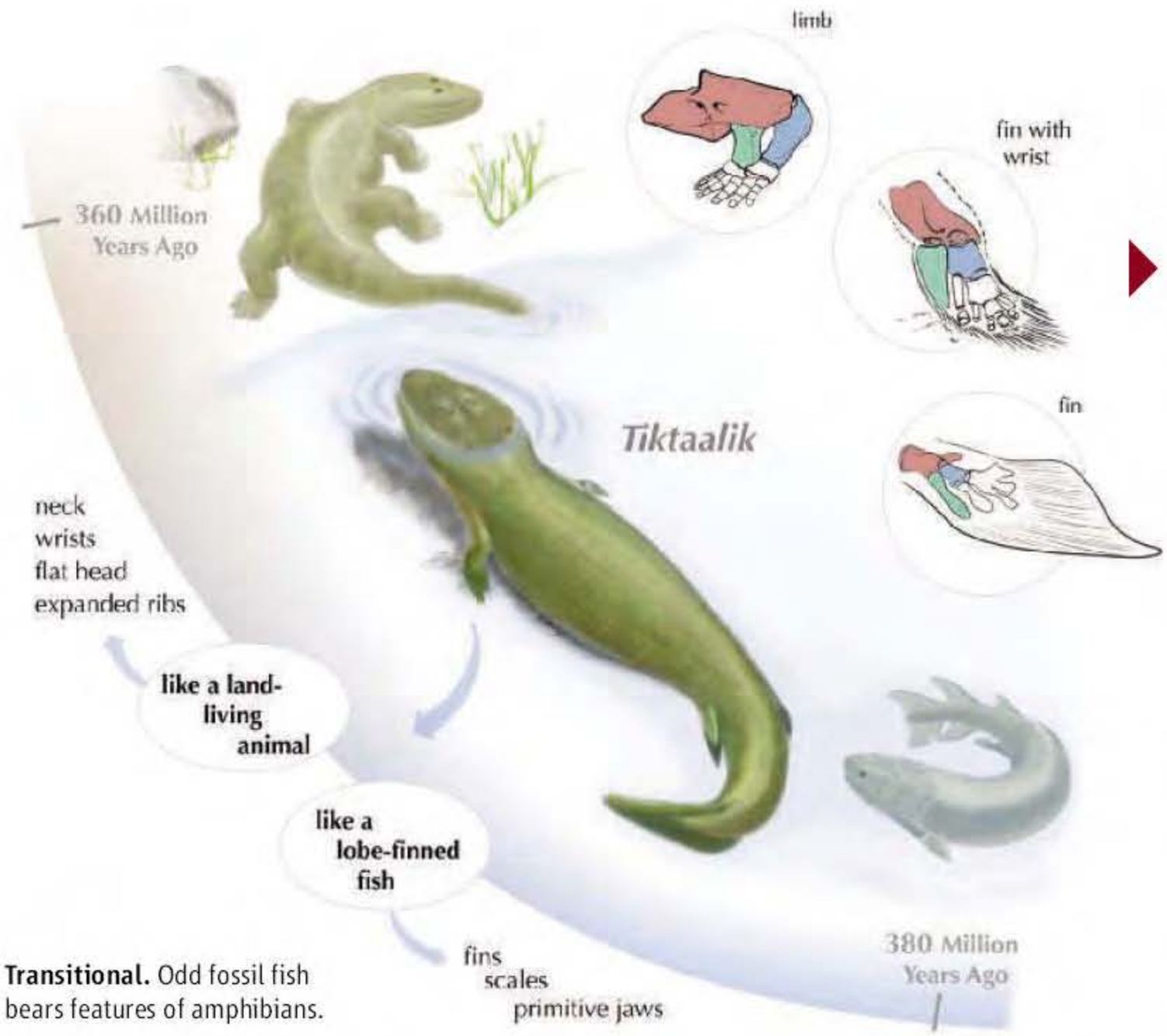

Transitional. Odd fossil fish bears features of amphibians.

4 NEITHER FISH NOR FOWL.

Paleontologists made a major splash this year with the debut of a fossil fish that long ago took a deep breath and made some tentative but ultimately far-reaching steps onto land. With its sturdy, jointed fins, the 375-million-year-old specimen fills an evolutionary gap and provides a glimpse of the features that helped later creatures conquer the continents.

All limbed vertebrates, known as tetrapods, evolved from lobe-finned fishes some 370 million to 360 million years ago. Many of these sophisticated fishes had skeletons with modifications, such as enlarged bones in their fins, that would ultimately prove useful for weight-bearing limbs. The new species is the most tetrapodlike fish yet discovered.

Three specimens were found during a 2004 field expedition to Ellesmere Island in the far north of Nunavut, Canada. They were named *Tiktaalik roseae* for "large freshwater fish" in the Inuktitut language and a donor who helped fund the expedition, respectively. With fins and scales, the 3-meter-long *Tiktaalik* is clearly a fish. It had a flat head with eyes on top and lived in shallow streams.

What makes *Tiktaalik* unique among fish is that each of the front fins has a wrist and elbow, providing flexible motion. Also unlike other fish, *Tiktaalik* sported a neck—the oldest one known in the fossil record—and could move its head. Achieving that flexibility required losing a bone called the operculum, which modern fish use to pump water over their gills. *Tiktaalik* still had well-developed gills, and it probably used its neck and stout limbs to push its head above water to inhale.

Another feature that makes *Tiktaalik* close kin to tetrapods is its robust, overlapping ribs.

now show that both Greenland and Antarctica have been losing ice over the past 5 to 10 years. In the north, Greenland is shedding at least 100 gigatons each year. In the south, the figure is less certain but lies in the range of tens of gigatons per year or more.

Current ice sheet losses aren't raising sea level faster than 0.1 meter per century, but researchers fear that the rate could rise to a meter per century or more in the near future. As recently as 5 years ago, they assumed that global warming would simply melt more and more ice from the ice sheets, as it is melting mountain glaciers. But it turns out the ice isn't just melting faster, it is moving faster. Radar mapping shows that in recent years, glaciers carrying ice away from the sheets have sped up by as much as 100%. In West Antarctica, warming ocean waters seem to have attacked the floating tongues of ice that hold back the ice sheet's outlet glaciers. Around southern Greenland, something else seems to be quickening the pace of outlet glaciers, perhaps lubrication by increasing amounts of surface meltwater seeping to a glacier's base.

Now glaciologists are wondering how the next chapter will play out. Will the relatively strong warming around the ice continue, or will it be weakened by natural variations of climate? Will the ice sheets adjust to the new warmth by eventually slowing their ice loss? And will more glaciers succumb to the spreading warmth? A few more breakthroughs are definitely in order.

CREDIT: KALLIOPI MONOYIOS

Small worlds. As predicted, microbial evolution and ecology emerged among the most exciting areas of biology. Researchers got a better grasp of what a prokaryote species might be, despite promiscuous lateral gene transfer. And it became clear that symbioses involving microbes (bacteria in the human gut, for example) are pervasive and sometimes extreme.

Seconding supersolidity. Two groups reproduced the subtle signal that could be evidence that crystalline helium flows—as predicted. But one group reported that the effect disappeared if the frigid crystal was gently heated and cooled to remove imperfections. That suggests that the crystal itself doesn't budge, but thin layers of liquid flow between crystalline grains. The upshot: *Something* is happening, but what?

Homing in on high T_c. We can dream, can't we? The 20th anniversary of high-temperature superconductivity passed without any consensus being reached on how the materials carry electricity without resistance at temperatures as high as 138 kelvin. Experimenters are producing exquisitely precise data, but it seems that every theoretical concept has data pointing in its direction.

Bird to watch for. We hoped new sightings would prove that the ivory-billed woodpecker is alive and pecking. But indirect evidence from trees in Florida failed to sway the skeptics, and the original Arkansas sightings of the bird are looking increasingly shaky. Maybe it drowned in a rogue gravitational wave.

Outta sight. Although not as fashionable as this electronic garment, a cloak unveiled this year is a step toward true invisibility.

Although their function isn't completely clear, researchers think they could have helped support its body out of water and aided in breathing. Forays onto land would have offered an escape from sharks and other predators, as well as insects to eat. *Tiktaalik* isn't a perfect tetrapod, of course—among other traits, it lacks fingers and toes—but it was certainly a big step in the right direction.

5 THE ULTIMATE CAMOUFLAGE. Science veered toward science fiction this year as physicists cobbled together the first rudimentary invisibility cloak. Although far from perfect—the ring-shaped cloak is invisible only when viewed in microwaves of a certain wavelength traveling parallel to the plane of the ring—the device could usher in a potentially revolutionary approach to manipulating electromagnetic waves.

The disappearing act began in May, when two independent analyses predicted that it should be possible to ferry electromagnetic waves around an object to hide it. All that was needed was a properly designed shell of "metamaterial," an assemblage of tiny metallic rods and c-shaped rings. The waves churn the electrons in the rods and rings, and the sloshing affects the propagation of the waves. Both analyses specified how to sculpt the properties of the metamaterial and left it to experimenters to design the materials to meet those specs.

In October, the team that made one of the predictions did just that—almost. Physicists at Duke University built a ring instead of an all-concealing sphere. They made some approximations that rendered the cloak slightly reflective. Still, the thing whisked microwaves around a plug of copper, proving that the method works. Cloaks for visible light are likely years off, as researchers must figure out how to make metamaterials that work at such short wavelengths. Even then, the cloak would be a bust for spying because it would be impossible to see out of it.

The real breakthrough may lie in the theoretical tools used to make the cloak. In such "transformation optics," researchers imagine—à la Einstein—warping empty space to bend the path of electromagnetic waves. A mathematical transformation then tells them how to mimic the bending by filling unwarped space with a material whose optical properties vary from point to point. The technique could be used to design antennas, shields, and myriad other devices. Any way you look at it, the ideas behind invisibility are likely to cast a long shadow.

6 A RAY OF HOPE FOR MACULAR DEGENERATION PATIENTS. The year brought good news to the many people suffering from the vision-robbing disease known as age-related macular degeneration (AMD). In October, *The New England Journal of Medicine* published the results of two clinical trials showing that treatment with the drug ranibizumab improves the vision of roughly one-third of patients with the more serious wet form of AMD and stabilizes the condition of most of the others. Other approved treatments can only slow the progression of AMD.

Vision loss in the wet form of AMD is caused by the growth and leakage of abnormal blood vessels in the macula, the central region of the retina. Ranibizumab, a monoclonal antibody fragment produced by Genentech Inc. does better than other treatments because it specifically targets a protein called VEGF that stimulates that vessel growth. The U.S. Food and Drug Administration approved ranibizumab for AMD treatment this year, but researchers are also looking at a related antibody made by Genentech. That drug, known as bevicizumab, is approved for treating certain cancers but so far not for use in AMD. If it works, however, it could be a cheaper alternative to ranibizumab, which costs $1950 per monthly dose.

AMD researchers are making progress on another front as well. Over the past year and a half, they have uncovered several genes that influence an individual's susceptibility to the eye disease. One of them is the gene for VEGF itself, and another makes a protein that might also help regulate blood vessel growth. In addition, several groups have zeroed in on genes encoding proteins involved in inflammation, which can damage tissues if not controlled properly. Identifying those genes could help physicians determine whether a person is at high risk for AMD and thus should take preventive steps such as consuming more antioxidants and not smoking. And by shedding light on the causes

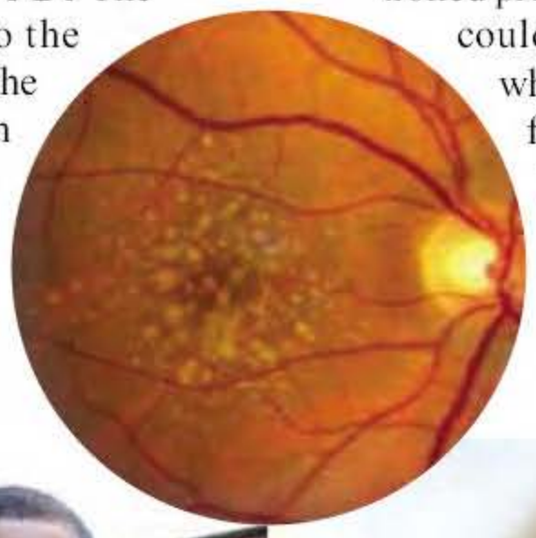

CREDITS (TOP TO BOTTOM): SHIZUO KAMBAYASHI/AP; MAURICIO LINARES; GREGORY HAGEMAN; NATIONAL EYE INSTITUTE, NATIONAL INSTITUTES OF HEALTH

of AMD, genetic studies should also provide targets for devising even better therapies.

7 DOWN THE BIODIVERSITY ROAD. It doesn't take much to send an organism down speciation's path. Several studies these past 12 months have uncovered genetic changes that nudge a group of individuals toward becoming a separate species by giving them an edge in a new environment. The year's results speak to the power of genomics in helping evolutionary biologists understand one of biology's most fundamental questions: how biodiversity comes about.

For Florida beach mice, a single base difference in the melanocortin-1 receptor gene accounts for up to 36% of the lighter coat color that distinguishes the beach mice, evolutionary biologists reported in July. For cactus finches, the activity of the calmodulin gene is upregulated, causing their relatively long beaks, researchers reported in August.

Genes help drive speciation in other ways as well. Since the late 1930s, researchers have realized that as two incipient species diverge, the sequences of two or more interacting genes can evolve along different paths until the proteins they encode no longer work together in any crossbred offspring. Working with *Drosophila melanogaster* and a sister species, *D. simulans*, evolutionary geneticists have pinpointed the first such pair of incompatible genes, demonstrating in transgenic flies the genes' killing effects in hybrids of the two species. In October, a separate team found another fast-evolving gene and is homing in on its partner. They both seem to be nuclear pore proteins that are no longer compatible in fruit-fly hybrids. In September, fruit-fly researchers found that hybrids had problems because a particular gene was in a different place in the two species, likely because of duplication and loss of the original copy in one of them.

But in at least one case, hybrids do just fine. In June, evolutionary biologists detailed the most convincing case yet of a species that arose through hybridization. They bred two species of passion vine butterflies and got the red and yellow stripe pattern of a third species (image above). The pattern proved unattractive to the parent species, helping to reproductively isolate the hybrid.

CREDIT: CHUNG SUNG-JUN/GETTY IMAGES

Breakdown of the Year: Scientific Fraud

One year ago, as *Science* was assembling its 2005 Breakthrough of the Year issue, the need for a last-minute change became uncomfortably clear. A shadow was creeping across one of this journal's landmark papers, in which a team of South Korean and American researchers, led by Woo Suk Hwang at Seoul National University, claimed to have created the first-ever human embryonic stem cell lines that matched the DNA of patients. After anonymous allegations of irregularities in that paper appeared on a Korean Web site, South Korean authorities launched an investigation. As the story unfolded, *Science*'s news editors hastily pulled an item about the Hwang achievements from the issue's roster of runners-up.

Today, the fallout from the Hwang case is plain. Multiple inquiries discredited two papers Hwang published in *Science* in 2004 and 2005, which claimed some of the greatest accomplishments to date with human embryonic stem cells. The papers were retracted. But the scientific fraud, one of the most audacious ever committed, shattered the trust of many researchers and members of the public in scientific journals' ability to catch instances of deliberate deception.

As it turned out, the Hwang debacle marked the beginning of a bad year for honest science. Incidents of publication fraud, if not on the rise, are garnering more attention, and the review process is under scrutiny. In June, European investigators reported that the bulk of papers by Jon Sudbø, formerly a cancer researcher at the Norwegian Radium Hospital in Oslo, contained bogus data. Those included two articles in *The New England Journal of Medicine* that described a new way of identifying people at high risk of oral cancer, a strategy that many clinicians were keen to apply to patients.

Busted. The unraveling of Hwang's stem-cell papers was the first and worst of the year's research scandals.

Eric Poehlman, formerly a menopause and obesity researcher at the University of Vermont in Burlington, garnered perhaps the most dubious distinction of all: He became the first researcher in the United States to go to jail for scientific misconduct unrelated to patient deaths.

The Hwang case, however, was unique for its combustible mix of startling achievements in a high-profile field and publication in a high-visibility journal. Manipulated images, purportedly of distinct stem cells matched to patients but in fact showing cells drawn from fertilized embryos, handily fooled outside reviewers and *Science*'s own editors. "The reporting of scientific results is based on trust," wrote Editor-in-Chief Donald Kennedy in a January 2006 editorial explaining why journals are not designed to catch fraud. It's a comment echoed often by journal editors facing the nightmare of faked data in their own pages.

But the shock of the Hwang deception, along with other recent fraud cases, is jolting journals into a new reality. Five scientists and a top editor of *Nature* examined *Science*'s handling of the Hwang papers, at the journal's request. Their report, published on *Science*'s Web site earlier this month (www.sciencemag.org/sciext/hwang2005), concluded that operating in an atmosphere of trust is no longer sufficient. "*Science* must institutionalize a healthy level of concern in dealing with papers," the group wrote. It recommended "substantially stricter" requirements for reporting primary data and a risk assessment for accepted papers. *Science* and some other journals are also beginning to scrutinize images in certain papers, in an effort to catch any that have been manipulated.

Stem cell researchers, meanwhile, endured deep disappointment as a remarkable scientific advance evaporated before their eyes. Cloning early-stage human embryos, and crafting customized stem cell lines, is not the cakewalk some scientists hoped Hwang's papers had shown it to be. Stem cell researchers are backpedaling to more modest goals, just as *Science* and other journals consider how to prevent a breakdown of this magnitude from striking again. **–JENNIFER COUZIN**

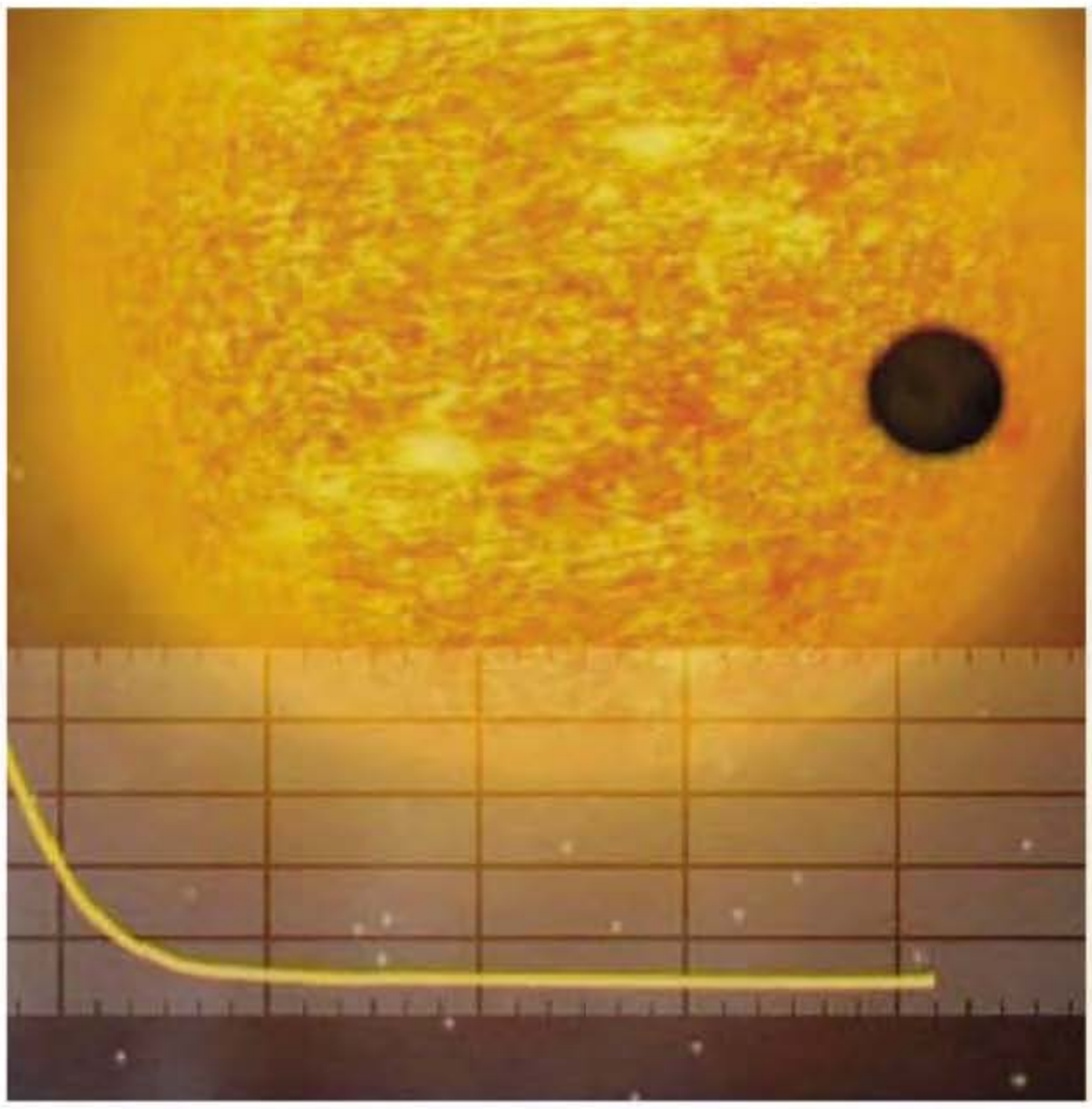

Areas to Watch in 2007

World-weary? Hardly. Four fledgling spacecraft will give planetary scientists plenty to ponder in 2007. Europe's COROT orbiting exoplanet hunter, scheduled for launch 27 December, should detect dozens of new "hot Jupiters" around other stars and may even bag its big quarry: signs of rocky planets just a few times the size of Earth. Closer to home, the Mars Reconnaissance Orbiter will take the sharpest-ever pictures of the martian surface and will use radar to look for rock layers—and ice—as much as 1 kilometer deep. The Venus Express orbiter will be going full tilt, and in February, New Horizons will send back snapshots of Jupiter en route to its 2015 rendezvous with Pluto.

Skulls and bones. In recent years, paleoanthropologists have uncovered new skulls, teeth, and lower limbs of the earliest members of our genus *Homo* at sites in the Republic of Georgia, China, and Kenya. In 2007, the first descriptions of these fossils should give clues to the identity of the first human ancestors to leave Africa about 1.8 million years ago—such as whether the bones all belong to one species (*Homo erectus*) or to two or more. Meanwhile, the long-awaited partial skeleton of *Ardipithecus ramidus*, an early human ancestor that lived in Ethiopia 4.4 million years ago, promises to shed light on how upright walking evolved in early hominids.

8 PEERING BEYOND THE LIGHT BARRIER.

Biologists got a clearer view of the fine structure of cells and proteins this year, as microscopy techniques that sidestep a fundamental limit of optics moved beyond proof-of-principle demonstrations to biological applications. The advances could open a new realm of microscopy.

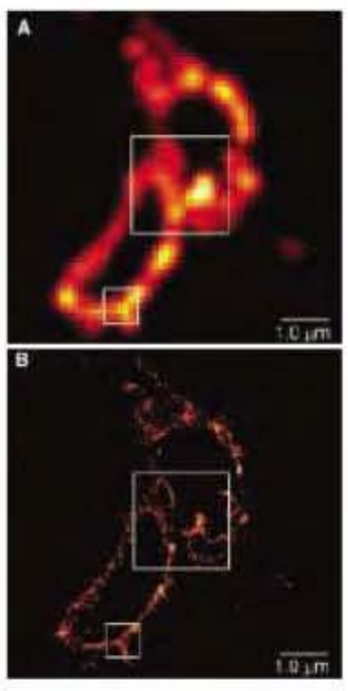

Clearly. New microscopy techniques resolve nanometer-sized features of proteins.

An ordinary microscope cannot resolve features smaller than half the wavelength of the light used to illuminate an object—about 200 nanometers for visible light. For years, physicists and engineers have devised schemes to get around the "diffraction limit," and this year, researchers used those techniques to do some real biology.

In April, researchers in Germany used a technique known as stimulated emission depletion (STED) to study the tiny capsules in nerve cells called synaptic vesicles. Each vesicle releases its load of neurotransmitter when it merges into the cell membrane. The team showed that a protein in the vesicle remains clumped after the merger, suggesting that the clumps do not form from scratch when the process reverses to form new vesicles. The researchers tagged the proteins with a fluorescent dye and zapped the specimen with laser light to excite a spot as small as the diffraction limit allows. Then, by applying a pulse from a second beam with a dark "hole" in the middle, they squeezed the fluorescent spot down to a much smaller pinpoint of light. By scanning the beams across the sample and recording the level of fluorescence, the researchers assembled an image with a resolution of tens of nanometers. The team followed up with two other biological studies.

In August, another team imaged proteins within cells using a simpler technique known as photoactivated localization microscopy (PALM). The researchers used a fluorescent tag that had to be turned on with a pulse of light of one wavelength before it could be excited to fluoresce by light of another wavelength. By applying the first laser at a very low level, the researchers could turn on one tag molecule at a time. The molecule still produced a blurry spot when viewed through the microscope, but the researchers could nail down its position very precisely by finding the center of the blob. Repeating the process over and over, the team mapped proteins in cells with nanometer resolution. Two other groups introduced similar techniques this year.

Just how widely the techniques will be used remains to be seen. PALM is too slow to track dynamic processes, and STED requires fluorescent tags that can withstand intense excitation. Still, researchers are optimistic that more applications will follow, now that the diffraction limit is no longer a limit.

9 THE PERSISTENCE OF MEMORY.

How the brain records new memories is a central question in neuroscience. One attractive possibility involves a process called long-term potentiation (LTP) that strengthens connections between neurons. Many neuroscientists suspect that LTP is a memory mechanism, but proving it hasn't been easy. Several findings reported this year strongly bolstered the case.

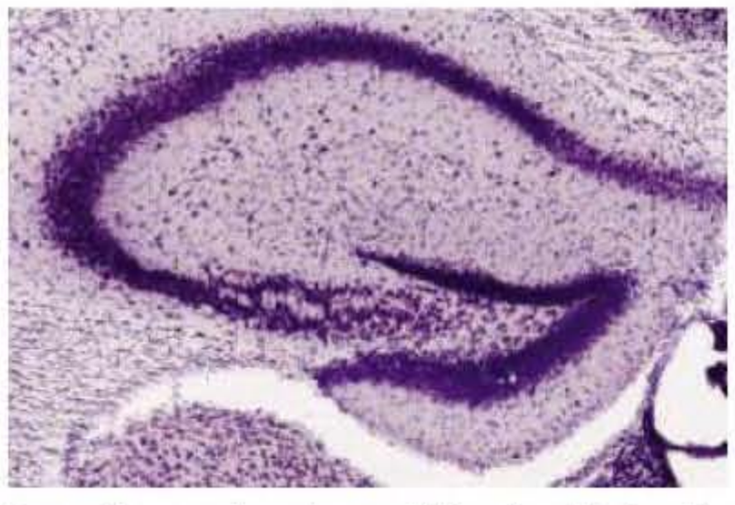

Record keeper. Learning and LTP go hand in hand in the rodent hippocampus.

CREDITS (TOP TO BOTTOM): CNES; E. BETZIG *ET AL.*/*SCIENCE* (2006); BRAINMAPS.ORG

Loads of new primate genes. With the human and chimpanzee genomes sequenced, genetic research into our evolutionary past is scrambling up other branches of the primate family tree. Low-resolution maps of gorilla, rhesus macaque, orangutan, marmoset, and gibbon genomes are already available, and refined, error-free versions should be ready in 2007. In addition, look forward to rough drafts of the genomes of the galago, tree shrew, and mouse lemur. If things go as planned, a comparative analysis of all these genomes might finally begin to explain what sets humans apart.

A climate of change? The case for human-induced warming will grow even more ironclad as the Intergovernmental Panel on Climate Change releases its report in February. Meanwhile, the International Polar Year, opening in March, will feature climate research on Earth's coldest climes. And the world is watching the U.S. Congress, which, under Democratic control, is expected to pass some sort of mandatory emission regime, and President George W. Bush, whose response will be sure to shape the debate.

Whole-genome association studies. The trickle of studies comparing the genomes of healthy people to those of the sick is fast becoming a flood. Already, scientists have applied this strategy to macular degeneration, memory, and inflammatory bowel disease, and new projects on schizophrenia, psoriasis, diabetes, and more are heating up. But will the wave of data and new gene possibilities offer real insight into how diseases germinate? And will the genetic associations hold up better than those found the old-fashioned way?

Light crystals. Ultracold atoms continue to be one of the hottest areas in physics. Now researchers are loading the atoms into corrugated patterns of laser light known as optical lattices. The lattices work like artificial crystals, with the spots of light serving as the ions in the crystal lattice and the atoms playing the role of electrons moving through it. Optical lattices could help crack problems such as high-temperature superconductivity and seem sure to produce interesting new physics. Look for rapid progress in this burgeoning effort.

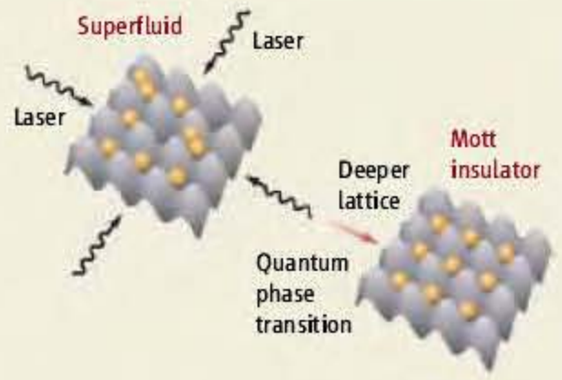

Scientists discovered LTP in the early 1970s, when experiments with rabbits showed that a brief barrage of electrical zaps could bolster synaptic connections between neurons in the hippocampus, a brain region tied to memory. Later studies revealed that drugs that block LTP, when given to an animal before it learns a new task, prevent new memories from being formed.

But some predictions of the LTP-memory hypothesis have been harder to test. One is that it should be possible to observe LTP in the hippocampus when an animal learns something. In January, Spanish scientists reported just such an observation in mice conditioned to blink upon hearing a tone. In August, another research team described LTP in the hippocampus of rats that had learned to avoid an area where they'd previously received a shock.

A study published in August addressed another prediction: that abolishing LTP *after* learning should erase what was learned. Researchers injected a compound that blocks an enzyme needed to sustain LTP into the hippocampus of rats after they'd been trained to avoid a "shock zone" in their enclosure. The treatment eradicated both LTP and the memory of the shock zone's location.

Although the new results add to evidence that LTP is a molecular mechanism of memory, much work remains. For example, researchers still haven't figured out how the many forms of LTP identified in brain tissue relate to different kinds of memory. And they may have a while to wait for the ultimate test, which some call the "Marilyn Monroe criterion": inducing LTP at select synapses to create the vivid memory of an event, such as an evening with the voluptuous movie star, that never happened.

10 MINUTE MANIPULATIONS. Small RNA molecules that shut down gene expression have been hot, hot, hot in recent years, and 2006 was no exception. Researchers reported the discovery of what appears to be a new and still-mysterious addition to this exclusive club: *Piwi*-interacting RNAs (piRNAs). Abundant in the testes of several animals, including humans, piRNAs are distinctly different from their small RNA cousins, and scientists are racing to learn more about them and see where else in the body they might congregate.

PiRNAs made their grand entrance last summer, when four independent groups released a burst of papers describing them. In a sense, their sudden prominence is not surprising. The *Piwi* genes to which piRNAs bind belong to a gene family called Argonaute, other members of which help control small RNAs known as microRNAs (miRNAs) and small interfering RNAs (siRNAs). Scientists already believed that the *Piwi* genes regulate the development and maintenance of sperm cells in many species. With the discovery of piRNAs, they may be close to figuring out how that happens.

Particularly intriguing to biologists is the appearance of piRNAs: Many measure about 30 RNA bases in length, compared with about 22 nucleotides for miRNAs and siRNAs. Although that may not sound like much of a difference, it has gripped biologists and convinced them that piRNAs are another class of small RNAs altogether. Also striking is the molecules' abundance and variety. One group of scientists found nearly 62,000 piRNAs in rat testes; nearly 50,000 of those appeared just once.

But beyond characterizing what piRNAs look like and finding hints that they can silence genes, scientists are mostly in the dark. Still to be determined: where they come from, which enzymes are key to their birth, and perhaps most important, what they do to an organism's genome. Stay tuned.

–THE NEWS STAFF

CREDITS (TOP TO BOTTOM): JUPITER IMAGES; CIRAC AND ZOLLER/*SCIENCE* (2003); BERNARD HOFFMAN/TIME LIFE PICTURES/GETTY IMAGES

A dolphin's demise 1860

Indians wary of nuclear pact 1863

SCIENTIFIC PUBLISHING

A Scientist's Nightmare: Software Problem Leads to Five Retractions

Until recently, Geoffrey Chang's career was on a trajectory most young scientists only dream about. In 1999, at the age of 28, the protein crystallographer landed a faculty position at the prestigious Scripps Research Institute in San Diego, California. The next year, in a ceremony at the White House, Chang received a Presidential Early Career Award for Scientists and Engineers, the country's highest honor for young researchers. His lab generated a stream of high-profile papers detailing the molecular structures of important proteins embedded in cell membranes.

Then the dream turned into a nightmare. In September, Swiss researchers published a paper in *Nature* that cast serious doubt on a protein structure Chang's group had described in a 2001 *Science* paper. When he investigated, Chang was horrified to discover that a homemade data-analysis program had flipped two columns of data, inverting the electron-density map from which his team had derived the final protein structure. Unfortunately, his group had used the program to analyze data for other proteins. As a result, on page 1875, Chang and his colleagues retract three *Science* papers and report that two papers in other journals also contain erroneous structures.

"I've been devastated," Chang says. "I hope people will understand that it was a mistake, and I'm very sorry for it." Other researchers don't doubt that the error was unintentional, and although some say it has cost them time and effort, many praise Chang for setting the record straight promptly and forthrightly. "I'm very pleased he's done this because there has been some confusion" about the original structures, says Christopher Higgins, a biochemist at Imperial College London. "Now the field can really move forward."

The most influential of Chang's retracted publications, other researchers say, was the 2001 *Science* paper, which described the structure of a protein called MsbA, isolated from the bacterium *Escherichia coli*. MsbA belongs to a huge and ancient family of molecules that use energy from adenosine triphosphate to transport molecules across cell membranes. These so-called ABC transporters perform many essential biological duties and are of great clinical interest because of their roles in drug resistance. Some pump antibiotics out of bacterial cells, for example; others clear chemotherapy drugs from cancer cells. Chang's MsbA structure was the first molecular portrait of an entire ABC transporter, and many researchers saw it as a major contribution toward figuring out how these crucial proteins do their jobs. That paper alone has been cited by 364 publications, according to Google Scholar.

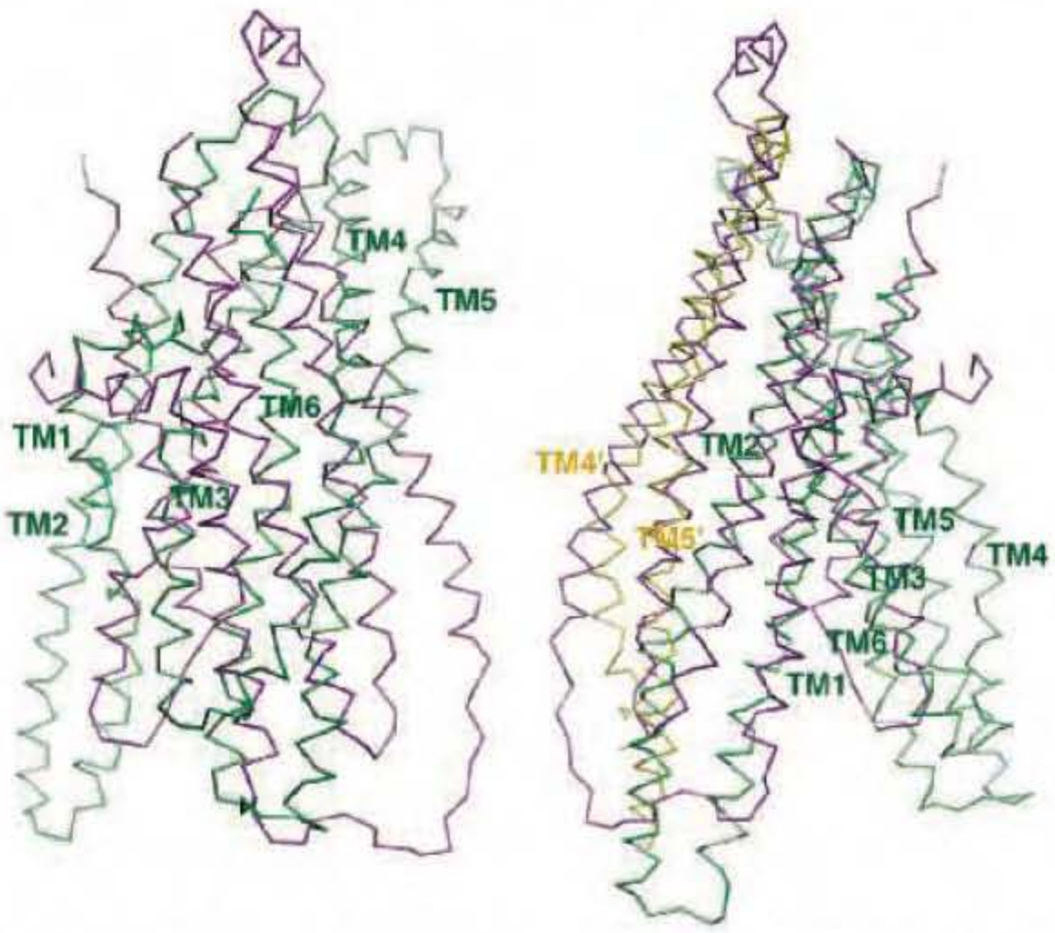

Flipping fiasco. The structures of MsbA (purple) and Sav1866 (green) overlap little (*left*) until MsbA is inverted (*right*).

Two subsequent papers, both now being retracted, describe the structure of MsbA from other bacteria, *Vibrio cholera* (published in *Molecular Biology* in 2003) and *Salmonella typhimurium* (published in *Science* in 2005). The other retractions, a 2004 paper in the *Proceedings of the National Academy of Sciences* and a 2005 *Science* paper, described EmrE, a different type of transporter protein.

Crystallizing and obtaining structures of five membrane proteins in just over 5 years was an incredible feat, says Chang's former postdoc adviser Douglas Rees of the California Institute of Technology in Pasadena. Such proteins are a challenge for crystallographers because they are large, unwieldy, and notoriously difficult to coax into the crystals needed for x-ray crystallography. Rees says determination was at the root of Chang's success: "He has an incredible drive and work ethic. He really pushed the field in the sense of getting things to crystallize that no one else had been able to do." Chang's data are good, Rees says, but the faulty software threw everything off.

Ironically, another former postdoc in Rees's lab, Kaspar Locher, exposed the mistake. In the 14 September issue of *Nature*, Locher, now at the Swiss Federal Institute of Technology in Zurich, described the structure of an ABC transporter called Sav1866 from *Staphylococcus aureus*. The structure was dramatically—and unexpectedly—different from that of MsbA. After pulling up Sav1866 and Chang's MsbA from *S. typhimurium* on a computer screen, Locher says he realized in minutes that the MsbA structure was inverted. Interpreting the "hand" of a molecule is always a challenge for crystallographers, Locher notes, and many mistakes can lead to an incorrect mirror-image structure. Getting the wrong hand is "in the category of monumental blunders," Locher says.

On reading the *Nature* paper, Chang quickly traced the mix-up back to the analysis program, which he says he inherited from another lab. Locher suspects that Chang would have caught the mistake if he'd taken more time to obtain a higher resolution structure. "I think he was under immense pressure to get the first structure, and that's what made him push the limits of his data," he says. Others suggest that Chang might have caught the problem if he'd paid closer attention to biochemical findings that didn't jibe well with the MsbA structure. "When the first structure came out, we and others said, 'We really ▶

CREDIT: R. J. P. DAWSON AND K. P. LOCHER, *NATURE* **443**, 180 (2006)

don't quite believe this is right,' " says Higgins. "It was inconsistent with a lot of things."

The ramifications of the software snafu extend beyond Chang's lab. Marwan Al-Shawi, a biochemist at the University of Virginia in Charlottesville, says he's now holding on to several manuscripts he was about to submit. Al-Shawi has been using Chang's MsbA structure to build computer models of an ABC transporter involved in human cancer drug resistance. David Clarke of the University of Toronto in Canada says his team had a hard time persuading journals to accept their biochemical studies that contradicted Chang's MsbA structure. Clarke also served on grant panels on which he says Chang's work was influential. "Those applications providing preliminary results that were not in agreement with the retracted papers were given a rough time," he says.

At Scripps, colleagues are standing behind the young researcher. "He's doing some really beautiful work, and this is just an absolute disaster that befell him," says Chang's department chair, Peter Wright. "I'm quite convinced he'll come out of it, and he'll go on to do great things." Chang meanwhile has been reanalyzing his original data and expects to submit papers on the corrected structures soon. The new structures "make a ton of sense" biologically, he says. "A lot of things we couldn't figure out before are very clear."

–GREG MILLER

U.S. OCEAN POLICY

Fisheries Bill Gives Bigger Role to Science—But No Money

New rules governing the U.S. fishing industry offer scientists much greater power to keep marine populations from collapsing. But although advocates for marine conservation are celebrating the changes in a 30-year-old law that Congress adopted earlier this month, they are disappointed that the focus remains on managing individual species rather than ecosystems. And they worry that the responsible agency—the National Oceanic and Atmospheric Administration (NOAA)—may not have enough money to implement many of the provisions in the revised law.

The bill, a reauthorization of the 1976 Magnuson-Stevens Fishery Conservation and Management Act, requires the eight regional fishery councils to follow the advice of their scientific committees, prevents continued overfishing, and calls for more research by NOAA on deep-sea corals. "We're very excited," says Steven Murawski, chief science adviser for NOAA Fisheries. The bill awaits the president's signature after legislators gave their approval in the final hours of the 109th Congress. Yet that same Congress failed to complete work on the 2007 budgets of most agencies, including NOAA's (*Science*, 15 December, p. 1666), raising doubts about how the agency will manage existing operations, let alone take on new ones. "Where is the money for all this?" wonders John Ogden, director of the Florida Institute of Oceanography in Tampa.

The new version is the first update in a decade. Environmentalists and researchers had feared that the revision might weaken the current law, because the House Resources Committee had proposed abolishing a rule requiring depleted stocks to be rebuilt within 10 years. But the deadline remains in place. "I'm very gratified," says Carl Safina of Stony Brook University in New York.

The bill breaks new ground by telling councils to end overfishing within 2 years after a species is deemed overfished. The current law was vague, and some councils allowed continued overfishing on the way to a rebuilding target, a practice that has made recovery harder for some species. "It's a significant improvement," says Gerald Leape of the National Environmental Trust in Washington, D.C.

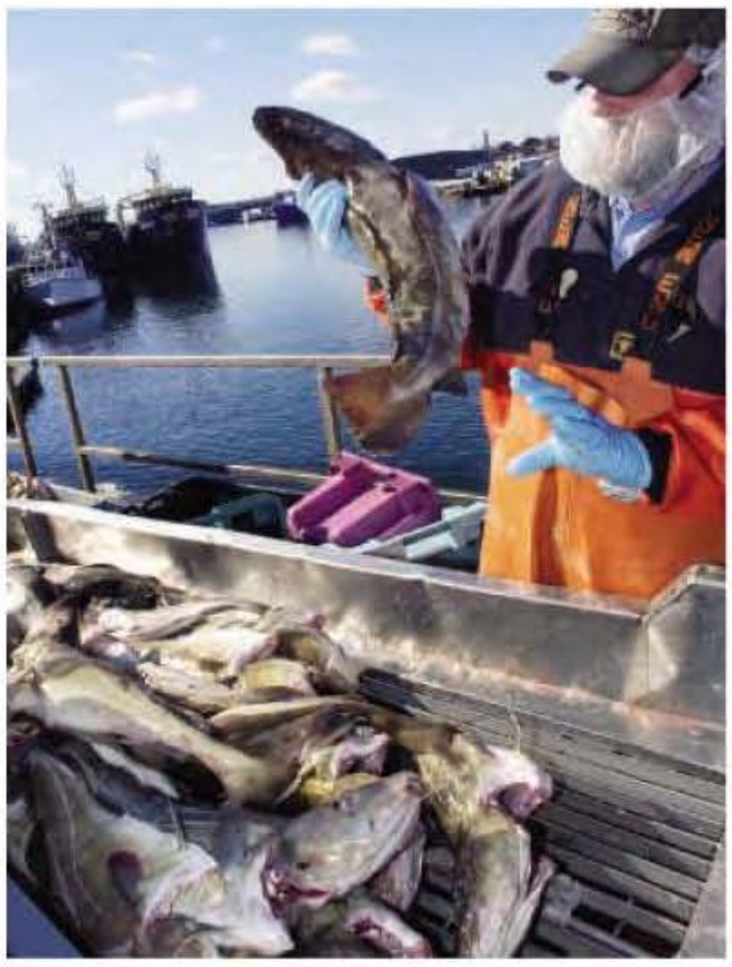

CREDIT: LISA POOLE/AP PHOTO

Catch phrases. New fishery legislation is intended to stop overfishing of species whose populations have crashed, such as these cod in Gloucester, Massachusetts.

In addition, councils will now be required to set catch limits and to follow scientific advice, two practices that are voluntary under the current law. But a Senate provision for penalties when fishers end up exceeding an annual limit was removed before final passage, and even setting all the catch limits is in question. The six NOAA fishery science centers that crank out most of the limits will require more resources, as well as more data from observers and NOAA survey vessels. This workload "is certainly a challenge," admits Murawski, referring to a pending 2007 spending plan that could shrink NOAA Fisheries' budget from $667 million to $541 million.

The same budget uncertainties imperil several other directives. A registry for recreational marine fishing and grant licenses would allow the agency to better estimate the impact of noncommercial catches (*Science*, 24 September 2004, p. 1958). But Murawski warns that "it's not going to be a cheap program." Another mandate would create a research program to map and monitor deep-sea corals.

Many scientists are deeply disappointed that the bill does not require an ecosystem-based approach to managing fisheries, as was recommended by several recent commissions. Instead, the bill continues the current species-by-species approach, while requesting a 180-day NOAA study of the state of the science of ecosystem management. It also authorizes the agency to begin funding pilot programs based on the study but doesn't set a level. "It's a major missed opportunity," says Ellen Pikitch of the University of Miami's Pew Institute for Ocean Science in Florida.

–ERIK STOKSTAD

IMMUNOLOGY

Mouse Studies Question Importance Of Toll-Like Receptors to Vaccines

Toll-like receptors (TLRs), once an obscure class of cell-surface proteins, have become hot targets for drugs and vaccines. And many immunologists have come to regard these key microbial sensors as the long-sought link between the immune system's initial inflammatory response and its more tailored and enduring antibody and cellular response (*Science*, 14 April, p. 184).

Now, however, a new study casts doubt on the importance of TLRs as general-purpose immune stimulators, particularly for the type of long-lasting immunity required by vaccines. On page 1936, immunologist Amanda Gavin at the Scripps Research Institute in San Diego, California, and her colleagues report that mice lacking the ability to respond to all TLR signals can nevertheless mount impressive antibody responses to four different vaccine adjuvants, two of which were thought to work through TLRs.

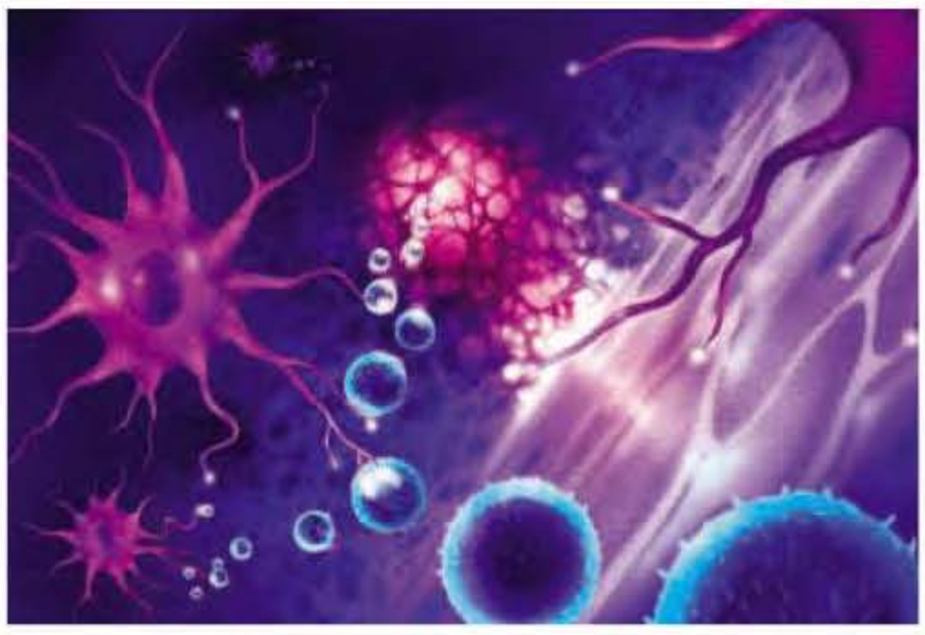

No Toll? A new study questions whether dendritic cells (pink) need proteins called Toll-like receptors to turn on other immune cells (blue) in response to vaccines.

CREDIT: JIM DOWDALLS/PHOTO RESEARCHERS INC.

Although the new work doesn't contest the role of TLRs in innate immunity, the early containment of microbial infection, it does challenge the notion that TLRs are necessary for turning on the adaptive immune response, in which T and B cells become armed against a specific microbe and remember it to deploy defenses against subsequent attacks. "This paper shows that TLRs are not the essential link between the innate and adaptive immune systems where classical adjuvants are concerned," says Scripps immunologist Bruce Beutler, a co-author of the paper. "A large body of literature has to be reexamined."

The work "is wonderfully provocative," says Thomas Hawn, an infectious-disease specialist at the University of Washington, Seattle. "It reminds the field that there are alternative pathways for the innate immune response to influence an adaptive immune response." Some of those pathways might provide superior targets for vaccine adjuvants, he adds; Hawn and others worry that stimulating TLRs could lead to serious side effects.

Yet some immunologists dismiss the new study, citing its use of an "artificial" antigen as one of several flaws in its methodology. Others, such as Arthur Krieg, chief scientific officer at the TLR firm Coley Pharmaceutical Group in Wellesley, Massachusetts, point out that immune stimulators thought to work through TLRs appear safe so far in human trials and have shown preliminary signs of efficacy.

The controversial Scripps work began some 20 months ago when Gavin, along with graduate student Bao Duong and Scripps immunologist David Nemazee, wanted to test whether TLRs were required for antibody-making B cells to respond to synthetic molecules belonging to a narrow class known as T-cell independent antigens. They injected a large molecule made of linked sugars into a strain of mice whose TLR signaling is defective. These mice generated just as many antibodies to the antigen as did ordinary mice.

The researchers then tested both the TLR-disabled and normal rodents' immune responses to a protein antigen. This time, Gavin added an adjuvant called alum, because proteins typically are weakly immunogenic. Her team saw the same strong antibody response in both kinds of mice. Just as they got this result last year, Yale University immunologists Ruslan Medzhitov and Chandrashekhar Pasare reported in *Nature* that work with a different strain of TLR-disabled mice, including cell-transfer studies, led them to conclude that TLRs on B cells as well as dendritic cells are required for optimal antibody responses. In a letter to *Nature*, the Scripps team disputed that conclusion, supplying some of their then-unpublished data. In a reply, Medzhitov and Pasare argued, among other points, that the Scripps team would have obtained different results with other vaccines or adjuvants. ▶

SCIENCESCOPE

Canada Tackles Chemicals

Canadian regulators last week began banning 350 chemicals after government scientists concluded a 7-year review of almost 23,000 chemicals. The list includes bisphenol A, marking the first time that any government has banned the common additive, found in plastics. "We're not afraid. There's an awful lot of science supporting the safety of bisphenol A," says Steven Hentges of the American Plastics Council. In addition, scientists will look at some 4000 of the most worrisome chemicals under a $300 million program aimed at identifying dangerous and environmentally persistent toxic substances.

Richard Denison, a senior scientist with Environmental Defense in Washington, D.C., applauds the move, noting that the U.S. government has only examined "a few thousand of the 82,000 chemicals in its inventory."

–PAUL WEBSTER

China Seeks Academic Partners

BEIJING—The Chinese government is hoping that its top research institutes and universities will team up with basic research laboratories around the world. And it plans to set up a special fund to help make those partnerships happen. Shang Yong, vice minister of science and technology, last week called for top institutions with "good international cooperation records" to participate in the 5-year plan. Chinese universities will need to apply for the money, which the government hopes will be matched by the non-Chinese partner.

–JIA HEPENG

Targeting Tropical Diseases

SINGAPORE—A new partnership for clinical research could make Indonesia the first country to field-test drugs against dengue, a burgeoning, occasionally fatal disease that causes fever and wrenching muscle aches. The partnership—between the Novartis Institute for Tropical Diseases (NITD) in Singapore and two Indonesian institutes—will also focus on tuberculosis.

NITD, co-funded by Novartis and the Singapore government, aims to develop diagnostics and drugs for diseases of the poor and polish up the company's image in the process (*Science*, 7 February 2003, p. 811). Next month, it will join officials from Hasanuddin University in Sulawesi and the Eijkman Institute for Molecular Biology in Jakarta to launch a $5 million effort to build clinical research capacity in the world's fourth most populous nation. "We hope there will be a snowball effect," says Irawan Yusuf, dean of Hasanuddin's medical school. **–MARTIN ENSERINK**

Responding to that challenge, the Scripps team injected both TLR-disabled and normal mice with a chemically modified protein antigen and other immune boosters, including Freund's complete adjuvant (FCA), an oily microbial mixture that includes TLR ligands, and Ribi adjuvant, a TLR4 activator used in a hepatitis B vaccine. They saw robust antibody responses to the antigen for all the adjuvants in both types of mice. "We were surprised," Gavin says. "We too had been sucked into the misconception that TLRs are the only road there is" to a strong antibody response.

Medzhitov believes the study is fatally flawed, however. The robust B-cell responses in the TLR-signaling mutants, he claims, result from the use of a chemically modified protein. If Gavin's team were to use a regular antigen, he predicts, they would see a big difference between the mice. "TLRs are not the only possible target for vaccines," Medzhitov maintains, "but as far as we know, most of the major adjuvants work through TLRs."

Whether TLR stimulants are safe and effective adjuvants should be resolved as large-scale human trials come to a close in the next several years. But if Gavin and her colleagues are correct, biotech firms may want to shift gears. "TLRs are moving rapidly in the clinic," Krieg says. "But could there be something better in the future? Absolutely. Clearly, you can generate strong immune responses without TLRs." **–INGRID WICKELGREN**

WILDLIFE CONSERVATION

River Dolphins Down for the Count, and Perhaps Out

The world's rarest cetacean is nowhere to be found. Last week, a 3500-kilometer survey along China's Yangtze River failed to turn up a single river dolphin, or baiji (*Lipotes vexillifer*). "It's going to take a rescue effort of epic proportions to save this species," says Karen Baragona, director of the World Wildlife Fund's China programs. But it may already be too late for the nearly blind, pale creature. Expedition organizer August Pfluger, head of the Swiss-based baiji.org Foundation, says bluntly: "The baiji is functionally extinct."

The gloomy appraisal has prompted researchers to redouble efforts to save another endangered Yangtze cetacean, the finless porpoise, known in China as the jiangzhu, or river pig. (Cetaceans include whales, dolphins, and porpoises.) The survey recorded fewer than 300 of the world's only freshwater porpoise (*Neophocaena phocaenoides asiaorientalis*). Experts now estimate a total population of at most 1400, a 50% decline from the last major survey in 1991. "Without further intervention, the finless porpoise will be the next baiji," says survey member Zhang Xianfeng of the Wuhan Institute of Hydrobiology.

Although biologists knew the baiji was scarce, coming home empty-handed after a 6-week survey up and down the Yangtze was unexpected. A team from China, the United Kingdom, and the United States had planned to follow the survey with a $400,000 "rescue mission" to transfer any captured baiji to Tian-e-Zhou Lake in Hubei Province, a sanctuary holding 30 finless porpoises. That plan has been shelved, says Pfluger.

The baiji split from other dolphins 20 million years ago. Since then, the baiji's eyes have shrunk to pea size. It can discern only light and dark, so it relies on a finely tuned sonar to hunt prey in the silty Yangtze. The last comprehensive survey in 1997 found 13 baiji; from this figure, experts pegged the population at fewer than 100. "For us to see zero means there might be 10" left in the wild, says survey member Barbara Taylor, a marine biologist with the U.S. National Oceanic and Atmospheric Administration (NOAA). Or, as Pfluger notes, zero may mean zero. If so, the baiji would follow the Stellar's sea cow, Caribbean monk seal, and Japanese sea lion into oblivion as the fourth large marine mammal to go extinct in the last 3 centuries. It would be the first cetacean lost in modern times.

Unhappy hunting. Expedition members search fruitlessly for signs of baiji on the hazy Yangtze River. The last baiji in captivity (*inset*) died in 2002.

Although the baiji's fate is uncertain, the dangers it faces are all too apparent. The most immediate threat is the use of rolling hooks, says expedition co-director Robert Pitman, a NOAA marine biologist. These illegal fishing lines are stretched across a river and are known to snag and drown baiji. During the survey, says Pitman, "we saw hundreds of fishermen using rolling hooks."

Long-term hazards are pollution and choking boat traffic. Near Poyang Lake in Jiangxi Province, connected to the Yangtze by a narrow channel, Taylor counted some 1200 boats in a span of 2 hours. Between the heavy traffic and numerous factories hard up against the lakeshore, Taylor declares Poyang the "biggest environmental disaster" she's ever seen. That's bad news, as Poyang, China's largest lake, is one of the last redoubts of the finless porpoise: It has the biggest intact population, estimated at 400, with 80 spotted during the survey.

Plucking the porpoise from peril won't be simple. Proposed megadams may fragment remaining populations, says Zhang. "There's no hope to change the environmental conditions on the Yangtze," he says. Pfluger says his organization will educate fishers about the impact of illegal fishing and finance a sustainable-fishing initiative at Tian-e-Zhou Lake. There, two or three porpoises are born each year, and captive breeding has resulted in a pregnancy last year, says expedition co-director Wang Ding of the Institute of Hydrobiology. "We have to set up more seminatural reserves like Tian-e-Zhou," Wang says.

Sadly, that approach may no longer be applicable to the baiji, an apparent victim of China's booming economy and the attendant environmental degradation of a mighty river. "It seems the baiji is the only thing that is not made in China anymore," says Pitman.

–JERRY GUO

Jerry Guo is a writer in New Haven, Connecticut.

CREDITS: BARBARA TAYLOR/NOAA/U.S. DEPARTMENT OF COMMERCE; (INSET) WANG XIAOQIANG

ENVIRONMENT

Spain's *Prestige* Oil Spill Resurfaces

BARCELONA—The hulk of the *Prestige* tanker that sank off the coast of Spain in 2002 is a disaster waiting to happen, according to a study released in Madrid last week. Although a private firm was hired to remove oil from the tanker and carry out bioremediation, a new analysis finds that as much as 23,000 tons of oil may still be in the ship. Bacteria that corrode the hull, according to the report, could soon trigger a rupture. The authors, led by José Luis De Pablos, a physicist at Madrid's Center for Energetic and Environmental Research, urged the government to take "prompt" action.

Some observers have disputed De Pablos's analysis but agree that an investigation is warranted. Oceanographic chemist Joan Albaiges, vice president of a government scientific advisory commission for the *Prestige* incident, said, "It's clear to me that bioremediation didn't work." The recent discovery that the tanker is leaking undegraded fuel, he says, "raises doubts about the success" of the 2004 cleanup. The company that carried out the bioremediation work, Repsol of Madrid, declined to comment.

Repsol used remotely operated submersibles to suck oil into giant plastic bags (*Science*, 28 November 2003, p. 1485). When the work ended in August 2004, the government said that only 700 to 1300 tons of oil remained in the tanker. An advisory scientific committee predicted that corrosive cracks were not likely to appear in the hull before 2025.

In March 2006, however, new oil slicks were detected near the *Prestige*. Scientists from several public institutions took samples and concluded that the petroleum at the surface matched the type carried by the *Prestige*. Their report, handed over to the government in mid-November, concluded that the fuel "did not have signs of degradation," indicating that the bioremediation effort had not been fully effective.

The independent analysis released by De Pablos on 12 December concluded that between 16,000 and 23,000 tons of oil remain in the wreck and could be released rapidly. For example, De Pablos claimed that the level of fuel in the tanker before Repsol began its cleanup was "double" that estimated by the company's formula. And he cited research published in 2004 describing the corrosive action of the bacteria *Desulfovibrio desulfuricans*, which produces an acid capable of destroying more than 2 mm of steel per year. He estimated that holes would form in the tanker's hull within 4 years of its sinking. In addition, De Pablos said the angle at which the tanker lies on the floor could stress bulkheads, leading to a catastrophic leak. De Pablos recommended that the government treat the oil with a neutralizing agent and build a sarcophagus over the wreck.

Cleanup. A fishing boat unloads tons of spilled oil from the stricken tanker *Prestige* in 2003.

But Albaiges says that some of De Pablos's data appear to be "flawed and based on speculation rather than strong evidence." For instance, Albaiges says, the tanker's position on the ocean floor isn't a key factor, and a massive spill "isn't possible." Yet he also doubts Repsol's claim that only 1000 tons of oil remain in the tanker. "I will believe them when they show the results of their studies," he contends.

The company referred questions to the government's Center for the Prevention and Fight Against Marine and Coast Pollution. Center Director Purificación Morandeira says that De Pablos's calculations underestimate the rate of flow of the recovery bags during the oil cleanup 2 years ago. Morandeira says the government has asked Repsol to examine the wreck again in 2007.

–XAVIER BOSCH

Xavier Bosch is a science writer in Barcelona, Spain.

CREDIT: VINCENT WEST/REUTERS

SCIENCESCOPE

South Pole Death Probed

More than 6 years after Australian astrophysicist Rodney Marks died of methanol poisoning while wintering over at the South Pole, New Zealand authorities continue to investigate the circumstances surrounding his death. And the willingness of the National Science Foundation (NSF) and other U.S. agencies to share information lies at the heart of the inquiry.

Last week, a coroner's inquest in Christchurch, New Zealand, heard 2 days of testimony about events shortly before Marks ingested a fatal dose of methanol, a common alcohol-based solvent that is also often used in homemade spirits. Marks was working on the Antarctic Submillimeter Telescope and Remote Observatory located at NSF's Amundsen-Scott South Pole Station. NSF originally reported that the 32-year-old Marks "apparently died of natural causes" on 12 May 2000. The body was sent to Christchurch once flights from the pole resumed in the fall, and in November 2000, an autopsy revealed lethal levels of methanol. Christchurch coroner Richard McElrea then asked police to investigate.

At the inquest, Detective Senior Sergeant Grant Wormald testified that the police department has been frustrated by what he characterized as a lack of cooperation from U.S. authorities in contacting the 49 people who were living at the South Pole station at the time of Marks's death. As a consequence, Wormald said that police have yet to determine whether the poisoning was accidental or deliberate.

NSF spokesperson Jeffrey Nesbit says that New Zealand authorities asked NSF for help in 2002 and that the following year the agency sought clarification of the request. "There are complex jurisdictional and privacy issues involved," says Nesbit, in explaining the delay. In 2005, NSF and its contractor, Raytheon Polar Services, distributed a questionnaire to those who had wintered over in 2000 and asked them to send their responses directly to New Zealand. "We didn't get any returns, so we assume that they went to the right addresses," Nesbit added. Wormald testified that the police eventually received nine replies.

New Zealand officials say they hope the additional publicity will lead people to come forward with new information. McElrea declined comment on his plans. But the case remains open, and the inquest is expected to resume in February.

–JEFFREY MERVIS

ARCHAEOLOGY

Researchers Helpless as Bosnian Pyramid Bandwagon Gathers Pace

LONDON—An unusual soirée took place here at the Bosnian embassy last week. The star of the show, Semir Osmanagić, presented a slide show of his discovery of ancient pyramids northwest of Sarajevo and other evidence of what he calls a "supercivilization" that flourished in Bosnia 12,000 years ago—a time when most archaeologists believe small groups of hunter-gatherers were struggling to survive in a frozen Europe. He then posed for photographs in front of a pyramid-shaped cake baked in his honor.

Osmanagić, a Bosnian businessman, has riled professional archaeologists who see his pyramid hypothesis as completely unfounded. Last week, the European Association of Archaeologists published an open letter to the Bosnian government calling Osmanagić's project "a cruel hoax on an unsuspecting public [which] has no place in the world of genuine science." U.K. archaeologists are disturbed at the lack of criticism. "Support for this raft of nonsense has only increased," says Richard Carlton, an archaeologist at the University of Newcastle, but "I have no idea what to do other than to continue to present reasonably argued opposition."

Half-baked. Semir Osmanagić poses with Bosnian ambassador to the U.K. Tanja Milašinović.

Osmanagić declared last year that a series of pyramid-shaped hills near Visoko were structures built by a previously unknown Neolithic civilization, and he set up a foundation to excavate and exploit them. Bosnia's fragmented archaeological community is struggling to convince the public that the pyramids are simply natural features (*Science*, 22 September, p. 1718), but Osmanagić's influence and popularity have only grown. He is planning to expand his "archaeological park" scheme across the country to include newly discovered stone sphere "megaliths" and stone temples—both of which scientists say are just geology. He is currently in Malaysia meeting business leaders interested in funding the parks.

Osmanagić began his lecture by saying that his excavation team includes an Oxford University archaeologist who "agrees that these are massive, manmade structures." And after the embassy event, the Bosnian Pyramid Foundation Web site claimed that "Robert Harris, member of the British Parliament," hailed "the significance of this discovery."

"There is no British parliamentarian called Robert Harris," says Colin Renfrew, a member of the House of Lords, and the Oxford archaeologist is Alex Cartwright, an undergraduate student. "Mr. Cartwright does not have any expertise and in no way represents the university," fumes Peter Mitchell, an Oxford archaeologist.

In contrast to this academic turmoil, most conversations at the embassy gathering centered on the 200,000 tourists Osmanagić says have visited Visoko this year.

–JOHN BOHANNON

2007 U.S. BUDGET

NIH Trims Award Size as Spending Crunch Looms

The National Institutes of Health (NIH) is asking most of its grantees to tighten their belts. The agency decided last week to cancel a scheduled inflationary boost for scientists with multiyear awards. Like other U.S. science agencies, NIH is preparing for an anticipated flat budget in 2007 that would freeze any new activities and take a bite out of existing programs.

The looming crunch is a result of a breakdown in the annual budget cycle. The 109th Congress adjourned earlier this month after completing only two of 11 spending bills—for homeland security and the military. Every other agency was ordered to operate, at best, at current funding levels until 15 February. Last week, the incoming Democratic chairs of the appropriations panels said they hoped the new Congress would extend the so-called continuing resolution (CR) through 30 September, the end of the 2007 fiscal year (*Science*, 15 December, p. 1666).

NIH decided not to wait. On 15 December, it eliminated a 3.4% inflationary boost in 2007 for "noncompeting renewals," some three-quarters of the pool of grants held by principal investigators. The savings will be used to fund as many new awards as possible in 2007. That number, about 9600, would be similar to 2005 levels and nearly 600 more than in 2006, when NIH's $28.6 billion budget actually shrunk by $100 million.

"The new policy is consistent with NIH's concerns for new investigators, those who will be applying for their first renewal grants, and those solely supported by NIH," says Patrick White of the Association of American Universities. "And while we appreciate that NIH is trying to spread the pain, the critical thing is [fighting for] a reasonable increase in 2008."

Some other agencies will be even worse off. A CR will decimate the first step in the proposed budget doubling of the National Science Foundation, the Department of Energy's Office of Science, and the National Institute of Standards and Technology. It could also wipe out a $1 billion increase that a Senate spending panel had approved for NASA to help the space agency recover from the 2003 Columbia space shuttle tragedy and damage from Hurricane Katrina in 2005. NASA officials say a CR would leave it with a $700 million shortfall that could eat into the agency's $5.2 billion science portfolio.

Many lawmakers are unhappy about funding the government on a CR but see no better alternative. "In some sense, a CR is like Iraq," says the incoming chair of the House Science Committee, Representative Bart Gordon (D–TN). "It's a matter of the least worst option ... and then going forward in 2008."

–JEFFREY MERVIS

CREDIT: ELMA OKIC/HUNGRY EYE IMAGES

NONPROLIFERATION

Indo–U.S. Nuclear Pact in Jeopardy

NEW DELHI—A landmark nuclear deal between India and the United States is in danger of unraveling. Top nuclear scientists in the Indian government, speaking on condition of anonymity, have told *Science* that they oppose provisions of new U.S. legislation that paves the way for civilian nuclear cooperation between the two nations. "The costs to the U.S. appear minimal. The price India will have to pay may well be a total loss of control over its future nuclear policies," asserts M. R. Srinivasan, a member of India's Atomic Energy Commission.

Most egregious, Srinivasan and others say, is language in the law that equates to a de facto ban on further nuclear tests. "The U.S. has shifted the goalposts," grouses one top government scientist. The Indian government is mulling a formal response.

The legislation would end a U.S. ban on the sale of nuclear technology and fuel to India, imposed after India's first nuclear test in 1974. U.S. President George W. Bush signed it into law on Monday, paving the way for negotiations on the "123 Agreement," a bilateral treaty spelling out each country's commitments under the pact. In the meantime, India must conclude safeguards agreements with the International Atomic Energy Agency (IAEA), and the 45-member Nuclear Suppliers Group must amend its rules to permit trade, even though India is not party to the Nuclear Nonproliferation Treaty. U.S. nuclear firms are eager to make sales: India estimates that over the next 25 years it will install almost 50,000 megawatts of nuclear power at a cost of $75 billion.

From the start, however, negotiations over implementing the nuclear accord, inked in July 2005, have been fraught. An early bone of contention was India's plan for separating its nuclear establishment into military and civilian facilities, with only the latter open to foreign commerce. After several rounds of talks, the two sides last March agreed on an implementation plan that was denounced by U.S. nonproliferation experts (*Science*, 10 March, p. 1356).

Now key Indian leaders are turning against it. Officials say their chief concern is provisions of the legislation that they claim aim to cap India's nuclear weapons program. In a statement last week, the main opposition party, the Bhartiya Janata Party, called for an "outright rejection" of the deal. And after a meeting on 15 December in Mumbai convened by the chair of India's Atomic Energy Commission, Anil Kakodkar, several retired atomic scientists in a statement called the U.S. legislation "objectionable" and argued that "India must not directly or indirectly concede our right to conduct future nuclear weapon tests."

Indian scientists see a major bugbear in the "joint explanatory statement" from the U.S. congressional conference committee that drafted the legislation. They claim the text makes India vulnerable to a repeat of the U.S. fuel blockade after India's 1974 test. Then, the United States banned the supply of uranium fuel for General Electric–built reactors at Tarapur, in western India. During the recent negotiations, India demanded that any future imported reactors come with assurances of a lifetime fuel supply. The U.S. legislation states that provisions "should be commensurate with reasonable reactor operating requirements." That's fine, Indian officials say, but they are riled by wording in the explanatory statement that fuel cannot be assured in the event of "Indian actions ... such as a nuclear explosive test."

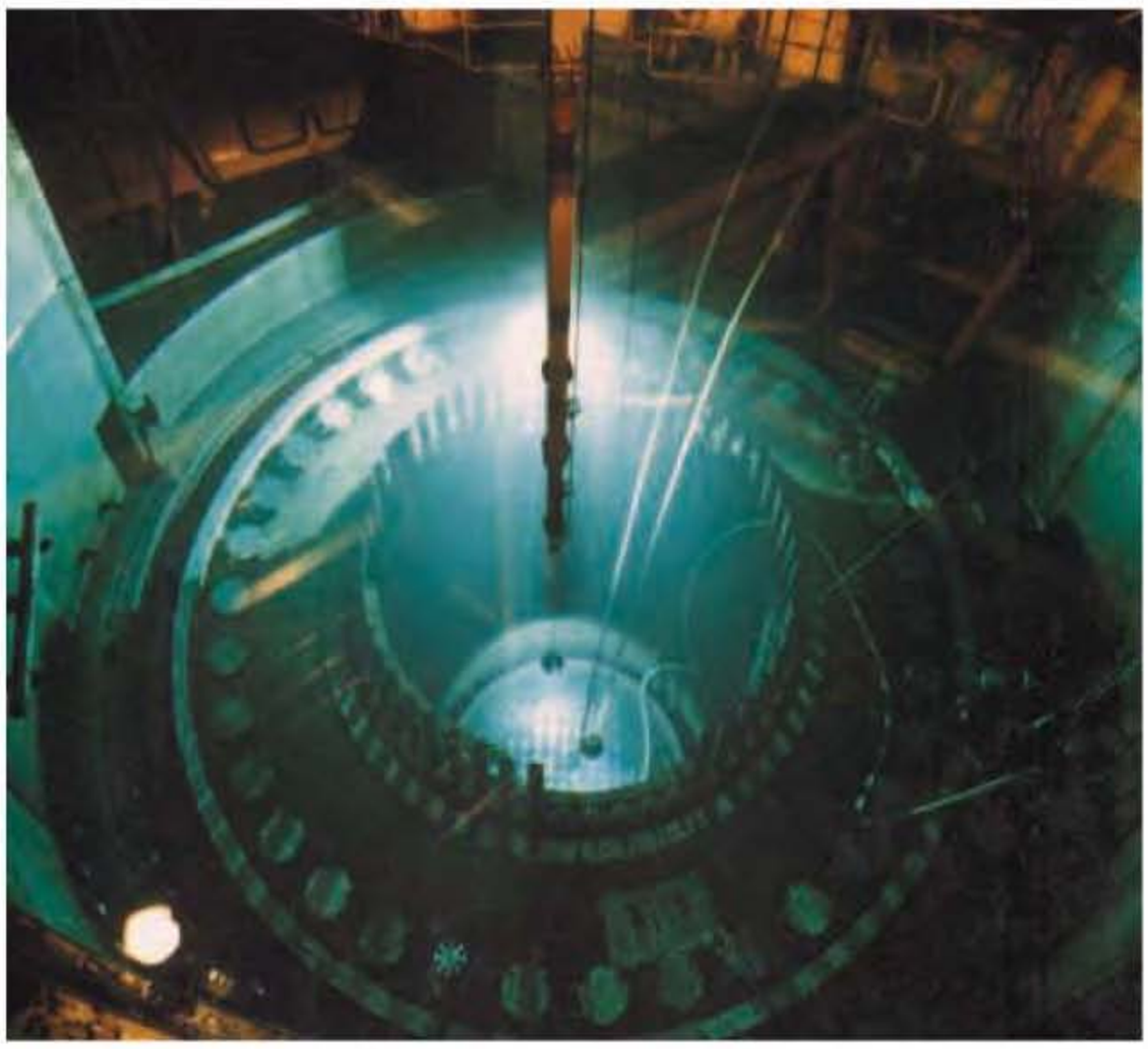

Core concern. Indian scientists assert that new U.S. legislation makes India vulnerable to a repeat of a nuclear fuel blockade of U.S.-built reactors at Tarapur (one shown *above*) in 1974.

CREDIT: DEPARTMENT OF ATOMIC ENERGY

"This is most unacceptable," says Srinivasan. Currently, he asserts, the deal would barter away India's right to conduct nuclear tests, particularly if India's electricity grid comes to depend on nuclear power. After tests in 1998, India declared a unilateral moratorium. "There is no question of accepting any such agreement that binds India beyond its voluntary hold on nuclear testing," says a top government scientist. Last week, India's foreign minister, Pranab Mukerjee, hinted at a hard line when he told Parliament, "We will not allow external scrutiny of or interference with the strategic program."

India also was hoping for an explicit allowance to reprocess imported fuel. India reprocesses domestic spent fuel, extracting plutonium for future breeder reactors. (U.S. analysts estimate that India has stockpiled 360 kilograms of plutonium for weapons.) The U.S. legislation does not refer to reprocessing, although "in future, it might get addressed," U.S. Under Secretary of State R. Nicholas Burns told *Science*; he declined to give further details.

Indian officials also object to wording in the legislation calling for free access for U.S. inspectors to any safeguarded nuclear facility in the event that IAEA were to fail to carry out routine inspections. Last August, Indian Prime Minister Manmohan Singh told Parliament that "there is no question of allowing American inspectors to roam around our nuclear facilities."

The fate of the nuclear pact hinges on negotiations over the 123 Agreement. Three rounds of talks have been held on the treaty, with no date set yet for the next round. If the two sides do find common ground, Indian and U.S. nuclear scientists could be spending a lot more time together—on nonproliferation. The legislation calls for the U.S. National Nuclear Security Administration to work with scientists from the U.S. National Academies and Indian government to establish a cooperative nuclear nonproliferation program. At least so far, Indian government scientists haven't objected to that. **–PALLAVA BAGLA**

A Gut Germ Goes AWOL

If you've ever suffered after eating undercooked chicken, chances are you had a bellyful of *Campylobacter jejuni* bacteria. At the meeting, researchers reported one possible explanation for the intestinal interloper's nastiness, showing that it evades a cellular defense that minces other bacteria.

C. jejuni sends more people to the doctor than any other food-dwelling bacterium. Recent tests by the magazine *Consumer Reports*, for instance, detected the microbe in 81% of supermarket chickens. Along with short-term misery, the germ occasionally triggers protracted problems such as Guillain-Barre syndrome, a paralyzing autoimmune reaction. The bacterium's gut-wrenching potential stems in part from its ability to infiltrate intestinal cells: Strains that are better invaders provoke more severe illness.

Campylobacter is tricky to study in a lab, however, and researchers aren't sure how it slips past a cell membrane and what it does once it gets inside. But graduate student Robert Watson of Yale University School of Medicine and his adviser, microbiologist Jorge Galan, improved the culturing method for the germ, allowing them to more easily watch it invade intestinal cells.

Many kinds of bacteria ride into a cell via the endocytic pathway, which the cell normally uses to ingest useful molecules. The cell first bags what it wants to import, creating a capsule called an endosome. Anything the cell doesn't remove from the endosome travels to another interior compartment, the lysosome, which brims with digestive enzymes potentially fatal to any trapped bacterium.

By observing molecular markers that decorate endosomes, Watson and Galan determined that *Campylobacter* does get snared by the endocytic pathway. But it avoids a deadly bath. Two tracking molecules that tag endosomes destined for the lysosome didn't mark containers holding *C. jejuni*. These findings indicate that *C. jejuni* makes its break from the endocytic pathway quickly, Watson says.

Other pathogens have evolved ways to escape destruction by lysosomes. The foodborne germ *Shigella* slips out of the endosome. In contrast, *Campylobacter* remains inside, but the endosome docks near the organelle known as the Golgi apparatus. What the germs are doing there isn't clear, Watson says. They don't appear to be reproducing, but they do settle in, switching their metabolism to run without oxygen. The Golgi apparatus serves as a cell's distribution center for proteins and other molecules, which the bacteria could be filching, Watson says.

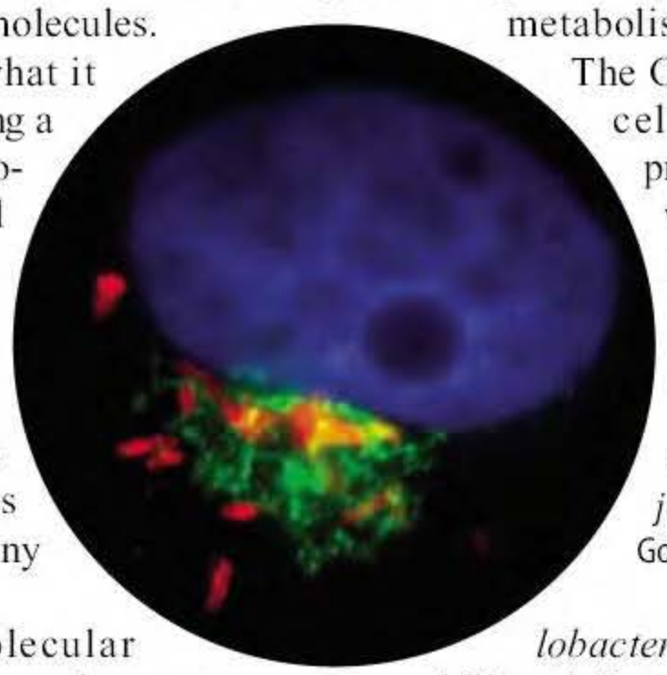

Wayward bug. *Campylobacter jejuni* (red) beds down near the Golgi apparatus (green).

The new results "define the step where *Campylobacter* eludes the host system for killing it," says microbiologist Patricia Guerry of the Naval Medical Research Center in Silver Spring, Maryland. The next step is to determine how it gets away, she says. "The study could potentially provide insight into how this bug makes us sick, which is a big black box," adds microbiologist Erin Gaynor of the University of British Columbia in Vancouver, Canada. For example, she says, researchers could test whether *Campylobacter* interacts differently with human and chicken cells, because the birds harbor the bacteria but don't become ill.

–MITCH LESLIE

Sprayed-on Growth Factors Guide Stem Cells

Researchers hoping one day to fashion intricate replacement parts that depend on multiple cell types—joints, for example—need to crack a vexing problem: how to coax adjacent stem cells to follow different developmental pathways. In San Diego, California, scientists reported a step toward this goal with the use of an unusual technology: an ink-jet printer.

Cell biologist Julie (Jadlowiec) Phillippi of Carnegie Mellon University in Pittsburgh, Pennsylvania, and colleagues used a custom-built printer to direct the growth of stem cells into two lineages side by side. They programmed their machine to squirt microscopic drops of a growth factor called bone morphogenetic protein (BMP)—which spurs bone cell specialization—into square shapes on a bed of extracellular matrix. They then planted adult muscle stem cells on the surface. Within 3 days, the cells growing on the squares differed visibly and biochemically from neighboring cells growing where no BMP had landed. The cells on the squares cranked out an enzyme that indicated they had diverted into the bone lineage. Meanwhile, the cells living on extracellular matrix alone manufactured the myosin heavy chain protein, showing that they had continued on the road toward muscle.

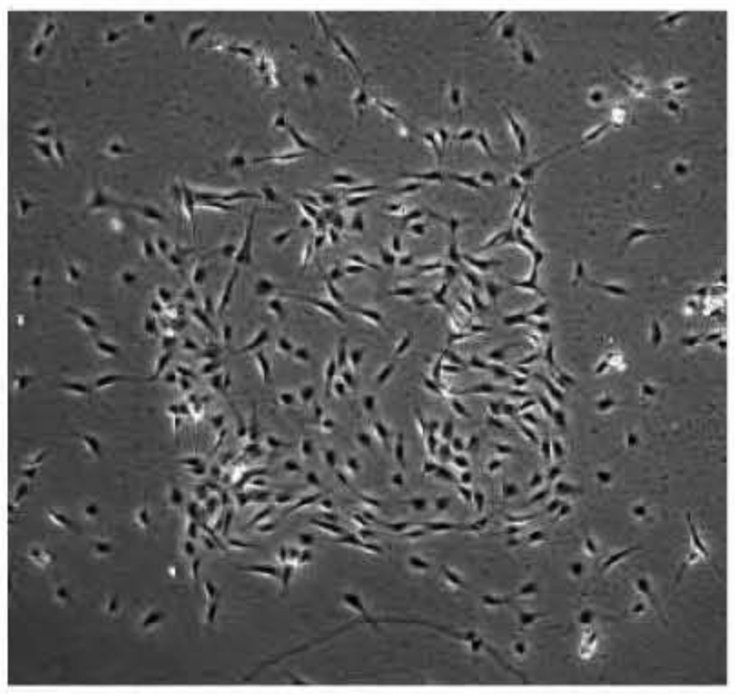

Stem cells square up. Prebone cells cluster inside the box where a growth factor was sprayed, whereas premuscle cells remain outside.

The team is experimenting with more complex patterns, including three-dimensional "stacks" made from alternating layers of growth factors and extracellular matrix, Phillippi says. She and her colleagues are also testing whether the ink-jet method can promote healing of skull punctures in rats. They apply patches of extracellular matrix to the wounds, and then spray on growth factors to encourage the animals' own cells to close the punctures.

The scientists aren't the first to turn to ink-jet printers. Biologists have used them to spray cells and molecules into particular patterns to study everything from muscle development to crystallography (*Science*, 24 September 2004, p. 1895). Much of this work has focused on the machines' technical capabilities, says materials scientist Brian Derby of the University of Manchester in the U.K. Phillippi and her colleagues, he says, "are the first people to show that the [ink-jet] technique is not just practical but useful."

–MITCH LESLIE

CREDITS (TOP TO BOTTOM): ROBERT WATSON; PHIL CAMPBELL AND ERIC MILLER

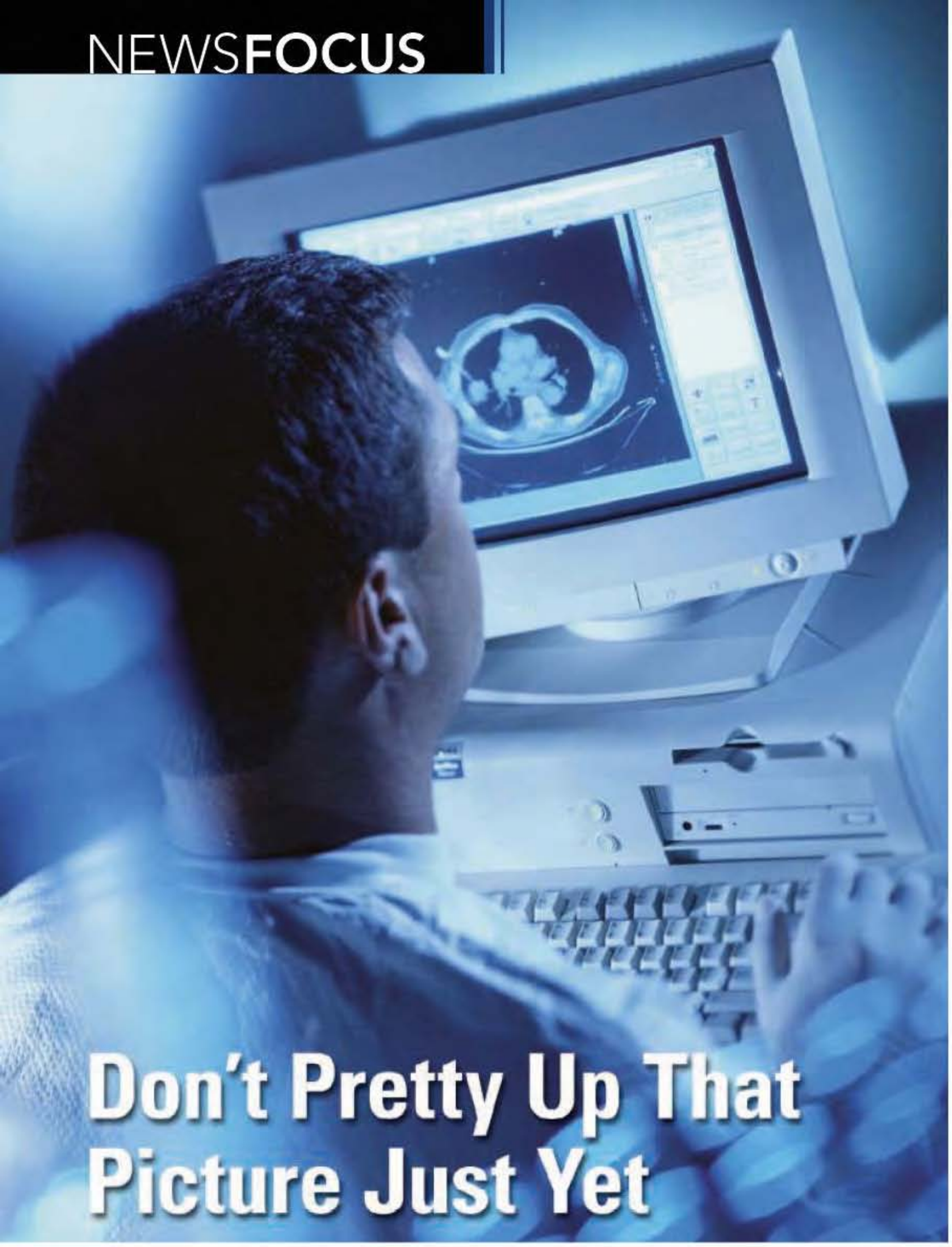

Don't Pretty Up That Picture Just Yet

Scientists are used to enhancing images, but journal editors worry that the results can be misleading and are cracking down on the practice—some more forcefully than others

WHEN HE TRAINS COLLEAGUES TO capture images of cells and their squishy contents in microscopes at the Wistar Institute in Philadelphia, Pennsylvania, James Hayden sees certain behaviors again and again. Some biologists become so excited by a weak signal suggesting the presence of a particular molecule that "they'll take a picture of it, they'll boost the contrast, and they'll make it look positive," says Hayden, who runs Wistar's microscopy core facility. And often, he adds, scientists discard the original, ambiguous image and preserve only the modified one.

Hayden himself, who has worked for years helping scientists ready images for publication, wrestles with the fine line between appropriate and misleading image alterations. "We've all seen gels that look like a complete disaster," with "splotches" everywhere from artifacts related to processing. "In the past, I would take those out," says Hayden. "I wouldn't do that now."

That's because scientific journals, concerned about a growing number of cases of image manipulation, are cracking down on such practices with varying degrees of aggressiveness. At one end of the spectrum is the biweekly *Journal of Cell Biology*, which for the past 4 years has scrutinized images in every paper accepted for publication—and reports that a staggering 25% contain at least one image that violates the journal's guidelines. That number has held steady over time, says Mike Rossner, the journal's managing editor.

Increasingly, journals are offering authors detailed instructions on how digital images should be handled, but many doubt that this will be much of a deterrent to "improving" them. And although troubled by a mounting stack of problem images, usually picked up by reviewers or readers, most journals are reluctant to devote much staff time and money to hunting for images that have been inappropriately modified. Vanishingly few are emulating the *Journal of Cell Biology*, although more are beginning to consider it.

Last month, *Nature* and its suite of specialized journals began spot checks of all images in one paper for each issue of every journal. Editors were driven in part by several cases of inappropriate image manipulation, including a *Nature Immunology* paper that was retracted after a reader noticed that flow cytometry data were identical in supposedly different experiments. "It's a little embarrassing to publish papers with figures like this," admits Linda Miller, the U.S. executive editor at *Nature* and the *Nature* research journals.

Mounting concern

Most journals don't keep statistics on cases of dubious images, and it's unclear whether image manipulation is really on the rise or whether readers and journals are more attuned to it than in the past. Awareness of the problem was certainly raised by the discovery that Woo Suk Hwang, formerly of Seoul National University, and his colleagues had faked data in two blockbuster stem cell papers in *Science*. In one, published in 2005, images purporting to be of different cell lines were in fact overlapping pictures of the same cells.

A review commissioned by *Science* and led by six outsiders, including Miller, recommended last month that *Science* more often request primary data, including images. This past summer, *Science* began screening all papers close to acceptance that contain images of gels or cells, about 15 to 20 per week.

Regardless of whether the frequency of image manipulation has changed, there's no question that digital technology has made it far easier. Anyone familiar with image-based computer software can cut and paste portions of pictures, duplicate images and reuse them, delete blemishes, or selectively adjust the contrast of an image—for example, by darkening the band of a gel, which would suggest that a molecule's presence or

CREDIT: ANDREW YATES/GETTY IMAGES

characteristics are stronger than they really are. "People are very agile" at performing these modifications, says James Ihle, editor-in-chief of *Molecular and Cellular Biology* and a molecular biologist at St. Jude Children's Research Hospital in Memphis, Tennessee. His biweekly journal has detected at least a half-dozen cases of inappropriate image manipulation so far this year. Five years ago, just one case would have been a surprise, he says.

A general consensus is emerging among journals about what constitutes inappropriate image manipulation, although in some disciplines defining it can be tricky. Astronomers, for example, are "taking pictures, and they enhance what they get" in order to "see things they would not see with the naked eye, and that's legitimate," says Martin Blume, editor-in-chief of the American Physical Society (APS), which publishes nine journals. So what represents improper manipulation? In Blume's mind, that would include inserting data points or adding a light spot, which might represent a planet.

Broadly speaking, "the big issue is whether such manipulation, which is done to enhance an image, actually changes its meaning," says Kathleen Case, the publisher at the American Association for Cancer Research (AACR), which puts out five journals. Next month, AACR plans to post new guidelines on image modification. The association recently encountered its first case of improper modification, caught by an astute reader. "Most authors don't feel this is particularly wrong; they're just trying to make the illustration look better," says Case.

In general, certain types of manipulation are considered acceptable—such as adjusting brightness or color across an entire image—particularly if those changes are disclosed by the authors. Hayden of Wistar feels strongly that scientists ought to preserve all original image files, no matter how much the files are subsequently "cleaned up."

> "Most authors don't feel this is particularly wrong; they're just trying to make the illustration look better."
>
> —Kathleen Case, AACR

News of the journals' stricter stance has not reached all the scientists for whom it's designed. "I almost died when I heard they didn't think it was a true picture," says one biologist, who asked not to be named because he was reluctant to be known for image modification. A member of the biologist's lab had created a collage of images. Editors of the journal in which it was published, tipped off by a reader, deemed the collage unethical because it was presented as a single picture. A correction was subsequently published, noting that the modification, although inappropriate, did not affect the paper's conclusions. "We thought it was obvious that it was a collage," says the biologist, adding that he vehemently opposes altering images.

Policing, or not

Even as they urge scientists to adjust images sparingly, if at all, journals are mired in a debate about how far their own responsibility for catching rule breakers extends. Like AACR's five journals, the 11 journals published by the American Society for Microbiology (ASM) will release new guidelines on digital image modification in January. In 2006, the *Proceedings of the National Academy of Sciences*, *Science*, and *Nature* all created restrictions for authors on modifying digital images. Most image guidelines are targeted to certain fields of biology, such as molecular biology and genetics.

ASM's journals, which include the one edited by Ihle, have together experienced roughly a dozen cases of image manipulation deemed misleading in the past 6 months, estimates Samuel Kaplan, chair of the society's publications board and a microbiologist at the University of Texas, Houston, Medical School. In some cases, editors concluded that the manipulations were a deliberate attempt to mislead, and the guilty parties were banned from publishing in ASM journals for 3 to 5 years. In other instances, authors were asked to supply original images for a paper not yet published, or a correction for a paper that had already appeared.

The pattern is troubling enough to Kaplan and others at ASM that late this month, an editors' meeting in Washington,

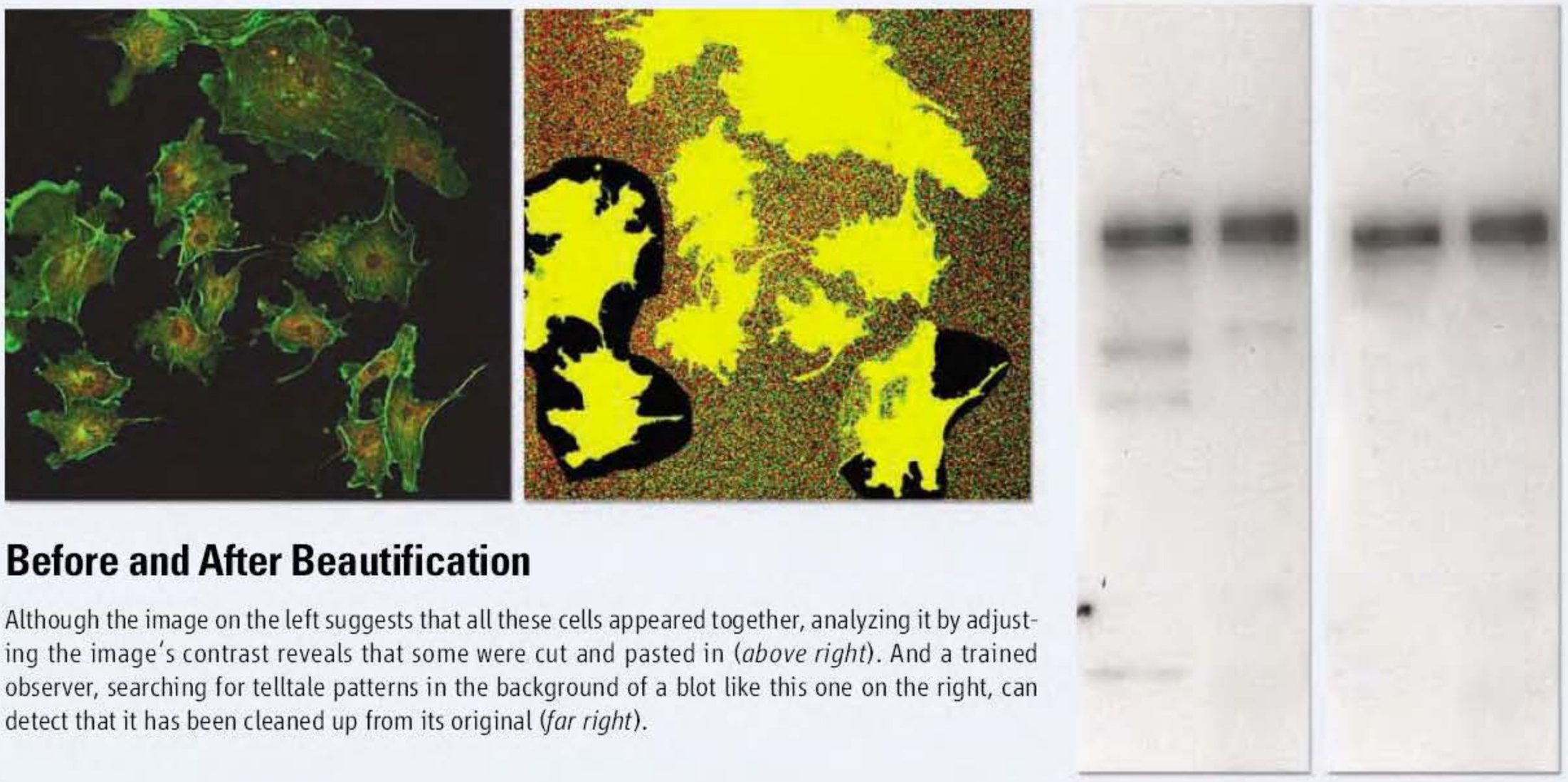

Before and After Beautification

Although the image on the left suggests that all these cells appeared together, analyzing it by adjusting the image's contrast reveals that some were cut and pasted in (*above right*). And a trained observer, searching for telltale patterns in the background of a blot like this one on the right, can detect that it has been cleaned up from its original (*far right*).

CREDITS (LEFT TO RIGHT): ROSSNER *ET AL.*, *JCB* **166** 11–15 (2004)

D.C., will take up the problem. ASM journals collectively publish about 8000 papers every year, out of 17,000 submitted. "Should we prescreen every manuscript that comes in?" asks Kaplan, acknowledging that, however desirable, this would be "a horrendous task."

In fact, few journals perform any kind of systematic screening of papers. Among the exceptions are the *Journal of Cell Biology* and its two sister journals, which have a dedicated staffer who reviews the roughly 800 papers accepted by all three each year prior to publication. *Science*'s screening is principally designed to pick up selective changes in contrast and images that are cut and pasted. *Nature* has its spot checks. The biweekly *Journal of Neurochemistry* also does systematic screening; one of its chief editors was inspired by Rossner of the *Journal of Cell Biology*, who has heavily promoted the cause.

The editors say that the rates of manipulation at *Science* and the *Journal of Neurochemistry* are far lower than at Rossner's journal. Katrina Kelner, deputy editor for the life sciences at *Science*, says that since initiating image analysis earlier this year, *Science* has seen "some number less than 10," or a few percent at most. She speculates that the difference might be due to the subject matter—cell biology images are considered more prone to manipulation, and that discipline makes up only a fraction of *Science*'s papers—or the fact that Rossner's staffer, originally the office manager, is now unusually experienced at hunting for modifications. Either way, there's no evidence that this intensive review is having much effect on behavior, as the rates of manipulation recorded by the *Journal of Cell Biology* haven't changed with time. That worries Miller, who says she is hoping the extra scrutiny at *Nature* will act as a deterrent.

Most journals say extensive screening is not possible for them. "There is no way in which we can search everything that comes in or even everything that's published," a total of 17,000 papers, says APS's Blume. Adds Lynn Enquist, editor-in-chief of ASM's *Journal of Virology* and a molecular biologist at Princeton University, "We're not a for-profit sort of thing; everything is done by the grace of people who give up their time. ... We're concerned about it, but I don't see any new staff getting hired."

That situation is common. Journals are "looking for a cheap fix," says Hany Farid, a computer scientist at Dartmouth College who is designing software that can pick up airbrushing, cutting-and-pasting, and other alterations made to images. Farid says the journals he has spoken with are reluctant to embark on widespread image analysis. But, he says, "they have some obligation to be a better gatekeeper than they are now." Rossner, who pioneered image review, agrees wholeheartedly.

Regardless of the policies instituted by journals, it's widely agreed that a generational disconnect has left students agile at handling digital images while many older lab leaders shy away from it, presuming that their students understand the rules. After his own journal experienced its second case of improper image manipulation, Enquist says, "I spoke up at a lab meeting and said, 'This is the second time I've seen someone do something really dumb; I hope you guys aren't doing this.' Then we had this discussion, and people said, 'I turned the contrast up here and there.' "

The experience drove home for Enquist that "students really aren't being told what's right or wrong, what's acceptable or not. We're just assuming that they know."

–JENNIFER COUZIN

DATA STORAGE

Is the Terabit Within Reach?

Makers of computer hard disk drives have a good idea for how they'll keep disk capacities rising through the end of the decade. After that, they'll likely have to reinvent disk-drive technology with a lot of help from nanotechnology

BOSTON—Makers of magnetic disk drives are perpetual victims of their own success. The more storage capacity they pack into their disks, the more people want. Today, the top disk drives pack more than 100 billion bits, or 100 gigabits (Gb), of data into a single square inch of hard disk space. (Bits/in^2 is the industry's standard unit.) That makes it possible to hold thousands of songs and pictures on one of the 1" disks in an Apple iPod. But with digital video recorders now gobbling up to 6 Gb for an hourlong TV show, all of a sudden that 120-Gb disk drive doesn't seem so big anymore. As for that 20-Gb hard drive that came with your desktop a few years ago, forget it.

Computer hard disks store data by defining the magnetic orientation of small regions of a spinning platter. For 50 years, diskmakers have boosted the capacity of their disks by shrinking the size of those regions. So far, that strategy has worked splendidly. Disk drives today hold 100 million times as much data as the first devices that IBM researchers turned out in 1956. Diskmakers predict that tweaks to the current technology will keep making bits smaller until around 2010, when disk drives are expected to pack an estimated 500 Gb/in^2. Past that, it'll be time to get creative. "We believe new media technology will be needed to take areal density beyond 500 Gb/in^2," says Dieter Weller, who directs research on magnetic media at Seagate, a major disk drive manufacturer in Fremont, California.

Today's disks are made by laying down a thin film of a magnetic alloy, which is composed of a mosaic of tiny grains that act as independent magnetic elements. The leading contender for next-generation technology is to replace this layer of granulated material with prepatterned magnetic islands in a background of nonmagnetic material. Such "patterned media" could strengthen the magnetic signal coming from each island, thus enabling diskmakers to pack the islands—or bits of data—closer together.

But getting there won't be easy. Patterned media are complicated to make, and many industry experts worry that the costs of hard drives could rise significantly. "In the past, patterned media looked very good in theory," says Zvonimir Bandic, a physicist with Hitachi Global

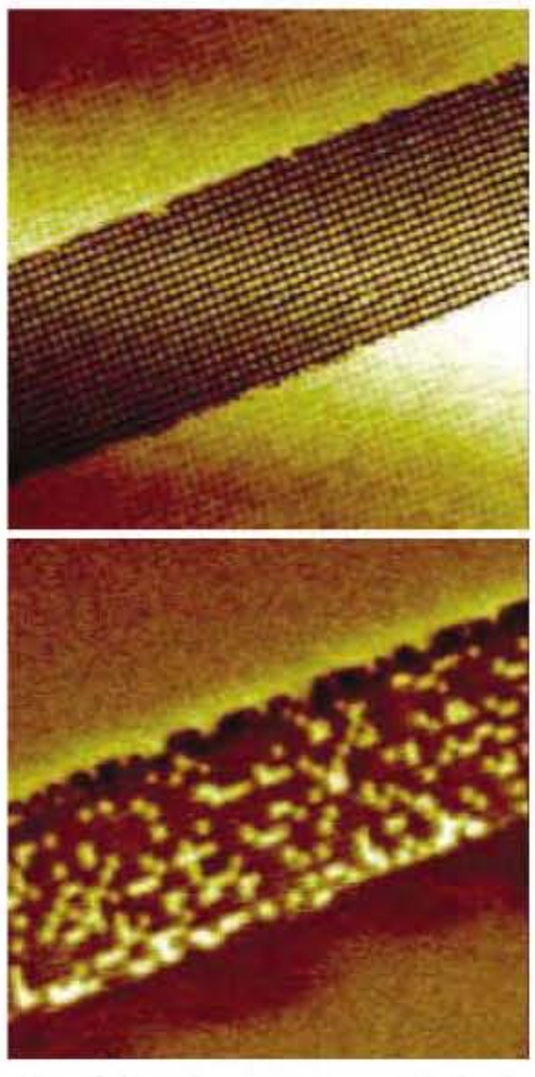

Bits of the future. Patterned islands in an array (*top*) reveal their magnetic orientations (*bottom*).

CREDIT: Z. BANDIC/HITACHI GLOBAL STORAGE TECHNOLOGIES

Storage Technologies (Hitachi GST) in San Jose, California. "The question was, 'Could it be manufactured at low cost?' Today, that's starting to look possible." Many of the latest advances in patterned media were on display here at a recent conference.*

Bandic and others say advances in the field are coming thick and fast. Particularly promising are efforts to marry the top-down lithographic patterning used by the semiconductor industry with a bottom-up approach to making regular arrays of features called self-assembly. "I wouldn't be surprised to see [this combination] in products in 5 to 10 years," Bandic says.

Still, there's a long way to go to ensure that the technology will work on a manufacturing scale. And cost is critical because today disk-drive makers create the magnetic platters at the heart of their devices for only about $6, and it's unlikely that consumers will be willing to see a big jump in their storage costs. "No one will transition to patterned media unless we have to do it," says Weller. So the question is can magnetic disk researchers hurdle the obstacles in the few short years before the technology is likely to be called on to do heavy lifting?

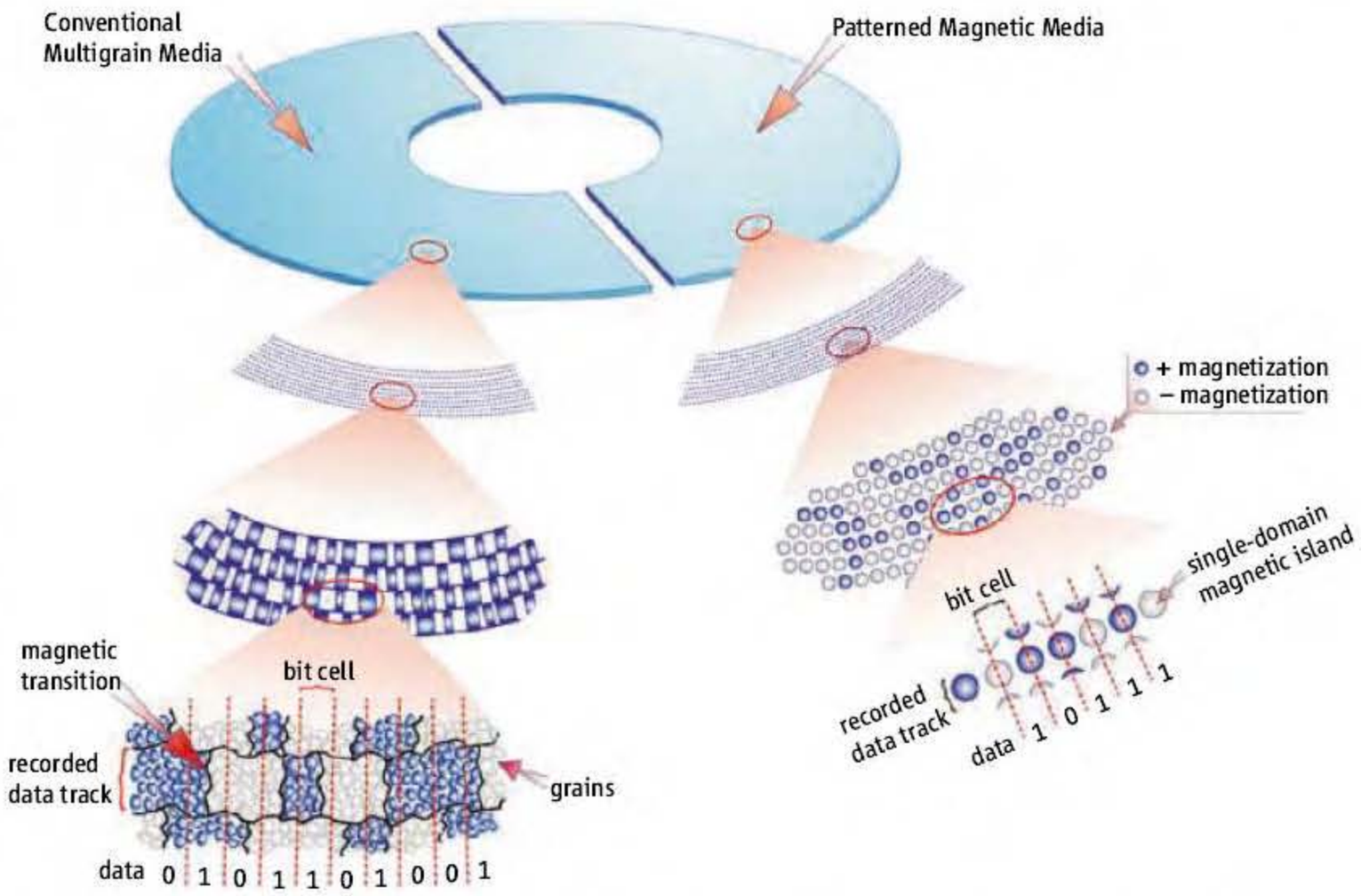

What's next. Bits currently stored as multiple grains (*left*) could give way to magnetic islands (*right*).

Diminishing returns

The current disk-drive technology has already been doing yeoman's work for decades. Inside these disks, a magnetic "write head" surfs just above the surface as the disk spins, writing bits of digital data—1s and 0s—as it goes. Reversing the magnetization between neighboring regions encodes a "1"; leaving it alone, a "0". The magnetic orientation of those bits is frozen in place and can be read back until it is erased and rewritten.

But peering deeper within a single bit reveals another level of complexity. A disk's magnetic material is made up of millions of tiny grains, each of which holds its magnetic orientation independently. A single bit is typically made up of 50 to 100 of them. If a single stray grain within a bit flips its magnetization spontaneously, there's no harm done. But if too many of its neighbors start to flip, you've just lost your bit of data. The upshot is that there's safety in numbers. To shrink the size of a region that makes up a bit without imperiling your data, you have to shrink the grains as well.

There's the rub. Throughout much of the 1990s, grain sizes dwindled fast enough for manufacturers to increase the data capacity of disk drives by about 100% a year. Today, however, that increase has dropped to about 40% per year. One problem is that the grains are now becoming so small that they are approaching what is known as the "superparamagnetic limit," where ambient heat can trigger their magnetic orientation to flip.

To deal with the problem, diskmakers have started reducing the cross section of magnetic regions by orienting bits perpendicularly, or up and down relative to the surface of the spinning disk. (Up to now, the magnetic orientation of bits has always switched horizontally.) Disks using "perpendicular recording" went on the market earlier this year and are soon expected to dominate the industry. Some manufacturers hope to make similar gains by co-opting an old enemy, heat. Augmenting the disk drive's write head, which magnetizes the tiny regions as it flies over the spinning disk, with a tiny heater should briefly make the magnetic orientation of the material under the head easier to flip. That trick would enable them to switch to new, more magnetically stable materials such as an alloy of iron and platinum, in which the magnetic orientations of grains are harder to flip. Between perpendicular recording and adding tiny heaters, industry leaders are confident that they can achieve data densities of about 500 Gb/in^2 around the end of the decade, a density that would give a laptop a hard disk capable of storing between 320 and 640 Gb. "It's in this regime where we expect patterned media to take effect," says Elizabeth Dobisz, a data-storage expert with Hitachi GST.

Seeing patterns

Patterned media would walk diskmakers back from the superparamagnetic limit. In contrast to grainy conventional media, in patterned media each bit is made from a single magnetic island that's not broken into smaller grains. Because these islands can be larger than single grains, they are less apt to be influenced by ambient temperature fluctuations and thus are more stable. That in turn should allow diskmakers to pack those islands closer together than the bits made from bunches of grains today. With that advantage in sight, "the hard disk drive industry is investing heavily in patterned media," Bandic says.

The $64,000 question is how to accomplish the patterning. The standard patterning technology of the semiconductor industry, known as photolithography, can now pattern features down to 65 nanometers. But to beat a data density of 500 Gb/in^2, diskmakers will have to make their magnetic islands a mere 22 nanometers across with just 36 nanometers between the bits. "Historically, the disk-drive industry has had it easy, lithographically," by adapting semiconductor techniques, says Dobisz. But "we're not going to be able to ride on the coattails of the semiconductor industry for this one."

Photolithography could still ride to the rescue, however. At the Materials Research Society meeting, Harun Solak, a nanofabrication expert at the Paul Scherrer Institute in Villigin, Switzerland, reported that he and colleagues have created a patterning system that directs multiple beams of extreme ultraviolet light at a thin organic layer called a photoresist. Where the beams intersect, they create an interference pattern, much like the classic double-slit physics experiment. A pair of

* Materials Research Society, Boston, 27 November–1 December 2006.

CREDITS: HITACHI GLOBAL STORAGE TECHNOLOGIES

intersecting beams creates an array of lines; four intersecting beams creates an array of squares. Photoresist exposed to those lines and squares can be chemically etched to transfer the pattern to a new material. At the meeting, Solak reported that the system could make perfect arrays of 15 to 20 nanometer dots in photoresist at a density of 516 Gb/in^2, an accomplishment that Bandic calls "a very impressive result." Solak says his group hasn't yet converted these high-density arrays into arrays of magnetic islands but has done it at lower densities.

Another patterning option many groups are exploring is a technique known as electron-beam lithography, which uses a styluslike beam of electrons to write features in a resist. Dobisz reported that her group at Hitachi GST has used e-beams to create arrays of magnetic islands at a density of 520 Gb/in^2. They've done even better when it comes to just punching holes in various films—the first step to patterning magnetic islands—creating arrays with densities as high as 1.6 Tb/in^2.

The trouble is that e-beam technology is slow. At a density of 1 Tb/in^2, it takes days to scratch out all the bits on a disk. That's unacceptable for manufacturers that have to turn out hundreds of disks an hour. Tetsuya Nishida of Hitachi's Central Research Lab in Tokyo, Japan, hopes to speed things up by building an e-beam machine that spins the substrate as it's being patterned. At the meeting, Nishida reported that his group can quickly pattern pits in a resist and substrate at a density of 100 Gb/in^2—not high enough for commercial disks, but a start.

One strategy that could offer some help would be to use e-beam lithography to create a "master" disk that could then be replicated using a relatively new technique called nanoimprint lithography. Developed 12 years ago by Princeton University engineering professor Stephen Chou, nanoimprint lithography first creates a master stamp with tiny features, then presses it into a malleable plastic. The plastic can be used as a mold for shaping metals, magnetic materials, silicon, or other materials, or as a resist for chemically etching patterns into a separate substrate. Using e-beams to create masters instead of for manufacturing makes speed less critical, Dobisz notes: "If we only need one master, it gives us a bit more leeway." Nanoimprint lithography isn't quite ready for prime time, but at the Boston meeting, several groups reported making steady progress with the technique.

Other potential solutions are in the works as well. Researchers are making arrays from materials that naturally assemble themselves into regular patterns. Last year, for example, researchers led by Manfred Albrecht, a nanoscientist at the University of Konstanz in Germany, reported in *Nature Materials* that they had created regular arrays of polystyrene spheres, each just 50 nanometers across. They then laid down a thin magnetic layer of a cobalt-palladium alloy on top, creating a regular pattern of undulations that could be used to define separate magnetic islands. At the meeting, Albrecht reported that his team is now working on making a similar array with 20-nanometer particles.

Another approach gaining popularity is to make a resist layer out of two-part polymers, known as diblock copolymers. The starting materials for these plastics consist of individual polymer chains with two distinct components stitched together, like a strand of linguini attached at one end to a piece of macaroni. In bulk, each component organizes to associate with its own kind. By mixing the polymers in the right proportions, researchers can create arrays of tiny pillars of one polymer inside a matrix of the other. Then they can either dissolve the pillars to create an array of holes, or dissolve the matrix, leaving an array of pillars, which can be filled with or surrounded by magnetic materials. Numerous teams have shown in recent years that they can create arrays of such pillars and holes at a density of hundreds of gigabits per square inch. Unfortunately, the pillars and holes in diblock films don't stay in an ordered pattern over large areas. That's a serious problem, notes Hiroshi Yoshida of Hitachi's Materials Research Lab in Ibarki, Japan, because read and write heads need to be placed exactly over the bit they must read, write, and erase.

In an effort to solve this problem, several groups are marrying top-down lithographic patterning with bottom-up self-assembly. Katsuyuki Naito of Toshiba's Corporate Research Center in Kawasaki, Japan, reported progress on what his team calls artificially assisted self-assembly. Naito and his colleagues first pattern a nickel disk with a series of fine, circular grooves, then fill the grooves with a diblock copolymer made of hybrid molecules of polymethylmethacrylate (PMMA) and polystyrene (PS). The copolymer self-assembles into arrays of PMMA pillars in a PS matrix, which the grooves' confined geometry forces into a regular pattern. That pattern ranges from a single row of pillars inside 60-nanometer grooves on up to six rows of pillars side by side in 400-nanometer grooves. Naito says his group has managed to turn out arrays of polymer pillars up to 800 Gb/in^2 and in separate work has used lower-density polymer patterns to create arrays of magnetic cobalt-platinum dots. The trick now, he says, is putting it all together. Bandic says he finds the work impressive. "It's looking very serious now that self-assembly may find its first application in information storage," he adds.

At this point, however, no one is under the illusion that researchers are close to their target. "Patterned media is an aggressive nanofabrication challenge," Dobisz says. Among the biggest hurdles will be to integrate novel patterned media approaches with the rest of the components of a hard disk drive—such as read and write heads that are sensitive enough to spot the magnetic islands and servo systems that can steer the heads to just the right bits on the disk. "We've got to do quite a bit of innovation and development in patterned media," Dobisz adds. True enough. But quite a bit of innovation is already under way.

–ROBERT F. SERVICE

Progress in Hard Disk Drive Technology

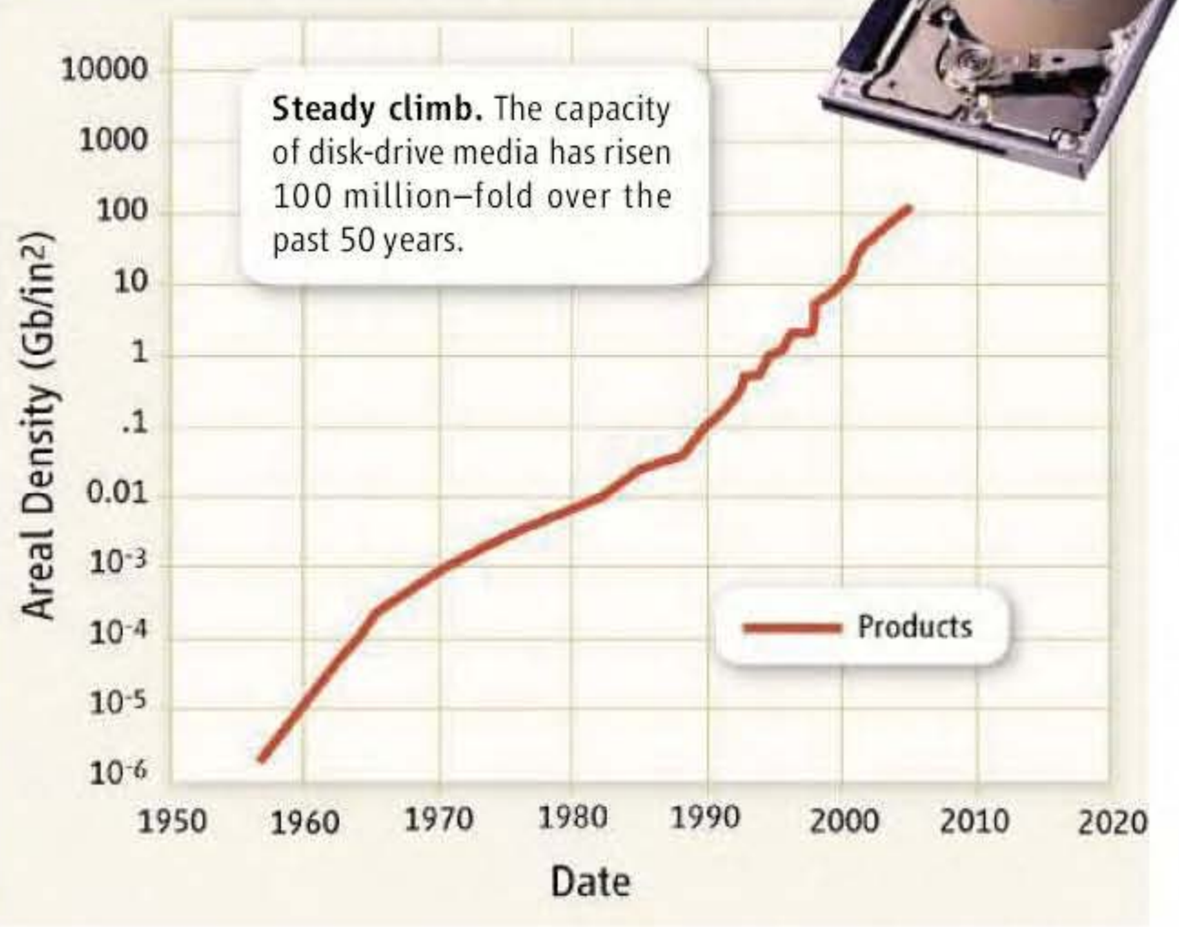

Steady climb. The capacity of disk-drive media has risen 100 million–fold over the past 50 years.

CREDIT: ADAPTED FROM D. WELLER/SEAGATE

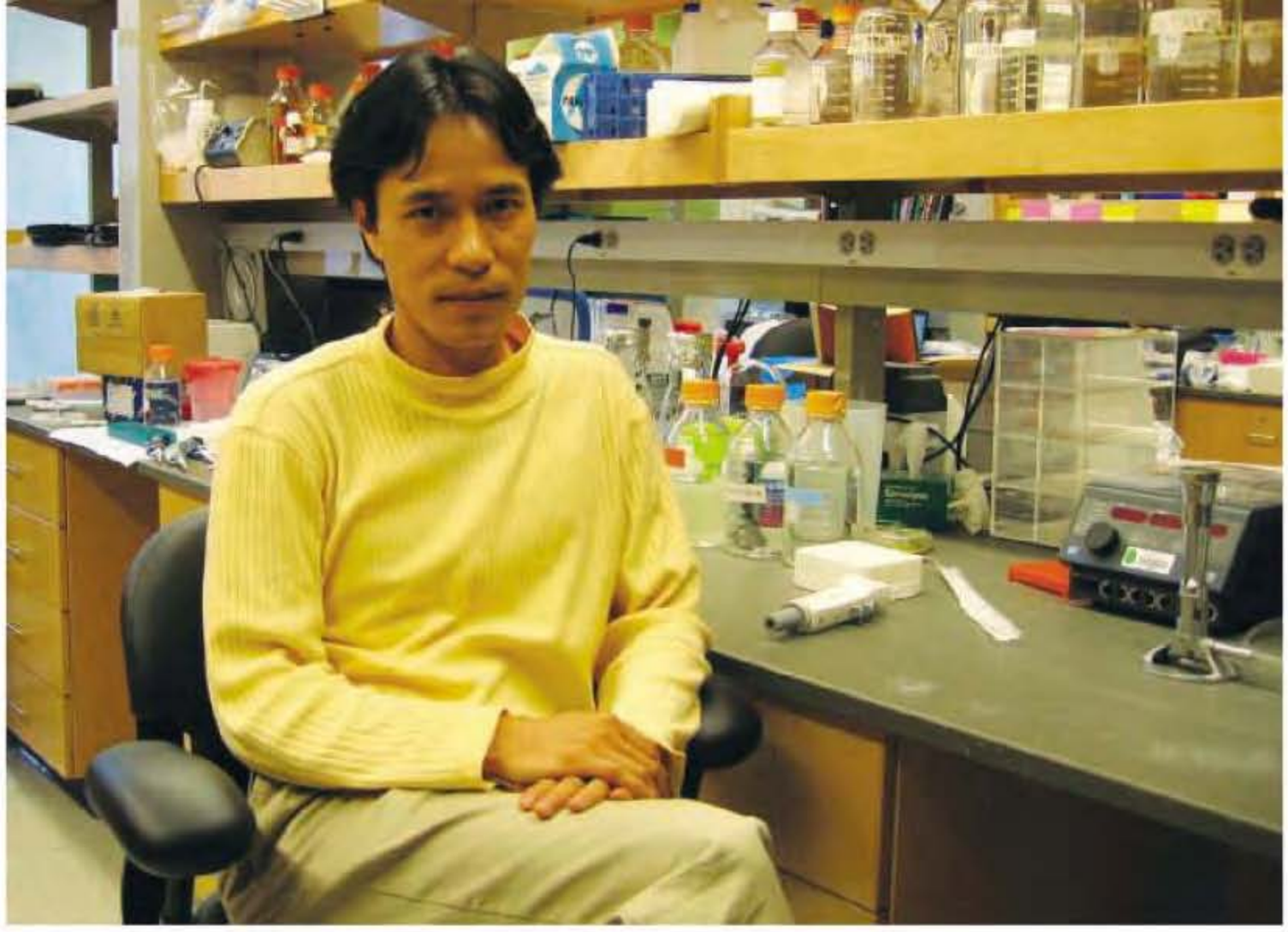

Golden hands. Lahn's lab skills led swiftly to a University of Chicago post.

PROFILE: BRUCE LAHN

Brain Man Makes Waves With Claims of Recent Human Evolution

Geneticist Bruce Lahn's quest to understand the biology of human differences lands him in the minefield of debates over race and IQ

CHICAGO—In 1993, not long after Bruce Lahn joined David Page's genetics lab at the Massachusetts Institute of Technology (MIT), Page invited all lab members on a 2-day hike in New Hampshire's rugged White Mountains. Page circulated a list of items to pack and stressed bringing enough food and water. Everyone showed up with stuffed backpacks—everyone, that is, except Lahn, who arrived toting only a small shoulder bag. When asked, Lahn pulled out the bag's sole contents: a gallon jar of Chinese pickled eggs.

"That was classic Bruce," Page recalls. "He didn't follow instructions." Lahn's insistence on doing things his way has made him one of the fastest rising stars in genetics and also one of the most controversial. His work with Page to decipher the evolutionary history of the human Y chromosome was a major landmark in genome research. It led directly to a position at the University of Chicago in Illinois, where Lahn achieved tenure in an unusually rapid 5 years, and to an investigator award from the Howard Hughes Medical Institute.

But Lahn's more recent work, seeking to identify the genes behind our species' superior cognition, has sparked skepticism (see sidebar, p. 1872) and plunged this Chinese-American scientist into contentious debates over genetics, race, and intelligence. Two *Science* papers concluding that purportedly beneficial brain mutations are common in Eurasia but rare in Africa have made Lahn a darling of right-wing commentators seeking evidence of racial differences in cognition. Some scientists say Lahn overinterpreted and sensationalized his findings, and one coauthor has distanced herself from one of the paper's more speculative conclusions.

The papers have such serious social implications that they needed to meet a higher standard of proof, says David Altshuler of the Broad Institute in Cambridge, Massachusetts—and they didn't. The links to cognition in particular were "wild speculation," he says. "We have a powerful responsibility to think about how society will interpret [such work]."

> **"You can't deny that people are different at the level of their genes."**
>
> —Bruce Lahn

Lahn finds the political fallout discomfiting, insisting that he is a staunch antiracist and "extremely liberal" in his personal politics. He says he is a lifetime member of the National Association for the Advancement of Colored People and gives money to Democratic candidates. Yet Lahn is fascinated by differences among people and says he has long wondered whether variations in social status have genetic underpinnings. "You can't deny that people are different at the level of their genes," Lahn says, citing the examples of skin color and physical appearance. "This is not to deny the role of culture, but there may be a biological basis [for differences] above and beyond culture."

Becoming Bruce

Lahn, 38, is slim and handsome, with expressive hands that gesture animatedly as he speaks. He was born in China to two physicists who both suffered from the country's political turmoil. His mother was branded a "rightist" by the Communist Party during the 1950s, leading his maternal grandmother to commit suicide out of shame. His paternal grandfather died in a Communist labor camp. "From early on, I had a sense of what had happened to my family, and that made me a bit of a rebel," Lahn says. "I was hyperactive and always in trouble at school."

Lahn's rebelliousness made him keenly interested in China's social inequalities. He was particularly struck by the privileges foreigners received when they visited China. "I was deeply traumatized by that," Lahn says. He wondered whether there might be a genetic basis for these class differences. "But I didn't know what genes were exactly."

In 1986, Lahn began studying genetics at Beijing University. He soon got caught up in the nascent democracy movement, putting up one of the first wall posters on campus. "We were very naive," he recalls. "We really thought that we had the power to change the government." When Lahn heard he was on a watch list, he decided to leave China and was accepted at Harvard University in 1988.

When he arrived in the United States, Lahn was still going by his Chinese name, Lan Tian. But one day, a McDonald's janitor told him he looked like the late martial arts actor Bruce Lee, and Lahn's friends started calling him "Bruce." Lahn soon adopted it as his legal first name and Anglicized the spelling of his last name.

Lahn thrived at Harvard. Geneticist James Birchler, now at the University of Missouri, Columbia, supervised Lahn's senior thesis. "He had golden hands" in the lab, Birchler recalls, "and he was intellectually fearless and adventuresome."

In 1991, after beginning Ph.D. studies at MIT, Lahn asked Page to take him on as a student. But Page says at first he was not

Continued on p. 1873

CREDIT: M. BALTER/*SCIENCE*

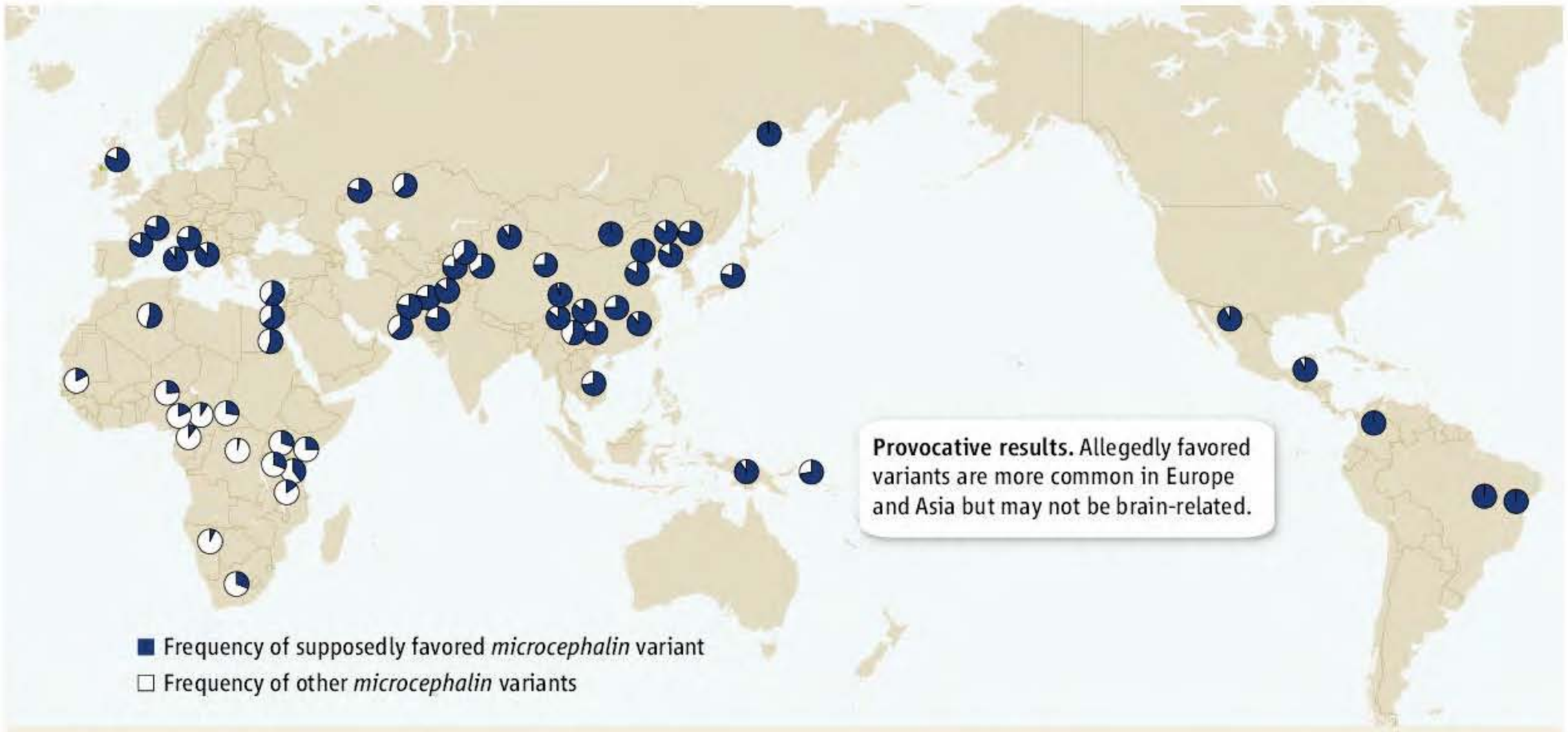

Links Between Brain Genes, Evolution, And Cognition Challenged

Some of Bruce Lahn's provocative claims are running into heavy fire. Last year, the University of Chicago geneticist reported, in two papers in *Science*, that he had uncovered genes that are still evolving in humans, and he suggested that they confer a brain-related boost—perhaps even a cognitive one (see main text). His university even applied for patents on a test that would reveal whether individuals carry the possibly advantageous genetic variants. Some researchers have since argued, however, that selection may have favored the variants for a non-neural function. Others have questioned whether the variants were under recent selection at all. And Lahn's own work with other scientists has failed to correlate variants of the genes *ASPM* and *microcephalin* with IQ. At this point, concedes Lahn, "we don't know what the variants do."

Soon after the *Science* papers were published, Lahn set out to see whether the variants give a cognitive advantage. In one study, Lahn helped controversial psychologist Philippe Rushton of the University of Western Ontario in London, Canada, test whether people who carry the favored variants have higher IQs. Rushton is well known for his claims that African Americans have lower intelligence than whites, and Lahn had found that some genetic variants are common in Europeans and Asians but less frequent among sub-Saharan Africans. But Rushton reported last week at the annual meeting of the International Society for Intelligence Research in San Francisco, California, that he had struck out: The variants conferred no advantage on IQ tests. "[We] had no luck," Rushton told *Science*, "no matter which way we analyzed the data." Lahn was not a co-author, but his group genotyped the 644 adults of differing ethnicity in the study.

Lahn is a leading author, however, of a similar international study of about 2500 subjects. Most of the results are unpublished, but findings from Australia were presented at a meeting in Brisbane last August. Nicholas Martin's team at the Queensland Institute of Medical Research in Brisbane found no statistically significant correlations between the supposedly favored variants and IQ. In large part due to this raft of negative results, Lahn says, the patenting effort has now been dropped.

If the variants aren't boosting IQ scores, what are they doing? Some mutations in *microcephalin* and *ASPM* lead to microcephaly, or very small brains, so Lahn had hypothesized that the variants might influence brain growth in normal people. But that idea was challenged last May by neuroscientist Roger Woods of the University of California, Los Angeles. Woods's team found no correlation between brain volume and the variants in 120 normal subjects, as reported in *Human Molecular Genetics*. Woods suggested—and Lahn agrees—that the variants might be involved in some more subtle neurological function, with Lahn arguing that a brain-related function is still the most likely target of selection.

But genome researcher Chris Ponting of the University of Oxford, U.K., notes that *microcephalin* and *ASPM* are also expressed outside the brain. In last May's issue of *Bioinformatics*, he reported that part of *ASPM*'s DNA sequence resembles that of genes involved in the function of flagella, which propel sperm. Earlier work had shown that *ASPM* is expressed during sperm production. Ponting suggests that natural selection might have acted on flagellar function rather than brain growth. "These genes could well have many functions in many parts of the body," Ponting says, "and any one of these could have driven their adaptive sequence changes."

Meanwhile, other researchers have questioned the basic finding that the variants have been under recent natural selection. In a Technical Comment published 14 July online in *Science*, Sarah Otto of the University of British Columbia in Vancouver, Canada, and colleagues argued that Lahn's findings reflected not a signature of selection but rather the genetic traces of population movements as modern humans migrated out of Africa. And in October, a team led by geneticist David Reich of the Broad Institute in Cambridge, Massachusetts, reported at the meeting of the American Society of Human Genetics that it found no evidence for recent selection on *ASPM* when it used a method of analysis it considered superior to Lahn's. But Lahn, who is familiar with Reich's results, stands by his conclusions: "Their method has lower resolution ... and is less reliable," he says.

All the same, Lahn says he has mixed feelings about the failure to date to correlate the variants of *microcephalin* and *ASPM* with differences in intelligence: "On the scientific level, I am a little bit disappointed. But in the context of the social and political controversy, I am a little bit relieved." **–M.B.**

CREDIT: EVANS *ET AL.*, *SCIENCE* **309**, 1719 (2005)

Continued from p. 1871

keen to do so: "A number of people in the lab were unsure about whether it was wise. He seemed brash and cocky and too self-confident." Page put Lahn on a small project investigating a rare defect in the human Y chromosome. "But Bruce thought [the project's] range was too limited. He started conducting secret experiments in the lab that he thought I wasn't aware of." Finally, Lahn announced that he wanted to isolate all of the Y chromosome's genes. Page let him go ahead. Within 18 months, Lahn had cloned about half of the dozen genes then known on the male part of the chromosome. Page and Lahn went on to show that the human Y chromosome evolved from a series of rearrangements of the mammalian X chromosome (*Science*, 29 October 1999, p. 877).

"Bruce had a deadly killer instinct," Page says. "He kept his eye on the prize. And he was very charismatic. … After he left, some of us felt that we would never see the likes of him again."

Tackling the evolving brain

Soon after Lahn's move to the University of Chicago in 2000, he began looking for genes that might explain the evolution of the human brain, motivated in part by his long-standing interest in human differences. In 2004, his team reported that two genes thought to regulate brain growth, called *microcephalin* and *ASPM*, appeared to have undergone strong natural selection since the human and chimpanzee lineages split between 5 million and 7 million years ago. These genes are implicated in regulating cell division in developing neural cells, and some mutations in them result in a tiny brain, or microcephaly. But their function in normal humans is not clear, and they are expressed in non-neural tissues as well.

Then, in two papers in *Science* last year, Lahn reported that variants of the two genes appear to have been strongly favored by recent natural selection (*Science*, 9 September 2005, pp. 1717 and 1720). That implies that the variants conferred a survival or reproductive benefit, perhaps a cognitive one. In media interviews, Lahn conceded that there was no real evidence natural selection had acted on cognition or intelligence. But both papers pointed out that the mutations arose when key events in human cultural development occurred: The *microcephalin* variant was dated to about 37,000 years ago, when the first art and symbolism showed up in Europe, and the *ASPM* variant to 5800 years ago, when the first cities arose.

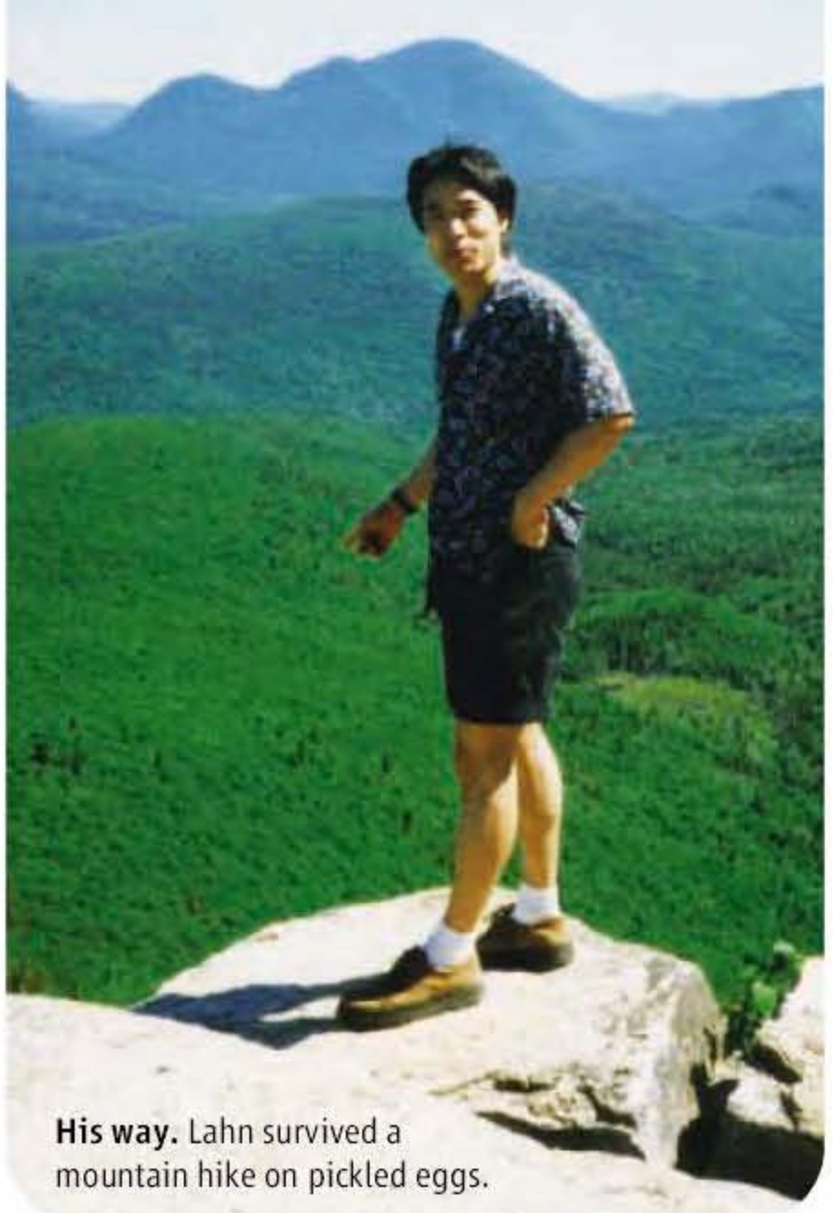

His way. Lahn survived a mountain hike on pickled eggs.

CREDIT: LAURA BROWN

Lahn's papers also reported the skewed geographic distribution of the genetic variants. Variants in *microcephalin* turned up in 75% or more of some Europeans and Asians Lahn studied, but in less than 10% of some African groups. The *ASPM* variant was also much less frequent in Africa.

Bloggers jumped on the news, trumpeting the papers as support for the idea that African Americans have lower intelligence than whites. Two months later, in the conservative *National Review Online*, columnist John Derbyshire wrote that the research implied that "our cherished national dream of a well-mixed and harmonious meritocracy … may be unattainable."

Among some geneticists, there was consternation. "There was no evidence whatsoever that these [genetic variants] have any effect" on differences between people, Altshuler says, adding that the controversy over the work was "easily anticipated." Harvard geneticist Richard Lewontin goes further, criticizing both Lahn and *Science* for publishing such speculative links to cultural advances. "These two papers are particularly egregious examples of going well beyond the data to try to make a splash," he says. And archaeologist Scott MacEachern of Bowdoin College in Brunswick, Maine, says the archaeological links in the papers are simplistic and outdated. The symbolic revolution, agriculture, and urbanism developed "over many thousands of years, and none was restricted to Europe and the Middle East," he says.

Even one of the co-authors of the papers, Sarah Tishkoff of the University of Maryland, College Park, has now distanced herself from the attempt to link the *ASPM* variant to human advances, saying that she didn't see the wording until page proofs.

Lahn points out that the papers include disclaimers, stating, as one of them put it, that it was "formally possible" that natural selection had acted on the genes' roles outside the brain. And in media interviews he emphasized that a number of genes other than *microcephalin* and *ASPM* are probably involved in cognition. But he insists that the evidence points to some sort of brain function as the most likely target of selection.

Lahn asserts that some scientists "start with a political agenda and fit the evidence to that." This political bias, he argues, "takes credibility away from an antiracist program that I agree with. … If someday we discover that there are genetic differences in cognitive abilities, would that mean that racism is now justified?"

And some scientists believe that Lahn has shown courage in pursuing his research. "There is widespread fear of this [research] among scientists," says geneticist Henry Harpending of University of Utah in Salt Lake City, who has suggested evolutionary explanations for high IQ scores in Ashkenazi Jews. Even some researchers who scoff at racial differences in intelligence think the research should go on. Geneticist Michael Hammer of the University of Arizona in Tucson says he's not worried about the end result: "I have no serious concerns that Europeans or Asians are going to be proven to be more intelligent, so I say go at it, let the chips fall where they may."

Lahn says the controversy has made him back away "from going after these kinds of questions aggressively," although he continues to test whether the variants affect IQ. He has begun diverting his energies to another high-profile project: stem cells. He became interested in the topic after running into a Chinese colleague at a meeting and is collaborating with a center at Sun Yat-sen University in Guangzhou. He was motivated in part by China's relatively liberal attitude toward this research and also, he says, by his desire to help China modernize.

Time, and further research, will tell if Lahn was right about *microcephalin* and *ASPM*. But Page says that few other scientists would have been willing to get involved in such controversial questions in the first place: "That willingness to venture into this territory without his guard up is entirely in keeping with who Bruce is. Anybody who would have packed their bag as instructed for that White Mountain hike would have steered clear of all this."

–MICHAEL BALTER

LETTERS

edited by Etta Kavanagh

Retraction

WE WISH TO RETRACT OUR RESEARCH ARTICLE "STRUCTURE OF MsbA from *E. coli*: A homolog of the multidrug resistance ATP binding cassette (ABC) transporters" and both of our Reports "Structure of the ABC transporter MsbA in complex with ADP•vanadate and lipopolysaccharide" and "X-ray structure of the EmrE multidrug transporter in complex with a substrate" (*1*–*3*).

The recently reported structure of Sav1866 (*4*) indicated that our MsbA structures (*1*, *2*, *5*) were incorrect in both the hand of the structure and the topology. Thus, our biological interpretations based on these inverted models for MsbA are invalid.

An in-house data reduction program introduced a change in sign for anomalous differences. This program, which was not part of a conventional data processing package, converted the anomalous pairs (I+ and I–) to (F– and F+), thereby introducing a sign change. As the diffraction data collected for each set of MsbA crystals and for the EmrE crystals were processed with the same program, the structures reported in (*1*–*3*, *5*, *6*) had the wrong hand.

The error in the topology of the original MsbA structure was a consequence of the low resolution of the data as well as breaks in the electron density for the connecting loop regions. Unfortunately, the use of the multicopy refinement procedure still allowed us to obtain reasonable refinement values for the wrong structures.

The Protein Data Bank (PDB) files 1JSQ, 1PF4, and 1Z2R for MsbA and 1S7B and 2F2M for EmrE have been moved to the archive of obsolete PDB entries. The MsbA and EmrE structures will be recalculated from the original data using the proper sign for the anomalous differences, and the new Cα coordinates and structure factors will be deposited.

We very sincerely regret the confusion that these papers have caused and, in particular, subsequent research efforts that were unproductive as a result of our original findings.

GEOFFREY CHANG, CHRISTOPHER B. ROTH, CHRISTOPHER L. REYES, OWEN PORNILLOS, YEN-JU CHEN, ANDY P. CHEN

Department of Molecular Biology, The Scripps Research Institute, La Jolla, CA 92037, USA.

References

1. G. Chang, C. B. Roth, *Science* **293**, 1793 (2001).
2. C. L. Reyes, G. Chang, *Science* **308**, 1028 (2005).
3. O. Pornillos, Y.-J. Chen, A. P. Chen, G. Chang, *Science* **310**, 1950 (2005).
4. R. J. Dawson, K. P. Locher, *Nature* **443**, 180 (2006).
5. G. Chang, *J. Mol. Biol.* **330**, 419 (2003).
6. C. Ma, G. Chang, *Proc. Natl. Acad. Sci. U.S.A.* **101**, 2852 (2004).

Aquaculture in Offshore Zones

THE EDITORIAL BY ROSAMOND NAYLOR, "Offshore aquaculture legislation" (8 Sept., p. 1363), suggests that the motivation for moving aquaculture into the open ocean is that "marine fish farming near the shore is limited by state regulations." Although unworkable regulations may exist in a few states, in the larger scheme this is irrelevant. Of the offshore aquaculture projects currently under way, none are occurring in the U.S. Exclusive Economic Zone (EEZ); rather, they are happening in state waters. Even historically, only two aquaculture projects have ever occurred in federal waters (*1*).

Much of Naylor's stated concern over offshore aquaculture is based on historical experience with near-shore fish farms. This is in spite of years of more relevant offshore operations that reveal little, if any, negative impact on the environment or local ecosystems (*2*, *3*). Naylor criticizes the National Offshore Aquaculture Act of 2005 because it lacks specific environmental standards. Yet, she recommends California's recent Sustainable Oceans Act as a legislative model, although it is similarly silent, leaving those details to rule-making in response to the best available science.

Naylor criticizes the use of fishmeal as an aquaculture ingredient, ignoring the fact that industrial fisheries are well managed and would occur with or without aquaculture's demand. Naylor ignores the higher efficiency of using fishmeal to feed fish compared with its use in land-based livestock operations (*4*). Also ignored is the inefficiency of using small pelagic fish in the natural setting to feed predator fish (*5*).

Researchers and entrepreneurs currently developing the technologies needed for offshore aquaculture share a vision of a well-managed industry governed by regulations with a rational basis in the ecology of the oceans and the economic realities of the marketplace.

CLIFFORD A. GOUDEY

Massachusetts Institute of Technology, Cambridge, MA 02139, USA.

References and Notes

1. The SeaStead project a decade ago, four miles off Massachusetts (see www.nmfs.noaa.gov/mb/sk/saltonstallken/enhancement.htm) and the recent Offshore Aquaculture Consortium experimental cage operation 22 miles off Mississippi (see www.masgc.org/oac/).
2. See www.lib.noaa.gov/docaqua/reports_noaaresearch/hooarrprept.htm/.
3. See www.blackpearlsinc.com/PDF/hoarpi.pdf.
4. See www.salmonoftheamericas.com/env_food.html.
5. D. Pauly, V. Christensen, *Nature* **374**, 255 (2002).

IN HER PROVOCATIVE EDITORIAL "OFFSHORE aquaculture legislation" (8 Sept., p. 1363), R. Naylor raises valid points regarding regulation of oceanic aquaculture, since it is sure to grow in the future because of dwindling global fishery supplies. This growth is

bound to bring with it many possibilities for resource and environmental degradation. The whole prospect reminds me of my research with a group of entrepreneurs more than a decade ago into the possibility of coupling offshore oil and gas production with operations designed to farm fish and shellfish in deep water. The idea was to establish mariculture (sea farming) technologies that would utilize offshore oil and gas production platforms located in the clear, oceanic-quality, deep waters of the Gulf of Mexico, beyond near-shore land runoff and related pollution.

The economic incentives for such a plan included the fact that when oil and gas production rigs are near the end of their life, it is more economically prudent to cease production because of the excessive costs of drawing additional resources. After useful life, the production companies are also required by U.S. law to remove the oil and gas structures from their deep water settings.

These platforms have usually supported an extensive, highly productive underwater ecosystem of attached and foraging marine life that is not only important for its inherent natural value but also important economically to tourism and recreational fishing. Our investigations in the early 1990s focused on maintaining these ecologically important environments while capitalizing on their economic value by designing vertically integrated mariculture operations for spawning, cultivation, harvesting, processing, and sale of marine species that would be based on the rig infrastructure.

The concept of utilizing offshore oil and gas production platforms for mariculture purposes is not new. If the legislative concerns for offshore mariculture expressed by Naylor can be met, imagine the possibilities for this technology in food production. The use of offshore oil and gas platforms for growing fish offers a way to turn the liabilities of an energy production business into assets, continuing the sustainable economic life of these platforms as well as their ecological and societal importance.

R. WARREN FLINT

Five E's Unlimited, 1221 1st Avenue, #231, Seattle, WA 98101, USA.

Response

MY EDITORIAL EMPHASIZED THE NEED FOR environmental safeguards in the drafting of the National Offshore Aquaculture Act (S.1195). Unlike near-shore aquaculture, the farming of fish in the open ocean occurs in marine environments with rapid currents, high flushing rates (rapid currents), and minimal interference with other human

activities. It is for these reasons, perhaps, that Goudey objects to the comparisons between near-shore and offshore farming in justifying the need for stronger environmental language in the current bill. However, it is misleading to suggest that there are no environmental impacts from offshore fish farming. Very few offshore facilities currently operate at a commercial scale. Therefore, the cumulative impacts on the benthic environment, on the surrounding environment through chemical discharge, and on wild fish populations through genetic and competitive interactions and the spread of pathogens have not yet been demonstrated for the type of intensive, industrial production that would be made possible through S.1195. There is evidence from existing offshore operations of predator attacks (*1*, *2*), farm fish escapes (*2*–*4*), and high fishmeal and fish oil use in feeds (*5*). Although livestock also uses fishmeal and fish oil in feeds, these ingredients are more essential for many aquaculture species. Moreover, aquaculture's use of fishmeal and fish oil is expected to increase in the future and does not represent a balanced, ecologically sound use of these resources. Contrary to Goudey's statement, there is little evidence that industrial forage fisheries are now well managed throughout the world.

There are some existing commercial farms operating several miles offshore within state boundaries that have demonstrated strong environmental stewardship. My Editorial recommended that business leaders from these operations become engaged in a redrafting of the bill; such leaders would certainly promote environmental safeguards and would have no problem operating profitably under stronger legislation. Flint's Letter reinforces this idea and suggests that offshore oil and gas platforms be used for mariculture activities—provided that they meet the environmental requirements of a stronger national legislation. I commend Flint's confidence that aquaculture can proceed under more rigorous environmental standards. For offshore platforms to be used for aquaculture, however, additional approval must be sought through the Department of the Interior in connection with the Outer Continental Shelf Lands Act.

Finally, I recommended environmental language similar to that found in the California Sustainable Oceans Act (SB 201) for the revision of the national bill. The California legislation incorporates many features that the national bill does not, including the requirement of environmental impact assessments before granting of leases, stronger language (e.g., minimize escapes, disease transfers, and pollution, rather than just "consider" these potential impacts), and transparent oversight and public participation in the process. As the rule-making process is set to begin, California is now in a position to ensure that any marine aquaculture facilities operating in state waters will be environmentally sound. Whether open ocean aquaculture develops within state boundaries or in federal waters, the legislative process should incorporate environmental safeguards to protect marine ecosystems for all species—not just humans—in the long run.

ROSAMOND L. NAYLOR

Center for Environmental Science and Policy, Stanford University, Stanford, CA 94305–6055, USA.

References

1. NOAA/SBIR Project Summary Form for SnapperFarm, Inc. (see www.snapperfarm.com/content/research_and_development/NOAA%20SBIR%202005%20Pred%20P1.pdf).
2. "Seas of doubt: upstart fish farms feed on theory, not fact" (Food and Water Watch, Washington, DC, June 2006) (available at http://www.foodandwaterwatch.org/fish/pubs/reports/seas-of-doubt).
3. M. L. Weber, "What price farmed fish: A review of the environmental and social costs of farming carnivorous fish" (SeaWeb Aquaculture Clearinghouse, Silver Spring, MD, 2003) (available at www.seaweb.org/resources/aquaculturecenter/documents/WhatPriceFarmedFish_high.pdf).
4. ABC Australia, "Fish farm escape creates environment fears," 9 Feb. 2006 (http://www.abc.net.au/news/newsitems/200602/s1565651.htm).
5. A. G. J. Tacon, "State of information on salmon aquaculture feed and the environment," report presented at the World Wildlife Federation Salmon Aquaculture Dialogue, 29 Apr. 2005 (available at www.worldwildlife.org/cci/pubs/Feed_final_resaved2.pdf).

CREDIT: KEN HAMMOND/USDA

CORRECTIONS AND CLARIFICATIONS

This Week in *Science*: "Not lost in translation" (1 Dec., p. 1351). The image accompanying this item should have appeared with the preceding item "Turing patterning in the mouse hairs." The image should have been credited to Sick *et al.*

This Week in *Science*: "Making RNA, one molecule at a time" (17 Nov., p. 1045). The second sentence describes RNA polymerase, not RNA, and should begin, "How RNAP translocates relative to DNA in the initial transcribing complex has been controversial..." The next-to-the-last sentence should describe "scrunching" as follows: "RNAP remains fixed on the promoter and pulls downstream DNA into itself."

Reports: "Giant ringlike radio structures around galaxy cluster Abell 3376" by J. Bagchi *et al.* (3 Nov., p. 791). On page 794, column 1, paragraph 2, line 15, the number 50 should be changed to 5, to read "5×10^{19} eV."

Table of Contents: (3 Nov., p. 717). The one-sentence summary for the Report "Protrudin induces neurite formation by directional membrane trafficking" by M. Shirane and K. I. Nakayama was incorrect. It should have read, "Nerve growth factor promotes extension of neurites by local phosphorylation of a newly described protein that then promotes membrane trafficking."

Letters to the Editor

Letters (~300 words) discuss material published in *Science* in the previous 6 months or issues of general interest. They can be submitted through the Web (www.submit2science.org) or by regular mail (1200 New York Ave., NW, Washington, DC 20005, USA). Letters are not acknowledged upon receipt, nor are authors generally consulted before publication. Whether published in full or in part, letters are subject to editing for clarity and space.

News of the Week: "Small RNAs reveal an activating side" by K. Garber (3 Nov., p. 741). There were two errors in the article. It incorrectly referred to an Angela Ling, when it should have been Angela Ting, and Long-Cheng Li is now an Assistant Researcher at UCSF, not a postdoc.

Policy Forum: "An ambitious, centrist approach to global warming legislation" by D. D. Doniger *et al.* (3 Nov., p. 764). On page 764, the key to the figure misrepresents the options for U.S. CO_2 emission reductions: The red line shows a prompt implementation of emission reductions (450 prompt), and the blue line shows the effects of delayed implementation (-450 delay).

Perspectives: "Cosmic rays track the rotation of the Milky Way" by M. Duldig (20 Oct., p. 429). The first sentence of the first full paragraph on page 430 was incorrect. It should read, "The motion of cosmic rays in a magnetic field is described by a transport equation that takes into account the convection, diffusion, drift, and adiabatic gain (if the field is converging) or loss (if the field diverges)."

News Focus: "AAS High Energy Astrophysics Division: Snapshots from the meeting" by T. Siegfried (20 Oct., p. 411). The item "Galactic jet fuel" describes a finding reported at the meeting by Rita Sambruna of NASA's Goddard Space Flight Center on the composition of jets from active galactic nuclei. Sambruna and collaborators have since discovered a calibration error in their instruments and have retracted their finding.

Table of Contents: (13 Oct., p. 219). The caption for the image that related to the *Science*'s STKE article by S. J. Mulligan and B. A. MacVicar that appeared on the *Science* Online table of contents on page 219 was incorrect. The correct caption is "Communication between astrocytes and neurons."

Reports: "Nonrandom processes maintain diversity in tropical forests" by C. Wills *et al.* (27 Jan., p. 527). The analysis presented in the paper was flawed because of a programming error. The error affects the analysis presented in Table 1 and alters the ordinate of Fig. 4, which was derived from the same analysis. Sentence 2 of paragraph 4 of column 3 of page 529 should read, "Each of these differences consisted of the difference between the observed mortality or recruitment rate of the species in the quadrat and the mortality or recruitment rate of that species in a random sample of the same size taken from that quadrat." Sentences 2 and 3 of the next paragraph should read, "Table 1 lists the average *t* values and degrees of freedom of all these analyses. In most cases, the *t* value was positive and highly significant, but the size of the *t* value diminished as quadrat size increased." Corrected versions of Table 1 and Fig. 4 are shown here with their corrected captions.

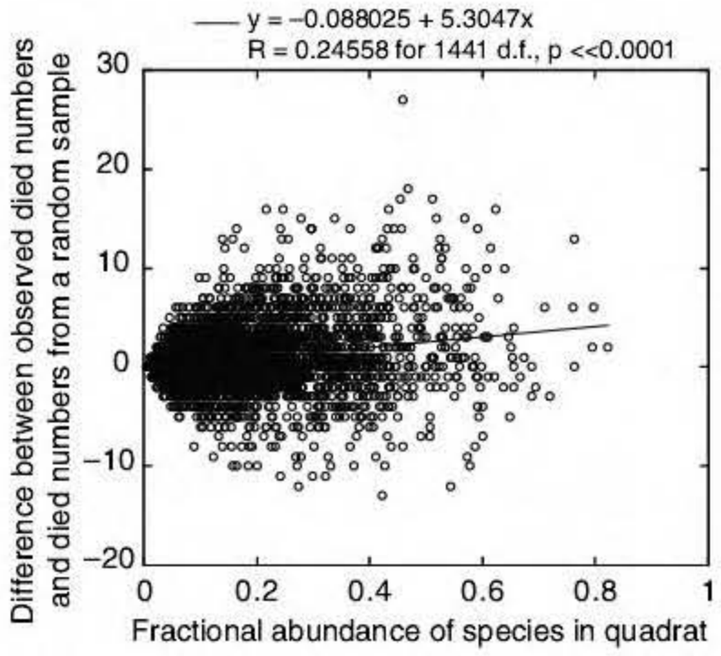

Fig. 4. Plot of Luquillo 10-m quadrat mortality data, in which the frequency of each species in a quadrat (abscissa) is plotted against the difference between the number of trees of the species that died in that quadrat and the number that "died" in a random sample of the same size taken from survivors + died in that quadrat (ordinate). Solid line, linear regression fit to the data.

	10 m quadrats			20 m quadrats			30 m quadrats			40 m quadrats			50 m quadrats		
	Mean number of trees per species		Paired t-value, *df*	Mean number of trees per species		Paired t-value, *df*	Mean number of trees per species		Paired t-value, *df*	Mean number of trees per species		Paired t-value, *df*	Mean number of trees per species		Paired t-value, *df*
	Real	Random		Real	Random		Real	Random		Real	Random		Real	Random	
Mortality															
Lambir	1.279	1.096	26.0, ***4505***	1.482	1.195	23.9, ***1299***	1.629	1.294	21.7, ***578***	1.747	1.407	19.6, ***325***	1.897	1.539	17.5, ***200***
Pasoh	1.149	1.108	15.3, ***4981***	1.373	1.309	14.1, ***1249***	1.615	1.543	11.7, ***577***	1.917	1.830	10.6, ***324***	2.280	2.188	8.8, ***199***
BCI	1.550	1.435	18.4, ***4971***	2.221	2.082	12.3, ***1249***	2.869	2.740	8.2, ***577***	3.635	3.527	4.8, ***324***	4.544	4.469	2.8, ***199***
Sinharaja	1.490	1.463	2.2, ***2377***	2.101	2.136	−1.3, ***624***	2.792	2.843	−1.2, ***288***	4.072	4.269	−1.5, ***91***	5.522	5.872	−2.1, ***50***
HKK	1.540	1.362	14.0, ***3750***	1.891	1.644	9.4, ***1243***	2.345	2.068	10.0, ***577***	2.880	2.556	11.6, ***324***	3.571	3.209	8.9, ***199***
Luquillo	3.046	2.265	23.0, ***1443***	5.020	3.729	16.0, ***399***	7.091	5.432	12.5, ***186***	9.734	7.598	10.2, ***103***	11.891	9.584	8.1, ***69***
Mudum	2.660	1.908	22.8, ***1696***	3.643	2.076	14.3, ***974***	4.681	2.556	8.1, ***543***	5.532	3.200	9.5, ***318***	6.872	4.142	7.3, ***199***
Recruitment															
Lambir	1.239	1.114	19.6, ***4558***	1.451	1.244	21.0, ***1281***	1.632	1.375	21.7, ***578***	1.849	1.533	19.4, ***325***	2.092	1.719	18.4, ***200***
Pasoh	1.123	1.075	13.3, ***4350***	1.266	1.197	13.9, ***1247***	1.439	1.352	12.6, ***577***	1.635	1.546	10.5, ***324***	1.895	1.789	9.2, ***199***
BCI	1.454	1.353	15.0, ***4816***	2.066	1.903	13.3, ***1249***	2.701	2.490	11.8, ***577***	3.436	3.166	10.5, ***324***	4.299	4.006	8.7, ***199***
Sinharaja	1.440	1.340	5.8, ***1499***	1.811	1.692	4.6, ***559***	2.233	2.089	3.8, ***282***	3.062	2.885	2.4, ***92***	3.970	3.748	2.1, ***51***
HKK	1.975	1.456	19.4, ***2730***	2.442	1.596	14.9, ***1138***	2.947	1.884	14.7, ***567***	3.404	2.268	12.2, ***323***	4.078	2.776	12.8, ***199***
Luquillo	1.771	1.487	11.3, ***1367***	2.530	2.109	8.9, ***397***	3.334	2.874	6.4, ***186***	4.255	3.794	5.0, ***103***	5.162	4.681	4.1, ***69***
Mudum	1.591	1.363	2.7, ***67***	1.694	1.370	3.6, ***84***	1.673	1.370	3.5, ***93***	1.935	1.460	3.3, ***80***	1.815	1.472	2.9, ***79***

Table 1. The mean number of trees per species of trees that died and were recruited in each quadrat was compared with the mean number of trees per species of samples of trees of the same size that were drawn at random from survivors + died or survivors + recruited in the same quadrat. Sampling of all quadrats with two or more trees that died or were recruited was carried out 100 times. The mean *t* values of the paired comparisons between the real and randomized values, along with their degrees of freedom (df), are shown. The expectation was that if trees that died or recruits were a random sample of the trees in the quadrat, there should be no difference in mean numbers of trees per species between the real died or survived categories and the randomized samples from the same quadrats. In almost all cases, the observed mean numbers of trees per species were significantly larger than the mean numbers of trees per species of random samples of the same size. This is the result that would be expected if commoner species were overrepresented and rarer species underrepresented among the trees that died and the trees that were recruited. The significance of the difference between real and random data sets diminished with increasing quadrat size, as expected if the nonrandom effects were strongest in the local regions represented by small quadrat sizes.

MATHEMATICAL BIOLOGY

Master Class in Evolutionary Modeling

Steven A. Frank

How does one identify a significant idea? From the purely intellectual perspective, the great mathematician G. H. Hardy gave perhaps the best answer: "We may say, roughly, that a mathematical idea is 'significant' if it can be connected, in a natural and illuminating way, with a large complex of other mathematical ideas. Thus a serious mathematical theorem, a theorem which connects significant ideas, is likely to lead to important advances in mathematics itself and even in other sciences" (*1*). Hardy's definition of significance applies not just to mathematics but to any discipline.

Evolutionary Dynamics
Exploring the Equations of Life

by Martin A. Nowak

Harvard University Press, Cambridge, MA, 2006. 377 pp. $35, £22.95, €32.30. ISBN 0-674-02338-2.

Martin Nowak is certainly not alone when he argues, in *Evolutionary Dynamics*, that evolution is the single most significant idea in biology. But almost all major mathematical syntheses of evolution have been confined to population genetics—the study of gene frequency changes in populations. By contrast, Nowak (a professor of biology and mathematics at Harvard) follows up on Hardy's last qualification for a great idea by showing the many ways in which the mathematics of evolution lead to advances in diverse subjects, including cancer, game theory, and language.

Nowak's way of linking classical population genetics to the somatic evolution of cancer illustrates his approach. In one chapter, he gives a clear, step-by-step introduction to how sampling in small populations causes frequencies to fluctuate and how the directionality of selection balances against the randomness induced by sampling. Simple figures and basic equations lead the reader along to intuition and some classical results. The text emphasizes getting a start on the logic and translating the logic into basic mathematics.

With simple mathematical tools for finite populations in hand, Nowak turns in a later chapter to cancer. In many organs prone to cancer, such as the colon or skin, the tissue separates its cells into many small compartments. Each compartment renews continuously throughout life from a few long-lived stem cell lineages. Nowak develops the population genetics of these numerous isolated compartments to explore how somatic mutations accumulate over time in these populations. Using simple figures that match the biology of cancer genetics to the fundamental processes of population genetics, he shows how to write basic equations for the rate at which cancer progresses under different assumptions about how tissue architecture controls the size of local populations of cells and how particular genetic loci affect the processes of cellular birth and death.

The book does not emphasize new results; most of the theory Nowak discusses has been published previously. Nonetheless, the lucid presentation, drawing frequently on the author's own research, provides a uniquely compelling introduction to mathematical biology. Nowak aims to demonstrate the power of simple mathematics to illuminate diverse aspects of evolutionary analysis. He comments, "I will start with the basics and in a few steps lead you to some of the most interesting and unanswered research questions in the field. Having read the book, you will know what you need to embark on your own journey and make your own discoveries."

I have often wondered how to teach theoretical biology. There does not seem to be any decisive piece of knowledge or method. I know superb mathematicians who have written many mathematically elaborate papers about biology, each one missing the essence of the biological problem and so consigned to be neither good mathematics nor good biology. I know biologists with a vast knowledge of their subject who could never let go of the idea that mathematical models must incorporate every known fact of biology, rendering their models incomprehensibly complex expressions of biological fact forced into the austerely unforgiving language of mathematics.

When my own research on the sex ratios of fig wasps led me to some very abstract but powerful models on the evolution of sex ratios, I set out my own course for learning how to understand biological theory and how to make models. I decided to find a master work and to copy from it each day until the strokes seemed natural, and I could then modulate the technique to my own ends. Each day, I started with a blank piece of paper and tried to recreate the master work. I chose as my target W. D. Hamilton's famous model on sex ratio evolution in which males competed against their brothers in the mating arena (*2*). This was, perhaps, a lucky choice, because Hamilton's work easily satisfies Hardy's dictum for significance: no model has taught us more about the evolution of cooperation and competition and about how to formulate models that illuminate evolutionary process and can be tested empirically.

Evolutionary Dynamics provides a new generation with an

Learning from the masters. An art student copying an oil painting in the Louvre, Paris.

CREDIT: © DAVE BARTRUFF/CORBIS

The reviewer is at the Department of Ecology and Evolutionary Biology, University of California, Irvine, CA 92697–2525, USA. E-mail: safrank@uci.edu

opportunity to draw from the masters. To begin, read a chapter and get a feeling for the picture. Close the book. On a blank sheet, recreate the mathematical models. The math is very simple, but Nowak has nicely chosen significant problems that run deeply. At first, the task may seem impossible. But after numerous failures, each followed by a check against the book, you will start to feel the way of construction. Soon enough, you will be able to recreate the models. Then the fun begins. You will not like some of Nowak's assumptions about, say, how to model the evolution of language, or you will have your own ideas about how HIV evolves over the many years of an infection. The master becomes your foil rather than your target; you have started on your own research.

References

1. G. H. Hardy, *A Mathematician's Apology* (Cambridge Univ. Press, Cambridge, 1967).
2. W. D. Hamilton, *Science* **156**, 477 (1967).

10.1126/science.1136579

HEALTH, GENES, & ENVIRONMENT

Prosperous People, Penurious Genes

Steve Jones

Time, said Hamlet on seeing his father's ghost, is out of joint: he was no longer in the world he knew, but in a strange and alien sphere where the old laws no longer held. And that, according to Peter Gluckman and Mark Hanson in *Mismatch*, is becoming a global predicament: a man-made universe of riches in which man himself no longer feels at home.

Shakespeare had an old-fashioned view of genetics: of Caliban, in *The Tempest*, he said: "On thy foul nature, nurture shall never stick." Mendel felt much the same, while Lamarck and Lysenko were each certain that the environment had an influence upon the next generation. All were to some degree right, and the boundaries of nature and nurture are far less distinct than once they seemed. Perhaps, developmental biologists Gluckman (University of Auckland, New Zealand) and Hanson (University of Southampton) suggest, today's lifestyle diseases can be traced to the mismatch between our current rich environment and our parsimonious genes—between the way we are and the way we used to be.

Fat runs in families but so do frying pans, which makes it hard to know whether DNA or dripping is more to blame for today's plague of obesity. My own generation—those now in middle age—may be the longest-lived in history, for they gained from the healthy diet of the 1950s while their successors are losing to the pressure to eat more and exercise less.

Fat cats tend to have fat owners because of shared lifestyle rather than shared genes. Even so, changes in DNA can cause drastic changes in body weight. The *obese* mouse, with its fault in the satiety hormone leptin, offered the first hint of the complex mechanism of appetite control. The few children born with that mutation can be treated with the missing protein (although a vaccine against another such hormone as a means of weight loss has just been abandoned). Within the normal range, too, genes are involved, for identical twins experimentally gorged or starved tend to gain, or lose, avoirdupois to the same degree.

The search for other molecular culprits has been, if anything, too successful. The Human Obesity Gene Map has swollen to 250 loci, a number that beggars belief. Gluckman and Hanson make a convincing case that the environment and, crucially, the ghost of environments past each play a major role not just in fat but in many other attributes once confidently ascribed to simple Mendelism.

Mothers who smoke, or who have a poor diet, tend to have skinny babies (and the British press has put out scare stories about pregnant women smoking to ensure an easier birth). A tough time in the uterus damages the child in many ways. Underweight babies are at higher risk of adult hypertension and diabetes. They are also more likely to become obese in the modern world of surfeit, which does not match their deprived uterine experience, although in ancient times an impoverished fetus could expect a hard life as an adult and stored up reserves to match. Perhaps the best escape from that dilemma is to concentrate on the health of young women in the hope of helping the next generation

Birth weight has rather a small genetic component, but its effects continue into the next generation. More remarkable, recent studies in Scandinavia hint that even the health of grandfathers influences the well-being of their grandsons. Quite how, in this brave new epigenetic world, their fate is inherited is far from clear, but the discovery is another stake through the heart of Shakespeare's, and Weissman's, dogma that the germ line is kept safe from the thousand natural shocks that flesh is heir to.

Gluckman and Hanson make a good case for a modern mismatch for diet, but there is more to life than cheeseburgers. We often manage the world to fit our lifestyles. Social primates as we are, we flip open mobile phones to ensure that our networks stay in good shape. In the same way, we take the climate of the savannah with us (and pay the price in furs, tropical holidays, and air conditioning). Even so, *Mismatch* is a salutary reminder that the old genetics, with its rigid separation of nature from nurture, is giving way to a murkier model of inheritance in which the environment, almost as much as the DNA, plays a central part as generations succeed one another. In this brave and unexpected new world, it pays us all to—unlike Hamlet—choose our parents, and even our grandparents, well.

10.1126/science.1136273

CREDIT: JOE SUTLIFF

Mismatch
Why Our World No Longer Fits Our Bodies

by Peter Gluckman and Mark Hanson

Oxford University Press, Oxford, 2006. 297 pp. $29.95, £16.99. ISBN 0-19-280683-1.

The reviewer is at the Galton Laboratory, University College London, Wolfson House, 4 Stephenson Way, London NW1 2HE, UK. E-mail: j.s.jones@ucl.ac.uk

INQUIRY LEARNING

Teaching Scientific Inquiry

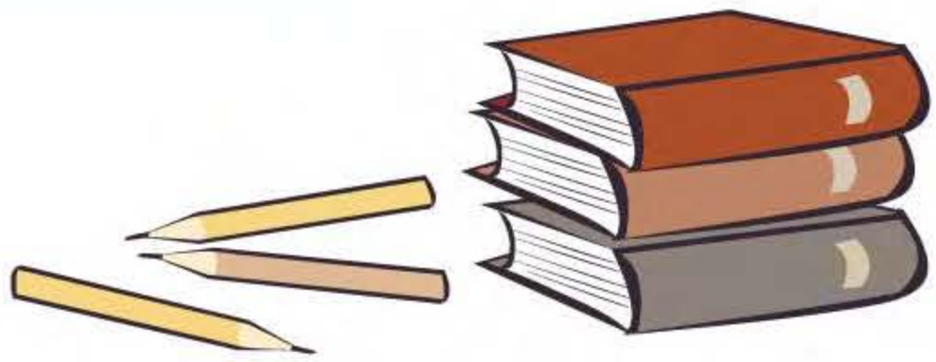

David I. Hanauer,[1]* Deborah Jacobs-Sera,[2] Marisa L. Pedulla,[3]
Steven G. Cresawn,[2] Roger W. Hendrix,[2] Graham F. Hatfull[2]*

Working in research laboratories to generate new scientific information can give high school students a taste of real scientific investigation.

Science teachers in kindergarten to 12th grade (K–12) classrooms face a curious paradox. On one hand, according to the generally accepted theory, scientific inquiry in the classroom is "at the heart of the science and science learning" (*1*). In essence, the teaching of science should mirror the processes used by professional scientific researchers. On the other hand, a school classroom is not a research laboratory. Scientific research typically involves complex methods and problem-solving approaches (*2*), resulting in conclusions that are subjected to worldwide evaluation (*3–6*). Capturing these characteristics of professional science within the K–12 school classroom is daunting (*7*).

The goals of scientific research and current pedagogical practice are at odds (*8*, *9*). In our culture, schools are designed to present established understandings, not to promote discovery of new knowledge. The focus on persuading students of the correctness of stated information is intensified by increased reliance on broad-based standardized testing, which—especially in the United States and the United Kingdom—has become a popular mechanism for making schools accountable. The ensuing culture of conformity with established knowledge is the very antithesis of scientific inquiry (*8*).

Problems with implementing scientific inquiry in the classroom include the following: (i) Teachers may manipulate classroom science to obtain the expected results (*10*). (ii) Teachers' demonstrations merely simulate scientific inquiry. (iii) The incomplete development of students' reasoning abilities may limit their ability to construct complex scientific arguments (*9–12*). (iv) Scientific inquiry often requires detailed knowledge of a topic that students have yet to master.

[1]Graduate Program in Composition and TESOL, Department of English, Indiana University of Pennsylvania, Indiana, PA 15705, USA. [2]Department of Biological Sciences, University of Pittsburgh, Pittsburgh, PA 15260, USA. [3]Department of Biological Sciences, Montana Technology of the University of Montana, Butte, MT 59701, USA.

*Authors for correspondence. E-mail: gfh@pitt.edu (G.F.H.); hanauer@iup.edu (D.I.H.)

Beyond the Classroom

If the classroom cannot be readily transformed into a research laboratory, can a research laboratory be used as a classroom? The advantages of successfully doing so are obvious: The research laboratory is where scientific advances are made and where professional scientists—at different levels of career development—work, and scientific inquiry is their core activity. Undergraduates benefit from doing research (*13*, *14*), and similar benefit may be expected for high school students. Integration of students into the laboratory environment thus seems desirable for the students, provided that they are the designers, executors, and interpreters of their experiments, not simply spectators of the performances of others.

Because K–12 students are limited in knowledge and available time, one challenge in facilitating their participation in research lies in finding appropriate research projects that are within reach of their skills and knowledge, are readily adapted to more than just one or two high-achieving students, and reflect substantial rather than incremental scientific discovery.

Playing with PHIRE

At the University of Pittsburgh, the Phage Hunters Integrating Research and Education (PHIRE) program was founded on the concept that bacteriophage discovery and comparative genomics allow students at multiple levels of development to engage in true scientific inquiry. In PHIRE, undergraduate and high school students may isolate a novel bacteriophage, grow it and extract its DNA, sequence the genome, and analyze the sequence relative to other genomes (see the chart below). The key scientific assumption is that the bacteriophage population is vast (estimated at 10^{31} particles globally), enormously diverse, and poorly understood. We have found that the genetic diversity is so great that phages isolated from the environment have a low probability of being identical to a previously characterized isolate. The prospect of discovering a genuinely new virus or many new genes provides strong motivation. The knowledge and technical skills required to isolate a phage from the environment are modest, ensuring that even middle school students can participate. The barriers to being a successful phage hunter and

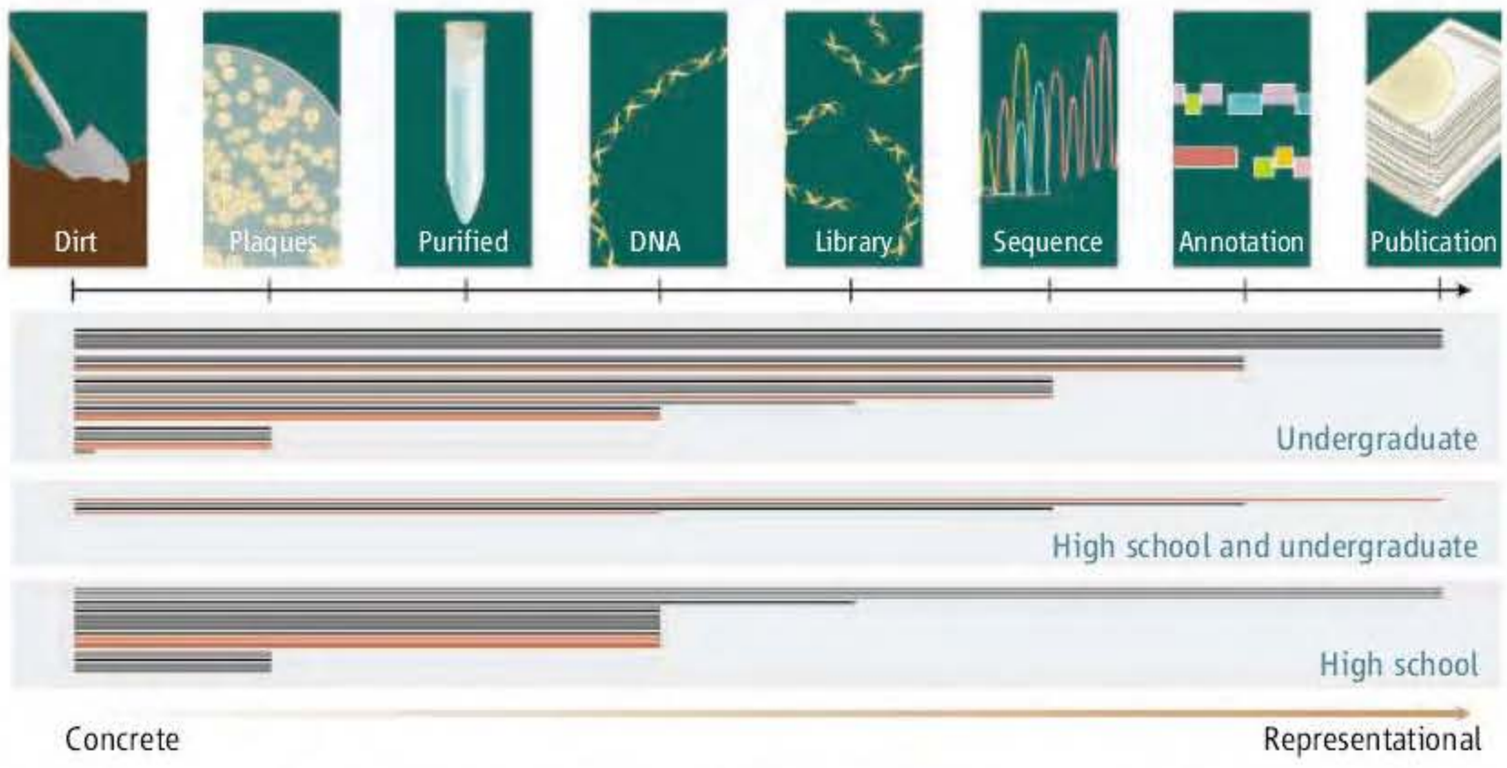

The PHIRE program. The phage-discovery process begins with a concrete activity and proceeds through increasingly representational milestones. The progress of each student is shown by a horizontal line; red lines indicate students still in the program. Most high school students participated for one summer term; four continued as undergraduates. Undergraduates average more than three terms in the program.

research scientist are minimal, opening the laboratory doors to all students, not just those labeled as academically gifted.

Comparative genomic analysis reveals that bacteriophage genomes are characteristically mosaic, composed of unique assemblages of individual and interchangeable modules (*15*). This fluid genetic exchange confuses attempts at taxonomic classification of entire phage genomes, because each of the constituent pieces has a different evolutionary history. We have therefore adopted a nonsystematic nomenclature that reflects this genetic individuality, leading to phage names such as Barnyard, Corndog, and Pipefish. The opportunity to name a new virus is exciting, and our student phage hunters often report that they consider their discoveries as being of great importance. Furthermore, the isolation of a new biological entity confers a strong sense of project ownership, and this—together with the thrill of discovery and the understanding that genomic analysis brings new knowledge of value to other scientists—promotes further engagement in the project.

We have used parallel research projects as a compromise between research independence and the ability to engage substantial numbers of students. The combination of undergraduate students and high school students facilitates peer- and near-peer mentoring, with undergraduates mentoring high school students, experienced undergraduates mentoring starting undergraduates, and experienced high school students mentoring starting undergraduates. Training mentors through programs such as the "Entering Mentoring" system (*16*) promotes an apprenticeship system (*17*) as part of the larger, multimodal structure with collective written experiences of detailed protocols, notebook reports, and published papers. The spirit of collective project ownership translates directly into collective authorship (see the chart on page 1880) (*18*, *19*). Integration of the research and educational missions promotes intertwined learning and understanding (see the chart above). The students progress from the concrete (handling biological specimens) to the representational (annotating genome sequences) (chart, page 1880). Students can participate at any or all of multiple points along this path of phage discovery and characterization (chart, page 1880).

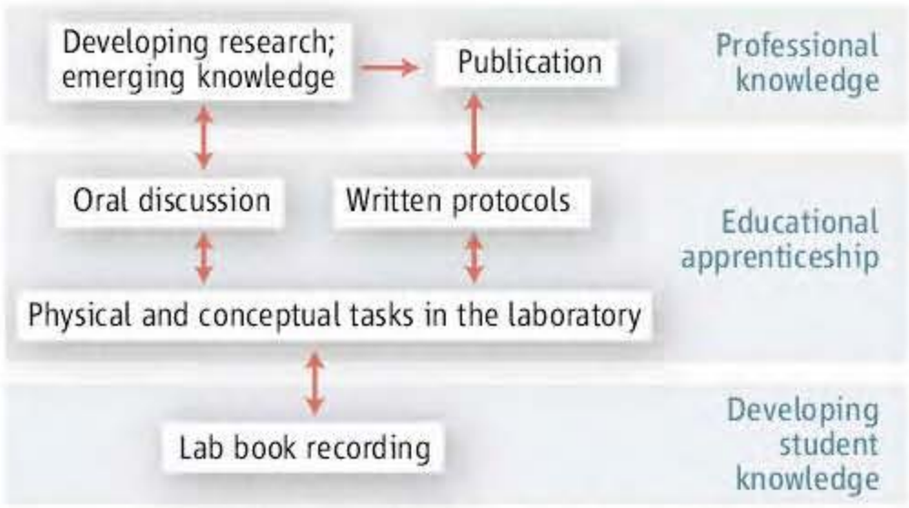

The professional apprenticeship model. The three levels of knowledge defined within the laboratory are interconnected throughout the educational program.

Does PHIRE Work?

Early results (chart, page 1880) from the PHIRE program show that virtually every student succeeded in phage isolation and at least 75% of students achieved phage purification and DNA isolation. Of the total of 54 students from 2002 to 2006, 27 are female and achieved progress through the project similar to that of male students [attaining an average of 4.8 (female) and 4.7 (male) of the eight milestones]. More than 18% of all students in the program have coauthored a scientific publication, and another 22% have contributed to a body of work that warrants future coauthorship. Characteristics of PHIRE that set it apart from other research-like activities to which students may be exposed include scientific discovery, project ownership, time flexibility, technical facility, mentorship structure, and the potential for publication.

Adding Fuel to the PHIRE

The transition of a research laboratory into an educational facility is an evolutionary process that requires constant planning and evaluation. The educational program needs to be integrated with the scientific aims of the laboratory. Integrating education and research is relevant to other research settings beyond genomics. For example, in the field of astronomy, a Web-based program titled the "Sloan Digital Sky Survey" takes on the ambitious endeavor of mapping the universe. High school students are invited to study time-lapse, color-filtered photographs of the night sky with the purpose of identifying asteroids that are close to Earth. The asteroids' motion relative to that of the stars and planets is revealed as colored dots against the backdrop of space and more distant celestial objects. As with the PHIRE program, the specificities of the research project allow the creation of an integrated educational program that enhances high school science without degrading the quality or the aims of the research (*20*).

The PHIRE platform can be translated cost-effectively into numerous other settings. The most costly part of the project is the genomic analysis, but technological advances continue to lessen the per-base-pair cost of sequencing. Implementation of PHIRE should be within reach of many universities. We have also implemented the phage isolation component in high school classrooms. High school students isolate phages and can send them to the Pittsburgh Bacteriophage Institute for genomic sequencing. The sequence information is then returned to the student class for annotation and analysis. Since 2003, a total of 57 high schools and 3534 high school students have participated in the phage-isolation program (at a cost of about $8 per student), leading to the isolation of 94 bacteriophages; three of these have been completely sequenced. Student surveys indicate at the conclusion of the experience that more than 90% of students were able to identify key concepts in microbiology research and that more than 92% would recommend the program to other students.

References and Notes

1. National Research Council, *National Science Education Standards* (National Academies Press, Washington, DC, 1996).
2. Y. Qin, H. A. Simon, *Cognit. Sci.* **14**, 281 (1990).
3. K. Dunbar, in *Mechanisms of Insight*, R. J. Sternberg, J. Davidson, Eds. (MIT Press, Cambridge, 1995), pp. 365–395.
4. K. Dunbar, in *Conceptual Structures and Processes: Emergence, Discovery, and Change*, S. M. S. T. B. Ward, S. Vaid, Eds. (APA Publishers, Washington, DC, 1997), pp. 461–493.
5. R. A. Harris, *Landmark Essays on the Rhetoric of Science: Case Studies* (Erlbaum, Mahwah, NJ, 1997).
6. L. J. Prelli, *A Rhetoric of Science: Inventing Scientific Discourse* (Univ. of South Carolina Press, Columbia, SC, 1989).
7. National Research Council, *America's Lab Report: Investigations in High School Science*, S. R. Singer, M. L. Hilton, H. A. Schweingruber, Eds. (The National Academies Press, Washington, DC, 2006).
8. D. Hanauer, paper presented at the American Association of Applied Linguistics conference, Montreal, Canada, 17 to 20 June 2006.
9. D. Hanauer, *Scientific Discourse: Multiliteracy in the Classroom* (Continuum Press, London, 2006).
10. M. Nott, R. Smith, *Int. J. Sci. Educ.* **17**, 399 (1995).
11. J. L. Lemke, *Talking Science: Language, Learning, and Values* (Ablex, Norwood, NJ, 1990).
12. D. Kuhn, *Sci. Educ.* **77**, 319 (1993).
13. E. Seymour *et al.*, *Sci. Educ.* **88**, 493 (2004).
14. D. Lopatto, *Cell Biol. Educ.* **3**, 270 (2004).
15. R. W. Hendrix, M. C. Smith, R. N. Burns, M. E. Ford, G. F. Hatfull, *Proc. Natl. Acad. Sci. U.S.A.* **96**, 2192 (1999).
16. C. Pfund *et al.*, *Science* **311**, 473 (2006).
17. J. R. Lewis *et al.*, *Cell Biol. Educ.* **1**, 26 (2002).
18. G. F. Hatfull *et al.*, *PLoS Genet.* **2**, e92 (2006).
19. M. L. Pedulla *et al.*, *Cell* **113**, 171 (2003).
20. Z. Ivezic, *J. Astron.* **122**, 2749 (2001).
21. We thank all of the students and their teachers that have contributed to or supported the PHIRE program. We also thank B. Jacobs and his laboratory personnel for helpful discussions throughout, and we acknowledge their related programs in supporting high school student summer research. Supported by the Howard Hughes Medical Institute through a grant to G. F. H. from the Howard Hughes Medical Institute Professors program, and in part by NIH grants GM51975 and RR16455.

Supporting Online Material
www.sciencemag.org/cgi/content/full/314/5807/1880/DC1

10.1126/science.1136796

BIOCHEMISTRY

Proteins in a Small World

Layering three-dimensional structural information on top of protein interaction networks reveals two different kinds of highly connected proteins or "hubs."

Todd O. Yeates and Morgan Beeby

Networks of interacting components have been put forward as models for understanding systems as diverse as food webs (*1*), the topology of the Internet, the social ties of guests at a cocktail party, and the collaboration networks of hip-hop acts in popular music (*2*). In the area of systems biology, networks of interacting proteins have been explored as models for understanding cellular processes (*3*–*6*). Many of these networks exhibit a "small world" property (*7*), meaning that a connection can be established between any two elements of the network by following only a small number of links. The small world property of some networks is due in part to the presence of hubs, which are elements connected to many other elements in the network. In protein interaction networks, hubs play an important role, and their properties have been investigated (*8*). On page 1938 of this issue, Kim *et al.* (*9*) add a new chapter to the analysis of hubs in protein interaction networks, clarifying some previously murky issues about how they operate in the cell and how they may have evolved.

In some protein networks, a link can denote a variety of different kinds of relationships between two proteins: direct physical interaction, correlated expression of proteins in the cell, performance of successive steps in a metabolic pathway, and so on. Kim *et al.* focus on direct physical interactions between proteins, but they take a further step by using the database of known three-dimensional structures to make inferences about what parts of the protein surfaces are involved in the various interactions.

This simple but elegant advance adds considerable information to the network view. With the added information it becomes possible to determine which of the multiple interactions or connections that are made to a given protein can occur simultaneously, and which are mutually exclusive due to overlapping binding surfaces. The thrust of their work is that they are able to distinguish between two different kinds of hubs in protein interaction networks (see the figure). One type, referred to as a single-interface hub, makes interactions to numerous other proteins using just one binding surface; these interactions are mutually exclusive. The other type, a multi-interface hub, makes simultaneous interactions to multiple other proteins using multiple distinct binding surfaces. The distinction between the different kinds of hubs makes it possible to ask new questions and to see new features in protein networks. It also provides a way to begin to factor out spatial versus temporal complexities in networks, which are otherwise convoluted in generic protein interaction networks.

After discriminating between the two kinds of protein hubs, the authors are able to clarify a number of issues that had been examined previously. There has been some disagreement over whether hub proteins evolve at a slower rate than more peripheral proteins (*10*, *11*). Kim *et al.* clarify the topic by showing that the rate of mutation of a hub is constrained by the amount of the protein surface involved in interactions with other proteins, not simply by the number of proteins with which the hub interacts. Thus, multi-interface hubs evolve more slowly than typical cellular proteins, whereas single-interface hubs generally do not. They also note that, compared to single-interface hubs, multi-interface hubs show more highly correlated cellular expression with their interacting partners. This parallels the recent observation of a division of hubs into "date" hubs, which tend to be coexpressed with only one binding partner at a time, and "party" hubs that are co-transcribed alongside multiple partners (*12*). The interacting partners of multi-interface hubs are more often involved in stable multisubunit complexes, whereas interactions to single-interface hubs are apparently more transient and temporally variable.

Kim *et al.* also argue that the distinction between the two kinds of hubs bears on issues of network growth and evolution. Networks with hubs and small-world properties can arise by preferential attachment of new nodes to nodes that already participate in multiple interactions (*13*). This kind of preferential attachment is generally consistent with evolution by gene duplication. However, Kim *et al.* note that this seems to apply only to single-interface hubs. Two homologous proteins that arose within the same organism by gene duplication would tend to bind to the same surface of a hub protein; the data support this contention. The gene duplication and preferential attachment mechanism therefore appears to provide a route mainly to single-interface hubs. This leaves questions about the evolution of hubs of the multi-interface type.

A particularly interesting and perhaps unanticipated finding of the analysis concerns the degree to which hub proteins are essential to cell function. This topic has been examined before (*8*). Kim *et al.* find that, compared to single-interface hubs, multi-interface hubs are twice as likely to be essential. This suggests the idea that multi-interface hubs are somehow more highly integrated into the network of the cell. This makes some sense in view of the persistence of the interactions involved. Any given interaction to a single-interface hub will tend to be transient to a degree, in that it may be

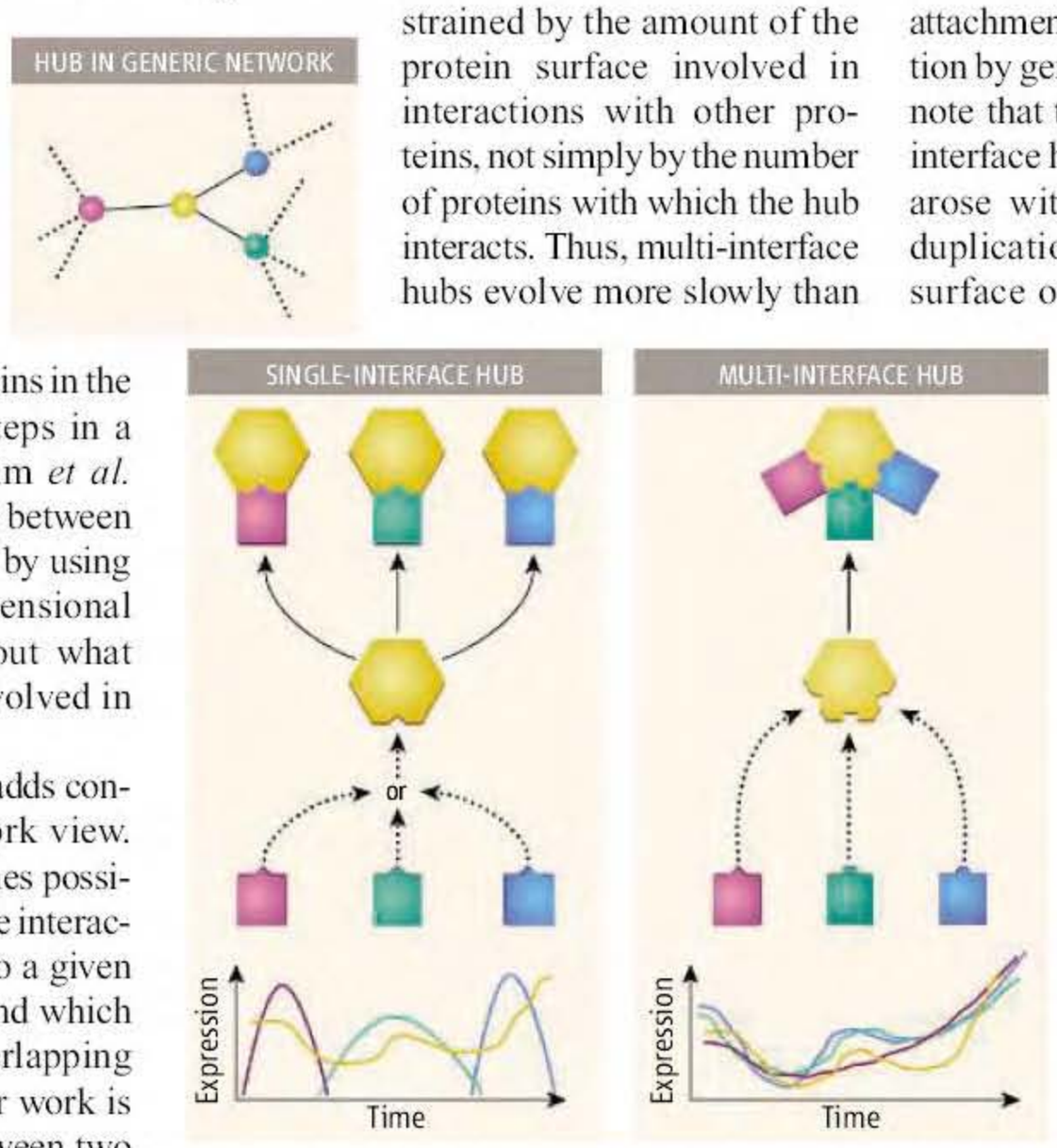

Hub connections. (**Top**) In this simplified network diagram, a hub protein (yellow) connects three other proteins. There may be two kinds of hubs: (**left**) a single-interface hub or (**right**) a multi-interface hub. Idealized gene expression levels are indicated on graphs to reflect the generally low correlation between expression levels for single-interface hubs and the high correlation for multi-interface hubs.

The authors are in the Department of Chemistry and Biochemistry, University of California Los Angeles, Los Angeles, CA 90024–1569, USA. E-mail: yeates@mbi.ucla.edu

replaced at another time by interaction to a different partner. In contrast, interactions to multi-interface hubs may be persistent, and might therefore reflect necessity.

The idea that multi-interface hubs are more highly integrated into cellular networks may also affect the issue of horizontal gene transfer as an evolutionary mechanism. It has been argued that the more integrated a protein is into cellular organization, the less likely it is that a horizontally transferred gene will displace it (*14*). It will be interesting to see if there is a notable difference in horizontal gene transfer tendencies between single-interface and multi-interface hubs.

After years of fruitful work in systems biology, network analysis, bioinformatics, and structural genomics, cross-fertilization of these inherently related perspectives is beginning to take place (*15*). The work of Kim *et al.* shows the shift toward increased integration of multiple perspectives. Future progress in understanding cellular networks will require more complete data sets describing the underlying interactions. A knowledge of which proteins are interacting in the yeast cell is approaching some degree of completion, but only a fraction of those interactions can presently be mapped onto protein surfaces in three dimensions, which is required for the analysis developed by Kim *et al.* The insights drawn by their methods of analysis will be further strengthened as more structural data become available.

References

1. R. J. Williams, E. L. Berlow, J. A. Dunne, A. L. Barabasi, N. D. Martinez, *Proc. Natl. Acad. Sci. U.S.A* **99**, 12913 (2002).
2. R. D. Smith, *J. Stat. Mech.* **P02006**, 10.1088/1742-5468/2006/02/P02006 (2006).
3. A. L. Barabasi, Z. N. Oltvai, *Nat. Rev. Genet.* **5**, 101 (2004).
4. E. M. Marcotte, M. Pellegrini, M. J. Thompson, T. O. Yeates, D. Eisenberg, *Nature* **402**, 83 (1999).
5. L. Salwinski *et al.*, *Nucleic Acids Res.* **32**, D449 (2004).
6. R. Milo *et al.*, *Science* **298**, 824 (2002).
7. D. J. Watts, S. H. Strogatz, *Nature* **393**, 440 (1998).
8. H. Jeong, S. P. Mason, A. L. Barabasi, Z. N. Oltvai, *Nature* **411**, 41 (2001).
9. P. M. Kim, L. J. Lu, Y. Xia, M. B. Gerstein, *Science* **314**, 1938 (2006).
10. I. K. Jordan, Y. I. Wolf, E. V. Koonin, *BMC Evol. Biol.* **3**, 1 (2003).
11. H. B. Fraser, A. E. Hirsh, L. M. Steinmetz, C. Scharfe, M. W. Feldman, *Science* **296**, 750 (2002).
12. J. D. Han *et al.*, *Nature* **430**, 88 (2004).
13. G. P. Karev, Y. I. Wolf, F. S. Berezovskaya, E. V. Koonin, *BMC Evol. Biol.* **4**, 32 (2004).
14. C. R. Woese, *Microbiol. Mol. Biol. Rev.* **68**, 173 (2004).
15. S. A. Levin, *PLoS Biol.* **4**, e300 (2006).

10.1126/science.1137400

EVOLUTION

The Origin of Insects

Recent molecular evidence suggests that crustaceans may have successfully invaded land as insects.

Henrik Glenner, Philip Francis Thomsen, Martin Bay Hebsgaard, Martin Vinther Sørensen, Eske Willerslev

Although hexapods—those arthropods having six legs, including insects—are the most diverse group of contemporary animals in terms of biological niches and number of species, their origin is highly debated. A key problem is the almost complete absence of fossils that connect hexapods to the other major arthropod subphyla, namely Crustacea, Myriapoda (such as centipedes and millipedes), and Chelicerata (such as scorpions and spiders). Over the years, hexapods (insects, springtails, proturnas, and diplurans) have been phylogenetically linked to all of these major arthropod taxa (*1*).

Traditionally, hexapods and the multi-legged myriapods have been united in a group named Atelocerata on the basis of morphological similarities between their tracheal respiration systems and head appendages. However, recent evidence from phylogenetic analyses of molecular sequence data from a variety of genes, as well as from newer morphological studies, points to a relationship between hexapods and crustaceans (*2–9*), a grouping commonly referred to as Pancrustacea. Furthermore, studies on neurological development in the major arthropod groups have pointed out similarities between the myriapods and chelicerates (*10*). Hence, pancrustacean monophyly seems to be gaining more support. So, what does this view tell us about the possible origin of hexapods?

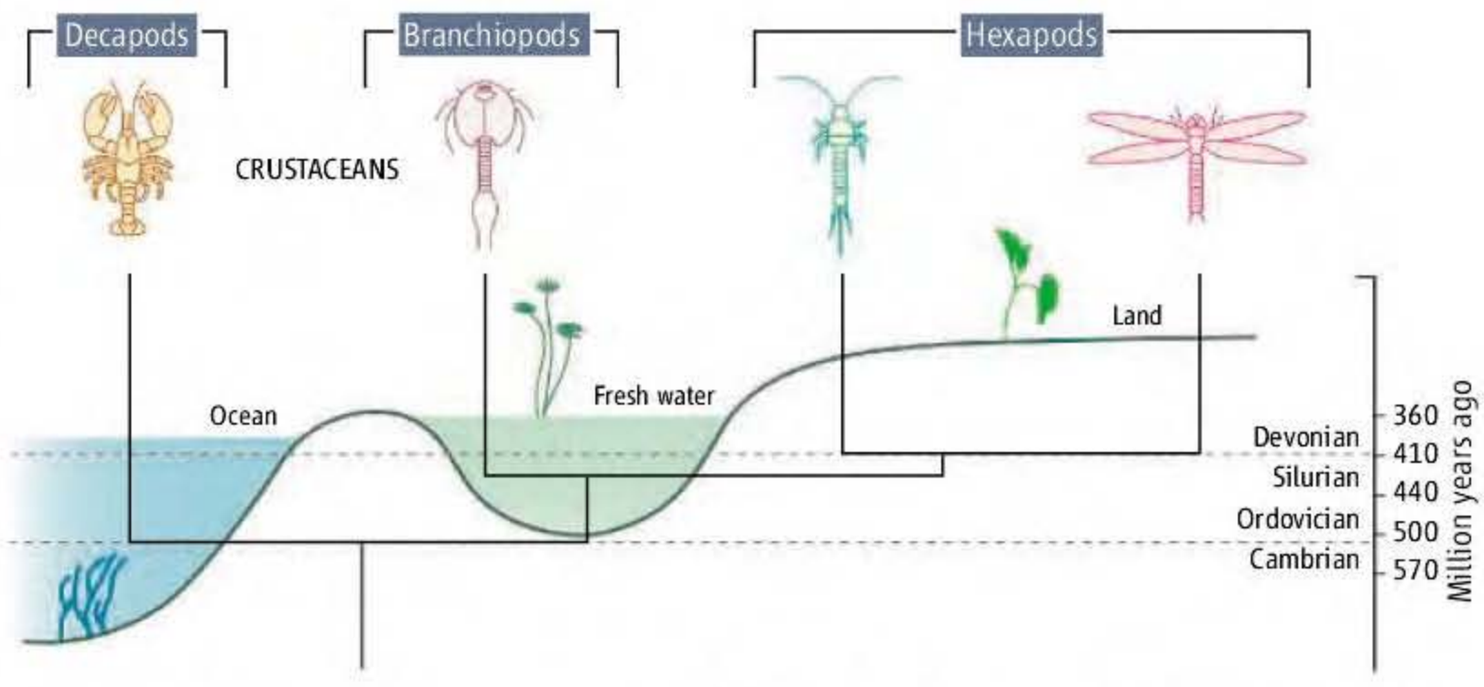

Hexapod evolution. The last common ancestor of hexapods and crustaceans (branchiopods, specifically) may have originated in freshwater during the Late Silurian, giving rise to extant freshwater dwelling branchiopods (fairy shrimps, water fleas, and tadpole shrimps) and insects. This hypothesis accounts for the missing fossil record of branchiopods and hexapods before the Devonian.

The crustaceans are recorded at least as far back as the Upper Cambrian, about 511 million years ago (*11*), where they are found in marine sediments (see the figure). However, except for the debated *Devonohexapodus bocksbergensis* specimen (*12*, *13*), all hexapod remains are found only in freshwater or terrestrial strata no earlier than the Devonian, around 410 million years ago (*14*). This leaves a gap of 100 million years to the earliest crustaceans. The common explanation has been that earlier traces of hexapods have been erased from the fossil record and that hexapods, like other major groups of terrestrial animals, have closely related ancestors to be found in the marine environment.

The recent morphological and molecular-based studies suggest an alternative interpretation—that hexapods originated within the crustaceans rather than as a sister group (*15–20*). Although the morphological studies mainly favor a close phylogenetic connection between

The authors are at the Centre for Ancient Genetics, Department of Evolutionary Biology, Biological Institute, University of Copenhagen, Universitetsparken 15, DK-2100 Copenhagen, Denmark. E-mail: ewillerslev@bi.ku.dk

hexapods and malacostracan crustaceans (crabs and crayfish) (*15*, *16*), recent molecular sequence data suggest that hexapods are closely related to branchiopods (*17*, *19*, *20*), a freshwater dwelling group of crustaceans that includes water fleas and fairy shrimp. This hypothesis is supported by analysis of Hox genes that demonstrates homology between development of the pregenital trunk region in insects and the thorax in branchiopods (*21*). The new molecular results correspond well with the fossil record and suggest an evolutionary origin of the hexapods in freshwater around 410 million years ago rather than in the marine Cambrian environment (*17*).

The vast majority of extant branchiopods are freshwater animals, and the few that are found in saltwater are believed to have invaded the sea secondarily. From the fossil record, it is known that modern branchiopods date back to the Early Devonian, by which time they were fully adapted to freshwater habitats (*22*). This late appearance of the freshwater branchiopods corresponds exactly with the emergence of hexapods and suggests that their last common ancestor swam around in a freshwater pond sometime in the Late Silurian (423 to 416 million years ago) or Early Devonian. This corresponds well with the time split between the crustacean and hexapod lineages estimated from molecular clock analyses (*23*). If correct, the early marine ancestor of the hexapods might have appeared more similar to *Rehbachiella kinnekullensis*, a close marine relative to branchiopods from Upper Cambrian (*24*), than to *D. bocksbergensis* or other hexapods.

The successful colonization of the terrestrial environment by hexapods seems to coincide with other major groups of land pioneering animals such as the chelicerates and the myriapods in the Late Silurian and the tetrapods (amphibians, reptiles, birds, and mammals) in the Late Devonian. All these events appear to have occurred through a freshwater dwelling phase in their evolutionary transition from marine to true terrestrial animals. The Devonian is believed to have been a time of severe drought, which might have forced these animals (at least hexapods and tetrapods) onto land as their freshwater habitats vanished.

It has been a puzzle as to why hexapods—in particular insects, which possess a morphology that apparently enables them to adapt to virtually all types of terrestrial environments—have not been able to diversify successfully in the marine environment. It is likewise remarkable that the crustaceans—fulfilling a biological role in the sea comparable to the insects on land—have not been able to invade land to a greater extent despite their considerable age. The recent phylogenetic analyses of molecular sequence data suggest a paradigm shift concerning the phylogenetic position of hexapods—that crustaceans successfully invaded land as insects. It is possible that when insects entered terrestrial habitats, their crustacean ancestors had already diversified in marine environments and occupied all potential niches, which could explain why insects were prevented from colonizing the sea subsequently. Most important, however, the new molecular results offer a solution to the enigma concerning the absence of marine hexapod remains in the fossil records prior to the Devonian.

References and Notes

1. G. Giribet, C. Ribera, *Cladistics* **16**, 204 (2000).
2. J. M. Mallatt *et al.*, *Mol. Phy. Evol.* **31**, 178 (2004).
3. J. C. Regier, J. W. Shultz, *Mol. Phy. Evol.* **20**, 136 (2001).
4. J. W. Shultz, J. C. Regier, *Proc. R. Soc. London Ser. B* **267**, 1011 (2000).
5. U. W. Hwang *et al.*, *Nature* **413**, 154 (2001).
6. G. Giribet *et al.*, *Nature* **413**, 157 (2001).
7. C. E Cook *et al.*, *Curr. Biol.* **11**, 759 (2001).
8. Y.-x. Luan *et al.*, *Mol. Biol. Evol.* **22**, 1579 (2005).
9. W. Dohle, *Ann. Soc. Ent.* France **37**, 85 (2001)
10. H. Dove, A. Stollewerk, *Development* **130**, 2161 (2003).
11. G. E. Budd *et al.*, *Science* **294**, 2047a (2001).
12. F. Hass *et al.*, *Org. Divers. Evol.* **3**, 39 (2003).
13. R. Willmann, *Org. Divers. Evol.* **5**, 199 (2005).
14. M. S. Engel, D. A. Grimaldi, *Nature* **427**, 627 (2004).
15. S. Harzsch, *Integrative Comp. Biol.* **46**, 162 (2006).
16. N. J. Strausfeld, *Arthropod Struct. Dev.* **34**, 235 (2005).
17. J. C. Regier, J. W. Shultz, *Mol. Biol. Evol.* **14**, 902 (1997).
18. C. E. Cook, Q. Y. Yue, M. Akam, *Proc. R. Soc. London Ser. B* **272**, 1295 (2005).
19. J. C. Regier *et al.*, *Proc. R. Soc. London Ser. B* **272**, 395 (2005).
20. J. Mallatt, G. Giribet, *Mol. Phy. Evol.* **40**, 772 (2006).
21. M. Averof, M. Akam, *Nature* **376**, 420 (1996).
22. S. R. Fayers, N. H. Trewin, *Trans. R. Soc. Edinburgh Earth Sci.* **93**, 355 (2003).
23. M. W. Gaunt, M. A. Miles, *Mol. Biol. Evol.* **19**, 748 (2002).
24. D. Walossek, *Fossils Strata* **32**, 54 (1993).

25. This work was supported by The Danish Natural Science Council, The Velux Foundation, The Carlsberg Foundation, and The Wellcome Trust.

10.1126/science.1129844

EPIDEMIOLOGY

Influenza Escapes Immunity Along Neutral Networks

Erik van Nimwegen

Given that influenza virus continues to escape immunity, why is it that only one strain dominates each year? The answer may lie in neutral networks and mapping viral genotypes to antigenic phenotypes.

In the late 1960s, Kimura (*1*) made the then-revolutionary proposal that many amino acid substitutions are neutral in terms of evolutionary selection. There is now little doubt that essentially any genotype can undergo a substantial number of amino acid substitutions without substantially changing its fitness. This implies that there are large collections of selectively neutral genotypes that are connected through point mutations. Indeed, such "neutral networks" are observed in genotype-to-phenotype mappings of biomolecules (*2*, *3*). On page 1898 of this issue, Koelle *et al.* (*4*) provide compelling evidence that neutral networks play a key role in the evolution of human influenza A (H3N2).

Computer simulations and analytical studies (*5*–*7*) have shown that intertwined neutral networks have profound consequences for evolutionary adaptation. Evolving populations typically exhibit "epochs" of phenotypic stasis, punctuated by sudden changes in phenotype. However, phenotypic stasis is not accompanied by genotypic stasis. During each phenotypic epoch, the population is dominated by genotypes belonging to one neutral network, and neutral mutations cause the population to drift continuously through this neutral network (see the figure). Mutations to neighboring neutral networks (those networks that can be reached by a point mutation from one of the genotypes in the current neutral network) occur as well and enable the population to explore other phenotypes until, eventually, a mutant on a neutral network with higher fitness is generated. The offspring of this beneficial mutant will then spread through the population, causing a sudden shift in phenotype. Until the study by Koelle *et al.*, this "epochal evolution" scenario (see the figure) had been observed mostly in silico and from in vitro evolution experiments (*5*–*8*).

The author is in the Division of Bioinformatics, Biozentrum, University of Basel, 4056 Basel, Switzerland. E-mail: erik.vannimwegen@unibas.ch

One of the main influenza antigens targeted by our immune system is the viral surface protein hemagglutinin (HA), which binds to host cells. The virus is therefore under strong evolutionary pressure to alter the shape of its HA protein (*9*) so as to escape the immune response. A major breakthrough in understanding this dynamic came from measuring cross-immunity between different strains of influenza (*10*). The study produced "antigenic maps" in which each viral strain corresponds to a point in an abstract "antigenic space" and the distance between points quantitatively reflects the amount of cross-immunity between the corresponding strains. Strains of influenza A (H3N2) separate into distinct clusters in antigenic space, each cluster corresponding to the set of strains from a particular time period. Whereas the genetic distance of strains to the ancestral strain increases smoothly, periods of relative phenotypic stasis (corresponding to antigenic clusters) are punctuated by sudden transitions from one antigenic cluster to another. Koelle *et al*. studied the genetic differences between strains from different antigenic clusters and provide evidence that antigenic clusters correspond to neutral networks. In particular, they find that there is no simple relationship between antigenic and genetic distance and no simple relation between changes at particular amino acids and cluster transitions.

To model influenza A (H3N2) evolution, Koelle *et al*. couple an epidemiological model that treats individuals as susceptible to, infected by, or recovered from each of the existing strains (*11*) with a neutral network model (*12*) for mapping genotypes to antigenic phenotypes. The figure illustrates the epochal evolution cycle exhibited by this model. At the start of the epochal evolution cycle, the viral population is distributed over the neutral network of one antigenic cluster (purple) and a mutation creates an individual on another neutral network (orange). Because a substantial fraction of the host population is no longer susceptible to strains from the purple neutral network at this time, the orange mutant has a high fitness advantage, and its descendants take over the viral population in a selective sweep. This "innovation" is associated with a peak in infections. After this phase, the viral population starts an exploratory phase in which it drifts over the orange neutral network, away from the ancestral strain, increasing its genotypic diversity without a substantial change in phenotype, while the fraction of hosts that are susceptible to strains from the orange neutral network declines. Eventually a mutant is created on a new neutral network (blue) and the cycle repeats itself.

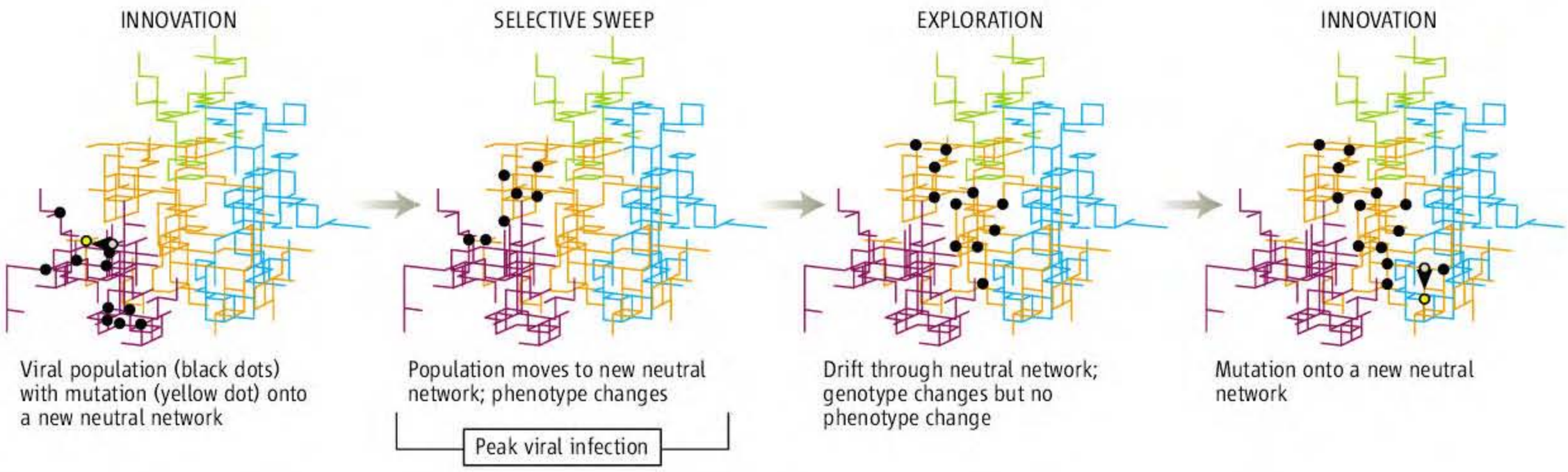

Cycling through networks. Schematic representation of the epochal model of influenza A evolution. Entangled neutral networks of genotypes (sets of genotypes, each with the same antigenic phenotype) are connected by single point mutations. By drifting through and switching between these neutral networks, the viral population exhibits periods of phenotypic stasis punctuated by sudden phenotypic transitions.

The model of Koelle *et al.* elegantly explains several observed features of the evolution of influenza A (H3N2). First, the model produces phylogenetic trees that are structured much like those observed for influenza, a feature that has been one of the main puzzles regarding influenza evolution (*13*). Second, an innovation typically causes a strong peak in infections. Third, because every innovation involves one or very few mutants, genetic diversity in the population will drop steeply at each cluster transition, after which the genetic diversity will rebound during the exploration phase of the epochal cycle.

These results indicate that the structure and interconnectivity of the neutral networks corresponding to different antigenic clusters of HA are key features determining influenza A (H3N2) evolution. In silico (*14*) and in vitro evolution studies (*15*) have suggested that by combining data on protein structure with sequence data and computational modeling, some of the structural features of neutral networks can be reconstructed. For example, probably a major constraint shaping HA neutral networks is the requirement to maintain HA's affinity to the host receptor that it binds. In addition, much is understood about how parameters such as mutation rates and effective population sizes affect epochal evolutionary dynamics (*16*), and this should enable more detailed modeling of influenza A's evolutionary dynamics. For species with high mutation rates, such as RNA viruses, it has been established both theoretically (*17*) and from sequence analysis (*18*) that populations do not drift randomly through the neutral networks but rather tend to converge to the most connected areas of the neutral network. These areas typically also correspond to sequences that fold robustly into their target shape (*19*).

Epochal evolution may also occur in the evolution of other pathogens. Particularly interesting in this regard is the fact that the intrahost phylogenetic trees of HIV and hepatitis C virus (HCV) show topologies that are very similar to those observed for influenza A (H3N2) (*20*). The key to investigating the possible role of epochal evolution in these systems will be to develop a quantitative antigenic understanding—for example, by reconstructing antigenic maps for HIV and HCV strains, as was done for influenza strains.

References

1. M. Kimura, *Nature* **217**, 624 (1968).
2. K. F. Lau, K. A. Dill, *Proc. Natl. Acad. Sci. U.S.A.* **87**, 638 (1990).

3. P. Schuster, Fontana, P. F. Stadler, I. L. Hofacker, *Proc. Biol. Sci.* **255**, 279 (1994).
4. K. Koelle, S. Cobey, B. Grenfell, M. Pascual, *Science* **314**, 1898 (2006).
5. M. A. Huynen, P. F. Stadler, W. Fontana, *Proc. Natl. Acad. Sci. U.S.A.* **93**, 397 (1996).
6. E. van Nimwegen, J. P. Crutchfield, M. Mitchell, *Phys. Lett. A* **229**, 144 (1997).
7. W. Fontana, P. Schuster, *Science* **280**, 1451 (1998).
8. S. F. Elena, V. S. Cooper, R. E. Lenski, *Science* **272**, 1802 (1996).
9. R. M. Bush, C. A. Bender, K. Subbarao, N. J. Cox, W. M. Fitch, *Science* **286**, 1921 (1999).
10. D. J. Smith *et al.*, *Science* **305**, 371 (2004); published online 24 June 2004 (10.1126/science.1097211).
11. J. R. Gog, B. T. Grenfell, *Proc. Natl. Acad. Sci. U.S.A.* **99**, 17209 (2002).
12. M. E. J. Newman, R. Engelhardt, *Proc. Biol. Sci.* **265**, 1333 (1998).
13. W. M. Fitch, R. M. Bush, C. A. Bender, N. J. Cox, *Proc. Natl. Acad. Sci. U.S.A.* **94**, 7712 (1997).
14. U. Bastolla, M. Porto, M. H. Eduardo Roman, M. H. Vendruscolo, *J. Mol. Biol.* **56**, 243 (2003).
15. C. A. Voigt, S. L. Mayo, F. H. Arnold, Z. G. Wang, *Proc. Natl. Acad. Sci. U.S.A.* **98**, 3778 (2002).
16. E. van Nimwegen, J. P. Crutchfield, M. Mitchell, *Theor. Comp. Sci.* **229**, 41 (1999).
17. E. van Nimwegen, J. P. Crutchfield, M. A. Huynen, *Proc. Natl. Acad. Sci. U.S.A.* **96**, 9716 (1999).
18. A. Wagner, P. F. Stadler, *J. Exp. Zool.* **285**, 119 (1999).
19. E. Bornberg-Bauer, H. S. Chan, *Proc. Natl. Acad. Sci. U.S.A.* **96**, 10689 (1999).
20. B. T. Grenfell *et al.*, *Science* **303**, 327 (2004).

10.1126/science.1137300

BIOCHEMISTRY

If the RNA Fits, Use It

A crystal structure of RNA bound to the IRP1 protein explains how this protein can perform two entirely different functions.

Tracey A. Rouault

Cells and organisms use a wide variety of regulatory mechanisms to sense and respond to changes in the extracellular environment. Cells can regulate gene expression at several steps after a gene has been transcribed. On page 1903 of this issue, Walden *et al.* (*1*) shed light on one such posttranscriptional regulatory mechanism. They show how a single protein—iron regulatory protein 1 (IRP1)—responds to changing conditions by performing two entirely different functions.

In iron-replete cells, IRP1 functions as an aconitase enzyme, which interconverts citrate and isocitrate in the cytosol (*2*, *3*). However, in cells that are iron-depleted and oxidatively stressed, the fragile and exposed iron-sulfur cluster in the aconitase active site disassembles and is lost from the protein. The protein transforms into apo-IRP1, which can bind RNA stem-loops within transcripts of iron metabolism genes known as iron-responsive elements (IREs) (see the figure) (*4*). Walden *et al.* now report the crystal structure of IRP1 bound to a ferritin IRE. Together with the previous structure of cytosolic aconitase (*3*), this cocrystal structure reveals how apo-IRP1 binds with high affinity to IREs, whereas cytosolic aconitase does not.

Cytosolic aconitase has four domains. Residues from each domain contribute to the enzymatic active site, including three cysteines that bind to the iron-sulfur cluster. In the IRE-IRP1 cocrystal, domain 4 has moved and rotated relative to its position in cytosolic aconitase (see the figure). Domain 3 has also substantially shifted its position relative to the central core formed by domains 1 and 2, opening up a hydrophilic cavity between the core and domain 3.

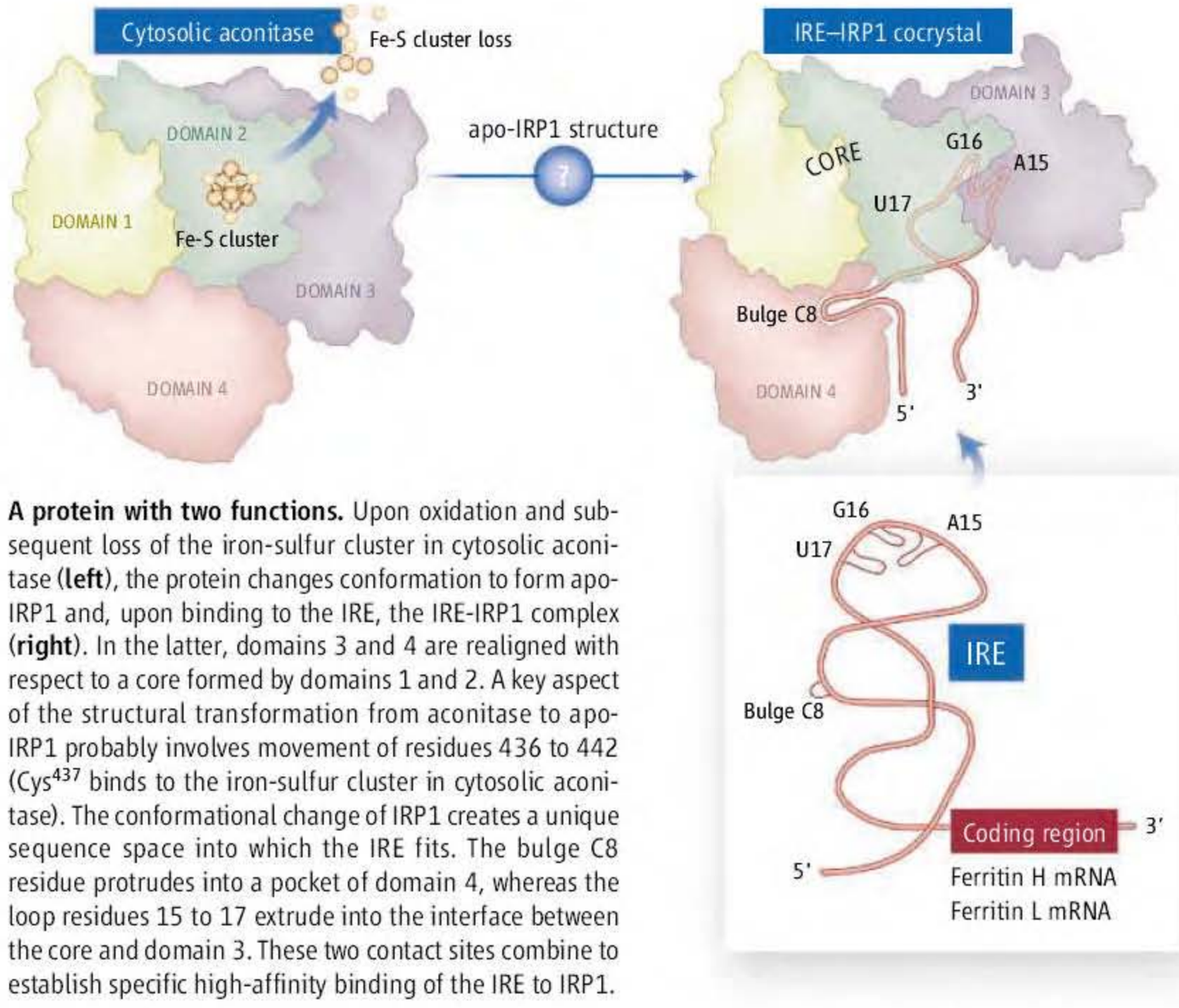

A protein with two functions. Upon oxidation and subsequent loss of the iron-sulfur cluster in cytosolic aconitase (**left**), the protein changes conformation to form apo-IRP1 and, upon binding to the IRE, the IRE-IRP1 complex (**right**). In the latter, domains 3 and 4 are realigned with respect to a core formed by domains 1 and 2. A key aspect of the structural transformation from aconitase to apo-IRP1 probably involves movement of residues 436 to 442 (Cys^{437} binds to the iron-sulfur cluster in cytosolic aconitase). The conformational change of IRP1 creates a unique sequence space into which the IRE fits. The bulge C8 residue protrudes into a pocket of domain 4, whereas the loop residues 15 to 17 extrude into the interface between the core and domain 3. These two contact sites combine to establish specific high-affinity binding of the IRE to IRP1.

Previous structural and mutagenesis studies of IREs, which have conserved structural and sequence elements but are not identical in different transcripts, indicated that the most important residues for high-affinity binding to IRP1 would be the unpaired residues of the terminal loop and an unpaired cytosine that interrupts the double-helical structure of the upper and lower stems. In the cocrystal, these unpaired residues contribute to two discrete binding sites between the IRE and IRP1. In one site, the terminal-loop residues A15, G16, and U17 interact with residues in the cavity between the core and domain 3. In the second binding site, separated by 1.0 nm from the first, the C8 bulge residue fits into a pocket of domain 4 (see the figure).

The structure of the IRE in the complex is similar to its structure in solution, except that the purine bases of the terminal loop (residues A15 and G16) reorient from a tucked position to extrude into the cavity between the core and domain 3. IRE is thus an ideal binding partner for apo-IRP1, because it can bind to apo-IRP1 while minimally reorganizing its terminal loop.

Apo-IRP1 accumulates in cells that cannot

The author is with the Cell Biology and Metabolism Branch, National Institute of Child Health and Human Development, Bethesda, MD 20892, USA. E-mail: trou@helix.nih.gov

retain an intact iron-sulfur cluster because of iron depletion and/or because of oxidative degradation of the cluster. The conformation of IRP2, a duplicated gene important in regulation, probably mimics that of apo-IRP1, although there are differences in its IRE binding site (*5*). Similar but not identical IREs found in many different transcripts can be regulated by either IRP1 or IRP2. These transcripts encode proteins involved in iron sequestration, red-cell heme biosynthesis, and iron export. An iron-starved cell would be expected to benefit from repressing translation of these transcripts. IREs are also found in an isoform of the iron importer, divalent metal transporter (DMT1), and transferrin receptor (TfR1), where stabilization of the TfR transcript by IRP binding increases TfR synthesis and iron uptake.

The appearance of nonidentical IREs in transcripts of multiple genes suggests that numerous independent evolutionary selection events created the IRP-IRE posttranscriptional regulatory network in mammalian cells. Because IREs are located in the untranslated ends of transcripts (see the figure), they can vary without affecting the protein sequence. Therefore, untranslated regions can develop new stem-loops or other features that favorably alter cellular iron conditions. Short RNA sequences such as stem-loops can provide good ligands for a wide variety of targets, in part because their shape and contact sites can vary appreciably, while stable underlying conformations are readily maintained (*6*). Aconitase arose early in evolution (*7*), and some researchers postulate that life itself arose in an iron-sulfur world (*8*), but the IRE-IRP system likely developed later in evolution and matured into an important regulatory system mainly in mammals.

The conformational shift of IRP1 from its cytosolic aconitase form to the apo-conformation thus appears to have created a new sequence space that could be sampled over time by mRNA sequences. mRNAs that contained IREs were repeatedly selected and retained, because by binding to apo-IRP1, they improved the ability of organisms to respond to iron deprivation. A new regulatory system likely took shape not through creation of new regulatory genes, but by enabling one of the oldest work-horses in the cell—aconitase—to acquire a new regulatory function. In the words of François Jacob, "Evolution does not produce novelties from scratch. It works on what already exists, either transforming a system to give it new functions or combining several systems to produce a more elaborate one" (*9*).

References

1. W. E. Walden *et al.*, *Science* **314**, 1903 (2006).
2. H. Beinert, R. H. Holm, E. Munck, *Science* **277**, 653 (1997).
3. J. Dupuy *et al.*, *Structure* **14**, 129 (2006).
4. T. A. Rouault, *Nat. Chem. Biol.* **2**, 406 (2006).
5. J. Butt *et al.*, *Proc. Natl. Acad. Sci. U.S.A.* **93**, 4345 (1996).
6. L. Gold, B. Polisky, O. Uhlenbeck, M. Yarus, *Annu. Rev. Biochem.* **64**, 763 (1995).
7. M. J. Gruer, P. J. Artymiuk, J. R. Guest, *Trends Biochem. Sci.* **22**, 3 (1997).
8. G. Wachtershauser, *Philos. Trans. R. Soc. London B Biol. Sci.* **361**, 1787 (2006).
9. F. Jacob, *Science* **196**, 1161 (1977).

10.1126/science.1137174

EARTH SCIENCE

A Submarine Volcano Is Caught in the Act

Ocean-bottom seismometers have recorded the seismic activity associated with a submarine volcanic eruption, revealing important differences from eruptions on land.

William W. Chadwick Jr.

In April 2006, Maya Tolstoy, a geophysicist at Columbia University, received some good news and some bad news during a research expedition at sea. The submarine volcano that she and her colleague Felix Waldhauser had been monitoring for years had recently erupted. This was exciting, because only a handful of other deep-sea eruptions have been detected (*1*), and it was the first time ocean-bottom seismometers were in place during such an event. However, two-thirds of the instruments were stuck in the new lava on the sea floor (see the figure). Would the remaining third yield the data needed to gain new insights into this fundamental but poorly understood geological process?

In the end, the good news outweighed the bad. The instruments that were recovered provided some remarkable results, as Tolstoy *et al.* report on page 1920 of this issue (*2*). Also, this may only be the first installment in this story, because there is hope that more instruments can be rescued from the sea floor.

The eruption took place on the East Pacific Rise, a huge ridge on the ocean floor west of Mexico where two of Earth's giant tectonic plates gradually spread apart. As the plates spread, molten rock rises in the gap to feed periodic eruptions on the sea floor, creating new ocean crust. Three quarters of Earth's volcanism takes place along such seafloor spreading centers, but we know very little about these events. Seismometers on land generally cannot sense them, because they are too far away and the associated earthquakes are too small. Before 1990, not a single eruption was documented on the mid-ocean ridge system, even though many probably occur each year. Since then, swarms of small earthquakes associated with seafloor spreading events have been detected by remote hydrophone arrays (*1*, *3*) and by local networks of ocean-bottom seismometers such as those used by Tolstoy *et al.*

We learn the most about Earth's active processes such as eruptions when we can observe them as they are happening. This is the philoso-

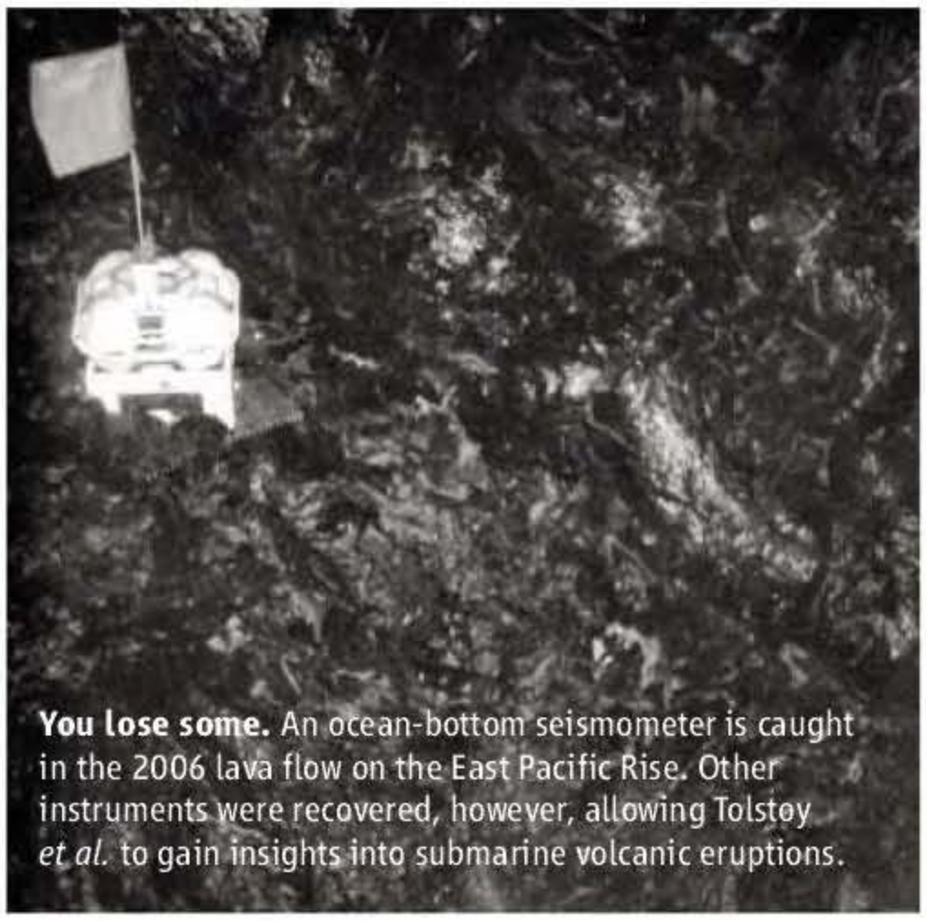

You lose some. An ocean-bottom seismometer is caught in the 2006 lava flow on the East Pacific Rise. Other instruments were recovered, however, allowing Tolstoy *et al.* to gain insights into submarine volcanic eruptions.

CREDIT: WHOI, NSF, AND RIDGE2000 PROGRAM

The author is at Oregon State University/NOAA, Hatfield Marine Science Center, Newport, OR 97365, USA. E-mail: william.w.chadwick@noaa.gov

phy behind the "integrated study sites" set up by the National Science Foundation's RIDGE2000 Program (*4*) on the global mid-ocean ridge system. The program funds long-term, focused, interdisciplinary monitoring at these sites, with the hope of capturing dynamic events and their impact on hydrothermal vents and associated biological communities. The East Pacific Rise at latitude 9°50′N is one of these sites.

Long-term monitoring of this kind is inherently risky, because you could monitor for several years and not capture an eruption. But the potential reward is great. Tolstoy *et al.* (*2*) document a gradual buildup of seismicity for at least 2 years leading up to the 2006 eruption, a pattern that may have predictive value in the future. The long duration of this increase in earthquake activity is unusual when compared with volcanoes of this type on land, where seismic precursors to eruption often last only hours to days (*5*). This observation implies that pressurized magma was accumulating beneath the ridge crest for years before the eruption and that there may be other measurable manifestations (like inflation of the sea floor) that could aid eruption forecasting.

The eruption itself was associated with an intense 6-hour peak in seismicity, when magma from the reservoir (~1.4 km beneath the ridge) rose to the surface. The earthquakes reflect the breaking of rock as the magma forced its way upward. Once this conduit was formed, the eruption probably did not generate as many earthquakes. It is unclear how long the eruption itself lasted, but the duration of magma intrusion appears to have been very brief.

This is the first time that an exact eruption recurrence interval has been documented on the mid-ocean ridge, because evidence of a previous eruption that had occurred just weeks before was found by chance at this site in 1991 (*6*). Knowing the exact date and time of the 2006 eruption will be very valuable to other interdisciplinary studies at the site, such as those focusing on biological colonization of the new lavas.

It is unfortunate that more ocean-bottom seismometers could not be initially recovered, but there is hope that more might be rescued from the lava flow. In 1998, an underwater eruption that I studied trapped a monitoring instrument at Axial Seamount, an active submarine volcano in the northeast Pacific where long-term monitoring is coordinated by the Vents Program of the National Oceanic and Atmospheric Administration (*7*). When we were eventually able to pull the instrument out of the lava, it was in remarkably good condition, even though it had been caught in lava that probably erupted at ~1190°C. Apparently, the unlimited supply of cold seawater and the strong insulating properties of a cooled lava crust kept the ambient water temperature modest. The data recorded by the instrument revealed the duration, rate, and character of a submarine lava eruption (*8*).

Therefore, if the ocean-bottom seismometers from the East Pacific Rise can be extracted, there is a very good chance that the data they recorded during the 2006 eruption are still intact. Data from more instruments would be extremely valuable, allowing us to determine the locations and depths of earthquakes, the three-dimensional distribution of events with time, and the temporal and spatial variation in earthquake magnitudes. We could learn how magma moved from depth to the surface as well as its extent along the plate boundary, and perhaps uncover more clues about how the next event might be forecast. These rewards are definitely worth the risks involved in trying to catch a submarine volcano in the act.

References

1. J. P. Cowen, E. T. Baker, R. W. Embley, in *The Subseafloor Biosphere at Mid-Ocean Ridges*, W. S. D. Wilcock *et al.*, Eds. (Geophys. Monograph 144, American Geophysical Union, Washington, DC, 2004), pp. 227–243.
2. M. Tolstoy *et al.*, *Science* **314**, 1920 (2006).
3. R. P. Dziak *et al.*, *Eos* **87**, 37 (2006).
4. www.ridge2000.org
5. S. R. McNutt, in *Encyclopedia of Volcanoes*, H. Sigurdsson, Ed. (Academic Press, San Diego, 2000), pp. 1095–1119.
6. R. M. Haymon *et al.*, *Earth Planet. Sci. Lett.* **119**, 85 (1993).
7. www.pmel.noaa.gov/vents/nemo
8. C. G. Fox, W. W. Chadwick Jr., R. W. Embley, *Nature* **412**, 727 (2001).

10.1126/science.1137082

PHYSICS

Gaps and Our Understanding

A. J. Millis

The binding of electrons in pairs within superconductors gives rise to energy gaps. Two studies of gaps may shed light on mechanisms underlying high-temperature superconductivity.

Superconductivity arises in metals when electrons bind into pairs and the phases of the quantum wave functions that describe the pairs become coherent throughout the solid. The onset of this phase coherence produces the spectacular properties of superconductivity (such as vanishing electrical resistivity) that define the superconducting phase, while pair binding gives rise to an energy gap observable in many spectroscopies. Several recent papers (*1*–*4*), including one by Tanaka *et. al.* on page 1910 (*1*) and one by Valla *et al.* on page 1914 (*2*) of this issue, reveal new aspects of the energy gap structure of high-temperature superconductors and may provide long-sought insights into the mechanism of high-temperature superconductivity.

In conventional superconductors, phase coherence and pair binding go hand in hand. Electrons in a pair are bound together by interaction with quantized lattice vibrations (phonons). The observable consequence of the binding, a spectroscopic gap, appears at (or very close to) the transition temperature T_c at which the resistance vanishes. High-temperature copper oxide–based superconductors, which lose resistance at temperatures up to 150 K, seem different. They are created by doping (adding carriers to) an insulating parent compound (see the figure, top panel), and over wide regions of the phase diagram, spectroscopic evidence of a gap remains long after signatures of phase coherence have vanished (brown region in figure). This has come to be known as the pseudogap; its origin and physical interpretation are fundamental questions in the physics of high-temperature superconductivity.

One broad class of theories can be traced to a paper by Anderson that appeared shortly after the discovery of high-T_c superconductivity (*5*). He argued that the key to high-T_c materials is the parent compound, which is a Mott (or correlation-induced) insulator. The strong electron-electron interactions responsible for the insulating behavior would force the electrons into a paired state, which becomes superconducting once doping allows the carriers to move. In this view the pseudogap is the continuation of the superconducting gap into the non–phase-coherent regime and reflects the intrinsic paired nature of the underlying electronic state. A competing view holds that the key to the high-T_c phenomenon is an instability toward a different, nonsuperconducting phase. Fluctuations that occur near the point of

The author is in the Department of Physics, Columbia University, New York, NY 10027, USA. E-mail: millis@phys.columbia.edu

instability provide the glue leading to pairing (analogously to phonons in conventional materials), but the instability itself competes with superconductivity. In this view, the pseudogap is a manifestation of the new instability. It is not directly related to the superconducting gap, so materials in the pseudogap regime should exhibit two gaps, a small one associated with the superconductivity and a larger one associated with the (as yet unidentified) additional instability.

The question of "one gap or two?" has been with us for years and has eluded resolution. Part of the difficulty in finding an answer is that in the high-temperature superconductors, even the basic superconducting gap has structure. The materials are electronically two-dimensional; conventionally the electrons are considered to be moving in the x-y plane. The pairing symmetry is d-wave, implying an energy gap that vanishes at four or more symmetry-related nodes and is maximal at four antinodes. The standard d-wave gap function is $\Delta(\theta) = \Delta_0 \cos(2\theta)$, where θ is an angle representing the position along the Fermi surface (see the blue solid line in the bottom panel of the figure). Some nonsuperconducting mechanism might produce an energy gap in the antinodal region (solid red line in the bottom panel), leaving a weaker superconducting instability in the remaining portion of the Fermi surface (dotted blue line). From a purely experimental point of view, the issue is to decide between these two gap functions. The task is difficult: Many spectroscopies are sensitive mainly to the maximum value of the gap, or to its average value over the momentum structure. Also, disorder or thermal smearing may smear the gap in the region where it is small, causing a system that has only one gap to appear to have the structure associated with two gaps.

Le Tacon *et al.* (*3*) have used Raman spectroscopy to address the question. By studying the dependence of the scattering cross section on the polarizations of the incident and outgoing photons, they were able to obtain two averages over the momentum dependence of the gap–function; one peaked at the antinodal point and one at the nodal point. Two issues with the Raman measurements in high-T_c materials are that the overall intensities depend on so many factors that they are not knowable in practice, and that there is a large background of unknown (but probably electronic) origin. Le Tacon *et al.* presented a clever analysis (backed up by calculations) that, they argued, allowed them to get around these problems; they concluded that their data favored a two-gap scenario.

Hawthorn *et al.* (*4*) measured the thermal transport at ultralow temperatures. These data allow one to infer the way the gap opens very near to the node. They found that over a wide range of carrier concentrations, their values, when extrapolated away from the node by means of the simple $\cos(2\theta)$ form, lead to antinodal gaps in quantitative agreement with those measured by a wide range of other spectroscopies. Thus, except near the lowest carrier concentration at which superconductivity exists, they concluded that their data favored a one-gap scenario.

The momentum structure of the gap can in principle be directly measured in angle-resolved photoemission experiments, which have yielded much data. In practice the measurements present difficulties of interpretation because thermal smearing and disorder-induced pair breaking broaden the gap function in the near-node region in ways that are still not understood. Tanaka *et al.* overcome some of these difficulties, presenting substantially improved measurements of the gap function. Particularly important are the results for low carrier concentrations, down near the small-p endpoint of the superconducting phase, where they find, even in the superconducting state, a gap function given by the sum of the red and dotted blue curves in the bottom panel of the figure. They thus conclude that at low concentrations there is definitive evidence for two gaps.

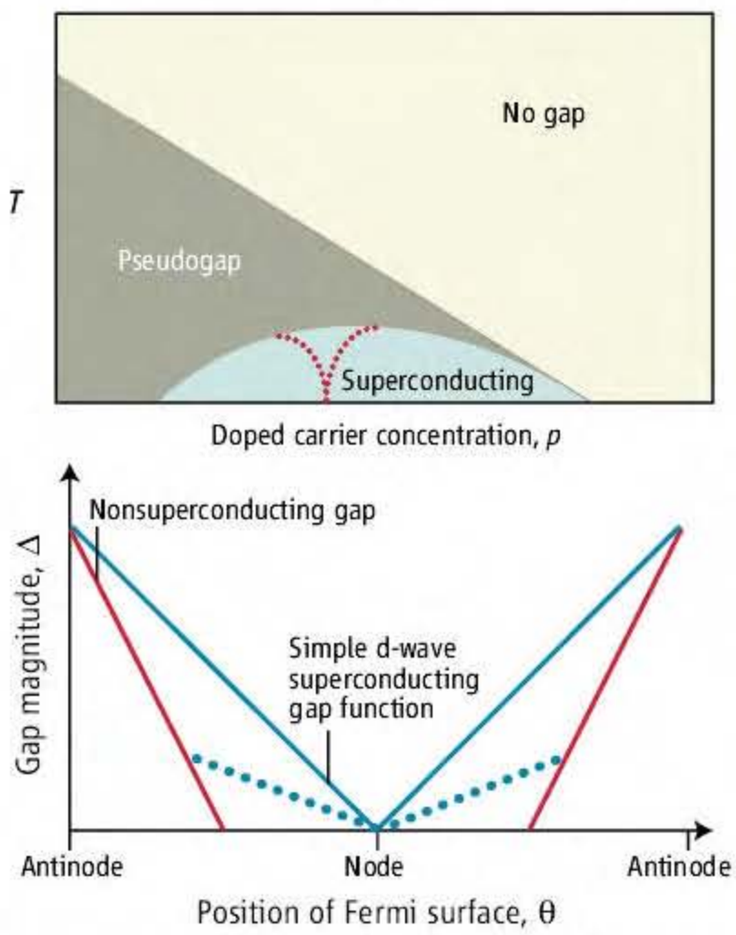

Superconductor phase diagram and gap structures. (**Top**) Schematic high-T_c superconductor phase diagram plotted as function of carrier concentration (p) and temperature (T). The superconducting phase is shown in blue and the pseudogap regime is shown in brown. The red dotted line shows the superconducting phase boundary of the material studies by Valla *et al.* (*2*). (**Bottom**) Gap magnitude Δ around the Fermi surface. Solid blue line: simple d-wave gap function appropriate to one-gap scenario favored by Valla *et al.* (*2*) and Hawthorn *et al.* (*4*); dotted blue line: superconducting gap appropriate to two-gap scenario favored by Tanaka *et al.* (*1*) and Le Tacon *et al.* (*3*). Red line: gap of nonsuperconducting origin.

Valla *et al.* approached the problem differently, using photoemission techniques to study lanthanum barium copper oxide, which at a particular carrier concentration $p = 0.125$ (that is, one-eighth added carrier per unit cell) is not superconducting (see the figure, top panel) but exhibits long-range antiferromagnetic and charge order (*6*). Even at the nonsuperconducting composition, Valla *et al.* find that the electronic spectrum is characterized by a gap that takes essentially the same simple d-wave form and has the same magnitude as at higher carrier concentrations where the superconductivity is robust. Thus, they conclude that there is one gap, even though superconductivity is suppressed by a different instability.

What does the future hold? Different experiments must now be reconciled, which means verifying the consistency of the gap values or tracing differences to variations in sample or to assumptions made in interpreting the data. But Valla *et al.* seem to have discovered a clear example of that much-discussed entity "a new state of matter"—in this case, a paired but nonsuperconducting electronic state that either coexists with antiferromagnetism or is antiferromagnetic itself. Thermal conductivity measurements at low carrier concentrations in which the superconductivity is destroyed by a magnetic field have been interpreted in a similar way (*7*). This novel state is sure to be the focus of extensive study in the near future, and its discovery provides additional impetus for understanding the pseudogap in terms of pairing, and thus additional support for theories based on Anderson's resonating valence bond picture. The results of Tanaka *et al.*, however, suggest that the ultimate fate of superconductivity at low carrier concentrations is destruction by a competing phase. The gaps in our understanding of the high-T_c phenomenon are perhaps slowly closing.

References

1. K. Tanaka *et al.*, *Science* **314**, 1910 (2006); published online 16 November 2006 (10.1126/science.1133411).
2. T. Valla, A. V. Fedorov, J. Lee, J. C. Davis, G. D. Gu, *Science* **314**, 1914 (2006); published online 16 November 2006 (10.1126/science.1134742).
3. M. Le Tacon *et al.*, *Nature Phys.* **2**, 537 (2006).
4. D. G. Hawthorn *et al.*, http://arxiv.org/cond-mat/0502273.
5. P. W. Anderson, *Science* **235**, 1196 (1987).
6. J. M. Tranquada, B. J. Sternlieb, J. D. Axe, Y. Nakamura, S. Uchida, *Nature* **375**, 561 (1995).
7. N. Doiron-Leyraud *et al.*, *Phys. Rev. Lett.* **97**, 207001 (2006).

This work was supported by NSF-DMR-0431350.

10.1126/science.1137173

ELECTION SCIENCE

AAAS Forum: Research, Action Needed to Improve U.S. Elections

With concerns mounting about the integrity of United States elections, AAAS and Carnegie Corporation of New York convened a panel of influential election experts to chart a course of research for improving the voting process.

What emerged from 2 days of meetings in Washington, D.C., was a shared view that elections need a 21st-century makeover—better technology, more training, and a renewed commitment to ballot box access and accuracy. To achieve that, many participants said, researchers and election administrators should collaborate more closely to assess problems and find practical solutions.

Critics say that long lines at polling places sometimes discouraged people from voting in recent elections.

"Experiments are being done, but we have no way to capture the knowledge that is gained in a systematic way," said Shirley Malcom, head of AAAS Education and Human Resources and a member of the commission convened in 2005 by former President Jimmy Carter and former Secretary of State James A. Baker III. "As a result, we're constantly reinventing the wheel—or the flat tire."

The meeting at AAAS "illustrated you can bring a variety of disciplines together to tackle the continuing problems facing the U.S. election system, especially by teaming with those election administrators from the field willing to explore new and better ways to increase voter confidence in the system," said Geri Mannion, chair of Carnegie's Strengthening U.S. Democracy Program. "There are still a lot of challenges, but it's clear there are solutions, if talent and funding can continue to be invested in ensuring that all American voters have the election system they deserve."

The conference came just after U.S. mid-term elections that featured extensive problems, including long lines at polling places, shortages of paper ballots, and mysterious glitches in high-tech electronic voting machines. A post-election *New York Times* review [26 November 2006] found that such problems affected tens of thousands of voters in more than 25 states.

The conference, held at AAAS on 27 and 28 November, featured 40 policy-makers, election administrators, scholars, and activists, including Utah Lt. Gov. Gary Herbert. It was organized by Mark S. Frankel, director of the AAAS Scientific Freedom, Responsibility and Law Program.

Dana DeBeauvoir, left, and Shirley Malcom

The conference was a sequel to a 2004 forum at AAAS at which 18 experts called for a crash course of study and reform to make results more reliable and to promote better access by voters, especially those who historically have encountered impediments to voting.

This year, too, the participants discussed specific problems that plague voting at every step of the process—arcane election laws, anomalies in voter registration databases, long lines at polling places, confusing ballot designs, and inaccurate vote counts.

But another, less obvious, theme was persistent: Researchers are frustrated that they are unable to gain access to useful election data, and election administrators often feel undermined by critical research that fails to account for real-world limitations.

"There is a big gulf right now between practitioners and voters and researchers," said Dana DeBeauvoir, the elected clerk of Travis County, Texas, who has served as an election monitor in South Africa and Bosnia. "Are we working on improvement in the voting system, which is what our goal is? Researchers' goals are publishing and advancing the field."

Thad Hall, a voting scholar at the University of Utah, acknowledged that narrowly focused research, without context, can exaggerate problems. But, he added, election officials may be sensitive even to accurate criticism. "They have an interest in promoting trust and confidence," Hall said, "and they don't want to do things that diminish that."

An initiative in Colorado's Larimer County offered a possible model of positive collaboration between election administrators and researchers.

Responding to the 2002 passage of the Help America Vote Act, Larimer pioneered the use of "vote centers," said County Clerk Scott Doyle. The county committed to voter education, then opened easy-access, electronically linked sites at which voters from any precinct could go to cast ballots. Researchers from Rice University in Texas followed up with a study of this year's election in Colorado, finding that the centers get high marks from voters and may help attract some who otherwise might not vote.

Many of the experts agreed that means are available now to improve voting, but that research is needed to help persuade elected officials and policy-makers to back reform and pay for it.

CREDIT: GETTY IMAGES

ANNUAL MEETING

See the Stars of Science

The 173rd AAAS Annual Meeting convenes in San Francisco 15 to 19 February with a program that features fascinating symposia and lectures and accomplished researchers from across the fields of science, technology, and policy.

The theme of the meeting is "Science and Technology for Sustainable Well-Being." Among the plenary speakers will be Susan Solomon, co-chair of the working group that is assessing the scientific basis of climate change for the Intergovernmental Panel on Climate Change. Other plenaries will be delivered by Steven Chu, a Nobel laureate in physics, and Larry Page, co-founder of Google.

Family Science Days, the free annual event for children and their parents, will feature Adam Savage and Jamie Hyneman, hosts of the popular "MythBusters" program on the Discovery Channel.

To find out more and to register, visit www.aaasmeeting.org.

Still, a number of critical election issues won't be easily resolved. Participants disagreed on the value of electronic voting machines that have paper trails versus those that don't. Activists criticized voting machine manufacturers, but administrators stressed the need for constructive engagement with them. Malcom, among others, suggested that election administration should strive to be nonpartisan. But these and other issues are ripe for research, and that, participants said, is the value of the meeting.

The day after the meeting at AAAS, officials from Carnegie Corporation of New York and several other private foundations gathered in Washington, D.C., to discuss funding strategies for future election-related research.

Frankel told participants at the AAAS forum that in early 2007 the Association will launch the first-ever searchable, Web-based database on election research. Also, he said, a report summarizing the meeting will be issued early next year.

SCIENCE DIPLOMACY

Chinese Fellowship Winners Headed To San Francisco

Six young Chinese journalists are the winners of the 2007 AAAS Fellowships for Science Reporters in Developing Regions. The award, sponsored by the publisher Elsevier, brings science writers to the AAAS Annual Meeting, where they can cover the latest research and mingle with their fellow science writers from around the world.

This year's winners are Gong Yidong , *China Features;* Wu Chong, *China Daily;* Yanhong Wang, *Xinhua News;* and Guo Kun, *Beijing Times,* along with honorary fellows Ding Yimin, *Xinhua News,* and Jia Hepeng, *China Daily/SciDev.net.*

The Fellowship "gives me a unique opportunity to participate in a marvelous science festival held by one of the largest scientific societies," Wang said, adding that she is especially looking forward to talking with her colleagues in the United States.

This year's Annual Meeting theme, "Science and Technology for Sustainable Well-Being," is "extremely important for China, which is undergoing overwhelming changes," Yidong said.

Chong said news of the Fellowship was "an inspiration to my career" and that it came as a surprise "because I still considered myself too young a reporter to win any prestigious award like this."

The Fellowship pays for travel, lodging, and meals at the San Francisco meeting. Four fellows were chosen from a pool of reporters nominated by their editors at leading Chinese media organizations. The two honorary fellows were chosen in recognition of their excellence in science reporting. William Chang of the U.S. National Science Foundation's Beijing office was the independent judge for the award.

Chang said that open and unbiased news reporting is on the rise in China, "but there is still great room for further improvement. I feel that all the applicants recognized this, and made their best efforts under the present constraints."

The Fellowship winners "will be included in the AAAS writers' family, where they can seek support from this network and help the world community to better understand Chinese science," Chang added.

The program is an important part of AAAS's mission to encourage international scientific dialogue and development, according to Vaughan Turekian, AAAS's chief international officer.

"China is clearly an emerging important place for science, and one key piece of trying to develop a scientific infrastructure is making sure that science journalism is also strong," Turekian said.

The Fellowship is a program of EurekAlert!, AAAS's editorially independent Web site for reporters. Rahman Culver, who works with Karen Yuan to oversee the fellowships, said that past winners have praised the program for its role in connecting reporters in developing countries to a wider audience

The Fellowships were launched in 2004 with a seed grant from the William T. Golden Endowment Fund for Program Innovation, with additional support in 2005 from the Global Alliance for Vaccines & Immunization, The Vaccine Fund, and the Rotavirus Vaccine Program. Past winners include science reporters from Africa, Latin America, and China.

From left, Gong Yidong, Yanhong Wang, and Wu Chong are among winners of the 2007 AAAS Fellowships for Science Reporters in Developing Regions.

"Elsevier would like to help equip science journalists from all over the world with the necessary skills and insights in order to write accurate 'good science' articles that benefit their communities," said Shira Tabachnikoff, the publisher's director of corporate relations.

"Being able to support independent science reporting in China is incredibly meaningful," said Ginger Pinholster, director of AAAS's Office of Public Programs. "In their lifetimes, these promising young journalists will be in a position to tell the story of China's transformation."

Information about this year's Fellowship recipients, including their winning entries, will be posted to EurekAlert!'s Multi-Language Portal at http://www.eurekalert.org/language/.

—Becky Ham

SCIENCE COMMUNICATION

AAAS Names Science Journalism Winners

A compelling story on the current scientific understanding of Alzheimer's disease, a series on the impact of climate change in the American West, and a lively look at efforts to grow a better banana are among the winners of the prestigious 2006 AAAS Science Journalism Awards.

Large Newspaper—(Circulation >100,000): Stacey Burling, *The Philadelphia Inquirer,* for "Probing a Mind for a Cure," 26 February 2006.

Small Newspaper—(Circulation <100,000): Michelle Nijhuis, *High Country News,* for "The Ghosts of Yosemite," 17 October 2005; "Save Our Snow," 6 March 2006; and "Dust and Snow," 29 May 2006.

Magazine: Craig Canine, *Smithsonian,* for "Building a Better Banana," October 2005.

Television: Samuel Fine, Julia Cort, Vincent Liota, Peter Doyle, and Dean Irwin, NOVA scienceNOW, for a program on RNA interference; the chemistry of fuel cells; two wizards of supercomputing; and the fastest moving glacier in the world, 26 July 2005.

Radio: Bruce Gellerman, Steve Curwood, Terry Fitzpatrick, and Chris Ballman, Public Radio International's "Living on Earth" program, for "Some Like it Hot..."; "Cold Fusion: A Heated History"; and "Pebble Bed Technology—Nuclear Promise or Peril?" 30 September 2005.

Online: Larisa Epatko, Leah Clapman, Rich Vary, and Katie Kleinman, "Online NewsHour with Jim Lehrer," for "The 1906 San Francisco Earthquake: 100 Years Later," 20 March 2006.

Children's Science News: Beth Geiger, *Current Science,* for "Fade to White," 6 January 2006.

The awards, which have been given to nearly 400 journalists since the competition began, are sponsored by Johnson & Johnson Pharmaceutical Research & Development, L.L.C. Each category carries a $3,000 award. The winners will pick up their plaques at the AAAS Annual Meeting in San Francisco in February.

—Earl Lane

Ancient Noncoding Elements Conserved in the Human Genome

Byrappa Venkatesh,[1]* Ewen F. Kirkness,[2]* Yong-Hwee Loh,[1] Aaron L. Halpern,[3] Alison P. Lee,[1] Justin Johnson,[3] Nidhi Dandona,[1] Lakshmi D. Viswanathan,[3] Alice Tay,[1] J. Craig Venter,[3] Robert L. Strausberg,[3] Sydney Brenner[1]

Comparisons of the human genome with distantly related vertebrate genomes are valuable for identifying evolutionarily conserved regulatory elements in the human genome. For example, genome-wide comparisons of human with teleost fishes, such as *Fugu* and zebrafish, that diverged from the human lineage about 450 million years (My) ago (*1*) were able to identify a large number of conserved noncoding elements (CNEs). Several of the CNEs were shown to function as tissue-specific enhancers (*2*, *3*). Cartilaginous fishes represent the living group of jawed vertebrates that diverged from the common ancestor of mammals and teleost fishes about 530 My ago (*1*). Here, we report the identification of ancient vertebrate CNEs by comparison of genome sequences of a cartilaginous fish, the elephant shark (*Callorhinchus milii*), with the human genome.

The elephant shark, with its compact genome (Materials and Methods), was recently proposed as a model cartilaginous fish genome (*4*). We generated ~1.4× sequence coverage of the elephant shark genome and compared it with the human genome to identify CNEs with the use of discontiguous MegaBLAST (Materials and Methods). A total of 4782 CNEs associated with 1189 human genes (table S1) were identified. The mean length of CNEs is 210 base pairs (bp), with identity ranging from 71% to 98% (mean = 83%) and a combined length of 1.0 Mb (Table 1). The longest CNE is 937 bp and is found in the second intron of ZNF407 (table S2). We also aligned a representative CNE with orthologous sequences from other vertebrates (fig. S1). BLASTN search (*e*-value cutoff at 1×10^{-5}) of the CNEs against *Ciona*, fruit fly, and nematode worm genomes indicated that nearly all of them (with the exception of six CNEs that show similarity to *Ciona* or fly sequences) are specific to vertebrates. The genes associated with CNEs are statistically enriched for functions such as regulation of transcription, DNA binding, and transcription factor activity ($P = 0$) (table S3). They are also significantly enriched in protein domains such as homeobox; helix-turn-helix motif, lambda-like repressor; and POU ($P < 10^{-32}$, χ^2 analysis) (table S4). A significant number of CNEs identified previously in the human and *Fugu* genomes was also found to be associated with similar genes (*3*). Most of the human-*Fugu* CNEs assayed functioned as enhancers mediating tissue-specific expression (*3*). We predict that most of the human–elephant shark CNEs identified are likely to function as tissue-specific enhancers, influencing the gene regulatory networks in vertebrates.

Given that only 1.4×-coverage sequence of the elephant shark (estimated genome coverage of ~75%) was analyzed, we estimate that the human and elephant shark genomes contain about 6300 CNEs (totaling 1.3 Mb). For comparison, we identified CNEs in the whole-genome sequences of human-*Fugu* and human-zebrafish by using the same protocol used for human–elephant shark comparison (Materials and Methods). Both teleost fishes genomes contain fewer CNEs than the elephant shark gemone. The *Fugu* genome contains a total of 2107 CNEs (totaling 0.38 Mb), whereas the zebrafish genome contains 2838 CNEs (totaling 0.53 Mb) (Table 1). Thus, more than twice as many noncoding sequences are conserved between elephant shark and human genomes compared with those conserved between teleost fishes and human genomes. Comparisons of the top 20 genes associated with elephant shark (table S5), *Fugu* (table S6), and zebrafish (table S7) CNEs show that the same genes are targeted for highly conserved CNEs in these genomes. For example, *NR2F1*, *ARRDC3*, *EBF3*, *FOXP1*, and *FOXP2* contain large numbers of CNEs in all three genomes. However, overall only 652 and 782 genes are associated with human-*Fugu* and human-zebrafish CNEs, respectively, in contrast to 1189 genes associated with human–elephant shark CNEs. Indeed, human–elephant shark CNEs associated with 518 human genes are not identifiable by human–teleost fish comparisons. Thus, the elephant shark genome comparison was able to uncover a large number of ancient regulatory elements in the human genome that could not be identified by comparison with teleost fishes.

Comparative analysis of noncoding regions of the *HoxA* cluster from human, teleost fishes, and horn shark had indicated that the regulatory elements in teleost fishes are more divergent than those in human and horn shark (*5*). Thus, it appears that, even though cartilaginous fishes diverged from the human lineage before teleost fishes, higher proportions of regulatory elements are conserved between cartilaginous fishes and human than between teleost fishes and human. This implies that the regulatory regions of teleost fishes have been evolving faster since their common ancestor diverged from the lineage that led to mammals. The divergent regulatory regions in teleosts may be partly explained by the partitioning of regulatory elements between duplicate gene loci that arose from the fish-specific whole-genome duplication event in the ray-finned fish lineage (*6*, *7*). Teleost fishes, with about 25,000 extant species, are the largest group of vertebrates and exhibit vast diversity in their morphology and adaptations. The accelerated rate of evolution of regulatory regions may be an important factor in the rapid radiation and diversity of teleost fishes. The highly conserved regulatory regions in the elephant shark compared with the divergent regulatory regions in teleosts underscore the importance of the elephant shark as a critical reference vertebrate genome.

Table 1. Human noncoding elements conserved in the elephant shark, *Fugu*, and zebrafish genomes.

CNEs	Human/elephant shark	Human/*Fugu*	Human/zebrafish
Number	4782	2107	2838
Total length (kb)	1003	379	530
Average length (bp)	210	180	187
Maximum length (bp)	937	982	880
Mean identity (range) (%)	83 (71–98)	83 (71–98)	84 (73–99)

References and Notes

1. S. Kumar, S. B. Hedges, *Nature* **392**, 917 (1998).
2. J. T. Shin *et al.*, *Nucleic Acids Res.* **33**, 5437 (2005).
3. A. Woolfe *et al.*, *PLoS Biol.* **3**, e7 (2005).
4. B. Venkatesh, A. Tay, N. Dandona, J. G. Patil, S. Brenner, *Curr. Biol.* **15**, R82 (2005).
5. C. H. Chiu *et al.*, *Proc. Natl. Acad. Sci. U.S.A.* **99**, 5492 (2002).
6. A. Christoffels *et al.*, *Mol. Biol. Evol.* **21**, 1146 (2004).
7. J. Postlethwait, A. Amores, W. Cresko, A. Singer, Y. L. Yan, *Trends Genet.* **20**, 481 (2004).
8. This project was supported by the Agency for Science, Technology, and Research (A*STAR), Singapore. We thank J. G. Patil for help in collecting the elephant shark and the Sanger Institute for making available the zebrafish assembly for comparative analysis. A.P.L. is supported by the A*STAR Graduate Scholarship. B.V. is an adjunct staff of the Department of Pediatrics, Yong Loo Lin School of Medicine, National University of Singapore.

Supporting Online Material

www.sciencemag.org/cgi/content/full/314/5807/1892/DC1
Materials and Methods
Fig. S1
Tables S1 to S7
References

1 June 2006; accepted 27 October 2006
10.1126/science.1130708

[1]Institute of Molecular and Cell Biology, 61 Biopolis Drive, Singapore 138673. [2]Institute for Genomic Research, 9712 Medical Center Drive, Rockville, MD 20850, USA. [3]J. Craig Venter Institute, 9704 Medical Center Drive, Rockville, MD 20850, USA.

*To whom correspondence should be addressed. E-mail: mcbbv@imcb.a-star.edu.sg (B.V.); ekirknes@tigr.org (E.F.K.)

Untemplated Oligoadenylation Promotes Degradation of RISC-Cleaved Transcripts

Fadia Ibrahim,* Jennifer Rohr,* Won-Joong Jeong, Jennifer Hesson, Heriberto Cerutti†

In the best-characterized mechanism of RNA-mediated silencing, small interfering RNAs (siRNAs), incorporated into the RNA-induced silencing complex (RISC), guide the endonucleolytic cleavage of complementary RNAs (*1*). In *Drosophila melanogaster*, these RISC-generated products are eventually degraded by exoribonucleases: Xrn1, a 5′-to-3′ exonuclease, and exosome, a 3′-to-5′ multisubunit exonuclease (*2*). Interestingly, in *Arabidopsis thaliana* and in mammals, an oligouridine or oligoadenine [oligo(U/A)] tail is added to the 5′ RNA fragments resulting from microRNA-directed cleavage (*3*). However, the biological role of this tail remains unclear.

An RNA interference–defective mutant strain of the alga *Chlamydomonas reinhardtii* provided some insight into this process. We had previously generated a strain (Maa7-IR44) that expresses an inverted repeat (IR) homologous to ~60 base pairs (bp) in the 3′ untranslated region (UTR) of the *MAA7* gene (encoding tryptophan synthase β subunit) (fig. S1). In this line, the *MAA7* transcripts are present at reduced quantities compared with the amounts in the nontransgenic wild-type strain (CC-124) (Fig. 1A). In contrast, in a mutant strain, Mut-68, obtained by insertional mutagenesis of Maa7-IR44, we detected increased amounts of the full-length *MAA7* mRNAs and a faint smear of RNA degradation products (Fig. 1A). Unexpectedly, Mut-68 also showed higher quantities of siRNAs than those of the Maa7-IR44 parental strain (Fig. 1B). This result suggested that Mut-68 was deficient in the decay of siRNA-targeted mRNAs.

DNA flanking the tagging plasmid was obtained by polymerase chain reaction (PCR), and Southern blot analyses revealed that Mut-68 contained a deletion at the *MUT68* locus that abolished mRNA expression (Fig. 1A). To confirm that this deletion was responsible for the observed phenotype, we used the *MUT68* coding sequence under the control of *PsaD* (encoding a photosystem I component) regulatory sequences to successfully complement the mutant strain [Fig. 1A, Mut-68(*MUT68*) lines].

The MUT68 protein ($MUT68_p$) belongs to the noncanonical polyadenylate [poly(A)] polymerase family (fig. S1). Two other homologs, *Caenorhabditis elegans* RDE-3 and *Schizosaccharomyces pombe* Cid12, have recently been implicated in siRNA production and/or stabilization (*4*, *5*). However, *Chlamydomonas* Mut-68 is not defective in siRNA production. Thus, we examined whether MUT68p might be responsible for the addition of an oligo(U/A) tail to RISC-generated RNA fragments. By using a reverse transcription PCR (RT-PCR) approach that relies on RNA circularization (*3*), we inspected the 3′ ends of *MAA7* 5′ RNA fragments resulting from siRNA-directed cleavage. The clones from Maa7-IR44 were quite heterogeneous at their 3′ ends, and some terminated before the region of homology to the transgene-produced double-stranded RNA (dsRNA) (Fig. 1C), suggestive of 3′-to-5′ degradation. Interestingly, nearly 45% of the examined clones contained an untemplated oligo(A) tail (Fig. 1D). In contrast, the clones sequenced from Mut-68 ended at fairly discrete sites, and none included untemplated nucleotides (Fig. 1C). The complemented strain, Mut-68(*MUT68*)-3, showed a clonal distribution similar to that of the Maa7-IR44 strain. We also transformed Maa7-IR44 with a second IR transgene designed to suppress the CSL4 exosome subunit to test whether this would result in stabilization of the RISC-generated 5′ RNA products. Indeed, in this strain (Csl4-IR2) most *MAA7* 5′ RNA fragments had very discrete 3′ ends, terminating at two sites within the region of homology to the *MAA7* dsRNA (Fig. 1C and fig. S1).

These results suggest that untemplated oligoadenylation by MUT68p stimulates the degradation of RISC-generated 5′ RNA fragments by a 3′-to-5′ exonuclease, most likely the exosome. This is reminiscent of the proposed role of the Trf4/Air2/Mtr4 polyadenylation complex in the decay of nuclear transcripts in *S. cerevisiae* (*6*). Moreover, MUT68p may also participate in the degradation of siRNAs, because their amounts are increased in Mut-68 and U and/or A addition to small RNAs has been detected in *Arabidopsis* (*7*).

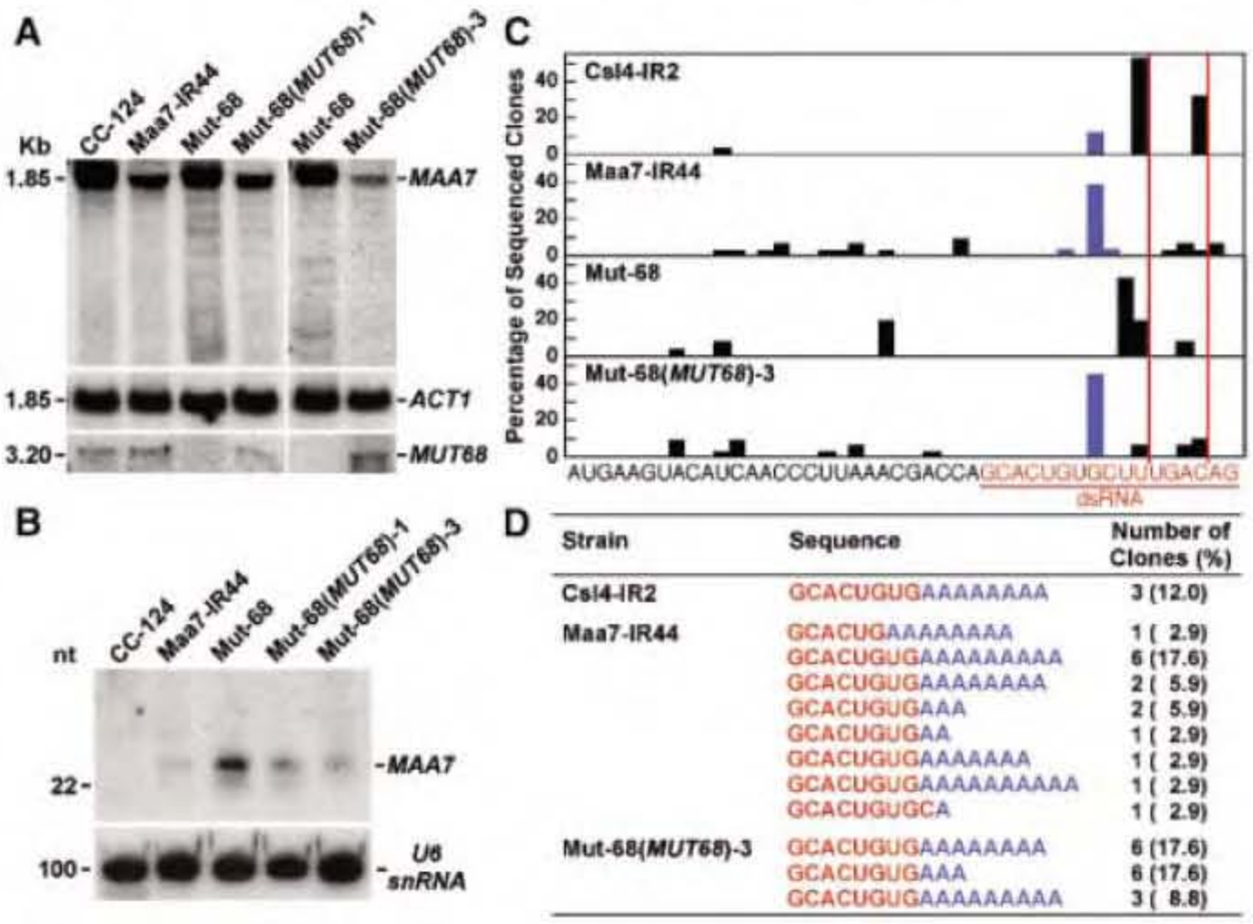

Fig. 1. (**A**) Northern blot analysis of the indicated strains using probes specific for the 5′ end of the *MAA7* coding sequence, the *ACTIN1* 3′ UTR sequence, and the *MUT68* coding sequence. (**B**) Detection of *MAA7* siRNAs by Northern hybridization. nt, nucleotide. (**C**) Frequency of circularized RT-PCR products ending at specific sites within the *MAA7* transcript (fig. S1). Clones containing untemplated adenines are denoted by blue bars, and the sites of RISC-directed cleavage (determined in the *CSL4*-suppressed strain) are shown by vertical red lines. (**D**) Sequence of circularized RT-PCR products displaying nonencoded adenines (blue).

References and Notes

1. P. D. Zamore, B. Haley, *Science* **309**, 1519 (2005).
2. T. I. Orban, E. Izaurralde, *RNA* **11**, 459 (2005).
3. B. Shen, H. M. Goodman, *Science* **306**, 997 (2004).
4. C. C. Chen *et al.*, *Curr. Biol.* **15**, 378 (2005).
5. M. R. Motamedi *et al.*, *Cell* **119**, 789 (2004).
6. J. LaCava *et al.*, *Cell* **121**, 713 (2005).
7. J. Li, Z. Yan, B. Yu, J. Liu, X. Chen, *Curr. Biol.* **15**, 1501 (2005).
8. Supported by NIH (grant GM62915) and NSF (grant MCB-0544448). MUT68 has GenBank accession number DQ989285.

Supporting Online Material

www.sciencemag.org/cgi/content/full/314/5807/1893/DC1
Materials and Methods
Fig. S1

18 September 2006; accepted 4 October 2006
10.1126/science.1135268

Biological Sciences and Plant Science Initiative, University of Nebraska, Lincoln, NE 68588, USA.

*These authors contributed equally to this work.
†To whom correspondence should be addressed. E-mail: hcerutti@unl.edu

The Heartbeat of the Oligocene Climate System

Heiko Pälike,[1*] Richard D. Norris,[2] Jens O. Herrle,[1,3] Paul A. Wilson,[1] Helen K. Coxall,[4] Caroline H. Lear,[4] Nicholas J. Shackleton,[5]† Aradhna K. Tripati,[5] Bridget S. Wade[6]

A 13-million-year continuous record of Oligocene climate from the equatorial Pacific reveals a pronounced "heartbeat" in the global carbon cycle and periodicity of glaciations. This heartbeat consists of 405,000-, 127,000-, and 96,000-year eccentricity cycles and 1.2-million-year obliquity cycles in periodically recurring glacial and carbon cycle events. That climate system response to intricate orbital variations suggests a fundamental interaction of the carbon cycle, solar forcing, and glacial events. Box modeling shows that the interaction of the carbon cycle and solar forcing modulates deep ocean acidity as well as the production and burial of global biomass. The pronounced 405,000-year eccentricity cycle is amplified by the long residence time of carbon in the oceans.

Attempts to understand Quaternary glacial-interglacial changes in ice volume and temperature have shown that the coupling between external forcings, the carbon cycle, atmospheric greenhouse gas concentrations, and glaciations is extremely complex. Nevertheless, records from the past few hundred thousand years indicate that glaciations lag changes in the carbon cycle and orbital forcing (*1*). An insight into the mechanisms that link these three elements of the Earth system is crucial to successfully modeling past and future climates accurately. A good understanding of the carbon cycle response to external forcing requires data series several times longer than the longest orbital variations, which are on the order of millions of years and which we show here are an important feature of climatic records during the Oligocene.

Although geologically older periods experienced the most prominent transient climatic events during the Cenozoic [(the past ~65 million years (My)] (*2*), records and analyses of high enough resolution and fidelity to provide data of astronomically directed climate variations over longer intervals of Earth's history are rare. The Oligocene is of particular interest because it represents an early "icehouse" epoch that is thought to have commenced with the initiation of large ice sheets on Antarctica (*3*), experienced extensive variations of sea level (*4*, *5*), and culminated in a major transient glaciation across the Oligocene-Miocene (O-M) boundary [(~23 million years ago (Ma)] (*6*).

Site 1218 Oligocene stable isotope records. Here we present a high-resolution [5 to 10 cm, ~4-thousand-year (ky) interval)] climate proxy record (*7*–*9*) spanning the entire Oligocene (~23 to 33.9 Ma), incorporating new and recently published (*3*, *5*, *10*, *11*) benthic foraminiferal stable isotope data from Ocean Drilling Program (ODP) Leg 199, Site 1218, equatorial Pacific (8°53.378′N, 135°22.00′W, 4.8-km water depth) (*12*). The 13-My-long record has been astronomically age-calibrated and is used here to explore the influence of Earth's orbital variations on Oligocene climate. In addition, we include previously published stable isotope data from planktonic foraminifera (*5*) and new bulk sediment stable isotope and $CaCO_3$ (*13*) data along a high-resolution composite depth scale (*14*) (fig. S2). The ODP Leg 199 records are complemented by an uninterrupted set of well-defined geomagnetic reversals across the Oligocene, as well as detailed calcareous and siliceous biostratigraphic datum events (*12*, *14*, *15*).

Foraminiferal stable isotope measurements are controlled by a number of processes, including changes in dominant deep-water masses, ocean circulation, and paleoproductivity, which vary between regions. No single site can represent whole ocean conditions; nevertheless, proxy records from the deep Pacific ocean can be regarded as those most closely resembling globally averaged temperature and ice-volume conditions because of the large size of the Pacific reservoir and its isolation from surface temperature variations. The data set from Site 1218 provides a means to tie future records to this high-resolution archive in order to develop a more global proxy record and to further assess the potential role of substantial changes in ocean circulation, for example, in response to opening Southern Ocean gateways and closure of the Tethys Ocean.

The basis of our astronomical age model is a new orbital integration (*16*) that has been shown (*17*) to fit geological data, specifically the past 30 My, better than a previous solution (*18*), by using present-day values for the dissipative Earth model (*19*). Building on the shipboard stratigraphy (*12*), an initial astronomical age model was generated from physical property proxy records reflecting the percentage of $CaCO_3$ contents (*14*). This initial age model was then improved using the stable isotope measurements. The astronomically calibrated age for the O-M boundary [~23 Ma, as recognized in studies of *Sphenolithus delphix* (*20*) and magnetostratigraphy (*21*, *14*)] agrees well with independently calibrated ages for this boundary (*22*–*24*), if adjusted to the new astronomical solution.

Our new single-site Oligocene data set from ODP Site 1218 is presented against astronomical age in Fig. 1. The composite record displays features on temporal scales from thousands to millions of years, chiefly (i) two large-scale glaciation events bracketing the Oligocene, (ii) substantial longer-term (multi-My) secular changes, and (iii) a striking rhythm corresponding to Earth orbital variations, including lead-lag relationships and the time-evolutive behavior of cycle amplitudes. In this study, we use the term "heartbeat of the Oligocene" for three main observations in the data: (i) a persistent 405-ky eccentricity pacing of the carbon cycle as indicated by benthic $\delta^{13}C$, (ii) intervals of recurring "glacial" episodes that broadly follow the ~1.2-My-long amplitude modulation of Earth's obliquity, and (iii) higher-amplitude $\delta^{18}O$ variations during individual short and long eccentricity minima.

Two previously described large transient glaciation events are known as Oi-1 (*4*, *25*) immediately after the Eocene-Oligocene (E-O) boundary (*3*, *26*), and Mi-1 at the O-M boundary (*6*, *22*, *24*, *27*). Under a recent astronomical naming scheme based on the 405-ky cycle of Earth's eccentricity (*5*), these two events correspond to cycles $84_{Eo\text{-}C13n}$ (Oi-1) and $58_{Ol\text{-}C6Cn}$ (Mi-1) (*28*). Within cycle $67_{Ol\text{-}C9n}$, the data show a period of coldest temperatures and/or largest ice volumes during the Oligocene. The transition into the Oligocene icehouse world, represented by a rapid increase in benthic $\delta^{18}O$ and $\delta^{13}C$, commenced around cycle $85_{Eo\text{-}C13r}$. It has been shown to have occurred in a stepwise manner (*3*) and was followed by a ~0.4- to 0.8-My-long recovery phase of decreasing $\delta^{18}O$ and $\delta^{13}C$ to values representative for the early Oligocene. This recovery likely represents a readjustment response of the carbon cycle to the rapid deepening of the oceanic carbonate compensation depth (*3*), well illustrated by bulk (fig. S2) and benthic carbon isotope measurements (Fig. 1C).

At the O-M boundary, we observe an increase of $\delta^{18}O$ values by 0.7 to 0.9 per mil (‰),

[1]National Oceanography Centre, Southampton, School of Ocean and Earth Science, European Way, Southampton SO14 3ZH, UK. [2]Scripps Institution of Oceanography, University of California at San Diego, 308 Vaughn Hall, La Jolla, CA 92093–0244, USA. [3]Department of Earth and Atmospheric Sciences, University of Alberta, 1–26 Earth Sciences Building, Edmonton, AB, T6G 2E3, Canada. [4]School of Earth, Ocean and Planetary Sciences, Cardiff University, Main Building, Park Place, Cardiff CF10 3AT, UK. [5]Department of Earth Sciences, University of Cambridge, Downing Street, Cambridge CB2 3EQ, UK. [6]Institute of Marine and Coastal Science, Rutgers, State University of New Jersey, 71 Dudley Road, New Brunswick, NJ 08901–8521, USA.

*To whom correspondence should be addressed. E-mail: H.Palike@soton.ac.uk

†Deceased (24 January 2006).

comparable with records from other ocean basins, and with similar absolute values as those from the subantarctic Southern Ocean (*22*). Benthic $\delta^{13}C$ increases rapidly during cycle $58_{Oi\text{-}C6Cn}$ (Mi-1) but with a preceding 1- to 2-My trend toward heavier values before the Miocene. Although both transient events, Oi-1 and Mi-1, have clear climatic and paleoceanographic importance (*2*, *3*), the intervening variation and longer-term (multi-My) trends in stable isotope records are of equal interest, and indeed are notable.

The Site 1218 time series show clear oscillations, with typical amplitudes of 0.5 to 1.0‰ in $\delta^{18}O$ and $\delta^{13}C$, at periods related to the Earth's orbital evolution. These oscillations are superimposed on longer term (multi-My) changes throughout the Oligocene that prompt us to recognize at least four distinct phases of the Oligocene (Fig. 1): The first ~2.5 My of the Oligocene (Phase I) are initiated by cycle $84_{Eo\text{-}C13n}$ and constitute the Oi-1 recovery phase. This phase is characterized by a smaller amplitude of Earth's orbital imprint and by the subsequent establishment of longer-term climatic oscillations with a clear 405-ky pattern, typical of the Oligocene, particularly in benthic $\delta^{13}C$, in response to orbital forcing. After the initial 2.5 My of Oligocene time, during Phase II, $\delta^{13}C$ briefly exhibits a minimum of ~0.5‰, followed by a positive excursion and succeeded by a 2-My-long $\delta^{13}C$ decrease to close to 0‰ within cycle $73_{Oi\text{-}C10m}$. During this phase, $\delta^{18}O$ values show increased variability at higher frequencies in the Milankovitch band. Once this pattern is established, the stable isotope variations continue along a similar baseline for a further 2.5 My during Phase III, albeit with strong orbital scale variations, following Earth's 405-ky eccentricity cycle. Within cycle 67, equatorial Pacific benthic $\delta^{18}O$ reaches peak maximum values (*29*). During Phase IV, $\delta^{13}C$ displays high-amplitude 405-ky cyclicity, whereas $\delta^{18}O$ undergoes a distinct longer-term trend toward increasingly light values over ~1.2 to 2.4 My, with peak warmth at this location, or minimum ice volume, around magnetic polarity chron C6Cr. This feature is also shown in data from the equatorial Atlantic (ODP Leg 154, fig. S3). Phase IV culminates with the transient glacial event Mi-1, during cycle $58_{Oi\text{-}C6Cn}$, which marks the onset of a period of strong and rapid early Miocene climate variability (*6*, *22*).

Our carbonate content and mass accumulation rate determinations (fig. S2) partly reflect the evolution of the stable isotope records, for example, the rapid increase of carbonate content across cycle $84_{Eo\text{-}C13n}$ at ~33.9 Ma, a subsequent overshoot (*3*), and maximum carbonate content during the coldest middle Oligocene, within cycle 67. During the middle Oligocene cold phase, $\delta^{18}O$ reaches heavier values than during either the Oi-1 or Mi-1 events. This observation points to two possible scenarios: Either the record at Site 1218 is not a perfect recorder of global carbon cycle dynamics, temperature, and ice volume, or there are additional factors that influence the overall evolution of climate, independent of the detailed orbital configuration, such as weathering patterns, deep water mass reorganization, and tectonic processes.

The pattern of orbital-scale oscillations superimposed on multi-My trends in the Site 1218 stable isotope record reveals an Earth system that appears sensitive to Earth's orbital variations (*3*, *5*, *6*). First, there is a very clear imprint in the benthic isotope series of the long (405 ky) Earth eccentricity variation, particularly in the $\delta^{13}C$ record. Second, the $\delta^{18}O$ record exhibits strong variability at the shorter eccentricity periods (126 and 96 ky). $\delta^{18}O$ also shows correspondence of high isotopic values during periods of low-obliquity amplitude variations, except during cycles 63/64 and 78/79. Oi-1 experiences a temporal delay with respect to low-obliquity amplitude that is presumably related to the initial establishment of large ice volumes on Antarctica. This observation was made previously during the middle Oligocene (*5*) and the Mi-1 event (*6*). The observed pattern correlates the most extreme $\delta^{18}O$ events with low-amplitude obliquity variations (marked in Fig. 1), and minimum eccentricity (a near circular orbit). This pattern is important in that these Oi- glacial events (*4*) have been correlated with sequence stratigraphic studies to estimate magnitudes of eustatic

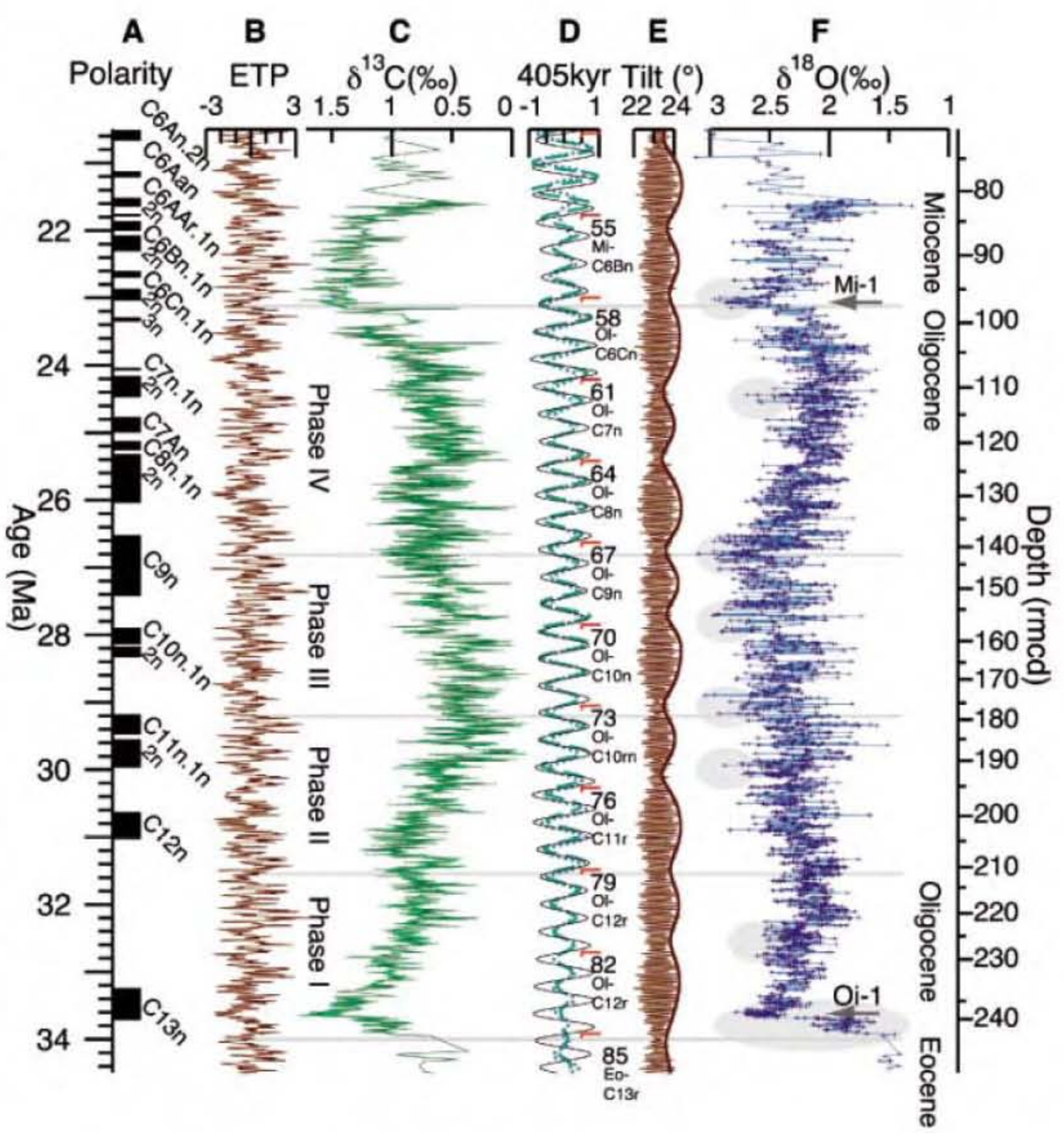

Fig. 1. Oligocene Pacific benthic stable isotope data from ODP Site 1218. (**A**) Astronomically age-calibrated magnetic polarity record for Leg 199, based on (*12*, *14*, *15*, *21*). (**B**) Calculated normalized mix of the orbital parameters eccentricity, obliquity (tilt), and climatic precession [ETP, devised in (*40*)], using (*16*). (**C**) Benthic carbon isotope measurement from foraminiferal calcite. (**D**) Bandpass filtering (*41*) to extract the 405-ky eccentricity component from astronomical eccentricity (solid line), benthic inverted $\delta^{13}C$ isotopes (dashed line), and benthic inverted $\delta^{18}O$ isotopes (dotted line). Values close to −1 mark near-circular orbits (minimum 405-ky eccentricity). Also marked are absolute 405-ky eccentricity cycle numbers, counted from the present, following the naming scheme of (*5*). (**E**) Obliquity, and obliquity amplitude envelope (in degrees), from (*16*). (**F**) Benthic oxygen isotope measurements from foraminiferal calcite, Site 1218. Foraminiferal isotope measurements were adjusted to seawater equilibrium by adding 0.64‰ (*42*). Mi-1 and Oi-1 isotope events (*2*) are indicated along the core depth axis by arrows. Depth values are revised meters composite depth (rmcd) (*14*). Horizontal lines mark long-term Oligocene phases. Gray ellipses mark maximum $\delta^{18}O$ during low obliquity amplitudes.

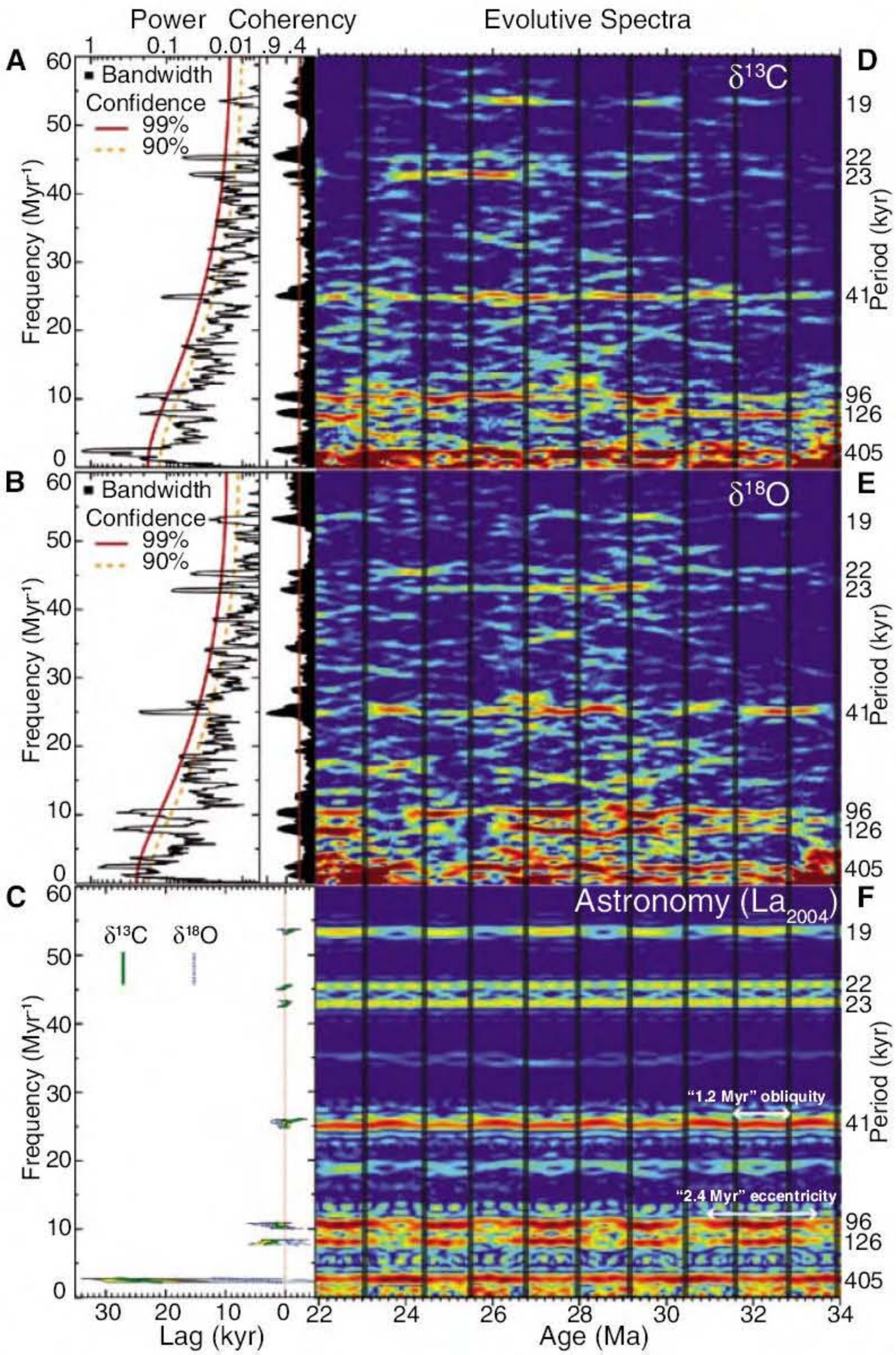

Fig. 2. (**A** and **B**) Log-power spectrum of benthic $\delta^{13}C$ and $\delta^{18}O$ time series, determined by the multitaper method (*43*). Before analysis, records were linearly detrended, and a Gaussian notch filter removed periods longer than ~1 My. The time series was interpolated at the average sample resolution (~5 ky).We show coherency estimates between data and astronomical eccentricity, tilt, and precession mix (ETP), using the Blackman-Tukey method, with 280 lags (10% of series from 20.5 to 34.5 Ma). The 99% (solid) and 90% (dashed) confidence levels are shown. $\delta^{13}C$ shows a relatively stronger signal at the longer eccentricity frequencies. (**C**) Blackman-Tukey cross-spectral phase estimates between stable isotopes and ETP curve, converted to lag times in ky (with 95% confidence intervals) (*39*). For climatic precession, obliquity, and short eccentricity, the phase angles are essentially zero. For long eccentricity (405 ky) periods, there is a relative lag of $-\delta^{13}C$ compared with $-\delta^{18}O$ of ~20 ky. (**D** to **F**) Evolutive multitaper method log-power spectra for $-\delta^{13}C$, $\delta^{18}O$, and astronomical ETP showing the temporal evolution of spectral power throughout the Oligocene. Note the correspondence of amplitude variations (high power with hot colors) for the (96 and 126 ky) eccentricity cycles and $\delta^{18}O$, and between the strong 405-ky eccentricity cycle and the 41-ky obliquity cycle between $\delta^{13}C$ and ETP, supporting previous analysis (*17*). Vertical bars mark obliquity amplitude minima every ~1.2 My (also see fig. S2).

Oligocene sea-level variations (*30*), which our data help to constrain. Our extended time series show that the relationship between astronomical patterns and more extreme Oligocene glaciation periods (*5*) holds throughout most of the Oligocene (Fig. 1), with additional events that do not appear to be correlated to astronomical forcing.

Time series and spectral analysis. Power spectra for $\delta^{18}O$ and $\delta^{13}C$ (Fig. 2) exhibit peaks at astronomical frequencies that are significantly above 99% confidence estimates using a red-noise model. Our results confirm the observation that both time series exhibit strong power at eccentricity periods (405, 126, and 96 ky). $\delta^{13}C$ shows a stronger response at longer periods (405 ky), whereas $\delta^{18}O$ shows more sensitivity at shorter eccentricity periods (96 and 126 ky). Both records also show a significant response at the main obliquity period (41 ky), with a weaker response at the lower-amplitude obliquity periods (29 and 54 ky). Because of its length, our data set allows us to trace intervals carrying a signal of climatic precession with higher statistical significance than has been possible in previous studies (*3*, *6*).

Phase estimates between astronomy and data (Fig. 2C) determine a ~20 ky lag of $\delta^{13}C$ compared to $\delta^{18}O$ for long eccentricity cycles (405 ky), with close to zero lags for other astronomical terms. Phase estimates between $\delta^{13}C$ compared to $\delta^{18}O$ suggest that $\delta^{13}C$ shows increased lag times for correspondingly longer periods, a behavior that we are able to model as part of this study. A similar pattern has been recognized previously in late Oligocene records (*6*, *22*). This observation is compatible with the long residence time of carbon in the oceans [~0.1 My (*31*)] that transfers energy from climatic precession into eccentricity bands through a nonlinear process, resulting in a frequency-dependent phase lag of $\delta^{13}C$.

We also calculated evolutive spectra for $\delta^{13}C$ (Fig. 2D), $\delta^{18}O$ (Fig. 2E), and astronomical time series [Fig. 2F, (*16*)]. Our results reveal a consistent imprint of the eccentricity and obliquity signals in the $\delta^{18}O$ record, following closely the amplitude modulation terms that coincide with most of the Oligocene glacial events (*5*), including events around cycle $58_{Ol\text{-}C6Cn}$ (~23 Ma) (*6*). The ~2.4-My modulation of the 96- and 126-ky eccentricity cycles is notably similar in the astronomy and in $\delta^{18}O$. All three precession frequencies intermittently appear in the evolutive spectra, and for $\delta^{18}O$ the 19-ky amplitude variation follows the predictions of calculated eccentricity. The strength of the climatic precession traces are at least partially related to higher sedimentation rates, with more consistent responses where sample resolution is higher, mostly ~24 to 27 Ma. However, during the earliest part of the record (*3*), the response to climatic precession is weak, despite higher mass accumulation rates that occurred after the dramatic shift in the depth of carbonate compensation (*3*, *32*).

Box modeling results. A previous modeling study that focused on the E-O transition found that an imposed astronomical forcing has a considerable effect on the Earth's climate system (*33*). Loutre *et al.* (*34*) demonstrate that climatic precession and obliquity are the dominant astronomical periods in insolation calculations that use the traditional Milankovitch summer insolation hypothesis, with only a very minor contribution by Earth's eccentricity periods. Our data for the Oligocene, in contrast, exhibit an unexpectedly strong ~405-ky signal in $\delta^{13}C$ as well as in the carbonate flux. The mismatch between the strongest periodicities in most insolation calculations and the climate system response recorded in our data prompt us to evaluate the response of the carbon cycle to astronomical climate forcing. We do this by using a suite of carbon cycle box models, with the aim to gain a better understanding of how astronomical forcing terms are transferred through the carbon cycle. We modified two previously published carbon cycle box models of varying complexity [Model A (*35*); Model B (*36*)] and combined them with astronomical forcing time series to investigate whether we can qualitatively explain basic features of our data (*37*).

By first applying a white-noise signal as forcing input, we established that fundamental properties of both models are the preferential amplification of lower-frequency components and the attenuation of higher-frequency components, resulting in a red-noise transfer function from model input to output (*37*). In the models used, sea-level variations influence the weathering of silicate rocks directly by changing the land area available for weathering on Antarctica and indirectly through the change of carbonate ion concentration. We currently do not model the influence of sea-level on basin-to-shelf fractionation (*38*) and the deposition of carbonate on shallow shelf areas directly. This process would exert additional positive feedback between sea level and the carbon cycle.

Figure 3 shows the model response to astronomical forcings that are dominated by climatic precession and obliquity. We found that applying astronomical forcing terms to globally averaged temperature alone does not result in a response of both $\delta^{18}O$ and $\delta^{13}C$, as observed in our data. Yet, a good match between model output and our data is achieved by also applying astronomical forcing to key components of the carbon cycle. Specifically, we force the effective solar constant in the model by simultaneously applying scaled annual and boreal (65°N) summer orbital insolation changes. The actual temperature is then calculated as a function of both solar constant and carbon dioxide concentration. Here we use 65°N summer insolation to obtain a representative model response for a larger suite of possible insolation forcings (*34*). The same result could have been achieved by applying a seasonal insolation curve from lower latitudes with a smaller obliquity imprint. For the carbon cycle, we use seasonal insolation to modulate the downward flux of particulate organic matter (loosely termed "productivity"); during warmer climates, this downward flux is reduced.

By forcing both global annual temperature and carbon burial in the model of (*35*) by a synthetic insolation curve, we are able to reproduce the strong ~405-ky cyclicity seen in our $\delta^{13}C$ data. Interestingly, some of our model configurations show that by imposing a gradual decrease in atmospheric CO_2 levels some time before the E-O transition, similar to (*33*), we obtain a rapid onset of glaciation at the time that it is observed in our records. We find that onset of glaciation is independent of the exact timing of CO_2 reduction and is triggered by astronomical forcing as soon as atmospheric CO_2 levels are close to a threshold value. Our model results therefore confirm the view (*33*) that a decrease in atmospheric CO_2 is a possible mechanism to explain the record across the E-O transition.

Within the astronomically driven carbon cycle we also investigated the possible response of the oceanic carbonate ion (CO_3^{2-}) concentration by combining astronomical forcing terms with the more sophisticated model of (*36*), which includes individual representations of the Atlantic, Indian, and Pacific deep oceans, the thermocline, surface waters, and carbon reservoirs. In this case, we forced global temperature by the annual and mean monthly summer insolation (65°N) and carbon burial by mean monthly summer insolation (Fig. 3C). We are able to reproduce a strong eccentricity-driven response in the modeled lysocline depth (Fig. 3D) from a forcing term that is dominated by climatic precession. The model output matches the first-order features of our sedimentary $CaCO_3$ content record, which we interpret as a proxy for lysocline depth variations on orbital time scales.

Global carbon cycle implications. Earth seems to "breathe" on time scales ranging from the annual to the orbital. We hypothesize that in all cases these cycles are driven by the expansion and contraction of biosphere productivity in response to changes in solar insolation. Our modeling studies show that the main reasons for the strength of the 405-ky cycle in the carbon isotope data appear to be the long residence time of carbon in the oceans amplifying longer forcing periods, as well as a smaller contribution attributable to the dampening effects of dissolution of sea-floor carbonate on the shorter-term forcing. In addition, we find that applying astronomical forcing to key variables of the carbon cycle, rather than to temperature alone, is necessary to model the principal features of our data set, adding strength to the view (*1*) that the effect of orbital forcing is imprinted upon paleoclimatic records through an influence on the carbon cycle as well as temperature.

References and Notes

1. N. J. Shackleton, *Science* **289**, 1897 (2000).
2. J. C. Zachos, M. Pagani, L. Sloan, E. Thomas, K. Billups, *Science* **292**, 686 (2001).
3. H. K. Coxall, P. A. Wilson, H. Pälike, C. H. Lear, J. Backman, *Nature* **433**, 53 (2005).

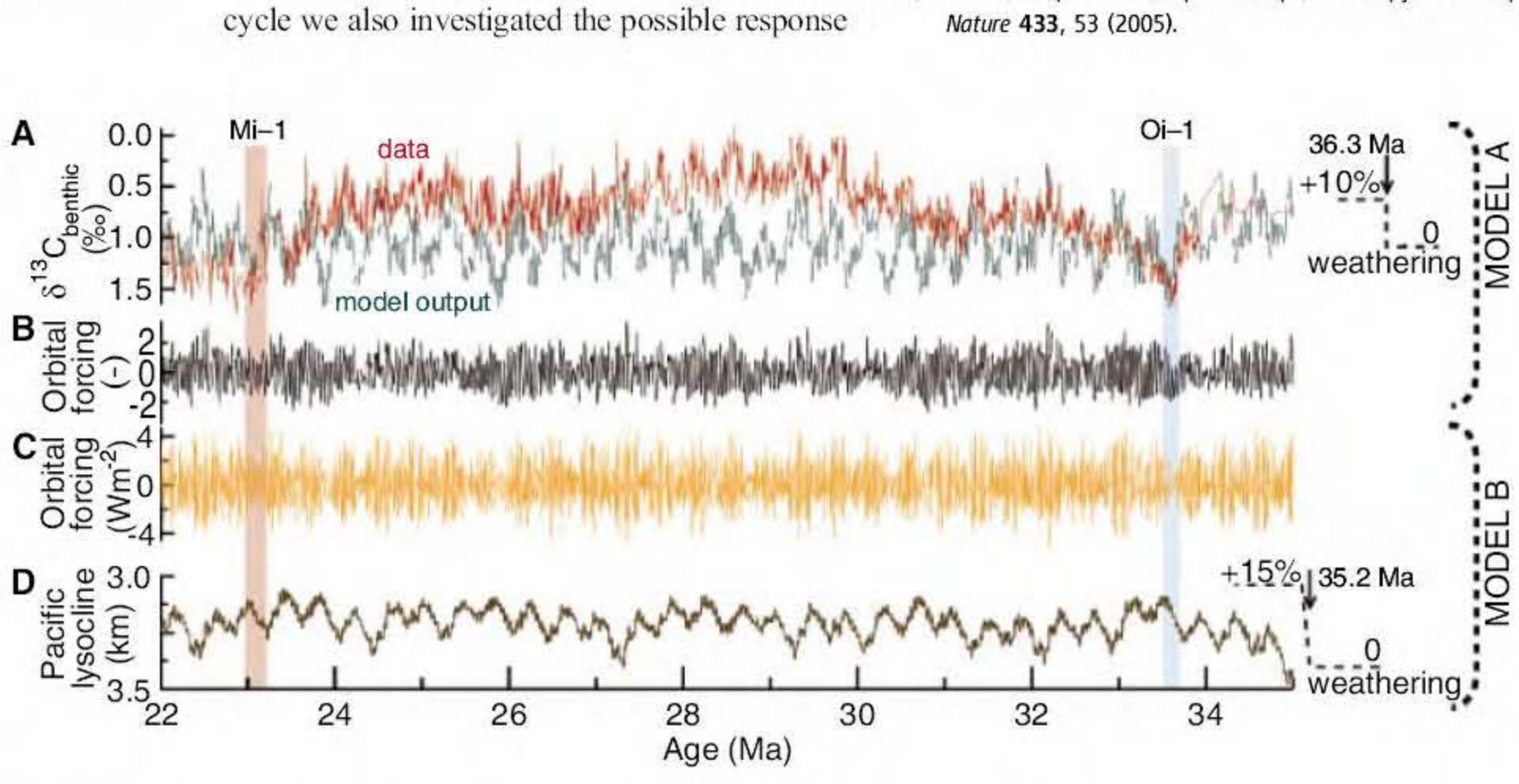

Fig. 3. (**A** and **B**) Model A, adapted from (*35*). (**C** and **D**) Model B, adapted from (*35*, *36*). Ages and step functions on right side illustrate change in silicate weathering applied to both models to simulate the onset of the Oligocene icehouse. (A) $\delta^{13}C$ data and model A output. Note the close correspondence between model and data at the 405-ky eccentricity period. (B) Orbital forcing applied to Model A. This forcing is dominated by obliquity, with smaller contributions from eccentricity and climatic precession. (C) Main summer insolation (65°N, June and July) forcing applied to Model B. (D) Pacific lysocline depth variations from Model B. Note strong 405-ky cyclicity compared with forcing (C).

4. K. G. Miller, J. D. Wright, R. G. Fairbanks, *J. Geophys. Res. Sol. Earth Planets* **96**, 6829 (1991).
5. B. S. Wade, H. Pälike, *Paleoceanography* **19**, PA4019 (2004).
6. J. C. Zachos, N. J. Shackleton, J. S. Revenaugh, H. Pälike, B. P. Flower, *Science* **292**, 274 (2001).
7. Our detailed Oligocene Pacific data set is available in electronic form at a designated data repository (www.pangaea.de). Accession codes are http://doi.pangaea.de/10.1594/PANGAEA.547942, http://doi.pangaea.de/10.1594/PANGAEA.547798, and http://doi.pangaea.de/10.1594/PANGAEA.547800.
8. Data were generated in five laboratories. A lower-resolution record across the entire interval (*10*) shows that there are no discernible interlaboratory offsets.
9. Methods are available as supporting material on *Science* Online.
10. C. H. Lear, Y. Rosenthal, H. K. Coxall, P. A. Wilson, *Paleoceanography* **19**, PA4015 (2004).
11. A. Tripati, H. Elderfield, L. Booth, J. Zachos, P. Ferretti, *Sci. Res., Proc. Ocean Drill. Prog.* (Ocean Drilling Program, College Station, TX, 2006), vol. 199.
12. M. Lyle *et al.*, *Init. Rep., Proc. Ocean Drill. Prog.* (Ocean Drilling Program, College Station, TX, 2002), vol. 199.
13. Measured $CaCO_3$ content was used to calibrate calculated $CaCO_3$ from physical property measurements (*12*).
14. H. Pälike *et al.*, *Sci. Res., Proc. Ocean Drill. Prog.* (Ocean Drilling Program, College Station, TX, 2005), vol. 199.
15. L. Lanci, J. M. Parés, J. E. T. Channell, D. V. Kent, *Earth Planet. Sci. Lett.* **237**, 617 (2005).
16. J. Laskar *et al.*, *Astron. Astrophys.* **428**, 261 (2004).
17. H. Pälike, J. Laskar, N. J. Shackleton, *Geology* **32**, 929 (2004).
18. J. Laskar, F. Joutel, F. Boudin, *Astron. Astrophys.* **270**, 522 (1993).
19. H. Pälike, N. J. Shackleton, *Earth Planet. Sci. Lett.* **182**, 1 (2000).
20. I. Raffi, *Phil. Trans. R. Soc. London Ser. A* **357**, 1975 (1999).
21. L. Lanci, J. M. Parés, J. E. T. Channell, D. V. Kent, *Earth Planet. Sci. Lett.* **226**, 207 (2004).
22. K. Billups, H. Pälike, J. E. T. Channell, J. C. Zachos, N. J. Shackleton, *Earth Planet. Sci. Lett.* **224**, 33 (2004).
23. N. J. Shackleton, M. A. Hall, I. Raffi, L. Tauxe, J. Zachos, *Geology* **28**, 447 (2000).
24. H. Pälike, J. Frazier, J. C. Zachos, *Quat. Sci. Rev.*, in press; available online at http://dx.doi.org/10.1016/j.quascirev.2006.02.001.
25. J. P. Kennett, N. J. Shackleton, *Nature* **260**, 513 (1976).
26. J. C. Zachos, T. M. Quinn, K. A. Salamy, *Paleoceanography* **11**, 251 (1996).
27. H. A. Paul, J. C. Zachos, B. P. Flower, A. Tripati, *Paleoceanography* **15**, 471 (2000).
28. The cycle naming scheme (*5*) incorporates the 405-ky cycle number, the geological epoch, and the nearest magnetic polarity chron.
29. S. Van Simaeys, H. Brinkhuis, J. Pross, G. L. Williams, J. C. Zachos, *Geology* **33**, 709 (2005).
30. S. F. Pekar, N. Christie-Blick, M. A. Kominz, K. G. Miller, *Geology* **30**, 903 (2002).
31. W. S. Broecker, T.-H. Peng, *Tracers in the Sea* (LDGO Press, Palisades, NY, 1982).
32. T. H. van Andel, *Earth Planet. Sci. Lett.* **26**, 187 (1975).
33. R. M. DeConto, D. Pollard, *Nature* **421**, 245 (2003).
34. M. F. Loutre, D. Paillard, F. Vimeux, E. Cortijo, *Earth Planet. Sci. Lett.* **221**, 1 (2004).
35. J. C. Zachos, L. R. Kump, *Global Planet. Change* **47**, 51 (2005).
36. J. C. G. Walker, J. F. Kasting, *Palaeogeogr. Palaeoclimatol. Palaeoecol.* **97**, 151 (1992).
37. A description of the modified model equations can be found in (*9*).
38. B. N. Opdyke, J. C. G. Walker, *Geology* **20**, 733 (1992).
39. D. Paillard, L. Labeyrie, P. Yiou, *EOS Transactions AGU* **77**, 379 (1996).
40. J. Imbrie *et al.*, *Milankovitch and Climate, Part 1*, A. L. Berger, *et al.*, Eds. (Reidel, 1984), pp. 269–305.
41. The central bandpass frequency was 2.5 My^{-1}, with a bandwidth of ±0.5 My^{-1}. Filtering was performed using (*39*).
42. N. J. Shackleton, N. D. Opdyke, *Quat. Res.* **3**, 39 (1973).
43. M. Ghil *et al.*, *Rev. Geophys.* **40**, 3.1 (2002).

44. This research used samples and data provided by the Ocean Drilling Program (ODP). ODP is sponsored by the U.S. National Science Foundation (NSF) and participating countries under the management of Joint Oceanographic Institutions (JOI), Inc. We thank the crew and shipboard scientists of ODP Leg 199, particularly I. Raffi and J. Backman for their biostratigraphy work. We thank L. Kump, J. Zachos, J. Walker, and J. Kasting for providing code and information for their models.

Supporting Online Material

www.sciencemag.org/cgi/content/full/314/5807/1894/DC1

Methods
SOM Text
Figs. S1 to S3
Tables S4 to S6
References

14 August 2006; accepted 6 November 2006
10.1126/science.1133822

Epochal Evolution Shapes the Phylodynamics of Interpandemic Influenza A (H3N2) in Humans

Katia Koelle,[1,2]*† Sarah Cobey,[1]† Bryan Grenfell,[2,3] Mercedes Pascual[1]

Human influenza A (subtype H3N2) is characterized genetically by the limited standing diversity of its hemagglutinin and antigenically by clusters that emerge and replace each other within 2 to 8 years. By introducing an epidemiological model that allows for differences between the genetic and antigenic properties of the virus's hemagglutinin, we show that these patterns can arise from cluster-specific immunity alone. Central to the formulation is a genotype-to-phenotype mapping, based on neutral networks, with antigenic phenotypes, not genotypes, determining the degree of strain cross-immunity. The model parsimoniously explains well-known, as well as previously unremarked, features of interpandemic influenza dynamics and evolution. It captures the observed boom-and-bust pattern of viral evolution, with periods of antigenic stasis during which genetic diversity grows, and with episodic contraction of this diversity during cluster transitions.

Interpandemic influenza causes substantial morbidity and mortality in humans. Annual winter epidemics yield cumulative attack rates between 10 and 20% for influenza A (subtypes H3N2 and H1N1), and influenza B infections (*1*) and contribute heavily to deaths caused by respiratory infections worldwide. The virus is capable of evading immune recognition through continual antigenic drift of its surface glycoproteins, hemagglutinin (HA) and neuraminidase (NA), complicating long-term control of the disease through vaccination (*2*). An understanding of the ecological and immunological processes driving influenza dynamics and evolution is therefore critical for anticipating and ultimately mitigating the effect of this infectious disease. Here we focus on the phylodynamics (*3*) of H3N2, which has been present worldwide since its pandemic appearance in 1968.

One of the most striking characteristics of influenza A evolution is the limited standing diversity of the HA gene, despite the virus's high mutation rate. This limited diversity is evident in its phylogeny: The tree consists of a long trunk with short side branches that are indicative of high extinction rates of the lineages (*4*) (Fig. 1A). Epidemiological factors that contribute to this pattern include the short infectious period of the host and partial cross-immunity between similar strains (*3*). However, the most detailed model of interpandemic influenza to date suggests that these factors alone cannot account for limited diversity and that temporary strain-transcendent (generalized) immunity is necessary to restrict diversity (*5*).

More recently, differences between the genetic and antigenic evolution of the H3N2 virus's HA glycoprotein have been highlighted (*6*). A key unexplained pattern is that, although genetic change is gradual, antigenic change is punctuated. HA inhibition (HI) assays show that H3N2 sequences fall into groups, or clusters, with unique antigenic properties. Between 1968 and 2003, these clusters emerged and replaced each other within 2 to 8 years, exerting a major influence on vaccine strategy (*2*). Empirical evidence suggests that there is almost complete immunity between strains within a cluster (*7*). In contrast, cross-immunity is as low as 60 to 85% between clusters adjacent in time (*7*, *8*) and is undetectable between temporally distant clus-

[1]Department of Ecology and Evolutionary Biology, 2019 Kraus Natural Science Building, University of Michigan, 830 North University Avenue, Ann Arbor, MI 48109-1048, USA. [2]Center for Infectious Disease Dynamics (CIDD), Department of Biology, 208 Mueller Lab, Eberly College of Science, The Pennsylvania State University (PSU), University Park, PA 16802, USA. [3]Fogarty International Center, National Institutes of Health, Bethesda, MD 20892, USA.

*To whom correspondence should be addressed. E-mail: kkoelle@psu.edu
†These authors contributed equally to this work.

ters (*9*). A time series of influenza-related deaths highlights the importance of clusters and the timing of their transitions: Anomalously high mortality rates accompany cluster transitions (*10*, *11*) (Fig. 1B).

Here we present a model that offers an explanation for both limited HA diversity and punctuated antigenic changes. It is a phylodynamic model, in that it simulates the interaction of epidemiological dynamics and pathogen evolution using a single underlying framework (*3*). Unlike previous models that focus on individual strains [e.g. (*5*, *12*)], our model emphasizes the concept of clusters. We first looked at the genetic sequences analyzed by Smith and coauthors (*6*) by cluster designation (Fig. 1C). Within a cluster, the HA sequences can differ by a substantial number of amino acids while retaining their antigenic similarity. For example, two sequences in the HK68 cluster differ by 19 amino acids. Furthermore, transitions between clusters, and therefore large changes in antigenic properties, can result from as few as one amino acid change (as in the case of the SI87 to BE89 and the BE92 to WU95 cluster transitions).

Traditional multistrain disease models (including those for influenza) directly relate the degree of cross-immunity between strains to the distances between their sequences. Distance metrics often employ the Hamming distance between two strain sequences, and they are used in both bit-string models (with alleles 0 or 1 at each locus) (*13*, *14*) and in more realistic models of amino acid evolution (*5*). By design, distance metrics set the degree of cross-immunity high between strains with high sequence similarity and low between strains with low sequence similarity. However, these distance metrics are incongruent with observations of cross-immunity between influenza clusters (Fig. 1C). They cannot provide a framework in which a single amino acid change can markedly release a strain from population-level host immunity and in which 19 changes can have little antigenic effect.

Although it may be argued that amino acid changes that precipitate cluster jumps occur at key influential sites, a closer investigation of the substitutions associated with cluster transitions suggests that few sites fit this model. Of the 43 sites associated with cluster transitions, 35 also exhibited some degree of neutral polymorphism (*6*). (We categorize a site as carrying some degree of neutral polymorphism if the site exhibits any variation in amino acid use within at least one cluster.) In the remaining eight sites, substitutions were always accompanied by cluster transitions (table S1); however, these sites could not account for every transition. Four transitions were associated only with sites capable of showing neutral polymorphism. Site-directed mutagenesis of strains belonging to different clusters also showed that identical substitutions can have different effects on hemadsorption, depending on differences in local structure (*15*). Thus, a model of invariably influential and neutral sites is unlikely to generate a realistic topology.

Neutral networks map genetic-to-antigenic change. We therefore take an alternative approach for modeling cross-immunity–one in which phenotype is determined by a context-dependent interaction of amino acids. Every amino acid site in an epitope is potentially important. Whether an amino acid replacement in a site precipitates a cluster jump is determined

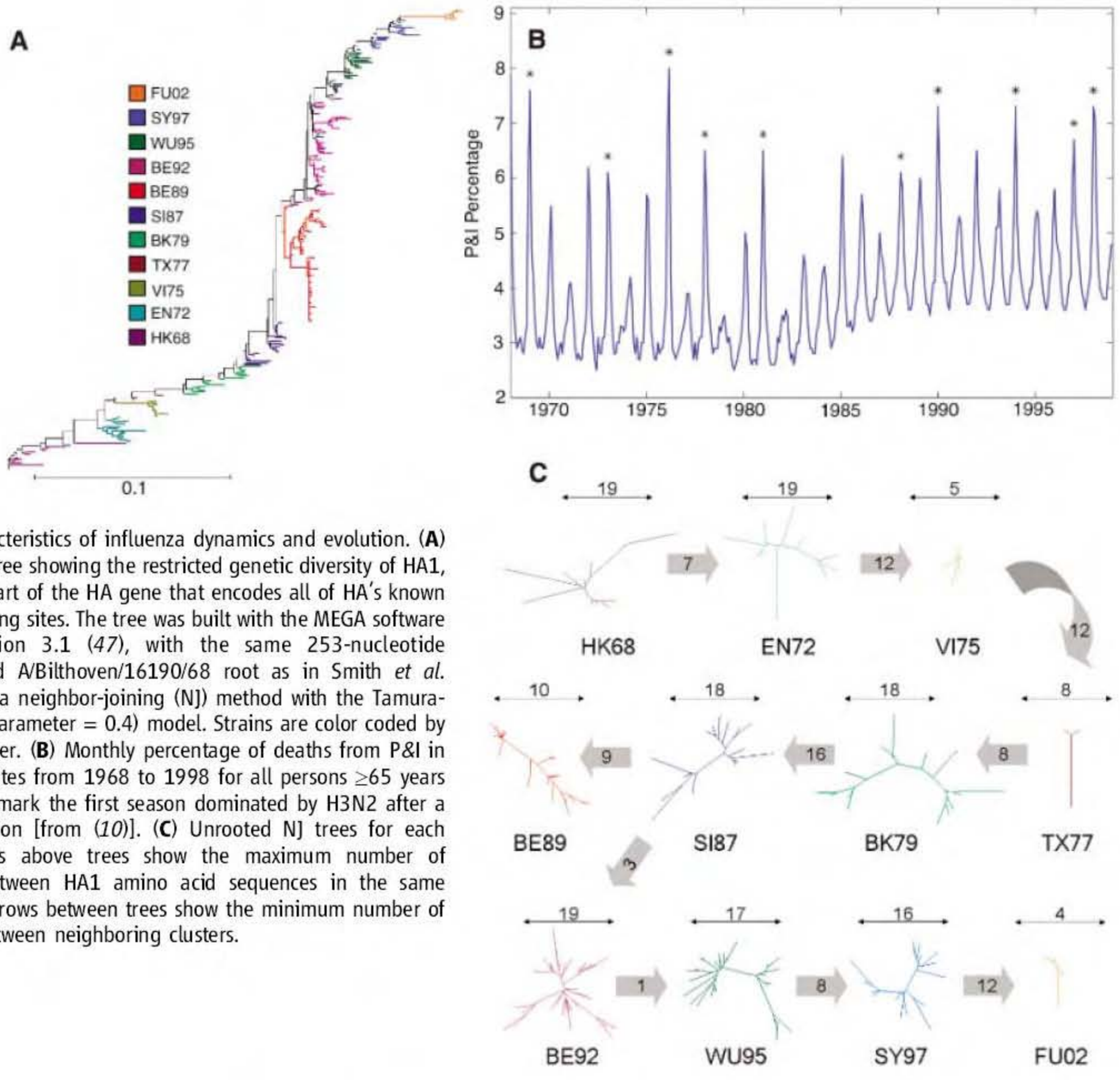

Fig. 1. Characteristics of influenza dynamics and evolution. (**A**) Phylogenetic tree showing the restricted genetic diversity of HA1, which is the part of the HA gene that encodes all of HA's known antibody binding sites. The tree was built with the MEGA software package version 3.1 (*47*), with the same 253-nucleotide sequences and A/Bilthoven/16190/68 root as in Smith *et al.* (2004), using a neighbor-joining (NJ) method with the Tamura-Nei (gamma parameter = 0.4) model. Strains are color coded by antigenic cluster. (**B**) Monthly percentage of deaths from P&I in the United States from 1968 to 1998 for all persons ≥65 years old. Asterisks mark the first season dominated by H3N2 after a cluster transition [from (*10*)]. (**C**) Unrooted NJ trees for each cluster. Arrows above trees show the maximum number of differences between HA1 amino acid sequences in the same cluster, and arrows between trees show the minimum number of differences between neighboring clusters.

not only by the change at that site, but also by the genetic background in which the change is made. Epitope structure is thus mediated through high-level interactions between the amino acids of a HA sequence. Extensive theoretical and empirical studies have focused on understanding protein genotype-to-phenotype mapping in light of these interactions. These studies have shown that sequence space is inhabited by "neutral networks" (*16*–*20*). Neutral networks for proteins are defined as sets of amino acid sequences (of length L) that are connected by one-mutation neighbors and map into the same conformation. The number of sequences folding into the same conformation varies, with the size distribution of the conformational sets consisting of many rare shapes and only a few highly designable, or frequent, shapes (*21*). The presence of an underlying neutral network topology affects evolutionary dynamics on the phenotype landscape: In simulations where an optimal shape (phenotype) is defined exogenously, an initial phenotype will evolve toward this target shape in punctuated steps (*22*, *23*). During the periods of phenotypic stasis separating the punctuated shape changes, sequences diffuse through genotype space along neutral or almost neutral networks (*24*, *25*). This diffusion is critical for gaining access to adjacent networks that enable more dramatic phenotypic change (*22*, *26*). The stepwise emergence of these phenotypic innovations, guided by the process of neutral diffusion, has been termed epochal evolution (*27*, *28*).

We can now interpret influenza clusters in terms of neutral networks (Fig. 1C). Within each cluster, strains have similar conformations of their HA epitopes; host antibodies are thus more likely to recognize these strains as antigenically equivalent, and strain cross-immunity is close to complete. These strains can therefore be classified as belonging to a set of neutral networks with similar antigenic phenotypes. Sharply reduced cross-immunity between influenza clusters arises from antigenic escape by the HA protein and is precipitated by amino acid substitutions that substantially change the structure of one or more epitopes.

Dynamical consequences of the genetic-antigenic map. To determine the effect of this genotype topology on the dynamics and evolution of influenza, we modeled the disease by coupling an epidemiological transmission model to a genotype-phenotype (GP) model that implements neutral networks. The GP model is used to map strains, or genotypes, into antigenic phenotypes. To this end, we extended a simple model that allows for a tunable degree of neutrality (*29*, *30*). It is a generalization of the NK fitness-landscape model, which allows epistatic interactions between loci to affect fitness (*31*).

We modeled influenza's HA as five distinct epitopes, with each epitope represented by a separate GP map (*32*). At a given epitope, amino acids interact with a small number of their neighbors [$K = 1$, where K is the degree of epistasis or context dependency] to determine the epitope's overall shape. This level of context dependency captures the size distribution of the neutral networks seen in lattice models of protein folding (*21*) (Fig. 2A). Our genetic-antigenic map for HA assumes statistical properties of cross-immunity between strains that are one amino acid apart (Fig. 2B). Specifically, point mutations resulting in an amino acid replacement in an epitope belong to one of three types. Mutations are neutral (100% cross-immunity) if the epitope in which the replacement occurs does not change its conformation. This occurs when the two sequences belong to the same neutral network at the mutated epitope. When the mutated sequence belongs to another neutral network, two different cases are considered: Mutations are almost neutral (93% cross-immunity) if the epitope changes its conformation only slightly, whereas they are classified as escape mutations if the epitope changes its structure significantly (80% cross-immunity). These escape mutations precipitate cluster transitions and occur relatively infrequently (*32*) (Fig. 2).

Given this underlying genotype space topology, we simulated the dynamics of influenza and the concurrent evolution of its HA in a temperate-latitude population. We based our influenza transmission model on a multistrain model that uses a status-based approach for tracking classes of hosts (*12*). However, instead of modeling the number of individuals susceptible, infected, and recovered to each individual strain, we modeled the number of individuals susceptible, infected, and recovered to each neutral ensemble. We define a neutral ensemble i as the set of strains that have identically shaped epitopes; i.e., that reside on the same neutral network at each epitope. This compartmental formulation eliminates the need to track the infection histories of individual hosts and facilitates future mathematical analyses of the dynamics. Without mutation, the dynamics of a system with n neutral ensembles are given by Eqs. 1a and 1b:

$$\frac{dI_i}{dt} = [\beta(t)I_i + mp_i]\frac{S_i}{N} - (\nu + \mu_D)I_i \quad (1a)$$

$$\frac{dS_i}{dt} = \mu_B N - \sum_{j=1}^{n} [\beta(t)I_j + mp_j]\sigma_{ij}\frac{S_i}{N} - \mu_D S_i \quad (1b)$$

where the subscript i denotes the neutral ensemble, and σ_{ij} denotes the degree of cross-immunity between neutral ensembles i and j. As in standard epidemiological models, $\beta(t)$ is the seasonally varying transmission rate, ν is the recovery rate,

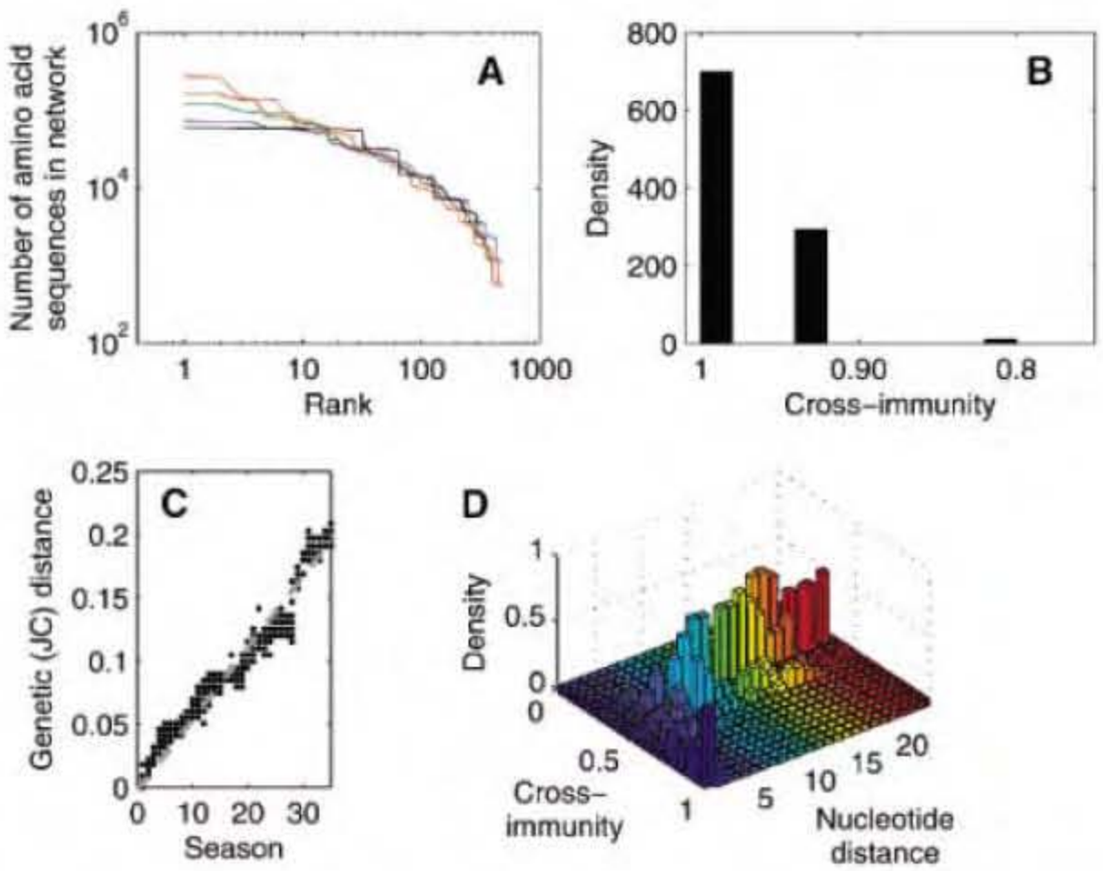

Fig. 2. Statistical properties of the model's neutral networks and patterns of genetic and antigenic change under the neutral-network framework. (**A**) Distribution of neutral-network sizes for each of the five modeled HA epitopes. Epitopes one to five each contain approximately $1.5^L = 438$ neutral networks, or distinct conformations. For each epitope, the networks were generated with a neutralized NK fitness-landscape model (*30*), with $L = 15$, $K = 1$, alphabet size (A) = 2, and neutrality parameter (F) = 2 (see supporting online material text). (**B**) Cross-immunity σ_{ij} between strains i and j that differ by a single amino acid. We let a neutral mutation of an epitope ε result in $x_{ij}(\varepsilon) = 100\%$ recognition, an almost-neutral mutation result in $x_{ij}(\varepsilon) = 65\%$ recognition, and an escape mutation result in $x_{ij}(\varepsilon) = 0\%$ recognition. The degree of cross-immunity between two strains is assumed to depend additively on recognition at each epitope, such that $\sigma_{ij} = \frac{1}{5}\sum_{\varepsilon=1}^{5} x_{ij}(\varepsilon)$. In the case of a non-neutral mutation, we let there be a low chance [$\rho = 1/40$ (1 out of 40)] that the adjacent neutral networks have conformations that are antigenically very different, yielding an escape mutant that may precipitate a cluster transition. The remainder of the time, a non-neutral mutation is considered almost neutral, yielding an antigenically similar conformation. With cross-immunity additive across epitopes, two sequences that are one mutation apart have either full cross-immunity, 93% cross-immunity, or 80% cross-immunity. The distribution was generated by computing the degree of cross-immunity between two strains of Hamming distance that are one amino acid apart for 1000 randomly sampled strain pairs. (**C**) Genetic [Jukes-Cantor (JC)] distance from the founder strain to the annual strain samples over the time course of the simulation. (**D**) Frequency distribution of the degree of cross-immunity between the simulation-generated HA strains shown in Fig. 3D.

μ_B is the birth rate, and μ_D is the death rate. Because clusters consist of neutral ensembles with high levels of cross-immunity, the model formulation yields dynamics that are essentially susceptible-infected-recovered (SIR) within single clusters. The model without immigration results in the stochastic extinction of influenza during the summer troughs; we therefore introduced the immigration rate parameter m to allow an influx of strains from areas outside the region. We let p_i represent the proportion of strains in the outside region that belong to neutral ensemble i. For simplicity, rather than modeling the outside region dynamically, we assumed that the strains in this region are derived from the strains present in the temperate region during the previous year (*32*). A more complex model that incorporates the region dynamically produces similar results as long as there is sufficient asynchrony between the geographic patches and provided that no genetic bottlenecks are otherwise produced.

The resulting disease dynamics reproduce influenza's well-known annual outbreaks in temperate regions, with seasonal attack rates of 1 to 13% (Fig. 3, A and B). The model also captures the sequential replacement of influenza clusters that is seen empirically, with cluster-transition years having higher incidence levels (Fig. 3A) and correspondingly higher annual attack rates (Fig. 3B), echoing the pneumonia and influenza (P&I) mortality rates that are representative of influenza's time series (*10*) (Fig. 1B). The temporal patterns of genetic and antigenic change can now also be visualized (Fig. 2, C and D). Figure 2C shows that genetic distances increase gradually from the founder strain, consistent with the gradual genetic change of H3N2's HA1 observed by Smith and coauthors (*6*). However, antigenic change, as measured by cross-immunity, evolves in punctuated steps between clusters. In Fig. 2D, we plotted cross-immunity between genetically distinct strains that were sampled over the time course of the simulation. Under influenza's epochal evolution, a roughly linear relationship between antigenic differences and genetic differences emerges. This relationship is in agreement with the previously observed relationship between genetic and antigenic distances (*6*). However, the roughly linear relationship between these distances over the long run does not imply that genetic and antigenic differences are linearly related at shorter time scales. Figure 1C and the previous findings of punctuated antigenic change by Smith and colleagues (*6*) clearly show that antigenic and genetic distances can be uncorrelated at this temporal scale. The neutral network topology thus accounts for both the short and the long time-scale patterns of antigenic and genetic distance relationships.

The model also predicts an emergent dynamic property of influenza that arises from the interaction between cluster jumps and herd immunity. Specifically, the model frequently generates a refractory year of low attack rates after cluster-transition years. During cluster transitions, many hosts become infected and recover, and hence there are few susceptible hosts to infect in the following year. Two years after a cluster-transition year, enough susceptible hosts have been replenished to cause another large annual outbreak. The replenishment of susceptible hosts comes from a combination of new births and the slight antigenic evolution of the strains that compose the cluster. The existence of this refractory period is empirically suggested–a pattern that, to our knowledge, has gone unnoticed. After a year dominated by a new cluster (and not immediately followed by another cluster), the incidence of H3N2 often drops below that of the following "normal" year—a year that is neither dominated by an invading cluster nor possibly refractory (*10*, *33*, *34*). This pattern occurs in six out of seven cases after the HK68 cluster. Interestingly, also in six out of seven potentially refractory years, subtypes H1N1 and/or B predominate.

We compared our model's results with the characteristic phylogenetic patterns of H3N2 HA1. A phylogenetic reconstruction of the sequences obtained from yearly sampling of the model's infected individuals generated a tree with a long trunk and short side branches that is characteristic of influenza (*4*) (Fig. 3D). To better understand the factors that determine the shape of this phylogenetic tree, we tracked the diversity of strains present in the population over time, as measured by average pairwise nucleo-

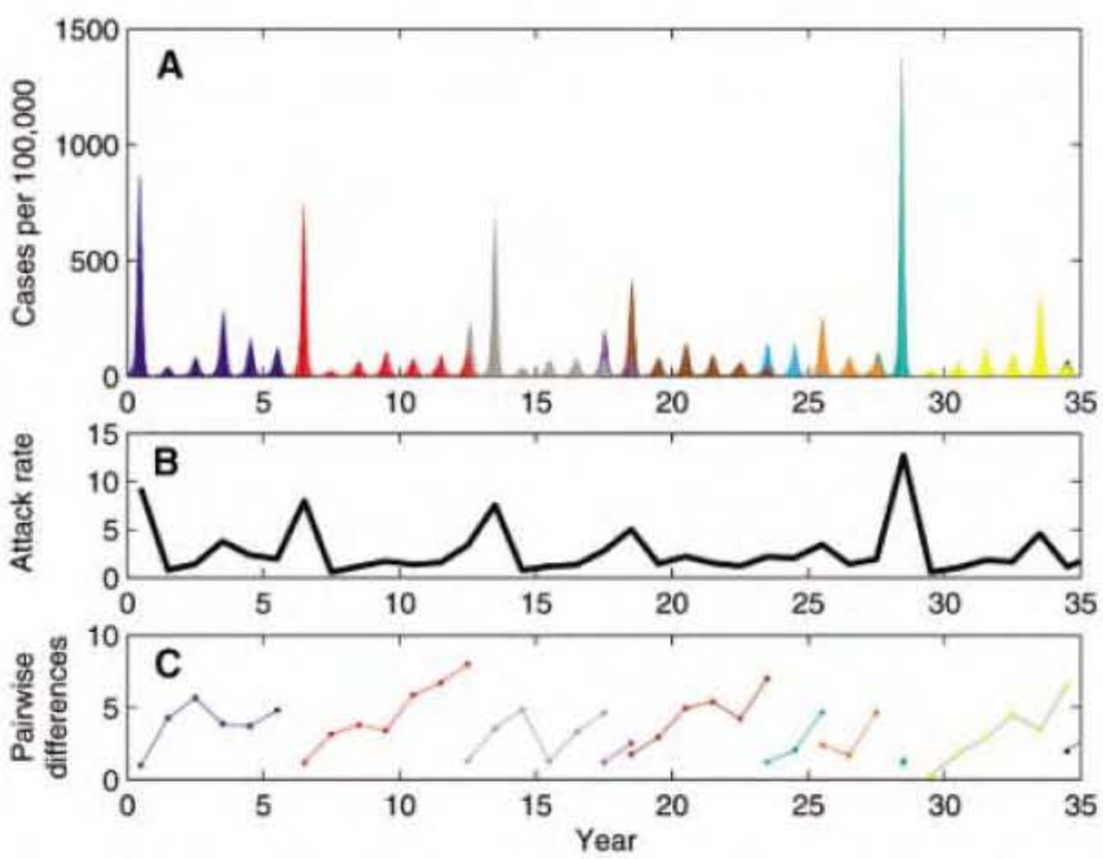

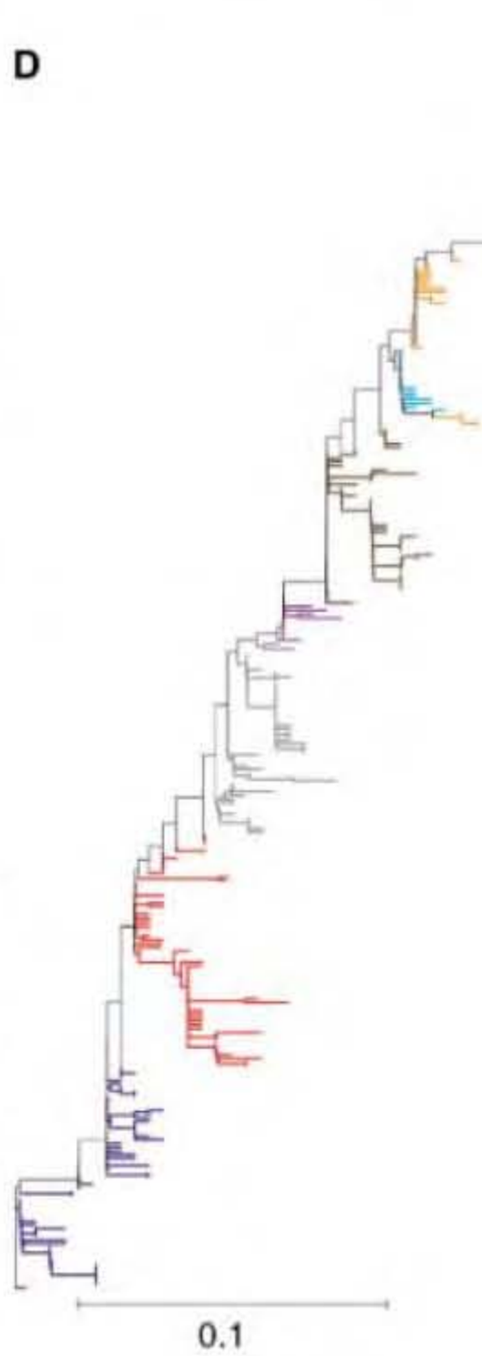

Fig. 3. Influenza dynamics and evolution from model simulations. (**A**) Time series of infected cases, color coded by cluster designation. Clusters remained dominant for less than a decade, in congruence with the empirically suggested two- to eight-season dominance of H3N2's clusters (*6*). (**B**) Annual attack rates, showing increases during cluster-transition years and a refractory period during each subsequent year. (**C**) Average pairwise nucleotide differences over time, showing a boom-and-bust pattern of genetic diversity that is associated with cluster-transition years. Nucleotide differences were calculated annually from 20 randomly sampled strains along cluster designations. Simulations were started at the endemic equilibrium of a single random strain. (**D**) Phylogenetic tree showing the restricted HA diversity generated by the model. The neighbor-joining (JC distance) tree was built with 10 randomly sampled strains from every year. Lineages are color coded by antigenic cluster. Simulations were run with an initial population size of two million. We let the duration of infection $\nu^{-1} = 8$ days (*48*), the birth rate $\mu_B = 14/1000$ per year, the death rate $\mu_D = 8/1000$ per year, the mutation rate $\delta = 2 \times 10^{-5}$ per base per day, and the probability of an adjacent network being antigenically discontinuous $\rho = 1/40$. We used an average basic reproductive rate R_0 of 5 [consistent with estimates from (*49*)], with seasonal sinusoidal forcing $c = 0.35$. The strength of the interaction between the temperate region and the outside region is determined by the transmissibility-reduction factor $r^{-1} = 1/150$ and the immigration rate of $m = 50$ per day (*32*).

tide differences between strains (Fig. 3C). As a cluster emerges and spreads, strains diffuse through genotype space with weak positive selection from the slight antigenic changes accumulating at the epitopes, increasing strain diversity. The appearance of a novel phenotype severely curtails diversity in the old cluster. This contraction results from a selective sweep, with the mutant strain having higher fitness (because of the higher levels of susceptible hosts available to it), thereby allowing it to competitively exclude all the strains in the previous cluster. The invasion of the new cluster is facilitated by the accumulated diversity of the old cluster: The novel antigenic cluster can have up to 80% cross-immunity with strain variants of the old cluster that share four out of five of its epitopes; however, it has only 52% cross-immunity with strain variants of the old cluster that differ slightly in four out of five of the epitopes. The emergence of new clusters, their rapid expansion, and their decline create a boom-and-bust cycle of explosive diversity and contraction.

To validate this model, we computed the average pairwise nucleotide differences in the H3N2 sequences given by Smith and coauthors (*6*). Despite the limited number of antigenically typed samples, a boom-and-bust pattern is evident. There is a significant increase in nucleotide differences as the clusters age ($P < 0.02$) (Fig. 4A), suggesting diffusion in genotype space. A plot of diversity over time (1968 to 2003) shows that this overall increase occurs in seven out of nine clusters and is greatest while the cluster is still dominant (Fig. 4B). This pattern in diversity also holds when analysis is restricted to residues located in the five epitopes, with pairwise nucleotide differences growing from 0 to 3 to approximately 5 to 13 in 3 to 4 years. A further match between the model and H3N2 HA1 is observed when tree-balance metrics are employed to determine the degree of skewness within clusters (*32*). These types of quantitative measures should be used in the future to compare different phylodynamic models.

A minimal theory for influenza. By incorporating a GP mapping based on neutral networks into a simple multistrain transmission model, we have shown that major features of influenza's interpandemic ecology and evolution can be explained. These features include sequential cluster transitions and limited standing HA diversity in the viral population. Another model, which assumes that genotypic differences approximate phenotypic differences, has been successful in reproducing clustered strain appearances (*12*). However, this model is deliberately restricted to a much lower dimensional space [one-dimensional (1D) or 2D], which constrains the direction of evolution. Models that incorporate higher dimensions of mutational possibilities have not shown evidence for self-organized clusters; thus, explosive diversity results instead (*5*, *14*). To limit viral diversity, these models have had to invoke temporary strain-transcending immunity (*5*, *14*). Both of these models also predict fluctuations in strain diversity; however, these decreases in diversity are not associated with increases in the attack rate. It is also unclear whether or not these models generate antigenic clusters. The existence of generalized immunity is suggested by cellular immune responses in mice [(*35*, *36*), but see (*37*)], although the amount of protection required in models of human populations appears to be comparatively greater. Here, we have shown that generalized immunity is unnecessary to restrict the interpandemic diversity of HA. Our model indicates that weak within-cluster selection and the selective sweeps that accompany cluster transitions are sufficient. Empirical patterns corroborate this model (Fig. 1B and Fig. 4).

This model made several simplifying assumptions that should be investigated. We assumed that only HA determines the antigenic phenotype. This is certainly not the whole story: Antibody responses to NA and internal proteins, cellular immune responses, and non–immune-mediated traits contribute to viral fitness and hence might affect influenza's dynamics and diversity patterns (*38*, *39*). However, the fact that HA diversity and associated variations in herd immunity allow our model to explain emergent evolutionary and epidemic properties underlines the fact that HA is the major (phylo)dynamical component to build on. Teasing out whole-genome influences on influenza cluster transitions is an important area for future work. We have also assumed that there is no interaction between H3N2, H1N1, or influenza B, despite suggestive instances of subtype replacement (e.g., of H1N1 by H2N2 and H2N2 by H3N2). Although the model presented here predicts refractory periods after cluster-transition years during which H1N1/B outbreaks often occur, it does not include a mechanism to explain why H1N1/B outbreaks do not seem to occur in seasons with high H3N2 incidence. Some degree of generalized immunity (*5*) or ecological interference (*40*) may be needed to account for these interannual subtype patterns and pandemic subtype replacements. These processes do not, however, seem necessary to restrict the intrasubtype diversity of HA, nor can they parsimoniously explain aspects of H3N2's interannual variability.

Our model also opens up general questions about the time-series analyses of influenza dynamics at the population level. In the absence of strain data, influenza has been modeled as a simple SIRS system (*41*–*43*), with viral evolution causing transition from the recovered class to the susceptible class. In light of the punctuated cluster transitions identified by Smith and colleagues (*6*) and the implications of the transitions expanded upon in this paper, it is becoming evident that influenza dynamics can be approximated as a serial SIR system, with abrupt changes in the level of susceptible hosts when a new cluster appears. The development of such mathematical and statistical approaches may allow the short-term dynamics of influenza to be predicted without recourse to complex evolutionary models. Improved subtype-specific flu surveillance is the key to full utilization of such methods (*44*).

Further investigation of the biological basis of neutrality in GP mappings could yield new

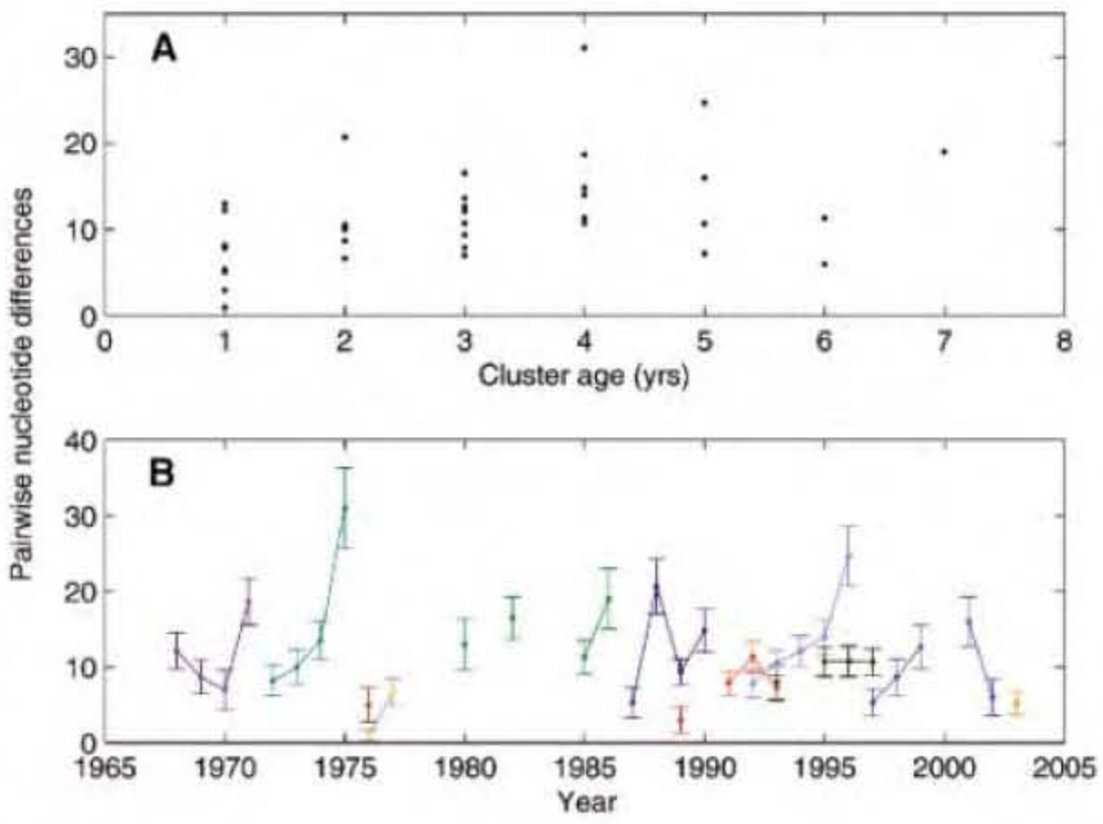

Fig. 4. Patterns of genetic diversity in HA1. (**A**) Average pairwise nucleotide differences between the HA1 regions of circulating strains as a function of cluster age. Cluster age was calculated from the first year in which a strain from the cluster appeared in the data set. Each strain was assumed to circulate only during the year it was isolated. Average pairwise differences were calculated as the means within groups of isolates, distinguished by cluster and year, using the MEGA software package version 3.1 (*47*). The slope is significantly positive ($P < 0.02$), as was determined by least-trimmed-squares regression (LTSR) and 1000 bootstrap samples. (**B**) Average pairwise nucleotide differences in HA1 by cluster and year. The average number of nucleotide differences increased in all nine clusters for which between-year comparisons are possible using least-squares regression, and in seven of nine clusters (EN72, VI75, BK79, SI87, BE89, BE92, and SY97) using LTSR. Vertical bars indicate 95% confidence levels, inferred from 500 bootstrap samples. More sequences were available for EN72, SI87, BE89, BE92, WU95, and SY97 than for other clusters (fig. S1). The patterns in diversity shown in (A) and (B) were similar when considering only the subset of codons belonging to epitopes A to E, as identified in (*50*) and (*6*). For some clusters, the growth in pairwise nucleotide differences was interrupted by sampling discontinuities (i.e., years for which one or no sequences of that cluster were sampled; see fig. S1).

insights into the phylodynamics of disease systems in general. Critically, neutrality is mediated not only by the accessibility of different structures to the pathogen but also by the hosts' abilities to detect these differences. The phenotype of the pathogen thus depends on the specificity of the host response. The availability of different phenotypes under this framework may establish major differences between the phylogenetic characteristics of different diseases [e.g., influenza A and measles (*3*)] and the same disease in different hosts experiencing different ecologies (e.g., influenza A in swine, avian, and equine hosts). There is also evidence that the specificity of the host antibody response to influenza varies within a host population (*45*). This heterogeneity might have important consequences for the diffusion of strains along antigenically similar networks in genotype space.

This study highlights the necessity of coupling molecular evolution with population-level models to understand the basic aspects of a biological system. In the case of influenza, a more detailed understanding of the structural basis of antigenicity and the dynamics of immune recognition of viral epitopes is of utmost importance. The roles that neutrality and context dependency play in enabling phenotypic change (*46*) need to be addressed in virological studies. These efforts could help to identify the GP map of influenza's HA and are critical for vaccine development, because antigenic distances between epidemic strains and vaccine strains determine vaccine efficacy (*2*). Further inquiries into population-level processes that affect influenza dynamics and evolution, such as the extent of epidemiological mixing and the global circulation of the virus in humans and other host species, are also necessary parts of this research. Integrating findings from these fields will be critical to understanding and managing influenza.

References and Notes

1. N. J. Cox, K. Subbarao, *Annu. Rev. Med.* **51**, 407 (2000).
2. D. J. Smith, S. Forrest, D. H. Ackley, A. S. Perelson, *Proc. Natl. Acad. Sci. U.S.A.* **96**, 14001 (1999).
3. B. T. Grenfell *et al.*, *Science* **303**, 327 (2004).
4. W. M. Fitch, R. M. Bush, C. A. Bender, N. J. Cox, *Proc. Natl. Acad. Sci. U.S.A.* **94**, 7712 (1997).
5. N. M. Ferguson, A. P. Galvani, R. M. Bush, *Nature* **422**, 428 (2003).
6. D. J. Smith *et al.*, *Science* **305**, 371 (2004).
7. P. W. Gill, A. M. Murphy, *Med. J. Aust.* **2**, 761 (1977).
8. G. Meiklejohn, T. C. Eickhoff, P. Graves, I. Josephine, *J. Infect. Dis.* **138**, 618 (1978).
9. S. Nakajima, E. Nobusawa, K. Nakajima, *Virology* **274**, 220 (2000).
10. S. K. Greene, E. L. Ionides, M. L. Wilson, *Am. J. Epidemiol.* **163**, 316 (2006).
11. D. C. Wiley, I. A. Wilson, J. J. Skehel, *Nature* **289**, 373 (1981).
12. J. R. Gog, B. T. Grenfell, *Proc. Natl. Acad. Sci. U.S.A.* **99**, 17209 (2002).
13. M. Girvan, D. S. Callaway, M. E. J. Newman, S. H. Strogatz, *Phys. Rev. E Stat. Nonlinear. Soft Matter Phys.* **65**, 031915 (2002).
14. F. Tria, M. Lässig, L. Peliti, S. Franz, *J. Stat. Mech.* **1**, P07008 (2005).
15. K. Nakajima, E. Nobusawa, A. Nagy, S. Nakajima, *J. Virol.* **79**, 6472 (2005).
16. K. F. Lau, K. A. Dill, *Proc. Natl. Acad. Sci. U.S.A.* **87**, 638 (1990).
17. D. J. Lipman, W. J. Wilbur, *Proc. R. Soc. London Ser. B* **245**, 7 (1991).
18. A. Babajide *et al.*, *J. Theor. Biol.* **212**, 35 (2001).
19. E. Bornberg-Bauer, *Biophys. J.* **73**, 2393 (1997).
20. U. Bastolla, H. E. Roman, M. Vendruscolo, *J. Theor. Biol.* **200**, 49 (1999).
21. H. Li, R. Helling, C. Tang, N. Wingreen, *Science* **273**, 666 (1996).
22. P. Schuster, W. Fontana, *Phys. D.* **133**, 427 (1999).
23. W. Fontana, P. Schuster, *J. Theor. Biol.* **194**, 491 (1998).
24. M. A. Huynen, *J. Mol. Evol.* **43**, 165 (1996).
25. M. A. Huynen, P. F. Stadler, W. Fontana, *Proc. Natl. Acad. Sci. U.S.A.* **93**, 397 (1996).
26. E. van Nimwegen, J. P. Crutchfield, *Bull. Math. Biol.* **62**, 799 (2000).
27. E. van Nimwegen, J. P. Crutchfield, M. Mitchell, *Phys. Lett. A* **229**, 144 (1997).
28. E. van Nimwegen, J. P. Crutchfield, M. Mitchell, *Theor. Comput. Sci.* **229**, 41 (1999).
29. L. Barnett, in *Artificial Life VI: Proceedings of the Sixth International Conference on Artificial Life* (MIT Press, Cambridge, MA, 1998), pp. 18–27.
30. M. E. J. Newman, R. Engelhardt, *Proc. R. Soc. London Ser. B* **265**, 1333 (1998).
31. S. A. Kauffman, S. Johnsen, *J. Theor. Biol.* **149**, 467 (1991).
32. Materials and methods are available as supporting online material on *Science* Online.
33. T. A. Reichert *et al.*, *Am. J. Epidemiol.* **160**, 492 (2004).
34. W. W. Thompson *et al.*, *JAMA* **289**, 179 (2003).
35. P. G. Thomas, R. Keating, D. J. Hulse-Post, P. C. Doherty, *Emerg. Infect. Dis.* **12**, 48 (2006).
36. J. W. Yewdell, J. R. Bennink, G. L. Smith, B. Moss, *Proc. Natl. Acad. Sci. U.S.A.* **82**, 1785 (1985).
37. S. R. Crowe, S. C. Miller, D. L. Woodland, *Vaccine* **24**, 452 (2006).
38. J. R. Gog, G. F. Rimmelzwaan, A. D. M. Osterhaus, B. T. Grenfell, *Proc. Natl. Acad. Sci. U.S.A.* **100**, 11143 (2003).
39. E. C. Holmes *et al.*, *PLoS Biol.* **3**, e300 (2005).
40. P. Rohani, C. J. Green, N. B. Mantilla-Beniers, B. T. Grenfell, *Nature* **422**, 885 (2003).
41. J. Dushoff, J. B. Plotkin, S. A. Levin, D. J. D. Earn, *Proc. Natl. Acad. Sci. U.S.A.* **101**, 16915 (2004).
42. Y. Xia, J. R. Gog, B. T. Grenfell, *Appl. Stat.* **54**, 659 (2005).
43. S. K. Greene, J. S. Koopman, M. L. Wilson, in *Proceedings of the International Conference on Options for the Control of Influenza V*, Y. Kawaoka, Ed. (Elsevier, San Diego, CA, 2004), pp. 795–798.
44. D. J. Smith, *Science* **312**, 392 (2006).
45. K. Sato *et al.*, *Epidemiol. Infect.* **132**, 399 (2004).
46. A. Wagner, in *Robustness and Evolvability in Living Systems*, S. A. Levin, S. Strogatz, Eds. *Princeton Studies in Complexity* (Princeton Univ. Press, Princeton, NJ, 2005), pp. 223–227.
47. S. Kumar, K. Tamura, M. Nei, *Brief. Bioinform.* **5**, 150 (2004).
48. R. Douglas, in *The Influenza Viruses and Influenza*, E. Kilbourne, Ed. (Academic Press, New York, 1975), pp. 395–418.
49. C. C. Spicer, C. J. Lawrence, *J. Hyg. Camb.* **93**, 105 (1984).
50. R. M. Bush, W. M. Fitch, C. A. Bender, N. J. Cox, *Mol. Biol. Evol.* **16**, 1457 (1999).

51. We thank R. Fouchier, D. Smith, S. Greene, M. Boni, E. Holmes, D. Alonso, G. Sawicki, A. King, S. Allesina, I. Volkov, and J. Lloyd-Smith for useful discussions and comments; L. Fernando-Chaves and D. Ruiz-Moreno for feedback on statistical analyses; three anonymous reviewers for helpful comments; and the Center for the Study of Complex Systems at the University of Michigan and the High Performance Computing group at PSU for computing resources. This work was supported by the James S. McDonnell Foundation (through a Centennial Fellowship to M.P.), a CIDD postdoctoral fellowship to K.K., and an NSF Graduate Research Fellowship to S.C.

Supporting Online Material

www.sciencemag.org/cgi/content/full/314/5807/1898/DC1
Materials and Methods
SOM Text
Figs. S1 to S6
Table S1
References

19 July 2006; accepted 30 October 2006
10.1126/science.1132745

Structure of Dual Function Iron Regulatory Protein 1 Complexed with Ferritin IRE-RNA

William E. Walden,[1] Anna I. Selezneva,[1] Jérôme Dupuy,[2] Anne Volbeda,[2] Juan C. Fontecilla-Camps,[2] Elizabeth C. Theil,[3] Karl Volz[1]*

Iron regulatory protein 1 (IRP1) binds iron-responsive elements (IREs) in messenger RNAs (mRNAs), to repress translation or degradation, or binds an iron-sulfur cluster, to become a cytosolic aconitase enzyme. The 2.8 angstrom resolution crystal structure of the IRP1:ferritin H IRE complex shows an open protein conformation compared with that of cytosolic aconitase. The extended, L-shaped IRP1 molecule embraces the IRE stem-loop through interactions at two sites separated by ~30 angstroms, each involving about a dozen protein:RNA bonds. Extensive conformational changes related to binding the IRE or an iron-sulfur cluster explain the alternate functions of IRP1 as an mRNA regulator or enzyme.

Iron regulatory protein 1 (IRP1) is a cytosolic, RNA binding protein that regulates the translation or stability of mRNAs encoding proteins for iron transport, storage, and use. IRP1 has an alternate function as cytosolic (c-) aconitase when a [4Fe-4S] cluster is bound (*1*–*5*). The distribution of IRP1 between these mutually exclusive activities requires no new protein synthesis; iron excess or starvation promotes c-aconitase or RNA binding activity, respectively (*6*). Assembly and disassembly of the [4Fe-4S] cluster appears to be an effective mechanism for

regulating IRP1 activity, dependent on facile interchange between the two functional conformations.

IRP1 binds ~30-nucleotide-long stem-loop structures called iron-responsive elements (IREs) located within the 5′ or 3′ untranslated regions of the mRNA, where IRP1 blocks ribosome binding or nuclease degradation, respectively (*1*, *3*, *4*). IRP1:IRE interactions are strong (pM) and selective (*2*), and they do not involve canonical RNA binding motifs identified in other RNA binding proteins (*7*, *8*). Nuclease protection analysis suggests that IRP1 binding spans the entire length of the IRE stem-loop (*9*, *10*). The conserved nucleotides –CAGUG– (nucleotides 14 to 18 in the RNA used in this study) form a terminal –AGU– loop closed by a C14:G18 base pair, followed by an unpaired nucleotide (*2*, *11*–*14*). The IRE stem is interrupted by the conserved, unpaired cytosine C8, which divides the helix into a 5–base pair upper stem and a variable length lower stem (*2*). Sequence and base pairing surrounding the C8 mid-helix distortion are variable among members of the IRE-RNA family (*3*, *15*). A second iron regulatory protein, IRP2, binds the same family of IRE-mRNAs, but is a single-function protein lacking aconitase activity (*16*). IRP2 displays in vitro RNA binding that is more sensitive than IRP1 to distortions in the mid-helix (*15*). Variations in the IRE stem-loops among the mRNAs, exemplified by ferritin and mitochondrial aconitase IRE-RNAs, coincide with graded responses to iron signals in vivo (*17*) and different IRP binding stabilities in vitro (*2*, *15*).

The recently elaborated crystal structure of c-aconitase showed a compact protein conformation, with the residues known to function in enzyme activity or IRE binding buried and relatively inaccessible (*18*). Clearly, the protein accesses different conformations during binding of alternate ligands, as demonstrated by marked changes in radius of gyration (*19*). Localized structural changes also have a significant effect. For example, [4Fe-4S] cluster binding or oxidation of Cys^{437} blocked RNA binding. By contrast, a serine substitution at this position had no effect (*2*, *20*, *21*). To determine the nature of the conformational changes underlying the bifunctionality of IRP1, we solved the crystal structure of the $Cys^{437}Ser/Cys^{503}Ser$ double-mutant IRP1 in complex with ferritin H IRE [see Methods in supporting online material and (*22*)].

Overall structure of IRP1:IRE complex. The crystal structure of the IRP1:IRE complex shows

[1]Department of Microbiology and Immunology, University of Illinois at Chicago, Chicago, IL 60612–7344, USA. [2]Laboratoire de Cristallographie et de Cristallogénèse des Protéins, IBS, Institut de Biologie Structurale Jean-Pierre Ebel; CEA; CNRS; Université Joseph Fourier, 41 rue Jules Horowitz, F-38207 Grenoble, France. [3]Children's Hospital Oakland Research Institute, Oakland, CA 94609–1673, and Department of Nutritional Science and Molecular Toxicology, University of California, Berkeley, Berkeley, CA 94720–3104, USA.
*To whom correspondence should be addressed. E-mail: kvolz@uic.edu

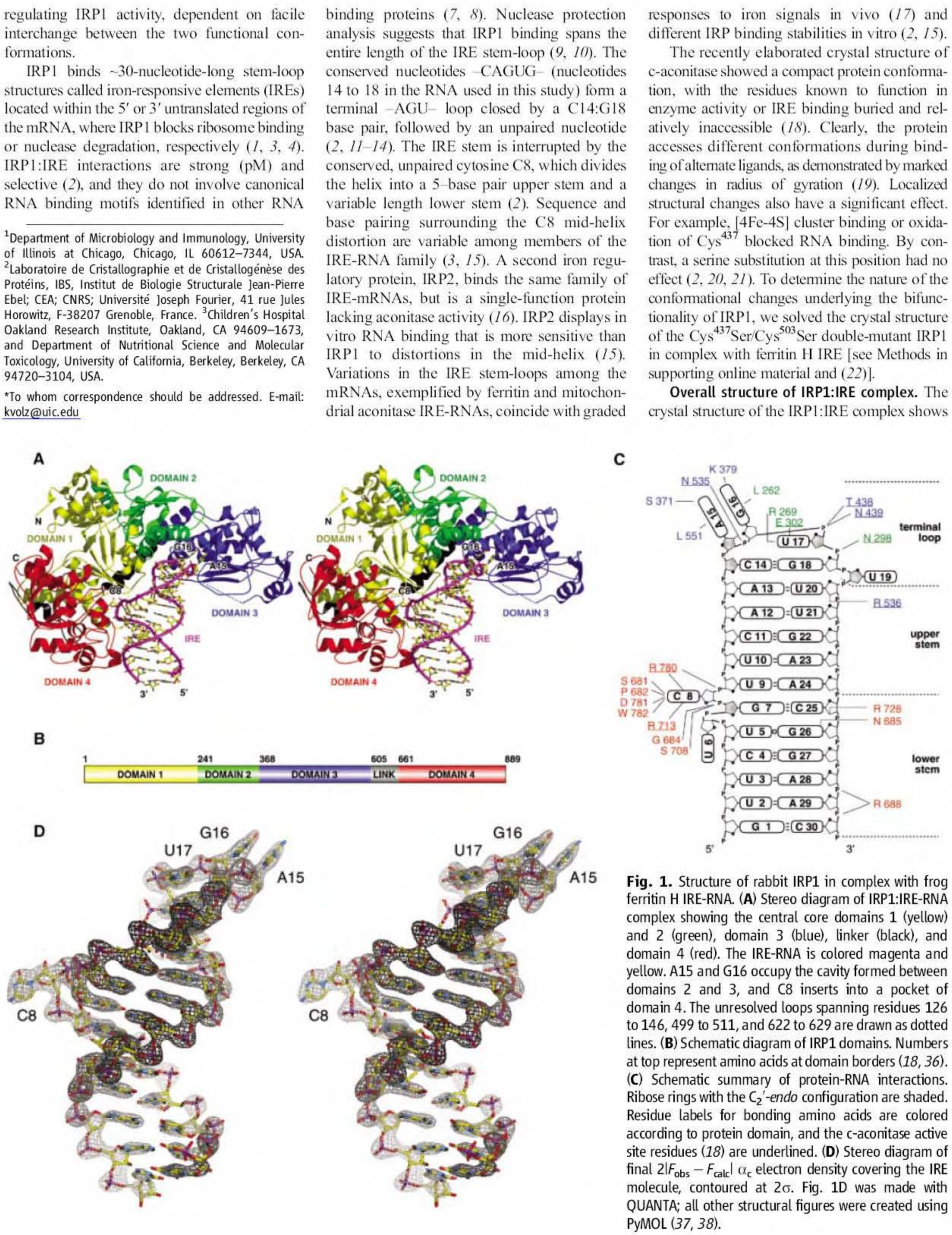

Fig. 1. Structure of rabbit IRP1 in complex with frog ferritin H IRE-RNA. (**A**) Stereo diagram of IRP1:IRE-RNA complex showing the central core domains 1 (yellow) and 2 (green), domain 3 (blue), linker (black), and domain 4 (red). The IRE-RNA is colored magenta and yellow. A15 and G16 occupy the cavity formed between domains 2 and 3, and C8 inserts into a pocket of domain 4. The unresolved loops spanning residues 126 to 146, 499 to 511, and 622 to 629 are drawn as dotted lines. (**B**) Schematic diagram of IRP1 domains. Numbers at top represent amino acids at domain borders (*18*, *36*). (**C**) Schematic summary of protein-RNA interactions. Ribose rings with the C_2'-*endo* configuration are shaded. Residue labels for bonding amino acids are colored according to protein domain, and the c-aconitase active site residues (*18*) are underlined. (**D**) Stereo diagram of final $2|F_{obs} - F_{calc}|\ \alpha_c$ electron density covering the IRE molecule, contoured at 2σ. Fig. 1D was made with QUANTA; all other structural figures were created using PyMOL (*37*, *38*).

that the protein binds a single IRE-RNA molecule through contacts at two spatially separate sites. The IRP1 molecule adopts an L-shape in the complex, with aconitase structural domains 3 and 4 extending perpendicularly from a central core composed of domains 1 and 2 (Fig. 1, A and B). The IRE stem-loop is bound across the concave opening of IRP1, with direct contacts from the RNA terminal loop and the RNA lower stem (Fig. 1, A and C). Exposed terminal loop residues A15 and G16 extend into a large protein cavity at the interface between domains 2 and 3. Bonds to A15, G16, and U17 provide specificity and stability to interactions at this site (Fig. 1C). Protein binding to the stem of the IRE is centered on the C8 nucleotide, which inserts into a pocket on the inner face of domain 4. A 31° bend in the RNA helix redirects the path of the lower stem along the same face of domain 4, which binds the side of the IRE lower stem farthest from the terminal loop (Fig. 1A). Mutagenesis and binding studies of IRP1:IRE interactions indicated that residues from each of the four structural domains of IRP1 contributed to IRE binding (*23*–*27*). Although the electron density for domain 1 residues 126 to 146 is unresolved, it suggests that some protein:RNA contacts here might be revealed with higher resolution data.

The high binding affinity and specificity of IRP1:IRE interactions are explained by the many protein:RNA contacts observed in the terminal loop and stem-binding regions (Fig. 1C). The interfaces cover ~1400 Å^2 for the terminal loop and ~1300 Å^2 for the stem, each comparable in area to individual binding sites for other protein:RNA complexes (*28*). The terminal loop and C8 of the IRE are separated by ~30 Å, held in their orientations by the 5–base-pair helix of the upper stem. Selectivity among different IREs may depend in part on helix parameters that reflect variations in the intersite distances, base pair sequences, and/or local distortions in the upper stem [e.g., (*29*)].

IRP1 structure and comparison with c-aconitase. The structural differences between IRP1 in the protein:RNA complex and c-aconitase are larger than those previously predicted from aconitase structures (*18*, *23*). Although most of aconitase domains 1 and 2 form a single core in IRP1 with moderate changes relative to each other, there are extensive changes in domains 3 and 4. To a first approximation, these changes can be described as rigid body motions relative to the core (Fig. 2 and movie S1). Domain 4 rotates by 32° and translates ~14 Å. This eliminates the interactions between domains 3 and 4 that are present in c-aconitase. Instead, most of these surfaces are incorporated into the two separate RNA binding sites. Domain 4 is attached to domain 1 through strong hydrophobic contacts (*18*). As a result, residues 90 to 170 of domain 1 move with domain 4 during the conformational changes (Fig. 2 and movie S1).

Domain 3 displays the largest conformational difference between c-aconitase and the IRP1:IRE complex, with a rotation of 52° resulting in a translation of ~13 Å (Fig. 2 and movie S1). This difference was unexpected and contrasts with the predicted, and observed, movement of domain 4 (*18*, *23*–*26*). Because the interface between domain 3 and the core domains 1 and 2 is only moderately buried in both conformations and is populated with more hydrogen-bonding groups than hydrophobic interactions, a major rearrangement is possible while adhesion is retained at the interface. A conformational change in the polypeptide linker joining domains 3 and 4 is central to their repositioning relative to the core. In c-aconitase, residues 593 to 614 in the linker comprise two helices α21 and α22, separated by a bend preceding Pro^{606} (*18*). In the IRP1:IRE complex, formation of a single continuous helix over residues 593 to 614 facilitates the large domain shifts (movie S1).

Regulation of IRE binding. The large-scale domain rearrangements necessary for IRP1 to switch between c-aconitase and IRE-binding functions appear coupled to key internal reconfigurations of the protein, ultimately linked to the ligand-binding groups. The shift of domain 3 is accompanied by reconfiguration of two functionally important segments at the interface of domains 2 and 3, the 430 region (residues 436 to 442), and the 530 loop (residues 534 to 544). These segments play dual structural and functional roles by forming the ligand-binding environment for the Fe-S cluster in c-aconitase or by making IRE contacts in the complex. In c-aconitase, Cys^{437} is one of the three iron-binding residues for the Fe-S cluster and is part of the tight, single-turn helix α14 [Fig. 3A and (*18*); Cys^{503} and Cys^{506} are the other cluster ligands]. In sharp contrast, α14 becomes an extended loop in the IRE-bound IRP1, which places residue 437, a serine in the mutant protein used here, in the terminal loop-binding cavity (Fig. 3B and movie S2). Ser^{437} has no direct RNA interactions, whereas Thr^{438} and Asn^{439} are in new positions and make direct contacts with the bound IRE.

The 530 loop contributes bonds to the RNA and occupies the space taken by the Fe-S cluster in c-aconitase. The configuration of the 530 loop in the protein:RNA complex is associated with the helix-to-loop change of α14 (Fig. 3 and movie S2). The 430 and 530 loops stabilize each other in the protein:RNA complex, forming a rim of the protein cavity that binds the RNA terminal loop. Mutation of Arg^{541} to either lysine or glutamine greatly reduces IRE binding affinity (*27*). This is rationalized by the network of hydrogen bonds that Arg^{541} makes to stabilize the entire 530 loop (movie S2). Replacing Arg^{536} with glutamine also decreases IRE binding (*27*), which is explained by the direct contact between Arg^{536} and the 2′OH of U20, over a distance too great to be spanned by a glutamine (Fig. 3B). Finally, a triple interaction between the 530 loop, the 430 region, and the IRE terminal loop stabilizes the protein:RNA complex, with Asn^{535} establishing four hydrogen bonds: two to Thr^{438} and two to the IRE.

The repositioning of domain 4 also occurs through key localized conformational changes. The pivot point for domain 4 movement is in domain 1 near Gly^{90} of α4, ~13 Å away from the Fe-S cluster in c-aconitase. α4 has an unusual sequence with two helix-destabilizing residues (Gly^{90} and Pro^{92}) occupying its 4th and 6th positions. In the IRP1:IRE complex, the amino-terminal residues 86 to 89 of α4 have collapsed

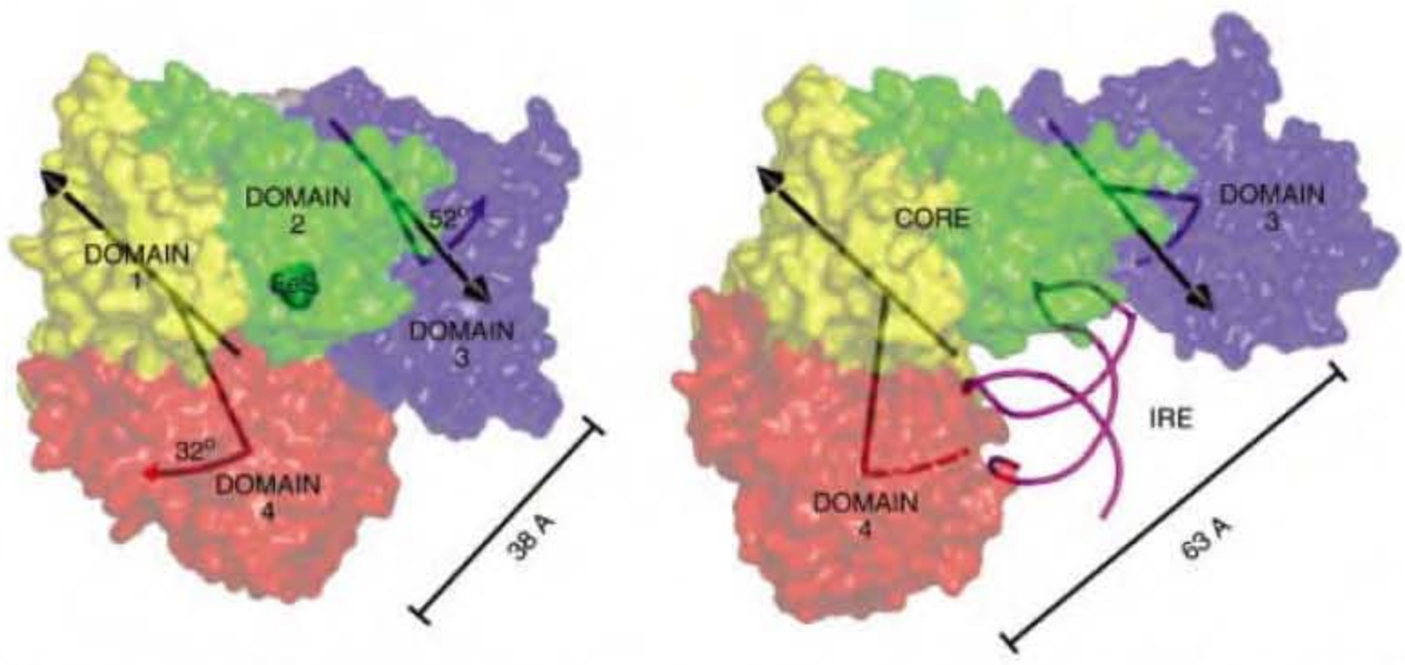

Fig. 2. Differences in domain positions between c-aconitase and IRP1:IRE-RNA complex. The c-aconitase structure is from Dupuy *et al.* [(*18*); Protein Data Bank 2B3X]. Domains 1 and 2 of c-aconitase (left) correspond to the core in the IRP1:IRE complex (right). The two molecules are displayed in the same orientation to show the displacements of domains 3 and 4. The molecular surfaces are semitransparent to reveal the internal [4Fe-4S] cluster in c-aconitase, and the axes of rotation around which domains 3 and 4 pivot. The arcs show the motion of the centers of mass of domains 3 and 4. Domain 4 remains attached to domain 1 through hydrophobic contacts between the carboxy-terminal helix α31 (residues 879 to 889) and the buried helix α4 (residues 87 to 106), plus surrounding hydrogen-bonding interactions. As a result, the pivot axis for domain 4 extends through domain 1 near α4 and α31. Domain 3 pivots around the axis on the interface between it and the core. See also movie S1.

to a β turn, and domain 4 has pivoted more than 30° with minimal internal distortion. The reversible disruption of α4 may be a mechanism linking the rotational freedom of domain 4 to the structural integrity of the Fe-S cluster.

Overall structure of ferritin H IRE in the complex. The ferritin IRE has 12 base pairs, all with Watson-Crick bonding, except for the wobble pair U5:G26 (Fig. 1C). Although the bound IRE retains the general stem-loop structure observed by nuclear magnetic resonance (NMR) spectroscopy (*13*, *14*), there are several significant differences. The IRE –CAGUGU– terminal loop forms a pseudotriloop (*30*) both in the complex and in solution. The defining elements of the ferritin H IRE pseudotriloop are the –AGU– triplet, isolated by the conserved C14:G18 base pair, followed by the unpaired U19. Neither base in the C14:G18 bridge makes direct contact with the protein, which suggests that the bridge serves only a structural role for IRP1 recognition. In the NMR structures of free IREs, A15 is stacked on top of the C14:G18 pair; G16 and U17 are disordered (*12*–*14*). In the complex, it is U17 that completes the base stacking of the helix, whereas A15 and G16 are extruded from the rest of the IRE molecule (Figs. 1D and 4A). A sharp turn in the RNA backbone, resulting from nonhelical conformations in the terminal loop, supports the extrahelical stacking of A15 and G16, which is maximized by a *syn* configuration of G16 (Fig. 4A). U19, a variable base in the IRE-RNA family, appears to be the most solvent-exposed nucleotide in the complex. In the NMR structures of unbound IREs, C8 is extrahelical but disordered (*13*, *14*). In the complex, C8 extends completely away from the stem, and is ordered by interaction with protein (Figs. 1D and 4B). The unpaired U6, conserved in ferritin IREs, lacks the stacking interactions indicated by NMR in the free IRE-RNA (*14*), but remains tucked into the minor groove of the bound RNA, where it can bond with Arg^{149}.

Details of IRP1:IRE-RNA interactions. The wide separation of the two IRE contact sites in IRP1 allows each to contribute individually to binding affinity and specificity. The terminal loop-binding cavity of IRP1 is generated by the displacement of domain 3 from domains 1 and 2 and, consequently, only exists in the IRE-binding conformation (movie S1). The IRP1:IRE terminal loop interactions are built around the main bonding features of the –AGU– pseudotriloop (Fig. 1C). As mentioned above, A15 and G16 extend into the terminal loop-binding cavity and make base-specific bonds with Ser^{371} and Lys^{379}, respectively, and van der Waal's contacts with residues lining the walls of the cavity (Figs. 1C and 4A). U17, the top stacked base of the upper stem, makes one base-specific bond with Arg^{269} at the cavity opening. Additional bonds to the RNA backbone of the terminal loop further strengthen the protein:RNA interaction (Figs. 1C and 4A). Differences between solution conformations of the IRE terminal loop and the conformation in the IRP1:IRE complex are consistent with a mutually induced fit mechanism of binding.

Conserved C8 is the focal point for IRE stem binding with IRP1 (Fig. 1C), consistent with mutagenesis studies that showed a preference for a cytidine at position 8 (*2*, *31*). As mentioned above, the base of C8 occupies a pocket on the inner surface of domain 4, sandwiched between Arg^{713} and Arg^{780}, two active site residues of c-aconitase (Fig. 4B). Arg^{780}, whose mutation to asparagine abolishes IRE binding (*27*), is also in range for ionic interactions with the 3′ phosphate of C8 (Figs. 1C and 4B). The base of C8 has hydrogen bonds to Ser^{681}, Pro^{682}, Asp^{781}, and Trp^{782} (Fig. 4B). An unusual feature of the C8 pocket is that three of the four intrapocket bonds (the exception is Ser^{681}) involve backbone atoms. Specificity likely comes from the small volume of the C8 pocket and the bonding pattern. Substitution of C8 to G or A is sterically prohibited, whereas a U substitution would cause the loss of the H-donor capacity of the N4 amino group.

An IRP-specific subdomain (residues 680 to 730), predicted to be involved in RNA binding (*18*, *25*), cradles the lower stem of the IRE, with residues 681 to 685 running along the minor groove of the lower stem of the ferritin H IRE. At the closest approach between the protein and RNA in this region, the side chain of Asn^{685}

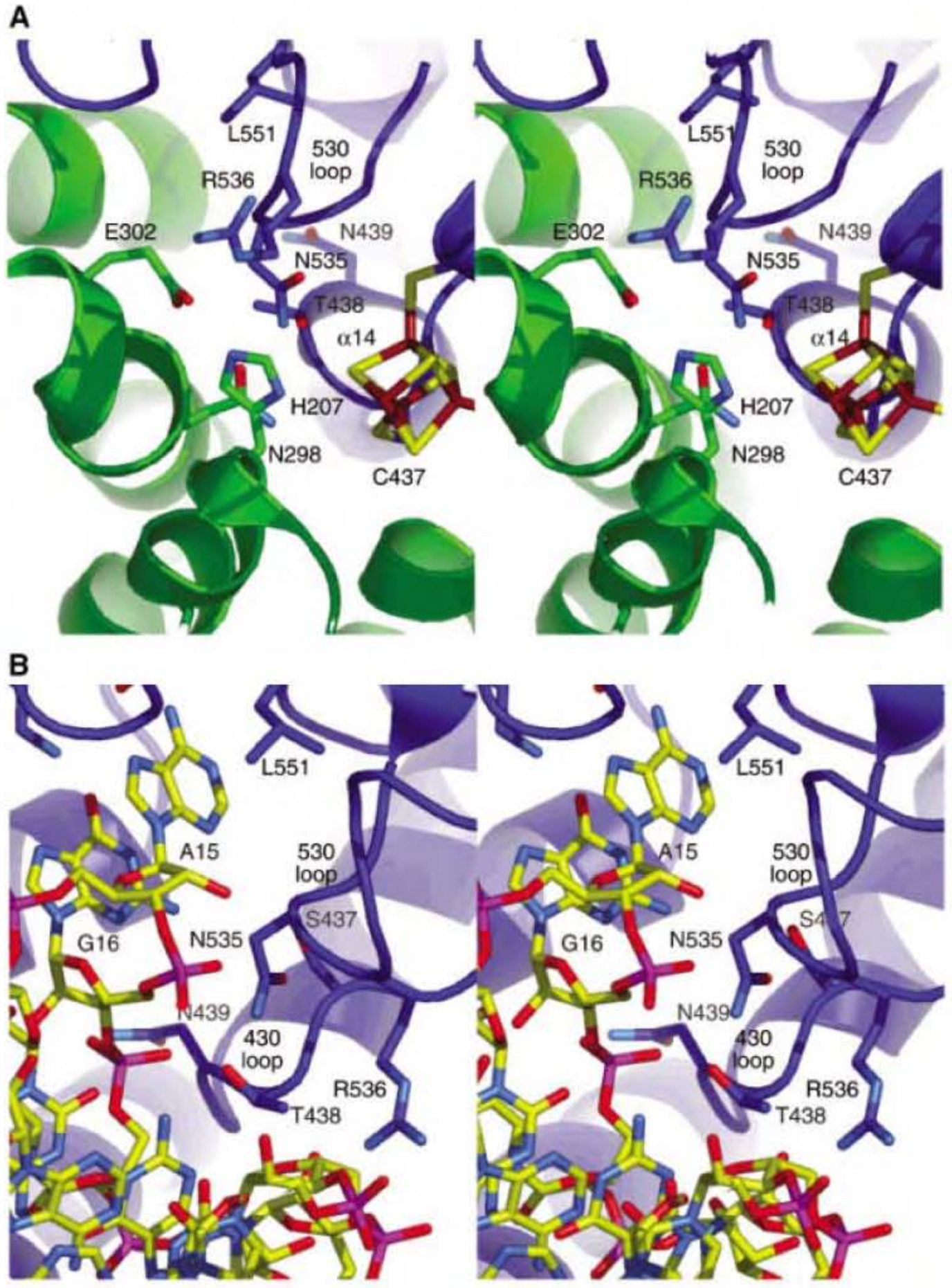

Fig. 3. Structural differences between ligand-binding regions in c-aconitase and IRP1:IRE-RNA complex. (**A**) Stereo diagram for c-aconitase. Shown is the environment of the Fe-S cluster where Cys^{437} from α14 and Asn^{535} from the 530 loop contribute to binding (*18*). (**B**) Stereo diagram of this region in IRP1:IRE-RNA complex, viewed in the same orientation. α14 (now labeled 430 loop) and the 530 loop of c-aconitase are rearranged, and residues from each contribute to RNA binding. A reference point for comparing these two views is the largely unchanged Leu^{551} and nearby loops at the top of the figures. See also movie S2.

protrudes into the minor groove and binds to the N2 of G26 (Fig. 4B). Displacement of G26 by nonstandard pairing with U5 facilitates the interaction. The U5:G26 wobble pair is not conserved in IREs, and asparagine is replaced by serine at the position equivalent to 685 in IRP2 and all non–IRE-binding homologs of IRP1, such as c-aconitase in plants and *Caenorhabditis elegans*. The natural variations in the IRE lower stem and the 685 position in IRPs may also be important determinants for IRP:IRE selectivity.

Basis for IRE-RNA selectivity. The effect of binding a single IRE molecule through interactions at two separate binding sites essentially eliminates the possibility of significant interactions with nonspecific RNAs. Two-point recognition in the IRP1:IRE complex is analogous to the transfer RNA (tRNA):aminoacyl-tRNA synthetase complexes, where the individual RNA binding sites relate to the dual requirements of tRNA selectivity and aminoacylation (*32*). An advantage of two-point recognition in IRP:IRE interaction may be the quantitatively different responses observed for different IRE-mRNAs to the same biological signal (*3*, *4*, *17*). Conserved sequence and structure at the IRE terminal loop and C8 is coupled with variation in helix sequence and mid-helix distortion near C8, known to influence IRP binding (*15*, *33*, *34*). Such IRE-mRNA–specific variations may establish different protein:RNA interactions. The excess IRP1 bonding capacity apparent in the IRP1:IRE complex supports such a model. Several amino acids are approximately in position for hydrogen bonding (e.g., Arg^{153}, His^{207}, Lys^{266}, Gln^{377}, Arg^{704}, and Ser^{778}), but too far (>3.7 Å) for direct contact with the ferritin H IRE. Thus, it is possible that in IRP1 (and, by inference, IRP2) alternate subsets of bonding groups are used for recognition of different IRE-RNAs. Such a combinatorial mode of binding would explain the graded response of different IRE-mRNAs to IRP regulation.

Conformational plasticity and dual functionality. The RNA-binding and enzyme active sites extensively overlap in IRP1, with many amino acids serving important, but different, roles in each functional state of the protein (Fig. 1C) (*18*). The functional plasticity of amino acids serving both catalytic and RNA binding roles reflects the conformational flexibility of the protein, particularly in the vicinity of the Fe-S and RNA binding sites. Given the high conservation of the RNA binding residues among c-aconitases, including those c-aconitases that lack IRE-binding ability [e.g., (*35*)], residues that confer the structural flexibility may be the key determinants of RNA binding.

Many of the details of IRP1:IRE interaction revealed in this work should also apply to IRP2, on the basis of the high sequence similarity and IRE-RNA–binding preferences shared between the IRPs. What remains to be determined is the evolutionary origin and selective advantage of such dramatic conformational plasticity and dual functionality encoded in IRP1.

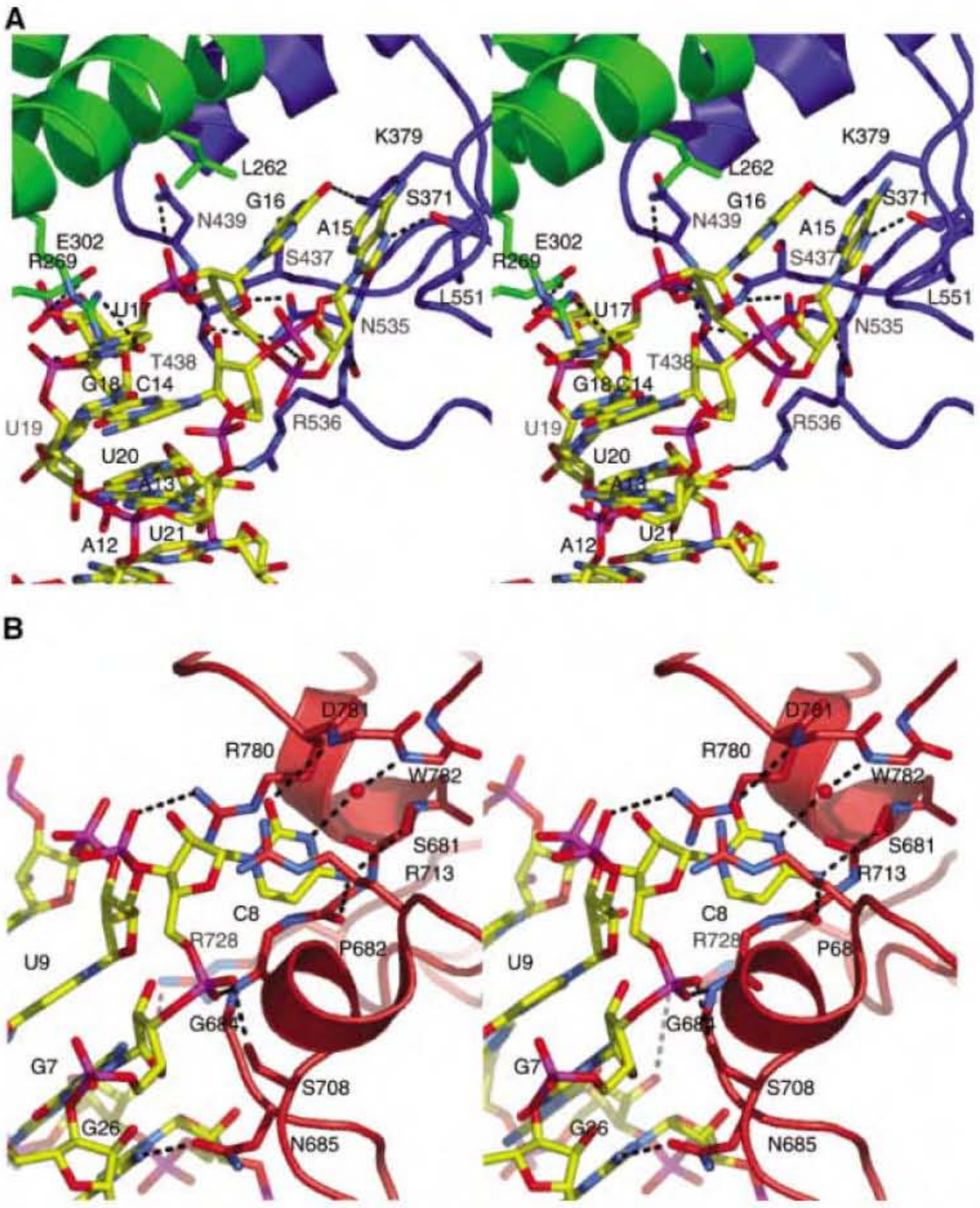

Fig. 4. Stereo diagrams of the interactions of IRP1 with the IRE-RNA. (**A**) Binding of the terminal loop within the cavity between domain 2 (green) and domain 3 (blue). The orientation is the same as that in Fig. 1A. A15 and G16 make base-specific bonds to Ser^{371} and Lys^{379}, respectively. Leu^{551} and Leu^{262} provide van der Waal's contacts to the exposed faces of A15 and G16. The cavity interior contains water molecules that hydrate the remaining groups of the two bases (not shown). At the cavity opening, the side chain of Arg^{269} specifically binds to U17, and the planar carboxyl group of Glu^{302} makes a stacking interaction with U17, the top stacked base of the IRE stem. (**B**) C8 binding pocket in domain 4. The orientation is from the reverse of Fig. 1A. The amide nitrogen of Asp^{781} binds to the O2 oxo group of C8, and the amide nitrogen of Trp^{782} binds to the ring N3 through an intervening water molecule. Ser^{681} and Pro^{682} provide the third and fourth hydrogen bonds to the base of C8, both to the N4 amino group.

References and Notes

1. M. W. Hentze, M. U. Muckenthaler, N. C. Andrews, *Cell* **117**, 285 (2004).
2. M. W. Hentze, L. C. Kühn, *Proc. Natl. Acad. Sci. U.S.A.* **93**, 8175 (1996).
3. E. C. Theil, R. S. Eisenstein, *J. Biol. Chem.* **275**, 40659 (2000).
4. R. S. Eisenstein, *Annu. Rev. Nutr.* **20**, 627 (2000).
5. M. C. Kennedy, L. Mende-Mueller, G. A. Blondin, H. Beinert, *Proc. Natl. Acad. Sci. U.S.A.* **89**, 11730 (1992).
6. B. R. Henderson, L. C. Kühn, *J. Biol. Chem.* **270**, 20509 (1995).
7. D. E. Draper, *J. Mol. Biol.* **293**, 255 (1999).
8. Y. Chen, G. Varani, *FEBS J.* **272**, 2088 (2005).
9. J. Schlegl *et al.*, *RNA* **3**, 1159 (1997).
10. C. M. Harrell, A. R. McKenzie, M. M. Patino, W. E. Walden, E. C. Theil, *Proc. Natl. Acad. Sci. U.S.A.* **88**, 4166 (1991).
11. B. R. Henderson, E. Menotti, L. C. Kühn, *J. Biol. Chem.* **271**, 4900 (1996).
12. L. G. Laing, K. B. Hall, *Biochemistry* **35**, 13586 (1996).
13. K. J. Addess, J. P. Basilion, R. D. Klausner, T. A. Rouault, A. Pardi, *J. Mol. Biol.* **274**, 72 (1997).
14. Z. Gdaniec, H. Sierzputowska-Gracz, E. C. Theil, *Biochemistry* **37**, 1505 (1998).
15. Y. Ke, J. Wu, E. A. Leibold, W. E. Walden, E. C. Theil, *J. Biol. Chem.* **273**, 23637 (1998).
16. T. A. Rouault, *Nat. Chem. Biol.* **2**, 406 (2006).
17. O. S. Chen, K. L. Schalinske, R. S. Eisenstein, *J. Nutr.* **127**, 238 (1997).

18. J. Dupuy *et al.*, *Structure* **14**, 129 (2006).
19. X. Brazzolotto, P. Timmins, Y. Dupont, J. M. Moulis, *J. Biol. Chem.* **277**, 11995 (2002).
20. C. C. Philpott, D. Haile, T. A. Rouault, R. D. Klausner, *J. Biol. Chem.* **268**, 17655 (1993).
21. H. Hirling, B. R. Henderson, L. C. Kühn, *EMBO J.* **13**, 453 (1994).
22. A. I. Selezneva, G. Cavigiolio, E. C. Theil, W. E. Walden, K. Volz, *Acta Crystallogr.* **F62**, 249 (2006).
23. J. P. Basilion, T. A. Rouault, C. M. Massinople, R. D. Klausner, W. H. Burgess, *Proc. Natl. Acad. Sci. U.S.A.* **91**, 574 (1994).
24. G. R. Swenson, W. E. Walden, *Nucleic Acids Res.* **22**, 2627 (1994).
25. P. Kaldy, E. Menotti, R. Moret, L. C. Kühn, *EMBO J.* **18**, 6073 (1999).
26. V. Gegout *et al.*, *J. Biol. Chem.* **274**, 15052 (1999).
27. C. C. Philpott, R. D. Klausner, T. A. Rouault, *Proc. Natl. Acad. Sci. U.S.A.* **91**, 7321 (1994).
28. S. Jones, D. T. Daley, N. M. Luscombe, H. M. Berman, J. M. Thornton, *Nucleic Acids Res.* **29**, 943 (2001).
29. Z. Kikinis, R. S. Eisenstein, A. J. Bettany, H. N. Munro, *Nucleic Acids Res.* **23**, 4190 (1995).
30. P. C. Haasnoot, J. F. Bol, R. C. Olsthoorn, *Proc. Natl. Acad. Sci. U.S.A.* **100**, 12596 (2003).
31. B. R. Henderson, E. Menotti, C. Bonnard, L. C. Kühn, *J. Biol. Chem.* **269**, 17481 (1994).
32. P. J. Beuning, K. Musier-Forsyth, *Biopolymers* **52**, 1 (1999).
33. R. Erlitzki, J. C. Long, E. C. Theil, *J. Biol. Chem.* **277**, 42579 (2002).
34. Y. Ke, E. C. Theil, *J. Biol. Chem.* **277**, 2373 (2002).
35. B. L. Gourley, S. B. Parker, B. J. Jones, K. B. Zumbrennen, E. A. Leibold, *J. Biol. Chem.* **278**, 3227 (2003).
36. Single-letter abbreviations for the amino acid residues are as follows: A, Ala; C, Cys; D, Asp; E, Glu; F, Phe; G, Gly; H, His; I, Ile; K, Lys; L, Leu; M, Met; N, Asn; P, Pro; Q, Gln; R, Arg; S, Ser; T, Thr; V, Val; W, Trp; and Y, Tyr.
37. QUANTA, 1997 (Molecular Simulations, Inc., San Diego, CA, 1997).
38. W. L. DeLano, *The PyMOL Molecular Graphics System* (DeLano Scientific, San Carlos, CA, 2002).
39. Supported by grants from the National Institutes of Health (DK47281 to W.E.W., DK20251 to E.C.T., and GM47522 to K.V.). We thank E. A. Craig, R. S. Eisenstein, H. Noller, T. A. Steitz, and D. S. Ucker for critical review of the manuscript. Data were collected at the Southeast regional collaborative access team (SER-CAT) 22-ID at the Advanced Photon Source, Argonne National Laboratory. Use of the Advanced Photon Source was supported by the Department of Energy under contract No. W-31-109-Eng-38. Structure factors and coordinates have been deposited in the Protein Data Bank (accession code 2IPY).

Supporting Online Material

www.sciencemag.org/cgi/content/full/314/5807/1903/DC1
Materials and Methods
Tables S1 and S2
References
Movies S1 and S2

27 July 2006; accepted 3 November 2006
10.1126/science.1133116

REPORTS

A Gaseous Metal Disk Around a White Dwarf

B. T. Gänsicke,* T. R. Marsh, J. Southworth, A. Rebassa-Mansergas

The destiny of planetary systems through the late evolution of their host stars is very uncertain. We report a metal-rich gas disk around a moderately hot and young white dwarf. A dynamical model of the double-peaked emission lines constrains the outer disk radius to just 1.2 solar radii. The likely origin of the disk is a tidally disrupted asteroid, which has been destabilized from its initial orbit at a distance of more than 1000 solar radii by the interaction with a relatively massive planetesimal object or a planet. The white dwarf mass of 0.77 solar mass implies that planetary systems may form around high-mass stars.

White dwarfs are the compact end products of stars with masses up to ~8 solar masses ($M_\odot$) (*1*). Because of the low luminosity of white dwarfs, the detection of low-mass stellar companions (*2*) or planets (*3*) is much easier around white dwarfs than around main-sequence stars. During a search for cool companions to white dwarfs, an excess infrared flux was discovered around the white dwarf G29-38 (*4*). The atmosphere of G29-38 has been found to be enriched with metals, i.e., elements heavier than helium. The sedimentation time scales of heavy elements in the high-gravity atmospheres of white dwarfs are short compared to the evolutionary time scale of these stars (*5*) and, hence, the high metal abundances in G29-38 imply that this star is accreting at a relatively high rate (*6*). Deep imaging and asteroseismological studies of G29-38 ruled out a brown dwarf companion (*7*, *8*) and led to the hypothesis of a cool dust cloud around the white dwarf. The presence of dust near G29-38 has been verified by infrared observations with the Spitzer Space Telescope (*9*). Infrared surveys of white dwarfs exhibiting metal-enriched atmospheres recently led to the discovery of three other potential dust disks (*10*–*12*). A possible origin of such dust disks is the tidal disruption of either comets (*13*) or asteroids (*14*). Asteroids appear to be more likely candidates because they can explain the large amount of metals accreted by the white dwarfs from the dusty environment, as well as the absence of hydrogen or helium. Although the detection of asteroid debris around G29-38 and the other white dwarfs represents a possible link to the existence of planetary systems around their main-sequence progenitor stars, modeling the excess infrared luminosity provides no direct information on the geometric location and extension of the dust, impeding a more detailed understanding of the nature and origin of the circumstellar material (*9*). A concentration of dust in the equatorial plane around G29-38 has been suggested on the basis of the relative amplitudes of non-radial white dwarf pulsations observed in the optical and infrared wavebands (*7*).

We identified SDSS J122859.93+104032.9 (henceforth SDSS 1228+1040) as a moderately hot white dwarf in the Data Release 4 of the Sloan Digital Sky Survey (SDSS) (*15*), but noted very unusual emission lines of the Ca II 850- to 866-nm triplet, as well as weaker emission lines of Fe II at 502 and 517 nm. The line profiles of the Ca II triplet display a distinct double-peaked morphology, which is the hallmark of a gaseous, rotating disk (*16*, *17*). Time-resolved spectroscopy (Fig. 1) and photometry do not reveal any radial velocity or brightness variations. These data exclude the possibility that SDSS 1228+1040 is an interacting white dwarf binary, in which an accretion disk around the white dwarf forms from material supplied by a nearby companion star. Furthermore, the absence of Balmer and helium emission lines implies that the gaseous disk around SDSS 1228+1040 must be extremely deficient in volatile elements, which independently rules out an interacting binary nature for this object.

Our detection of double-peaked metal emission lines from a circumstellar disk in SDSS 1228+1040 provides direct evidence for hydrogen- and helium-

Table 1. System parameter of SDSS 1228+1040. My, millions of years.

Distance	142 ± 15 pc
Effective temperature	22,020 ± 200 K
White dwarf mass	0.77 ± 0.02 $M_\odot$
White dwarf radius	0.0111 ± 0.0003 $R_\odot$
White dwarf cooling age	100 ± 5 My
Helium abundance	≤0.1 × solar
Calcium abundance	0.8 ± 0.15 × solar
Progenitor mass	4 to 5 $M_\odot$
Progenitor main-sequence life time	~ 70 My
Ca II full-width at zero intensity	1270 ± 35 km/s
Ca II peak separation	630 ± 5 km/s
Outer radius of the circumstellar disk	≅ 1.2 $R_\odot$
Ellipticity	0.021

Department of Physics, University of Warwick, Coventry CV4 7AL, UK.

*To whom correspondence should be addressed. E-mail: boris.gaensicke@warwick.ac.uk

depleted material rotating around a white dwarf at a very short distance in a flat, disklike structure. Assuming that the Ca II line profiles (Fig. 1) originate indeed in a circumstellar disk, it must have an azimuthal asymmetry to match the asymmetry in the profiles. Such asymmetries are known in the disks around B-type emission-line stars (Be stars) (*18*). Drawing upon this analogy, we developed a dynamical model of the Ca II line profiles [Fig. 2; supporting online material (SOM) text, section 1), which provides a robust constraint on the outer radius of the disk of ≅ 1.2 solar radii ($R_\odot$).

As the main-sequence stars hosting planetary systems evolve through the red-giant stage, they swell up and destroy planets and asteroids out to many hundred solar radii (*19*). The white dwarf mass of SDSS 1228+1040 implies a relatively massive main-sequence progenitor of ~4 to 5 $M_\odot$ (*20*), which will have expanded to a radius of ~1000 $R_\odot$ (*21*). It is therefore impossible that the material making up the present-day disk has survived the giant phase at its current location; it must instead have been brought inward from outside a distance of 1000 $R_\odot$. Planetary debris that migrated outward to large radii during the giant phase is expected to have relatively stable orbits unless perturbed by larger-mass objects (*13*). A likely scenario is therefore that one or more planets that survived the evolution of the progenitor of SDSS 1228+1040 destabilized the orbit of an asteroid sometime after the end of the planetary nebula phase. When it gets close enough to the compact star, the asteroid is tidally disrupted, forming a disk of metal-rich debris, which subsequently sublimates in the radiation field of the white dwarf. The radius derived from our dynamical model is indeed compatible with the tidal disruption radius for a rocky asteroid (*22*).

A strong Mg II 448-nm absorption line is detected in the spectrum of the white dwarf and implies a magnesium abundance in its atmosphere comparable to that of the Sun. This is extremely unusual for white dwarfs, which typically have pristine hydrogen atmospheres. The large abundance of magnesium can be explained only by sustained accretion, because the diffusion time scale for magnesium in a white dwarf atmosphere of 22,000 K (Fig. 3 and Table 1) is only ~5 days (*23*). Moreover, the accreted material must be of very low helium abundance, because small traces of helium already mixed into the radiative atmosphere of the white dwarf would cause noticeable He I 447-nm absorption, which is not observed. The absence of helium lines in the white dwarf spectrum places an upper limit on the helium abundance of the material accreted from the circumstellar disk of 0.1 times the solar value, which is independent evidence for a metal-rich composition of the disk around SDSS 1228+1040.

No infrared excess has been found around metal-polluted white dwarfs hotter than 15,000 K (*12*), which suggests that the radiation field of these hot white dwarfs causes sublimation of a dust disk. The case of SDSS 1228+1040 dem-

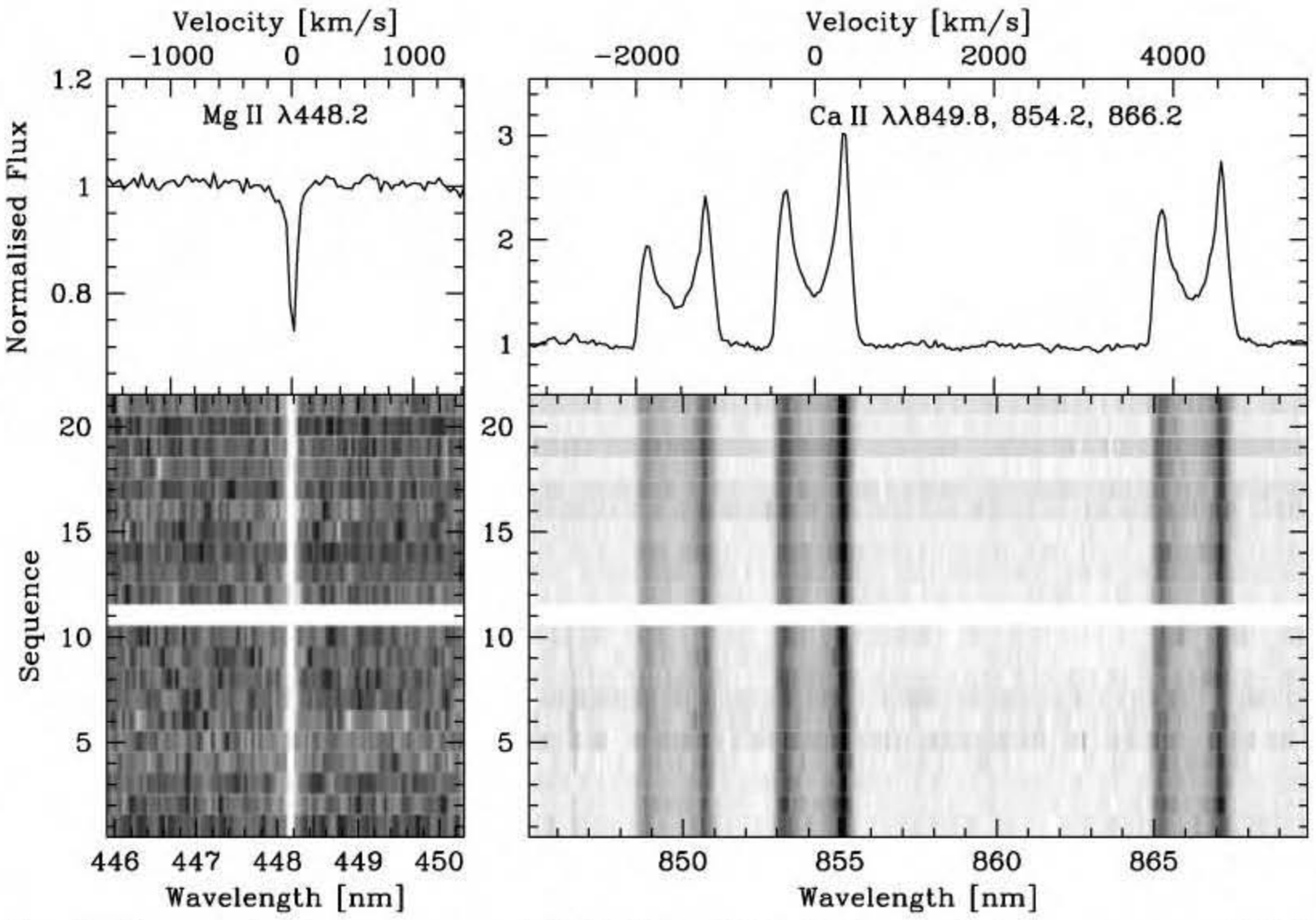

Fig. 1. Time-resolved spectroscopy of SDSS 1228+1040. Medium-resolution spectroscopy of SDSS 1228+1040 was obtained with the double-arm spectrograph ISIS on the 4.2-m William Herschel Telescope on La Palma, Canary Islands. Two sets of 10 consecutive spectra each were obtained on 30 June 2006 and 1 July 2006. The exposure times of the individual spectra were 600 s. The bottom panels show the two time series of spectra, each extending over 1.7 hours, centered on the calcium emission triplet (**right**) and the magnesium absorption line (**left**). The normalized average spectra are shown in the top panels. Radial velocities are given in the upper axes with respect to Ca II 854 nm (right) and Mg II 448 nm (left). The radial velocity of the Mg II line is stable to within ±4 km/s over time scales of 20 min to 1 day. Additional time-series photometry obtained at the Isaac Newton Telescope shows the star at constant brightness within ±0.01 mag.

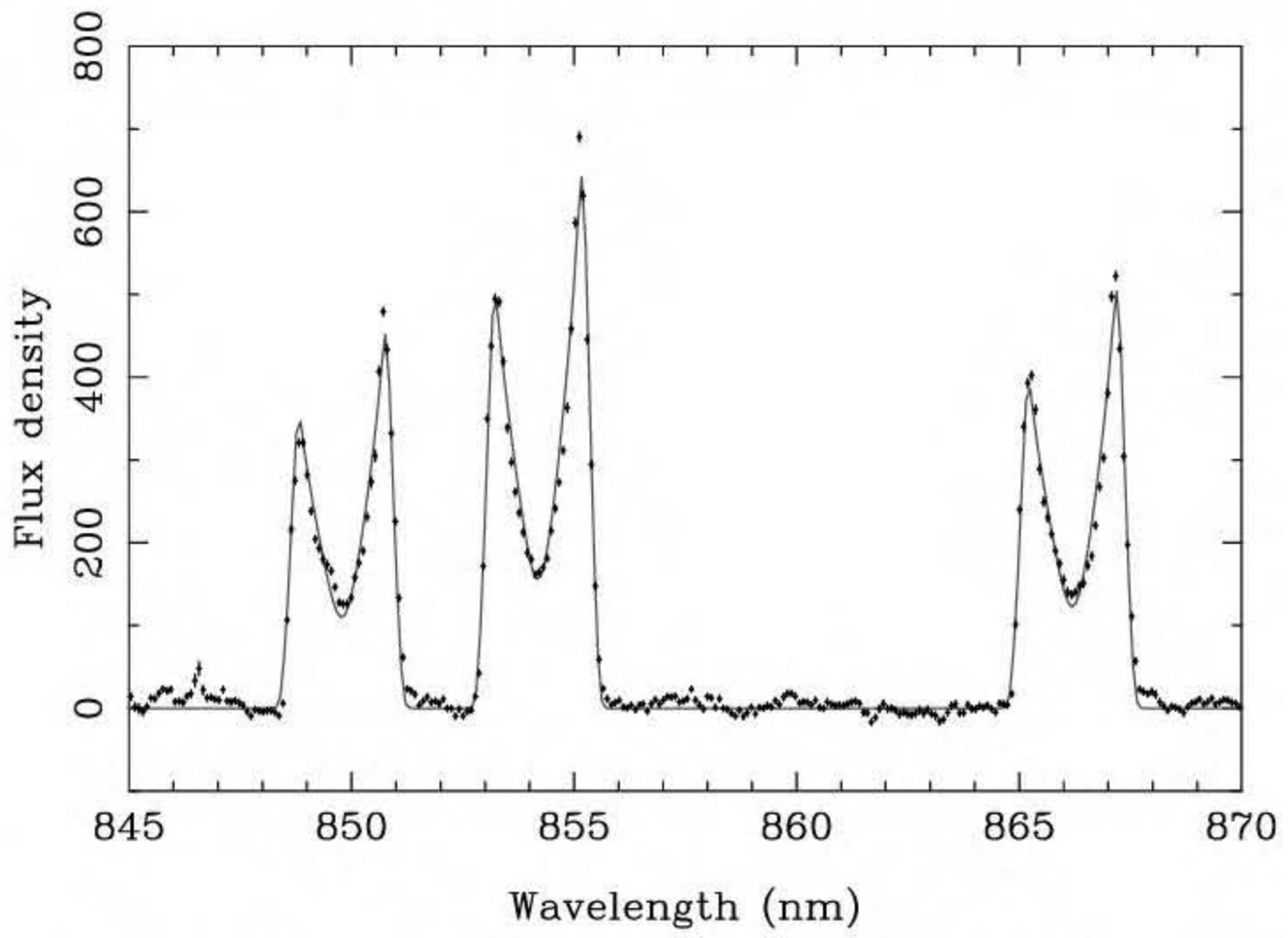

Fig. 2. A dynamical debris disk model. We modeled the observed Ca II emission line profiles (points) by assuming that the orbits in the disk took the form of a series of coaligned elliptical orbits of constant eccentricity (SOM text, section 1). We find an outer radius of 1.2 $R_\odot$ for an edge-on disk and an ellipticity of 0.021. The measured outer radius of the disk is relatively invulnerable to the detailed assumptions of the model because it is primarily fixed by the velocities of the emission-line peaks. The value given has to be interpreted as an upper limit because the radius scales as $\sin^2 i$ for disks inclined by angle i to the line of sight. The deep central dips of the profiles imply optically thick emission (*17*) and suggest that the orbital inclination must be quite high (>70°), and therefore the 1.2-$R_\odot$ upper limit should be close to the true value.

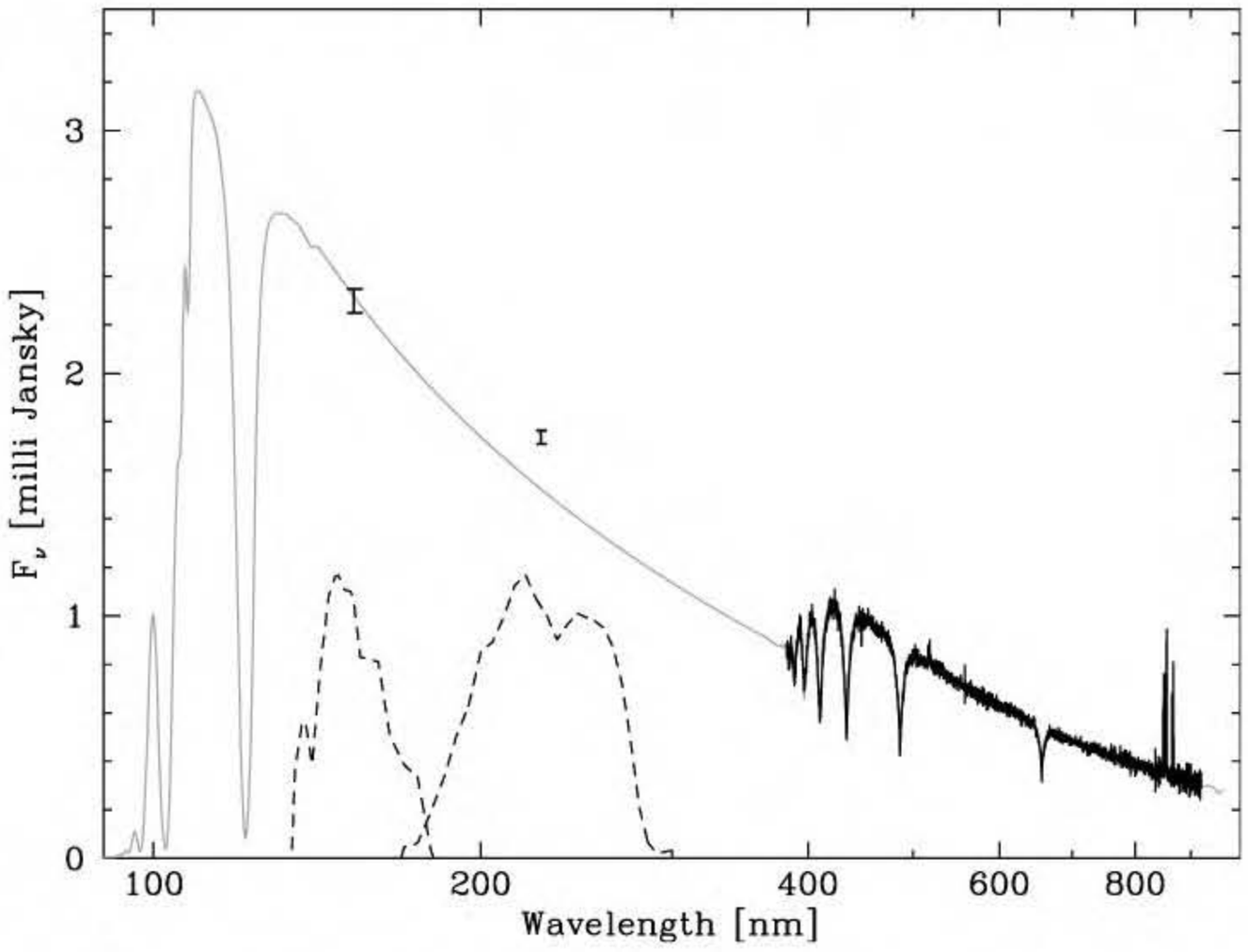

Fig. 3. A model of the white dwarf in SDSS 1228+1040. The optical SDSS spectrum of SDSS 1228+1040 is plotted in black. In addition to the Ca II emission lines seen in Fig. 1, Fe II 517 nm (and 502 nm, not visible at the plotted scale) is detected as well. The signal-to-noise ratio of the iron lines is too low to assess the shape of their profiles. The observed spectrum was modeled with synthetic white dwarf spectra (*25*), resulting in an effective temperature of $T_{WD} = 22{,}020 \pm 120$ K, a surface gravity of $\log g = 8.24 \pm 0.04$, an abundance of Mg II of 0.8 ± 0.15 with respect to solar abundances, and a limit of $v \sin i \leq 20$ km/s on the rotation rate of the white dwarf. The best-fit white dwarf model is plotted in gray. The ultraviolet fluxes detected by Galaxy Evolution Explorer (GALEX; http://galex.stsci.edu/GR2/) are indicated as black error bars, and the filter transmission curves of GALEX are shown by dashed lines. The best-fit white dwarf model is consistent with the far-ultraviolet GALEX flux, but a flux excess is observed in the near-ultraviolet. A host of Fe II transitions lie within the near-ultraviolet bandpass (*6*) and could be in emission in SDSS 1228+1040, explaining the observed flux excess.

onstrates that planetary debris material can be detected around younger and hotter white dwarfs in the form of gaseous disks. Prompted by the discovery of SDSS 1228+1040, we have inspected 406 SDSS spectra of white dwarfs with hydrogen-dominated atmospheres brighter than 17.5 in the *g*-bandpass that are contained in the SDSS Data Release 4 (*24*), and we find just one additional object that potentially exhibits flux excess in the region of the Ca II triplet (SDSS J104341.53+085558.2, fig. S1), so SDSS 1228+1040 is clearly a rare object. The detection of a metal-rich debris disk around this relatively massive white dwarf indicates that the formation of planetary systems can take place also around short-lived massive stars.

References and Notes

1. P. D. Dobbie *et al.*, *Mon. Not. R. Astron. Soc.* **369**, 383 (2006).
2. J. Farihi, E. E. Becklin, B. Zuckerman, *Astrophys. J. Suppl.* **161**, 394 (2005).
3. M. R. Burleigh, F. J. Clarke, S. T. Hodgkin, *Mon. Not. R. Astron. Soc.* **331**, L41 (2002).
4. B. Zuckerman, E. E. Becklin, *Nature* **330**, 138 (1987).
5. C. Paquette, C. Pelletier, G. Fontaine, G. Michaud, *Astrophys. J. Suppl.* **61**, 177 (1986).
6. D. Koester, J. Provencal, H. L. Shipman, *Astron. Astrophys.* **320**, L57 (1997).
7. J. R. Graham, K. Matthews, G. Neugebauer, B. T. Soifer, *Astron. J.* **357**, 216 (1990).
8. M. J. Kuchner, C. D. Koresko, M. E. Brown, *Astrophys. J. Lett.* **508**, L81 (1998).
9. W. T. Reach *et al.*, *Astrophys. J. Lett.* **635**, L161 (2005).
10. E. E. Becklin *et al.*, *Astrophys. J. Lett.* **632**, L119 (2005).
11. M. Kilic, T. von Hippel, S. K. Leggett, D. E. Winget, *Astrophys. J. Lett.* **632**, L115 (2005).
12. M. Kilic, T. von Hippel, S. K. Leggett, D. E. Winget, *Astrophys. J.* **646**, 474 (2006).
13. J. H. Debes, S. Sigurdsson, *Astrophys. J.* **572**, 556 (2002).
14. M. Jura, *Astrophys. J. Lett.* **584**, L91 (2003).
15. J. K. Adelman-McCarthy *et al.*, *Astrophys. J. Suppl.* **162**, 38 (2006).
16. P. Young, D. P. Schneider, S. A. Shectman, *Astrophys. J.* **245**, 1035 (1981).
17. K. Horne, T. R. Marsh, *Mon. Not. R. Astron. Soc.* **218**, 761 (1986).
18. A. Meilland, P. Stee, J. Zorec, S. Kanaan, *Astron. Astrophys.* **455**, 953 (2006).
19. I.-J. Sackmann, A. I. Boothroyd, K. E. Kraemer, *Astrophys. J.* **418**, 457 (1993).
20. T. Blöcker, *Astron. Astrophys.* **299**, 755 (1995).
21. J. R. Hurley, O. R. Pols, C. A. Tout, *Mon. Not. R. Astron. Soc.* **315**, 543 (2000).
22. B. J. R. Davidsson, *Icarus* **142**, 525 (1999).
23. D. Koester, D. Wilken, *Astron. Astrophys.* **453**, 1051 (2006).
24. D. J. Eisenstein *et al.*, *Astrophys. J. Suppl.* **167**, 40 (2006); preprint available at http://arxiv.org/abs/astro-ph/0606700 (2006).
25. I. Hubeny, T. Lanz, *Astrophys. J.* **439**, 875 (1995).

26. B.T.G., T.R.M., J.S., and A.R.M. were supported by an Advanced Fellowship from the Particle Physics and Astronomy Research Council (PPARC), a Senior Research Fellowship, a postdoctoral grant, and a joint PPARC-IAC (Instituto de Astrofísica de Canarias) studentship. The observations were obtained at the Spanish Observatorio del Roque de los Muchachos, IAC, with the William Herschel Telescope and Isaac Newton Telescope. We thank P. Wheatley for constructive comments on the manuscript, D. Koester for discussions on diffusion time scales, and I. Hubeny for ongoing support of the TLUSTY/SYNSPEC codes. Funding for the SDSS and SDSS-II was provided by the Alfred P. Sloan Foundation, the participating institutions, NSF, the U.S. Department of Energy, NASA, the Japanese Monbukagakusho, the Max Planck Society, and the Higher Education Funding Council for England. The SDSS Web site is at www.sdss.org/.

Supporting Online Material

www.sciencemag.org/cgi/content/full/314/5807/1908/DC1
SOM Text
Fig. S1
References

12 September 2006; accepted 25 October 2006
10.1126/science.1135033

Distinct Fermi-Momentum–Dependent Energy Gaps in Deeply Underdoped Bi2212

Kiyohisa Tanaka,[1,2] W. S. Lee,[1] D. H. Lu,[1] A. Fujimori,[3] T. Fujii,[4] Risdiana,[5] I. Terasaki,[5] D. J. Scalapino,[6] T. P. Devereaux,[7,8] Z. Hussain,[2] Z.-X. Shen[1]*

We used angle-resolved photoemission spectroscopy applied to deeply underdoped cuprate superconductors $Bi_2Sr_2Ca_{(1-x)}Y_xCu_2O_8$ (Bi2212) to reveal the presence of two distinct energy gaps exhibiting different doping dependence. One gap, associated with the antinodal region where no coherent peak is observed, increased with underdoping, a behavior known for more than a decade and considered as the general gap behavior in the underdoped regime. The other gap, associated with the near-nodal regime where a coherent peak in the spectrum can be observed, did not increase with less doping, a behavior not previously observed in the single particle spectra. We propose a two-gap scenario in momentum space that is consistent with other experiments and may contain important information on the mechanism of high–transition temperature superconductivity.

The pseudogap phase of underdoped cuprates has proven to be an important region for discoveries and surprises in the field of high-transition temperature (T_c) superconductors (*1*). Early angle-resolved photoemission spectroscopy (ARPES) (*2*) and electron tunneling experi-

ments from lightly underdoped samples (*3*) suggested that the pseudogap has similar characteristics to the superconducting gap below T_c, consistent with the idea that the pseudogap is a precursor to the $d_{x^2-y^2}$ superconducting state but lacks pair phase coherence. In this scenario, below T_c where the phase coherence of pairs is established, the pseudogap smoothly evolves into the superconducting gap. There is only one energy scale in the system, and it is associated with the magnitude of the gap at the antinode. This antinodal gap was found via ARPES (*4*), thermal conductivity (*5*), and tunneling measurements (*6*) to increase as the doping was reduced from optimum. However, the energy gap obtained by Andreev reflection (*7*), penetration depth (*8*), and recent Raman experiments (*9*, *10*) of cuprates exhibits the opposite trend with doping suggesting a rather different scenario from the one-gap picture.

We present ARPES data for deeply underdoped $Bi_2Sr_2Ca_{(1-x)}Y_xCu_2O_8$ (Bi2212) crystals with T_c values of 50 K, 40 K, and 30 K, finding evidence for the existence of two distinct energy gaps in the single-particle spectral function (Materials and Methods). One gap manifests itself as a spectral weight suppression near the Brillouin zone boundary (antinodal region); this antinodal gap becomes larger with decreased doping, consistent with previous ARPES studies (*4*). The other gap is resolved near the diagonal of the zone (nodal region), where a quasi-particle peak can be observed. We find that the gap size of this near-nodal gap determined by empirical methods does not increase by decreasing doping level. We attribute our result as evidence for two distinct Fermi momentum–dependent energy gaps, with the gap near the nodal region corresponding to the superconducting gap and the gap near the antinodal region corresponding to the pseudogap state.

We show energy distribution curves (EDCs) along the Fermi surface (FS) for samples with T_c values of 50 K, 40 K, and 30 K (Fig. 1). Compared to previous ARPES studies on underdoped Bi2212 with a similar doping level (*11*), our data have much-improved quality; even for the most underdoped sample (T_c = 30 K), a clear quasi-particle (or coherence) peak can still be observed near the nodal region (Fig. 1B), which has not been seen previously in Bi2212 for such a low doping. This improvement makes possible a more quantitative data analysis. We first note that the line shape of the spectra shows a marked change along the FS. The sharp coherence peak gradually loses spectral weight when moving from the nodal region toward the antinodal region. In the antinodal region, the peak disappears, and only a broad hump in the spectrum located far away from the Fermi level (E_F) can be observed for the T_c = 30 K and T_c = 40 K samples. This behavior is consistent with previous studies of other underdoped cuprates such as $La_{2-x}Sr_xCuO_4$ (LSCO) and $Ca_{2-x}Na_xCuO_2Cl_2$ (Na-CCOC) (*12*, *13*). Here, we operationally define the Fermi arc as the region where one can see a peak in the superconducting state EDCs. The length of the Fermi arc decreases as the doping level of the samples decreases (Fig. 1, B to G and H inset).

[1]Department of Physics, Department of Applied Physics, and Stanford Synchrotron Radiation Laboratory, Stanford University, Stanford, CA 94305, USA. [2]Advanced Light Source, Lawrence Berkeley National Laboratory, Berkeley, CA 94720, USA. [3]Department of Physics and Department of Complexity Science and Engineering, University of Tokyo, Kashiwa, Chiba 277–8561, Japan. [4]Cryogenic Center, University of Tokyo, Bunkyo-ku, Tokyo 113–0032, Japan. [5]Department of Applied Physics, Waseda University, Tokyo 169–8555, Japan. [6]Department of Physics, University of California, Santa Barbara, CA 93106–9530, USA. [7]Department of Physics, University of Waterloo, Ontario N2L3G1, Canada. [8]Pacific Institute for Theoretical Physics, University of British Columbia, Vancouver, British Columbia V6T 1Z1, Canada.

*To whom correspondence should be addressed. E-mail: zxshen@stanford.edu

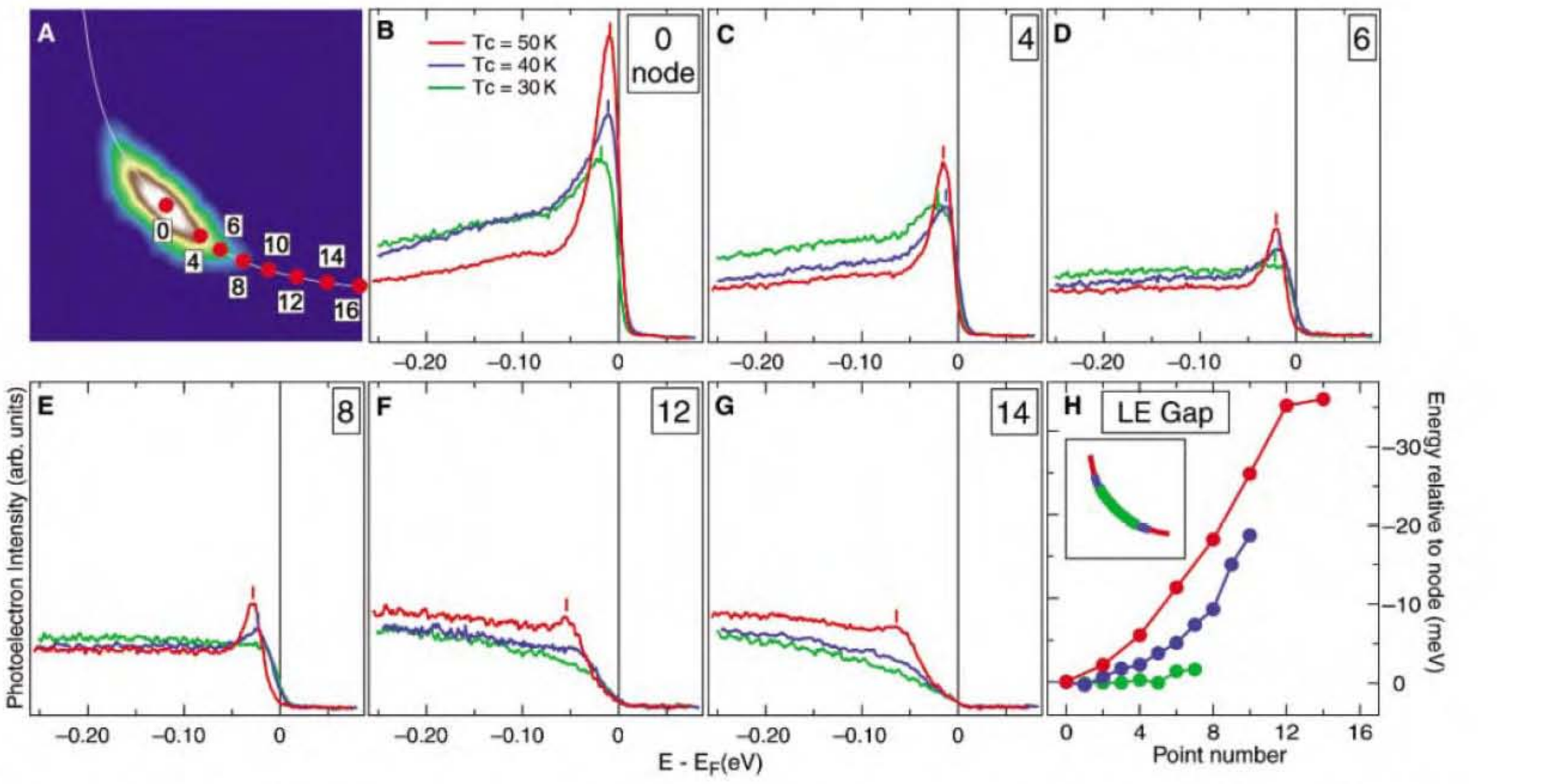

Fig. 1. Doping dependence of the ARPES spectra and leading edge position along the FS. (**A**) Intensity plot of the spectral weight of the T_c = 30 K sample, which is integrated within ±10 meV around E_F and symmetrized with respect to the diagonal of the zone. The intensity of diffraction replica due to supermodulation of the crystal structure has been cut off by color scale. The red dots labeled with numbers denote the k_F positions determined from the momentum distribution curves (MDC) at E_F. (**B** to **G**) The EDCs along the FS of the T_c = 30 K, T_c = 40 K, and T_c = 50 K samples. The number shown at the upper right corner corresponds to the k_F locations shown in (A). The vertical bars indicate the peak position of the EDC. The k_F region of the FS where a peak is visible in the EDCs is operationaly defined as the Fermi arc. (**H**) Doping dependence of the leading-edge position relative to that of the nodal spectrum within the Fermi arc. (Inset) The Fermi arc elongates toward the antinodal region of *k* space with increasing doping. The data shown were taken in the second Brillouin zone, where an enhancement of the spectra was observed (Materials and Methods).

We also plot the leading-edge gap (Fig. 1H), defined as the energy difference between the midpoint of the spectral leading edge and that of the nodal spectrum within the Fermi arc region. We find that the leading-edge gap is smaller for the lower T_c samples, suggesting that the energy gap associated with this Fermi arc region decreases with decreased doping. This doping dependence can be directly observed in the raw spectrum. The EDCs in the intermediate region (Fig. 1E) show that both the coherence peak position and the leading-edge gap of the T_c = 50 K sample are larger than the corresponding values for the T_c = 40 K and T_c = 30 K samples. Similar observations can also be deduced from Fig. 1, C and D, which are all still within the Fermi arc region. This gap-reduction trend within the Fermi arc region is opposite to the doping dependence of the energy gap in the antinodal region reported in previous ARPES studies (*4*) and is in conflict with the doping dependence of the energy gap inferred from thermal conductivity (*5*) and tunneling measurements (*6*).

In the antinodal region, the spectrum is characterized by a suppression of the spectral weight over a region that one associates with a pseudogap. To illustrate the difference in the doping dependence of the pseudogap and the energy gap associated with the Fermi arc, we have plot symmetrized EDCs (*14*) for the three samples for an intermediate Fermi arc k point (point 8) and an antinodal k point (point 16) (Fig. 2, A and B). As indicated by the shaded areas, the EDCs of point 16 show a larger gap with more underdoping, whereas the EDCs of point 8 exhibit

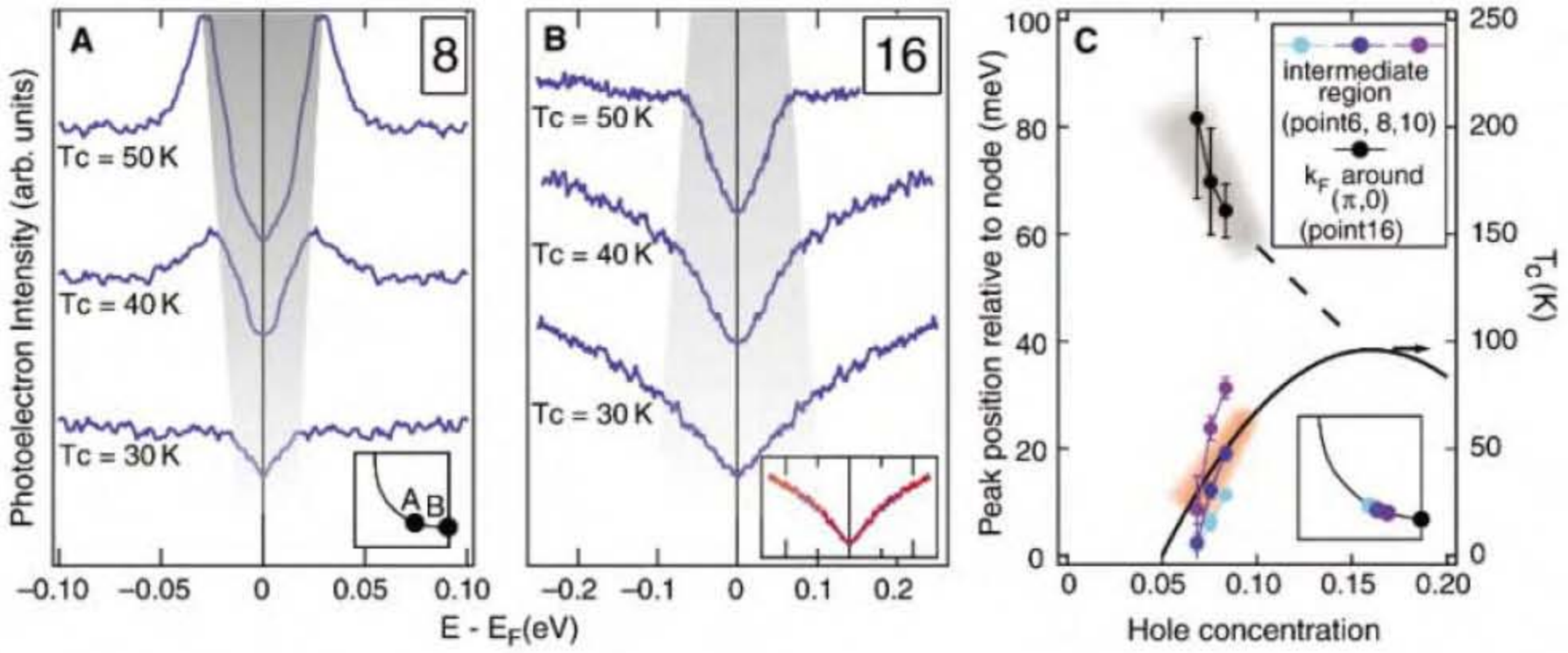

Fig. 2. Doping dependence of the symmetrized spectra at the intermediate region and the antinodal region. The symmetrized EDCs at (**A**) the intermediate region of the FS (point 8 in Fig. 1A) and (**B**) the antinodal region (point 16). Their corresponding locations on the FS are shown in the (A) inset. The shaded area denotes the region inside the gap determined by the peak positions of the EDCs. For the antinodal spectra, the position of the hump, which is determined from the second derivative of the spectra, is used as the peak position. (B) inset shows temperature dependence of the spectra of the T_c = 30 K sample taken at 10 K (blue) and 50 K (red) at the antinodal region. (**C**) Doping dependence of the peak position around the intermediate region (point 6, 8, and 10) and in the antinodal region (point 16), shown in the inset together with T_c. The dashed line indicates the pseudogap at the antinodal region reported by previous ARPES studies on Bi2212 system (*4*). The hole concentration (p) was estimated by using an empirical relationship, $T_c = 96[1 - 82.6(p - 0.16)^2]$. The error bars for the intermediate region measure the uncertainty of the gap due to the error of E_F and k_F, whereas the error bars for the antinodal region were estimated from the uncertainty of the peak position in second derivative spectra when applying different levels of smoothness to the raw spectra.

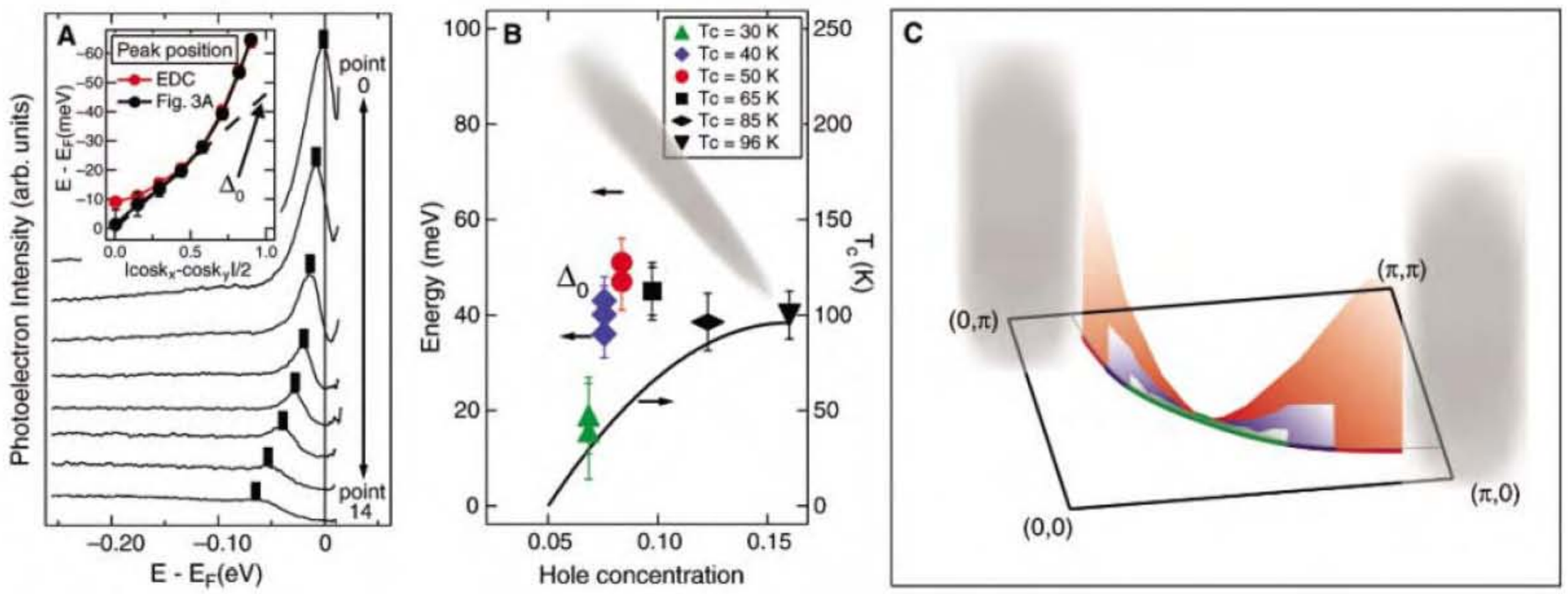

Fig. 3. Determination of Δ_0 and its doping dependence. (**A**) Spectra of the T_c = 50 K sample along the FS, which were divided by the FD function convoluted with the experimental resolution. The vertical bars indicate the peak position. (Inset) A comparison of the peak position in EDCs plotted against the d-wave function ($|\cos k_x - \cos k_y|/2$) for the raw EDCs and the FD function–divided EDCs. The dashed line illustrates an extrapolation of the straight section around the nodal region of the black curve, which leads to Δ_0 at $|\cos k_x - \cos k_y|/2 = 1$. (**B**) Doping dependence of the Δ_0. The gray shaded area is a guide to the eyes for the doping dependence of the energy gap at the antinodal region from data shown in Fig. 2C as well as existing published data (*27*). The values of Δ_0 for $T_c > 60$ K were taken from our ARPES studies of $Bi_2Sr_2Ca_{0.92}Y_{0.08}Cu_2O_{8+\delta}$ samples (Materials and Methods). (**C**) Doping dependence of the leading edge position in the k space. The same color assignment as (B) is used for an easy comparison.

the opposite trend with doping. There is essentially no change in the EDC of the $T_c = 30$ K sample between the superconducting ($T = 10$ K, blue line) and the normal ($T = 50$ K, red line) states in the antinodal region (Fig. 2B inset). This result also suggests that the broadening of the peak with temperature does not shift the leading-edge position downward in these deeply underdoped samples. For a more comprehensive view of the trend, we plotted the peak positions of EDCs relative to the node at various locations near the intermediate region (points 6, 8, and 10) and the antinodal region (point 16) (Fig. 2C). Apparently, the doping dependence of the energy gap along the Fermi arc differs from the dependence along the antinodal region. This behavior suggests that the energy gaps associated with the Fermi arc region and antinodal region represent two distinct energy gaps arising from different mechanisms. The antinodal gap appears to be related to the pseudogap and not related to superconductivity, whereas the nodal gap more likely represents the "real" superconducting gap because of the existence of a coherence peak in the spectrum. The distinction between the two gaps becomes smaller and harder to observe toward optimum doping (*1*–*4*). Although an earlier experiment near optimal doping had seen this same trend, the result was attributed to an anharmonic term in the *d*-wave gap (*15*). Uncovering the distinct spectral line shape in these deeply underdoped samples makes it possible to attribute to distinct energy gaps.

Because the energy gap in the antinodal region is primarily dominated by the pseudogap, it is not straightforward to estimate the magnitude of the maximum superconducting gap, Δ_0. We exploited a phenomenological method to estimate Δ_0. The EDCs along the Fermi arc were first divided by the Fermi-Dirac (FD) function at the measurement temperature convoluted with the experimental resolution (Fig. 3A). In this way, we could track the peak position of the single-particle spectral function without the complications of FD cutoff near E_F. We then plotted the peak position of these spectra with respect to the $d_{x^2-y^2}$ function ($|\cos k_x - \cos k_y|/2$) (Fig. 3A inset). The peak positions of these FD function–divided spectra lay on a straight line for k_F values in the nodal region, suggesting that the superconducting gap around the nodal region is consistent with this $d_{x^2-y^2}$ form. We then estimated Δ_0 by extrapolating this straight line to the boundary where $|\cos k_x - \cos k_y|/2 = 1$ (Fig. 3A inset). By using this method, we extracted Δ_0 for samples with various doping levels and summarized the result (Fig. 3B). The values of Δ_0 determined in this way increase as the doping changes from $T_c = 30$ K to $T_c = 50$ K, consistent with the behavior of the peak positions shown in Fig. 2C. Δ_0 reaches a maximum at a doping level of about 0.1 and then remains at the same size (or even slightly decreases) for doping levels up to the optimal doping level. Similar behavior appears in results obtained from Nernst effect measurements (*16*). Thus, taken at face value (*17*), the extrapolation of the nodal region data along with the behavior of the peak position at points 6, 8, and 10 suggest that the gap characteristic of the nodal region has a doping dependence distinct from that of the antinodal gap. Specifically, the nodal region gap has a *d*-wave momentum dependence with an amplitude that remains relatively constant for a range of doping below optimal doping and then decreases as the system becomes severely underdoped.

Let us summarize our momentum-space picture of this two-gap scenario. Beginning with the deeply underdoped Bi2212, there is a small Fermi arc where a peak can be observed in the EDCs at the Fermi crossing points, k_F. This arc, centered at the nodal k_F point, then extends out along the FS, increasing in length as the doping is increased. Along this arc, we find evidence for a *k*-dependent gap, consistent with a superconducting $d_{x^2-y^2}$ gap with an increasing magnitude as the hole doping increases. Another gap, which is much larger and decreases with doping, dominates the antinodal region. We believe that the smaller nodal region gap is the true superconducting gap because it exhibits a peak in the EDC. The pseudogap (antinodal gap) may arise from another mechanism, such as Umklapp scattering by the antiferromagnetic correlation, or from competing states, such as stripes (*18*, *19*), polaronic (*20*, *21*) behavior, or a charge-density wave (*13*, *22*, *23*).

This two-gap scenario is consistent with other experiments. First, thermodynamic data suggest a distinct pseudogap and a superconducting gap (*24*). Second, recent Raman studies (*9*, *10*) also suggest that energy gaps extracted from B_{1g} (dominated by the antinodal region) and B_{2g} symmetry (dominated by the nodal region) have different origins with opposite doping dependence. In addition, contradictive results of the superconducting gap deduced from different experimental tools can be resolved within this momentum-space two-gap picture. Andreev reflection (*7*) and penetration depth measurement (*8*) indicate that the superconducting gap declines with more underdoping, whereas tunneling spectroscopy (*3*, *6*) shows the opposite trend with the doping. Such inconsistencies are difficult to explain with a one-gap scenario but are naturally compatible with the two-gap scenario. We suggest that some measurements, such as Andreev reflection and the penetration depth, are sensitive to the superconducting condensate itself; thus, the superconducting gap near the nodal region is probed. On the other hand, the scanning tunneling microscopy (STM) spectrum is more sensitive to the antinodal gap because of larger phase space. Thus, the doping dependences of the energy gap obtained from STM, Andreev reflection, and penetration depth are different because they are sensitive to different gaps in the FS.

This two-gap scenario has two important implications, which could be very important for developing a microscopic theory of high T_c superconductivity. First, the pseudogap near the antinodal region in these deeply underdoped samples is unlikely to be a precursor state of the superconducting state. Second, our data suggest that the weakened superconductivity in the deeply underdoped region arises not only from the loss of phase coherence (*25*) caused by the decrease in the superfluid density but also a weakening of the pair amplitude. In this case, a mechanism for the superconducting gap reduction could be related to the shrinkage of the coherent FS with less doping, leading to a smaller phase space for pairing.

References and Notes

1. T. Timusk, B. Statt, *Rep. Prog. Phys.* **62**, 61 (1999).
2. A. G. Loeser *et al.*, *Science* **273**, 325 (1996).
3. Ch. Renner, B. Revaz, J.-Y. Genoud, K. Kadowaki, O. Fischer, *Phys. Rev. Lett.* **80**, 149 (1998).
4. J. C. Campuzano *et al.*, *Phys. Rev. Lett.* **83**, 3709 (1999).
5. M. Sutherland *et al.*, *Phys. Rev. B* **67**, 174520 (2003).
6. N. Miyakawa, P. Guptasarma, J. F. Zasadzinski, D. G. Hinks, K. E. Gray, *Phys. Rev. Lett.* **80**, 157 (1998).
7. G. Deutscher, *Nature* **397**, 410 (1999).
8. C. Panagopoulos, J. R. Cooper, T. Xiang, *Phys. Rev. B* **57**, 13422 (1998).
9. M. Opel *et al.*, *Phys. Rev. B* **61**, 9752 (2000).
10. M. Le Tacon *et al.*, *Nat. Phys.* **2**, 537 (2006).
11. J. M. Harris *et al.*, *Phys. Rev. B* **54**, R15665 (1996).
12. T. Yoshida *et al.*, *Phys. Rev. Lett.* **91**, 027001 (2003).
13. K. M. Shen *et al.*, *Science* **307**, 901 (2005).
14. J. Mesot *et al.*, *Phys. Rev. B* **63**, 224516 (2001).
15. J. Mesot *et al.*, *Phys. Rev. Lett.* **83**, 840 (1999).
16. Y. Wang, L. Li, N. P. Ong, *Phys. Rev. B* **73**, 024510 (2006).
17. We have fit the ARPES data by using various impurity scattering [Born, unitary, and forward scattering (*26*)] models and backgrounds. However, the large number of parameters and the choice of backgrounds make it hard to extract unique conclusions from fits. Therefore, we focused directly on the data.
18. J. M. Tranquada, B. J. Sternlieb, J. D. Axe, Y. Nakamura, S. Uchida, *Nature* **375**, 561 (1995).
19. K. Yamada *et al.*, *Phys. Rev. B* **57**, 6165 (1998).
20. K. M. Shen *et al.*, *Phys. Rev. Lett.* **93**, 267002 (2004).
21. A. S. Mishchenko, N. Nagaosa, *Phys. Rev. Lett.* **93**, 036402 (2004).
22. L. Benfatto, S. Caprara, C. DiCastro, *Eur. Phys. J. B* **17**, 95 (2000).
23. T. Hanaguri *et al.*, *Nature* **430**, 1001 (2004).
24. J. W. Loram, J. Luo, J. R. Cooper, W. Y. Liang, J. L. Tallon, *J. Phys. Chem. Solids* **62**, 59 (2001).
25. V. J. Emery, S. A. Kivelson, *Nature* **374**, 434 (1995).
26. L. Zhu, P. J. Hirschfeld, D. J. Scalapino, *Phys. Rev. B* **70**, 214503 (2004).
27. A. Damascelli, Z. Hussain, Z.-X. Shen, *Rev. Mod. Phys.* **75**, 473 (2003).

28. ARPES experiments were performed at Stanford Synchrotron Radiation Laboratory, which is operated by the Office of Basic Energy Science, U.S. Department of Energy, under contract DE-FG03-01ER45929-A001. This work was also supported by Office of Naval Research grant N00014-01-1-0048 and NSF grant 0304981. D.J.S. acknowledges the Center for Nanophase Materials Science at Oak Ridge National Laboratory for support.

Supporting Online Material

www.sciencemag.org/cgi/content/full/1133411/DC1
Materials and Methods
Figs. S1 to S3

3 August 2006; accepted 3 November 2006
Published online 16 November 2006;
10.1126/science.1133411
Include this information when citing this paper.

The Ground State of the Pseudogap in Cuprate Superconductors

T. Valla,[1]* A. V. Fedorov,[2] Jinho Lee,[3] J. C. Davis,[3] G. D. Gu[1]

We present studies of the electronic structure of $La_{2-x}Ba_xCuO_4$, a system where the superconductivity is strongly suppressed as static spin and charge orders or "stripes" develop near the doping level of $x = 1/8$. Using angle-resolved photoemission and scanning tunneling microscopy, we detect an energy gap at the Fermi surface with magnitude consistent with *d*-wave symmetry and with linear density of states, vanishing only at four nodal points, even when superconductivity disappears at $x = 1/8$. Thus, the nonsuperconducting, striped state at $x = 1/8$ is consistent with a phase-incoherent *d*-wave superconductor whose Cooper pairs form spin-charge–ordered structures instead of becoming superconducting.

There are several generally accepted phenomena in high-temperature superconductivity (HTSC) that make the cuprates so fascinating. One of these phenomena is a *d*-wave symmetry of the superconducting gap. Another feature is a normal-state gap (pseudogap) in underdoped materials, which exists above the temperature of the superconducting transition T_C (*1*, *2*). There are multiple aspects to the pseudogap phenomenon. In particular, the distinction is usually made between the "large" pseudogap in the overall density of states (DOS) and a "small" pseudogap in the excitations at the Fermi surface, which is seen in spectroscopic probes such as angle-resolved photoemission spectroscopy (ARPES) (*1*, *2*). Here, we consider the small pseudogap. It is generally believed and observed that the magnitude of the pseudogap monotonically decreases with increasing doping, whereas T_C moves in the opposite direction in the underdoped regime (*1*, *2*). The origin of the pseudogap and its relationship to superconductivity are some of the most important open issues in the physics of HTSC and represent the focal point of current theoretical interest (*3*–*6*). In one view, the pseudogap is a pairing (superconducting) gap, reflecting a state of Cooper pairs without global phase coherence. The superconducting transition then occurs at some lower temperature when phase coherence is established (*7*). In an alternative view, the pseudogap represents another state of matter that competes with superconductivity. However, the order associated with such a competing state has never been unambiguously detected. The first hints came from neutron-scattering studies in a magnetic field, where an incommensurate spin order was detected inside vortices (*8*). However, it was not until recent scanning tunneling microscopy (STM) experiments that more was learned about any potential candidate for such "hidden order." A charge-ordered state, energetically very similar to the superconducting state, has been found in the vortex cores (*9*), in the pseudogap regime (*10*) above T_C, and in patches of underdoped material in which the coherent conductance peaks were absent (*11*). We show that a similar state represents the ground state in a system with strongly suppressed superconductivity and with a static spin (*12*) and charge (*13*) orders: $La_{2-x}Ba_xCuO_4$ (LBCO) at doping level $x = 1/8$. The *k*-dependence of the gap in this state looks the same as the superconducting gap in superconducting cuprates: It has magnitude consistent with *d*-wave symmetry and vanishes at four nodal points on the Fermi surface. Furthermore, the single-particle gap, measured at low temperature *T*, has unexpected doping dependence with a maximum at $x \approx 1/8$, precisely where the charge-spin order is established between two adjacent superconducting domes. These findings reveal the pairing origin of the pseudogap and imply that the most strongly bound Cooper pairs at $x \approx 1/8$ are most susceptible to phase disorder and spatial ordering (*7*, *14*, *15*).

LBCO exhibits a sharp drop in superconducting transition temperature, $T_C \rightarrow 0$, when doped to $\sim 1/8$ holes per Cu site ($x = 1/8$) (*16*), while having almost equally strong superconducting phases at both higher and lower dopings, reaching maximal $T_C \approx 32$ K at $x = 0.095$ and $x = 0.155$. Therefore, the $x = 1/8$ case represents an ideal system to study the ground state of the pseudogap because the normal state extends essentially to $T = 0$ K. In scattering experiments on single crystals, a static local spin order with period of eight unit cells (*12*, *14*) and a charge order (*13*) with period of four unit cells—so-called stripes—has been detected at low *T*. While superconductivity is strongly reduced at $x = 1/8$, metallic behavior seems to be preserved. Optical studies have detected a loss of spectral weight at low frequencies with simultaneous narrowing of a Drude component, which suggests the development of an anisotropic gap (*17*). We used ARPES and STM to measure the electronic excitations and detailed momentum dependence of the single-particle gap in the ordered state of LBCO.

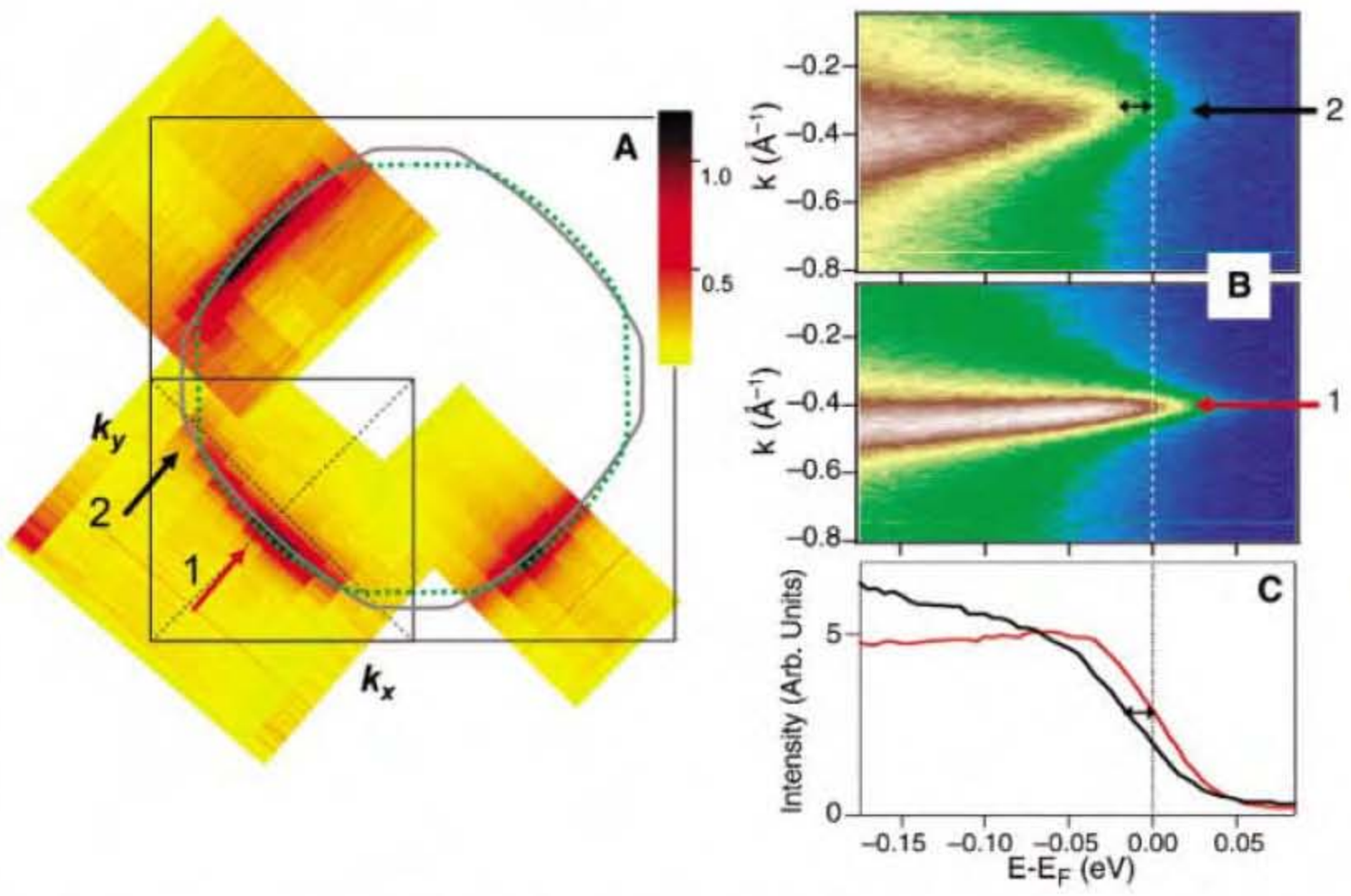

Fig. 1. Photoemission from LBCO at $x = 1/8$. (**A**) Photoemission intensity from a narrow interval around the Fermi level ($\omega = 0 \pm 10$ meV) is shown on a relative scale as a function of the in-plane momentum. High intensity represents the underlying Fermi surface. Lines represent fits to the positions of maxima in probed MDCs for LBCO ($x = 0.125$) (solid line) and LSCO ($x = 0.07$) (dashed line). Arrows correspond to the momentum lines represented in (B) and (C). k_y and k_x represent in-plane momenta spanning the Brillouin zone. (**B**) Photoemission intensity from LBCO sample as a function of binding energy along the momentum lines indicated in (A). (**C**) Energy distribution curves (EDCs) of spectral intensity integrated over a small interval $k_F \pm \Delta k$ along the two lines in *k*-space shown in (B), where $\Delta k = 0.08$ Å^{-1}. E-E$_F$, is energy measured from the Fermi level. The arrow represents the shift of the leading edge. The spectra were taken in the charge-ordered state at $T = 16$ K.

[1]Condensed Matter Physics and Materials Science Department, Brookhaven National Laboratory, Upton, NY 11973, USA. [2]Advanced Light Source, Lawrence Berkeley National Laboratory, Berkeley, CA 94720, USA. [3]Laboratory for Atomic and Solid State Physics, Department of Physics, Cornell University, Ithaca, NY 14853, USA.

*To whom correspondence should be addressed. E-mail: valla@bnl.gov

Figure 1 shows the photoemission spectra from LBCO at $x = 1/8$ in the ordered state (T = 16 K). The momentum distribution of the photoemission intensity from the energy window of ±10 meV around the Fermi level is shown within the Brillouin zone (Fig. 1A). From these and other contours measured for several samples, we extracted the Fermi surface as a line in momentum space that connects the maxima of each of the measured momentum distribution curves (MDC) at energy $\omega = 0$. In addition, we also show the extracted Fermi surface of $La_{2-x}Sr_xCuO_4$ (LSCO) at $x = 0.07$, which agrees well with published data (*18*). The areas enclosed by the Fermi lines correspond to $x = 0.06 \pm 0.015$, for LSCO and $x = 0.115 \pm 0.015$, for LBCO, in good agreement with the nominal doping levels, signaling that the bulk property has been probed. In both systems, we have detected an excitation gap (*19*) with a magnitude that depends on the k position on the Fermi surface, vanishing at the node and with maximum amplitude near the antinode as shown in Fig. 1, B and C.

In the detailed k-dependence for several samples (Fig. 2), two unexpected properties are uncovered. First, gaps in all samples have magnitudes consistent with d-wave symmetry even though superconductivity is essentially nonexistent in LBCO at $x = 1/8$. Second, the gap in LBCO is larger at $x = 1/8$ than at $x = 0.095$ and than in LSCO ($x \approx 0.07$). This finding contradicts a common belief that the excitation gap in cuprates monotonically increases as the antiferromagnetic (AF) phase is approached. Figure 2C shows the compilation of the maximal gap values, Δ_0, in LSCO and LBCO systems, as a function of doping, from this study and from previously published work. Values for LSCO for $x = 0.063$ and $x = 0.09$ are extracted from figure 4 in (*18*) and those for $x \geq 0.1$ are from (*2*). All the points have been measured at $T \approx 20$ K: in the superconducting state for $x = 0.09$, 0.095, 0.1, 0.165, and 0.22, and in the normal state for the other samples. It is clear from the figure that the total gap is not monotonic. Rather, in LBCO, it peaks at or near $x = 1/8$ when superconductivity vanishes and stripes are fully developed.

The momentum-resolved picture from ARPES is consistent with the STM data obtained from an LBCO sample at $x = 1/8$, cut from the same parent crystal used for ARPES. In Fig. 3A, a typical STM topographic image of a cleaved LBCO surface is shown. In addition, the differential conductance (dI/dV) spectra were taken at many points in a wide range of energies (fig. S2). In the averaged (over the whole field of view in Fig. 3A) conductance spectrum (Fig. 3B), a symmetric v-like shape at low energies, with zero-DOS falling exactly at the Fermi level, which is consistent with a pairing d-wave gap. The magnitude of this gap, $\Delta_0 \approx 20$ meV, as determined from the breaks in dI/dV curve agrees with the maximal gap Δ_0 measured in photoemission.

Our study provides the evidence for a d-wave gap in the normal ground state of a cuprate material. Previous studies on underdoped $Bi_2Sr_2CaCu_2O_{8+\delta}$ (BSCCO) were always affected by the superconductivity: The disconnected "Fermi arcs" were seen, shrinking in length as T was lowered below pseudogap temperature T^* and collapsing onto (nodal) points below T_C (*20*, *21*). As a result of this abrupt intervention of superconductivity, it was not clear whether the pseudogap ground state would have a Fermi arc of finite length or a nodal point or whether it would be entirely gapped. In LBCO, the absence of superconductivity at $x = 1/8$ has enabled us to resolve this puzzle and to show that the normal-state gap has isolated nodal points in the ground state. This result points to the pairing origin of the pseudogap, in general agreement with recent thermal transport measurements (*22*). With increasing T, a finite-length Fermi arc forms, as suggested in Fig. 2B, in accord with results on BSCCO (*20*, *21*).

What might be the origin of the observed d-wave gap in LBCO if superconductivity is absent? Neutron- and x-ray–scattering studies on the same crystal have identified a static spin order

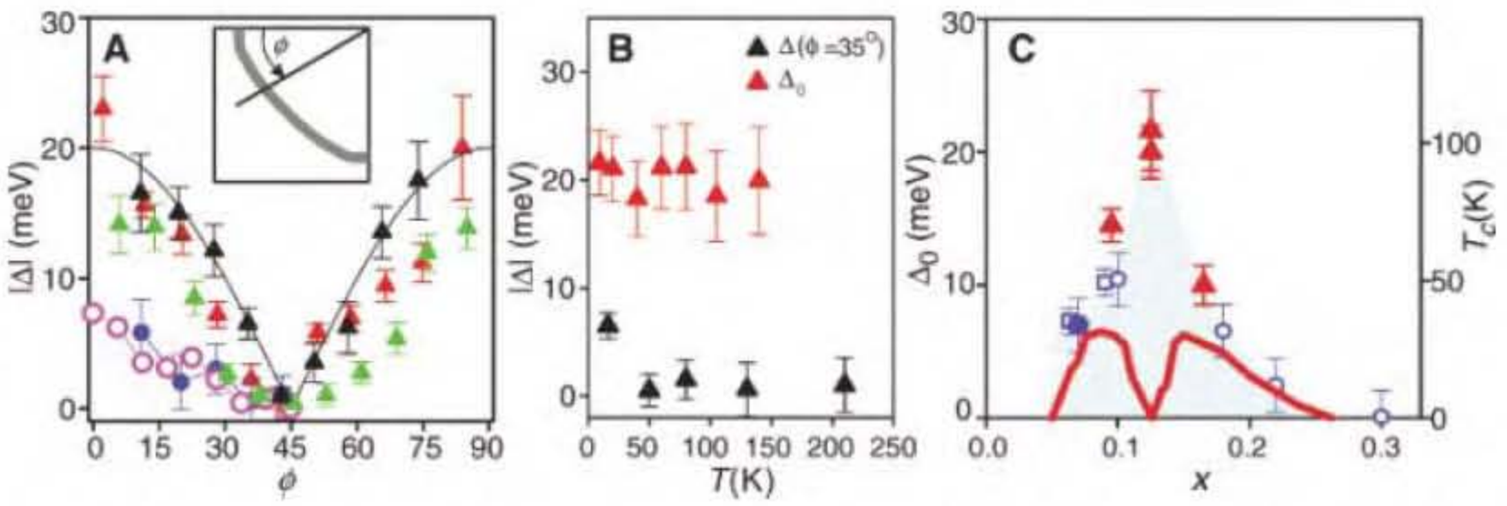

Fig. 2. k- and doping dependence of the single-particle gap. (**A**) Magnitude of single-particle gap (leading-edge gap) at $T = 16$ K as a function of an angle ϕ around the Fermi surface, as defined in the inset, for LBCO at $x = 1/8$ (black and red triangles), $x = 0.095$ (green triangles), and LSCO at $x = 0.07$ (blue circles) have been measured. Points for LSCO at $x = 0.063$ (magenta circles) have been extracted from figure 4A in (*18*). The line represents a d-wave gap amplitude, $\Delta_0|\cos(2\phi)|$ with $\Delta_0 = 20$ meV. (**B**) Temperature dependence of Δ_0 (red triangles) and Δ at $\phi \approx 35°$ (black triangles) for LBCO at $x = 1/8$. (**C**) Doping dependence of Δ_0 in LBCO (triangles) and LSCO (circles and squares). Solid symbols, this study; open squares, (*18*); open circles, (*2*). The red line represents doping dependence of T_C for LBCO from (*16*). Error bars in (A) to (C) indicate fitting uncertainty in position of inflection point (or the leading edge) of EDCs.

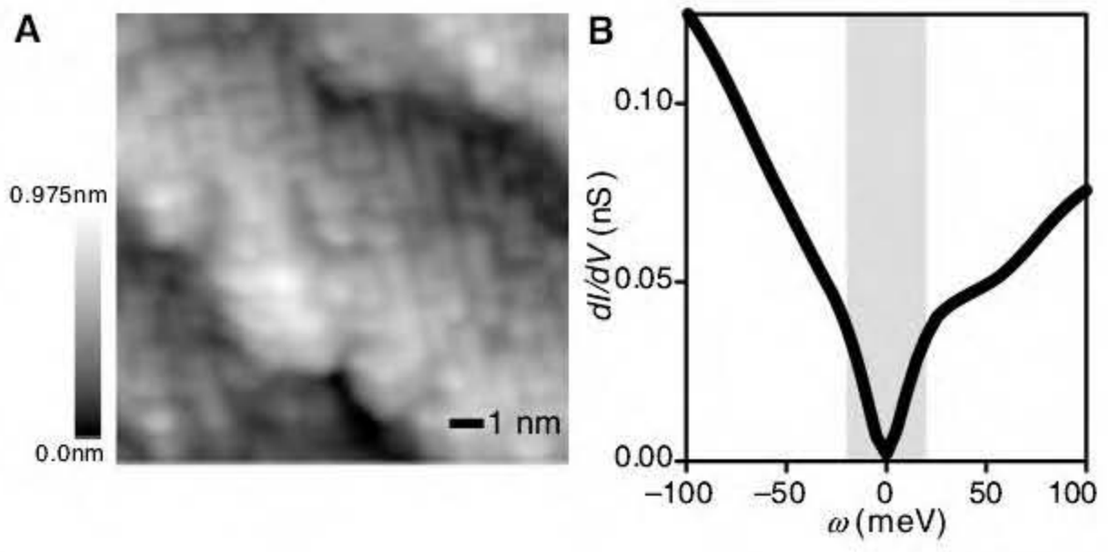

Fig. 3. STM of LBCO. (**A**) High-resolution STM topographic image of the cleaved sample. The image was taken at 4.2 K. (**B**) A tunneling conductance spectrum averaged over the area shown in (A). A v-like profile of DOS for energies $|\omega| \leq 20$ meV (gray region) is consistent with a d-wave gap observed in ARPES.

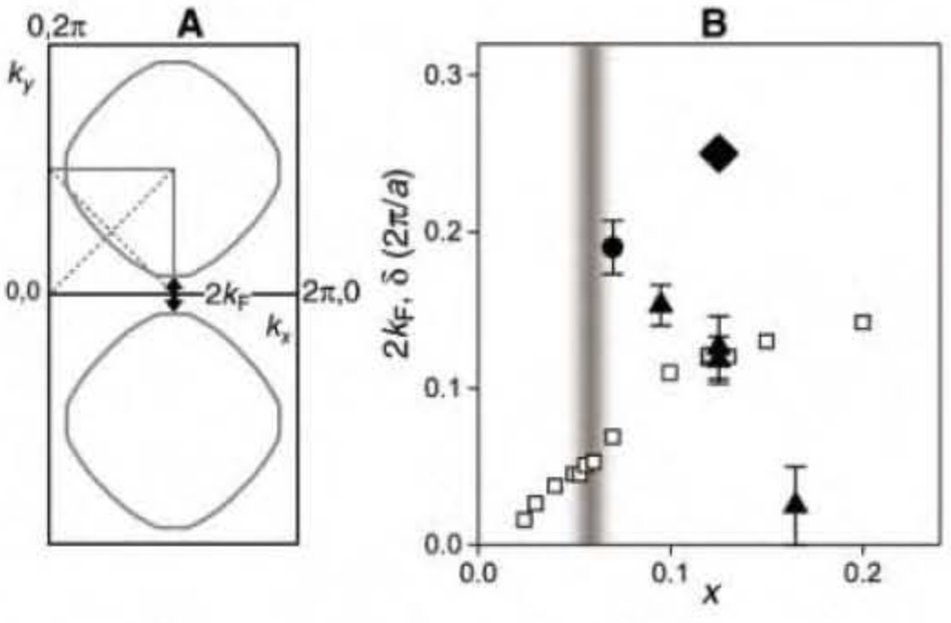

Fig. 4. A compilation of relevant wave vectors from neutron and x-ray scattering and ARPES on 214 materials. (**A**) A sketch of relevant vectors in the k-space. (**B**) Doping dependence of the antinodal k_F, indicated in (A) by the arrow, in LBCO (triangles) and LSCO (circle). The wave vector for charge order (*13*) (diamond) and the incommensurability δ from (π,π) point from neutron-scattering experiments (*31*, *32*) (squares) are also shown. The gray vertical bar represents the boundary between the "diagonal" and "parallel" spin superstructures and the onset of superconductivity. Error bars indicate fitting uncertainty in peak positions of MDC, used to extract k_F.

and a charge order (*12*, *13*). Therefore, it would be tempting to assume that at least a portion of the measured gap is due to the charge order, in analogy with conventional two-dimensional (2D) charge density wave (CDW) systems. It has been suggested that, in cuprates, the spin-charge–ordered state forms in a way where carriers doped into the AF insulator segregate into 1D charge-rich structures (stripes) separated by the charge-poor regions of a parent antiferromagnet (*14*, *23*–*25*). However, questions have often been raised on how to reconcile these unidirectional structures with an apparent 2D Fermi surface and a gap with *d*-wave symmetry. In the more conventional view, doped carriers are delocalized in the planes, forming a 2D Fermi surface that grows in proportion with carrier concentration. The charge-spin–ordered state may then be formed in the particle-hole channel by nesting of Fermi surface segments, producing a divergent electronic susceptibility and a Peierls-like instability and pushing the system into a lower energy state with a single-particle gap at nested portions of the Fermi surface. An example of a cuprate where such a "nesting" scenario is proposed to be at play is $Ca_{2-x}Na_xCuO_2Cl_2$ (CNCOC) (*26*). STM studies have detected checkerboard-like modulations in local DOS on the surface of this material, with $4a \times 4a$ periodicity, independent of doping (*27*). Subsequent ARPES studies on the same system have shown a Fermi surface with a nodal arc and truncated antinodal segments (*26*). The antinodal segments can be efficiently nested by the charge-ordering wave vectors $q_{CDW} = 2k_F = \pi/(2a)$ and $3\pi/(2a)$, observed in STM for charge superstructure, making the nesting scenario viable, at least near the surface of CNCOC. Here, k_F represents the antinodal Fermi wave vector. However, if we apply the same nesting scenario to LBCO at $x = 1/8$, we obtain $q_{CDW} \approx 4k_F$ ($= \pi/2a$) for charge order instead of $2k_F$ nesting, which is suggested to be at play in CNCOC. Moreover, the nesting of antinodal segments would produce a wave vector that shortens with doping, opposite of that observed in neutron-scattering studies in terms of magnetic incommensurability. This result is illustrated in Fig. 4, where we compile the doping dependences of several relevant quantities.

There is another, more fundamental problem with the nesting scenario: Any order originating from nesting (particle-hole channel) would open a gap only on nested segments of the Fermi surface, preserving the non-nested regions. The fact that only four gapless points (nodes) remain in the ground state essentially rules out nesting as an origin of the pseudogap. In addition, a gap caused by conventional spin-charge order would be pinned to the Fermi level only in special cases. The observation that the gap is always pinned to the Fermi level (independent of *k*-point, as measured in ARPES and of doping level, as seen in STM on different materials) and that it has *d*-wave symmetry undoubtedly points to its pairing origin [interaction in the particle-particle singlet channel (*28*)]. In contrast to the low-energy pairing gap, STM at higher energies shows a DOS suppressed in a highly asymmetric manner, indicating that some of the nesting-related phenomena might be at play at these higher energies (Fig. 3B).

The unexpected anticorrelation of the low-energy pairing gap and T_C over some region of the phase diagram suggests that, in the state with strongly bound Cooper pairs, the phase coherence is strongly suppressed by quantum phase fluctuations. Cooper pairs are then susceptible to spatial ordering and may form various unidirectional (*14*, *24*, *25*) or 2D (*15*, *27*–*30*) superstructures. Quantum phase fluctuations are particularly prominent in cases where such superstructures are anomalously stable. For some of the proposed structures, this occurs at the doping of $1/8$, in general agreement with our results: $1/8$ represents the most prominent "magic fraction" for a checkerboard-like "CDW of Cooper pairs" (*15*), and it locks the stripes to the lattice in a unidirectional alternative. The presence of nodes in the ground state of the pseudogap represents a new decisive test for validity of models proposed to describe such structures.

References and Notes

1. T. Timusk, B. Statt, *Rep. Prog. Phys.* **62**, 61 (1999).
2. A. Damascelli, Z. Hussain, Z.-X. Shen, *Rev. Mod. Phys.* **75**, 473 (2003).
3. G. Baskaran, Z. Zou, P. W. Anderson, *Solid State Commun.* **63**, 973 (1987).
4. P. A. Lee, N. Nagaosa, X.-G. Wen, *Rev. Mod. Phys.* **78**, 17 (2006).
5. E. W. Carlson, V. J. Emery, S. A. Kivelson, D. Orgad, *The Physics of Superconductivity: Conventional and Unconventional*, vol. 2, K. H. Benneman, J. B. Ketterson, Eds. (Springer, Berlin, 2003).
6. M. Franz, Z. Tešanović, *Phys. Rev. Lett.* **87**, 257003 (2001).
7. V. J. Emery, S. A. Kivelson, *Nature* **374**, 434 (1995).
8. B. Lake *et al.*, *Science* **291**, 1759 (2001).
9. J. E. Hoffman *et al.*, *Science* **295**, 466 (2002).
10. M. Vershinin *et al.*, *Science* **303**, 1995 (2004).
11. K. McElroy *et al.*, *Phys. Rev. Lett.* **94**, 197005 (2005).
12. J. M. Tranquada *et al.*, *Nature* **429**, 534 (2004).
13. P. Abbamonte *et al.*, *Nat. Phys.* **1**, 155 (2005).
14. J. M. Tranquada, B. J. Sternlieb, J. D. Axe, Y. Nakamura, S. Uchida, *Nature* **375**, 561 (1995).
15. Z. Tešanović, *Phys. Rev. Lett.* **93**, 217004 (2004).
16. A. R. Moodenbaugh, Y. Xu, M. Suenaga, T. J. Folkerts, R. N. Shelton, *Phys. Rev. B* **38**, 4596 (1988).
17. C. C. Homes *et al.*, *Phys. Rev. Lett.* **96**, 257002 (2006).
18. X. J. Zhou *et al.*, *Phys. Rev. Lett.* **92**, 187001 (2004).
19. Materials and methods are available as supporting material on *Science* Online.
20. M. R. Norman *et al.*, *Nature* **392**, 157 (1998).
21. A. Kanigel *et al.*, *Nat. Phys.* **2**, 447 (2006).
22. M. Sutherland *et al.*, *Phys. Rev. Lett.* **94**, 147004 (2005).
23. J. Zaanen, O. Gunnarson, *Phys. Rev. B* **40**, 7391 (1989).
24. V. J. Emery, S. A. Kivelson, *Physica C* **235-240**, 189 (1994).
25. M. Granath, V. Oganesyan, S. A. Kivelson, E. Fradkin, V. J. Emery, *Phys. Rev. Lett.* **87**, 167011 (2001).
26. K. M. Shen *et al.*, *Science* **307**, 901 (2005).
27. T. Hanaguri *et al.*, *Nature* **430**, 1001 (2004).
28. M. Franz, *Science* **305**, 1410 (2004).
29. H.-D. Chen, O. Vafek, A. Yazdani, S.-C. Zhang, *Phys. Rev. Lett.* **93**, 187002 (2004).
30. D. Podolsky, E. Demler, K. Damle, B. I. Halperin, *Phys. Rev. B* **67**, 094514 (2003).
31. M. Fujita *et al.*, *Phys. Rev. B* **65**, 064505 (2002).
32. J. M. Tranquada *et al.*, *Phys. Rev. Lett.* **78**, 338 (1997).

33. The authors thank P. Anderson, A. Chubukov, E. Fradkin, C. Homes, P. Johnson, S. Kivelson, W. Ku, A. Millis, Z. Tešanović, A. Tsvelik, and J. Tranquada for useful discussions and Z-H. Pan for technical help. T.V., A.V.F., and G.D.G. are supported by the Office of Science, U.S. Department of Energy (DOE). J.C.D and J.L. are supported by the Office of Science, DOE, the Office of Naval Research, and by Cornell University.

Supporting Online Material

www.sciencemag.org/cgi/content/full/1134742/DC1
Materials and Methods
Figs. S1 and S2
References

5 September 2006; accepted 3 November 2006
Published online 16 November 2006;
10.1126/science.1134742
Include this information when citing this paper.

Nondestructive Optical Measurements of a Single Electron Spin in a Quantum Dot

J. Berezovsky, M. H. Mikkelsen, O. Gywat, N. G. Stoltz, L. A. Coldren, D. D. Awschalom*

Kerr rotation measurements on a single electron spin confined in a charge-tunable semiconductor quantum dot demonstrate a means to directly probe the spin off-resonance, thus minimally disturbing the system. Energy-resolved magneto-optical spectra reveal information about the optically oriented spin polarization and the transverse spin lifetime of the electron as a function of the charging of the dot. These results represent progress toward the manipulation and coupling of single spins and photons for quantum information processing.

The prospect of quantum computation in conventional material systems has spurred much research into the physics of carrier spins in semiconductor quantum dots (QDs) (*1*). An important element necessary for spin-based quantum computing is the readout of the qubit spin state. Previously demonstrated schemes for single spin readout in a QD include optical measurements, such as photoluminescence (PL) polarization (*2*, *3*) or polarization-dependent absorption (*4*–*6*). Single spins can also be read out electrically by measuring the spin-dependent probability for an electron to tunnel out of the

Center for Spintronics and Quantum Computation, University of California, Santa Barbara, CA 93106, USA.

*To whom correspondence should be addressed. E-mail: awsch@physics.ucsb.edu

dot (*7*). However, these methods are destructive, in that they either remove the spin from the dot or drive transitions in the system with a resonant optical field. In contrast, we describe measurements of a single electron spin using Kerr rotation (KR), in which the spin state is probed nonresonantly, thus minimally disturbing the system. This effective spin-photon interaction has been shown to allow for Schrödinger's cat–type measurements to probe quantum effects such as measurement-induced decoherence and spin squeezing (*8*, *9*), as well as the implementation of quantum information protocols involving spin-photon entanglement (*10*) and optically mediated spin-spin entanglement (*11*–*13*).

In the present work, the electrons were confined to a single charge-tunable QD formed by monolayer fluctuations at the interfaces of a gallium arsenide (GaAs) quantum well (QW). The QD layer was centered within an optical microcavity with a resonance chosen to enhance the interaction of the optical field with the QD at energies well below the lowest interband transition. By the application of a transverse magnetic field, the electron spins can be depolarized in a Hanle-type measurement, thereby yielding information about the spin lifetime.

The magneto-optical Kerr effect results in a rotation of the plane of polarization of linearly polarized light with energy E upon reflection off the sample and is analogous to the Faraday effect for transmitted light. For both effects, the rotation angle is determined by the difference of the dynamic dielectric response functions for left and right (σ^+ and σ^-) circularly polarized light, which are proportional to the interband momentum matrix elements $\langle\psi_c|\hat{p}_x \pm i\hat{p}_y|\psi_v\rangle$, where ψ_c (ψ_v) is a conduction (valence) band state (*14*, *15*), and $\hat{p}_x$ and $\hat{p}_y$ are the components of the electron momentum operator perpendicular to the growth direction. As a result of the microcavity, both reflection and transmission contribute to the measured polarization rotation. For simplicity, we refer only to KR. For a single conduction-band energy level in a QD containing a spin-up electron in a state $|\psi_\uparrow\rangle$, optical transitions to the spin-up state are Pauli-blocked, and the KR angle θ_K is then given by

$$\theta_K(E) = CE \sum_{\alpha=\pm 1;v} \alpha|\langle\psi_\downarrow|\hat{p}_x + \alpha i\hat{p}_y|\psi_v\rangle|^2 \frac{E - E_{0,v}}{(E - E_{0,v})^2 + \Gamma_v^2} \quad (1)$$

where C is a constant, and $E_{0,v}$ and Γ_v are the energy and linewidth of the transition involving $|\psi_v\rangle$, respectively. We focus on a single transition in the sum in Eq. 1 and drop the index v. For $\Gamma << |\Delta| << E$, where $\Delta = E - E_0$, we note that $\theta_K \sim \Delta^{-1}$, which decays slower than the absorption line ($\sim\Delta^{-2}$) (*15*, *16*). Therefore, for a suitable detuning Δ, KR can be detected whereas photon absorption is strongly suppressed.

The sample structure (Fig. 1A) is grown by molecular beam epitaxy and consists of a single 4.2-nm GaAs QW in the center of a planar aluminum GaAS ($Al_{0.3}Ga_{0.7}As$) λ-cavity (*17*). The reflectivity of the sample at 10 K (Fig. 1D) shows a cavity resonance centered at 763.6 nm (1.624 eV) with a quality factor of 120. The probe light effectively interacts with the spin many times as it is reflected back and forth within the cavity. As a result, the polarization rotation described by Eq. 1 occurs repeatedly, enhancing the small, single spin KR angle (*18*). Based on previous measurements with similar cavities (*19*, *20*), we expect the KR at the peak of the cavity resonance to be enhanced by a factor of ~15.

The band profile for our structure (*17*), calculated with a one-dimensional self-consistent Poisson-Schrödinger solver, is shown in Fig. 1B. By the application of a bias voltage V_b across the structure, the conduction-band minimum in the QW can be made to plunge beneath the Fermi level, charging first the QDs, then the well itself (*21*, *22*). The onset of this charging occurs around 0.5 V (Fig. 1C) according to the band-structure calculation.

A continuous wave (cw) Ti-sapphire laser (1.654 to 1.662 eV) is focused through a microscope objective (spot size ~ 2 μm) on the sample at temperature T = 10 K to excite electron-hole pairs into the continuum of states in the QW. The carriers then relax into the QDs, and the subsequent PL is collected through the same objective, dispersed in a spectrometer, and detected by a liquid nitrogen–cooled charge-coupled device. In a typical single-dot PL spectrum as a function of the applied bias (Fig. 2A), the sharp features (linewidth ~100 μeV) are characteristic of single-dot PL (*23*), demonstrating the presence of only one QD within the laser focus. Above 0.5 V, a single line is observed at 1.6297 eV, which is attributed to recombination from the negatively charged exciton (trion or X^-) state. Below 0.5 V, this line persists faintly, and a bright line appears 3.6 meV higher in energy because of the neutral exciton (X^0) transition. The presence of the X^- line at $V_b < 0.5$ V implies that occasionally a single electron is trapped in the dot, forming an X^- when binding to an electron and a hole. In addition, a faint line at 1.6292 eV is visible from radiative decay of the biexciton (XX). These assignments of the observed lines are consistent with measurements on

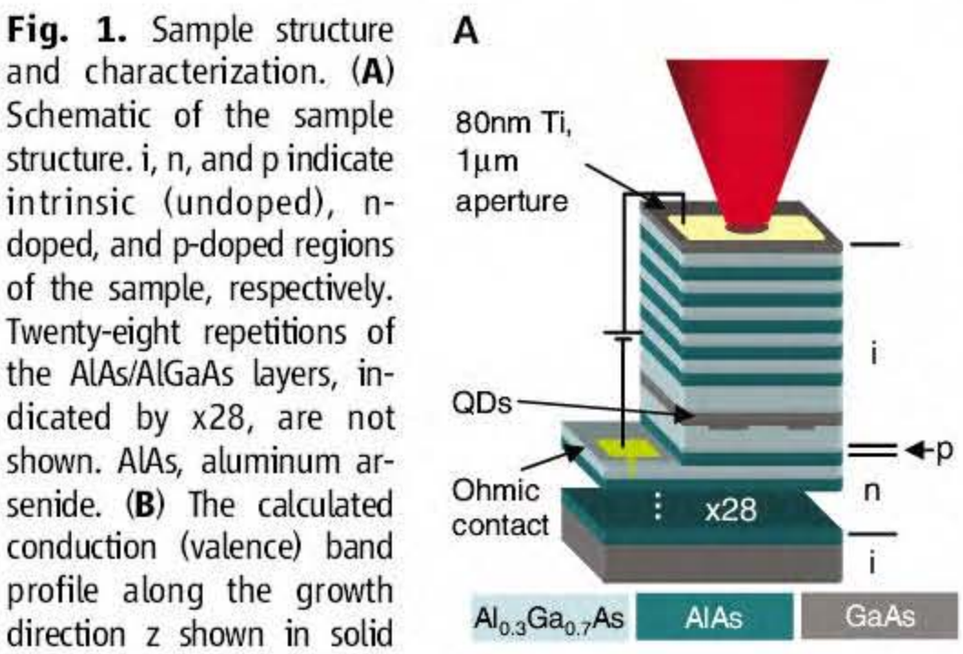

Fig. 1. Sample structure and characterization. (**A**) Schematic of the sample structure. i, n, and p indicate intrinsic (undoped), n-doped, and p-doped regions of the sample, respectively. Twenty-eight repetitions of the AlAs/AlGaAs layers, indicated by x28, are not shown. AlAs, aluminum arsenide. (**B**) The calculated conduction (valence) band profile along the growth direction z shown in solid (dashed) lines. Raising the bias voltage V_b from −1 to 1 V lowers the QW conduction-band minimum past the Fermi level (blue). (**C**) The calculated electron density n in the QW showing the onset of charging at V_b = 0.5 V. (**D**) The reflectivity R of the cavity at T = 10 K versus wavelength λ, with a resonance at 763.6 nm.

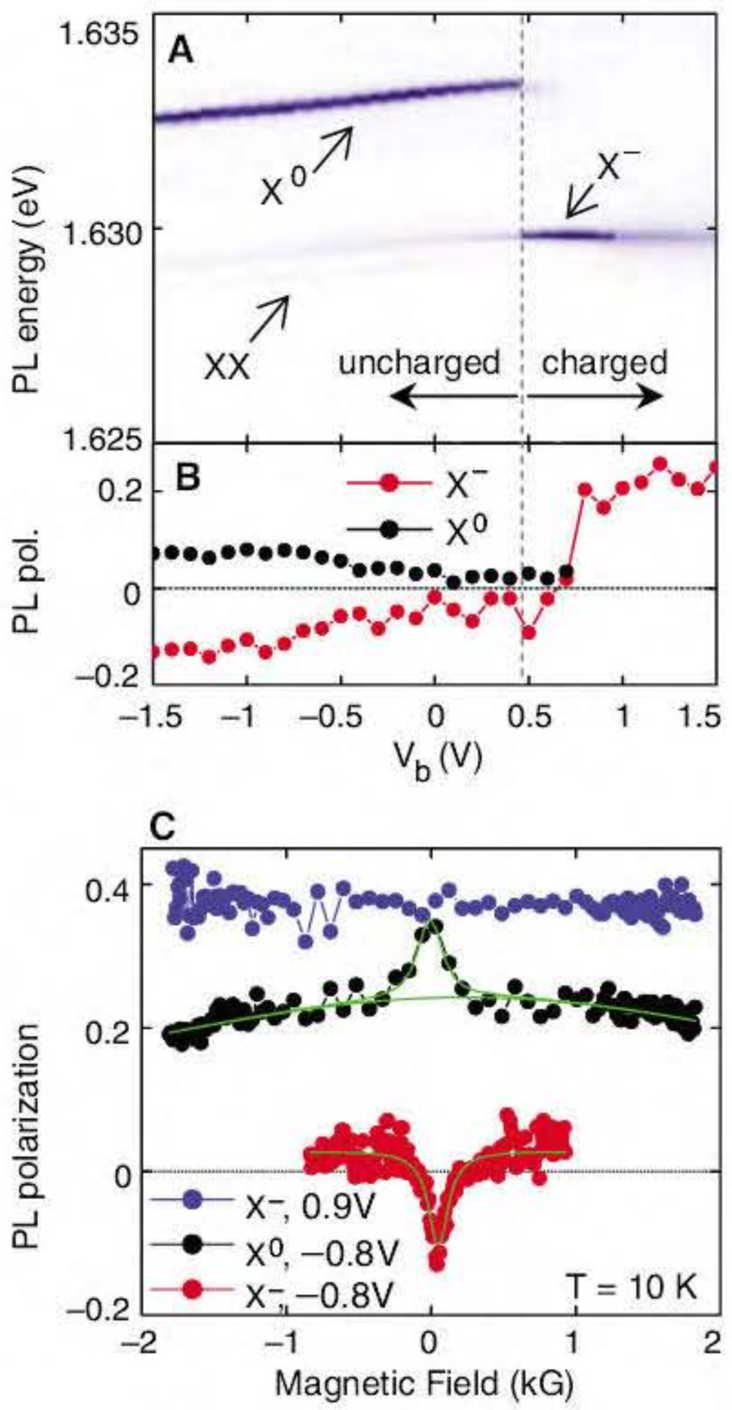

Fig. 2. Single-dot PL and Hanle measurements. (**A**) PL of a single QD as a function of V_b. A jump in the PL energy indicates the onset of QD charging. (**B**) The polarization (pol.) of the X^- and X^0 PL lines as a function of bias. (**C**) Hanle curves in the charged regime (blue) and in the uncharged regime (black and red).

similar structures (*2*, *22*) and are further supported by the linear dependence of the X^- and X^0 lines and the quadratic dependence of the XX line on the excitation intensity. Figure 3C illustrates these three optical transitions. In this QD, we see no evidence of a positively charged exciton.

With circularly polarized excitation, spin-polarized electrons and heavy holes can be pumped into the QD because of the optical selection rules of the GaAs QW (*2*, *24*). For the purposes of this discussion, spin polarization parallel to the optically injected electron spin polarization will be referred to as "spin up" and the opposite spin as "spin down." Information about the spin polarization in the QD can be gained from the polarization of the PL (*2*). The circular polarization of the PL is determined by switching the helicity of the pump from σ^+ to σ^- and measuring the intensity of the σ^+-polarized PL (I^+ and I^-, respectively). The polarization is then defined as $P = (I^+ - I^-)/(I^+ + I^-)$ and is shown for the X^0 and X^- lines in Fig. 2B, in agreement with earlier results (*2*, *22*).

The polarization of the X^- line is determined by the hole spin, as the two electrons in the trion form a spin-singlet state. In the uncharged regime ($V_b < 0.5$ V), the negative polarization of the X^- PL indicates that the heavy hole undergoes a spin flip before recombination in most cases. Hole spin flips may occur either during energy relaxation in the QW (*25*) or by an exchange-mediated electron-hole spin flip (*26*). Regardless of the hole spin-flip process, after the recombination of the X^-, the electron left in the QD is polarized in the spin-up direction. In this way, both optical injection and trion recombination serve to pump lone spin-up electrons into the QD.

When the dot is initially charged near V_b = 0.5 V, the now dominant X^- line remains negatively polarized, resulting in continued pumping of the spin-up state. As the electron density in the QW increases with higher applied bias, the X^- polarization becomes positive, as has been previously observed (*2*, *22*).

In a transverse applied magnetic field, the electron spins precess, depolarizing the PL. The hole spins do not precess (*27*) because the heavy and light hole states are split [by ~20 meV in our sample (*28*)], leading to an effective heavy-hole g factor of zero in the plane of the QW. Hanle measurements on this dot are summarized in Fig. 2C. In the charged regime, at V_b = 0.9 V, no depolarization of the X^- PL is observed, as expected for polarization resulting from the hole spin. The case is markedly different at V_b = –0.8 V, in the uncharged regime. Here, the (negatively polarized) X^- line is depolarized with a half-width $B_{1/2}$ = 80 G. With an estimated electron g factor of g_e = 0.2 (*2*), $B_{1/2}$ = 80 G corresponds to a time-averaged transverse spin lifetime $T_2^* = h/B_{1/2}g_e\mu_B$ = 7 ns, where μ_B is the Bohr magneton and $\hbar$ is Planck's constant h divided by 2π. This sharp Hanle peak has been previously attributed to the electron spin in the QD, before X^- formation (*2*). The X^0 line shows a much broader peak ($B_{1/2}$ = 4.1 kG), with a small narrow component at low field. The broad component is consistent with the radiative lifetime of the exciton (~50 ps) (*4*). The narrow component has a $B_{1/2}$ = 95 G, which is similar to the X^- width. Indeed, this narrow peak is expected if a lone electron in the dot can bind and recombine with a subsequently injected hole. Similar features have been observed in ensemble Hanle measurements in GaAs QWs (*29*).

In the uncharged regime, spin-polarized excitons or electrons can be pumped into the dot. Both optical injection and trion recombination

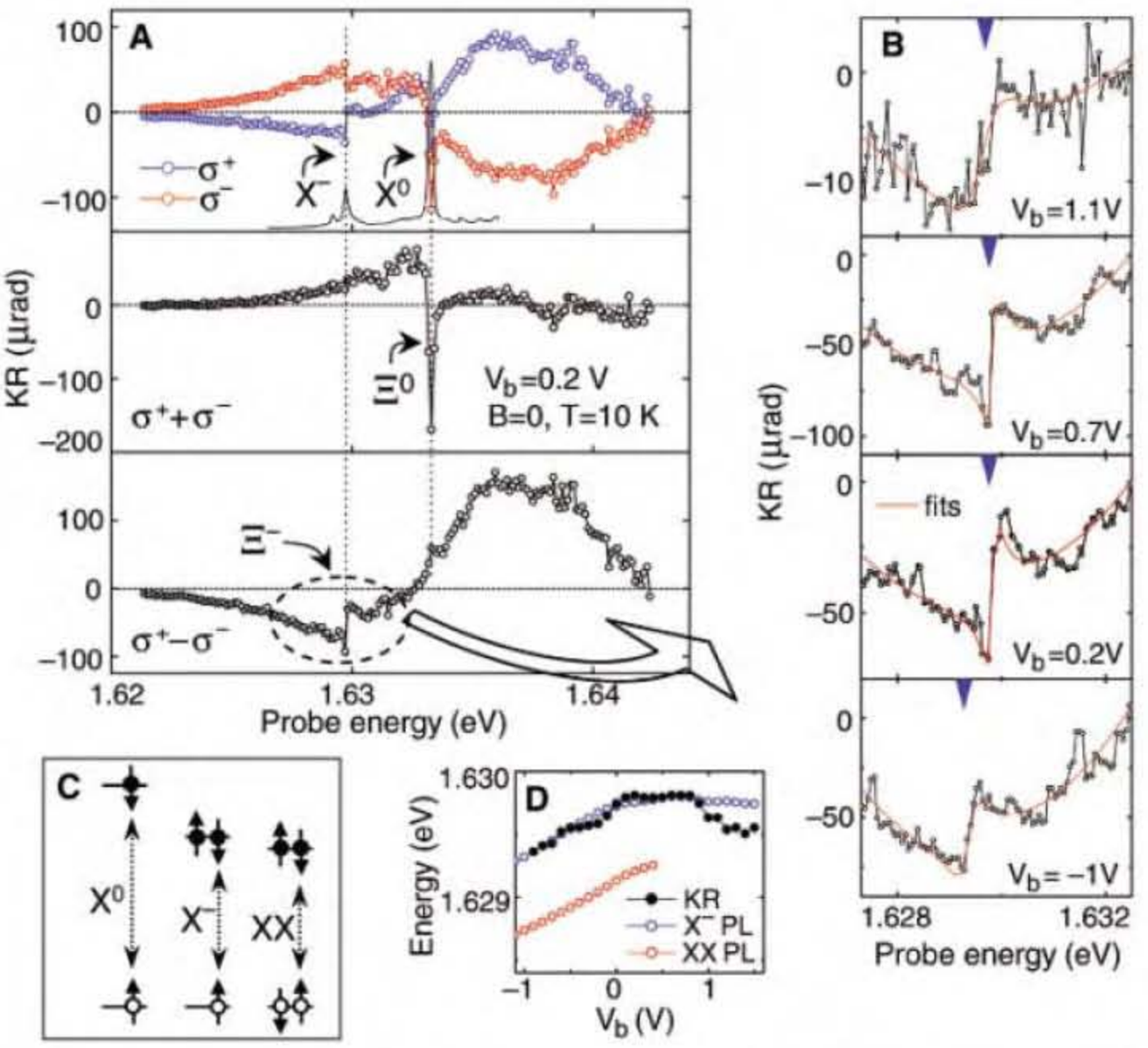

Fig. 3. Single-dot KR spectra. (**A**) Top panel, KR measured with a σ^+- and σ^--polarized pump at V_b = 0.2 V. The PL at this bias is also shown. Middle panel, the sum of the σ^+ and σ^- data showing a spin-independent feature Ξ^0 at the X^0 energy. Bottom panel, the difference of the σ^+ and σ^- data with the feature Ξ^- at the X^- energy circled. The circled feature is shown in more detail in (B), as indicated by the large arrow. (**B**) Single spin KR (Ξ^-) at various bias voltages. The blue triangle indicates the energy of the X^- PL line. Fits to the data are shown in red. (**C**) Illustration of three relevant optical transitions. Solid circles represent electrons, and open circles represent holes. (**D**) The agreement between the X^- PL energy and the Ξ^- energy. The biexciton PL energy is also shown for comparison.

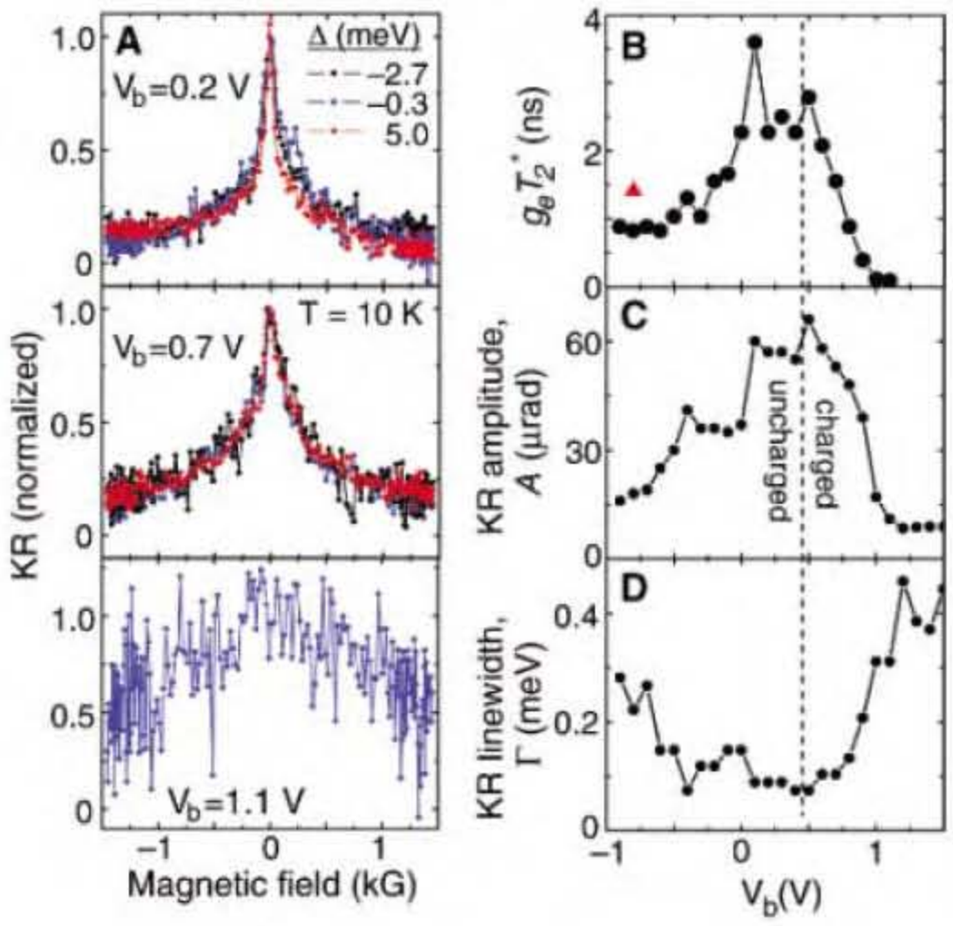

Fig. 4. KR depolarization and analysis. (**A**) KR as a function of transverse magnetic field for various bias voltages. The top two panels show measurements with the probe at various detunings Δ from the X^- energy. (**B**) $g_eT_2^*$ determined from the KR half-width. The red triangle indicates the value obtained from the Hanle measurement. (**C** and **D**) The amplitude and width of the KR Ξ^- feature as a function of applied bias.

serve to pump spin-up electrons. At high bias in the charged regime (V_b = 0.9 V), the PL polarization is due to the hole spin, obscuring any information about the electron spin polarization. To address this issue, we require a more direct probe of the spin polarization.

To probe spins in the dot through KR, we focused a second, linearly polarized, cw Ti-sapphire laser onto the sample, spatially overlapping the pump laser (*17*). The data in the top panel of Fig. 3A show the KR signal as a function of probe energy for σ^+ and σ^- pump helicity. Here, the applied bias is $V_b = 0.2$ V and the QD is in the uncharged regime. The PL at this bias is also shown, with the X^- and X^0 energies indicated by the dotted lines. These energies coincide spectrally with two sharp features observed in the KR data, which we will refer to as Ξ^- and Ξ^0, respectively. In the bottom two panels of Fig. 3A, the sum and difference of the σ^+ and σ^- data are shown. The feature Ξ^0 at the X^0 energy clearly does not depend on the sign of the injected spin and is similar to features seen in single-dot absorption measurements (*30*). We attribute this peak to polarization-dependent absorption in the QD. We focus here on the (σ^+–σ^-) data, which represent KR due to the optically oriented spin polarization. The feature Ξ^- at the X^- energy only appears in the difference data, indicating that it is due to the injected spin polarization, shown in Fig. 3B at four different bias voltages. For all voltages, the Ξ^- feature is centered at the X^- transition energy, indicated by the blue triangles. We can fit these data to Eq. 1 including only a single transition in the sum, on top of a broad background (red lines, Fig. 3B). From the free parameters in these fits, we determine the transition energy E_0, amplitude A (defined as half the difference of the local maximum and minimum near E_0), and width Γ of the Ξ^- KR feature.

Figure 3D shows E_0 compared to the energy of the X^- PL line as a function of the applied bias. The two energies agree well and show the same quantum-confined Stark shift. Only at the highest bias, where substantial broadening sets in, do we observe a small anti-Stokes shift between E_0 and the X^- PL energy. This effect may be caused by interactions with electrons in the QW. For a single electron spin in the QD ground state, the lowest-energy optical transition contributing in Eq. 1 is the X^- transition (Fig. 3C). Thus, the Ξ^- KR feature is due to the measurement of a single electron spin in the QD. We have repeated this measurement on another QD and observed the same Ξ^- feature, also at the X^- PL energy. The large, broad KR background is likely due to transitions involving excited electron and hole states, which are typically a few milli–electron volts above the lowest transition (*23*).

If present, a KR feature due to the X^0 spin should appear centered at the XX transition energy. The signal-to-noise ratio in our measurement is not high enough to conclusively identify such a feature. Despite the large amplitude of the X^0 PL compared to the X^- PL in the uncharged bias regime (~10:1), the short radiative lifetime of the X^0 state results in a low steady-state X^0 population and therefore in a low KR signal.

By applying a transverse magnetic field B, we can monitor the depolarization of the single electron spin through the KR signal. In contrast to the Hanle measurements described above, the KR probes the spin in the QD directly and nondestructively, as opposed to being inferred from the spin-dependent formation of the X^-. The KR as a function of B is shown for three different bias voltages (Fig. 4A). At $V_b = 0.2$ V, in the uncharged regime, a narrow peak is observed with a $B_{1/2}$ = 52 G, which is consistent with the X^- Hanle width measured in this regime. At V_b = 0.7 V, where the dot has charged but the PL remains negatively polarized, we measure a somewhat wider KR depolarization curve, with $B_{1/2}$ = 150 G. When the QW is charged further, the spin lifetime decreases as shown at V_b = 1.1 V, with $B_{1/2}$ = 1.4 kG. Assuming an effective electron g factor of 0.2 (*2*), these half-widths correspond to transverse spin lifetimes of 11, 3.3, and 0.8 ns, respectively.

The electron spin depolarization curves measured at probe energies detuned from the X^- transition by an energy Δ are shown in the top two panels of Fig. 4A for Δ = –0.3 meV (at the maximum of the Ξ^- feature), Δ = –2.7 meV (in the low-energy tail), and Δ = +5.0 meV (on the broad, high-energy feature). The curves have been normalized by their peak values, which vary with probe energy, but show identical lineshapes for a given bias. This suggests that, in this entire range of detuning, the KR of the same spin-polarized electron state in the QD is being probed.

Figure 4B shows $g_e T_2^* = h/B_{1/2}\mu_B$ as a function of the applied bias, measured at a probe energy E = 1.6288 eV, near the X^- transition. The dashed line indicates the onset of QD charging. The spin lifetime is largest in the uncharged regime. Here, $g_e T_2^* \sim 3$ ns is consistent with previous measurements (*2*) in which the spin dephasing is attributed to the random, fluctuating hyperfine field (*31*, *32*). As the dot and well are charged, the electron spin lifetime decreases dramatically. This result can be caused by the increasingly rapid capture of a second electron in the dot, which forms a spin-zero singlet state. Also, as discussed below, spin flips with electrons in the QW are likely to be a relevant mechanism in this regime.

The amplitude of the Ξ^- KR signal is shown as a function of V_b (Fig. 4C). A decreases in the charged regime, reflecting the lower spin lifetime. We have argued above that spin-up electrons are pumped into the QD in the uncharged regime. Therefore, the constant sign of the KR over the entire range of bias indicates spin-up polarization in the charged regime as well. Contrary to this observed polarization, the positively polarized X^- PL leaves a spin-down electron in the QD. However, this electron interacts with the bath of electrons in the QW, which is, on average, optically oriented in the spin-up direction. The predominant spin in the QW may be transferred to the electron in the dot via a higher-order tunneling process (*33*). The finite spin-up polarization measured up to a large bias suggests that these electron-electron spin flips dominate over the X^--mediated spin pumping in the charged regime.

As the bias increases above V_b = 0.5 V, the width of the Ξ^- KR feature, Γ, grows by a factor of six, as shown in Fig. 4D. A similar increase in linewidth is seen in the X^- PL in the charged regime. This provides further evidence for an increased coupling of the QD to other electronic states as the charging increases.

By probing a single electron in a QD through KR nonresonantly, we demonstrate a direct measurement of the electron spin with minimal perturbation to the system. As a first application, this method reveals information about spin dynamics in single QDs and constitutes a pathway toward quantum nondemolition measurements and optically mediated entanglement of single spins in the solid state. This scheme may also prove useful for nondestructive measurements in a variety of solid-state qubits, such as electrically gated (*7*) or chemically synthesized (*20*) QDs.

References and Notes

1. D. D. Awschalom, D. Loss, N. Samarth, Eds., *Semiconductor Spintronics and Quantum Computation* (Springer, Berlin, 2002).
2. A. S. Bracker *et al.*, *Phys. Rev. Lett.* **94**, 047402 (2005).
3. A. Ebbens *et al.*, *Phys. Rev. B* **72**, 073307 (2005).
4. T. H. Stievater *et al.*, *Appl. Phys. Lett.* **81**, 4251 (2002).
5. X. Li, Y. Wu, D. G. Steel, D. Gammon, L. J. Sham, *Phys. Rev. B* **70**, 195330 (2004).
6. A. Högele *et al.*, *Appl. Phys. Lett.* **86**, 221905 (2005).
7. J. M. Elzerman *et al.*, *Nature* **430**, 431 (2004).
8. J. M. Geremia, J. K. Stockton, H. Mabuchi, *Science* **304**, 270 (2004).
9. A. Kuzmich, L. Mandel, N. P. Bigelow, *Phys. Rev. Lett.* **85**, 1594 (2000).
10. F. Meier, D. D. Awschalom, *Phys. Rev. B* **70**, 205329 (2004).
11. B. Julsgaard, A. Kozhekin, E. S. Polzik, *Nature* **413**, 400 (2001).
12. M. N. Leuenberger, M. E. Flatté, D. D. Awschalom, *Phys. Rev. Lett.* **94**, 107401 (2005).
13. M. N. Leuenberger, *Phys. Rev. B* **73**, 075312 (2006).
14. D. V. Kupriyanov, I. M. Sokolov, *Quantum Opt.* **4**, 55 (1992).
15. F. Meier, D. D. Awschalom, *Phys. Rev. B* **71**, 205315 (2005).
16. J. R. Guest *et al.*, *Phys. Rev. B* **65**, 241310(R) (2002).
17. Materials and methods are available as supporting material on *Science* Online.
18. M. Sugita, S. Machida, Y. Yamamoto, preprint available at http://arXiv.org/abs/quant-ph/0301064.
19. G. Salis, M. Moser, *Phys. Rev. B* **72**, 115325 (2005).
20. Y. Q. Li *et al.*, *Appl. Phys. Lett.* **88**, 193126 (2006).
21. R. J. Warburton *et al.*, *Nature* **405**, 926 (2000).
22. A. S. Bracker *et al.*, *Phys. Rev. B* **72**, 035332 (2005).
23. D. Gammon, E. S. Snow, B. V. Shanabrook, D. S. Katzer, D. Park, *Science* **273**, 87 (1996).
24. F. Meier, B. Zakharchenya, Eds., *Optical Orientation: Modern Problems in Condensed Matter Sciences* (North Holland, Amsterdam, 1984).
25. R. I. Dzhioev *et al.*, *Phys. Solid State* **40**, 1587 (1998).
26. S. Cortez *et al.*, *Phys. Rev. Lett.* **89**, 207401 (2002).
27. J. G. Tischler, A. S. Bracker, D. Gammon, D. Park, *Phys. Rev. B* **66**, 081310(R) (2002).
28. Y. El Khalifi, B. Gil, H. Mathieu, T. Fukunaga, H. Nakashima, *Phys. Rev. B* **39**, 13533 (1989).

29. R. I. Dzhioev *et al.*, *Phys. Rev. B* **66**, 153409 (2002).
30. A. Zrenner *et al.*, *Phys. Rev. Lett.* **72**, 3382 (1994).
31. A. V. Khaetskii, D. Loss, L. Glazman, *Phys. Rev. Lett.* **88**, 186802 (2002).
32. I. A. Merkulov, Al. L. Efros, M. Rosen, *Phys. Rev. B* **65**, 205309 (2002).
33. J. Lehmann, D. Loss, *Phys. Rev. B* **73**, 045328 (2006).
34. We thank Y. K. Kato for useful advice and discussions and acknowledge support from NSF and the Air Force Office of Scientific Research.

Supporting Online Material
www.sciencemag.org/cgi/content/full/1133862/DC1
Materials and Methods
References

14 August 2006; accepted 1 November 2006
Published online 9 November 2006;
10.1126/science.1133862
Include this information when citing this paper.

A Sea-Floor Spreading Event Captured by Seismometers

M. Tolstoy,[1]* J. P. Cowen,[2] E. T. Baker,[3] D. J. Fornari,[4] K. H. Rubin,[5] T. M. Shank,[4] F. Waldhauser,[1] D. R. Bohnenstiehl,[1] D. W. Forsyth,[6] R. C. Holmes,[1] B. Love,[7] M. R. Perfit,[8] R. T. Weekly,[1] S. A. Soule,[4] B. Glazer[2]

Two-thirds of Earth's surface is formed at mid-ocean ridges, yet sea-floor spreading events are poorly understood because they occur far beneath the ocean surface. At 9°50'N on the East Pacific Rise, ocean-bottom seismometers recently recorded the microearthquake character of a mid-ocean ridge eruption, including precursory activity. A gradual ramp-up in activity rates since seismic monitoring began at this site in October 2003 suggests that eruptions may be forecast in the fast-spreading environment. The pattern culminates in an intense but brief (~6-hour) inferred diking event on 22 January 2006, followed by rapid tapering to markedly decreased levels of seismicity.

The ocean floor is episodically created by injections of magma in dikes that commonly erupt along divergent boundaries that separate tectonic plates. The timing and mechanics of these sea-floor spreading events must normally be inferred from remote seismic or hydroacoustic data and from sea-floor geology. Along fast-spreading ridges, most on-axis seismicity is too small in local magnitude (<2 M_L) to be recorded by global seismic networks or regional hydrophone arrays (*1*). A long-standing goal of mid-ocean ridge (MOR) research has been to capture the seismic precursors, signature, and aftermath of a sea-floor spreading event and eruption within a network of ocean-bottom seismometers (OBSs).

The East Pacific Rise (EPR) near 9°50'N spreads at a full rate of ~110 mm year^{-1} (*2*) and is one of the best-studied MOR segments in the world. Ever since an eruption was documented in 1991 (*3*, *4*), scientists have regularly returned to document ecosystem progression (*5*, *6*), to study changes in vent-fluid chemistry and temperature (*7*, *8*), and to conduct detailed geological mapping (*9*). Based on the predicted decadal-scale repeat rate of eruptions at the northern EPR (*10*), we initiated a 3-year OBS monitoring program in October 2003 as part of the National Science Foundation's Ridge2000 Program of coordinated research at this integrated study site (*11*). Since then, an array of up to 12 OBSs has been deployed in an ~4-by-4–km area between 9°49'N and 9°51'N, with approximately annual data recovery (Fig. 1).

The OBSs, which are deployed from a ship, each contain a seismometer that records the velocity of ground motion, a data-recording package, and an acoustic transponder that allows basic communication with the surface, including instrument release. The release system, when triggered by a coded acoustic pulse, separates the instrument from its anchor, allowing it to rise to the surface for recovery.

In the fast-spreading ridge environment, upper-crust microseismicity is dominated by small cracking events. This activity is driven largely by hydrothermal cooling (*12*) as well as stress concentrations associated with the shallow (1430 meters below the sea floor) axial magma chamber (*13*). The upper crust is therefore sensitive to crustal inflation and/or heating, as well as to increasing extensional stresses. A clear trend of increasing seismicity (*14*) from tens to many hundreds of events per day from October 2003 to May 2005 (Fig. 2) was thus interpreted as reflecting conditions within the system that were building toward an eruption (*15*). The average daily seismicity rate in 1995 was ~2.7 events per day, detected between 9°49'N and 9°51'N with a similarly designed array of nine OBSs (*12*). This activity is about one to two orders of magnitude lower than that observed from 2003 to 2006, indicating substantial differences on multiyear-to-decadal time scales, through different phases of the volcanic/tectonic cycle.

On 25 April 2006, during an expedition of the research vessel (R/V) *Knorr* to service the array, only 4 of 12 instruments were recovered (Fig. 1). Five OBSs were silent, and three were acknowledging anchor-release commands but not leaving the sea floor. In the context of the preceding years' seismicity and a pattern of instrument loss nearest the axial summit trough (AST), an eruption was immediately suspected to have occurred since the last OBS servicing in May 2005.

Corroborating evidence for this theory came from anomalies in water-column measurements of temperature and light scattering made from R/V *Knorr*. During a subsequent R/V *New Horizon* cruise (May 2006), an along-axis conductivity-temperature-depth (CTD)–optical and sample-bottle rosette tow confirmed ex-

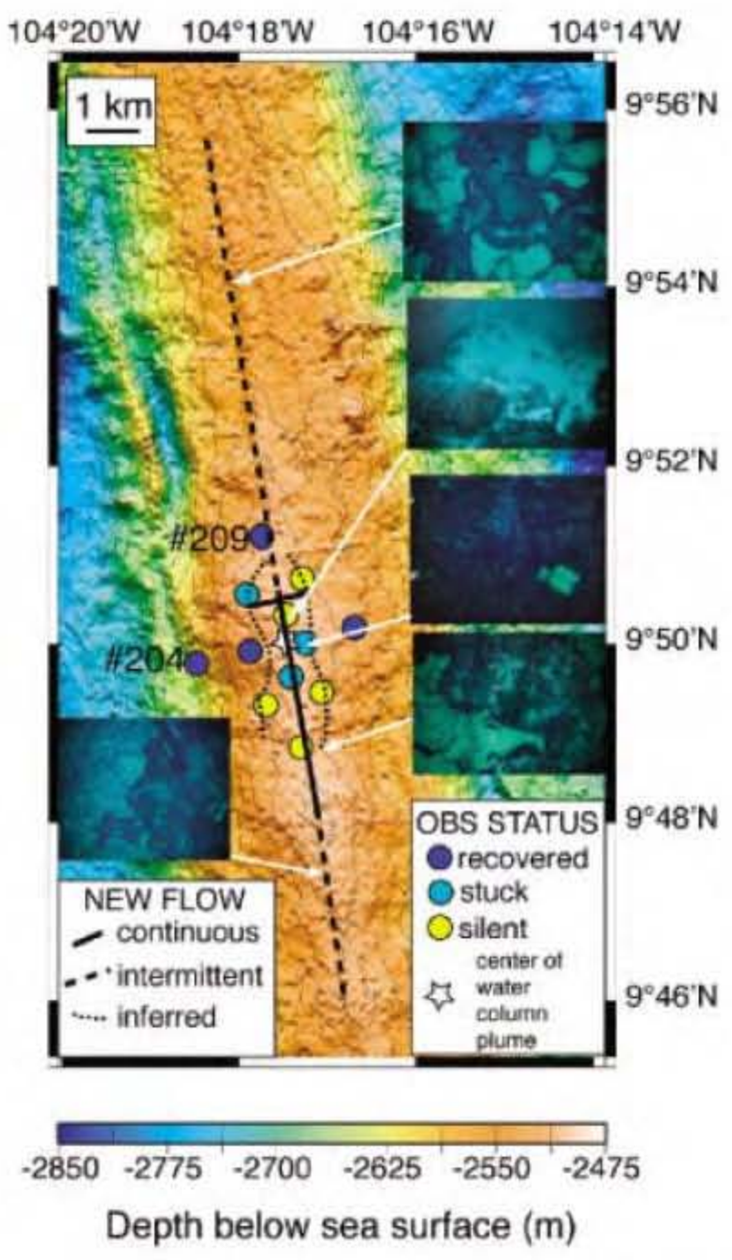

Fig. 1. Map of the EPR 9°50'N area (*26*) showing the OBS locations and estimated extent of the new flow. Insets are TowCam photographs showing contact relationships of the new lava flows and OBS no. 210 stuck in lava (images ~4 to 6 m across). In some locations, the on-axis new flow is continuous [e.g., 9°48'N to 9°50.5'N (solid black line)], whereas further north and south there are 50- to 200-m-long sections where it is discontinuous.

[1]Lamont-Doherty Earth Observatory (LDEO) of Columbia University, Palisades, NY 10964, USA. [2]Department of Oceanography, School of Ocean and Earth Science and Technology (SOEST), University of Hawaii at Manoa, Honolulu, HI 96822, USA. [3]Pacific Marine Environmental Laboratory (PMEL), National Oceanic and Atmospheric Administration (NOAA), WA 98115, USA. [4]Woods Hole Oceanographic Institution, Woods Hole, MA 02543, USA. [5]Department of Geology and Geophysics, University of Hawaii at Manoa, Honolulu, HI 96822, USA. [6]Department of Geological Sciences, Brown University, Providence, RI 02912, USA. [7]School of Oceanography, University of Washington, Seattle, WA 98195, USA. [8]Department of Geological Sciences, University of Florida, Gainesville, FL 32611, USA.

*To whom correspondence should be addressed. E-mail: tolstoy@ldeo.columbia.edu

ceptionally high light attenuation (Δc) values (>0.15 m^{-1}) (Fig. 3), indicative of vigorous discharge of high-temperature hydrothermal fluids. Maximum Δc was centered precisely over the OBS array during both cruises, with density-inversion layers found throughout the bottommost 100 m, especially between 9°48.5′N and 9°50.5′N. Their magnitude, variability, and near ubiquity over this area, along with exceptionally high methane concentrations, are symptomatic of a sea floor that discharges hot, potentially low-chlorinity, hydrothermal fluid. These qualities also suggest that an eruption had occurred less than 7 months before May 2006 (*14*).

Sea-floor images collected using a digital towed camera system [TowCam (*16*)] confirmed the existence of new lavas and constrained the eruption's spatial extent (Fig. 1). The new lavas appear to be erupted from fissures within the AST, which reestablished quickly after the event by drain-back and collapse. Comparison of TowCam bathymetry with pre-eruption Alvin mapping (*17*) suggests that the AST is now 10 to 15 m narrower and a few meters shallower at 9°50.4′N than it was previously. Lava flow morphologies indicate that the highest effusion rates were near 9°50′N (*18*).

Radiometric dating (*14*) of 10 rocks collected from the young terrain is under way, using ^{210}Po (*4*). Preliminary ^{210}Po results indicate that nine of the rocks were erupted within a year before their collection, with dates ranging from late summer 2005 to January 2006.

Based on the sea-floor images, the extent of water column anomalies, the preliminary lava ages, and the distribution of OBSs that failed to return, we estimate that the flow extended intermittently for ≥18 km along the ridge axis, from 9°46′N to 9°55.7′N, with off-axis extent ranging from 0 to ≥1 km. The eruption occurred on the same segment (segment B) as the 1991 to 1992 eruption, with a similar length scale.

Data from only two of the four OBSs recovered in 2006 are presently available because of hard-drive problems, but efforts are being made to recover these data and more OBSs (*14*). The available data come from the northernmost instrument (no. 209), ~0.15 km west of the AST at 9°51′N, and the westernmost instrument (no. 204), ~1.8 km west of the AST near 9°50′N (Fig. 1). Automatic phase picks (Fig. 2), combined with visual inspection of the seismograms, provide a picture of year-long high earthquake rates and abundant harmonic tremors visible at a range of frequencies, particularly in the 5- to 25-Hz band. Periods of pronounced harmonic tremors reduce the signal-to-noise ratio, making automatic detection of earthquakes a less reliable indicator of large swarm activity. To better quantify the variation of seismic activity over time, we summed the root mean square (RMS) amplitude of the seismic vertical channel in the 3- to 18-Hz band within 10-min windows (Fig. 4). High-amplitude events observed on only one instrument may indicate the presence of swarms to the north or south of the array or very close to that instrument. The event on 22 January is clearly the largest event at either station and is well correlated between instruments, indicating local activity over a spatial scale important to both sensors.

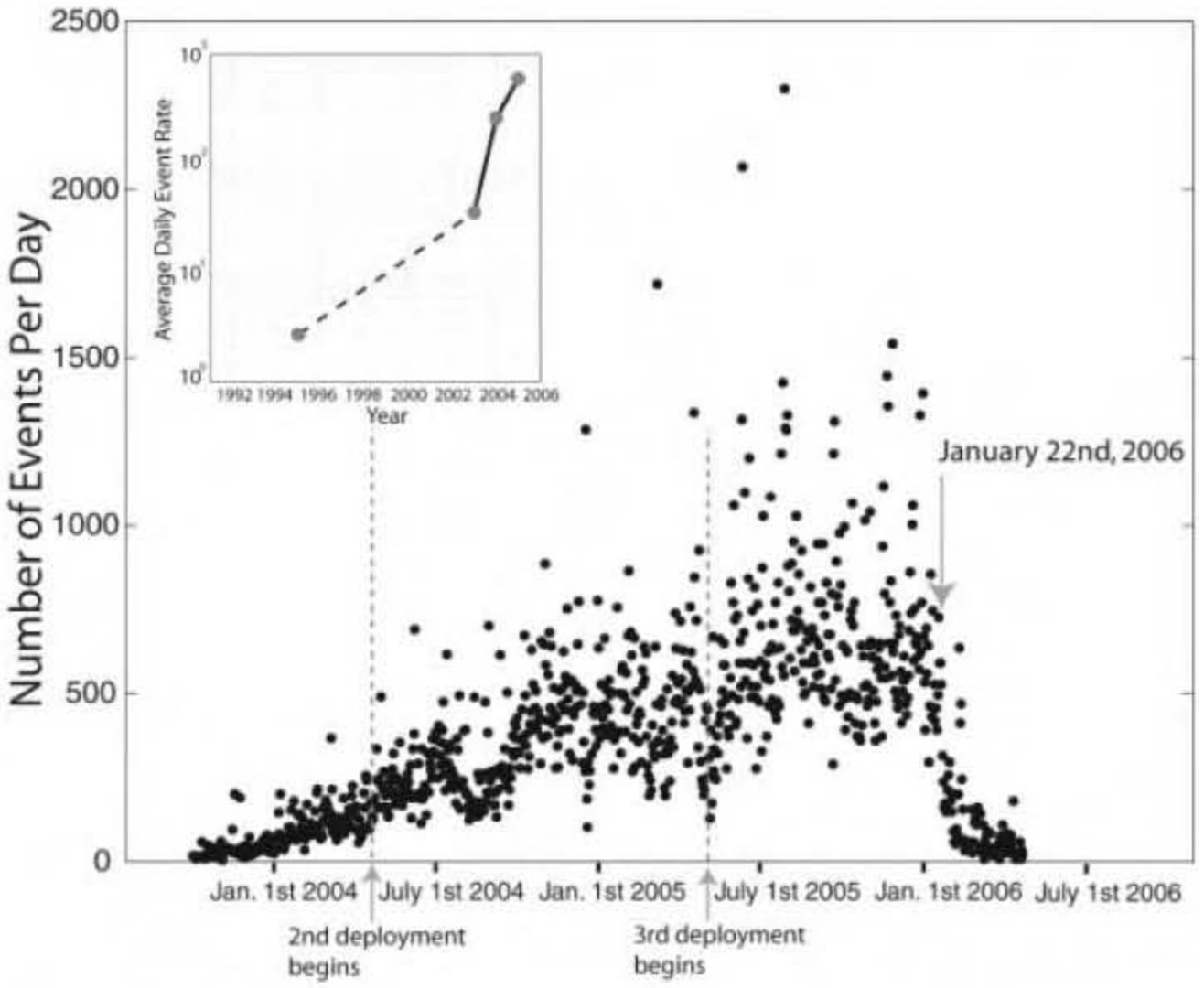

Fig. 2. Plot of the event rate from 3 October 2003 to 23 April 2006. Array turnarounds in April 2004 and May 2005 are marked with vertical dotted lines. Different methods were used to estimate event rates for the various deployments (*14*). Results were normalized by comparing periods of array overlap. The inset plot shows the average daily event rates by year, including data from a 1995 deployment (*12*).

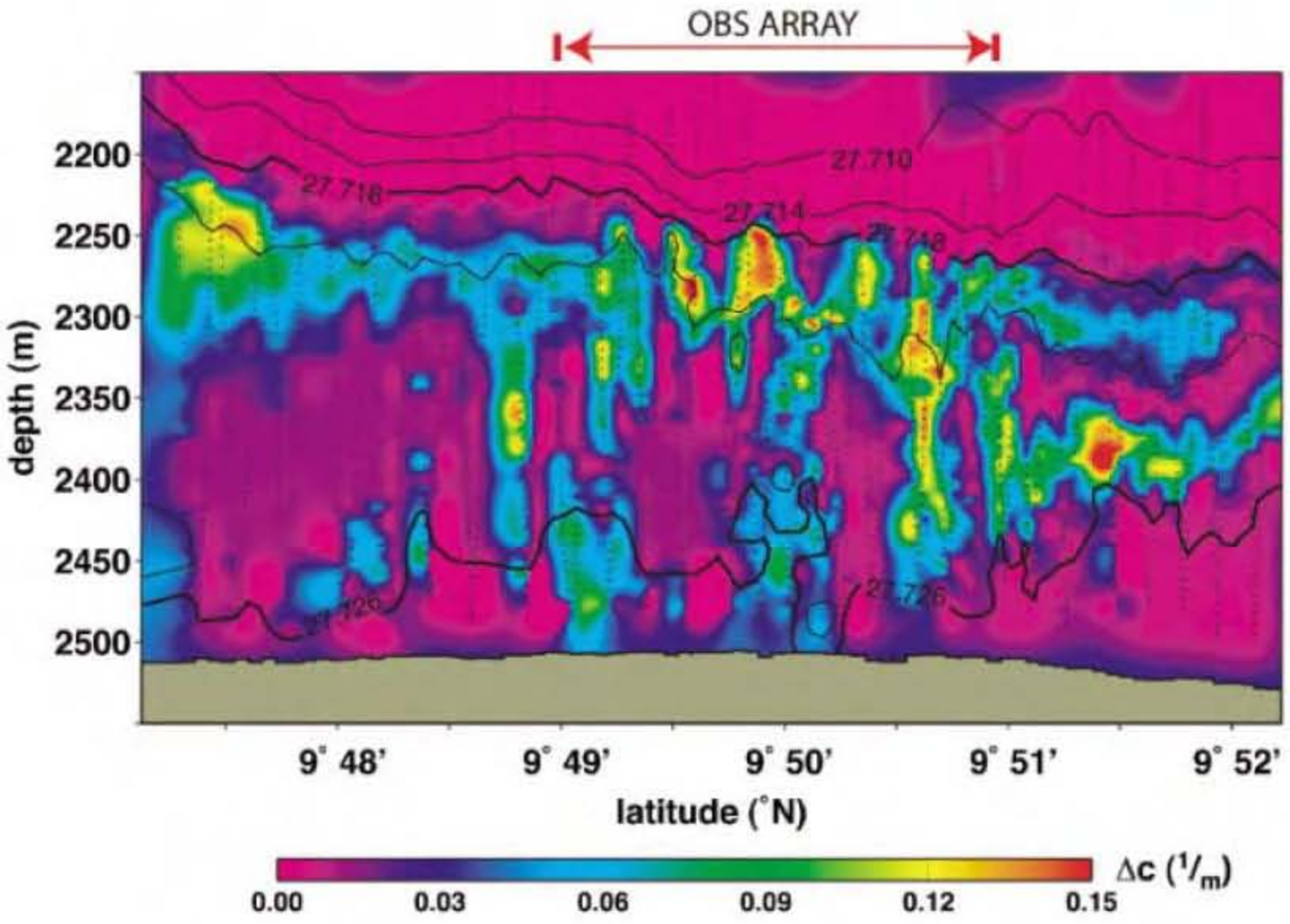

Fig. 3. Contour plot of Δc versus depth and latitude for an along-axis (ridge summit) tow-yo cast. Δc intensity is represented by colors. Potential density (sigma-theta; in kg m^{-3}) contours (solid black lines) are superimposed over Δc. The dotted line indicates the saw-toothed tow pattern of the CTD-transmissometer-bottle rosette instrument package. The deepest density line indicates localized areas of instability in the lower part of the water column; the strong correlation between the vertical structures in Δc and the deep density contour line suggest that strong localized hydrothermal venting is driving the entrainment and subsequent rise of ambient bottom water.

Seismograms and spectrograms from 22 January clearly show exceptionally high-amplitude seismic signals starting around 1345 (GMT) and continuing at high intensity for ~6 hours. Substantial earthquake activity lasted more than a week thereafter. The initial 6 hours were dominated by strong harmonic tremors and a single-station earthquake event rate often exceeding 250 events per hour [compared with single-station rates of ~1.6 events per hour reported after the 1991 eruption (*19*)]. Both OBSs exhibit tremors at similar but not identical frequencies, indicating differences in the character of the resonator proximal to 9°51'N (no. 209) and 9°50'N (no. 204). We interpret this period of most-intense activity, associated with the major spike in the seismic RMS amplitude (Fig. 4B), as propagation of the primary dike that fed this eruption. Plume distributions and high lava effusion rates inferred from lava morphology imply a dike that originated near 9°50′N. This is consistent with 80 secondary wave–minus–primary wave measurements of the largest earthquakes (*14*), which indicate that the events were concentrated near 9°50.5′N before and during the first hour of the 6-hour period, and then were dispersed throughout the 9°49.2'N to 9°50.5′N region for the remaining ~5+ hours. This supports the idea that individual eruptions occur at the fourth-order segment scale, defined by local axial discontinuities, even though volcanic systems may be organized at the third-order scale, defined by discontinuities with off-axis expressions (*20*, *3*, *21*, *22*).

At ~1445 (GMT), seismic amplitudes peaked at about five times higher than during the rest of the 6-hour high-intensity interval (Fig. 4B). This hour-long peak may coincide with the dike rising to the surface from the axial magma chamber depth of 1.43 km (*13*), implying a vertical propagation rate of ~1.4 km hour^{-1}, consistent with typical dike propagation rates at MORs (*23*). Thus, the vertical propagation of the crack may have been preceded by ~1 hour of precursory cracking and/or magma injection at depth, manifested by lower-amplitude but intense tremor and earthquake activity. Over the weeks after the inferred diking event, tremor and seismic activity tapered rapidly to background levels substantially lower than those in the preceding months. However, brief pulses of activity were evident through April 2006.

Swarms of tremor and seismicity were observed during the preceding months as far back as May 2005 (Fig. 4A), when the last Alvin dives were conducted in this region (confirming an eruption at 9°50'N had not yet occurred). It is possible that periods of high activity may have been associated with either local minor intrusive diking/eruptive events or events north or south of the 9°50'N area, consistent with preliminary radiometric dating evidence for a mid-2005 eruption at the southern end of the flow, observed contact relationships within the new flow, and evidence that the 1991-to-1992 eruptive activity lasted ~1 year (*4*). However, it is evident in the seismic data that the primary diking event in the immediate 9°50'N area began on 22 January 2006, consistent with the relative strength of the water-column signal and the stage of ecosystem recovery (*14*). Records from three recording temperature probes (*8*) deployed in high-temperature vents at the site also provide evidence that substantial changes occurred in the hydrothermal system in the January 2006 time frame (*24*).

This event documents a known MOR eruption surface being paved over by lava from a repeat eruption, thereby completing an ~15-year full volcanic cycle that has been scrutinized by regular multidisciplinary monitoring. Our documentation of how seismic activity builds up before an eruption may make it possible to forecast future eruptions a year or more in advance. The brevity and intensity of the culminating dike event suggest rapid tapping of the axial magma chamber as compared with slower-spreading ridges (*23*, *25*). A 6-hour window for the primary diking event emphasizes the need for multidisciplinary in situ monitoring to fully characterize the geological, chemical, and biological phenomena associated with this fundamental process that shapes our planet.

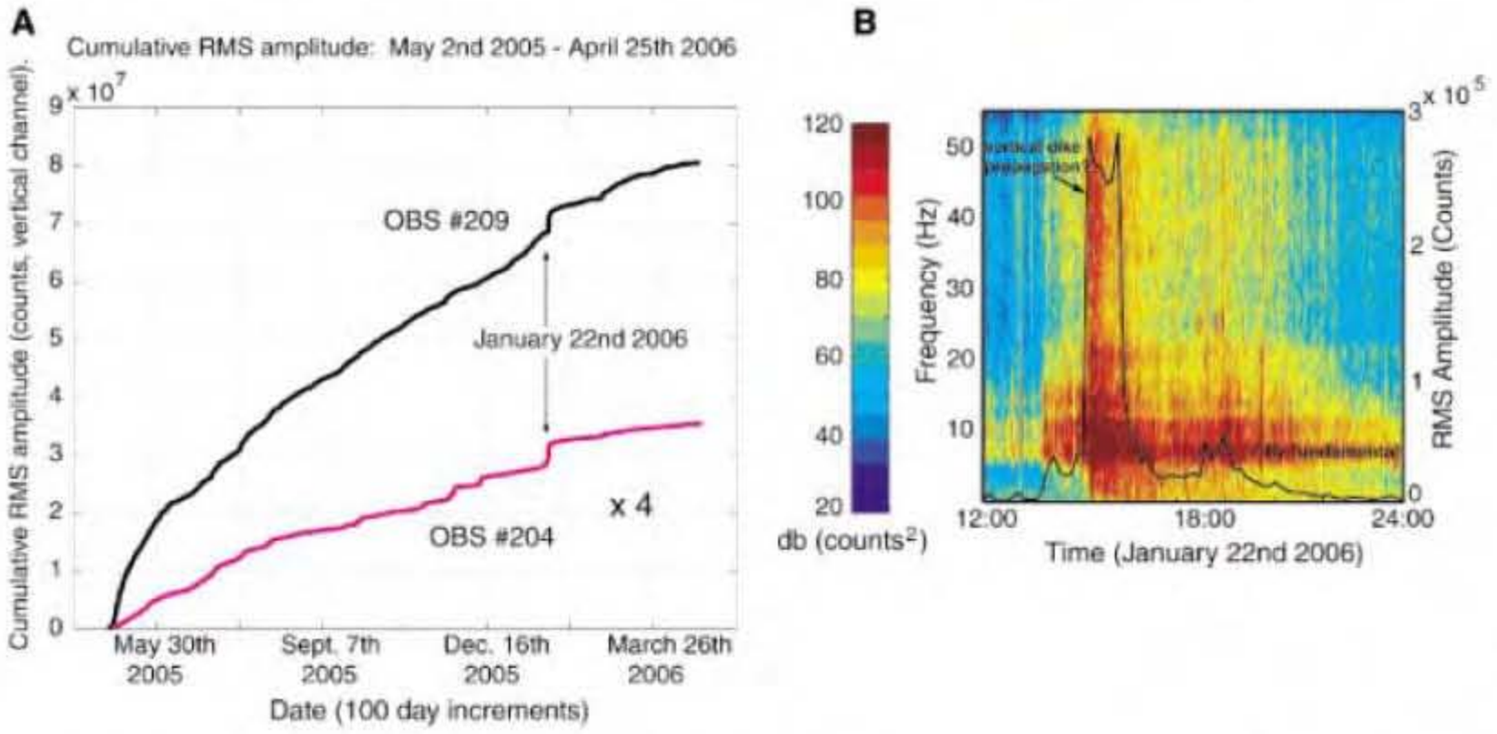

Fig. 4. (**A**) Cumulative plot of RMS amplitude of the waveforms. OBS no. 204 is multiplied by 4 to assist comparison with OBS no. 209. (**B**) Spectrogram of seismic data from 1200 to 2400 on 22 January 2006 from no. 209, showing the most intense activity of the year interpreted as the propagation of a dike from depth. The black line shows the RMS amplitude from Fig. 4A, which provides a quantitative measure of signal strength. db, decibels.

References and Notes

1. C. G. Fox, H. Matsumoto, T.-K. A. Lau, *J. Geophys. Res.* **106**, 4183 (2001).
2. S. M. Carbotte, K. C. MacDonald, *J. Geophys. Res.* **99**, 13609 (1994).
3. R. M. Haymon *et al.*, *Earth Planet. Sci. Lett.* **119**, 85 (1993).
4. K. H. Rubin, J. D. MacDougall, M. R. Perfit, *Nature* **368**, 841 (1994).
5. R. A. Lutz *et al.*, *Nature* **371**, 663 (1994).
6. T. M. Shank *et al.*, *Deep-Sea Res. II* **45**, 465 (1998).
7. K. L. Von Damm, M. D. Lilley, *AGU Monogr.* **144**, 245 (2004).
8. D. J. Fornari *et al.*, *J. Geophys. Res.* **103**, 9827 (1998).
9. M. R. Perfit *et al.*, *Geology* **22**, 375 (1994).
10. M. R. Perfit, W. W. Chadwick Jr., *AGU Monogr.* **106**, 59 (1998), and references therein.
11. www.ridge2000.org
12. R. A. Sohn, J. A. Hildebrand, S. C. Webb, *J. Geophys. Res.* **104**, 25367 (1999).
13. G. M. Kent, A. J. Harding, J. A. Orcutt, *J. Geophys. Res.* **98**, 13945 (1993).
14. Materials and methods are available as supporting material on *Science* Online.
15. M. Tolstoy, F. Waldhauser, in report of the Ridge 2000 *EPR* ISS Science and 2006 Field Planning *Workshop*, 10 to 12 April 2006, Palisades, NY; available at (www.ridge2000.org/science/downloads/meetings/EPRwksp_report_final.pdf).
16. D. J. Fornari, *Eos* **84**, 69 (2003).
17. V. L. Ferrini *et al.*, *Geochem. Geophys. Geosys.*, in press.
18. S. A. Soule *et al.*, *Geochem. Geophys. Geosys.* **6**, Q08005 (2005).
19. J. A. Hildebrand, S. C. Webb, L. M. Dorman, *RIDGE Events* **2**, 6 (1991).
20. K. C. Macdonald *et al.*, *Nature* **335**, 217 (1988).
21. S. M. White *et al.*, *J. Geophys. Res.* **107**, B000571 (2002).
22. R. M. Haymon, S. C. White, *Earth Planet. Sci. Lett.* **226**, 367 (2004).
23. R. P. Dziak, C. G. Fox, *Geophys. Res. Lett.* **26**, 3429 (1999).
24. K. L. Von Damm, personal communication.
25. M. Tolstoy, D. R. Bohnenstiehl, M. Edwards, G. Kurras, *Geology* **29**, 1139 (2001).
26. S. M. White, R. M. Haymon, S. M. Carbotte, *Geochem. Geophys. Geosys.*, in press.

27. This work was supported by NSF under grant OCE-0327283 (M.T., F.W., D.R.B., R.C.H., and R.T.W.), grant OCE-0222069 and University of Hawaii–NASA Astrobiology Institute (J.P.C.), NOAA Vents Program (E.T.B.), grant OCE-9819261 (D.J.F.), grant OCE-0525863 (D.J.F. and S.A.S.), and grant OCE-0636439 (K.H.R.). We thank S. C. Solomon, K. C. Macdonald, and W. W. Chadwick for constructive reviews and the captain, crew, and science parties of the R/V *New Horizon* and R/V *Knorr*. M.T. thanks J. Cameron; Disney; Walden Media; and the captain, crew, and science party led by A. M. Sagalevitch of the R/V *Keldysh* for enabling early OBS deployment. This is LDEO contribution number 6983, SOEST contribution number 6996, and PMEL contribution number 2951.

Supporting Online Material

www.sciencemag.org/cgi/content/full/1133950/DC1
Materials and Methods
Fig. S1
References and Notes

16 August 2006; accepted 7 November 2006
Published online 23 November 2006;
10.1126/science.1133950
Include this information when citing this paper.

Homoploid Hybrid Speciation in an Extreme Habitat

Zachariah Gompert,[1] James A. Fordyce,[2] Matthew L. Forister,[3] Arthur M. Shapiro,[4] Chris C. Nice[1]*

According to theory, homoploid hybrid speciation, which is hybrid speciation without a change in chromosome number, is facilitated by adaptation to a novel or extreme habitat. Using molecular and ecological data, we found that the alpine-adapted butterflies in the genus *Lycaeides* are the product of hybrid speciation. The alpine populations possess a mosaic genome derived from both *L. melissa* and *L. idas* and are differentiated from and younger than their putative parental species. As predicted, adaptive traits may allow for persistence in the environmentally extreme alpine habitat and reproductively isolate these populations from their parental species.

Homoploid hybrid speciation is characterized by hybridization between parental species that results in a derivative hybrid species without a change in chromosome number (*1*–*6*). A growing list of possible examples, such as African cichlids (*7*), cyprinid fishes (*8*), *Rhagoletis* fruit flies (*9*), *Heliconius* butterflies (*10*), and swallowtail butterflies (*11*), suggest that homoploid hybrid speciation in animals may be more common than previously thought. Models predict that ecological isolation spurs homoploid hybrid speciation, especially when the hybrids invade novel or extreme habitats (*12*). Colonization of a novel habitat by an incipient hybrid species may allow it to avoid introgression and competition with the parental species (*4*, *12*). Although these predictions have been borne out in plants (*13*), no examples of homoploid hybrid speciation in animals have involved adaptation to a novel habitat, although a switch to a novel host plant species has been documented (*9*).

The ecologically, morphologically, and behaviorally distinct species *L. melissa* and *L. idas* (*14*–*17*) have come into secondary contact in the Sierra Nevada of western North America (*18*) (Fig. 1). *Lycaeides melissa* populations occur in Great Basin habitats on the east side of the Sierra Nevada, whereas *L. idas* populations occupy wet meadows at mid-elevation on the west slope of these mountains. Unnamed populations of *Lycaeides* occur in the alpine habitat above the tree line of the Sierra Nevada, an environmentally extreme habitat not occupied by *L. melissa* or *L. idas*. The alpine habitat is characterized by a short growing season and severe fluctuations in ambient temperature and relative humidity on a daily and seasonal basis (*19*). These alpine butterflies have male genitalia that are intermediate in size and shape compared with those of *L. melissa* and *L. idas* (*18*), with wing pattern elements that are qualitatively similar to those of *L. melissa* (*14*). However, analysis of mitochondrial DNA variation shows that the alpine populations' haplotypes share a more recent common ancestor with haplotypes of *L. idas* than those of *L. melissa* (fig. S1) (*20*). These discordant patterns suggest that hybridization may have played a role in the evolutionary history of alpine *Lycaeides* populations.

If the alpine *Lycaeides* populations are a hybrid species, they should possess a genome that is a blend of alleles derived from both *L. melissa* and *L. idas*. We tested this using a large multilocus genomic data set consisting of 128 amplified fragment length polymorphism (AFLP) markers, three microsatellite markers (*Msat201*, *Msat4*, and *MsatZ12-1*), and sequence data from three nuclear genes (*Nuc1*, *Nuc3*, and *Ef1α*) and two mitochondrial genes (*COI* and *COII*) (*20*). To assess the overall genomic composition of the alpine *Lycaeides* populations, we used the Bayesian program STRUCTURE version 2.1 to cluster *L. melissa*, *L. idas*, and alpine individuals on the basis of their multilocus genotypes (*20*, *21*) under the assumption that the data represented two separate populations ($K = 2$). Individuals from *L. melissa* and *L. idas* clustered to different groups with high probability, whereas alpine *Lycaeides* individuals were assigned to both groups with moderate probability (Fig. 2A and table S1). This pattern is inconsistent with a bifurcating mode of speciation, in which alpine butterflies originated from a single parental species, and suggests that the alpine genome is a mosaic of the two species. In further support of this hypothesis, five AFLP fragments were shared between *L. melissa* and *L. idas* to the exclusion of the

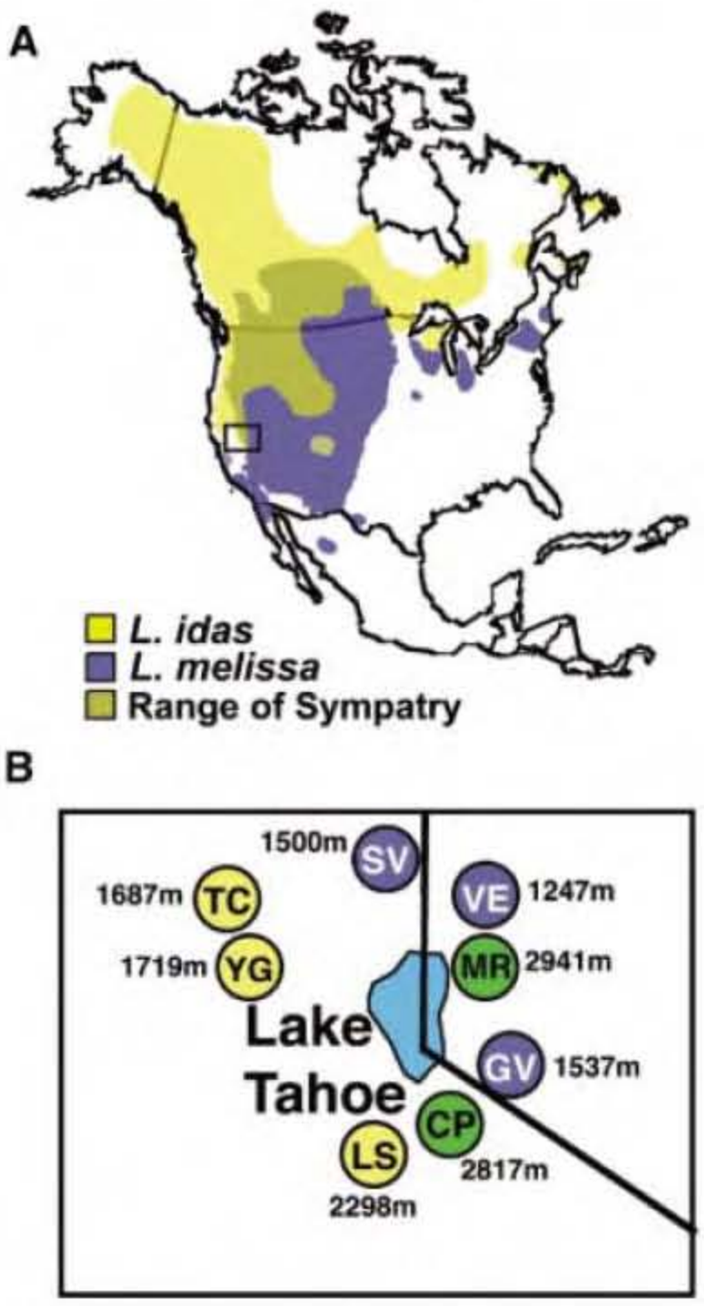

Fig. 1. Approximate range of *L. melissa* and *L. idas* in North America (**A**) and sampling localities for this study (**B**). The range map is based on Nabokov (*23*), Stanford and Opler (*24*), and Scott (*25*). *Lycaeides idas* is shown in yellow, *L. melissa* is shown in blue, and regions of sympatry are shown in gray. The box denotes the focal region for this study. Sampling localities for *L. idas*, *L. melissa*, and alpine *Lycaeides* are shown in yellow, blue, and green, respectively. SV, Sierraville; VE, Verdi; MR, Mt. Rose; GV, Gardnerville; CP, Carson Pass; LS, Leek Springs; YG, Yuba Gap; TC, Trap Creek.

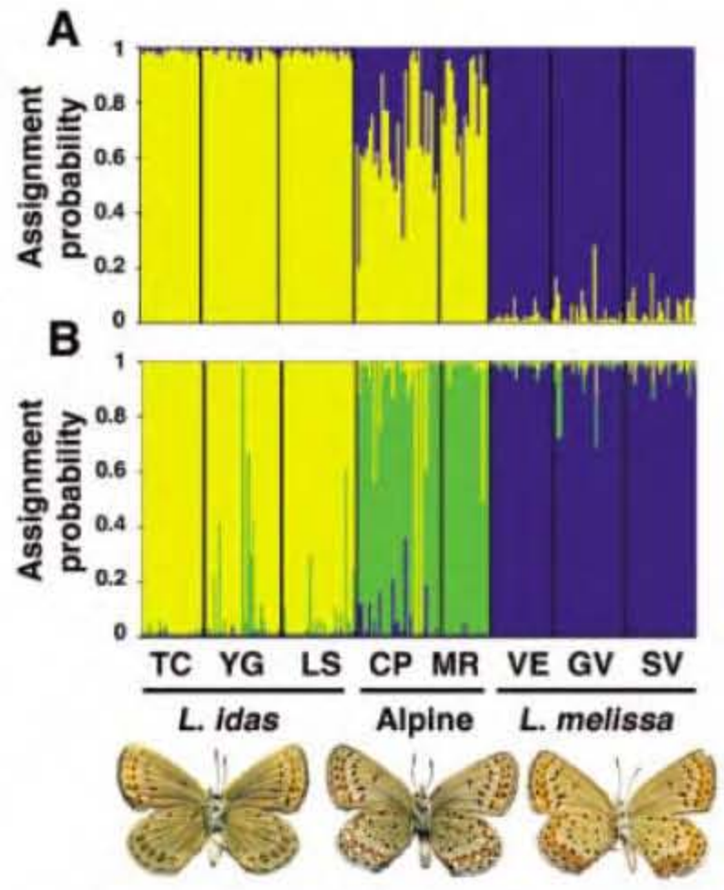

Fig. 2. Bar plots showing Bayesian assignment probabilities from the software STRUCTURE 2.1 (*21*) for two (**A**) and three (**B**) clusters (*20*). Each vertical bar corresponds to one individual. The proportion of each bar that is yellow, blue, and green represents an individual's assignment probability to clusters one, two, and three, respectively. See table S1 for mean population assignment probabilities. Location abbreviations are as in Fig. 1.

[1]Department of Biology, Population and Conservation Biology Program, Texas State University, San Marcos, TX 78666, USA. [2]Department of Ecology and Evolutionary Biology, University of Tennessee, Knoxville, TN 37996, USA. [3]Department of Natural Resources and Environmental Science, University of Nevada, Reno, NV 89512, USA. [4]Section of Evolution and Ecology, University of California, Davis, CA 95616, USA.

*To whom correspondence should be addressed. E-mail: ccnice@txstate.edu

alpine populations, whereas the alpine populations shared 12 unique alleles with *L. melissa* and 16 unique alleles with *L. idas*. Additionally, in *L. melissa* and *L. idas*, different alleles were fixed at the *Nuc1* locus (fig. S2 and table S1), whereas the alpine populations shared three *Nuc1* alleles with *L. melissa* and three *Nuc1* alleles with *L. idas*.

Although the mosaic genome of the alpine populations is consistent with homoploid hybrid speciation, a similar pattern could arise if the alpine populations have continuous gene flow with *L. melissa* and/or *L. idas*. If so, the alpine populations would not be genetically differentiated from *L. melissa* and *L. idas*, and there would be evidence of gene flow with these species. When STRUCTURE (*21*) was run under the assumption that the data represented three separate populations ($K = 3$), *L. melissa* and *L. idas* individuals were still assigned to their respective clusters, but the alpine *Lycaeides* individuals were assigned to a distinct, third cluster (Fig. 2B and table S1) (*20*). Additionally, alpine populations were fixed for unique alleles at the mitochondrial genes *COI* and *COII*, as well as the nuclear gene *Nuc3* (figs. S1 and S3 and table S1). These data and examination of pairwise F_{ST} (*20*) (table S2) suggest that alpine populations are differentiated from *L. melissa* and *L. idas*. We did not detect excess heterozygosity or deviations from linkage equilibrium for any microsatellite markers or nuclear gene sequences (*20*); such deviations would indicate ongoing gene flow between the alpine populations and either *L. melissa* or *L. idas*. We used the program NewHybrids, which uses the Bayesian assignment algorithm of Anderson and Thompson (*22*) to assess the probability that gene flow occurs between *L. melissa* and/or *L. idas* and the alpine populations (*20*). No individuals were identified that could be considered F_1's produced from crosses between *L. melissa* or *L. idas* and the alpine populations (fig. S4). Thus, we concluded that the alpine populations are genetically differentiated from *L. melissa* or *L. idas* and are not exchanging genes with either.

The genetic patterns we documented could have occurred if *L. melissa*, *L. idas*, and the alpine populations all developed rapidly from a single ancestral species distributed along a geographic cline with the alpine populations originating from the center of the cline. This scenario is unlikely for several reasons. Phylogeographic data suggest that the current distribution of *L. melissa* and *L. idas* is the result of post-Pleistocene range expansion and secondary contact and thus does not reflect the distribution of the ancestor of these species (*18*). The alpine populations also have a more recent origin than either *L. melissa* or *L. idas*. We calculated a coalescent-based estimate of the time to the most recent common ancestor (TMRCA) for mitochondrial variation for each of the three putative species: the alpine populations, *L. melissa*, and *L idas* (*20*). The estimated TMRCA for the alpine populations, 442,579 years before present (yr B.P.), is substantially younger than that of either *L. melissa* or *L. idas*, 1,902,995 and 1,267,885 yr B.P., respectively (*20*). Furthermore, pairwise estimates of τ (species divergence time multiplied by mutation rate) based on nuclear and mitochondrial sequence data were approximately four times greater for the divergence of *L. melissa* and *L. idas* [0.006576, 95% confidence interval (95% CI) 0.002823 to 0.009855] than for the divergence of the alpine populations and either *L. melissa* (0.001318, 95% CI 0.000638 to 0.002233) or *L. idas* (0.001468, 95% CI 0.000763 to 0.002454) (*20*) (fig. S5). Thus, *L. melissa*, *L. idas*, and the alpine populations did not arise rapidly from a single ancestral species.

Homoploid hybrid speciation is more likely when a hybrid species colonizes a novel habitat (*5*, *6*, *12*, *13*), such as the alpine habitat occupied by *Lycaeides*. Reproductive isolation between the hybrid and the parental taxa may be maintained by behavioral and ecological adaptations to the alpine habitat specifically associated with the alpine host plant. Females from the alpine populations have near-perfect host fidelity for their host plant, the perennial alpine endemic, *Astragalus whitneyi* (Fig. 3) (*20*). Indeed, alpine females have stronger host fidelity than has been recorded in other *Lycaeides* populations. Because males and females of *Lycaeides* locate mates and copulate on or near their larval host plants (*15*), strong fidelity with *A. whitneyi* may serve as a strong prezygotic barrier to gene flow between alpine *Lycaeides* populations and their putative parental species. In addition, host fidelity is coupled with a unique lack of egg adhesion in the alpine populations. Whereas *Lycaeides* females from nonalpine populations "glue" their eggs to their host plant when they oviposit, the alpine populations' eggs fall off the plant after oviposition and remain near the site of new plant growth in the following spring (*16*). Because *Lycaeides* overwinter as diapausing eggs (*16*) and the senesced aboveground biomass of the alpine host plant is blown away by strong winds in the winter (*16*), any eggs attached to the alpine host plant would be carried far from the site of new host plant growth, resulting in likely death of neonate larvae. Any females from nonalpine populations that oviposit on the alpine host plant would suffer a major reduction in fitness. Together, these alpine-associated adaptive traits—strong host fidelity for an alpine endemic host plant and the loss of egg adhesion—may act as an effective ecological barrier to gene flow.

Two other mechanisms may also contribute to reproductive isolation. Color pattern differences on the underside of the wings operate as species recognition cues, isolating the alpine populations from *L. idas* (*14*). Differences in male genital morphology have also been documented (*18*) and may operate in a similar manner to limit gene flow, although this was not explicitly tested in this study. Thus, morphological characters and adaptation to an extreme, novel habitat may create reproductive isolation between the hybrid species and its parental species.

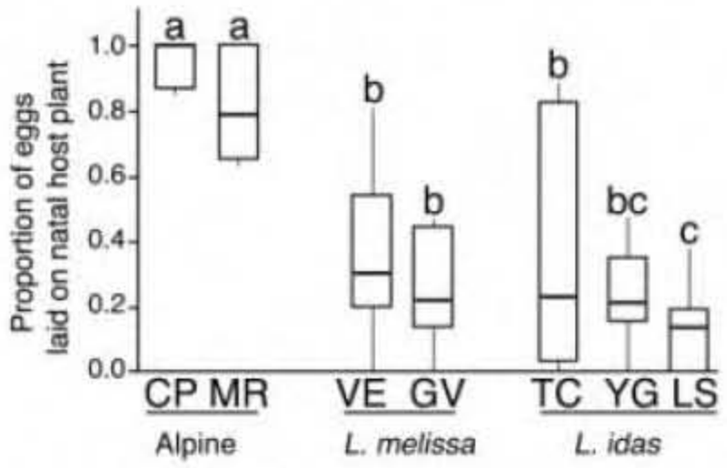

Fig. 3. Natal host plant fidelity from seven focal populations. Box plots show the median proportion of eggs laid on the natal host plant for each population. Kruskal-Wallis test indicates significant differences in natal host plant preference among populations ($T = 46.67$; $P < 0.0001$). Different letters (a, b, and c) indicate differences in strength of preference for natal host among populations ($\alpha < 0.05$). Natal host plants are listed in table S1. Location abbreviations are as in Fig. 1.

References and Notes

1. J. A. Coyne, H. A. Orr, *Speciation* (Sinauer Associates, Sunderland, MA, 2004).
2. V. Grant, *Plant Speciation* (Columbia Univ. Press, New York, 1981).
3. M. L. Arnold, *Natural Hybridization and Evolution* (Oxford Univ. Press, Oxford, 1997).
4. T. E. Dowling, C. L. Secor, *Annu. Rev. Ecol. Syst.* **28**, 593 (1997).
5. L. H. Rieseberg, *Annu. Rev. Ecol. Syst.* **28**, 359 (1997).
6. B. L. Gross, L. H. Rieseberg, *J. Hered.* **96**, 241 (2005).
7. R. Schelly, W. Salzburger, S. Koblmuller, N. Duftner, C. Sturmbauer, *Mol. Phylogenet. Evol.* **38**, 426 (2006).
8. B. D. Demarais, W. L. Minckley, *Copeia* **1992**, 697 (1992).
9. D. Schwarz, B. M. Matta, N. L. Shakir-Botteri, B. A. McPheron, *Nature* **436**, 546 (2005).
10. J. Mavarez *et al.*, *Nature* **441**, 868 (2006).
11. J. M. Scriber, G. J. Ording, *Entomol. Exp. Appl.* **115**, 247 (2005).
12. C. A. Buerkle, R. J. Morris, M. A. Asmussen, L. H. Rieseberg, *Heredity* **84**, 441 (2000).
13. L. H. Rieseberg *et al.*, *Science* **301**, 1211 (2003).
14. J. A. Fordyce, C. C. Nice, M. L. Forister, A. M. Shapiro, *J. Evol. Biol.* **15**, 871 (2002).
15. C. C. Nice, J. A. Fordyce, A. M. Shapiro, R. ffrench-Constant, *Ecol. Entomol.* **27**, 702 (2002).
16. J. A. Fordyce, C. C. Nice, *Ecol. Lett.* **6**, 23 (2003).
17. M. L. Forister, J. A. Fordyce, C. C. Nice, Z. Gompert, A. M. Shapiro, *Ann. Entomol. Soc. Am.* **99**, 933 (2006).
18. C. C. Nice, N. Anthony, G. Gelembiuk, D. Raterman, R. ffrench-Constant, *Mol. Ecol.* **14**, 1741 (2005).
19. M. V. Lomolino, B. R. Riddle, J. H. Brown, *Biogeography* (Sinauer Associates, Sunderland, MA, ed. 3, 2006).
20. Materials and methods are available as supporting material on *Science* Online.
21. J. K. Pritchard, M. Stephens, P. Donnelly, *Genetics* **155**, 945 (2000).
22. E. C. Anderson, E. A. Thompson, *Genetics* **160**, 1217 (2002).
23. V. Nabokov, *Bull. Mus. Comp. Zool.* **101**, 479 (1949).
24. R. E. Stanford, P. A. Opler, *Atlas of Western USA Butterflies, Including Adjacent Parts of Canada and Mexico* (Self-published, Fort Collins, CO, 1996).
25. J. A. Scott, *The Butterflies of North America, a Natural History and Field Guide* (Stanford Univ. Press, Stanford, CA, 1986).

26. This research was funded by a NSF graduate research fellowship to Z.G., the University of Tennessee, a Research Enhancement Grant from Texas State University to C.C.N., and NSF grant DEB-9306721 to A.M.S. We thank D. Bolnick, B. Fitzpatrick, S. Gavrilets, C. Jiggins, J. Ott, the EEB discussion group at Texas State University, and two anonymous reviewers for comments on an earlier version of this manuscript, and A. Stephenson for assistance in the lab. GenBank accession numbers for sequence data are EF 090312-EF090397.

Supporting Online Material

www.sciencemag.org/cgi/content/full/1135875/DC1
Materials and Methods
SOM Text
Figs. S1 to S10
Tables S1 to S4
References

3 October 2006; accepted 16 November 2006
Published online 30 November 2006;
10.1126/science.1135875
Include this information when citing this paper.

A Giant European Dinosaur and a New Sauropod Clade

Rafael Royo-Torres,* Alberto Cobos, Luis Alcalá

Fossils of a giant sauropod dinosaur, *Turiasaurus riodevensis*, have been recovered from terrestrial deposits of the Villar del Arzobispo Formation (Jurassic-Cretaceous boundary) of Riodeva (Teruel Province, Spain). Its humerus length (1790 millimeters) and estimated mass (40 to 48 metric tons) indicate that it may have been the most massive terrestrial animal in Europe and one of the largest in the world. Phylogenetic analysis indicates that the fossil represents a member of a hitherto unrecognized group of primitive European eusauropods that evolved in the Jurassic.

Most gigantic sauropods are neosauropods and have been found in the New World [such as *Seismosaurus* (*1*) and *Sauroposeidon* (*2*) in North America and *Argentinosaurus* (*3*) and *Puertasaurus* in South America (*4*)] or Africa [such as *Paralititan* (*5*) and *Brachiosaurus* (*6*)]. Here we describe a new giant European sauropod from Riodeva (Spain) as a new taxon, *Turiasaurus riodevensis* gen. et sp. nov., in Tithonian-Berriasian–aged deposits of the Villar del Arzobispo Formation (*7*) (figs. S1 and S2). The Barrihonda–El Humero site, where the new gigantic sauropod was found, has also yielded theropod teeth, postcranial remains of stegosaurs, and isolated elements of ornithopods, as well as fishes, turtles, and crocodylomorphs. The only other sauropod specimens reported from Riodeva were isolated elements from Pino de Jarque 2 and La Cautiva 2 (fig. S2): an ilium of a Diplodocidae indet (*8*) and a proximal caudal vertebra of a basal eusauropod (*9*).

Etymology. *Turiasaurus*, from Turia (word used since the 12th century from which Teruel derives) and *sauros* (Greek word, lizard); *riodevensis*, from Riodeva (village where the fossil site is located).

Holotype. An articulated left forelimb (Fig. 1, A to G) including humerus, radius, proximally incomplete ulna, carpal, five metacarpals, and seven phalanges (specimen numbers CPT-1195 to CPT-1210, housed in the Museo de la Fundación Conjunto Paleontológico de Teruel-Dinópolis, Teruel, Aragón, Spain).

Paratype. Remains attributed to the same individual, found close to each other in an area of 280 m^2 (fig. S3), consisting of skull fragments, eight teeth (Fig. 2), six cervical vertebrae (Fig. 1K) with ribs (Fig. 1, L and M) (probably cervicals 3 to 8), two proximal dorsal vertebrae, a middle dorsal vertebra (Fig. 1I), fragments of other dorsal vertebrae, eight dorsal ribs (five incomplete), a partial sacrum, two distal caudal vertebrae (Fig. 1T), a proximal fragment of the left scapula, a left sternal plate (Fig. 1J), a distal fragment of the left femur, a proximal fragment of the left tibia (Fig. 1, N and O), a distally incomplete left fibula (Fig. 1H), a complete left astragalus (Fig. 1, P and Q), two left pedal phalanges, and an incomplete right astragalus and pes (Fig. 1, R and S) (CPT-1211 to CPT-1261), housed in the Museo de la Fundación Conjunto Paleontológico de Teruel-Dinópolis, Teruel, Spain).

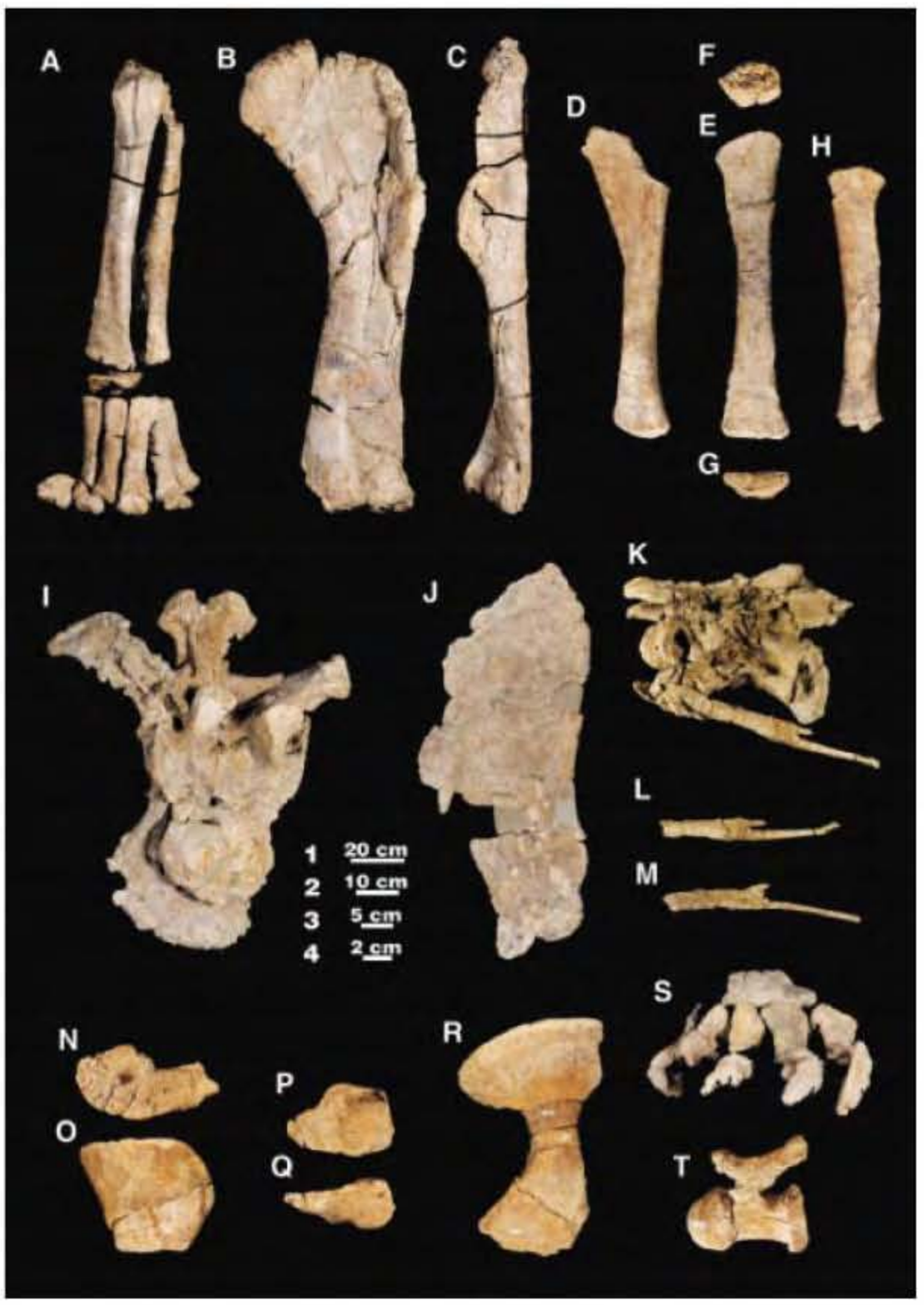

Fig. 1. Skeletal elements of *T. riodevensis* gen. et sp. nov.: left radius, ulna, carpal, and manus in cranial view (**A**); humerus in cranial (**B**) and lateral (**C**) views; left ulna in cranial view (**D**); left radius in medial (**E**), proximal (**F**), and distal (**G**) views; left fibula in medial view (**H**); middle dorsal vertebra in cranial view (**I**); left sternal plate in ventral view (**J**); cervical vertebra and rib in left lateral view (**K**); cervical rib in medial (**L**) and lateral (**M**) views; left tibia in proximal (**N**) and medial (**O**) views; left astragalus in proximal (**P**) and cranial (**Q**) views; metatarsal V in lateral view (**R**); right pes in cranial view (**S**); distal caudal vertebra in left lateral view (**T**). Scale bar 1 = 20 cm [(A) to (H), (N) to (Q), and (S)]; scale bar 2 = 10 cm [(I) to (M)]; scale bar 3 = 5 cm (R), and scale bar 4 = 2 cm (T).

Fundación Conjunto Paleontológico de Teruel-Dinópolis. Avenida de Sagunto, E-44002 Teruel, Spain.

*To whom correspondence should be addressed. E-mail: royo@dinopolis.com

Diagnosis. Autapomorphies of *Turiasaurus* include the following: prezygapophyseal and postzygapophyseal articular facets on middle dorsal vertebrae strongly convex and concave, respectively; strongly convex subcircular hyposphene on middle dorsal vertebrae; distal caudal vertebrae strongly opisthocoelous; accessory process projecting caudodorsally from the dorsal margin of the shafts of proximal cervical ribs; distal humeral condyles strongly expanded cranially and caudally; radius and ulna distal condyles very compressed mediolaterally; carpal with two subcircular distal processes separated by a depression; cnemial crest of tibia reduced and directed cranially; fibula with roughened oval medial trochanter on middle-distal part; and metatarsal V with strongly expanded distal end.

Locality and horizon. Riodeva (fig. S1), Teruel Province, Aragón, Spain (grid coordinates Universal Transverse Mercator 659049 and 4443553), site RD-10 (known as Barrihonda–El Humero), in the Villar del Arzobispo Formation (Tithonian-Berriasian), conformably overlying the Higueruelas Formation (*7*). In Riodeva, the top of the Higueruelas is dated as early Tithonian based on the occurrence of the foraminiferan *Anchispirocyclina lusitanica* (*10*).

The teeth of *Turiasaurus* (Fig. 2) have heart-shaped spatulate crowns that are arranged in the typical sauropodomorph overlapping imbricate arrangement. The tooth enamel is wrinkled, and crown-to-crown occlusion has produced V-shaped wear facets (*11*, *12*). There are also some isolated and very reduced marginal tooth denticles on the mesial and distal edges of the teeth. The cervical and dorsal vertebral centra are opisthocoelous and possess simple but well-developed pleurocoels. The neural spines appear to have been shallowly divided (bifurcate) on the midline, as in the distal cervicals and proximal dorsals of *Euhelopus* (*13*) and *Mamenchisaurus* (*14*). The dorsal neural spines are broader transversely than craniocaudally, a synapomorphy of Eusauropoda (*11*), and terminate dorsally in laterally directed triangular processes (Fig. 1I). The internal bone structure is solid in the presacral vertebrae and ribs. A potentially diagnostic character, previously observed only in the Late Cretaceous Asian titanosaurs *Opisthocoelicaudia* (*15*) and *Borealosaurus* (*16*), is the presence of strongly opisthocoelous articulations in distal caudal vertebrae (Fig. 1T). Based on our phylogenetic results, this appears to represent a convergence between these taxa and *Turiasaurus*. In contrast to that of *Brachiosaurus*, which has a deltopectoral crest medially projected (*11*), the humerus of *Turiasaurus* has a robust deltopectoral crest oriented cranially, and the proximal third of the bone slants noticeably medially in cranial view (Fig. 1B). The ulna has a triradiate proximal end, and the radius possesses a subrectangular distal condyle, as in other sauropods (*11*). The ratio of the length of the longest metacarpal (Mc II) to that of the radius is 0.369. The manual phalangeal formula is reduced to 2-2-2-2-?, with phalanges that are broader than they are long. The proximal end of the tibia is compressed mediolaterally, representing a primitive state recorded in basal sauropods (*11*, *12*). The astragalus is wedge-shaped in cranial view,

Fig. 2. Teeth of *T. riodevensis* (specimens CPT-1213, CPT-1215, and CPT-1217, from left to right). Lingual [(A), (D), and (G)], distal [(B), (E), and (H)], and labial [(C), (F), and (I)] views are shown.

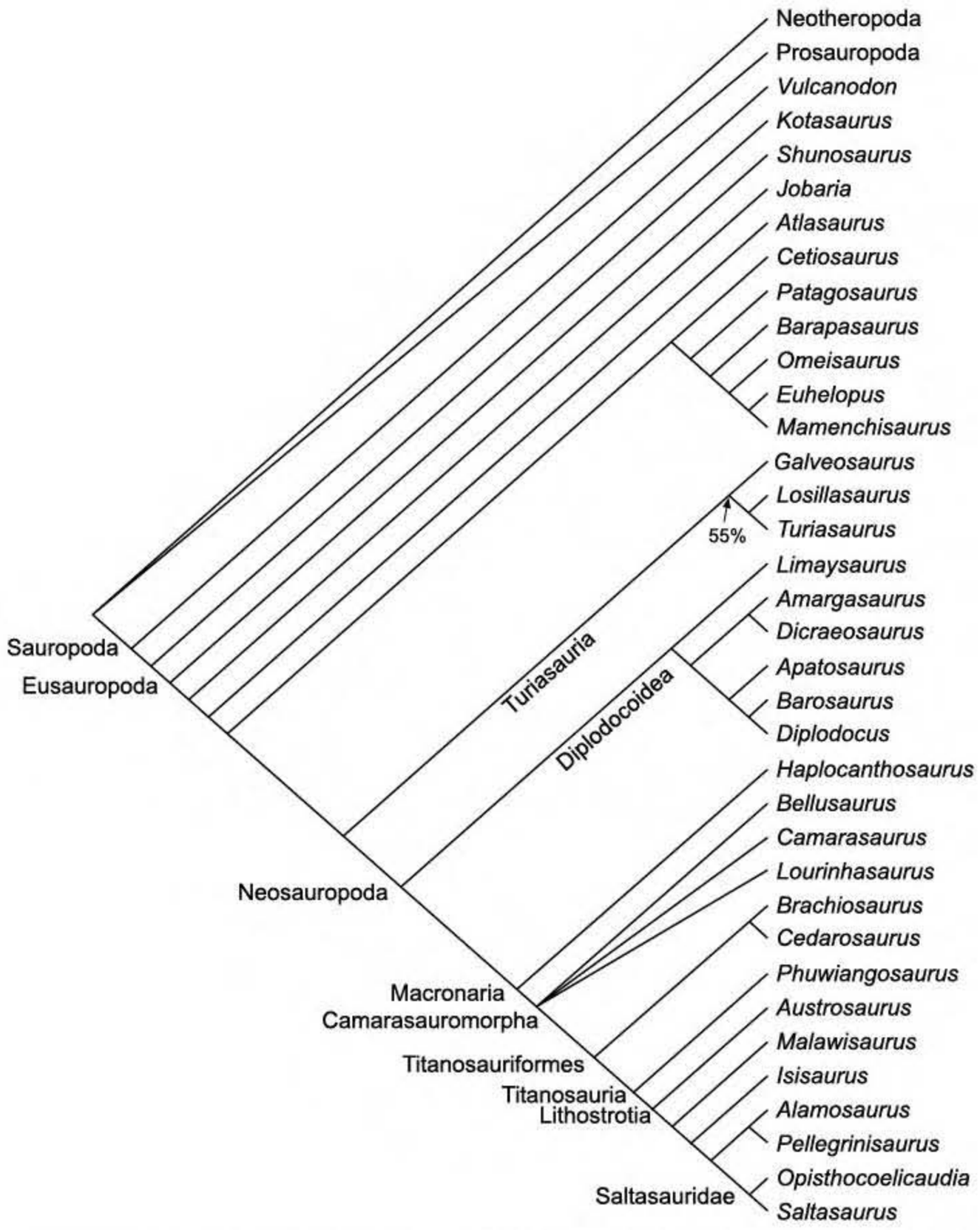

Fig. 3. Phylogenetic relationships of *Turiasaurus* gen. nov. and the newly recognized clade Turiasauria. This analysis also groups European, Asian, and South American Middle-Upper Jurassic Euhelopodidae-related sauropods in a monophyletic clade. The figure represents a 50% majority-rule consensus cladogram based on 11 most parsimonious trees. The data matrix contains 309 characters and 33 taxa (*12*), adding three genera from the Villar del Arzobispo Formation: *Galveosaurus*, *Losillasaurus*, and *Turiasaurus* (table S3). The analysis was done with PAUP* 4.0b 10 (*29*): tree length = 611; consistency index = 0.5205; retention index = 0.7233.

and its distal surface is convex mediolaterally. The ascending process of the astragalus extends over the cranial two-thirds of the proximal surface, unlike the condition in neosauropods where this process reaches the caudal margin (*11*). The metatarsals are robust and display the typical sauropod "spreading" graviportal morphology (*11*). The pedal phalanges are broader than they are long, and the unguals of digits II and III have mediolaterally compressed and dorsoventrally tall proximal ends, as in other sauropods (*11*, *12*).

Turiasaurus differs from other sauropods from the Iberian Range. *Aragosaurus* (*17*) is a taxon distinct from *Turiasaurus*, as demonstrated by differences in both morphology and age. *Losillasaurus* (*18*) and *Galveosaurus* (*19*–*21*), which also come from the Villar del Arzobispo Formation, are also different from the new Riodeva taxon. *Turiasaurus* possesses features that distinguish it from *Losillasaurus*, among them presacral vertebrae with bifurcate neural spines. Moreover, the prezygapophyses of *Turiasaurus* have a rugose ventral process that is better developed toward the proximal than toward the prezygapophyses themselves. A similar character is developed in the postzygapophyses but in a more dorsal position. Also, the dorsal vertebrae of *Turiasaurus* have convex and robust prezygapophyses and a convex hyposphene with a circular contour. Distal caudal vertebrae are opisthocoelous. With respect to the appendicular skeleton, the main differences are in the humeral condyles, which are well marked on the cranial face. Furthermore, in *Turiasaurus*, the radial and ulnar distal ends are strongly compressed mediolaterally, and the carpal has two distal processes. *Turiasaurus* also possesses features that distinguish it from *Galveosaurus*. In *Turiasaurus* the cervical vertebrae have a solid internal bone structure, the dorsal vertebrae are broader transversely, and the cervical and dorsal neural spines are bifid. Pleurocoels in dorsal vertebrae are smaller and shallower. The humeral distal condyles of *Turiasaurus* are more marked cranially. Furthermore, *Turiasaurus* also differs from Portuguese sauropods known from the Oxfordian-Kimmeridgian. The following features distinguish it from *Lourinhasaurus*: absence of a large postspinal lamina on the dorsal vertebrae, a differently shaped humerus with more marked distal condyles, and an elliptical morphology of the proximal end of the tibia (*12*, *22*). *Dinheirosaurus* possesses the following features that are absent in *Turiasaurus*: an elongate pneumatic fossa on the lateral surfaces of the cervical neural spines, robust horizontal lamina linking the hyposphene with the posterior centrodiapophyseal lamina in dorsal vertebrae, and prespinal and postspinal laminae on dorsal vertebrae (*23*).

Phylogenetic analysis (Fig. 3 and table S1) indicates that *Turiasaurus* lies outside of Neosauropoda and belongs to a new clade, named Turiasauria (*24*), together with *Losillasaurus* and *Galveosaurus*. Turiasauria is diagnosed by vertical cervical neural spines, posterior centroparapophyseal laminae on dorsal vertebrae, absence of prespinal and postspinal laminae on dorsal vertebrae, absence of the scapular acromial crest, proximal end of humerus deflected medially (Fig. 1B), prominent humeral deltopectoral crest, and finally by a vertical ridge developed on the caudal side of the distal half of the ulna. The geographic and stratigraphic ranges of this clade are uncertain, but Turiasauria probably represents a sauropod radiation that originated in Europe earlier than the Tithonian. Members of this clade may also have been present in France, Portugal, and England, where teeth similar to those of *Turiasaurus* have been recovered from the Jurassic [such as "*Neosodon*" (*12*, *25*) and *Cardiodon* (*12*)]. All of these teeth share the following characters, and may be referable to Turiasauria: heart-shaped crowns (when unworn), a pointed and asymmetrical crown apex that is strongly compressed labiolingually, and crowns with convex labial surfaces with a bulge that extends from the base toward the apex.

Many of the elements of *Turiasaurus* are comparable in size with those of some of the largest known sauropods (tables S2 and S3). For example, the humerus of the type specimen is 1790 mm long, similar to the value estimated for *Argentinosaurus* (1810 mm) (*5*) and longer than that of *Paralititan* (1690 mm) (*5*). Only the humeri of brachiosaurids, which can exceed 2000 mm in length (*6*, *22*) are longer. However, brachiosaurs, including *Brachiosaurus* itself, have apomorphically elongated forelimbs (*11*), which means that comparisons based solely on humerus length might underestimate the relative body size of a nonbrachiosaurid such as *Turiasaurus*. This explains why hindlimb elements of *Turiasaurus* are actually larger than those of the biggest *Brachiosaurus* specimens (table S3). For example, in *Turiasaurus*, the length of metatarsal II is 295 mm, whereas in *Brachiosaurus* (HMN SII) it is 276 mm (*6*). In *Turiasaurus*, the ungual phalanx on pedal digit I is 300 mm long, and 240 mm long in *Brachiosaurus* (HMN SII) (*6*). The largest sauropod specimens that had been reported from Europe are an isolated brachiosaurid cervical vertebra from the Lower Cretaceous Wessex Formation in southern England (*26*) and an isolated proximal caudal vertebra from another site in Riodeva (*9*). We estimate that *Turiasaurus* body mass was between 40 and 48 metric tons (*27*), weighing more than any other European sauropod. Particularly large sauropod genera, with body lengths exceeding 30 m and estimated masses of 40,000 kg or more, have previously been recognized only within the neosauropod radiations [diplodocoids (*1*) and titanosauriforms (*2*, *3*, *28*)], and it might have been supposed that truly gigantic forms were restricted to Neosauropoda. *Turiasaurus* however, demonstrates that at least one of the more basal (non-neosauropod) lineages achieved gigantic size independently.

References and Notes

1. D. D. Gillete, *J. Vertebr. Paleontol.* **11**, 417 (1991).
2. M. J. Wedel, R. L. Cifelli, R. K. Sanders, *J. Vertebr. Paleontol.* **20**, 109 (2000).
3. J. F. Bonaparte, R. A. Coria, *Ameghiniana* **30**, 271 (1993).
4. F. E. Novas, L. Salgado, J. Calvo, F. Agnolin, *Rev. Mus. Argent. Cienc. Nat. Bernardino Rivadavia* **7**, 37 (2005).
5. J. B. Smith *et al.*, *Science* **292**, 1704 (2001).
6. G. S. Paul, *Hunteria* **2**, 1 (1988).
7. L. Luque, A. Cobos, R. Royo-Torres, E. Espílez, L. Alcalá, *Geogaceta* **38**, 27 (2005).
8. R. Royo-Torres, A. Cobos, *Geo-Temas* **6**, 59 (2004).
9. R. Royo-Torres, A. Cobos, *Geogaceta* **38**, 23 (2005).
10. R. Fezer, *Arb Inst. Geol. Paläont. Univ. Stuttgart* **84**, 1 (1988).
11. J. A. Wilson, *Zool. J. Linn. Soc.* **136**, 215 (2002).
12. P. Upchurch, P. M. Barrett, P. Dodson, in *The Dinosauria*, D. B. Weishampel, P. Dodson, H. Osmólska, Eds. (Univ. of California Press, Berkeley, CA, 2004), pp. 259–322.
13. C. Wiman, *Palaeontol. Sinica* **6**, 1 (1929).
14. C. C. Young, H. C. Chao, *Vert. Paleontol. Paleoanthropol. Monogr.* **8**, 1 (1972).
15. M. Borsuk-Bialynicka, *Palaeontol. Polonica* **37**, 5 (1977).
16. H. You, Q. Ji, M. C. Lamanna, J. Li, Y. Li, *Acta Geol. Sin.* **78**, 907 (2004).
17. J. L. Sanz, A. D. Buscalioni, M. L. Casanovas, J. V. Santafé, *Estud. Geol.* **Galve-Tremp**, 45 (1987).
18. M. L. Casanovas, J. V. Santafé, J. L. Sanz, *Paleontol. Evolució* **32**, 99 (2001).
19. J. L. Barco, J. I. Canudo, G. Cuenca-Bescós , J. I. Ruiz-Omeñaca, *Nat. Aragonesa* **15**, 4 (2005).
20. B. Sánchez-Hernández, *Zootaxa* **1034**, 1 (2005).
21. B. Sánchez-Hernández, *Zootaxa* **1201**, 63 (2006).
22. A. F. Lapparent, G. Zbyszewski, *Mem. Serv. Géol. Portugal* **2**, 1 (1957).
23. J. F. Bonaparte, O. Mateus, *Rev. Mus. Argent. Cienc. Nat. Bernardino Rivadavia* **5**, 13 (1999).
24. Turiasauria is defined here as a stem-based taxon including all eusauropods more closely related to *T. riodevensis* than to *Saltasaurus loricatus*.
25. E. Buffetaut, M. Martin, *Rev. Paléobiol.* **7**, 17 (1993).
26. D. Naish, D. M. Martill, D. Cooper, K. A. Stevens, *Cretaceous Res.* **25**, 787 (2004).
27. See supporting material on *Science* Online.
28. G. V. Mazzetta, P. Chistiansen, R. A. Fariña, *Hist. Biol.* **16**, 71 (2004).
29. D. L. Swofford, *PAUP*. Phylogenetic Analysis Using Parsimony (*and Other Methods)*, version 4.0b 10 (Sinauer, Sunderland, MA, 2002).

30. We thank our colleagues at the Foundation; P. Upchurch; Gobierno de Aragón (Departamentos Educación, Presidencia, Industria, Economía, Ciencia); Projects FOCONTUR and 252/2002, 142/2003, 142/02/2004, and 197/2005 (Dirección General Patrimonio Cultural); Dinópolis; Diputación Provincial Teruel and Gabinete Geológico; Ayuntamiento Riodeva; the Spanish Army; and the Ministerio Educación (492839C1 and CGL2006-13903). V. Fonte and M. Prendergast helped in editing text. We thank two anonymous reviewers for their comments. We dedicate this work to the memory of J. Roig.

Supporting Online Material

www.sciencemag.org/cgi/content/full/314/5807/1925/DC1
SOM Text
Figs. S1 to S4
Tables S1 to S5
References

21 July 2006; accepted 25 October 2006
10.1126/science.1132885

Anticipatory Reproduction and Population Growth in Seed Predators

Stan Boutin,[1]* Lucas A. Wauters,[2] Andrew G. McAdam,[3] Murray M. Humphries,[4] Guido Tosi,[2] André A. Dhondt[5,6]

Mast seeding, the intermittent, synchronous production of large seed crops by a population of plants, is a well-known example of resource pulses that create lagged responses in successive trophic levels of ecological communities. These lags arise because seed predators are thought capable of increasing reproduction and population size only after the resource pulse is available for consumption. The resulting satiation of predators is a widely cited explanation for the evolution of masting. Our study shows that both American and Eurasian tree squirrels anticipate resource pulses and increase reproductive output before a masting event, thereby increasing population size in synchrony with the resource pulse and eliminating the population lag thought to be universal in resource pulse systems.

The reproductive output of any species is constrained by the availability of resources required for offspring production. As a consequence, reproductive rates are often correlated with resources available before and during parental care (*1*–*3*). All basic consumer-resource population models portray consumer rates of increase as a function of current or past rather than future resource availabilities (*4*, *5*). This has important ecological implications, including boom and bust consumer dynamics in systems characterized by intermittent resource pulses (*6*, *7*).

Seed masting, the intermittent production of large seed crops by a population of plants, is a well-known example of a resource pulse (*7*–*9*). There is growing evidence that the increased reproductive investment necessary for masting is an adaptive response by the plant rather than a simple resource-tracking strategy (*8*, *10*). A widely cited evolutionary explanation for this phenomenon is predator satiation (*8*, *11*). Seed consumers are forced into a starvation-saturation cycle whereby low resources before the masting event prevent the seed predator from increasing reproductive investment until after the resources have come and gone, creating a lagged population response. Although it would appear advantageous for seed predators to anticipate mast years by increasing reproduction and population growth before masting, doing so would require both a reliable cue signaling the upcoming mast event and the capacity to increase reproductive investment before the abundant food supply becomes available. Some insects use environmental cues to emerge in synchrony with seed masts (*12*, *13*), and there are rare examples of vertebrate species using unknown cues to trigger onset of reproduction in mast years only (*14*, *15*). Although many organisms initiate reproduction before regular seasonal resource peaks (*16*), irregular resource pulses represent a unique challenge to consumers, because they occur infrequently relative to the generation time of consumers and future resource availability is often not correlated with current or past availability.

Here, we provide evidence that two species of seed predators do not follow a resource-tracking strategy but instead adjust reproductive investment according to future rather than past seed crops. We studied red squirrels (*Tamiasciurus hudsonicus*, hereafter American reds) in Yukon Canada and Eurasian red squirrels (*Sciurus vulgaris*, Eurasian reds) in Belgium and Italy (*17*). For American reds, we used complete enumeration to track population size, survival, and reproductive output of individual females in two control populations from 1989 to 2004 (*17*). For Eurasian reds, we used capture-recapture techniques to collect similar data for two populations in northern Belgium and for a single population in northern Italy over a 3- to 9-year period (*17*).

The natural history of American and Eurasian red squirrels suggests that they are part of a classic consumer-resource pulse system, the key elements being that the resource pulse (seed mast) is highly variable (fig. S1) and is not mature and consumed until autumn, well after the consumer has committed to reproductive investment for that year (*17*). As a consequence, increased reproductive investment and population growth would not be expected to occur until the following spring, when females enter the breeding season in good condition after having fed on abundant seeds all winter (*18*). Thus, if red squirrels respond in the manner typical of consumer-resource pulse systems, we would expect reproduction to be constrained by seasonal resource limitation before a masting event but enhanced in the year after the masting event. We found limited evidence for this. For American reds in years after high seed production, females responded by breeding earlier and raising faster-growing offspring than in years after low seed production (Fig. 1, A and B), but the proportion of yearling females breeding and the litter size were not correlated with the previous year's seed crop (table S1). In Eurasian reds, only the proportion of females producing spring litters (Fig. 1C) was positively correlated with food abundance in the previous year, whereas litter

[1]Department of Biological Sciences, University of Alberta, Edmonton, Alberta T6G 2E9, Canada. [2]Department of Environment, Health, and Safety, University of Insubria, Varese, Via J. H. Dunant 3, I-21100 Varese, Italy. [3]Ecology, Evolutionary Biology, and Behavior Program, Department of Fisheries and Wildlife, Department of Zoology, 13 Natural Resources Building, Michigan State University, East Lansing, MI 48824, USA. [4]Natural Resource Sciences, Macdonald Campus, McGill University, Ste-Anne-de-Bellevue, Québec H9X 3V9, Canada. [5]Laboratory of Ornithology, Cornell University, 159 Sapsucker Woods Road, Ithaca, NY 14850–1999, USA. [6]Department of Biology, University of Antwerp, B-2610 Wilrijk, Belgium.

*To whom correspondence should be addressed. E-mail: stan.boutin@ualberta.ca

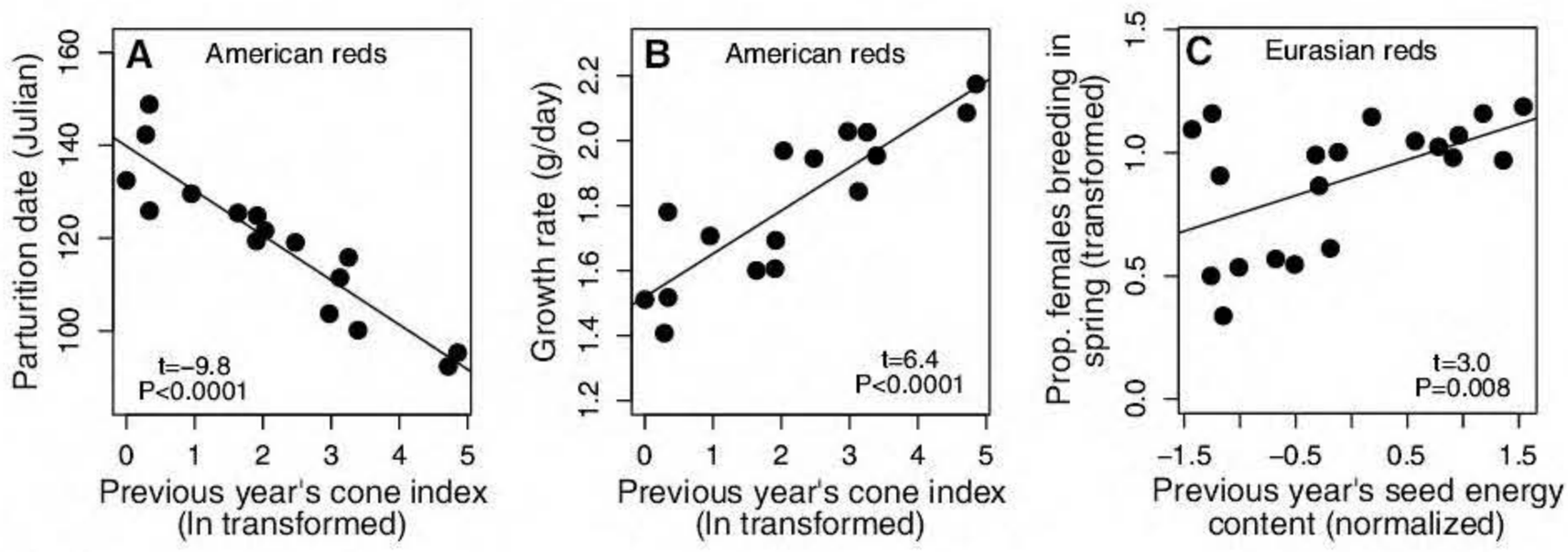

Fig. 1. Red squirrel life history characteristics that responded to the previous year's food abundance [indexed by cones or seed energy content (*17*)]. In American reds, parturition date (**A**) was advanced and juvenile growth rates (**B**) were higher after years of high cone production. In Eurasian reds, the proportion of females producing spring litters (**C**) was higher after years of high food abundance. Values shown are yearly averages, and proportions are arcsine square root transformed. See table S1 for statistical results.

size and the proportion of females producing a summer litter were not (table S1).

Reproductive investment was, however, correlated with future seed production (seed production in the current year but not available for consumption until after females have completed the bulk of their reproductive investment). American reds gave birth to larger litters in advance of high food production (Fig. 2A) and were more likely to breed as yearlings (Fig. 2B). The most striking effect was that females produced a second litter after a successful first litter (the equivalent of summer litters in Eurasian reds) in advance of high food production (Fig. 2C). In most cases, females were still lactating with the first litter when they conceived the second (litter one young were 35 to 87 days old, and weaning occurs at 70 days of age), suggesting that the normal physiological inhibition of ovulation by lactation characteristic of mammals (*19*) had been circumvented. These increases in reproductive effort when taken together resulted in a higher average number of offspring produced per female in advance of high food production (Fig. 2D). In Eurasian reds, summer litters were produced in all years, but the proportion of females doing so was positively correlated with future food abundance (Fig. 2E), as was summer litter size (Fig. 2F). In both species, none of these breeding parameters were correlated with the previous year's food abundance (table S1).

The ability to adjust reproductive output to match future food resources has the potential to alter typical lagged responses between the availability of food resources and the growth of consumer populations. In contrast to assumptions of resource-consumer population models, the summer population growth rates of both American and Eurasian reds were not correlated with the abundances of food produced the previous autumn (table S1). Instead, summer population growth rates were correlated with future food production (Fig. 3). This increased population growth before the maturation of the seed crop means that population size reached a maximum when the seed crop reached maturity in autumn. These results show that the temporal lag in population growth rate, common to consumer-resource pulse systems, can be circumvented through anticipatory reproductive investment.

The collective anticipatory reproductive responses observed in both systems represent a departure from the simple resource-tracking strategy characteristic of consumers in resource pulse systems. This raises two important questions. First, what cues do American and Eurasian red squirrels use to predict upcoming resources? We can rule out previous food abundance, because seed crop in the previous year was not correlated with seed crop in the current year (for American reds, the relevant statistics are $r = -0.07$, $t_{14} = -0.28$, and $P = 0.78$; for Eurasian reds, they are $r = -0.24$, $t_{18} = -1.0$, and $P = 0.32$). Other studies have suggested that visual (*20*) or chemical (*21*) stimuli, possibly linked to reproductive structures [buds, flowers, pollen cones (*15*)], can trigger onset of reproduction. These structures are also good cue candidates for American and Eurasian reds, because they are consumed by squirrels (*17*) and are present in advance of and may be correlated with the size of the forthcoming seed crop (*22*).

The second question is how American and Eurasian reds increase reproductive investment during what has been considered a seasonal resource bottleneck in other consumer-resource pulse systems. One possibility is that the squirrels are in fact following a resource-tracking strategy but that the resource being tracked is an alternative energy source whose abundance is correlated to the upcoming seed crop (*23*). Immature reproductive structures of trees are unlikely candidates, because they are only consumed in quantity when seed is not available and do not differ in energetic value from vegetative buds, which are always superabundant (*24*, *25*). American reds given buds in feeding trials lost weight (*24*); in the case of Eurasian reds, daily energy intake was low, time spent active in-

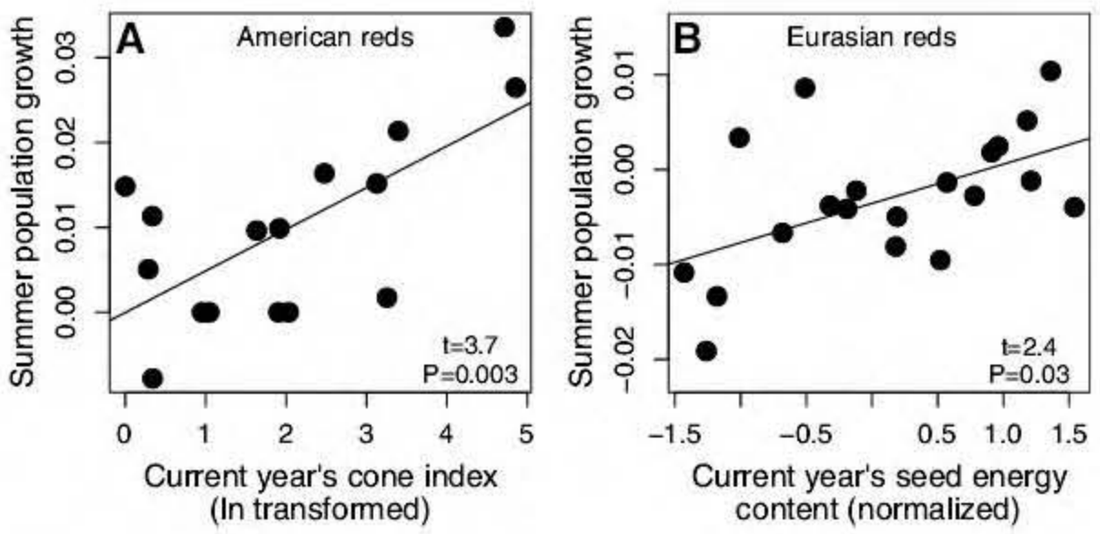

Fig. 3. Summer population growth rates of American (**A**) and Eurasian (**B**) reds were positively correlated to future food supply. Values are weekly rates measured between spring and autumn censuses (*17*).

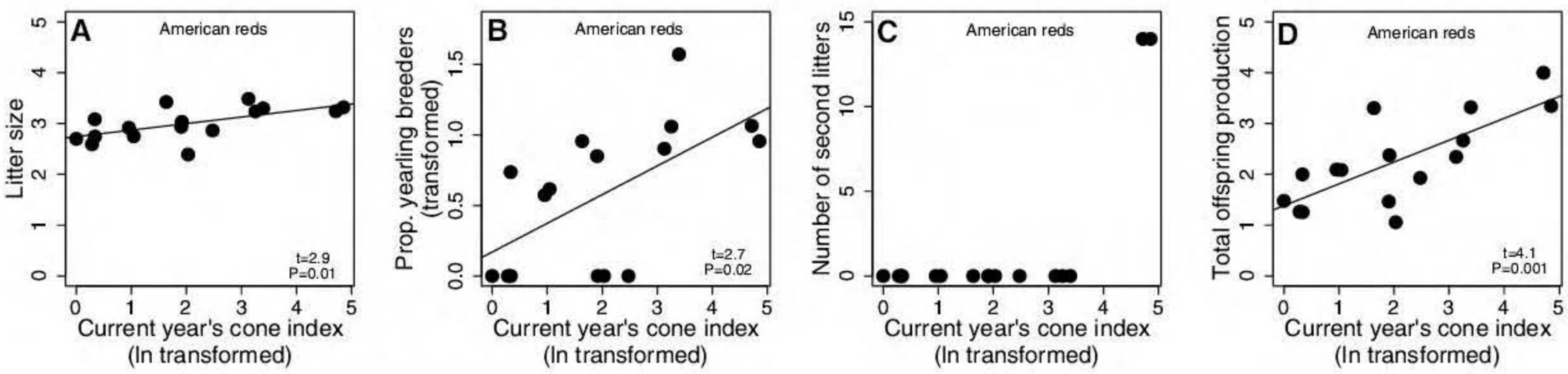

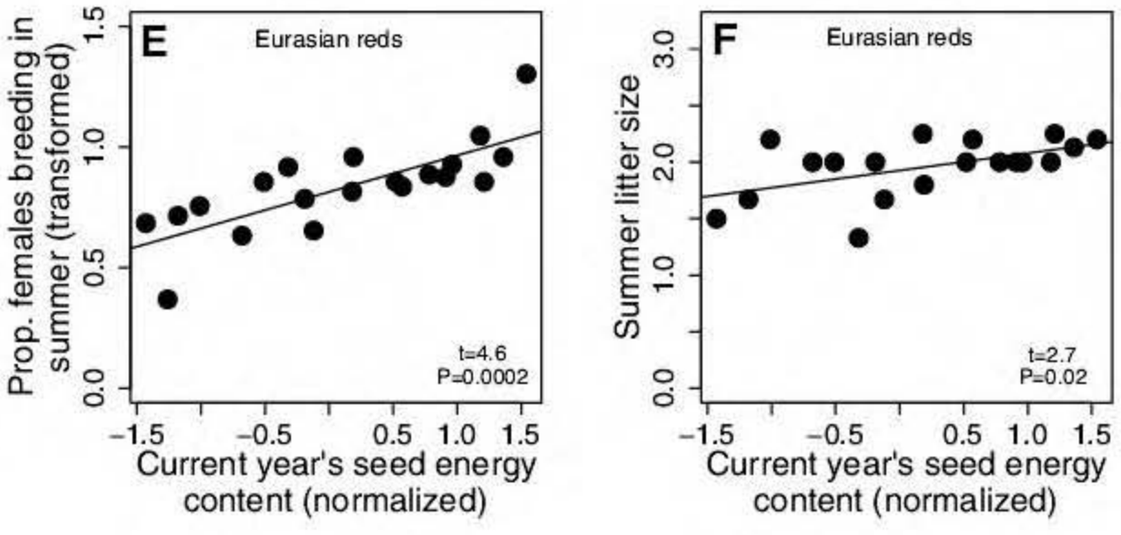

Fig. 2. Red squirrel life history characteristics that anticipated future food abundance. In American reds, litter size (**A**) and the proportion of yearlings breeding (**B**) increased when future food supply (as in Fig. 1 but measured in autumn of the current year) was high. This, combined with production of a second litter (those produced after successfully weaning a first litter) in mast years only (**C**), led to higher numbers of offspring being produced per female (**D**) when future food supply was high. In Eurasian reds, the proportion of females producing a summer litter (**E**) and the summer litter size (**F**) were higher when future food supply (as in Fig. 1 but measured in autumn of the current year) was high. Values shown are yearly averages, and proportions are arcsine square root transformed. See table S1 for statistical results.

creased, and body mass was lower when squirrels were feeding on these items as compared with feeding on seed (*26*, *27*). Lastly, food supplementation experiments of American reds have failed to produce increases in litter size or a second litter, providing strong evidence that the increased reproductive investment observed in our study cannot be triggered by increased energy availability alone (*17*, *28*, *29*). We hypothesize that, rather than following a resource-tracking strategy where reproductive investment is determined by current resource amounts, reproductive rates are driven by future fitness payoffs. During years of low seed production, competition among juveniles for available resources is intense, and, although litter augmentation experiments in American reds show that females are capable of supporting larger litters (*30*), they refrain from doing so because offspring recruitment is low (*30*). However, when mast years occur, competition among juveniles is reduced, and females produce more offspring, which successfully recruit into the population (*31*, *32*). Further, the increased production of young by females in mast years does not come with any obvious cost to the female, because overwinter survival is not reduced after years of increased reproductive investment (for American reds, offspring production in the previous year versus proportion of adult females surviving to spring has slope = -0.023 ± 0.034, $t_{15} = -0.7$, and $P = 0.51$; for Eurasian reds, proportion of estrous females in the previous year versus adult female survival to spring has slope = 0.37 ± 0.27, $t_{15} = 1.4$, and $P = 0.19$).

If masting has evolved as a swamp-and-starve adaptation against seed predation, then anticipatory reproduction and population growth represent a potent counteradaptation by the predators. Given that increased reproductive output in these systems coincides with low current but high future resources, our results suggest that reproductive investment in these systems is more responsive to future fitness prospects than present energetic constraints. The evolution of seed masting in trees is also driven by the survival prospects for progeny rather than simple resource tracking, suggesting an intriguing parallel in reproductive strategies of trees and the predators that consume their seed.

References and Notes

1. J. L. Gittleman, S. D. Thompson, *Am. Zool.* **28**, 863 (1988).
2. T. H. Clutton-Brock, *Reproductive Success* (Univ. of Chicago Press, Chicago, 1988).
3. T. H. Clutton-Brock, *The Evolution of Parental Care* (Princeton Univ. Press, Princeton, NJ, 1999).
4. G. Caughley, in *Theoretical Ecology*, R. M. May, Ed. (Blackwell, Oxford, 1981), ch. 6.
5. P. Bayliss, D. Choquenot, *Proc. R. Soc. London Ser. B* **357**, 1233 (2002).
6. C. G. Jones, R. S. Ostfeld, M. P. Richard, E. M. Schauber, J. O. Wolff, *Science* **279**, 1023 (1998).
7. R. S. Ostfeld, F. Keesing, *Trends Ecol. Evol.* **15**, 232 (2000).
8. D. Kelly, V. L. Sork, *Annu. Rev. Ecol. Syst.* **33**, 427 (2002).
9. L. M. Curran, M. Leighton, *Ecol. Monogr.* **70**, 101 (2000).
10. W. D. Koenig, J. M. H. Knops, *Am. Sci.* **93**, 340 (2005).
11. D. H. Janzen, *Annu. Rev. Ecol. Syst.* **2**, 465 (1971).
12. A. F. Hedlin, *For. Sci.* **10**, 124 (1964).
13. M. J. McKone, D. Kelly, A. L. Harrison, J. J. Sullivan, A. J. Cone, *N.Z. J. Zool.* **28**, 89 (2001).
14. P. R. Wilson, B. J. Karl, R. J. Toft, J. R. Beggs, *Biol. Conserv.* **83**, 175 (1998).
15. T. Ruf, J. Fietz, W. Schlund, C. Bieber, *Ecology* **87**, 372 (2006).
16. F. H. Bronson, *Reproductive Biology* (Univ. of Chicago Press, Chicago, 1989).
17. Materials and methods are available on *Science* Online.
18. J. O. Wolff, *J. Mammal.* **77**, 850 (1996).
19. A. S. McNeilly, *Reprod. Fertil. Dev.* **13**, 583 (2001).
20. J. D. Ligon, *Nature* **250**, 80 (1974).
21. P. J. Berger, N. C. Negus, E. H. Sanders, P. D. Gardner, *Science* **214**, 69 (1981).
22. S. Eis, J. Inkster, *Can. J. For. Res.* **2**, 460 (1972).
23. B. M. Fitzgerald, M. J. Efford, B. J. Karl, *N.Z. J. Zool.* **31**, 167 (2004).
24. M. C. Smith, *J. Wildl. Manag.* **32**, 305 (1968).
25. D. A. Rusch, W. G. Reeder, *Ecology* **59**, 400 (1978).
26. L. A. Wauters, C. Swinnen, A. A. Dhondt, *J. Zool.* **227**, 71 (1992).
27. L. A. Wauters, A. A. Dhondt, *J. Zool.* **217**, 93 (1989).
28. C. D. Becker, *Can. J. Zool.* **71**, 1326 (1993).
29. K. W. Larsen, C. D. Becker, S. Boutin, M. Blower, *J. Mammal.* **78**, 192 (1997).
30. M. M. Humphries, S. Boutin, *Ecology* **81**, 2867 (2000).
31. A. G. McAdam, S. Boutin, *Evolution* **57**, 1689 (2003).
32. L. A. Wauters, E. Matthysen, F. Adriaensen, G. Tosi, *J. Anim. Ecol.* **73**, 11 (2004).

33. We thank J. Herbers, C. Aumann, J. LaMontagne, M. Andruskiw, J. Lane, R. Boonstra, K. McCann, B. Thomas, Kluane Red Squirrel Project 2005 annual meeting participants, and three anonymous reviewers for very useful comments. We are indebted to the many field workers who helped collect the data and to A. Sykes and E. Anderson for management of the long-term data. Financed by Natural Sciences and Engineering Research Council of Canada, NSF (American reds), a Concerted Action of the Belgian Ministry of Education, and a Training and Mobility of Researchers grant from the Commission of the European Union (Eurasian reds). This is publication 30 of the Kluane Red Squirrel Project.

Supporting Online Material

www.sciencemag.org/cgi/content/full/314/5807/1928/DC1
Materials and Methods
SOM Text
Fig. S1
Table S1
References

25 September 2006; accepted 15 November 2006
10.1126/science.1135520

Human Catechol-*O*-Methyltransferase Haplotypes Modulate Protein Expression by Altering mRNA Secondary Structure

A. G. Nackley,[1] S. A. Shabalina,[2] I. E. Tchivileva,[1] K. Satterfield,[1] O. Korchynskyi,[3] S. S. Makarov,[4] W. Maixner,[1] L. Diatchenko[1]*

Catechol-*O*-methyltransferase (COMT) is a key regulator of pain perception, cognitive function, and affective mood. Three common haplotypes of the human *COMT* gene, divergent in two synonymous and one nonsynonymous position, code for differences in COMT enzymatic activity and are associated with pain sensitivity. Haplotypes divergent in synonymous changes exhibited the largest difference in COMT enzymatic activity, due to a reduced amount of translated protein. The major *COMT* haplotypes varied with respect to messenger RNA local stem-loop structures, such that the most stable structure was associated with the lowest protein levels and enzymatic activity. Site-directed mutagenesis that eliminated the stable structure restored the amount of translated protein. These data highlight the functional significance of synonymous variations and suggest the importance of haplotypes over single-nucleotide polymorphisms for analysis of genetic variations.

The ability to predict the downstream effects of genetic variation is critically important for understanding both the evolution of the genome and the molecular basis of human disease. The effects of nonsynonymous polymorphisms have been widely characterized; because these variations directly influence protein function, they are relatively easy to study statistically and experimentally (*1*). However, characterizing polymorphisms located in regulatory regions, which are much more common, has proved to be problematic (*2*). Here, we focus on the mechanism whereby polymorphisms of the cathechol-*O*-methyltransferase (*COMT*) gene regulate gene expression.

COMT is an enzyme responsible for degrading catecholamines and thus represents a critical component of homeostasis maintenance (*3*). The human *COMT* gene encodes two distinct proteins: soluble COMT (S-COMT) and membrane-bound COMT (MB-COMT) through the use of alternative translation initia-

[1]Center for Neurosensory Disorders, University of North Carolina, Chapel Hill, NC 27599, USA. [2]National Center for Biotechnology Information, National Institutes of Health, Bethesda, MD 20894, USA. [3]Thurston Arthritis Center, University of North Carolina, Chapel Hill, NC 27599, USA. [4]Attagene, Inc., 7030 Kit Creek Road, Research Triangle Park, NC 27560, USA.

*To whom correspondence should be addressed. E-mail: lbdiatch@email.unc.edu

tion sites and promoters (*3*). Recently, COMT has been implicated in the modulation of persistent pain (*4*–*7*). Our group demonstrated that three common haplotypes of the human *COMT* gene are associated with pain sensitivity and the likelihood of developing temporomandibular joint disorder (TMJD), a common chronic musculoskeletal pain condition (*4*). Three major haplotypes are formed by four single-nucleotide polymorphisms (SNPs): one located in the *S-COMT* promoter region (A/G; rs6269) and three in the *S-* and *MB-COMT* coding region at codons $his^{62}his$ (C/T; rs4633), $leu^{136}leu$ (C/G; rs4818), and $val^{158}met$ (A/G; rs4680) (Fig. 1A). On the basis of subjects' pain responsiveness, haplotypes were designated as low (LPS; GCGG), average (APS; ATCA), or high (HPS; ACCG) pain sensitive. Individuals carrying HPS/APS or APS/APS diplotypes were nearly 2.5 times as likely to develop TMJD. Previous data further suggest that *COMT* haplotypes code for differences in COMT enzymatic activity (*4*); however, the molecular mechanisms involved have remained unknown.

A common SNP in codon 158 ($val^{158}met$) has been associated with pain ratings and μ-opioid system responses (*7*) as well as addiction, cognition, and common affective disorders (*3*, *8*–*10*). The substitution of valine (Val) by methionine (Met) results in reduced thermostability and activity of the enzyme (*3*). It is generally accepted that $val^{158}met$ is the main source of individual variation in human COMT activity; numerous studies have identified associations between the low-activity *met* allele and several complex phenotypes (*3*, *8*, *10*). However, observed associations between these conditions and the *met* allele are often modest and occasionally inconsistent (*3*). This suggests that additional SNPs in the *COMT* gene modulate COMT activity. Indeed, we found that haplotype rather than an individual SNP better accounts for variability in pain sensitivity (*4*). The HPS and LPS haplotypes that both code for the stable val^{158} variant were associated with the two extreme-pain phenotypes; thus, the effect of haplotype on pain sensitivity in our study cannot be explained by the sum of the effects of functional SNPs. Instead, the $val^{158}met$ SNP interacts with other SNPs to determine phenotype. Because variation in the S-COMT promoter region does not contribute to pain phenotype (Fig. 1A), we suggest that the rate of mRNA degradation or protein synthesis is affected by the structural properties of the haplotypes, such as haplotype-specific mRNA secondary structure.

Previous reports have shown that polymorphic alleles can markedly affect mRNA secondary structure (*11*, *12*), which can then have functional consequences on the rate of mRNA degradation (*11*, *13*). It is also plausible that polymorphic alleles directly modulate protein translation through alterations in mRNA secondary structure, because protein translation efficiency is affected by mRNA secondary structure (*14*–*16*). To test these possibilities, we evaluated the affect of LPS, APS, and HPS haplotypes on the stability of the corresponding mRNA secondary structures (*17*).

Secondary structures of the full-length LPS, APS, and HPS mRNA transcripts were predicted by means of the RNA Mfold (*18*, *19*) and Afold (*20*) programs. The mRNA folding analyses demonstrated that the major *COMT* haplotypes differ with respect to mRNA secondary structure. The LPS haplotype codes for the shortest, least stable local stem-loop structure, and the HPS haplotype codes for the longest, most stable local stem-loop structure in the val^{158} region for both *S-COMT* and *MB-COMT*. Gibbs free energy (ΔG) for the stem-loop structure associated with the HPS haplotype is ~17 kcal/mol less than that associated with the LPS haplotype for both *S-COMT* and *MB-COMT* (Fig. 1B and fig. S1A). Additional evidence supporting predicted RNA folding structures was obtained by generating consensus RNA secondary structures based on comparative analysis of *COMT* sequences from eight mammalian species (fig. S2). The consensus RNA folding structures were LPS-like and did not contain highly stable local stem-loop structures analogous to the human HPS-like form. Thus, substantial deviation from consensus structure, as observed for the HPS haplotype, should have notable functional consequences. Additional studies were conducted to test this molecular modeling.

We constructed full-length S- and MB-COMT cDNA clones in mammalian expression vectors that differed only in three nucleotides corresponding to the LPS, APS, and HPS haplotypes (*17*, *21*). Rat adrenal (PC-12) cells were transiently transfected with each of these six constructs. COMT enzymatic activity, protein expression, and mRNA abundance were measured. Relative to the LPS haplotype, the HPS haplotype showed a 25- and 18-fold reduction in enzymatic activity for S- and MB-COMT constructs, respectively (Fig. 1C and fig. S1B). The HPS haplotype also exhibited marked reductions in S- and MB-COMT protein expression (Fig. 1D and fig. S1C). The APS haplotype displayed a moderate 2.5- and 3-fold reduction in enzymatic activity for S- and MB-COMT constructs, respectively, while pro-

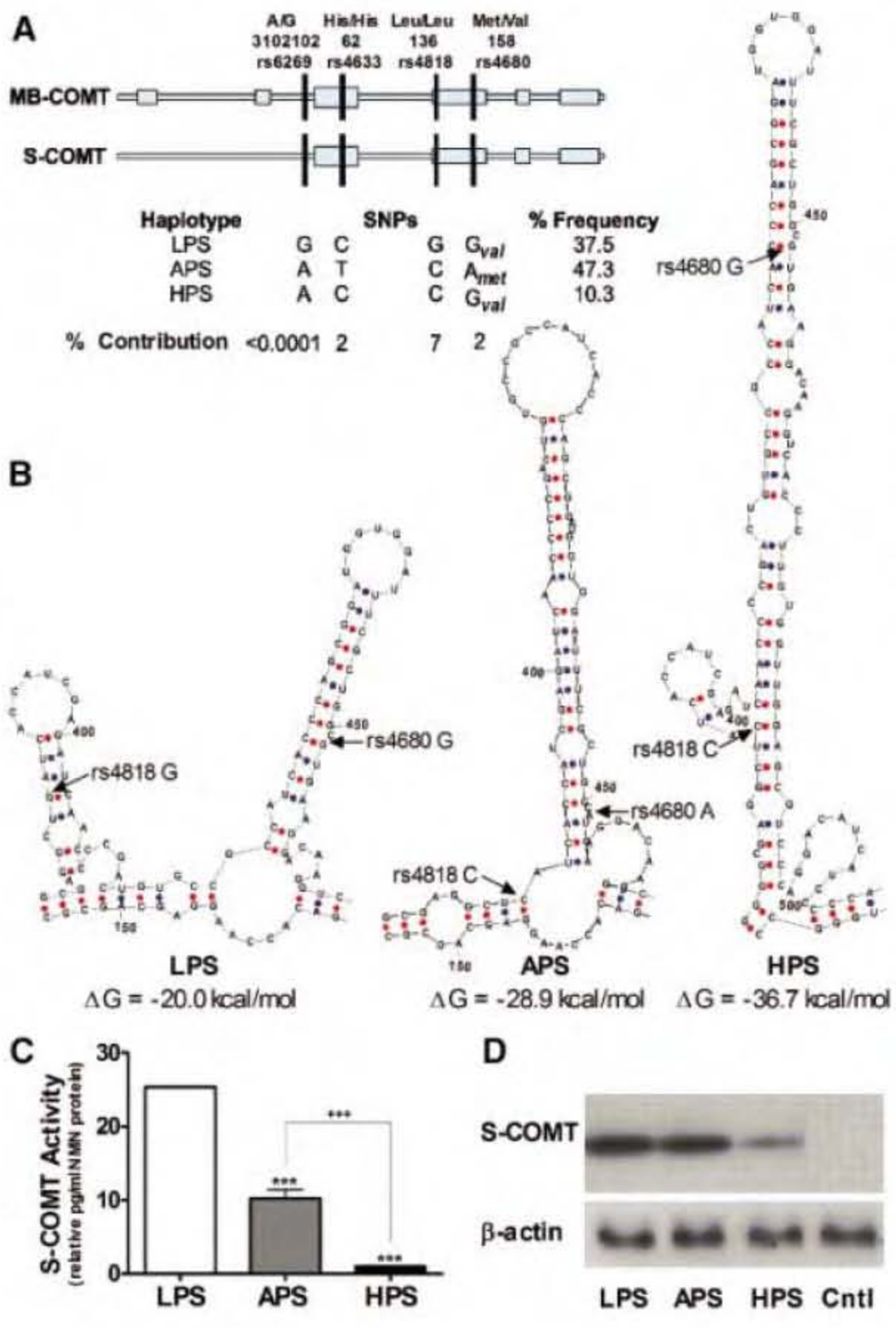

Fig. 1. Common haplotypes of the human *COMT* gene differ with respect to mRNA secondary structure and enzymatic activity. (**A**) A schematic diagram illustrates *COMT* genomic organization and SNP composition for the three haplotypes. Percent frequency of each haplotype in a cohort of healthy Caucasian females, and percent independent SNP contribution to pain sensitivity, are indicated. (**B**) The local stem-loop structures associated with each of the three haplotypes are shown. Relative to the LPS and APS haplotypes, the HPS local stem-loop structure had a higher folding potential. (**C** and **D**) The LPS haplotype exhibited the highest, while the HPS haplotype exhibited the lowest enzymatic activity and protein levels in cells expressing COMT. $^{***}P < 0.001$, ≠ LPS. $^{+++}P < 0.001$, ≠ APS.

tein expression levels did not differ. The moderate reduction in enzymatic activity produced by the APS haplotype is most likely due to the previously reported decrease in protein thermostability coded by the *met*^{158} allele (*3*). These data illustrate that the reduced enzymatic activity corresponding to the HPS haplotype is paralleled by reduced protein levels, an effect that could be mediated by local mRNA secondary structure at the level of protein synthesis and/or mRNA degradation. Because total RNA abundance and RNA degradation rates did not parallel COMT protein levels (fig. S2), differences in protein translation efficiency likely results from differences in the local secondary structure of corresponding mRNAs.

To directly assess this hypothesis, we performed site-directed mutagenesis (*17*). The stable stem-loop structure of *S-* and *MB-COMT* mRNA corresponding to the HPS haplotype is supported by base pairs between several critical nucleotides, including 403C and 479G in *S-COMT* and 625C and 701G in *MB-COMT* (Fig. 2A and fig. S3A). Mutation of 403C to G in *S-COMT* or 625C to G in *MB-COMT* destroys the stable stem-loop structure and converts it into a LPS haplotype–like structure (HPS Lsm). Double mutation of mRNA in position 403C to G and 479G to C in *S-COMT* or 625C to G and 701G to C in *MB-COMT* reconstructs the original long stem-loop structure (HPS dm). The single- and double-nucleotide HPS mutants (HPS Lsm and HPS dm, respectively) were transiently transfected to PC-12 cells. As predicted by the mRNA secondary-structure folding analyses, the HPS Lsm exhibited increased COMT enzymatic activity and protein levels equivalent to those of the LPS haplotype, whereas the HPS dm exhibited reduced enzymatic activity and protein levels equivalent to those of the original HPS haplotype (Fig. 2, B and C; fig. S3, B and C). These data rule out the involvement of RNA sequence recognition motifs or codon usage in the regulation of translation. In contrast to the HPS haplotype, protein levels did not parallel COMT enzymatic activity for the APS haplotype and site-directed mutagenesis confirmed that the *met*^{158} allele, not a more stable mRNA secondary structure, drives the reduced enzymatic activity observed for the APS haplotype (fig. S4). This difference is moderate relative to the mRNA structure–dependent difference coded by LPS and HPS haplotypes. These results were verified by an alternate approach of modifying mRNA secondary structure (fig. S5).

Our data have very broad evolutionary and medical implications for the analysis of variants common in the human population. The fact that alterations in mRNA secondary structure resulting from synonymous changes have such a pronounced effect on the level of protein expression emphasizes the critical role of synonymous nucleotide positions in maintaining mRNA secondary structure and suggests that the mRNA secondary structure, rather than independent nucleotides in the synonymous positions, should undergo substantial selective pressure (*22*). Furthermore, our data stress the importance of synonymous SNPs as potential functional variants in the area of human medical genetics. Although nonsynonymous SNPs are believed to have the strongest impact on variation in gene function, our data clearly demonstrate that haplotypic variants of common synonymous SNPs can have stronger effects on gene function than nonsynonymous variations and play an important role in disease onset and progression.

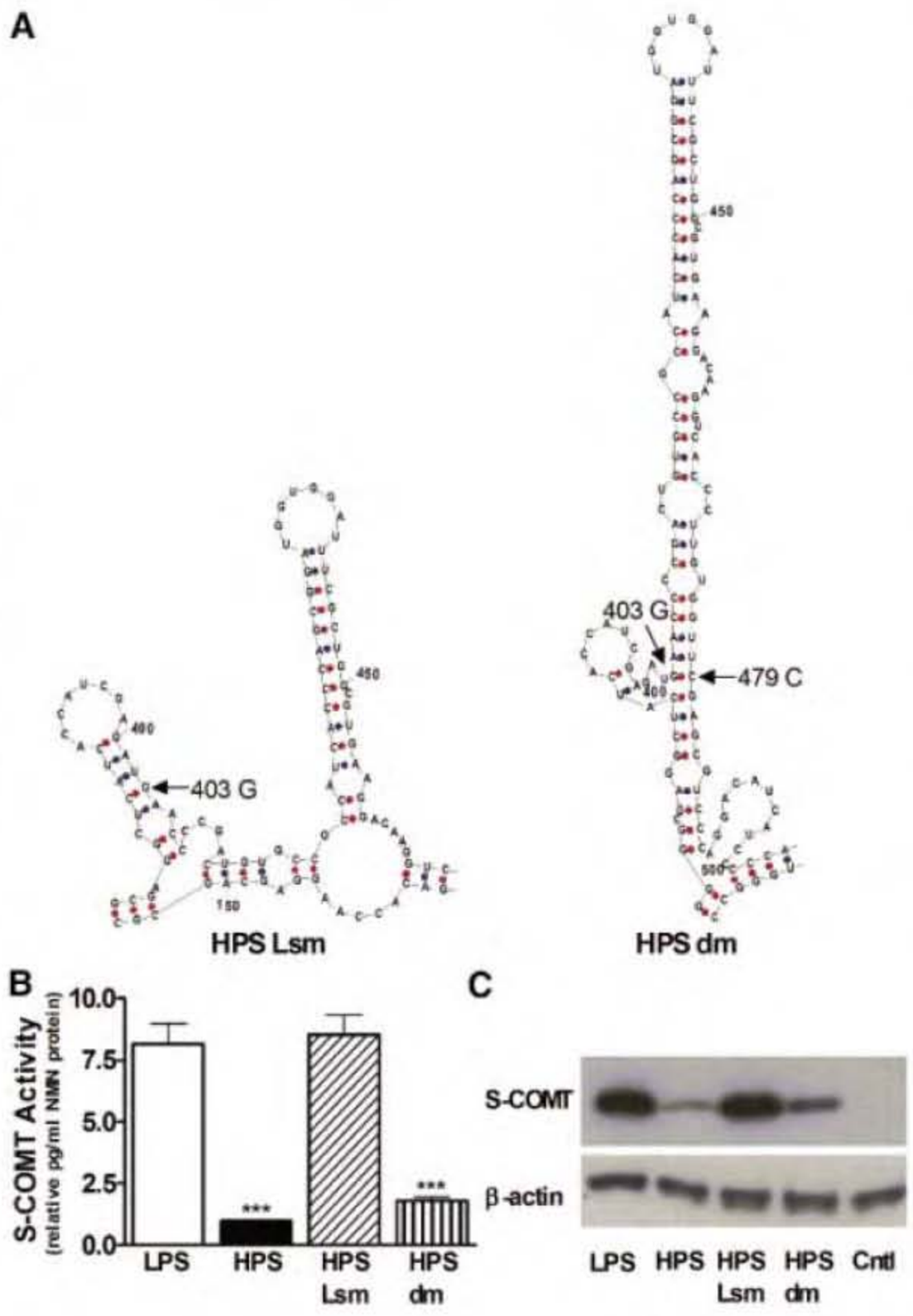

Fig. 2. Site-directed mutagenesis that destroys the stable stem-loop structure corresponding to the HPS haplotype restores COMT enzymatic activity and protein expression. (**A**) The mRNA structure corresponding to the HPS haplotype was converted to an LPS haplotype-like structure (HPS Lsm) by single mutation of 403C to G. The original HPS haplotype structure (HPS dm) was restored by double mutation of interacting nucleotides 403C to G and 479G to C. (**B** and **C**) The HPS Lsm exhibited COMT enzymatic activity and protein levels equivalent to those of the LPS haplotype, whereas the HPS dm exhibited reduced enzymatic activity. ***$P < 0.001$, ≠ LPS.

References and Notes

1. L. Y. Yampolsky, F. A. Kondrashov, A. S. Kondrashov, *Hum. Mol. Genet.* **14**, 3191 (2005).
2. J. C. Knight, *J. Mol. Med.* **83**, 97 (2005).
3. P. T. Mannisto, S. Kaakkola, *Pharmacol. Rev.* **51**, 593 (1999).
4. L. Diatchenko *et al.*, *Hum. Mol. Genet.* **14**, 135 (2005).
5. J. J. Marbach, M. Levitt, *J. Dent. Res.* **55**, 711 (1976).
6. T. T. Rakvag *et al.*, *Pain* **116**, 73 (2005).
7. J. K. Zubieta *et al.*, *Science* **299**, 1240 (2003).
8. G. Winterer, D. Goldman, *Brain Res. Brain Res. Rev.* **43**, 134 (2003).
9. B. Funke *et al.*, *Behav. Brain Funct.* **1**, 19 (2005).
10. G. Oroszi, D. Goldman, *Pharmacogenomics* **5**, 1037 (2004).
11. J. Duan *et al.*, *Hum. Mol. Genet.* **12**, 205 (2003).
12. L. X. Shen, J. P. Basilion, V. P. Stanton Jr., *Proc. Natl. Acad. Sci. U.S.A.* **96**, 7871 (1999).
13. I. Puga *et al.*, *Endocrinology* **146**, 2210 (2005).
14. K. Mita, S. Ichimura, M. Zama, T. C. James, *J. Mol. Biol.* **203**, 917 (1988).
15. T. D. Schmittgen, K. D. Danenberg, T. Horikoshi, H. J. Lenz, P. V. Danenberg, *J. Biol. Chem.* **269**, 16269 (1994).
16. A. Shalev *et al.*, *Endocrinology* **143**, 2541 (2002).
17. Materials and methods are available as supporting material on *Science* Online.
18. D. H. Mathews, J. Sabina, M. Zuker, D. H. Turner, *J. Mol. Biol.* **288**, 911 (1999).
19. M. Zuker, *Nucleic Acids Res.* **31**, 3406 (2003).
20. A. Y. Ogurtsov, S. A. Shabalina, A. S. Kondrashov, M. A. Roytberg, *Bioinformatics* **22**, 1317 (2006).
21. Sequence accession numbers: S-COMT clones BG290167, CA489448, and BF037202 represent LPS, APS, and HPS haplotypes, respectively. Clones corresponding to all three haplotypes and including the transcriptional start site were constructed by use of the unique restriction enzyme Bsp MI. The gene coding region containing all three SNPs was cut and inserted into the plasmids through use of the S-COMT (BG290167) and MB-COMT (BI835796) clones containing the entire COMT 5′ and 3′ ends as a backbone vector.
22. S. A. Shabalina, A. Y. Ogurtsov, N. A. Spiridonov, *Nucleic Acids Res.* **34**, 2428 (2006).

23. We are grateful to the National Institute of Child Health and Human Development, National Institute of Neurological Disorders and Stroke, and National Institute of Dental and Craniofacial Research at the NIH for financial support of this work. This research was also supported by the Intramural Research Program of the NIH, National Center for Biotechnology Information.

Supporting Online Material
www.sciencemag.org/cgi/content/full/314/5807/1930/DC1
Materials and Methods
SOM Text
Figs. S1 to S6
References

13 June 2006; accepted 16 November 2006
10.1126/science.1131262

Lineages of Acidophilic Archaea Revealed by Community Genomic Analysis

Brett J. Baker,[1] Gene W. Tyson,[2] Richard I. Webb,[3] Judith Flanagan,[2]*
Philip Hugenholtz,[2]† Eric E. Allen,[2]‡ Jillian F. Banfield[1,2]§

Novel, low-abundance microbial species can be easily overlooked in standard polymerase chain reaction (PCR)–based surveys. We used community genomic data obtained without PCR or cultivation to reconstruct DNA fragments bearing unusual 16*S* ribosomal RNA (rRNA) and protein-coding genes from organisms belonging to novel archaeal lineages. The organisms are minor components of all biofilms growing in pH 0.5 to 1.5 solutions within the Richmond Mine, California. Probes specific for 16*S* rRNA showed that the fraction less than 0.45 micrometers in diameter is dominated by these organisms. Transmission electron microscope images revealed that the cells are pleomorphic with unusual folded membrane protrusions and have apparent volumes of <0.006 cubic micrometer.

Our understanding of the variety of microorganisms that populate natural environments was advanced by the development of polymerase chain reaction (PCR)–based, cultivation-independent methods that target one or a small number of genes (*1*–*3*). Genomic analyses of DNA sequence fragments derived from multispecies consortia (*4*–*6*) and whole environments (*7*–*9*) have provided new information about diversity and metabolic potential. However, PCR-based methods have limited ability to detect organisms whose genes are significantly divergent relative to gene sequences in databases, and most cultivation-independent genomic sequencing approaches are relatively insensitive to organisms that occur at low abundance. Consequently, it is likely that low-abundance microorganisms distantly related to known species will be undetected members of natural consortia, even in low complexity systems such as acid mine drainage (AMD) (*10*).

An important way in which microorganisms affect geochemical cycles is by accelerating the dissolution of minerals. For example, microorganisms can derive metabolic energy by oxidizing iron released by the dissolution of pyrite (FeS_2). The ferric iron by-product promotes further pyrite dissolution, leading to AMD generation. AMD solutions forming underground in the Richmond Mine at Iron Mountain, California, are warm (30° to 59°C), acidic (pH ~0.5 to 1.5), metal-rich [submolar Fe^{2+} and micromolar As and Cu (*11*)] and host active microbial communities. Extensive cultivation-independent sequence analysis of functional and rRNA genes (*11*, *12*) revealed that biofilms contain a significant number of Archaea, but the diversity reported to date has been limited to the order Thermoplasmatales (*10*). Current models for AMD generation thus include only these species.

The genomes of the five dominant members of one biofilm community from the "5-way" region of the Richmond Mine (fig. S1) were largely reconstructed through the assembly of 76 Mb of shotgun genomic sequence (*4*). Previously unreported is a genome fragment that encodes part of the 16*S* rRNA gene of a novel archaeal lineage: Archaeal Richmond Mine Acidophilic Nanoorganism (ARMAN-1). Using an expanded data set that now comprises more than 100 Mb of genomic sequence, we reconstructed a contiguous 4.2-kb fragment adjacent to this gene. A second 13.2-kb genome fragment encoding a 16*S* rRNA gene from an organism that is related to ARMAN-1 (ARMAN-2) was reconstructed from 117 Mb of community genomic sequence derived from a biofilm from the A drift (fig. S1). Within the data sets from each site, results to date indicate that each ARMAN population is near-clonal.

Comparison of the ARMAN-1 and -2 DNA fragments revealed some gene rearrangements, insertions, and deletions (Fig. 1). Genes present in both organisms encode putative inorganic pyrophosphatases, a transcription regulator, and a gene shown to be an arsenate reductase (*13*). Comparative analysis of these genes with sequences in the public databases consistently

[1]Department of Earth and Planetary Sciences, University of California, Berkeley, CA 94720, USA. [2]Environmental Science, Policy, and Management, University of California, Berkeley, CA 94720, USA. [3]Centre for Microscopy and Microanalysis and Department of Microbiology and Parasitology, University of Queensland, Brisbane 4072, Australia.

*Present address: University of California, San Francisco, CA 94143, USA.
†Present address: Department of Energy Joint Genome Institute, Walnut Creek, CA 94598, USA.
‡Present address: University of California, San Diego, La Jolla, CA 92093, USA.
§To whom correspondence should be addressed. E-mail: jill@eps.berkeley.edu

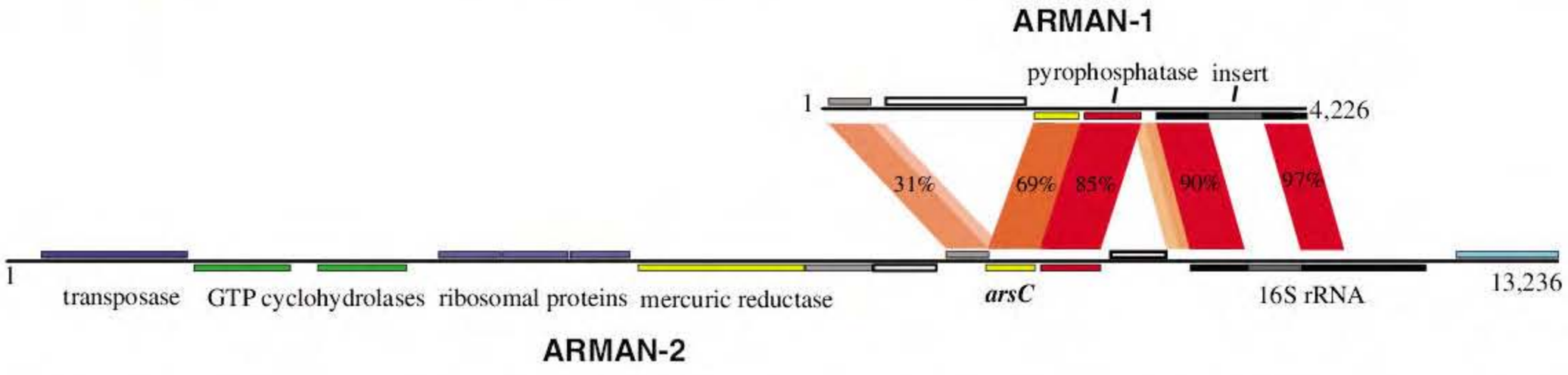

Fig. 1. Comparison of syntenous genomic regions of ARMAN-1 [from the "5-way" (CG) community (*4*)] and ARMAN-2 (from the UBA community). Orthologs and their protein identity are indicated by the red bands. The percentage similarity for the 16*S* rRNA gene sequences is also shown. Numbers at ends indicate length (number of nucleotides); predicted open reading frames for hypothetical proteins are indicated by boxes.

indicated that ARMAN-1 and -2 are representatives of a deeply branching lineage within Euryarchaeota with no cultivated representatives. The only other identified members of this lineage are uncultivated organisms from a hot pool (78°C, pH 7.5) with 85% similarity to ARMAN-2 (Fig. 2) (*14*), and organisms represented by clones from an acidic (pH 4.2 to 4.8) west Siberian peat bog [88% similarity to ARMAN-2 (*15*)]. In both of these studies, atypical 16*S* rRNA gene primers were used.

The 16*S* rRNA genes of ARMAN-1 and -2 have three to five mismatches with commonly used broad-specificity primers (four mismatches with Arc-23F and Univ-1492R; table S1), which explains why these organisms were missed in previous PCR-based surveys (*10*–*12*). The 16*S* rRNA genes both have 519–base pair inserts that encode predicted proteins. The inserts (1102–1103 *E. coli* numbering) share protein-level similarity to each other (*13*) and have weak homology with a functionally characterized homing endonuclease encoded within the 16*S* rRNA gene of *Aeropyrum pernix* (*16*). Excision of the inserts, probably at the bulge-helix-bulge (fig. S2), leaves complete and fully aligned rRNA genes. Insertion sequences (e.g., introns) in archaeal and bacterial rRNA genes are uncommon, although other instances have been reported in pathogens, symbionts, and the crenarchaeal orders Thermoproteales and Desulfurococcales (*17*).

To further explore the diversity and distribution of ARMAN-like microorganisms, we designed primers that target the 16*S* rRNA and putative *arsC* genes of ARMAN-1 and -2, and applied them to samples collected from throughout the Richmond Mine (*13*) (fig. S1). The primers amplified 16*S* rRNA genes from a third previously undetected lineage, ARMAN-3, that are 18% divergent from ARMAN-1 and -2 (Fig. 2). The ARMAN-3 organisms do not have inserts in their 16*S* rRNA genes. This observation, in combination with the relatively low similarity between inserts in the ARMAN-1 and -2 genes, suggests that insertion sequences were acquired after the divergence of the three groups. Both the *arsC* and 16*S* rRNA genes from an ARMAN-lineage organism were recovered from all samples tested, indicating that these organisms are present in most biofilms growing at the site. ARMAN group organisms are present in samples that differ significantly in habitat type (e.g., subaerial and subaqueous biofilms) and geochemical conditions (pH 0.5 to 1.5, temperature 30° to 47°C).

Fluorescently labeled oligonucleotide probes targeting the 16*S* rRNA (ARM980 and ARM1357) of all known ARMAN-lineage microorganisms enabled optical microscope–based visualization of the cells in the suite of biofilm samples (Fig. 3A). The specificity of probe binding was verified using an archaeal-ARMAN (ARC915-ARM915) competitor probe set (*13*). Notably, the cells labeled with the ARM probes are significantly smaller than other bacterial and archaeal cells in the samples. A filtration-based method was used to concentrate cells for ultrastructural characterization.

A biofilm from the A drift (fig. S1) was homogenized, and the fraction of the biomass that passed through 0.45-μm filters was collected (*13*). To verify that ARMAN-lineage organisms dominated the filtrate, we extracted genomic DNA and amplified the 16*S* rRNA genes with the ARMAN-, archaeal-, and bacterial-specific primers. Significant amplification product was obtained only with the ARMAN primers (fig. S3). Cloning and sequencing of this amplification product (24 clones) revealed that the filtrate was dominated by ARMAN-2 organisms but contained some ARMAN-1 organisms. Cells in the filtrate were labeled with ARMAN-specific fluorescent probes (Fig. 3B), and the resulting images were compared with those obtained from environmental samples (Fig. 3A). The results confirm that ARMAN organisms are highly enriched by filtration (Fig. 3B).

The filtrate was frozen under high pressure and cryo-substituted for transmission electron microscope (TEM)–based imaging of cell size and morphology (*13*). In addition to ruptured cell membranes, we detected some morphologies typical of *Leptospirillum* cells known to be present at low abundance in the filtrate, as well as rounded objects of highly variable size (average diameter ~85 nm;

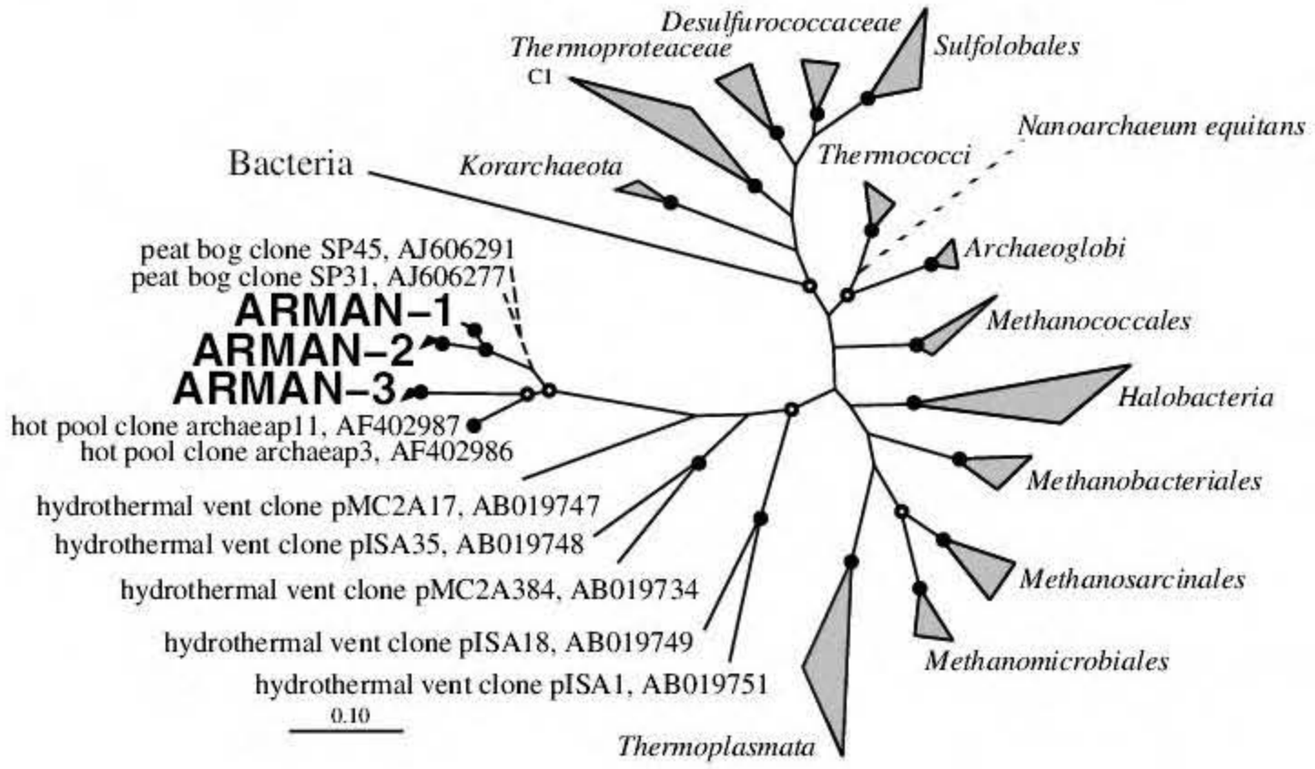

Fig. 2. Phylogeny of the ARMAN groups and several other archaeal phyla, based on 16*S* rRNA gene sequence analysis (maximum likelihood method). Bootstrap values are indicated at the nodes (solid circles, >75%; open circles, >50%). The dashed branch to *Nanoarchaeum equitans* and the uncultured peat bog clones SP31 and SP45 (*15*) signifies that we were unable to resolve these positions in our analyses.

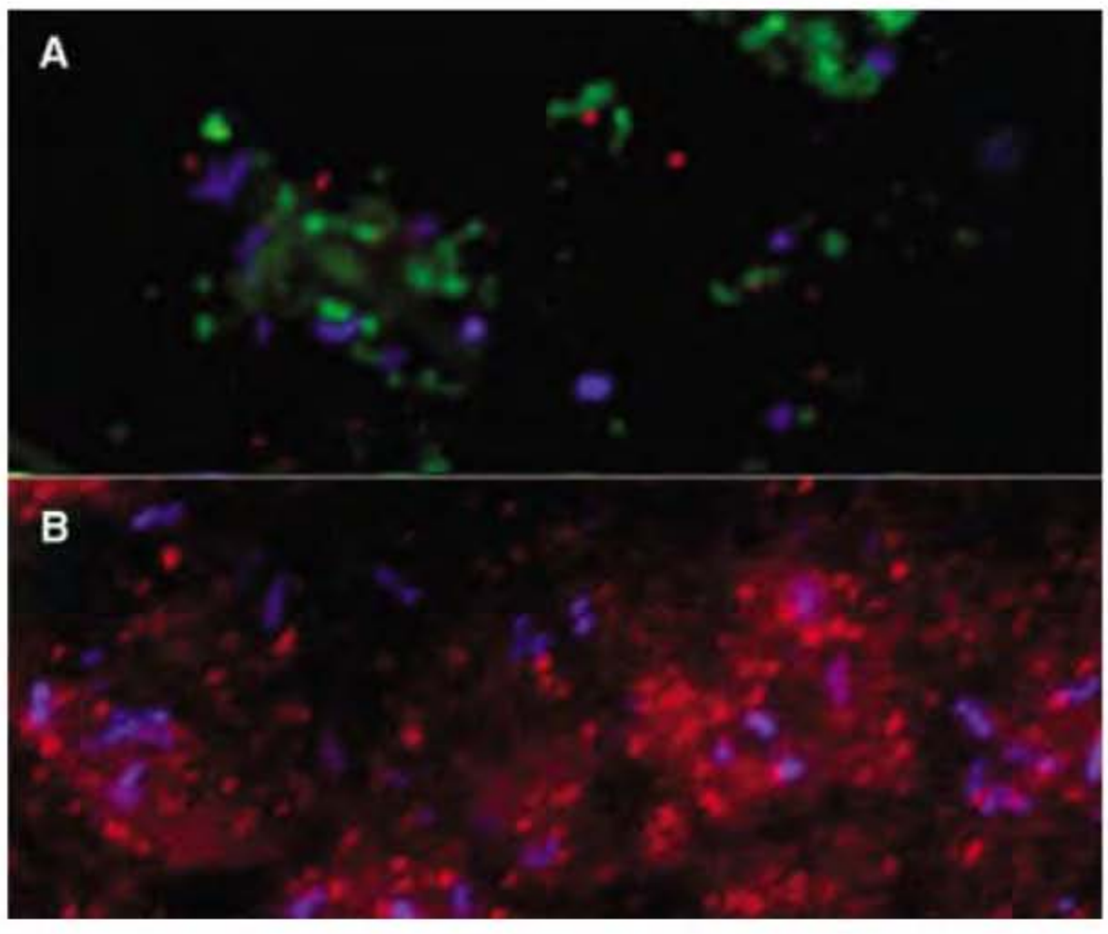

Fig. 3. Fluorescence in situ hybridization micrographs of Archaea (ARC915, fluorescein isothiocyanate in green), Bacteria (EUB338, Cy5 in blue), and ARMAN (ARM980 and ARM1357, Cy3 in red) in (**A**) an A-drift biofilm sample and (**B**) the 0.45-μm filtrate. Magnifications, 630×.

fig. S4) interpreted to be membrane buds. The other abundant cell-like objects are pleomorphic and surrounded by an archaeal-like cell wall with an S-layer. These objects have one or two folded membrane protrusions (Fig. 4 and fig. S5) that somewhat resemble structures of unknown function observed in the crenarchaeon *Pyrodictium abyssi* (*18*). On the basis of 60 measurements (excluding the protrusions), the sectioned cell-like objects have a mean length of 244 nm (range, 193 to 299 nm) and a mean width of 175 nm (range, 129 to 207 nm). The colocalization of DNA stain and probes binding specifically to ARMAN rRNA, the existence of clearly contiguous external membranes, and the presence of an archaeal-type cell wall indicate that these objects are the ARMAN cells. The apparently dense packing of the ribosomes may account for the strength of the fluorescence signal in optical microscope images, despite the small cell size. The TEM data confirm the inference from the filtration experiment that the ARMAN-lineage organisms are extremely small.

It has not escaped our attention that if the average cell size estimated from TEM observations is accurate, the ARMAN cells have volumes of $<0.006\ \mu m^3$ [calculated from the maximum size observed in ultramicrotomed sections (*13*)], making them smaller than any other known cellular life form. The smallest known Archaea, of the phylum Nanoarchaea, have cell volumes that range from 0.02 to $0.70\ \mu m^3$ (*19*). They are obligate parasites of other Archaea (*20*, *21*). The smallest Bacteria include those described from Greenland ice cores, with cell volumes of 0.04 to $0.10\ \mu m^3$ (*22*), and members of the SAR11 clade, which inhabit the oligotrophic open ocean and have cell volumes of 0.031 to $0.051\ \mu m^3$ (*23*, *24*). Note that these data do not rule out the possibility of larger cytoplasmic volumes if there are unobserved connections between the objects that appear to be cells.

If the ARMAN cells have volumes of $<0.006\ \mu m^3$, and half of the cell volume is occupied by ribosomes, then there is enough room for at least 350 ribosomes of normal size. However, the cells are smaller than the minimum size expected on the basis of theoretic considerations for free-living cells (*25*). We have no evidence to suggest that the ARMAN cells are parasitic on other community members. If future work demonstrates that ARMAN cells are viable and have cell volumes of $<0.006\ \mu m^3$, it may be necessary to reconsider existing paradigms for the minimum requirements for life.

The ARMAN groups expand the variety of archaea known to be associated with AMD. Further targeted genomic characterization of cells concentrated by filtration should help to elucidate the ecological roles of these tiny, enigmatic, uncultivated microorganisms. Our findings emphasize the possibility that novel organisms with unexpected characteristics remain to be discovered among the relatively low-abundance members of microbial communities.

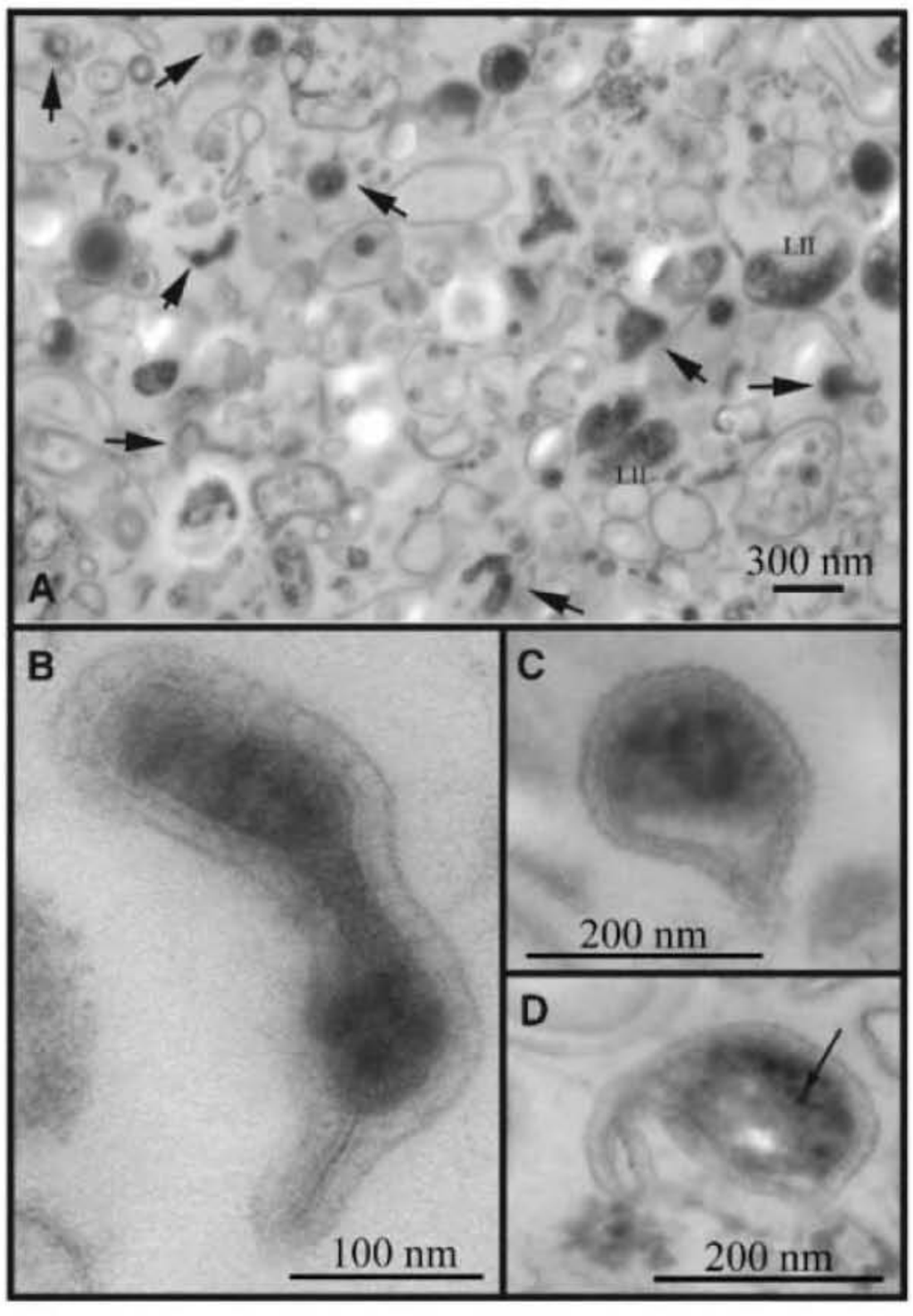

Fig. 4. Transmission electron microscope images of four cells inferred to belong to the ARMAN group. (**A**) A large area showing many cells of the ARMAN type, a subset of which are indicated by arrows. Also present are rounded objects, membrane debris, and a small number of *Leptospirillum* group II cells (LII). (**B**) Most cells exhibit one or two folded membrane-bounded protrusions (see fig. S5). (**C**) Most cells appear to be surrounded by an S-layer with periodicity in the cell surface. The dark internal contrast is consistent with densely packed ribosomes. (**D**) Some cells have very dark inclusions (arrow).

References and Notes

1. P. Hugenholtz *et al.*, *J. Bacteriol.* **180**, 4765 (1998).
2. B. J. Baker *et al.*, *Environ. Microbiol.* **5**, 267 (2003).
3. C. A. Francis *et al.*, *Proc. Natl. Acad. Sci. U.S.A.* **102**, 14683 (2005).
4. G. W. Tyson *et al.*, *Nature* **428**, 37 (2004).
5. O. Béjà *et al.*, *Science* **289**, 1902 (2000).
6. M. R. Rondon *et al.*, *Appl. Environ. Microbiol.* **66**, 2541 (2000).
7. E. F. DeLong *et al.*, *Science* **311**, 496 (2006).
8. S. G. Tringe *et al.*, *Science* **308**, 554 (2004).
9. J. C. Venter *et al.*, *Science* **304**, 66 (2004); published online 4 March 2004 (10.1126/science.1093857).
10. B. J. Baker, J. F. Banfield, *FEMS Microb. Ecol.* **44**, 139 (2003).
11. G. K. Druschel *et al.*, *Geochem. Trans.* **5**, 13 (2004).
12. P. L. Bond *et al.*, *Appl. Environ. Microbiol.* **66**, 3842 (2000).
13. See supporting material on *Science* Online.
14. A. Sunna, P. L. Bergquist, *Extremophiles* **7**, 63 (2003).
15. O. R. Kotsyurbenko *et al.*, *Environ. Microbiol.* **6**, 1159 (2004).
16. N. Nomura *et al.*, *J. Bacteriol.* **180**, 3635 (1998).
17. B. J. Baker *et al.*, *Appl. Environ. Microbiol.* **69**, 5512 (2003).
18. G. Rieger *et al.*, *J. Struct. Biol.* **115**, 78 (1995).
19. H. Huber *et al.*, *Res. Microbiol.* **154**, 165 (2003).
20. H. Huber *et al.*, *Nature* **417**, 63 (2002).
21. E. Waters *et al.*, *Proc. Natl. Acad. Sci. U.S.A.* **100**, 12984 (2003).
22. V. I. Miteva, J. E. Brenchley, *Appl. Environ. Microbiol.* **71**, 7806 (2005).
23. R. R. Malmstrom *et al.*, *Appl. Environ. Microbiol.* **70**, 4129 (2004).
24. S. J. Giovannoni *et al.*, *Science* **309**, 1242 (2005).
25. Steering Group for the Workshop on Size Limits of Very Small Microorganisms, National Research Council, *Size Limits of Very Small Microorganisms: Proceedings of a Workshop* (National Academies Press, Washington, DC, 1999).

26. Supported by the NSF Biocomplexity Program, the DOE Genomics:GTL program, and the NASA Astrobiology Institute. We thank T. Arman (owner, Iron Mountain Mines) and R. Carver for access to the site; K. Nealson, A. Driks, C. Wimpee, and B. Hedlund for their comments; K. MacDonald for assistance with preparation of sample for TEM analyses; J. R. Giska for assistance with *arsC* amplification, and J. C. Detter and P. Richardson for library construction and genome sequencing support. Genomic sequencing was carried out at the Joint Genome Institute. The fully annotated genomic fragment belonging to ARMAN-1 was deposited under GenBank accession number AY652726, and the ARMAN-2 fragment was deposited under number DQ848677.

Supporting Online Material

www.sciencemag.org/cgi/content/full/314/5807/1933/DC1
Materials and Methods
Figs. S1 to S5
Table S1
References

18 July 2006; accepted 14 November 2006
10.1126/science.1132690

Adjuvant-Enhanced Antibody Responses in the Absence of Toll-Like Receptor Signaling

Amanda L. Gavin,[1] Kasper Hoebe,[1] Bao Duong,[1,2] Takayuki Ota,[1] Christopher Martin,[1,2] Bruce Beutler,[1] David Nemazee[1]*

Innate immune signals mediated by Toll-like receptors (TLRs) have been thought to contribute considerably to the antibody-enhancing effects of vaccine adjuvants. However, we report here that mice deficient in the critical signaling components for TLR mount robust antibody responses to T cell–dependent antigen given in four typical adjuvants: alum, Freund's complete adjuvant, Freund's incomplete adjuvant, and monophosphoryl-lipid A/trehalose dicorynomycolate adjuvant. We conclude that TLR signaling does not account for the action of classical adjuvants and does not fully explain the action of a strong adjuvant containing a TLR ligand. This may have important implications in the use and development of vaccine adjuvants.

Adjuvants are vaccine additives that enhance the elicited levels of antibodies and T lymphocyte responses by promoting inflammatory responses of leukocytes in ways that presumably mimic natural infection. Toll-like receptor (TLR)–mediated recognition of microbial signature molecules is one of the cues normally used by leukocytes to react to real microbial challenges (*1*, *2*). Each of the 10 different functional TLRs in humans (12 in mice) has apparently evolved to recognize a specific set of evolutionarily conserved molecules, including components of bacterial cell walls, and endocytosed nucleic acids such as double-stranded RNA, single-stranded DNA, and unmethylated CpG dinucleotide-containing DNA (*1*, *2*). TLR recognition leads to the activation of transcription factors that drive cytokine expression, proliferation, survival, and inflammatory mediator expression. TLR signaling is initiated by four adapters—MyD88, Toll-interleukin 1 receptor (TIR) domain–containing adapter inducing interferon beta (TRIF), TIR domain–containing adapter protein (TIRAP)/MyD88 adapter–like (Mal), and TRIF-related adapter molecule (TRAM)—which associate with the cytoplasmic TIR domains of TLRs (*1*, *2*). MyD88 associates with all TLRs except TLR3, whereas TRIF associates with TLR3 and TLR4. TIRAP/Mal and TRAM appear to function as bridging adapters for MyD88 and TRIF, respectively (*1*, *2*). TIRAP/Mal and TRAM are essential for signaling by TLR4, with TIRAP/Mal also required for TLR2 function. MyD88 also contributes to signaling in B cells and is required for maximal B cell responses to foreign proteins when present in the context of TLR ligands (*3*). Nevertheless, there is debate about whether such signals are necessary for this class of response (*4*, *5*). Mice genetically deficient in both MyD88 and TRIF ($Myd88^{-/-}$;$Trif^{Lps2/Lps2}$ mice) have a complete lack of known TLR signaling (*6*–*8*), thus allowing an assessment of the TLR dependence of antibody responses. We took advantage of this to explore more precisely the role of TLR signaling in antibody responses to immunization and the augmenting roles of adjuvants in this response.

$Myd88^{-/-}$;$Trif^{Lps2/Lps2}$ and control C57BL/6 mice were immunized with the T cell–dependent antigen trinitrophenol-hemocyanin (TNP-Hy) given in Freund's complete adjuvant (FCA), and the titers of induced antibodies to TNP in the serum were determined (*9*). In these analyses, antibody responses of $Myd88^{-/-}$;$Trif^{Lps2/Lps2}$ mice were entirely comparable to those of C57BL/6 mice, indicating that signals transmitted by TRIF and MyD88 made no appreciable contribution to the antibody response (Fig. 1). This experiment included initial immunization, followed by a boost with TNP-Hy in phosphate-buffered saline (PBS) on day 21, and showed no significant defect in sera at any time point for immunoglobulin M (IgM), IgG1, IgG2b, IgG2c, IgG3, and IgE antibody responses to TNP. Furthermore, when the TNP-Hy challenge was given with the adjuvant alum, a frequently used adjuvant in human vaccines, antibody responses of $Myd88^{-/-}$;$Trif^{Lps2/Lps2}$ mice were also comparable to those of C57BL/6 mice (*5*) (fig. S1).

To reevaluate the augmenting effects of adjuvant on antibody production and its suggested dependence on MyD88 and TRIF, additional immunizations of C57BL/6 and of $Myd88^{-/-}$;$Trif^{Lps2/Lps2}$ mice were carried out

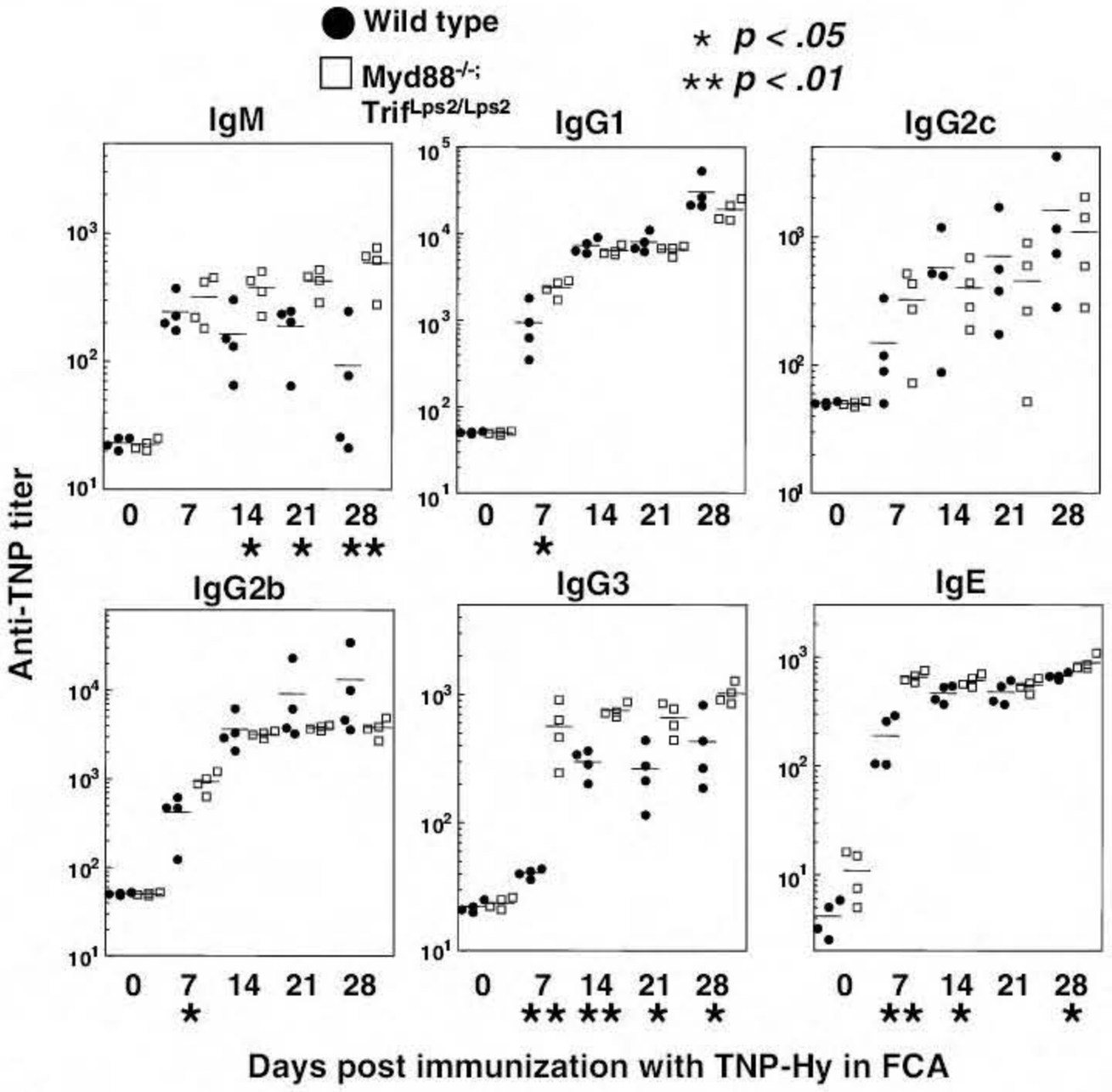

Fig. 1. T cell–dependent antibody responses of $Myd88^{-/-}$;$Trif^{Lps2/Lps2}$ and control mice using FCA. Two-month-old mice were immunized with TNP-Hy in FCA on day 0 and boosted with antigen in PBS on day 21. Each point represents the serum antibody titer to TNP for an individual mouse. IgE titers represent ng/ml, whereas other measurements represent reciprocal serum dilution yielding half-maximal signal. Closed circles, wild-type C57BL/6; open squares, $Myd88^{-/-}$;$Trif^{Lps2/Lps2}$ double knockout mice. *, $P < .05$; **, $P < .01$. For methods, see (*9*).

[1]Department of Immunology, The Scripps Research Institute, La Jolla, CA 92037 USA. [2]The Scripps Research Institute, Kellogg School of Science and Technology, Doctoral Program in Chemical and Biological Sciences, La Jolla, CA 92037, USA.

*To whom correspondence should be addressed. E-mail: nemazee@scripps.edu

with a second antigen, TNP–keyhole limpet hemocyanin (TNP-KLH), in which the adjuvants FCA, Freund's incomplete adjuvant (FIA), and monophosphoryl-lipid A/trehalose dicorynomycolate ("Ribi" adjuvant) were compared with responses in the absence of adjuvant. TNP-specific antibody responses were assessed 7 and 14 days later (Fig. 2). Ribi adjuvant contains the TLR4 ligand monophosphoryl-lipid A, whereas FIA is not known to contain any TLR ligand. Both C57BL/6 and *Myd88*$^{-/-}$;*Trif*$^{Lps2/Lps2}$ mice responded strongly to TNP-KLH only when given in adjuvant (Fig. 2). [The IgG1 responses to TNP-KLH given in PBS, although low, were significantly above preimmune background (titer < 10)]. Responses of *Myd88*$^{-/-}$;*Trif*$^{Lps2/Lps2}$ mice to antigen given in FCA or FIA were unimpaired, whereas responses to TNP-KLH given in Ribi adjuvant were reduced relative to those of wild-type mice at day 14 (Fig. 2). However, the reduction in antibody titers elicited in *Myd88*$^{-/-}$;*Trif*$^{Lps2/Lps2}$ mice was modest and observed mainly in the IgG2c and IgG2b responses (Fig. 2). We conclude that, under these experimental conditions, TLR signaling is not required for T cell–dependent antibody responses and makes a relatively small contribution to responses to antigen given in either alum or FCA.

It was notable that even in mice challenged with Ribi adjuvant, which contains a potent TLR ligand, most of the antibody-augmenting adjuvant effect was independent of MyD88/TRIF (Fig. 2). Consistent with this, Ribi, but not FIA or FCA, stimulated peritoneal macrophages to produce type I interferon (IFN) and tumor necrosis factor (TNF) when used to treat cells at concentrations approximating those achieved in vivo (fig. S2). As expected, isolated splenic B cells from *Myd88*$^{-/-}$;*Trif*$^{Lps2/Lps2}$ mice failed to proliferate in response to the TLR ligand lipopolysaccharide (LPS) (fig. S3B). By contrast, responses of *Myd88*$^{-/-}$;*Trif*$^{Lps2/Lps2}$ B cells to B cell receptor ligation were indistinguishable from those of normal cells (fig. S3, A and C). Nevertheless, it was apparent that the observed adjuvant effect on antibody responses in vivo failed to correlate with their potential to activate myeloid cells or B cells in vitro.

Thus far, the responses we had measured were for antigens that depend on T cell help, although another class of antibody response is independent of help from T cells. *Myd88*$^{-/-}$;*Trif*$^{Lps2/Lps2}$ mice were thus tested for their responses to the T cell–independent type 2 (TI-2) antigen TNP-Ficoll. Overall antibody responses did not generally differ significantly from normal controls (fig. S4). These results show for the first time that the antibody response to a typical TI-2 antigen is independent of TLR signaling.

Preimmune serum levels of Ig in *Myd88*$^{-/-}$;*Trif*$^{Lps2/Lps2}$ mice were next analyzed and found to have a complex pattern, with some isotypes reduced in amount and others increased relative to C57BL/6 levels (Fig. 3). Relative to control, IgG2b and IgG2c levels were lower in *Myd88*$^{-/-}$;*Trif*$^{Lps2/Lps2}$ mice, by 50% and 70%, respectively, a statistically significant but modest reduction (Fig. 3). Also, the serum levels of one Ig subclass (IgG3) in *Myd88*$^{-/-}$;*Trif*$^{Lps2/Lps2}$ mice were notably lower. By contrast, *Myd88*$^{-/-}$;*Trif*$^{Lps2/Lps2}$ mice displayed 3 times the levels of IgG1 ($P < .001$) and 20 times the levels of IgE ($P < .0001$). Collectively, such differences suggest that TLR signaling may control the class rather than the magnitude of Ig levels in naive mice, at least under specific pathogen-free conditions such as those found in our facility.

Consistent with the robust preimmune Ig levels and antibody responses of *Myd88*$^{-/-}$;*Trif*$^{Lps2/Lps2}$ mice, nearly normal B-1, marginal zone, and follicular B cell numbers were found in these animals. Compared with wild-type mice, the only consistent differences found in *Myd88*$^{-/-}$;*Trif*$^{Lps2/Lps2}$ mice tested at 2 and 6 months of age were a B cell surface level of CD23 about twice as high (fig. S5) and a slight reduction in splenic transitional type 1 B cells (T1) (tables S1 and S2). We conclude that TLR signaling is not required for preimmune B cell development but may partly affect the abundance and CD23 levels of B cell subsets. As levels of CD23, IgE, and IgG1 are up-regulated by interleukin 4, we speculate that environmental stimuli transduced by TLRs in a MyD88- and/or TRIF-dependent manner suppress the expression of, or response to, this cytokine.

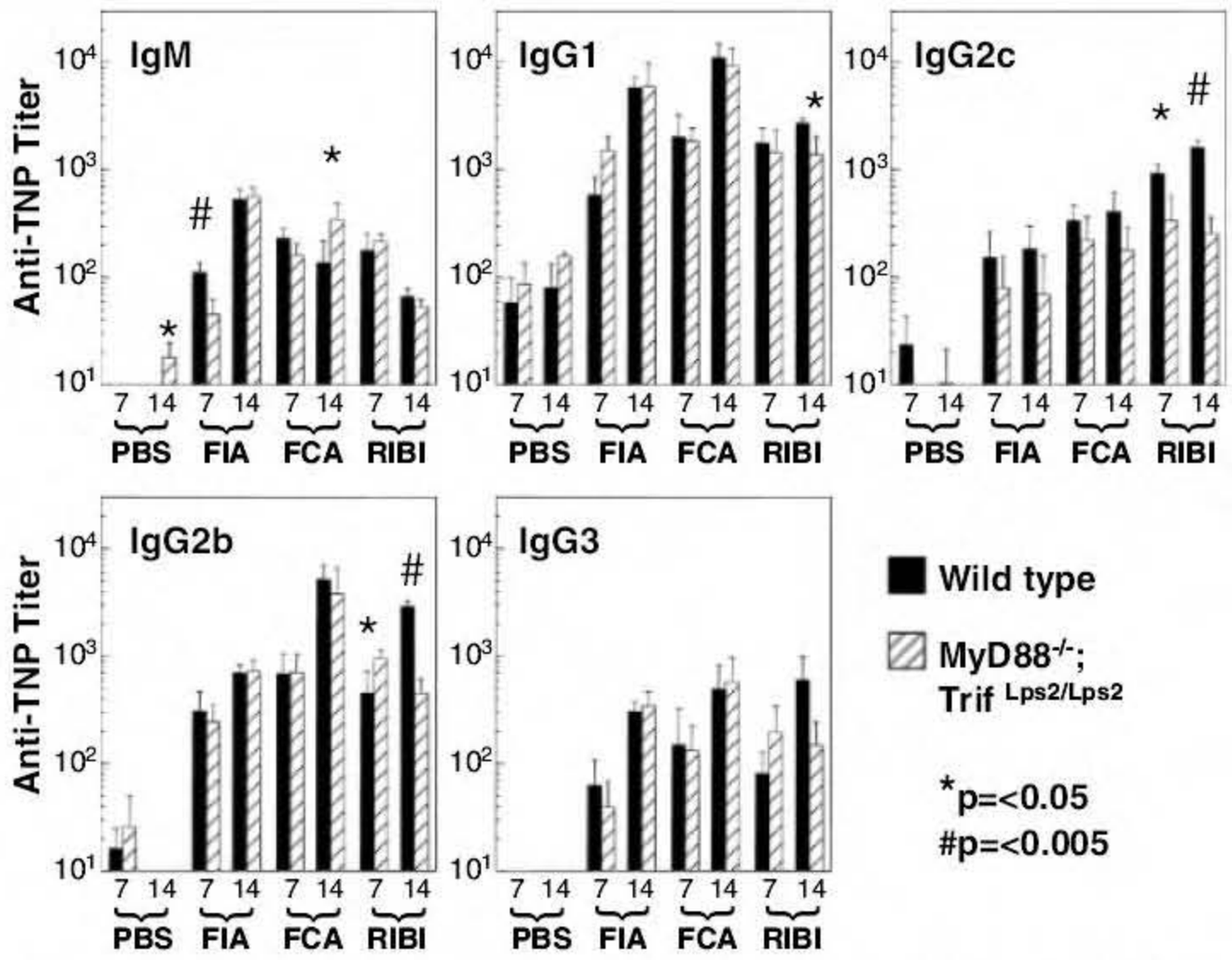

Fig. 2. Comparison of serum antibody responses of C57BL/6 and *Myd88*$^{-/-}$;*Trif*$^{Lps2/Lps2}$ mice given immunogen in different adjuvants. Groups of four mice were immunized with 100 μg TNP-KLH in PBS in the indicated adjuvants, and titers of antibody to TNP of the indicated immunoglobulin isotypes were determined on days 7 and 14.

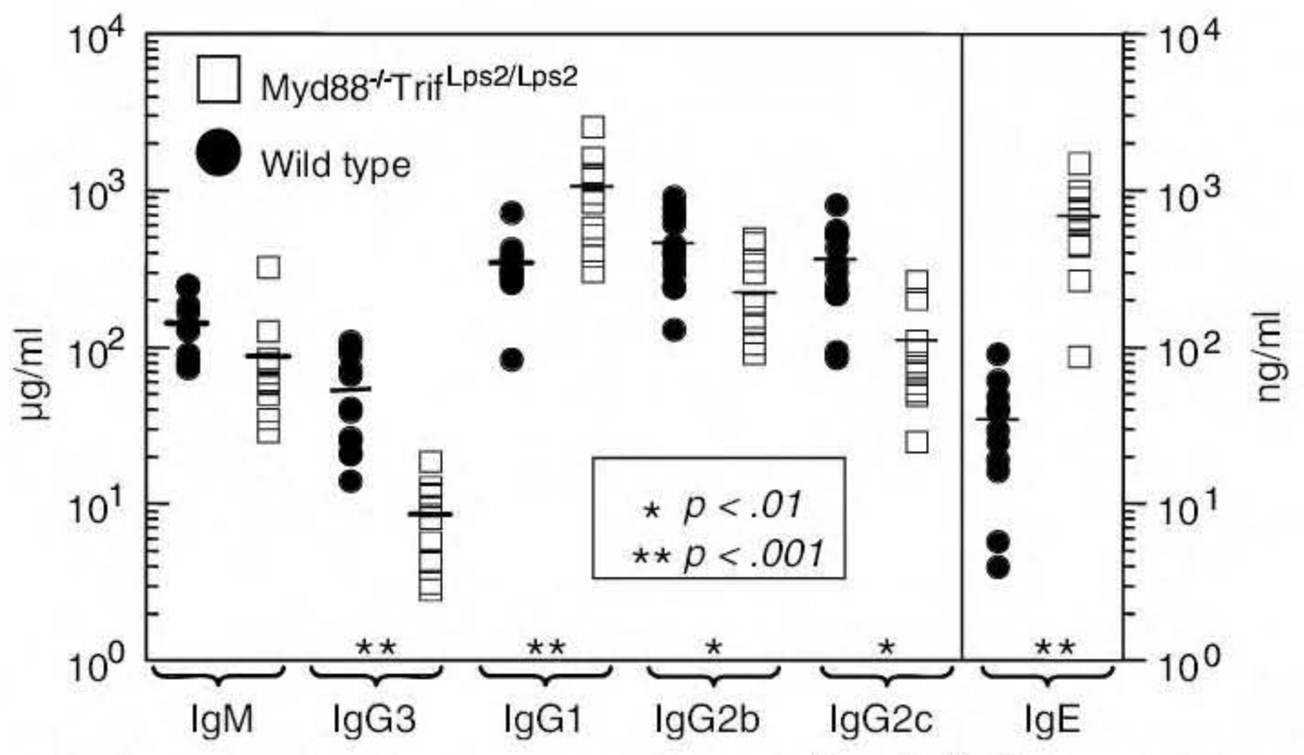

Fig. 3. Preimmune serum immunoglobulin levels in *Myd88*$^{-/-}$;*Trif*$^{Lps2/Lps2}$ compared with wild-type C57BL/6 controls as measured by enzyme-linked immunosorbent assay. Each point represents data from a different mouse. Closed circles, wild-type, C57BL/6; open squares, *Myd88*$^{-/-}$;*Trif*$^{Lps2/Lps2}$ mice.

Our findings reveal that TLR signaling is not required for robust antibody responses to antigen when given in four commonly used adjuvants, in particular FCA, which is widely thought to depend on TLR signaling for its adjuvant effect (*10*). However, ligands that signal through the MyD88 and TRIF pathways can costimulate these responses and affect the antibody class of the response, as has been known for LPS for many years (*3*), and is indicated by the modest boost seen in C57BL/6 mice immunized with Ribi adjuvant (Fig. 2). By exclusion, our data suggest the likelihood that non-TLR–mediated "innate" signals may be involved in the augmentation of adaptive antibody responses. It is also formally possible that MyD88/TRIF–independent modes of TLR signaling are yet to be discovered, possibly through TRAM and TIRAP, although so far there is no evidence for this.

Our results extend and clarify previous studies. A recent paper involving MyD88-deficient mice asserted that T cell–dependent antibody responses require activation of TLRs in B cells (*4*). However, that inference was based on the use of LPS as an adjuvant rather than more commonly used adjuvants such as FCA or alum. Indeed, an earlier study found that although MyD88-deficient mice failed to make an IgG2a response to ovalbumin given in FCA, they still made good IgG1 and IgE antibody responses, and antigen given in alum could promote an IgE response (*11*). However, in those studies, the remaining antibody responses in MyD88-deficient mice could conceivably have involved TLR signaling through TRIF-dependent pathways, a caveat that does not apply to our data. We clearly find that IgG2c (also known as IgG2a^b) responses to protein antigen given in alum or FCA are robust in $Myd88^{-/-}$;$Trif^{Lps2/Lps2}$ mice, in apparent contradiction to both studies of MyD88-deficient mice mentioned (*4*, *11*) and other studies implicating a requirement of MyD88 or TLR signaling in the generation of IgG2a antibodies. It may be that TLR ligand–driven suppression of IgG2c/a production occurs in mice with intact TRIF signaling that lack MyD88; for example, through cytokine-driven polarization of the T helper response (*11*, *12*). The IgG2c/a response is promoted by IFN-α/β or IFN-γ (*13*, *14*). In viral infection, the IgG2c/a response is lost in mice lacking both IFN-α/βR and IFN-γR (*15*). Because we found good IgG2c responses upon immunization of $Myd88^{-/-}$;$Trif^{Lps2/Lps2}$ mice, our results may indicate that these immunizations can stimulate TLR-independent IFN production.

The antibody response to the T cell–independent type II antigen TNP-Ficoll was relatively normal in $Myd88^{-/-}$;$Trif^{Lps2/Lps2}$ mice, although it was slightly lower at later time points. Interestingly, the IgG3 component of the antigen-specific response of $Myd88^{-/-}$;$Trif^{Lps2/Lps2}$ mice was not significantly lower than normal despite their reduced preimmune total serum IgG3 levels. It has been argued that the class switch to IgG3 requires cytokines produced by accessory cells (*16*). If this is so, it is clear from these results that production of the cytokines in question does not require TLR stimulation of B cells or accessory cells.

That B cells can respond to autologous DNA and RNA through TLR signaling (*17*, *18*) raised the possibility that TLRs could affect preimmune development or maintenance of B cell subsets, particularly the marginal zone and B-1 compartments. However, our findings that $Myd88^{-/-}$;$Trif^{Lps2/Lps2}$ mice generate abundant B-1 and marginal zone B cells appear to rule out definitively a required role for TLR signaling in their development.

Our data do not contest the long-held understanding that TLR ligands can augment antibody responses. However, it is surprising, given the recent emphasis on the importance of TLRs in the initiation of the adaptive immune response, that we fail to find a deficit in the early antibody responses of $Myd88^{-/-}$;$Trif^{Lps2/Lps2}$ mice using conventional antigens and immunization regimens. Our data are more consistent with a model in which TLRs play roles in early microbial suppression, regulation of the antibody class, and sustaining antibody secretion at late times after immunization, rather than as an essential component of the self/nonself discrimination of the adaptive immune response. These data have implications for vaccine design because they indicate that robust antibody responses to moderate doses of antigens can be achieved when given in the total absence of TLR ligands. Because TLR-mediated signals can be toxic, our findings raise the possibility that unwanted side effects of adjuvants may be avoided by excluding TLR ligands from adjuvants.

References and Notes

1. K. Takeda, S. Akira, *Int. Immunol.* **17**, 1 (2005).
2. B. Beutler *et al.*, *Annu. Rev. Immunol.* **24**, 353 (2006).
3. J. Andersson, O. Sjoberg, G. Moller, *Transplant. Rev.* **11**, 131 (1972).
4. C. Pasare, R. Medzhitov, *Nature* **438**, 364 (2005).
5. D. Nemazee, A. Gavin, K. Hoebe, B. Beutler, *Nature* **441**, E4 (2006).
6. K. Hoebe *et al.*, *Nature* **424**, 743 (2003).
7. M. Yamamoto *et al.*, *Science* **301**, 640 (2003).
8. E. Janssen *et al.*, *Immunity* **24**, 787 (2006).
9. Materials and methods are available as supporting material on *Science* Online.
10. C. Pasare, R. Medzhitov, *Curr. Opin. Immunol.* **15**, 677 (2003).
11. M. Schnare *et al.*, *Nat. Immunol.* **2**, 947 (2001).
12. T. Kaisho *et al.*, *Int. Immunol.* **14**, 695 (2002).
13. C. M. Snapper, W. E. Paul, *Science* **236**, 944 (1987).
14. F. D. Finkelman *et al.*, *J. Exp. Med.* **174**, 1179 (1991).
15. M. F. van den Broek, U. Muller, S. Huang, M. Aguet, R. M. Zinkernagel, *J. Virol.* **69**, 4792 (1995).
16. C. M. Snapper *et al.*, *J. Exp. Med.* **175**, 1367 (1992).
17. E. A. Leadbetter *et al.*, *Nature* **416**, 603 (2002).
18. C. M. Lau *et al.*, *J. Exp. Med.* **202**, 1171 (2005).

19. We thank D. Kono and A. Theofilopoulos for comments on the manuscript, A. Rolink for FGK4.5 antibody, and G. Nemerow and N. Sarvetnick for use of instruments. Supported by NIH grants RO1GM44809 to D.N., AI050241 to B.B., and T32AI07606 to B.D.

Supporting Online Material

www.sciencemag.org/cgi/content/full/314/5807/1936/DC1
Materials and Methods
Figs. S1 to S5
Tables S1 and S2
References

19 September 2006; accepted 15 November 2006
10.1126/science.1135299

Relating Three-Dimensional Structures to Protein Networks Provides Evolutionary Insights

Philip M. Kim,[1] Long J. Lu,[1] Yu Xia,[4,5] Mark B. Gerstein[1,2,3]*

Most studies of protein networks operate on a high level of abstraction, neglecting structural and chemical aspects of each interaction. Here, we characterize interactions by using atomic-resolution information from three-dimensional protein structures. We find that some previously recognized relationships between network topology and genomic features (e.g., hubs tending to be essential proteins) are actually more reflective of a structural quantity, the number of distinct binding interfaces. Subdividing hubs with respect to this quantity provides insight into their evolutionary rate and indicates that additional mechanisms of network growth are active in evolution (beyond effective preferential attachment through gene duplication).

Protein interaction networks are principal components of a systems-level description of the cell (*1*–*4*). Many previous studies have explored global aspects of network topology, clearly linking it to protein function, expression dynamics, and other genomic features (*5*–*9*). In particular, a protein's degree (number of interaction partners) is an important factor, and proteins with high degree (hubs) have been found to be essential (*3*, *7*). However, most network studies have not considered the structural and chemical aspects of interactions; only recently have there been proposals to use structural information for systems biology (*10*). One specific problem with the current treatment is that protein interaction networks do not differentiate between many types of relationships—e.g., high-affinity and direct versus loose and transient. Sometimes,

in fact, interactions are reported that connect two proteins that never touch each other physically but are only linked through a third protein (*11*, *12*).

Here we address this problem by combining structural modeling with network analysis. In particular, we compiled a consensus yeast interaction network from various sources (*13*), filtering out low-confidence interactions by using statistical methodologies (*4*). We then annotated many of the edges in this network structurally on the basis of sequence similarity to known complexes (Fig. 1). We used simple three-dimensional (3D)–structural exclusion to distinguish the interfaces of each interaction. Consider two or more proteins interacting with a common partner protein. If they use the same interface on the partner (as known from the structures), the interactions are classified as mutually exclusive. Conversely, if they use different interfaces, the interactions are simultaneously possible (Fig. 1). The network resulting from this analysis (the structural interaction network, SIN) contains 873 nodes (proteins) and 1269 edges (interactions), 438 of which are mutually exclusive (fig. S1). It contains parts of 147 complexes, suggesting that it covers a representative range of interactions. [For the SIN data set and further discussion, see SOM Text, tables S1 and S3, and (*13*)]

After building the SIN, we examined its two different kinds of interactions with respect to the properties of the linked proteins. As shown in Table 1, proteins connected by simultaneously possible interactions are more likely to share the same function than are those connected by mutually exclusive ones [in terms of Gene Ontology (GO) cellular component, molecular function, and biological process designations]; also, they are more likely to be expressed at the same time. Consequently, we expect most of the mutually exclusive interactions to be temporary or transient, because they cannot occur at the same time. Likewise, the simultaneously possible interactions are enriched in permanent associations, connecting members of the same complex (table S4).

Turning to global statistics of the SIN, we find that it has a degree distribution with a notably shorter tail than either the complete yeast interactome or a core, filtered subset of this (fig. S2). In particular, hubs in the SIN have a maximum of 14 interaction partners. This is similar to the number of close-packed neighbors in crystal lattices (12 in hexagonal packing) and reflects the direct, physical constraints on interactions in the SIN. In contrast, in early yeast interactomes some hubs had >200 interaction partners, and even in newer data sets, >30 partners are noted for some proteins (*7*, *14*).

Within hubs in the SIN, we compared those with many physical interfaces (as detected by our approach) to those with a few—to uncouple degree from interface number (which are correlated). We defined hubs by setting an arbitrary cutoff of ≥5 interaction partners; variations in this cutoff did not affect our results (table S5). We detected differences in the properties between multi- and single-interface hubs. However, more statistically significant differences were evident if we distinguished between hubs with one or two interfaces (singlish-interface) and those with more

[1]Department of Molecular Biophysics and Biochemistry, Yale University, New Haven, CT 06520, USA. [2]Department of Computer Science, Yale University, New Haven, CT 06520, USA. [3]Program in Computational Biology and Bioinformatics, Yale University, New Haven, CT 06520, USA. [4]Bioinformatics Program, Boston University, Boston, MA 02215, USA. [5]Department of Chemistry, Boston University, Boston, MA 02215, USA.

*To whom correspondence should be addressed. E-mail: mark.gerstein@yale.edu

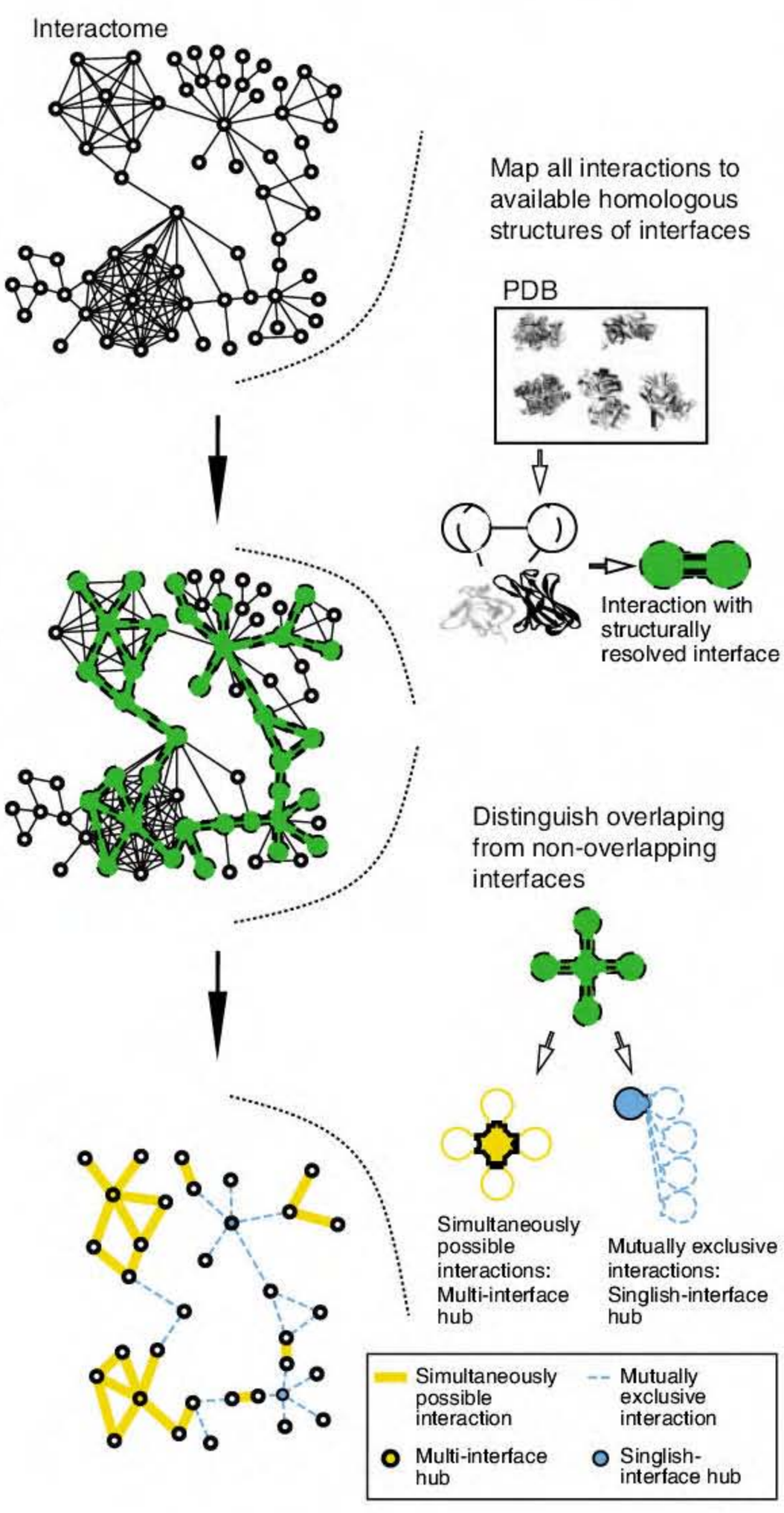

Fig. 1. The creation of the structural interaction network (SIN) data set. All interactions from the filtered protein interaction data set are mapped to Pfam domains (*30*). The Pfam domains are mapped to known structures of protein interactions by means of iPfam (*31*). Only those interactions in which both interaction partners (or a homologous domain of either) can be found in a 3D structure of a protein complex are kept. All interactions are then classified into mutually exclusive and simultaneously possible by 3D structural exclusion. When a protein has more than one simultaneously possible interaction, the number of interaction interfaces is counted.

Table 1. Differences of simultaneously possible versus mutually exclusive interactions with respect to GO annotations (shared by the interacting proteins) and coexpression correlation coefficients. GO biological process, molecular function, and cellular component are taken from SGD lite (*26*) and coexpression correlation from the compendium expression data set (*27*). All differences are significant, with $P << 0.01$.

	Simultaneously possible interactions	Mutually exclusive interactions
Fraction with same biological process	14%	24%
Fraction with same molecular function	18%	33%
Fraction with same cellular component	12%	27%
Coexpression correlation	0.17	0.23

than two interfaces (multi-interface). First, we examined the essentiality of both kinds of hubs. Although hubs in general are more likely than other proteins to be essential for cellular viability (*3*), as shown in Table 2, multi-interface hubs are twice as likely to be essential as singlish-interface ones, which, in turn, are no more likely to be essential than the average protein in the SIN. This result suggests the notion of hubs having a higher essentiality due to their network centrality is somewhat incomplete: It is the number of interaction interfaces that leads to higher essentiality.

Furthermore, Table 2 shows that multi-interface hubs are more likely to be coexpressed with their neighbors than are singlish-interface ones. This provides a straightforward structural explanation for the existence of two types of expression dynamics for hubs (*10*), date and party hubs (*7*). In particular, singlish-interface hubs seem to correspond to date hubs (which are expressed at different times than their interaction partners; table S7), and multi-interface hubs correspond to party hubs (which are expressed at the same times as their interaction partners). It is quite reasonable that the interaction partners of singlish-interface hubs are not coexpressed, because they would compete for the same binding interface. On the other hand, for the partners of multi-interface hubs, it makes sense to be expressed simultaneously, because they bind to different interfaces. Multi-interface hubs, in fact, correspond to central members of protein complexes, as is evident from cross-referencing them with known complexes (table S8). A representative multi-interface hub, for example, is Arp2p, a member of the Arp2/3 complex. Conversely, a good example for a singlish-interface hub is Snf1p, a central protein kinase (see SOM Text and table S6).

There has been some controversy over whether hubs are slower-evolving than other proteins (*15*–*18*). A commonly used measure of evolutionary rate is the *dN/dS* ratio (the ratio of nonsynonymous to synonymous substitutions, also referred to as K_a/K_s ratio). Table 2 shows that it is significantly lower for multi-interface hubs than for the average SIN protein, but not so for singlish-interface hubs. Although the dependence of evolutionary rate on protein degree has been attributed to an underlying effect of expression level (*18*), we find that the relationship of evolutionary rate to the number of interfaces is independent of expression level (whereas that to the degree is not) (fig. S4). The aforementioned controversy may have arisen because previous studies did not differentiate between singlish and multi-interface hubs. A larger number of interfaces may give rise to a lower evolutionary rate because a larger fraction of residues participate in interactions. Indeed, Fig. 2 shows that the variation in a protein's evolutionary rate can be accounted for better by changes in the fraction of its accessible surface area involved in interactions than by degree. This result can be explained simply from a structural point of view: The average mutational rate for exposed surface residues is more than twice as high as for those at an interface, which, in turn, is slightly higher than the one for buried residues (table S9) (*19*). Thus, as suggested previously (*20*) and shown in our analysis, the proportion of a protein's available surface area involved in interactions should correlate inversely with evolutionary rate.

Finally, we examined network evolution from a structural perspective. The existing scale-free network topology (the dominance of hubs) may have evolved through preferential attachment (*21*). Gene duplication is one possible cause of such an evolutionary process (*22*, *23*), but other factors, such as preferential rewiring, could contribute as well (*23*, *24*). As depicted in Fig. 3, if a hub evolves by duplication, its interaction partners are expected to be enriched in paralogs (products of homologous genes originating from within-genome duplications). As expected (*25*), we found that two proteins are significantly more likely to be

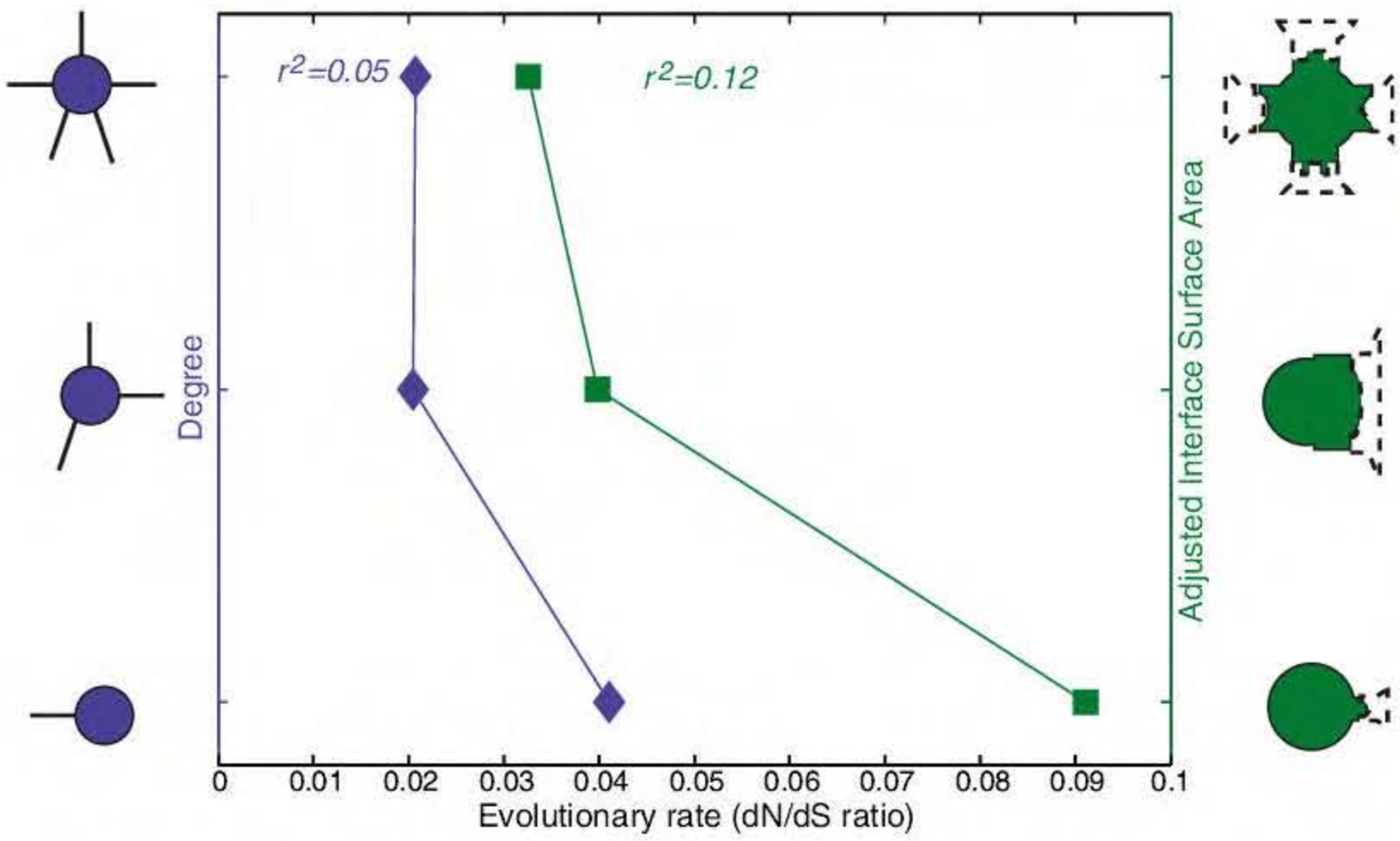

Fig. 2. Dependence of the average evolutionary rate (*dN/dS* ratio) of a protein with the degree and the interacting accessible surface area (adjusted by protein size, as estimated from molecular weight). For the degree correlation coefficient, we get $r^2 = 0.05$, and for the adjusted interface surface area, $r^2 = 0.12$, suggesting that more than twice as much of the variation in *dN/dS* is accounted for by adjusted interface surface area (12%) than by the degree (5%).

Table 2. Correlation of genomic features with singlish and multi-interface hubs. The fraction of proteins that are products of essential genes (*28*), the average expression correlation with their neighbors (*27*), and the evolutionary rate [*dN/dS* ratio, from (*29*)] was calculated for the entire proteome, the entire SIN, singlish-interface protein hubs, and multi-interface protein hubs. The *P*-values of the differences between the whole data set and the singlish interface hubs (all-singlish) and the singlish and multi-interface hubs (singlish-multi) were calculated with the Wilcoxon rank-sum test (see Methods in the SOM).

	Entire proteome	All in data set	*P*-value (all-singlish)	Singlish-interface hubs only	*P*-value (singlish-multi)	Multi-interface hubs only
Protein essentiality	18.6%	32.3%	0.9	31.8%	<0.01	64.9%
Expression correlation		0.20	0.3	0.17	<0.05	0.25
Evolutionary rate	0.077	0.047	0.5	0.051	<0.01	0.029

Table 3. Fraction of protein pairs that are paralogs of each other. Random pair: randomly chosen protein pair from our data set (average); Same partner: fraction of pairs with the same interaction partner that are paralogs; Same partner, same interface: Fraction of pairs that bind to the same interface that are paralogs; Same partner, different interface: fraction of pairs with the same interaction partner, but different interacting interface that are paralogs (calculated from the platinum standard set only; see Methods in the SOM).

	Random pair	Same partner	Same partner, same interface	Same partner, different interface
Fraction paralogs	0.23%	4.10%	8.10%	0.00%

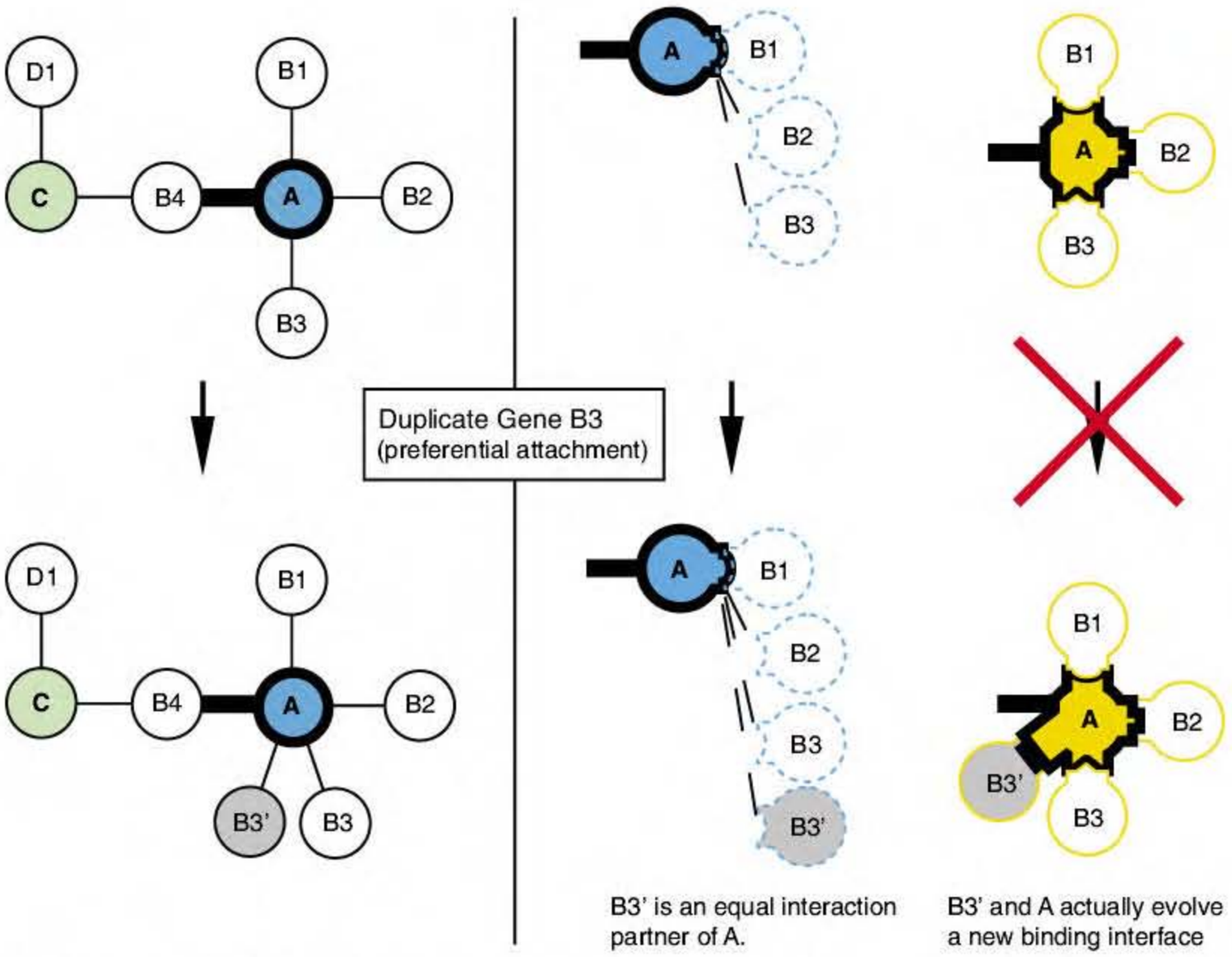

Fig. 3. The concept of network evolution by gene duplication. A given protein may acquire a new interaction by duplication of an existing one. Given equal likelihood of any gene to be duplicated, a protein with many partners is more likely to get a new partner than one with few—hence, there is effective preferential attachment. For singlish-interface hubs, this mechanism is straightforward. However, for multi-interface hubs, it would then require coevolution of the hub and the duplicated gene to form a new interface.

paralogs if they share a common partner (Table 3). However, this is true only if they also share an interaction interface. We did not find enrichment for paralogs among interaction partners binding to different interfaces (Table 3). That is, our analysis is consistent with the evolution of singlish-interface hubs through duplication-mutation, whereas it does not support such an evolution of multi-interface hubs (Fig. 3). Because multi-interface hubs are often parts of larger protein complexes, it appears that protein-complex evolution could follow a different mechanism.

From our 3D structural analysis of protein interaction networks, we find that we can distinguish two fundamentally different types of network edges. On the one hand, we find a group of interactions that are simultaneously possible and a set of multi-interface hubs associated with these. Multi-interface hubs correspond, in many respects, to our "classic" notion of network hubs. They are more likely to be essential and more conserved. They are most likely members of large and stable complexes. However, they do not follow canonical models of network evolution, growing through gene duplication. On the other hand, we find a second class of interactions, mutually exclusive ones, which have a transient character and occur in singlish-interface hubs. Singlish-interface hubs are distinctly "nonclassical": They are neither likely to be essential, nor conserved. However, in respect to network growth they do follow the canonical preferential gene duplication model.

References and Notes

1. A. L. Barabasi, Z. N. Oltvai, *Nat. Rev. Genet.* **5**, 101 (2004).
2. A. C. Gavin *et al.*, *Nature* **440**, 631 (2006).
3. H. Jeong, S. P. Mason, A. L. Barabasi, Z. N. Oltvai, *Nature* **411**, 41 (2001).
4. R. Jansen *et al.*, *Science* **302**, 449 (2003).
5. U. de Lichtenberg, L. J. Jensen, S. Brunak, P. Bork, *Science* **307**, 724 (2005).
6. R. Kelley, T. Ideker, *Nat. Biotechnol.* **23**, 561 (2005).
7. J. D. Han *et al.*, *Nature* **430**, 88 (2004).
8. I. Lee, S. V. Date, A. T. Adai, E. M. Marcotte, *Science* **306**, 1555 (2004).
9. P. M. Kim, thesis (MIT, Cambridge, MA, 2003), pp. 1–125.
10. P. Aloy, R. B. Russell, *Nat. Rev. Mol. Cell Biol.* **7**, 188 (2006).
11. P. Aloy, R. B. Russell, *Nat. Biotechnol.* **22**, 1317 (2004).
12. G. D. Bader, C. W. Hogue, *Nat. Biotechnol.* **20**, 991 (2002).
13. See supporting information on *Science* Online for details. For updates to the SIN and interactive viewing using tYNA, see http://sin.gersteinlab.org.
14. P. Uetz *et al.*, *Nature* **403**, 623 (2000).
15. H. B. Fraser, A. E. Hirsh, L. M. Steinmetz, C. Scharfe, M. W. Feldman, *Science* **296**, 750 (2002).
16. I. K. Jordan, Y. I. Wolf, E. V. Koonin, *BMC Evol. Biol.* **3**, 1 (2003).
17. S. Wuchty, *Genome Res.* **14**, 1310 (2004).
18. J. D. Bloom, C. Adami, *BMC Evol. Biol.* **3**, 21 (2003).
19. W. S. Valdar, J. M. Thornton, *Proteins* **42**, 108 (2001).
20. H. B. Fraser, A. E. Hirsh, *BMC Evol. Biol.* **4**, 13 (2004).
21. R. Albert, A. L. Barabasi, *Rev. Mod. Phys.* **74**, 47 (2002).
22. A. Vazquez, *Phys. Rev. E* **67**, 056103 (2003).
23. A. Wagner, *Proc. Biol. Sci.* **270**, 457 (2003).
24. E. Eisenberg, E. Y. Levanon, *Phys. Rev. Lett.* **91**, 138701 (2003).
25. J. Espadaler *et al.*, *Proc. Natl. Acad. Sci. U.S.A.* **102**, 7151 (2005).
26. L. Issel-Tarver *et al.*, *Methods Enzymol.* **350**, 329 (2002).
27. T. R. Hughes *et al.*, *Cell* **102**, 109 (2000).
28. G. Giaever *et al.*, *Nature* **418**, 387 (2002).
29. D. P. Wall *et al.*, *Proc. Natl. Acad. Sci. U.S.A.* **102**, 5483 (2005).
30. A. Bateman *et al.*, *Nucleic Acids Res.* **30**, 276 (2002).
31. R. D. Finn, M. Marshall, A. Bateman, *Bioinformatics* **21**, 410 (2005).

32. We thank J. Korbel, T. Gianoulis, A. Paccanaro, and H. Yu for helpful comments on the manuscript. We also thank the anonymous referees for valuable suggestions. This work was supported by the NIH. Y.X. was supported by a fellowship from the Jane Coffin Childs Memorial Fund for Medical Research.

Supporting Online Material

www.sciencemag.org/cgi/content/full/314/5807/1938/DC1
Materials and Methods
SOM Text
Figs. S1 to S4
Tables S1 to S9
References

11 October 2006; accepted 7 November 2006
10.1126/science.1136174

Characterizing a Mammalian Circannual Pacemaker

Gerald A. Lincoln,[1]* Iain J. Clarke,[2] Roelof A. Hut,[3] David G. Hazlerigg[4]

Many species express endogenous cycles in physiology and behavior that allow anticipation of the seasons. The anatomical and cellular bases of these circannual rhythms have not been defined. Here, we provide strong evidence using an in vivo Soay sheep model that the circannual regulation of prolactin secretion, and its associated biology, derive from a pituitary-based timing mechanism. Circannual rhythm generation is seen as the product of the interaction between melatonin-regulated timer cells and adjacent prolactin-secreting cells, which together function as an intrapituitary "pacemaker-slave" timer system. These new insights open the way for a molecular analysis of long-term timing mechanisms.

Endogenous circannual rhythms drive many long-term cycles in physiology and behavior in long-lived vertebrates (*1*, *2*) including reproduction (*3*), hibernation (*4*, *5*), migration (*6*), and pelage growth (*7*), but the anatomical and cellular bases of such rhythm generation remain a mystery. We investigated whether a circannual rhythm may be generated through a pituitary mechanism, itself dependent on the circadian system. We focused on the anterior pituitary control of prolactin secretion, but similar cell-cell interactions in the brain may

govern circannual rhythms for other physiological processes.

Circannual rhythms are self-sustaining under constant conditions of day length, temperature, and food supply, with a free-running period typically less than 1 year. Geophysical cues, including the annual cycle of day length (photoperiod), act to entrain the circannual rhythm to the precise 365-day periodicity of the Earth's year (*1*, *2*). Thus, many long-lived organisms use both an endogenous calendar and a day length–measuring mechanism to adjust physiological state precisely to the seasons.

In sheep, photoperiod-dependent changes in the duration of nocturnal melatonin secretion by the pineal gland synchronize circannual rhythms to time of year (*8*). Pinealectomy blocks photoperiodic responsiveness and leads to expression of variable and asynchronous long-term rhythms, whereas appropriate replacement with exogenous melatonin mimics the synchronizing effect of photoperiod. Melatonin replacement to simulate only a part of the overall annual cycle is sufficient to induce synchronous circannual rhythms (*9*). Short-duration daily melatonin signals (8 hours/day) given for 3 months once a year are notably more effective than long-duration melatonin signals (16 hours/day). This indicates that the summer photoperiod is the important zeitgeber for the circannual reproductive rhythm.

The neuroanatomical basis of melatonin-mediated photoperiodic control is well defined (*10*). In sheep and hamsters, melatonin acts within the hypothalamus to mediate control of seasonal changes in gonadotrophin secretion and gonadal activity and acts within the pars tuberalis (PT) of the pituitary gland to control prolactin secretion and its dependent biology. This differential control is strongly supported by studies in hypothalamopituitary-disconnected (HPD) Soay sheep, where ablation of the neural input to the median eminence and arcuate nucleus blocks the photoperiodic control of the reproductive and metabolic axes but spares the control of prolactin secretion, because of a direct action of melatonin within the pituitary gland (*11*, *12*). The HPD sheep thus provides a unique in vivo model for the study of pituitary gland function in the absence of complex neural inputs from the brain (*13*).

We investigated whether HPD sheep exhibit a circannual rhythm of prolactin secretion under a constant photoperiod, with the aim of localizing a circannual timer mechanism. HPD Soay rams were preconditioned to short photoperiod (SP) (8 hours light/day) for 16 weeks to entrain the seasonal physiology to a winter state with low blood concentrations of prolactin. The animals were then released into constant long summer photoperiod (LP) (16 hours light/day) for 144 weeks (Fig. 1). This period was selected to cover, potentially, three repeated circannual cycles.

The transfer to LP caused an initial synchronous increase in prolactin concentrations. This was followed by a robust cyclical decline and reactivation in prolactin release that persisted throughout the 144-week study. The oscillations dampened in amplitude and became asynchronous (Fig. 1B). The period of this free-running prolactin rhythm, determined by a nonlinear sine wave regression procedure (*13*), ranged from 37.6 to 46.9 weeks (mean of 40.9, SD of 2.8 weeks, $n = 10$). The mean period was significantly (one-sample t test; $P < 0.0001$) different from the period of the sidereal year (*13*). There was a periodic "spring" molt of the pelage (recorded for the scrotal hair) following each cycle of increasing blood prolactin concentrations (Fig. 1A), consistent with the known role of prolactin in the dermal papilla (*10*). The molt cycle became progressively less clearly defined in parallel with the dampening of the prolactin rhythm. The testes of the HPD rams remained permanently regressed, and there was no overt cyclicity in other seasonal characteristics, as previously observed after pituitary disconnection (*11*, *13*)

The daily blood melatonin rhythm was measured at regular intervals, and locomotor activity patterns were recorded continuously throughout the 144 weeks under constant LP (*13*). There was no significant ($P > 0.05$, analysis of variance) change either in the duration of the nocturnal melatonin peak or in the amplitude of the maximum 24-hour melatonin concentration recorded at eight different sampling occasions under LP. Locomotor activity was consistently diurnal, and there was no evidence of a change in the behavioral patterns with time under LP, or related to the progression of the circannual prolactin cycles. Thus, the circannual rhythm in prolactin secretion in HPD animals is not accompanied by any detectable changes in circadian rhythmicity.

In a second experiment, we tested whether an abrupt change in photoperiod would reset the circannual rhythm. The same HPD animals from experiment 1 were switched to SP (8 hours light/day) for 8 weeks and then reexposed to continual LP (16 hours light/day). The resulting prolactin patterns are shown in Fig. 2A. The exposure to SP induced a rapid decline in prolactin concentrations within a week in all animals, and values remained low during the 8-week treatment. The release back into LP reactivated a robust prolactin response and a high-amplitude prolactin rhythm with a corresponding pelage molt in most animals, very similar to that seen at the start of experiment 1 (Fig. 2A). Analysis of the phase of the new circannual rhythm after 8 weeks of SP, assessed by the sine wave regression procedure, revealed that full reentrainment had occurred. The new phase was not dependent on the phase imme-

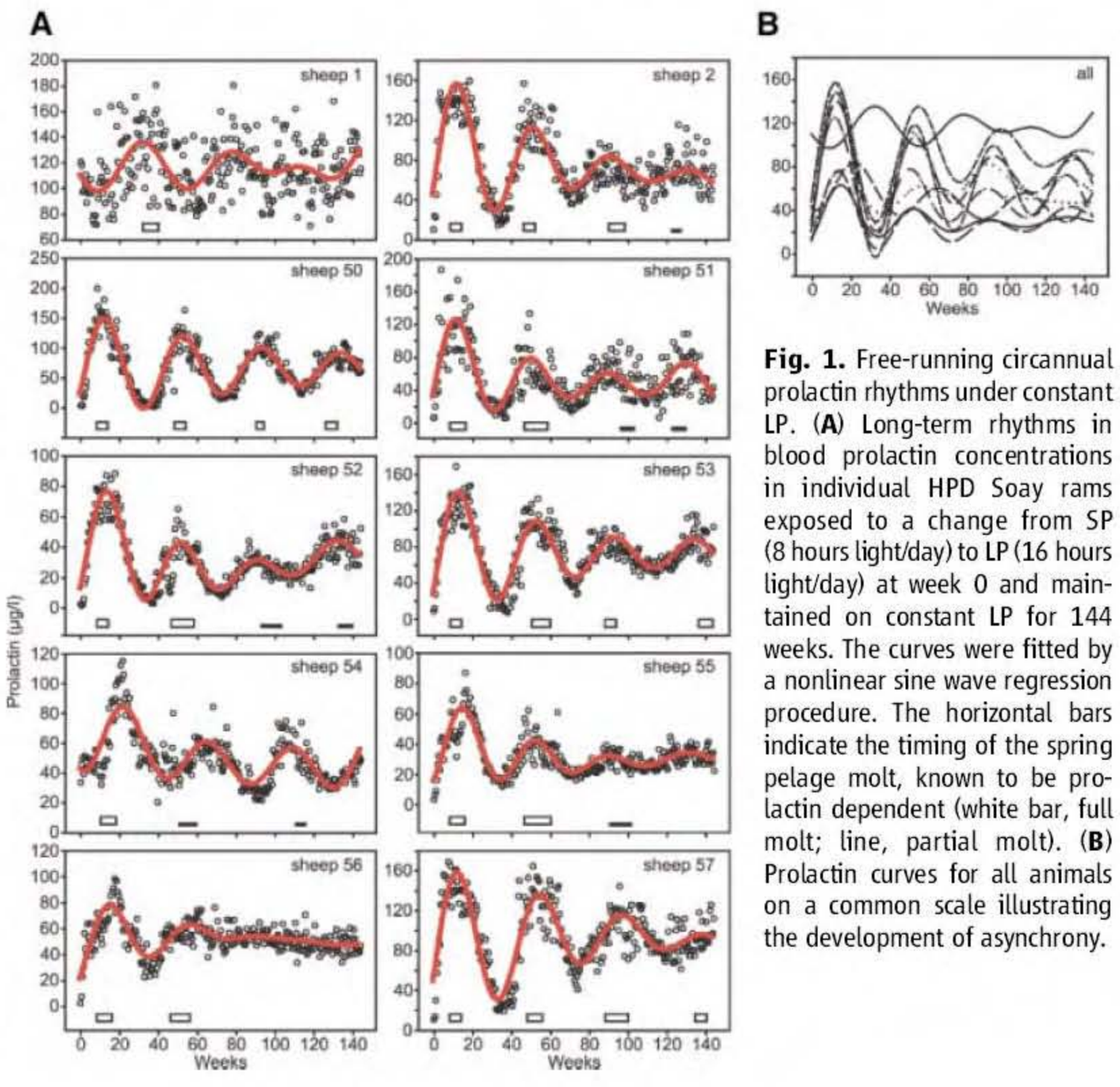

Fig. 1. Free-running circannual prolactin rhythms under constant LP. (**A**) Long-term rhythms in blood prolactin concentrations in individual HPD Soay rams exposed to a change from SP (8 hours light/day) to LP (16 hours light/day) at week 0 and maintained on constant LP for 144 weeks. The curves were fitted by a nonlinear sine wave regression procedure. The horizontal bars indicate the timing of the spring pelage molt, known to be prolactin dependent (white bar, full molt; line, partial molt). (**B**) Prolactin curves for all animals on a common scale illustrating the development of asynchrony.

[1]Centre for Reproductive Biology, University of Edinburgh, The Queen's Medical Research Institute, Edinburgh, Scotland. [2]Department of Physiology, Monash University, Melbourne, Australia. [3]Department of Chronobiology, University of Groningen, Haren, Netherlands. [4]School of Biological Sciences, University of Aberdeen, Aberdeen, Scotland.

*To whom correspondence should be addressed. E-mail: g.lincoln@hrsu.mrc.ac.uk

diately before SP exposure (Fig. 2B). This "type 0" resetting characteristic (*14*) indicates that the circannual oscillator expressed in the sheep is highly labile to altered photoperiodic input.

The pronounced effects of photoperiod on prolactin secretion in the HPD sheep are mediated by altered melatonin secretion (*11*). We therefore investigated whether the pineal melatonin signal is necessary for the expression of a circannual prolactin rhythm under constant photoperiod. In a new group of HPD Soay rams, the rhythmic secretion of melatonin was permanently blocked by superior cervical ganglionectomy, a procedure that denervates the pineal gland (*15*). The absence of a nocturnal increase in melatonin concentrations in these "HPDX" animals was confirmed by radioimmunoassay. The groups (HPD and HPDX) were exposed to a change from LP (16 hours light/day) to SP (8 hours light/day), and after 16 weeks returned to LP for 96 weeks. The standard HPD sheep showed the expected increase in blood prolactin concentrations under LP and a decrease in response to SP, with rapid transitions. The switch to constant LP produced a robust circannual prolactin oscillation, with two full cycles completed within 88 weeks (Fig. 3A). The removal of melatonin in the HPDX sheep disrupted both the initial photoperiodic response and the long-term expression of circannual prolactin rhythms (Fig. 3A). Alignment of the prolactin profiles to the time of the HPDX operation revealed that the loss of the LP melatonin signal because of the surgery caused an immediate and progressive decline in prolactin concentrations followed by partial recovery. This is akin to that seen in HPD animals transferred from LP to SP or given a constant-release melatonin implant (*16*) (Fig. 3B). Thereafter, prolactin concentrations remained in the intermediate range, with a variable long-term pattern in the individual animals. There was no consistent residual prolactin rhythm with a period close to 40 weeks and no regular pelage molt in the HPDX animals. Hence, an invariant LP melatonin signal is required for the expression of a robust, circannual prolactin rhythm in HPD sheep. This inference contrasts with the observations of Thrun and colleagues (*17*), who suggested that variability in melatonin secretion during continuous exposure to SP might lead to expression of circannual variation in reproductive status.

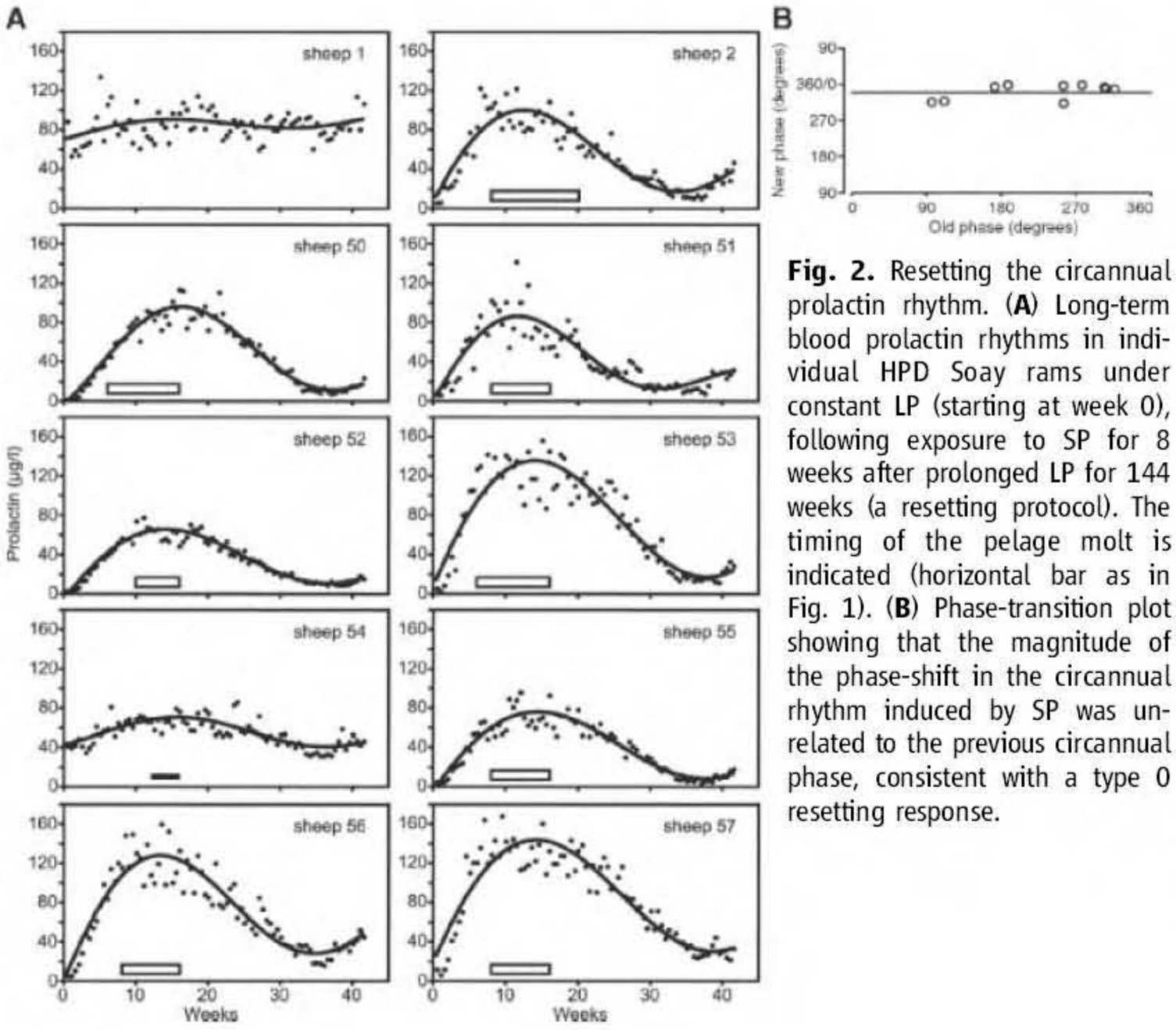

Fig. 2. Resetting the circannual prolactin rhythm. (**A**) Long-term blood prolactin rhythms in individual HPD Soay rams under constant LP (starting at week 0), following exposure to SP for 8 weeks after prolonged LP for 144 weeks (a resetting protocol). The timing of the pelage molt is indicated (horizontal bar as in Fig. 1). (**B**) Phase-transition plot showing that the magnitude of the phase-shift in the circannual rhythm induced by SP was unrelated to the previous circannual phase, consistent with a type 0 resetting response.

It has been suggested that circannual rhythms emerge as a subharmonic of circadian rhythms through "frequency demultiplication" (*1*). This idea has not gained favor, however, as the period of circannual rhythms appears to be independent of the period of the daily light-dark cycle on which animals are held (*1*, *18*, *19*). Given these findings, we prefer a model in which the dependence of the circannual prolactin rhythm on the circadian melatonin signal reflects a permissive requirement for circadian input. Thus, the circadian melatonin signal is required for circannual behavior to emerge, but does not determine the period of that behavior.

Two types of mechanism can be invoked to account for the generation of a circannual rhythm in the HPD sheep. The first is one in which the pituitary cells are driven by a timer in the brain or elsewhere that is responsive to pineal melatonin and that produces a rhythmical signal to control the pituitary gland. The pituitary is thus downstream from the putative circannual pacemaker. The second mechanism is where the timer exists within the pituitary gland and melatonin acts directly in the pituitary tissues. The latter model is consistent with the data from the HPD sheep where the surgery isolates the pituitary gland and blocks all known hypothalamopituitary-dependent changes in seasonal physiology (*13*). Melatonin receptors

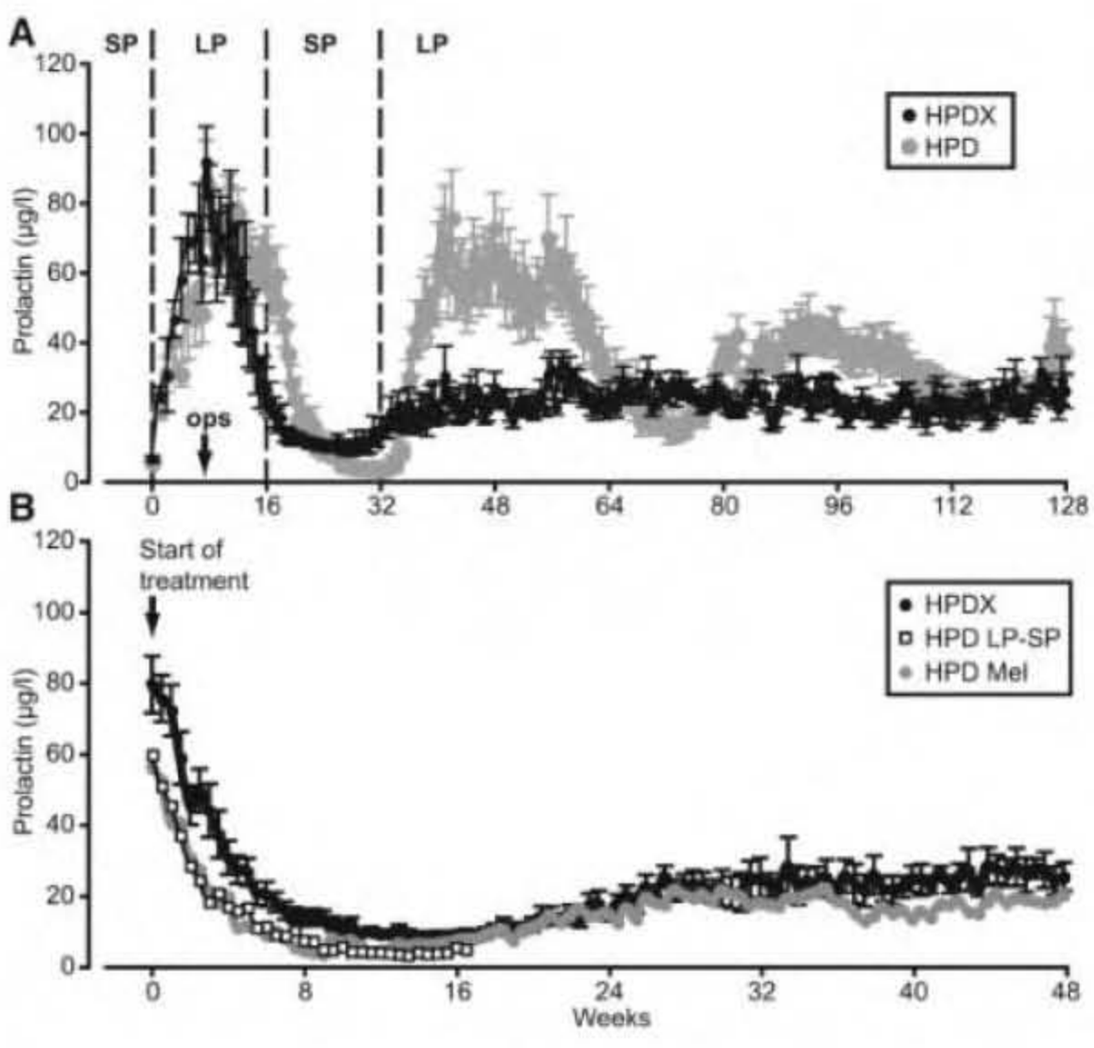

Fig. 3. Effect of removing the melatonin signal on circannual rhythmicity. (**A**) Long-term blood prolactin rhythms in HPD and HPDX Soay rams exposed to changes between SP and LP and then maintained under prolonged LP for 96 weeks. The time of the surgical operations is indicated (ops, arrow). Removal of the melatonin signal blocked both photoperiod responsiveness and circannual rhythm generation. (**B**) Blood prolactin concentrations in HPD Soay sheep aligned to the time of treatment comparing the effects of removal of melatonin (HPDX), transfer from LP to SP (HPD LP-SP), and treatment with a subcutaneous melatonin implant (HPD Mel) (*16*). All three treatments effectively blocked the LP melatonin signal and produced a similar winter-like default response.

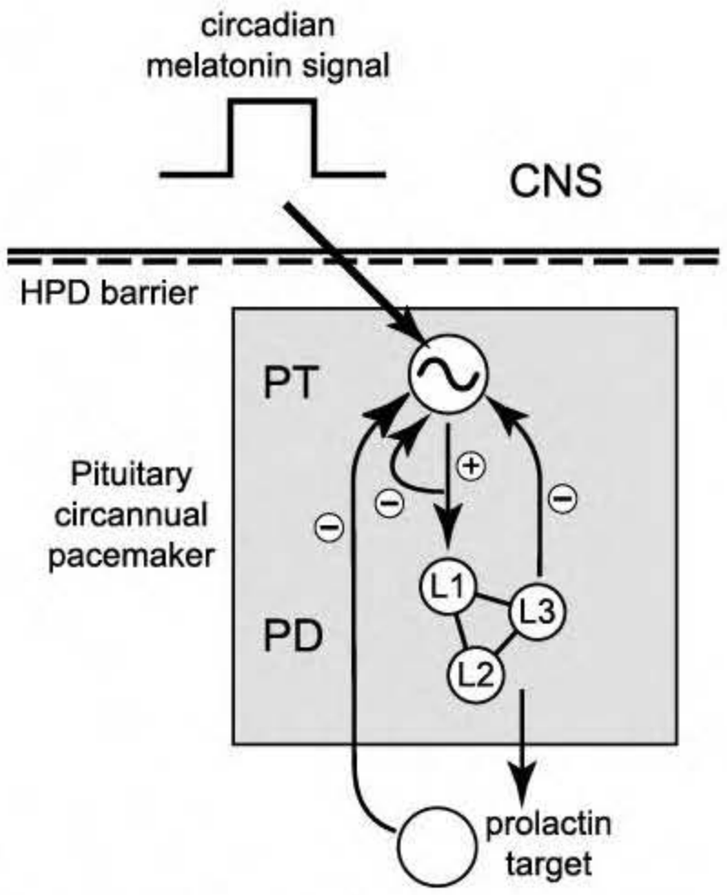

Fig. 4. Working hypothesis for a tissue autonomous circannual timer. The model proposes a pacemaker-slave mechanism operating within the pituitary gland. The pacemaker is the PT cell that receives circadian gating through the nocturnal melatonin signal, by means of the melatonin MT_1 receptor, and has interval timer properties. The slave is the PD lactotroph cell that has stochastic and heterogeneous properties and must be synchronized as a population of cells by a positive stimulus from the PT. The propagation of circannual oscillation is presumed to depend on feedback signals with long time-delays.

are highly expressed in the PT of the pituitary gland in HPD sheep, as in the normal animal (*20*), and can thus act as the local target for melatonin. The PT produces a prolactin-releasing factor modulated by melatonin that regulates the synthesis and release of prolactin by the lactotrophs that are located in the adjacent pars distalis (PD) of the pituitary gland (*21*). The local administration of melatonin close to the PT in sheep, using microimplants or programmed infusions, markedly affects prolactin secretion, with rapid suppression and slow recovery after 8 to 12 weeks, paralleling the change seen in response to SP (*10*). These treatments produce no detectable increase in the concentration of melatonin in the peripheral circulation. The result provides the strongest support for a localized timer mechanism within the pituitary. Other studies demonstrate that prolonged exposure to a fixed photoperiod produces changes in PT function [glycoprotein hormone, subunit α, and thyroid-stimulating hormone, subunit β, gene expression (*22*, *23*)] and in prolactin-releasing factor production (*21*) that preempt the endogenous cycle in prolactin secretion. This indicates that it is PT cells that drive the cycle in the lactotrophs.

We propose that the intrapituitary communication between PT photoperiod-relay cells and PD lactotroph cells is central to the propagation of a circannual prolactin rhythm. This is illustrated schematically in our working model for circannual rhythm generation within the pituitary gland (Fig. 4). We know that the nocturnal melatonin signal regulates circadian rhythms in clock gene expression in the mammalian PT (*24*, *25*), and that clock gene rhythmicity continues to reflect the ambient light-dark cycle, even during prolonged photoperiod treatments when photorefractoriness develops (*22*, *26*). This indicates that control depends on a stable melatonin signal and that the melatonin rhythm may be permissive because of its gating effect on processes in the PT that depend on clock gene expression. By contrast, endogenous changes in the PT appear to drive the circannual cycle in prolactin secretion. Moreover, we have shown that temporarily blocking prolactin secretion with bromocriptine fails to perturb the phase of this endogenous cycle (*27*). This favors our view that the PT cell may be the circannual pacemaker for this system (Fig. 4).

Lactotrophic cells are known to exhibit stochastic variability in prolactin gene expression and secretion over circadian and noncircadian time scales (*28*, *29*), and the heterogeneous population of lactotrophs is known to be activated by LP by means of a PT prolactin-releasing factor (*30*). We therefore propose that the function of the PT cells is to provide a coordinating signal for the lactotroph population that generates a slave response (Fig. 4). According to this hypothesis, ablation of the melatonin signal results in desynchronized activity within the lactotroph population, accounting for the winter-like default pattern in prolactin secretion, as well as loss of coordinated circannual rhythmicity, as observed in the HPDX animals (Fig. 3). Further studies will be required to determine whether long-term rhythmicity is an intrinsic property of the melatonin-regulated PT cells or whether it emerges through feedback interactions within the pituitary, or possibly involves peripheral prolactin target tissues.

References and Notes

1. E. Gwinner, *Circannual Rhythms: Endogenous Annual Clocks in the Organization of Seasonal Processes* (Springer-Verlag, Berlin, 1986).
2. I. Zucker, in *Handbook of Neurobiology*, vol. 12, J. S. Takahashi, F. W. Turek, R. Y. Moore, Eds. (Kluwer Academic/Plenum, New York, 2001), pp. 509–528.
3. F. J. Karsch, J. E. Robinson, C. J. I. Woodfill, *Biol. Reprod.* **41**, 1034 (1989).
4. E. T. Pengelly, S. J. Amundson, in *Circannual Clocks*, E. T. Pengelly, Ed. (Academic Press, New York, 1974), pp. 89–98.
5. N. Kondo *et al.*, *Cell* **125**, 161 (2006).
6. E. Gwinner, in *Frontiers of Life*, vol. 4, D. Baltimore, Ed. (Academic Press, New York, 2001), pp. 193–206.
7. L. Martinet, M. Mondain-Monval, R. Monnerie, *J. Reprod. Fertil.* **95**, 325 (1992).
8. B. Malpaux, M. Migaud, H. Tricoire, *J. Biol. Rhythms* **16**, 336 (2001).
9. C. J. I. Woodfill, N. L. Wayne, S. M. Moenter, *Biol. Reprod.* **50**, 965 (1994).
10. G. Lincoln, *Adv. Exp. Med. Biol.* **460**, 137 (1999).
11. G. A. Lincoln, I. J. Clarke, *J. Neuroendocrinol.* **6**, 251 (1994).
12. G. A. Lincoln, M. Richardson, *Comp. Biochem. Physiol. Part C Pharmacol. Toxicol. Endocrinol.* **119**, 283 (1998).
13. Supporting Online Material provides details of the hypothalamopituitary disconnection (HPD) sheep model (summary diagram, fig. S1), current materials and methods for the animals, experimental design, hormone assays and sine-wave analysis, results for melatonin rhythms and locomotor activity patterns in the sheep during prolonged exposure to LP (fig. S2), and results for the circannual rhythm analysis (two tables).
14. Y. Miyazaki, T. Nisimura, H. Numata, *J. Comp. Physiol. A Neuroethol. Sens. Neural. Behav. Physiol.* **191**, 883 (2005).
15. G. A. Lincoln, E. A. Libre, G. R. Merriam, *J. Reprod. Fertil.* **85**, 687 (1989).
16. G. A. Lincoln, I. J. Clarke, *Biol. Reprod.* **57**, 460 (1997).
17. L. A. Thrun, S. M. Moenter, D. O'Callaghan, *J. Biol. Rhythms* **10**, 42 (1995).
18. M. S. Carmichael, I. Zucker, *J. Biol. Rhythms* **1**, 277 (1986).
19. T. Nisimura, H. Numata, *Biol. Rhythm Res.* **33**, 255 (2002).
20. L. M. Williams *et al.*, *J. Neuroendocrinol.* **9**, 639 (1997).
21. J. A. Stirland *et al.*, *J. Neuroendocrinol.* **13**, 147 (2001).
22. G. A. Lincoln, J. D. Johnston, H. Andersson, *Endocrinology* **146**, 3782 (2005).
23. T. M. Bockers *et al.*, *Endocrinology* **138**, 4101 (1997).
24. D. G. Hazlerigg, H. Andersson, J. D. Johnston, *Curr. Biol.* **14**, 334 (2004).
25. A. Jilg *et al.*, *Eur. J. Neurosci.* **22**, 2845 (2005).
26. J. D. Johnston *et al.*, *FASEB J.* **17**, 810 (2003).
27. G. A. Lincoln, H. Andersson, I. J. Clarke, *Biol. Reprod.* **69**, 1416 (2003).
28. D. W. McFerran *et al.*, *Endocrinology* **142**, 3255 (2001).
29. G. M. Lederc, F. R. Boockfor, *Endocrinology* **146**, 2782 (2005).
30. J. D. Johnston, J. A. Stirland, M. R. White, *Gen. Comp. Endocrinol.* **134**, 182 (2003).

31. We dedicate this scientific contribution to the late Norah Anderson, who devoted a career to the Soay Sheep Research Programme and cared for the animals in the current study. We thank M. Thompson, I. Swanston, and I. Cooper for expert technical help, T. Pinner for the art work, and J. Johnston for constructive comments on the manuscript. The U.K. Medical Research Council provided the long-term funding.

Supporting Online Material

www.sciencemag.org/cgi/content/full/314/5807/1941/DC1
Materials and Methods
Figs. S1 and S2
Tables S1 and S2
References

3 July 2006; accepted 10 November 2006
10.1126/science.1132009

GPC Module

The GPCmax is an integrated pump, autosampler, and degasser module designed for gel permeation chromatography (GPC) applications. It mates seamlessly with Viscotek's Triple Detector Array, Dual Detector, or any concentration detector to form a complete GPC system. The GPCmax features a fixed loop autosampler capable of handling 2-ml or 20-ml vials (eliminating the need for sample transfer) and an isocratic pump for constant and pulseless solvent flow. The pump and autosampler can be programmed manually using the front instrument panel or through ViscoTek's OmniSEC software. The instrument comes equipped with an in-line solvent degasser to remove dissolved gasses and allow optimum performance of concentration, viscosity, and light-scattering detectors.

Viscotek For information 800-375-5966 www.viscotek.com

Microdialysis Systems

Two new methods for analysis of microdialysis perfusates will enable neuroscience researchers to achieve greater sensitivity more rapidly and efficiently. In the first method, researchers can measure norepinephrine, dopamine, and serotonin simultaneously with no interference. ESA's single chromatographic system provides simultaneous quantification of the three analytes in a single sample, making more efficient use of each sample and enabling researchers to obtain information about multiple pathways in a single analysis. In the other method, researchers can measure dopamine and serotonin together in less than four minutes at high sensitivity.

ESA Biosciences For information 978-250-7000 www.esainc.com

Hotplates and Magnetic Stirrers

The H4000 series of hotplates and magnetic stirrers features a durable, chemical-resistant ceramic work surface. Stirring speed (60 to 1500 rpm) and temperature (ambient +5 to 380 °C) are conveniently controlled with the advanced microprocessor and fine adjustment knobs. Designed to fit almost anywhere, their footprint is only 8 inches by 9 inches. The square 7.5-inch white ceramic work surface is durable, easy to clean, and compatible with a wide variety of popular sizes of glass beakers, flasks, bottles, and other vessels.

Biomega Research Products For information 908-769-5555 www.BiomegaResearch.com

mRNA Production

The mScript mRNA Production System provides researchers with a fast and simple method for producing superior eukaryotic messenger RNAs (mRNAs). Incorporating an in vitro transcription system, capping enzymes, and RNA poly(A) tailing reagents, the kit contains everything a researcher needs to produce transfection or microinjection-ready mRNA. The system provides the advantages of 100% capped messages, 100% proper cap orientation, and the natural Cap 1 structure, all of which increase in vivo mRNA translation efficiency.

Epicentre Biotechnologies For information 800-284-8474 www.EpiBio.com/mScript.asp

Gel-Imaging Systems

The Geliance series is a new line of high-performance bio-imaging systems for fluorescence and chemiluminescence applications. The instruments offer top-of-the-line optical performance, with easy-to-use hardware and software to provide researchers a choice of optics and lighting options for DNA, RNA, and protein chemiluminescent and fluorescent experiments. The series offers many integrated features for increasing productivity, including real-time image capture, which enables images to be instantly printed or analyzed. The Geliance 200 Imaging System is an affordable, advanced resolution system for one-dimensional documentation and analysis. It has a standard 1.4-megapixel camera, providing a wide range of capabilities for fluorescent stains. The Geliance 600 Imaging System is a high-performance, 1.4 megapixel, 16-bit-cooled charge-coupled device camera system for fluorescence and chemiluminescence applications. Its innovative design allows for a choice of optics and lighting options, allowing clear images of even faint luminescence for a wide range of applications.

PerkinElmer For information 781-431-4306 www.perkinelmer.com/geliance

Largescale Protein Production

The FreeStyle MAX System is designed for largescale protein production in the preferred cell lines for a number of biopharmaceutical and pre-clinical applications. This protein production system was developed for rapid generation of post-translationally modified, functional proteins of Chinese hamster ovary (CHO) and HEK-293 suspension cell cultures. It is the first commercially available largescale transient transfection system optimized with CHO suspension culture—the preferred cell line for preclinical testing and producing Food and Drug Administration-approved protein for therapeutic applications. Using suspension cultures and transient transfection methods, researchers can generate significantly higher levels of protein in the preferred cell lines for these applications in days, compared with months required for generating stable cell lines.

Invitrogen For information 800-955-6288 www.invitrogen.com/bioproduction783K

For more information visit Product-Info, *Science*'s new online product index at *http://science.labvelocity.com*

From the pages of Product-Info, you can:
- Quickly find and request free information on products and services found in the pages of *Science*.
- Ask vendors to contact you with more information.
- Link directly to vendors' Web sites.

Newly offered instrumentation, apparatus, and laboratory materials of interest to researchers in all disciplines in academic, industrial, and government organizations are featured in this space. Emphasis is given to purpose, chief characteristics, and availability of products and materials. Endorsement by *Science* or AAAS of any products or materials mentioned is not implied. Additional information may be obtained from the manufacturer or supplier by visiting www.science.labvelocity.com on the Web, where you can request that the information be sent to you by e-mail, fax, mail, or telephone.

POSITIONS OPEN

LIMNOLOGIST
ASSISTANT PROFESSOR, TENURE TRACK
Academic Year 100 Percent

The Department of Biology, University of Wisconsin, La Crosse, invites applications for an academic year, tenure-track position at the level of Assistant Professor. The successful candidate will teach limnology, water quality analysis, and develop a course in her/his area of expertise (biogeochemistry or large river ecology desirable), and participate in teaching introductory biology courses. Applicants must have a strong commitment to undergraduate education. A Ph.D. in a biological science is required. Some previous teaching experience is desirable. The successful candidate will be expected to develop an externally funded research program and direct undergraduate and graduate (M.S.) research. Academic year salary competitive and commensurate with experience. Start August 27, 2007. Applicants should submit letter of application, curriculum vitae, statements of teaching philosophy and research interests, graduate and undergraduate transcripts, and three letters of recommendation to: **Dr. Mark Sandheinrich, Department of Biology, University of Wisconsin-La Crosse, La Crosse, WI 54601.** Applications must be received by February 23, 2007, and electronic applications will not be accepted. *As an Affirmative Action/Equal Opportunity Employer, the University of Wisconsin, La Crosse, is engaged in an effort to be a leader in Wisconsin's movement toward increased diversity and indusiveness. Women, persons of color, and individuals with a disability are encouraged to apply. If you have a special need/accommodation to aid your participation in our hiring process, please contact* ***Mark Sandheinrich (e-mail: sandhein.mark@uwlax.edu)*** *to make appropriate arrangements.*

FACULTY POSITIONS AT THE UNIVERSITY OF VIRGINIA

A newly established Center for Molecular Design, emphasizing the identification and usage of new chemical tools, together with the Department of Pharmacology, seek to fill two faculty positions (open rank). Individuals conducting research in the broad areas of chemical biology and drug discovery of nuclear receptors or other drug targets are encouraged to apply. Ph.D. required in pharmacology, chemistry, biochemistry, or related discipline. The successful applicant will be provided with an attractive startup package, including laboratory space within Pharmacology **(website: http://www.healthsystem.virginia.edu/internet/pharmacology/)** and access to core facilities. To apply send curriculum vitae, research plan with names and addresses of at least three references (including e-mail address and telephone number) to: **Pharmacology Search Committee, Department of Pharmacology, University of Virginia, P.O. Box 800735, Charlottesville, VA 22908-0735 (e-mail: pharmsearch@virginia.edu).** Review of applications will begin January 15, 2007; however, the position will remain open until filled. *The University of Virginia is an Equal Opportunity/Affirmative Action Employer.*

ASSISTANT PROFESSOR OF BIOLOGY, University of South Carolina, Sumter, tenure track beginning fall 2007. Ph.D. required, preferably in plant biology. Twelve hours/semester all undergraduate; expectations include excellence in teaching and potential for research/scholarship. Ability to teach introductory and intermediate biology courses, and botany with accompanying field work to majors and nonmajors. May apply online at **website: http://uscjobs.sc.edu** or submit application letter (should describe the applicant's record, philosophy of teaching, and professional goals and interests), curriculum vitae, three current letters of recommendation, copies of all undergraduate and graduate transcripts, writing samples, and summary of teaching evaluations, or other evidence of excellence in teaching. Send materials to: **Dr. James E. Privett, Chair, Division of Science, Math, and Engineering, University of South Carolina, Sumter, 200 Miller Road, Sumter, SC 29150-2498.** Review of credentials will begin immediately. *Foreign nationals indicate current U.S. immigration status. Affirmative Action/Equal Opportunity Employer.*

POSITIONS OPEN

ASSISTANT PROFESSOR, ANATOMY AND PHYSIOLOGY

The Biology Department at the University of Nevada, Reno, seeks a faculty member for a state-funded **CONTINUING LECTURER** position at the level of Assistant Professor. This nontenure track, 12-month position, which starts August 2007, will teach human anatomy and physiology courses, comparative physiology, and another course such as endocrinology, cardiovascular, or introductory biology. Responsibilities include teaching two or more courses per semester, including summer semester, supervision of the anatomy and physiology laboratories, and Department service responsibilities. We seek an outstanding and enthusiastic Educator who is eager to interact with students. The Department has about 640 majors and 23 state-funded faculty. Reno, Nevada, sits on the eastern flank of the Sierra Nevada range, offers outstanding opportunities for outdoor recreation, and was recently rated one of the best small cities in the United States for overall quality of life. Minimum qualifications include an earned Ph.D. in biology, physiology, or related discipline, and previous teaching experience at the college level in a faculty position or as a graduate assistant. Applicants should apply online with curriculum vitae, letter of application, and statement of teaching philosophy. Also, three letters of recommendation should be sent to: **Dr. Carol Ort, Anatomy and Physiology Lecturer Search, Department of Biology/314, University of Nevada, Reno, NV 89557.** For complete position announcement and requirements, visit **website: http://jobs.unr.edu.** Applications received by February 2, 2007, will receive full consideration.

Equal Employment Opportunity/Affirmative Action. Women and underrepresented groups are encouraged to apply.

FACULTY POSITION IN MOLECULAR MICROBIOLOGY

The Department of Biological Sciences, University of Wisconsin, Milwaukee (UWM), invites applications for a faculty position in molecular microbial physiology at the **ASSISTANT, ASSOCIATE, or FULL PROFESSOR** level. Candidates conducting genome-sequence enabled research using model prokaryotic systems are especially encouraged to apply. The successful candidate will be expected to be an integral member of the microbiology and biotechnology group, develop an extramurally funded research program and contribute to the education of undergraduate and graduate (M.S. and Ph.D.) students.

Applicants must have a Ph.D. degree and postdoctoral experience. Applicants should submit curriculum vitae, a statement of research and teaching goals, and up to five recent reprints, and arrange to have three letters of recommendation sent to: **Chair of the Molecular Microbiology Search Committee, Department of Biological Sciences, University of Wisconsin-Milwaukee, P.O. Box 413, Milwaukee, WI 53201.** Review of applications will commence on February 1, 2007, and continue until the position is filled. More detailed information about this position, UWM, and the Department may be found at **website: http://www.uwm.edu/Dept/Biology/.** *The University of Wisconsin, Milwaukee, is an Equal Opportunity/Affirmative Action Employer.*

ORNITHOLOGIST. The University of Texas, Brownsville/Texas Southmost College (UTB/TSC) invites applications for a tenure-track position of avian ecology in the Department of Biological Sciences. Applicants must have a Ph.D. in a related field. Preference will be given to applicants with experience in the application of geographic information system in ecological studies, postdoctoral research, and teaching experience. Successful candidates will be expected to develop an extramurally funded research program and participate in both graduate and undergraduate programs in areas relevant to his/her expertise. To apply, submit curriculum vitae, copies of official transcripts, statements of research and teaching interests, and three letters of reference to: **Dr. Luis Colom, Chair, Department of Biology, LHSB 2.816, University of Texas Brownsville/Texas Southmost College, 80 Fort Brown, Brownsville, TX 78520.**

Positions @ NIH

THE NATIONAL INSTITUTES OF HEALTH

NIDDK

Postdoctoral Fellowship in Chemical Biology
Laboratory of Bioorganic Chemistry

The Laboratory of Bioorganic Chemistry, NIDDK, NIH, has fully funded postdoctoral positions available in the areas of chemical genetics, medicinal chemistry and proteomics. Research projects will focus on identifying novel protein substrates and small-molecule inhibitors of histone acetyltransferase (HAT) enzymes, which are key regulators of eukaryotic gene expression. Prospective candidates must have obtained a Ph.D. within the past four years, be highly motivated and have demonstrated experience in any or all of the following: synthetic organic/medicinal chemistry, protein biochemistry and proteomics. Located on the main NIH campus in Bethesda, MD, the NIDDK provides excellent opportunities for collaborative interactions with other research laboratories and access to advanced facilities dedicated to chemical biology, genomics, mass spectrometry and the NIH Chemical Genomics Center (NCGC).

Applicants should send a letter stating their research interests and goals, a CV including bibliography, and arrange for three letters of reference to be sent directly or by email to Dr. Hans Luecke, LBC/NIDDK/NIH, 9000 Rockville Pike, Bldg. 8, Room B2-A05, Bethesda, MD 20892, lueckeh@niddk.nih.gov

Department of Health and Human Services
National Institutes of Health
Clinical Center

Tenure-track Physician
Clinical Center/Nuclear Medicine Department

This position is located in The Warren G. Magnuson Clinical Center, Nuclear Medicine Department (NMD).

We are seeking a research-oriented physician for a possible tenure-track position. An M.D. or M.D. /PhD with U.S. Nuclear Medicine Board certification and CT training is needed to provide diagnostic and therapeutic nuclear medicine procedures as well as to participate in clinical research protocols of the NIH Intramural Program. U.S. citizenship or permanent residency status is required.

Please submit your curriculum vitae, bibliography, and a letter describing your clinical, research, and management experience to: **Mrs. Veronica Olaaje, HR Specialist, DHHS, NIH, OD/CSD-E, 2115 E. Jefferson Street, Rm. 2B209 MSC-8503, Bethesda, MD 20892-8503. Phone: 301-435-4748. Email: volaaje@mail.nih.gov**.

Salary is commensurate with experience. This appointment offers a full benefits package (including retirement, health, life and long term care insurance, Thrift Savings Plan participation, etc.). Application packages should be submitted as early as possible, but no later than **December 31, 2006**.

Selection for this position will be based solely on merit, without discrimination for non-merit reasons such as race, color, religion, sex, national origin, politics, marital status, sexual orientation, physical or mental handicap, age or membership or non-membership in an employee organization.

NIDA
NATIONAL INSTITUTE ON DRUG ABUSE

TENURE-TRACK INVESTIGATOR: The Department of Health and Human Services (DHHS), National Institutes of Health (NIH), announces a search for a tenure-track scientist, to lead the structural biology program at the Intramural Research Program (IRP), National Institute on Drug Abuse (NIDA). Candidates must have a terminal (MD and/or Ph.D.) degree. Candidates will be evaluated on (1) knowledge and experience in proteomics, lipidomics, glycomics, and their bioinformatics; (2) expertise in analytical chemistry, with a major emphasis on mass spectrometry and chromatography; (3) an understanding of mass spectrometric techniques applied to surface imaging, including MALDI, LDI, MALDI-Ion Mobility-oTOFMS - with UV and IR lasers and SIMS, particularly as applied to neuroscience and drug abuse; (4) knowledge of direct tissue imaging analysis of drug and biomolecular localization; (5) demonstrated ability to prepare biological tissue samples for quantitative and semi-quantitative spatial analysis of small and large molecules by laser and ion microprobe and laser capture microdissection; (6) application of these techniques, as well as ESI, Ion traps, Quadrupole and Q-TOF ESI, (GC, TLC and HPLC) /MS, to real-time monitoring of levels of molecules in blood, cerebrospinal fluid and saliva; (7) experience in correlating analytical results with three dimensional theoretical molecular modeling of physiological structure; and (8) successful collaboration with investigators from a wide range of disciplines. The successful candidate may be hired through the NIH Title 42(g) program at a competitive salary rate and with full Federal benefits. Candidates must submit a CV, a statement of proposed research objectives and goals of not more than three pages, and four (4) letters of recommendation (from noncollaborators) to: **Barry J. Hoffer, M.D., Ph.D., Scientific Director, NIDA, and Chief, Cellular Neurophysiology Section, Cellular Neurobiology Research Branch, IRP/NIDA, 5500 Nathan Shock Drive, Baltimore, Maryland 21224**. A copy of the terminal degree (with a certified English translation if foreign) should also be included. **Email: bhoffer@intra.nida.nih.gov**. Application materials must be received by COB on **January 31, 2007**. Applications received after that date will not receive consideration.

Staff Scientist (Core Laboratory)

The National Institute of Allergy and Infectious Diseases (NIAID), a major research component of the NIH and the Department of Health and Human Services, is recruiting for a Staff Scientist (Core Laboratory) in the Respiratory Viruses Section, Laboratory of Infectious Diseases (LID). LID has an active vaccine development program to generate live attenuated virus vaccines for flaviviruses including the four dengue, West Nile encephalitis, St. Louis encephalitis, and Tick-borne encephalitis viruses and respiratory viruses including the three parainfluenza viruses, two respiratory syncytial viruses, and the human metapneumoviruses. Vaccines are also being developed against viruses of interest to biodefense.

Responsibilities: 1) generate documents constituting the Investigational New Drug Application (IND) for the vaccines being developed; 2) work closely with members of the Sponsor of the IND, another unit of the Intramural program of NIAID, to generate final IND documents for submission to the FDA; 3) coordinate efforts of LID staff involving vaccine manufacture and preclinical testing of the vaccine candidates; and 4) organize the response of NIAID to the comments of the FDA regarding IND submissions.

The successful individual will ideally possess an M.D. or Ph.D. degree and have experience with IND preparation for infectious agents, but individuals without one of these degrees will also be considered if they have extensive experience in the field. Experience with generation of investigational vaccines, especially cDNA derived vaccines, and testing of investigational vaccines in animals and human subjects is desired. Salary range is $73,178 - $159,657 and is commensurate with research experience and accomplishments.

Please send CV/Bibliography and three references to **Dr. Alexander Schmidt, Bldg. 50, Room 6511, 50 South Drive, MSC 8007, Bethesda, MD 20892-8007**. Applications must be received by **January 5, 2007**. For additional information on this position, contact **Dr. Alexander Schmidt at schmidta@niaid.nih.gov**.